

BWIS 504

SECOND
INTERNATIONAL
KIMBERLITE
CONFERENCE
1977

Extended Abstracts

SPONSORS

American Geophysical Union	The San Carlos Apache Tribe
The Navajo Tribe, Museum & Research	International Association of
Carnegie Institution of Washington,	Volcanology and Chemistry
Geophysical Laboratory	of the Earth's Interior
U. S. Geological Survey	International Association
U. S. National Committee	of Geochemistry
for Geology	and Cosmochemistry
U. S. National Committee	Inter-Union Commission on
for Geochemistry	Geodynamics/IUGG
U. S. National Committee/IUGG	Commission on Experimental
U. S. Geodynamics Committee	Petrology/IUGS

Convenors: L. H. Ahrens, R.S.A.; F. R. Boyd, U.S.A.; J. B. Dawson, U.K.

Organizing Committee: O. L. Anderson, A. L. Boettcher, F. R. Boyd (Chmn.),
D. H. Eggler, S. R. Hart, T. H. Jordan, T. R.
McGetchin, W. G. Melson, H. O. A. Meyer, M. E.
McCallum, J. R. Smyth, G. A. Swann, H. G. Wilshire

Editorial and Program Committee: F. R. Boyd and H. O. A. Meyer

EXTENDED ABSTRACTS

contributed to

THE SECOND INTERNATIONAL KIMBERLITE CONFERENCE

Bishop's Lodge, Santa Fe, New Mexico

October 3-7, 1977

DIAMONDIFEROUS KIMBERLITE OF THE WAJRAKHARUR AREA,
SOUTHERN INDIA.

Jagannadham Akella: Univ. of California, Lawrence
Livermore Lab., Livermore, California 94550
Robert H. McCallister: Dept of Geoscience, Purdue University
Henry O.A. Meyer: West Lafayette, Indiana 47907

Although diamond has been known in India from antiquity the presence of kimberlite has been the subject of much speculation and controversy. However, in the late 19th Century igneous rocks, supposedly the hosts of diamond at Panna and Wajrakharur were described, but were discounted as being kimberlite (Foote, 1889; Lake, 1890). Subsequently, others studied the source of diamonds (Picamuthu and Rao, 1932; Mathur and Singa, 1963; and Mehr, 1953) but generally considered that kimberlite was not present. However, in 1963 Rao and Phadtre after examining the geology and petrography for four igneous bodies near Wajrakharur, Andhra Pradesh concluded they were kimberlitic. We report here preliminary data on the mineralogy and mineral chemistry of phases from two of these diatremes and confirm the conclusion of Rao and Phadtre that these are kimberlites.

Four pipe-like bodies are located in the region of Wajrakharur; two are near this village and the other two are near Lattavaram, about 6 miles SSW of Wajrakharur. The bodies are somewhat oval in shape, trending roughly N70°E, and have intruded pre-cambrian granite and gneiss. The material in the pipes is highly weathered near the surface and consists of serpentine, calcite, clay minerals and fragments of crustal and local host country-rock.

At Lattavaram the kimberlite is somewhat more durable and compact than at Wajrakharur and it is thus possible to distinguish slight mineralogical and petrographic differences between the two pipes. Rao and Phadtre (1963) report the occurrence of eclogite and peridotite xenoliths from this locality but unfortunately we have not yet been able to confirm this observation. For the most part xenoliths consist of amphibolite or other crustal fragments.

Petrographically the two kimberlites near Lattavaram are distinct. One kimberlite (L1) consists of relatively small (average about 1 mm) phenocrysts of olivine in a very dark, fine grained matrix of serpentine, calcite, phlogopite and magnetite-rich spinel. Minor monticellite and pectolite were also noted. Spinels in this rock appear to be of two types - a minor number are rich in chromium (7-11 wt% Cr₂O₃) whereas the second group have generally about 2-4 wt% Cr₂O₃.

The second kimberlite at Lattavaram (L2) is much more coarsely grained than L1. The phenocrysts of olivine are larger and more abundant although they are for the most part serpentized. Ilmenite and garnet, the latter with very thick kelyphitic rims, are also present in this kimberlite. The ground mass consists predominantly of serpentine, calcite, minor phlogopite and opaque phases,

including spinel and ilmenite. Minor phases such as sphene and perovskite have also been observed.

Chemical analyses of various phases from the two kimberlites at Lattavaram are presented in Tables 1 and 2. The analyzed olivine in L1 is generally close to Fo_{92} whereas that in L2 ranges between Fo_{88} and Fo_{92} . The garnets in L2 kimberlite are predominantly pyrope with subsidiary almandine and grossular. Cr_2O_3 is approximately 2.5 - 3.0 wt% in these garnets which are also relatively low in CaO (~5 wt%). The ilmenites so far analyzed vary in chromium content with some containing up to 4 wt% Cr_2O_3 . These ilmenites rich in Cr_2O_3 also contain high amounts of MgO relative to the Cr-poor ilmenites.

Serpentinized olivine phenocrysts in L1 kimberlite are interesting in that the veins of serpentine contain numerous minute needles of a nickel sulfide phase. A maximum content of 72 wt% Ni was obtained for this mineral which strongly suggests it is heazewoodite (Ni_3S_2). The occurrence of this phase is believed to be due to late stage sulfurization of the olivine, accompanying serpentinization, with the Ni being derived from the original olivine (0.2 - 0.3 wt% NiO).

The geological occurrence, plus the petrographic character of these rocks, and the similarity of mineral compositions with other known kimberlites are sufficient evidence to support Rao and Phadtre (1963) in their conclusion that these are true kimberlites.

References


1. Foote, R.B. (1889). Rec. Geol. Surv. Ind., v. 22.
2. Lake, P. (1890). Rec. Geol. Surv. Ind., v. 23.
3. Mathur, S.M. and Singa, H.N. (1963). Bull. Geol. Surv. Ind., no. 21.
4. Mehr, S. (1953). Quat. Jour. Min. Met. Soc. Ind., v. 24.
5. Picamuthu, C.S. and Rao, R. (1932). Proc. Ind. Sci. Cong., 19th Session.
6. Rao, P.S. and Phadtre, P.N. (1963). Geol. Soc. Ind., I. 118-123.

Table 1. Representative analyses of minerals from Lattavaram-1 kimberlite.

	Olivine	Spinel (1)	Spinel (2)	Monticellite	Pectolite	Serpentine
SiO ₂	41.50	-	-	37.25	52.40	42.57
TiO ₂	0.02	9.80	7.32	0.27	0.04	0.02
Al ₂ O ₃	-	0.95	1.17	0.06	0.50	0.97
Cr ₂ O ₃	0.09	2.63	10.69	-	0.04	0.13
FeO	7.84	79.25	71.94	8.05	0.52	1.07
MgO	50.86	6.69	7.16	21.63	0.23	39.46
CaO	0.10	-	-	32.46	33.73	0.77
MnO	0.12	0.54	0.58	0.29	0.13	0.23
Na ₂ O	-	-	-	0.06	9.34	0.09
K ₂ O	-	-	-	0.05	0.04	0.05
NiO	0.34	-	-	0.02	0.01	-
Co	-	0.12	0.14	-	-	-
Cu	-	0.07	0.03	-	-	-
Total	100.87	100.05	99.03	100.14	96.99 (+OH)	85.36 (+OH)

Table 2. Representative analyses of minerals in Lattavaram-2 kimberlite.

	Olivine	Garnet	Ilmenite (1)	Ilmenite (2)	Phlogopite	Serpentine	Sphene
SiO ₂	41.28	42.77	0.24	0.16	39.92	42.42	29.71
TiO ₂	0.05	0.11	53.37	53.18	0.58	0.05	37.08
Al ₂ O ₃	0.02	21.53	0.30	0.38	13.64	0.74	1.34
Cr ₂ O ₃	0.06	2.82	4.03	0.79	0.03	0.02	-
FeO	11.23	7.58	23.73	35.48	2.80	4.32	1.66
MgO	43.23	21.28	16.43	10.08	25.67	37.76	0.13
CaO	0.21	4.48	0.34	0.02	0.01	0.12	27.53
MnO	0.15	0.36	0.54	0.25	0.02	0.20	0.05
Na ₂ O	0.03	-	0.01	0.06	-	-	-
K ₂ O	-	-	-	-	10.10	-	0.01
NiO	0.23	-	0.05	-	0.01	0.19	0.01
Total	101.49	100.93	99.04	100.39	92.78 (+OH)	85.82 (+OH)	97.52



Digitized by the Internet Archive
in 2018 with funding from
University of Alberta Libraries

<https://archive.org/details/secondinternatio02inte>

PYROXENE-GARNET SOLID SOLUTION EQUILIBRIA IN THE EARTH'S MANTLE

Syun-iti Akimoto and Masaki Akaogi (Institute for Solid State Physics, University of Tokyo, Roppongi 7-22-1, Minato-ku, Tokyo 106, Japan)

Pyroxene-garnet solid solution equilibria have been studied in the pressure range 41 to 200 kbar over the temperature range 850 to 1450°C for the system enstatite-pyroxene and in the pressure range 30 to 105 kbar over the temperature range 1000 to 1300°C for the system ferrosilite-almundine. Preliminary investigations have also been progressing on the system $\text{Ca}_2\text{Mg}_2\text{Si}_4\text{O}_{12} - \text{Ca}_{1.5}\text{Mg}_{1.5}\text{Al}_2\text{Si}_3\text{O}_{12}$ in the pressure range 68 to 190 kbar at 1200°C. These phase equilibrium experiments were made using three types of high pressure apparatus — a tetrahedral anvil type, a cubic anvil type, and a double-staged cubic-octahedral anvil type. Pressure values in these multi-anvil apparatus were calibrated by means of several pressure fixed points. Latest data in our laboratory on the transformation pressure of high-Ba(126 kbar), Pb(142 kbar), ZnS(162 kbar), and GaAs(193 kbar) were adopted as fixed points between 100 and 200 kbar. High temperature correction was further made based on the phase boundary curves between coesite and stishovite, $P(\text{kbar}) = 80 + 0.011T(^\circ\text{C})$, and between pyroxene and ilmenite in ZnSiO_3 , $P(\text{kbar}) = 91 + 0.02T(^\circ\text{C})$, which were recently determined by means of in situ x-ray measurements.

Phase relationships in the system $\text{Mg}_4\text{Si}_4\text{O}_{12} - \text{Mg}_3\text{Al}_2\text{Si}_3\text{O}_{12}$ at 1000°C are shown in Figure 1. The solid solubility of enstatite in pyroxene increases gradually to 140 kbar and then suddenly in the pressure range 140 to 175 kbar, resulting in formation of homogeneous garnet with composition $\text{Mg}_3(\text{Al}_{0.8}\text{Mg}_{0.6}\text{Si}_{0.6})\text{Si}_3\text{O}_{12}$. In the MgSiO_3 rich field, the three phase assemblage of $\beta\text{Mg}_2\text{SiO}_4$ (or $\gamma\text{Mg}_2\text{SiO}_4$), stishovite and a garnet solid solution is stable at pressures above 175 kbar. Although these results support qualitatively

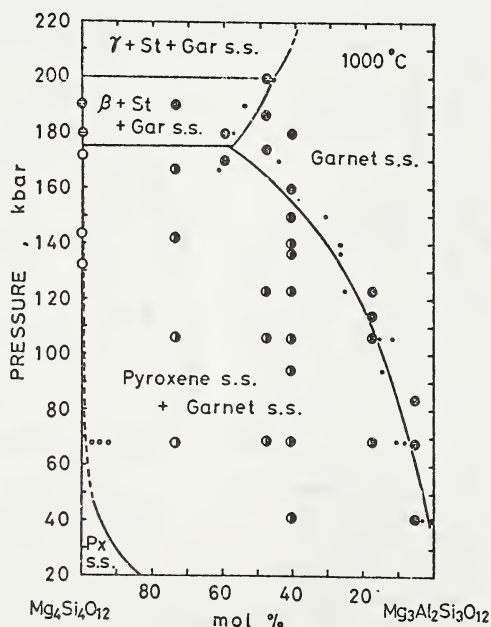


Figure 1

Ringwood's idea on the pyroxene-garnet transformation in the system $\text{Mg}_4\text{Si}_4\text{O}_{12} - \text{Mg}_3\text{Al}_2\text{Si}_3\text{O}_{12}$, some quantitative disagreements were found between these two investigations. He suggested

that a glass with the composition of $\text{MgSiO}_3 \cdot 10\% \text{Al}_2\text{O}_3$ (wt%), corresponding to $[\text{Mg}_4\text{Si}_4\text{O}_{12}]_{0.6} \cdot [\text{Mg}_3\text{Al}_2\text{Si}_3\text{O}_{12}]_{0.4}$, completely crystallized to the garnet structure at pressures around 110 kbar at 1000°C.

The system ferrosilite-almandine shows the similar trend of high pressure transformations (Figure 2): maximum solubility of ferrosilite in almandine for forming a homogeneous garnet solid solution is 40 mol% at 93 kbar and 1000°C. A systematic increase in the solid solubility of diopside component in $\text{Ca}_{1.5}\text{Mg}_{1.5}\text{Al}_2\text{Si}_3\text{O}_{12}$ garnet with increasing pressure was also observed at pressures above about 100 kbar at 1200°C.

If the pyrolite mantle is assumed and further high pressure transformations of pyroxenes with 10wt% R_2O_3 ($=\text{Al}_2\text{O}_3 + \text{Cr}_2\text{O}_3 + \text{Fe}_2\text{O}_3$) in the pyrolite mantle are approximated by those of a simple composition of $\text{MgSiO}_3 \cdot 10\% \text{Al}_2\text{O}_3$, from the present results, the following transformation scheme is suggested for the pyroxene-garnet assemblage. The pyroxene-garnet transformation is spread over more than 400 km in depth from about 120 to 540 km. At the latest range in depths between 450 and 540 km, pyroxenes transform effectively to a complex garnet solid solution. Complete disappearance of pyroxenes in the mantle takes place at about 540 km in depth. The complex garnet solid solution is expected to be stable at depths between 540 and 590 km. At deeper depths, it will decompose to a three-phase mixture of modified spinel (β phase) or spinel (γ phase), stishovite and garnet solid solutions dissolving lower amount of pyroxene component.

Zero pressure densities for the composition of $[\text{Mg}_4\text{Si}_4\text{O}_{12}]_{0.6} \cdot [\text{Mg}_3\text{Al}_2\text{Si}_3\text{O}_{12}]_{0.4}$ at varying pressures or depths are calculated and shown in Figure 3. In the range of depths from about 450 to 540 km, high gradient of the density increase appears. It is likely that this leads to about 2% increase in P-wave velocity at that depth range. It is concluded that the pyroxene-garnet transformation is responsible for the minor seismic discontinuity around 500 km in depth.

Since the garnets at depths below about 150 km

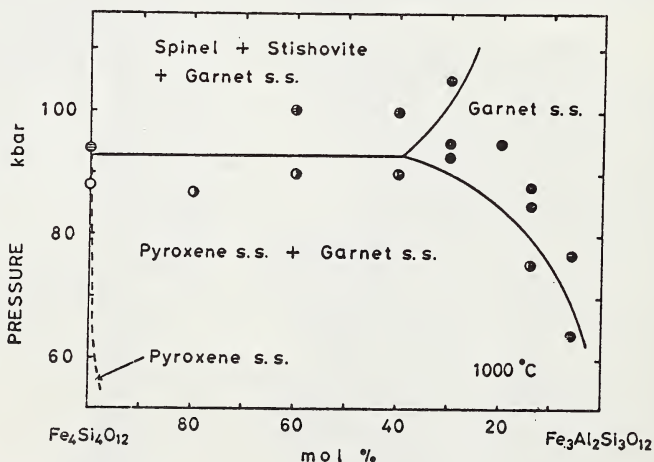


Figure 2

dissolve an appreciable amount of pyroxene component, natural finding of garnet with the atomic number of Si higher than 3 is very probable in the ultramafic inclusions in kimberlites.

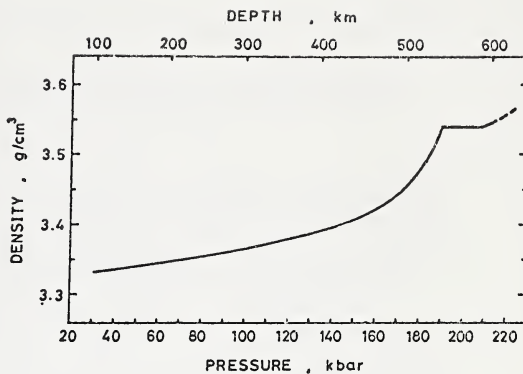


Figure 3

Pb, Sr AND Nd ISOTOPES IN MINERALS FROM ULTRAMAFIC NODULES IN KIMBERLITES.

C. J. Allègre, G. Manhès, P. Richard, D. Rousseau and N. Shimizu (Laboratoire de Géochimie et Cosmochimie, Institut de Physique du Globe, Université de Paris 6, Paris, France).

The major minerals were separated from garnet lherzolite nodules in kimberlites (from Lesotho and South Africa) and were analysed for isotopic compositions of Sr, Nd and Pb and for concentrations of Rb, Sr, Sm, Nd and Pb. The clinopyroxene, garnet and the whole-rock sample of a sheared garnet lherzolite (W 397) from the Premier Pipe define an isochron of 1.4 ± 0.02 b.y. with the initial $\text{Sr}87/\text{Sr}86 = 0.70241 \pm 0.00006$. Compared with the ages obtained by Barrett and Allsop (1973) for the Premier kimberlite pipe of 1.2-1.4 b.y., the present result suggests that these minerals had been in approximate isotopic equilibrium until pipe emplacement. This is consistent with the results of Erlank and Shimizu (1977) on a peridotite nodule in a Cretaceous pipe but diverges from those of Basu and Murthy (1977), who obtained a mineral isochron age of 3.4 b.y. for a peridotite nodule in a recent volcanic rock from San Quintin, Baja California.

The Rb (0.034 ppm) and Sr (96.4 ppm) concentrations of the clinopyroxene in W 397 lherzolite are very similar to those of the clinopyroxenes separated from sheared garnet lherzolites in Cretaceous pipes (Shimizu, 1975).

The isotopic composition and concentration of Pb were also determined in the clinopyroxene separate with a technique involving a chemical blank of 100 pg for Pb. The sample (40 mg) was washed four times with 0.5M HBr before HF decomposition. The first two steps of acid wash yielded significant amount of Pb (500 and 360 pg, respectively), while the third step showed only 30 pg, suggesting that most of the surface Pb was removed. The isotopic composition ($206/204 = 17.42$, $207/204 = 15.41$, $208/204 = 36.85$) is similar to the least radiogenic diopside sample reported by Kramers (1977), and plots on a primary growth curve with $\mu = 8.1$ and close to the meteoritic isochron (geochron).

References

- Barrett, D. R. and Allsop, H. L. (1973) Extended Abstract, First Kimberlite Conference, Cape Town, 23.
Basu, A. R. and Murthy, V. R. (1977) EPSL, 35, 239.
Erlank, A. J. and Shimizu, N. (1977) This Volume.
Kramers, J. D. (1977) EPSL, 34, 419.
Shimizu, N. (1975) Phys. Chem. Earth, 9, 655.

RB-SR AND U-PB AGE DETERMINATIONS ON SOUTHERN AFRICAN KIMBERLITE PIPES

H.L. Allsopp and J.D. Kramers (Bernard Price Institute of Geophysical Research, University of the Witwatersrand, Johannesburg, 2001, South Africa)

Radiometric age determinations were undertaken on 15 kimberlite occurrences in Southern Africa, emphasis being placed on a wide areal distribution of occurrences, and on occurrences for which pre-Karoo ages are indicated by field relationships. The Rb-Sr method, applied to mica (usually phlogopite), was used where possible. An alternative method, utilising the U-Pb isochron approach on whole rock and perovskite-enriched samples, was tested with a view to its application on samples devoid of mica.

Rb-Sr ages. New Rb-Sr age measurements are listed below. Other data by the same method are given in Allsopp and Barrett (1975). Further measurements are still in progress, for which reason the new data may be subject to minor revision. A value of $1.39 \times 10^{-11} \text{ yr}^{-1}$ was used for the ^{87}Rb decay constant.

Letseng-la-Terai, a pipe which cuts the uppermost Drakensberg basalts (age 180 m.y., Fitch and Miller, 1971) in Lesotho yielded mica ages of 380, 580 and 660 m.y. The pipe contains abundant basement xenoliths and the data may reflect incorporation of basement mica. Microprobe examination of the mica in question is in progress.

Finsch, in the northern Cape Province, yielded two ages of 130 and 170 m.y.. These data are compatible with the post-Karoo field relationship of this pipe.

Njoio and Tchivira, two intrusions with kimberlitic affinities in central Angola, were dated using mica and K-feldspar, and the result obtained was $130 \pm 10 \text{ m.y.}$

Swartruggens (Transvaal). The age of Swartruggens reported by Allsopp and Barrett (1975) was confirmed ($150 \pm 3 \text{ m.y.}$); no difference in age between the two fissures at Swartruggens could be discerned.

Colossus, a pipe situated in central Rhodesia, yielded a mica isochron age of $490 \pm 20 \text{ m.y.}$. The samples, available only from surface dumps, were all altered and the uncertainty in the result may have been underestimated.

National, a pipe situated close to the Premier pipe in the Transvaal, yielded a mica-isochron age of $1180 \pm 30 \text{ m.y.}$. The samples were again from weathered surface outcrops.

Premier data were previously reported by Barrett and Allsopp (1973) but not published in full because further work was intended. Unfortunately development in the mine has not yet permitted collection of fresh samples of the oldest type (2) kimberlite at distances sufficiently remote from the cross-cutting sill. Available Rb-Sr evidence indicates an age of 1250 m.y. for the type 1 and about 1200 m.y. for the type 4 kimberlites.

Camafuca, from Angola, yielded a mica isochron age of $1810 \pm 20 \text{ m.y.}$, a result in gross conflict with the supposed post-Karoo age of this intrusion. This result is further discussed below.

Discussion of Rb-Sr ages. In several cases the Rb-Sr ages obtained are in conflict with established geological relationships. Two mechanisms that could account for such anomalous results are considered.

(i) The mica analysed could have been derived from an older source. This older source could be the basement intruded by the kimberlite, in which case the mica is more likely to be biotite than phlogopite. An example of this is Camafuca: Microprobe analysis shows the mica to be biotite, the distinction being based largely on the Fe/Mg ratio. Allsopp and Barrett (1975) suggested that xenocrystic phlogopite could retain ages significantly, though not

greatly, in excess of the kimberlite age. The effect would be most significant for the youngest pipes, and may account for some of the scatter between different Rb-Sr ages from a particular pipe (e.g. Finsch), and for the differences between U-Pb zircon ages (Davis, private communication) and Rb-Sr ages from some occurrences (e.g. Finsch and Roberts Victor).

(ii) A linear or near-linear array of data points on an isochron diagram may also be the result of contamination by unradiogenic Sr. Micaceous whole-rock kimberlites have initial $^{87}\text{Sr}/^{86}\text{Sr}$ ratios of around .708 (Barrett and Berg, 1975), but the leachable carbonate component usually has an $^{87}\text{Sr}/^{86}\text{Sr}$ ratio of around .704 (Brookins, 1967). Therefore two different initial ratios can exist within the same kimberlite, and contamination of the radiogenic Sr in the mica with the Sr from the carbonate component might give rise to apparent ages which are too high. This effect would only be significant if the present-day $^{87}\text{Sr}/^{86}\text{Sr}$ ratios of the micas are less than about .75, and for most of the data reported here the influence of this factor is negligible.

U-Pb dating. Kleeman and Lovering (1973) have reported that uranium in the kimberlite matrix is very strongly concentrated into secondary perovskite and into alteration rims of ilmenite. Carbonate minerals of the kimberlite matrix are on the other hand extremely poor in uranium. The partitioning of uranium in this way presumably took place during, or shortly after, pipe formation. If closed-system behaviour prevailed since then, a mineral-isochron approach whereby $^{238}\text{U}/^{204}\text{Pb}$ is plotted against $^{206}\text{Pb}/^{204}\text{Pb}$, might yield the pipe age. The crudest approach to obtaining two "phases" of a matrix kimberlite suitable for such a plot is to leach the kimberlite in HCl, dissolving mainly the carbonate. The pair leach-residue is plotted in a $^{206}\text{Pb}/^{204}\text{Pb}$ vs. $^{238}\text{U}/^{204}\text{Pb}$ isochron diagram. Age-values were obtained in this way for the pipes Wesselton, Dutoitspan and Monastery. They are shown in Table 1 and compared with results reported by Allsopp and Barrett (1975).

Table 1: U-Pb and Rb-Sr ages.

<u>Sample</u>	<u>age U-Pb</u>	<u>age Rb-Sr</u> (Allsopp and Barrett, 1975)
Wesselton	90 \pm 4 m.y.	83, 84 m.y.
Dutoitspan	77 \pm 6 m.y.	--- (assumed same age as Wesselton)
Monastery	83 \pm 5 m.y.	90 m.y.

The perovskite in the kimberlite matrix is fine-grained (ϕ 5-50 micron). Separation of a perovskite-enriched fraction by heavy liquids and magnetic separation is easy, but handpicking is required to obtain a pure concentrate. Age determinations involving separation of a perovskite-enriched fraction were made on samples from the following pipes:

Table 2: U-Pb and Pb-Pb ages.

<u>Sample</u>	<u>age 206-238</u>	<u>age 207-206</u>
De Beers (Kimberley)	92 \pm 4 m.y.	120 \pm 100 m.y.
Colossus (Rhodesia)	660 \pm 20 m.y.	330 \pm 60 m.y.
Beit Bridge (")	420 \pm 20 m.y.	730 \pm 60 m.y.
Dokolwayo (Swaziland)	300 \pm 20 m.y.	400 \pm 200 m.y.
Goedgevonden (Transvaal)	117 \pm 4 m.y.	150 \pm 100 m.y.

Age determinations involving mineral separation were also attempted on five samples from the Premier mine, representing types 1, 2 and 3 as mapped by mine geologists. A good spread in U/Pb ratios and Pb isotopic compositions was only obtained for samples from type 3. The 207/206 age for this kimberlite

was 1250 ± 50 m.y., whereas values of 800 and 940 m.y. were obtained for the ^{206}Pb - ^{238}U age. In the case of type 1, the situation was complicated by sulphides which had apparently incorporated radiogenic lead at a time substantially after pipe formation.

Generally, it seems that ages obtained by the U-Pb mineral isochron method are roughly concordant for kimberlites round 100 m.y. old, but that lead loss (as in Premier, Type 3, and Beit Bridge) or uranium loss (as in Colossus) can occur in the more uranium-rich fraction analysed, if the samples are substantially older. However, the significance and relative precision of the lead 207/206 age of a sample increases with the actual sample age. For older samples, the effect of uranium- or lead loss is best visualised by the use of the concordia plot as commonly used for zircon data. In a concordia plot, the slopes of the $^{206}\text{Pb}/^{204}\text{Pb}$ vs. $^{238}\text{U}/^{204}\text{Pb}$ and the corresponding $^{207}\text{Pb}/^{204}\text{Pb}$ vs. $^{235}\text{U}/^{204}\text{Pb}$ "isochrons" can be plotted as $^{206}\text{Pb}/^{238}\text{U}$ and $^{207}\text{Pb}/^{235}\text{U}$ ratios.

While it appears that the U-Pb mineral isochron method, applied to kimberlitic minerals, can provide answers that are roughly correct, we feel that this method should only be used as a "last measure" in cases where no alternative method can be applied.

The data reported above shows that Southern African kimberlites range widely in age. With the establishment of this range, it becomes clear that no particular correlation in time and place between kimberlite occurrence and large-scale volcanic activity (such as the Karroo volcanism) can be maintained.

References

- H.L. Allsopp and D.R. Barrett (1975): Rb-Sr age determinations on South African kimberlite pipes. *Physics and Chemistry of the Earth*, 9 (Pergamon Press), pp 605-617
- D.R. Barrett and H.L. Allsopp (1973): rubidium-strontium age determinations on South African Kimberlite pipes. *First International Kimberlite Conference, extended abstract volume (University of Cape Town)*, pp 23-25.
- D.R. Barrett and G.W. Berg (1975): Complementary petrographic and strontium-isotope ratio studies of South African kimberlite. *Physics and Chemistry of the Earth*, 9 (Pergamon Press), pp619-635
- D.G. Brookins (1967): The strontium geochemistry of carbonates in kimberlites and limestones from Riley County, Kansas. *Earth and Planetary Science Letters*, 2, pp 235-240.
- F.J. Fitch and J.A. Miller (1971): Potassium-argon radioages of Karroo volcanic rocks from Lesotho. *Bulletin Volcanologique*, XXXV, pp 64-84.
- J.D. Kleeman and J.F. Lovering (1973): Uranium partitioning in kimberlites and their deep-seated inclusions. *First International Kimberlite Conference, extended abstract volume (University of Cape Town)*, pp 189-190.

STRESS CORROSION CRACK PROPAGATION AS A POSSIBLE MECHANISM FOR KIMBERLITE
PIPE FORMATION

O. L. Anderson (Institute of Geophysics and Planetary Physics, University of
California, Los Angeles, California 90024 U.S.A.)

The stress corrosion model is used whereby an igneous intrusion of magma within a crack is used to describe the physical processes of pipe eruption. A symbiotic relation exists between the crack and the fluid. The crack cannot go faster than the fluid within the crack can flow in the channel provided by the crack, and the speed of the fluid is limited by its own viscosity. A volatile phase at the tip of the crack at lithostatic pressures will allow the crack to accelerate to high speeds, since the viscosity of a volatile is small.

It is proposed that Kimberlite pipes occur in those rare regions of the earth where the composition of rocks at depth are rich in CO₂ compounds. A crack passing through such a region releases abundant CO₂ gas which accumulates in the tip of the crack. This provides the necessary low viscosity for the crack to accelerate. It becomes unstable, and the speed approaches the shear velocity of sound as the crack breaks through the earth's surface.

LHERZOLITE INCLUSIONS AND MEGACRYSTS FROM THE GERONIMO VOLCANIC FIELD, SAN BERNARDINO VALLEY, SOUTHEASTERN ARIZONA

R. J. Arculus (Research School of Earth Sciences, A.N.U., Canberra, A.C.T. 2600, Australia)

M. A. Dungan (NASA - Johnson Space Center, Houston, Texas 77058)

G. E. Lofgren (NASA-Johnson Space Center, Houston, Texas 77058)

J. M. Rhodes (Lockheed Electronics Co., Inc., Houston, Texas 77058)

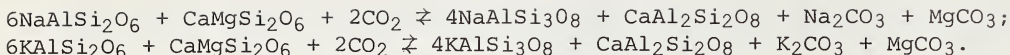
The Geronimo volcanic field of the San Bernardino Valley, southeastern Arizona is one of a number of upper Cainozoic basalt fields in the southwestern U.S.A. and northern Mexico. The lava flows and cinder cones of the Geronimo field are composed of mildly silica-undersaturated alkali olivine basalts with Mg/(Mg+Fe) ratios in the range 0.65 to 0.55, comparable with the other Cainozoic basalt fields. The basalts contain forsteritic olivine, calcic augite and occasionally plagioclase phenocrysts, and magnetite in addition to these phases in the groundmass (Analysis, Table 1).

These are apparently two distinct periods of volcanism in the San Bernardino Valley. The dissected "older" basalts are distributed on the flanks of the valley and are perched above the valley floor. These older flows were erupted prior to substantial north-south faulting on valley boundary faults. The "younger" cinder cones and flows are well preserved morphologically and a K-Ar age of approximately 50,000 years has been obtained for one of the largest cones (D. J. Lynch, pers. comm.). Several maars are present and the largest of these is approximately 1.5 km in diameter, 150 m deep and is rimmed by 30 m of basaltic tuff. In the vicinity of Palaeozoic limestone outcrops, a control on the distribution of vents by basement structure is apparent but elsewhere the structural control is not obvious.

Spinel lherzolite and megacrysts of calcic augite, kaersutite, feldspar, spinel and magnetite are present in the majority of the flows and cinder cones, but the absolute amounts and proportions of megacryst species and nodules varies considerably. Mineralogically the lherzolites are composed of olivine (Fo₉₁₋₈₈), calcic augite (Ca_{45.5}, Mg_{49.5}, Fe_{5.0}), orthopyroxene (Ca_{1.5}Mg_{89.0}Fe_{9.5}) and spinel. The spinel varies in colour from light brown and green through to dark red-brown, and also in composition but is predominantly a chromian spinel. Representative analyses of the lherzolititic phases are included in Table 1. Some of the nodules show signs of reaction with the host basalts. For example, the Cr-Al-rich spinels show an increasing magnetite component and are darker in colour where in close contact with the host. Also potassic feldspars are present in veins and cracks probably from host contamination.

Clinopyroxene megacrysts range in composition from those similar to lherzolite pyroxene to more Fe and Ca-rich varieties (Table 1). The megacrysts probably represent both disaggregated nodule material and high-pressure cognate phenocrysts. Banks of rods and spherules of pyrrhotite are present in some of the cognate megacrysts. It is conceivable that the sulfide globules were trapped during crystal growth although injection along annealed cracks is also a possibility.

Feldspar megacrysts range from potash oligoclase through lime anorthoclase to anorthoclase in composition and are similar to feldspar megacrysts in other Cainozoic basalt fields. Possible equilibria that may be involved in the genesis of these alkali feldspars are currently under experimental study at NASA-JSC and ANU-RSES. Preliminary results suggest an expansion of the primary phase field of feldspar in the presence of CO₂ relative to the volatile-free systems in the following equilibria studied at 7 and 15 kbar:-



Spinel megacrysts exhibit a wide range of composition and include some complex assemblages that permit estimates of T and f_{O_2} of equilibration. For example, some spinels included in augite megacrysts contain magnetite exsolved on {111} planes, ilmenite blebs and globular pyrrhotite. In rare samples, corundum is also present typically in veins and cracks. In one spinel inclusion, coexisting pyrrhotite and pyrite has been analyzed but this assemblage does not appear to be common.

If the assumption is made that the magnetite and ilmenite solid solutions have remained in equilibrium together with the host spinel, then the T and f_{O_2} of the last equilibration can be calculated (Buddington and Lindsley, 1964). Assuming this temperature also applies to the pyrrhotite compositions, then f_{S_2} can also be determined (Toulmin and Barton, 1964). The assemblage spinel_{ss} and titaniferous magnetite requires that $x_{\text{Fe}_3\text{O}_4}^{\text{spinel}}$ and $x_{\text{Fe}_3\text{O}_4}^{\text{mt}}$ be calculated from microprobe analyses with total Fe as FeO . The usual procedure for recalculating magnetite compositions (Carmichael, 1967) has been modified to group MgO (+ FeO) with Al_2O_3 in the ratio given by the host spinel. Excess FeO is then computed firstly as $2\text{FeO}\cdot\text{TiO}_2$ and then as Fe_3O_4 . Both the magnetites and ilmenites are aluminous and uncertainty may be attached to the application of the Buddington-Lindsley geothermometer/geobarometer, but temperatures in the range 830-700°C at $\log f_{\text{O}_2}$ of 10^{-12} to $10^{-15.5}$ are calculated ignoring any pressure effect. The lack of detectable Ti in the host spinel implies that the activity coefficients for Fe_2TiO_4 in magnetite are large and that the solvus between $(\text{Mg,Fe})\text{Al}_2\text{O}_4 - (\text{Fe}_2\text{TiO}_4\cdot\text{Fe}_3\text{O}_4)$ spinels is not regular.

The pyrrhotite compositions give $\log f_{\text{S}_2}$ in the range -1 to -0.5 and the pyrrhotite-pyrite pair appears to confirm the lower temperature limit (700°C) calculated from the host spinel plus Fe-Ti oxides. Some of the homogeneous Ti-Al-Mg-rich magnetite megacrysts may be cognate with the host lava but the more complex assemblages are apparently unrelated to the host.

The cause of the Upper Cainozoic basaltic volcanism in the southwestern U.S.A. has lately been related to the change in plate motions from compressional to tensional plus shear associated with the collision of the proto-East Pacific Rise with the Americas Plate (e.g. Christiansen and Lipman, 1972). It is suggested that a possible eruption trigger is through mantle diapirism following the eastward passage of the trailing edge of subducted Farallon Plate (Snyder et al., 1976), contemporaneous with Basin and Range Faulting.

References

- Buddington, A.F. and D.H. Lindsley, Iron-titanium oxide minerals and synthetic equivalents, *J. Petrol.* 5 (1964) 310-357.
- Carmichael, I.S.E., The iron-titanium oxides of salic volcanic rocks and their associated ferromagnesian silicates, *Contrib. Mineral. Petrol.* 15 (1967) 36-64.
- Christiansen, R.L. and P.W. Lipman, Cenozoic volcanism and plate-tectonic evolution of the western United States, Pt. 2, Late Cenozoic, *Phil. Trans. R. Soc. London A.* 271 (1972) 249-284.
- Snyder, W.S., W.R. Dickinson and M.L. Silberman, Tectonic implications of space-time patterns of Cenozoic magmatism in the western United States, *Earth Planet. Sci. Lett.* 32 (1976) 91-106.
- Toulmin, P. III and P.B. Barton, Jr., A thermodynamic study of pyrite and pyrrhotite, *Geochim. Cosmochim. Acta* 28 (1964) 641-671.

Table 1. Analyses of host basalt, individual lherzolite phases and megacrysts

	1	2	3	4	5	6	7
SiO ₂	44.41	40.96	51.35	54.71	0.00	48.30	64.52
TiO ₂	2.50	0.00	0.30	0.00	0.00	0.98	0.00
Al ₂ O ₃	15.50	0.00	6.56	4.50	58.94	9.25	21.09
Cr ₂ O ₃	0.00	0.00	0.88	0.27	9.03	0.13	0.00
FeO*	10.06	9.98	2.63	6.42	9.96	6.75	0.00
MnO	0.22	0.00	0.00	0.11	0.00	0.00	0.00
MgO	9.36	49.17	15.44	33.18	21.56	13.86	0.00
CaO	10.05	0.00	19.96	0.78	0.00	18.81	1.74
Na ₂ O	3.75	0.00	1.48	0.00	0.00	1.18	8.16
K ₂ O	1.94	0.00	0.00	0.00	0.00	0.00	4.01
Total	98.35	100.11	98.60	99.97	99.49	99.26	99.52

* Total Fe as FeO. Analyses are by TPD microprobe except for column 1 by XRF. Total in column 1 includes 0.56 wt.% P₂O₅ in host basalt; 2 = ol. in lherz.; 3 = cpx in lherz; 4 = opx in lherz; 5 = spinel in lherz; 6 = cpx megacryst; 7 = feldspar megacryst.

DENSE INCLUSIONS IN THE SULLIVAN BUTTES LATITE, CHINO VALLEY, YAVAPAI COUNTY, ARIZONA.

Richard J. Arculus (Research School of Earth Sciences, Australian National University, Canberra, A.C.T. 2600, Australia)

Douglas Smith (Department of Geological Sciences, University of Texas at Austin, Austin, Texas 78712, U.S.A.)

Dense inclusions are abundant in potassic latite about 25 m.y. in age which occurs in the southwestern structural transition zone of the Colorado Plateau (Krieger, 1965; Krieger and others, 1971). The host rock (1, Table 1) consists of shallow intrusions, breccias, and flows in Precambrian and Paleozoic country rock. Phenocrysts of biotite ($Mg/Mg+Fe = 0.65$), clinopyroxene ($Ca_{44}Mg_{46}Fe_{10}$), feldspar ($An_{55}Ab_{43}Or_2$) and apatite are present in the latite of Table 1; amphibole is prominent elsewhere. The inclusions are distributed on the order of 1 per 0.25 square meter on host rock surfaces and vary in size from 1 to 50 cm. Freshest samples are near country rock contacts.

Estimates of rock type abundances are based on grid counts and indicate approximately 60% of the nodules at the chief locality are eclogites. These are composed of variable proportions of garnet (near $Pyr_{37}Alm_{37}Gross_{26}$) and clinopyroxene (5-25 mol.% jadeite). Crystal sizes vary from 0.1 to 10 mm although most eclogites contain equant grains ≤ 2 mm. Amphibole is a common additional phase together with rutile, apatite, ilmenite and rare, altered clinzoisite. The eclogites are typically phase-layered and assemblages of strikingly different garnet/clinopyroxene proportions are in sharp contact. Compositional differences exist between different layers. Representative chemical analyses of eclogites of contrasted phase proportions together with microprobe analyses of individual phases are presented in Table 1.

Inclusions with major pargasitic amphibole comprise about 30% of the population at the chief locality and are more abundant elsewhere. Assemblages grade from eclogites with trace amphibole to those with 90% amphibole and minor clinopyroxene and garnet. Phlogopite, apatite, and Fe-Ti oxides are usually associated with amphibole-rich inclusions. In some samples, rutile and garnet are phase-layered with amphibole, giving rise to layers with up to 20 modal % rutile. In these nodules, amphibole crystals are up to 15 mm in length.

Websterites and orthopyroxenites form 2% of the inclusion population and typically contain deformed low-Ca pyroxene porphyroclasts with exsolved garnet in a groundmass of mosaic-textured garnet and pyroxene. The pyroxene porphyroclasts also contain exsolution lamellae of clinopyroxene, and broad beam microprobe analysis suggests that the assemblage results from the reaction of original aluminous pyroxene to an opx-cpx-gnt assemblage (8-10, Table 1). The porphyroclasts are up to 30-50 mm in length and display an undulatory schistosity defined by the garnet and cpx-opx lamellae, with superimposed kink deformation.

In general, the inclusions have metamorphic fabrics ranging from granular mosaic through to lineated. Rare undeformed biotite-apatite-clinopyroxenite inclusions may be cumulate from the host magma, but the other inclusions cannot be direct high-pressure cumulates from the host.

The occurrence of amphibole, phlogopite and biotite in association with eclogitic assemblages is of direct interest in relation to K₂O and H₂O budgets of the lower crust and upper mantle. Amphibole and phlogopite (Table 1) occur

as apparently primary crystals in some inclusions and have shared a common deformation history with garnet and pyroxene. However, at some host rock-eclogite contacts, amphibole and biotite are developed at gnt-cpx contacts. Amphibole without biotite is present along fractures in the eclogite and absent from the unfractured portions of the inclusion where clinopyroxene appears fresh. As a minor phase in eclogitic assemblages, amphibole commonly occurs as an anhedral, interstitial phase formed later than the original assemblage.

Late stage partial melting of some inclusions has resulted in distinctive textures and the formation of plagioclase, hercynite and corundum. Rare kyanite and quartz-feldspar veins in clinopyroxenite may also be related to a partial melting event.

The Fe-Ti oxide assemblages are complex and varied. For example, within a single amphibole-rich inclusion, the four phases rutile, pseudobrookite_{SS}, ilmenite_{SS} and ulvospinel-magnetite_{SS} occur. Rutile with exsolved pseudobrookite_{SS} is particularly common. Typically, all of the oxides other than rutile are highly magnesian with up to 10-13 wt.% MgO in ilmenite and spinel. Full characterization is incomplete but polybaric cooling and oxidation are likely factors involved in the generation of the assemblages.

Distribution coefficients for Fe and Mg between garnet and clinopyroxene in eclogites and websterites range from 3.4 to 7.0. Typical orthopyroxene coexisting with garnet contains 1.4 to 2.5 wt.% Al₂O₃. These data permit estimates of pressures and temperatures of equilibration in the region 650-900°C, <10-20 kbar using the empirical and experimentally-derived geobarometers and geothermometers of Wood (1974) and Raheim and Green (1974). A possible explanation for the petrographic relationships is that an original high-pressure cumulate assemblage of gnt-cpx-amph-phlog has been subjected to later (lower P) equilibration and partial melting events with generation of secondary amphibole, biotite and Al/Si-rich assemblages. The inclusions may be re-equilibrated samples of a cumulate sequence formed in the lower crust and uppermost mantle during Precambrian igneous activity (c. 1700 m.y.) in the last major magmatic event preceding the Tertiary (Anderson and Silver, 1976). The possible remelting of amphibole and phlogopite-bearing assemblages may have direct bearing on the formation of high-K ("shoshonitic") lavas in the Tertiary.

References

- Anderson, C. A. and L. T. Silver, Yavapai Series - a greenstone belt, Arizona Geol. Digest, 10 (1976) 13-26.
- Krieger, M. H., Geology of the Prescott and Paulden Quadrangles, Arizona, Geol. Surv. Prof. Pap., 467 (1965)
- Krieger, M. H., S. C. Creasey, and R. F. Marvin, Ages of some Tertiary andesitic and latitic volcanic rocks in the Prescott-Jerome area, north-central Arizona, U. S. Geol. Surv. Prof. Pap., 750-B, (1971) 157-160.
- Raheim, A. and D. H. Green, Experimental determination of the temperature and pressure dependence of the Fe-Mg partition coefficient for coexisting garnet and clinopyroxene, Contrib. Mineral. Petrol., 48 (1974) 179-203.
- Wood, B. J., The solubility of alumina in orthopyroxene coexisting with garnet, Contrib. Mineral. Petrol., 46 (1974) 1-15.

Table 1. Analyses of host latite, bulk eclogites and individual phases

	1	2	3	4	5	6	7	8
SiO ₂	61.61	51.62	45.24	53.65	54.37	39.93	40.32	51.40
TiO ₂	0.76	0.44	0.41	0.18	0.13	0.07	0.08	0.00
Al ₂ O ₃	13.89	6.59	15.62	4.31	3.88	22.40	22.59	6.68
FeO*	4.45	6.30	11.59	5.04	3.50	18.58	16.83	15.20
MnO	0.08	0.06	0.29	0.03	0.03	0.45	0.50	0.28
MgO	3.69	12.45	12.85	13.74	14.75	8.48	11.87	24.70
CaO	4.63	19.88	12.77	21.67	22.11	11.06	8.29	1.66
Na ₂ O	2.79	1.91	0.85	2.01	1.71	0.01	0.01	0.00
K ₂ O	5.49	0.02	0.04	0.00	0.00	0.01	0.00	0.00
P ₂ O ₅	0.36	0.09	0.11	—	—	—	—	—
CO ₂	0.00	0.00	0.00	—	—	—	—	—
H ₂ O ⁺	0.73	0.30	0.36	—	—	—	—	—
H ₂ O ⁻	0.31	0.06	0.06	—	—	—	—	—
Total	99.20	99.72	100.19	100.64	100.48	100.98	100.50	99.92

	9	10	11	12	13	14	15
SiO ₂	54.90	54.40	39.80	45.60	38.69	40.54	37.06
TiO ₂	0.02	0.11	0.00	1.05	0.24	0.49	2.17
Al ₂ O ₃	1.34	3.50	22.80	11.02	17.88	14.83	15.40
FeO*	14.00	4.50	20.70	8.08	16.03	4.53	17.25
MnO	0.00	0.00	0.68	0.00	0.00	0.01	0.00
MgO	29.90	14.50	12.10	17.26	10.12	23.58	13.63
CaO	0.17	20.75	5.35	10.77	11.40	0.00	0.13
Na ₂ O	0.04	2.34	0.00	2.81	1.69	0.38	0.36
K ₂ O	0.00	0.00	0.00	1.34	2.15	9.91	8.66
Total	100.37	100.10	101.43	97.88	98.19	94.68	94.66

* Total Fe as FeO for microprobe analyses and columns 2 and 3 due to problems of undecomposed garnet. Columns 1-3 are modified rapid method analyses by G. K. Hoops. See code for FeO/Fe₂O₃ in host latite.

Code: 1 = host latite (Fe₂O₃ = 4.14 wt.%, FeO = 0.72 wt.%); 2 = cpx-rich layer in eclogite; 3 = gnt-rich layer of same eclogite; 4 = cpx in cpx-rich layer; 5 = cpx in gnt-rich layer; 6 = gnt in cpx-rich layer; 7 = gnt in gnt-rich layer; 8 = broad beam average of px porphyroclast in websterite; 9 = opx lamella in porphyroclast; 10 = cpx lamella; 11 = mosaic gnt in websterite groundmass; 12 = possible "primary" amphibole; 13 = interstitial amphibole; 14 = phlogopite; 15 = biotite.

TRACE ELEMENTS AND SR-ISOTOPIC GEOCHEMISTRY OF THE CONSTITUENT MINERALS IN ULTRAMAFIC XENOLITHS FROM SAN QUINTIN, BAJA CALIFORNIA

Asish R. Basu and V. Rama Murthy (Department of Geology and Geophysics, University of Minnesota, Minneapolis, Minnesota 55455)

We report the abundances of K, Rb, Sr and Ba and the $^{87}\text{Sr}/^{86}\text{Sr}$ ratios of separated silicate minerals in a suite of ultramafic xenoliths, their host basalts, and plagioclase megacryst from San Quintin, Baja California, (Table 1).

Although the xenoliths are enriched in modal diopsides (up to 35%), the trace element abundances are extremely low in all the silicate phases. For example, the diopsides contain as low as 10.7 ppm K, 0.01 ppm Rb, 1.7 ppm Sr and 0.6 ppm Ba. The diopsides from the pyroxenite layers usually show slightly higher abundances, such as 107 ppm K, 0.07 ppm Rb, 22 ppm Sr and 33 ppm Ba.

In four lherzolites, the coexisting olivines, orthopyroxenes and clinopyroxenes were analyzed after separation by hand-picking. In three of these samples, each mineral fraction was analyzed twice - without washing and after washing in 2N add HCl for 3 minutes. In the acid washed minerals (AW), K, Rb, Sr and Ba abundances are reduced by about half from the unwashed abundances. In addition, $^{87}\text{Sr}/^{86}\text{Sr}$ ratios are also lowered by the acid washing. In one of these samples, the acid washed minerals and the acid washed whole rock reveal an isochron of $T = 3.41 \pm 0.3$ AE (2σ) and $I = 0.70057 \pm 0.004$ (2σ). In the other three samples the coexisting silicates show clear disequilibrium in their $^{87}\text{Sr}/^{86}\text{Sr}$ ratios.

The green chrome-diopsides in the spinel lherzolites, except in specimen 2-13, show $^{87}\text{Sr}/^{86}\text{Sr}$ ratios lower than 0.7030, whereas the more iron-rich black clinopyroxenites show much higher $^{87}\text{Sr}/^{86}\text{Sr}$ ratios. Therefore, these two groups of pyroxenes are not genetically related.

The extremely fine-grained (CPX+glass) whole rock vein, interpreted as a partially molten layer in the spinel lherzolite no. 2-68, show a $^{87}\text{Sr}/^{86}\text{Sr}$ ratio of 0.7030 - possibly the same ratio in the refractory chrome-diopside in the host rock.

In the plagioclase peridotite, no. 1-6-1, both plagioclase and clinopyroxene show the same $^{87}\text{Sr}/^{86}\text{Sr}$ ratios; possibly, this peridotite formed by crystal settling in an alkali basaltic magma chamber in the mantle with higher $^{87}\text{Sr}/^{86}\text{Sr}$ ratios than the surficial lava flows in San Quintin.

Plagioclase megacryst of andesine composition, Sp. No. 3-1, show essentially the same $^{87}\text{Sr}/^{86}\text{Sr}$ ratios as its host basalt. This plagioclase is, therefore, a true phenocryst. On this basis the partition coefficients between plagioclase/basalt for K, Rb, Sr and Ba are 0.688, 0.355, 4.09 and 0.916, respectively. These estimates are 2 to 10 times higher than the values commonly used. However, the andesine megacryst is likely to be a high pressure phenocryst, and the above distribution coefficients may be valid only at high pressures.

The clinopyroxenes from the different xenoliths show the lowest and the most variable $^{87}\text{Sr}/^{86}\text{Sr}$ ratios of all the silicates, from .70196±11 to .70445±5. Thus the data indicate that at least part of the vertical mantle profile beneath San Quintin, represented by the xenoliths studied here, is heterogeneous in its Sr-isotopic ratios. This heterogeneity must reflect complex processes in the mantle, such as partial melting, removal of melt, cumulus processes, recrystallization, etc.

Finally, the extreme depletion of the trace elements in the silicate phases of the lherzolites, as reported here, contrasts remarkably with the diopside-rich nature of the xenoliths. No simple scheme of partial melting of these xenoliths can produce any normal basalt with its appropriate trace elemental abundances and ratios.

Table 1

<u>Sample</u>	<u>Mineral</u>	<u>K</u> <u>ppm</u>	<u>Rb</u> <u>ppm</u>	<u>Sr</u> <u>ppm</u>	<u>Ba</u> <u>ppm</u>	<u>$^{87}\text{Rb}/^{86}\text{Sr}$</u>	<u>$^{87}\text{Sr}/^{86}\text{Sr}$</u>
2-82 Spinel Lherzolite	OL	13.6	.042	.380	.424	.3195	.70709±25
	OL(AW)	4.6	.018	.233	.114	.2233	-
	OPX	33.3	.059	.556	.280	.3068	.70680±18
	OPX(AW)	22.4	.034	.322	.172	.3053	-
	CPX	15.5	.049	1.951	1.490	.0726	.70340±12
	CPX(AW)	12.39	.038	1.703	.650	.0645	.70261±8
2-13 Spinel Lherzolite	OL	42.6	.100	2.643	16.00	.1094	.70723±5
	OL(AW)	17.5	.044	1.301	9.71	.0978	.70555±12
	OPX	52.2	.110	3.552	13.02	.0895	.70765±10
	OPX(AW)	28.7	.083	2.976	9.98	.0806	.70717±14
	CPX	50.9	.090	2.857	9.6	.0911	.70528±12
	CPX(AW)	23.9	.050	2.136	7.07	.0677	.70484±10
2-41 Spinel Lherzolite	OL	39.3	.063	4.32	13.0	.0422	.70684±11
	OL(AW)	21.2	.035	.953	8.48	.1062	.70585±18
	OPX	204.4	.186	5.74	8.82	.1094	.70702±7
	OPX(AW)	43.6	.057	1.51	6.34	.1091	.70579±7
	CPX	92.2	.123	11.17	12.72	.0318	.70545±12
	CPX(AW)	38.7	.054	5.295	12.58	.0295	.70196±11
	Whole Rock(AW)	33.6	.043	1.591	8.10	.0781	.70452±8
2-67 Spinel Lherzolite	OL(AW)	22.06	.050	.189	.321	.7648	.70644±16
	OPX(AW)	4.00	.003	.338	.827	.0256	.70302±13
	CPX(AW)	10.70	.011	7.353	.597	.0043	.70230±6
1-7-28 Spinel Lherzolite	Cr- Diopside (AW)	63.14	.059	5.643	.732	.0302	.70275±9

<u>Sample</u>	<u>Mineral</u>	<u>K</u> <u>ppm</u>	<u>Rb</u> <u>ppm</u>	<u>Sr</u> <u>ppm</u>	<u>Ba</u> <u>ppm</u>	$^{87}\text{Rb}/^{86}\text{Sr}$	$^{87}\text{Sr}/^{86}\text{Sr}$
2-68 Pxite layer in Spinel Lherzolite	CPX + glass (AW)	43.70	.050	32.83	.666	.0044	.70303±8
2-30 Cpxite layer	Cr- Diopside (AW)	107.9	.073	21.99	1.005	.0096	.70295±7
1-8-5 Black Cpxite (augite)	CPX (AW)	64.38	.049	18.707	-	.0076	.70413±8
2-81 Black Cpxite (augite)	CPX (AW)	31.61	.049	22.144	33.58	.0064	.70445±5
2-36 Sp-Lh W/ Opxite layer	OPX (AW)	94.96	.070	.449	.242	.4541	-
1-6-1 Plag - Peridotite	Plag (An ₉₈) (AW) CPX (AW)	36.80	.042	342.32	16.65	.00035	.70407±7
2-19 Plag- peridotite	Plag (AW)	143.61	.255	406.40	16.43	.0018	.70337±8
3-1 Plag Megacryst Andesine	Plag (AW)	10591	12.776	2503	348.7	.0148	.70317±9
1-2-6 Host Basalt	Whole Rock (AW)	15390	35.96	611.7	380.6	.1699	.70311±8
SQB Host Basalt	Whole Rock (AW)	13853	26.58	560.7	315.8	.1371	.70314±7

PRIMORDIAL 'PLANETARY' RARE GAS IN A MANTLE DERIVED AMPHIBOLE

Asish R. Basu, Kazuo Saito and E. Calvin Alexander, Jr. (Department of Geology and Geophysics, University of Minnesota, Minneapolis, Minnesota)

The abundances and the isotopic ratios of the five rare gases in a mantle derived amphibole (Kaersutite), from Kakanui, New Zealand, were measured (Table 1). The sample is a megacryst inclusion in an alkali basalt for which the geological age of lower Oligocene has been reported. The amphibole shows a low $^{87}\text{Sr}/^{86}\text{Sr}$ ratio of 0.7029. A K/Rb ratio of 1142 as well as the low $^{87}\text{Sr}/^{86}\text{Sr}$ ratio of the amphibole suggests that the source of the sample is similar to that of midoceanic ridge basalts.

The elemental abundances of the five rare gases are indistinguishable from 'planetary' rare gas as exemplified by some carbonaceous chondrites. The similarity is shown by plotting the data on a $^{84}\text{Kr}/^{130}\text{Xe}$ vs. $^{20}\text{Ne}/^{36}\text{Ar}$ diagram (Fig. 1), or by comparing the rare gas abundance with that in the carbonaceous chondrites (Fig. 2). In Fig. 2 the rare gas data of Mighei chondrite is plotted as a reference. In Fig. 3 the absolute abundances of rare gases is shown. The abundances of rare gases in the sample are high, especially Kr and Xe which show higher abundances than the earth's inventory (Atmospheric abundance/Mass of the earth). This high abundance may be either a result of concentration of rare gases in the mantle environment from which the amphibole crystallized or due to the efficient trapping of the rare gases in the partially empty 'A' site of kaersutite. In Fig. 3 the data of Mighei chondrite is also shown as a reference. Figure 3 shows a remarkable parallelism between the amphibole and the Mighei chondrite.

Table 1 shows the following salient aspects of the isotopic ratios of the gases in the amphibole.

He: $^3\text{He}/^4\text{He}$ ratio of 5×10^{-5} is obtained. This is one of the highest values ever found in terrestrial samples. The source of ^3He must be an originally trapped ^3He which still remains in the deep earth.

Ne: Excess ^{21}Ne was found. Although ^{21}Ne is produced by a $^{18}\text{O}(\alpha, p)^{21}\text{Ne}$ reaction, the ^4He abundance in the sample is too low to explain the ^{21}Ne anomaly by this reaction.

Ar: A $^{40}\text{Ar}/^{36}\text{Ar}$ ratio of 400 was measured. Almost complete exchange of the trapped Ar with the atmospheric argon can account for the $^{40}\text{Ar}/^{36}\text{Ar}$ of 400, but this explanation is incompatible with the He and Ne data. Making a correction of radiogenic ^{40}Ar accumulated after the solidification of the sample, the ratio becomes as low as 230.

Kr: ^{78}Kr and ^{80}Kr show anomalous abundance. Although the correction for the interference by $^{78}\text{H}_6\text{C}_6$ and $^{40}\text{Ar}_2^+$ were made, there still remains a little uncertainty in these corrections and ^{78}Kr and ^{80}Kr anomalies are doubtful. The other four isotopes of Kr show progressive enrichment in the heavier mass numbers as compared with the atmospheric abundance.

Xe: No significant difference from the atmospheric abundance was found.

Our data indicate that the earth has still retained its primordial rare gases and that the pattern of these gases is same as found in some 'planetary' type chondrites. However, the low $^{40}\text{Ar}/^{36}\text{Ar}$ ratio of 230 in the amphibole is difficult to explain by any degassing model.

TABLE 1. Abundance and isotopic composition of rare gases extracted from a 403.8 mg sample of handpicked, clear grains of amphibole from the Kakanui kaersutite megacryst.

Abundance

$$^4\text{He} = (3.93 \pm 0.13) \times 10^{-6} \text{ cm STP/g}$$

$$^{20}\text{Ne} = (3.59 \pm 0.19) \times 10^{-9} \text{ cm STP/g}$$

$$^{36}\text{Ar} = (1.477 \pm 0.038) \times 10^{-8} \text{ cm STP/g}$$

$$^{84}\text{Kr} = (6.85 \pm 0.80) \times 10^{-10} \text{ cm STP/g}$$

$$^{132}\text{Xe} = (5.35 \pm 0.18) \times 10^{-10} \text{ cm STP/g}$$

Isotopic Composition

^4He	^3He	^{20}Ne	^{21}Ne			
$\cong 1.000$	$4.92 \pm 0.60 \times 10^{-5}$	$\cong 1.000$	$(6.66 \pm 0.51) \times 10^{-3}$			
	^{22}Ne					
	0.1006 ± 0.0085					
	^{36}Ar	^{38}Ar	^{40}Ar			
	$\cong 1.000$	0.1836 ± 0.0032	400.0 ± 4.8			
^{78}Kr	^{80}Kr	^{82}Kr	^{83}Kr	^{84}Kr	^{86}Kr	
0.006497	0.04236	0.2014	0.2015	$\cong 1.000$	0.3065	
± 0.000065	± 0.00042	± 0.0006	± 0.0004		± 0.0006	
^{124}Xe	^{126}Xe	^{128}Xe	^{129}Xe	^{130}Xe	^{131}Xe	^{132}Xe
0.00351	0.00315	0.07145	0.9813	0.1498	0.7929	$\cong 1.000$
± 0.00011	± 0.00011	± 0.00071	± 0.0037	± 0.0015	± 0.0003	
^{134}Xe	^{136}Xe					
0.3935	0.3308					
± 0.0029	± 0.0025					

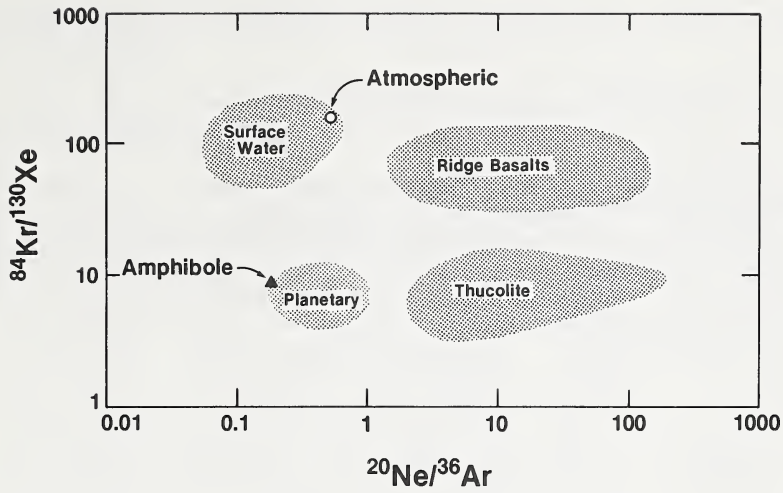


Fig. 1

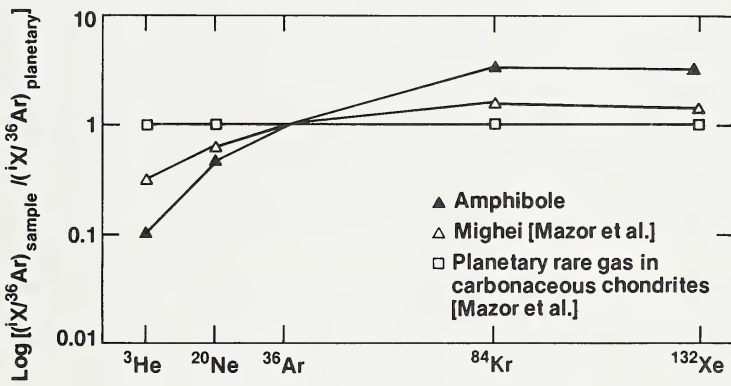


Fig. 2

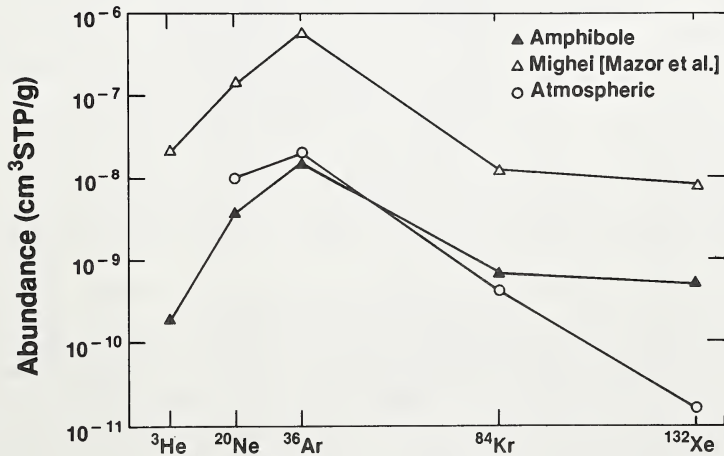


Fig. 3

THE DISTRIBUTION OF Fe^{2+} AND Mg BETWEEN PYROXENE AND ILMENITE IN INTERGROWTHS FROM KIMBERLITES

F. C. Bishop, Department of Geological Sciences, Northwestern University, Evanston, Illinois 60201

The effects of temperature, pressure and bulk composition on the iron-magnesium distribution coefficient, $K_D = (\text{MgO}/\text{FeO})_{\text{PX}}/(\text{MgO}/\text{FeO})_{\text{IL}}^{11}$, in the systems orthopyroxene-ilmenite and clinopyroxene-ilmenite have been experimentally calibrated with a piston-cylinder apparatus. Results in the orthopyroxene-ilmenite system are consistent with an ideal solution model for orthopyroxene and a regular solution model for ilmenite solid solutions near the ilmenite-geikielite join. At temperatures greater than 800°C , W_G is approximately 1.60 kcal for ilmenite. In the experiments in the clinopyroxene-ilmenite system, clinopyroxene compositions were restricted to the diopside-hedenbergite join. The regular solution model for ilmenite previously described and a regular solution model for clinopyroxene with $W_G = 2.5$ kcal are needed to account for the effect of bulk composition on the distribution coefficient in this system. There is a small pressure effect in both systems which increases the magnesium content of the silicates as the pressure is increased.

These results can help determine the physical parameters prevailing at the time of formation of the graphic and lamellar pyroxene-ilmenite intergrowths in kimberlites. A survey of the reported occurrences of these intergrowths reveals that they form a common paragenesis in kimberlite. They have been described from five kimberlites in South Africa, four in Lesotho, three in the U. S. A., three in the U. S. S. R., two in Namibia, two in Rhodesia and one in Angola. A similar clinopyroxene-ilmenite graphic intergrowth has also been found in alnöite from Malaita in the Solomon Islands.

Of five orthopyroxene-ilmenite nodules with published analyses of the coexisting phases, four have equilibration temperatures in the range $1130^\circ - 1180^\circ\text{C}$ (Fig. 1). K_D varies from 9.0 to 10.4 and $(\text{Fe}^{2+}/\text{Fe}^{2+}+\text{Mg})_{\text{IL}}^{11}$ from 0.56 to 0.65. In these calculations, pressure was assumed to be 50 kb, consistent with the estimate of Boyd and Nixon (1973). The calculated temperatures rise 5°C for every additional kilobar of pressure. The fifth orthopyroxene-ilmenite intergrowth, from Kharakhtakh, Yakutia, is unique since it also contains clinopyroxene lamellae. The calculated temperature of equilibration for this specimen is 1080°C .

Interpretation of K_D in clinopyroxene-ilmenite nodules is complicated by the presence of ferric iron in clinopyroxene. Four analyses of ferric iron in clinopyroxenes from intergrowths indicate that an average of 70% of the total iron present is in the ferrous state. When this correction is applied, a bimodal distribution in equilibration temperatures for clinopyroxene-ilmenite intergrowths is revealed (Fig. 1). Both groups indicate higher temperatures than the orthopyroxene-ilmenite intergrowths.

The low temperature group includes all but one of the Yakutian specimens and most of the Monastery specimens. The average temperature (1210°C) agrees well with the average temperature of 1190°C obtained on the same samples from the orthopyroxene-clinopyroxene miscibility gap determined by Davis and Boyd (1966) assuming that clinopyroxene has crystallized in equilibrium with orthopyroxene and garnet. The high temperature group contains all of the American and African specimens

except for those from Manastery previously mentioned. The average temperature of this group, 1330°C, is significantly higher than the average temperature calculated from the orthopyroxene-clinopyroxene miscibility gap.

Possible explanations of the bimodal temperature distribution include a difference in oxidation state of the clinopyroxene (although the specimens in which ferric iron has been determined fall into both groups), a difference in quench history resulting in subsolidus reequilibration for one group, or an actual difference in the temperature-pressure regime during the formation of each group. If the latter hypothesis is true, then the high temperature group apparently did not crystallize in equilibrium with orthopyroxene and garnet.

References

- Boyd and Nixon (1973), Carnegie Inst. Wash. Yearbk. 72, 431.
Davis and Boyd (1966), JGR 71, 3567.

The experimental work was supported by NSF DES74-22851.

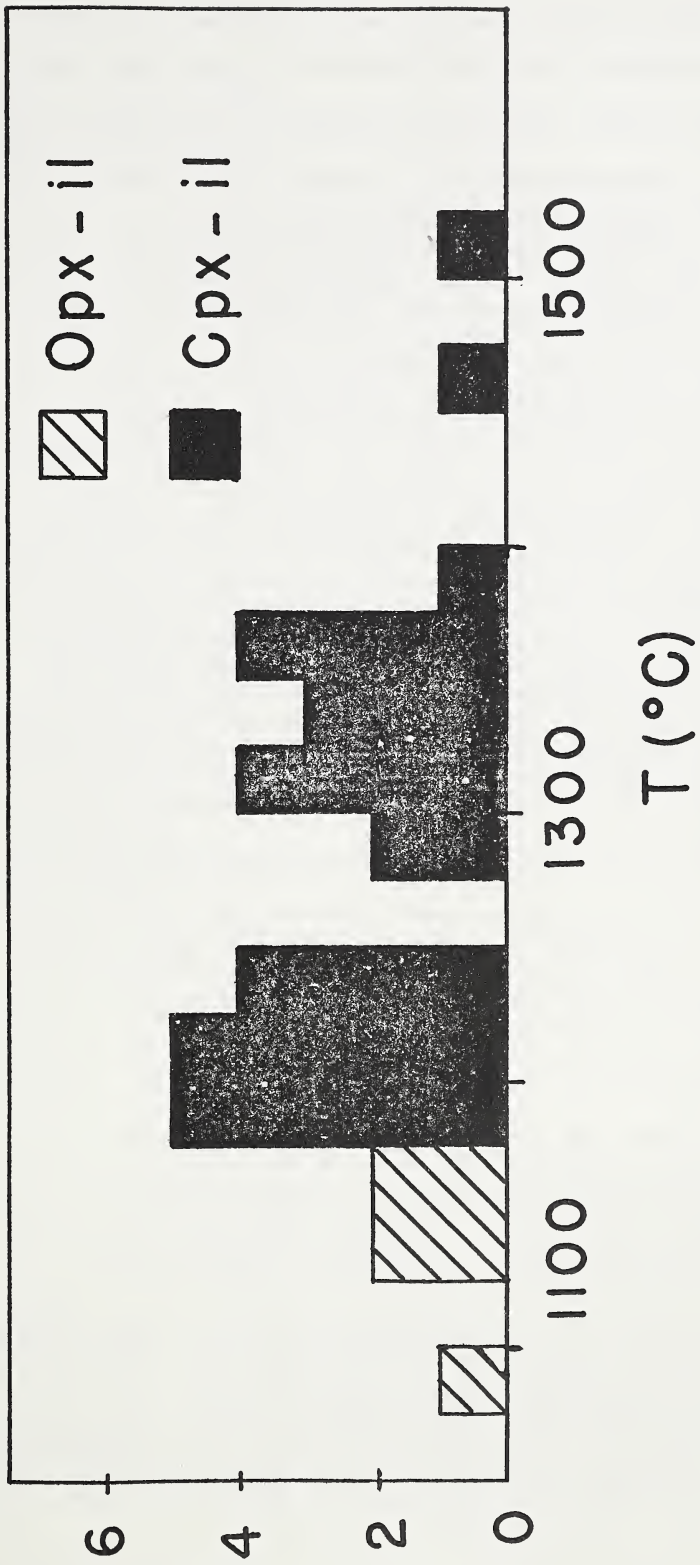


Figure 1. Number of specimens vs. calculated temperature for clinopyroxene-ilmenite and orthopyroxene-ilmenite intergrowths from kimberlites.

NA, K, P AND TI IN MINERALS IN XENOLITHS FROM AFRICAN KIMBERLITES.

F. C. Bishop, Department of Geological Sciences, Northwestern University,
Evanston, Illinois 60201

J. V. Smith, Department of Geophysical Sciences, The University of Chicago,
Chicago, Illinois 60637

J. B. Dawson, Department of Geology, St. Andrews University, Scotland

Little is known about the distribution of minor and trace elements in the upper mantle. Xenoliths provide the only direct information, although interpretation can be complicated by possible complex history. We report analyses for Na, K, P and Ti in garnet, pyroxenes and olivine in xenoliths from southern African kimberlites and the Lashaine ankaramite-carbonatite volcano (Tanzania). The xenoliths, mostly granular lherzolites, eclogites and a clinopyroxene megacryst, were chosen because their mineral homogeneity suggests equilibrium. Application of existing geothermometers and geobarometers indicates derivation from a range of depths (Boyd, 1973; Råheim and Green, 1974).

Presence of micron-sized impurities within mineral grains, especially for minerals in xenoliths that may have been subject to host-rock contamination, requires micro-analytical techniques whenever feasible. Ion microprobe techniques are still under development and are not yet fully established. Although electron microprobe analyses typically have a detection level of 0.02 wt.%, analyses conducted under conditions which maximized the sensitivity of the instrument lowered the detection level to 20 ppmw (2σ) for the elements studied. Operating conditions were 3 μ A beam current, 15 kV, several minutes counting times, beam size 5 to 10 μ m. Four background determinations symmetrically disposed around the peak wavelength were taken for each analysis. For concentrations less than 200 ppmw, the background was profiled at 60 wavelengths for each analysis. Matrix corrections for Na, Ti and K in the silicates were insignificant on the ARL-EMX instrument, but the correction for P averaged 1.27.

Ranges and means of Na, P, K and Ti concentrations in the minerals are summarized in Table 1.

Garnet contains ~0.01-0.1 wt.% Na₂O and P₂O₅ and 0.02-0.8% TiO₂. There is enough P + Ti in every analysis to account for all Na in components such as Na₃Al₂P₃O₁₂ and (Na₂Mg)Ti₂Si₃O₁₂; thus, there is no need to invoke octahedrally-coordinated Si, as proposed by Sobolev and Lavrentyev (1971). Although the atomic radii of Na+P sum to less than for Ca + Si, the P content of garnet does not correlate with the pressure estimated from the Al₂O₃ content of coexisting orthopyroxene. Our results corroborate Erlank's (1973) conclusion that K₂O in garnet does not exceed 20 ppmw.

Olivine Concentrations of Na, P and Ti in upper mantle olivines are low, but are important because of the high modal abundance of olivine in peridotites. The electron microprobe spectrum was carefully checked for possible higher-order interferences with the Na peak, and Pl40 olivine from an alpine peridotite (Balsam Gap, NC) was found to be Na-free. Upper mantle olivines were found to have a mean concentration of 90 ppmw. K₂O concentrations are below the limit of detection.

Orthopyroxene contains <100 ppmw K and P, although containing significant Na. Orthopyroxenes from granular peridotites have a moderate 1:1 correlation between Na and Cr. Sodium is >>Cr in opx megacrysts and grains from kimberlite concentrates, while Cr < Na in orthopyroxene from spinel peridotite xenoliths.

Clinopyroxene contains the highest amounts of K and Na. In fact, clinopyroxene is the only significant host for K₂O in all of the mica-free xenoliths. All diffractions in a long-exposure precession photograph of an

optically-homogeneous omphacite with 1600 ppmw K_2O can be indexed on the pyroxene cell, thereby precluding the presence of intergrown potassic richterite, which was previously suggested as the host for K.

Mica. Detailed analyses of micas are reviewed in another Extended Abstract. Three analyses showed up to 0.4 P_2O_5 . Thus, mica must be considered as a potentially important host for P at depths in which it is stable.

Distribution Coefficients. In general, a distribution coefficient for an element between two phases may vary with the composition of the phases as well as pressure, temperature and oxidation state. Since our xenoliths came from different depths within the earth, even for xenoliths from the same kimberlite, a simple correlation of the concentrations of an element between two minerals cannot be expected. For example, the ratio of P_2O_5 in garnet to cpx varies widely from 0.7 to 4.6 for xenoliths from the same kimberlite pipe. This indicates that caution should be exercised when using one distribution coefficient for models of the entire upper mantle.

$K_D(Fe/Mg) [= (FeO/MgO)^{gt}/(FeO/MgO)^{cpx}]$ was found experimentally to be relatively insensitive to bulk composition, while increasing with decreasing temperature and increasing pressure (Råheim and Green, 1974). We found that $K_D(Na) = (Na_2O)^{gt}/(Na_2O)^{cpx}$ correlates with $K_D(Fe/Mg)$ (Fig. 1) suggesting that it may also depend on P and T, and hence be a possible depth indicator. Fig. 2 shows the positive correlation between $K_D(Na)$ and both the Wood-Banno (1973) estimate of temperature and the MacGregor (1974) estimate of pressure. Until detailed syntheses under controlled conditions have been made, these correlations are only indicative, but the steepening of the trend in Fig. 1 for high $K_D(Na)$ suggests that it may prove more useful than $K_D(Fe/Mg)$ at pressures over 40kb. Note that values of $K_D(Na)$ for deformed peridotites are mostly higher than those for granular peridotites. Data for garnet and pyroxene inclusions in diamond are widely scattered, and the reason is unknown.

Trace Elements in the Mantle. Recognizing that problems arise because the upper mantle is inhomogeneous and peridotite xenoliths may be unrepresentative, we tentatively propose the following ideas as a guide to experimentation on trace element distribution and to speculation on the origin of the Earth.

Mean analyses for Na, P, K and Ti in the Table taken together with the estimated mode of the upper mantle (Harris *et al.*, 1967) give the following bulk values: Na_2O 2510 P_2O_5 180 K_2O 22 TiO_2 470 ppmw. K_2O would be greatly increased by addition of phlogopite. The P_2O_5 content is much lower than in bulk chemical analyses of Lashaine garnet peridotites, and even lower than estimates by Ringwood (1966). Apatite has recently been found in Lashaine peridotite, and may account for most P in upper-mantle peridotites. Since P is strongly partitioned into basaltic melt during partial melting (Anderson and Greenland, 1969; Thompson, 1975), residual peridotite could be strongly depleted.

In matching a cosmochemical model for the bulk chemistry of the Earth with mineralogical-geophysical data, Smith (1977) suggested that K_2O is confined to the crust and upper mantle, and that Na_2O is present to considerably greater depth in order that it be not depleted more than K. Perhaps Na is replacing Ca with a coupled substitution to give valence balance, e.g. as $NaPO_3$ in perovskite structure, or perhaps (Liu, 1977) in calcium ferrite structure ($NaAlSiO_4$).

References. Anderson & Greenland (1969), GCA 33, 493. Boyd (1973), GCA 37, 2533. Erlank (1973), Int. Conf. Kimberlites, Ext. Abstr., 103. Harris, Reay & White (1967), JGR 72, 6359. Liu (1977), EOS 58, no. 7, 613. MacGregor (1974), AM 59, 110. Råheim & Green (1974), CMP 48, 179. Smith (1977), Proc. 8th Lunar Sci. Conf. Rhodes & Dawson (1975), Phys. Chem. Earth 9, 545. Ringwood (1966),

Adv. in Earth Sci., Hurley, ed., MIT Press, 287. Sobolev & Lavrentyev (1971), CMP 31, 1. Thompson (1975), EPSL 26, 417. Wood & Banno (1973), CMP 42. 109.

Table Range and mean of some oxides.

	Na ₂ O	P ₂ O ₅	K ₂ O	TiO ₂
lherzolite and ultramafic rocks				
garnet	150-790(340)	200-1040(460)	<20	160-5190(1470)
olivine	40-130(90)	50-200(130)	<20	0-390(130)
orthopyroxene	530-1900(1070)	0-90(50)	10-110(30)	10-1650(480)
clinopyroxene	1.12-3.43(2.08)	90-630(350)	20-370(170)	100-4400(1630)
eclogites and cpx megacryst				
garnet	100-1420(610)	160-940(530)	<20	210-7800(2000)
clinopyroxene	1.9-9.1(4.3)	110-520(300)	50-1620(370)	330-3800(2000)

ppmw except for Na₂O in clinopyroxene given as wt.%.
NSF EAR 76-0304 and Materials Research Laboratory.

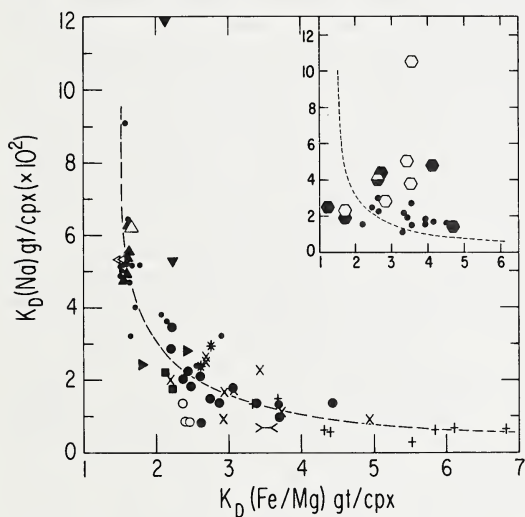


Fig. 1. Main diagram: eclogites, horizontal cross, Bobbejaan, inclined cross, Roberts Victor, star, Newlands, bridge, Vissuri; peridotites; large dot, S. Africa, circle, Lashaine; cpx megacryst, open triangle, Monastery; sheared lherzolite, small dot; enstatite megacryst, downward triangle; other symbols, see paper submitted to Lithos. Inset diagram: inclusions in diamond, hexagons; diamondiferous eclogites, dots.

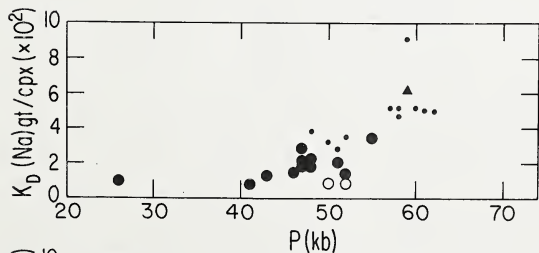
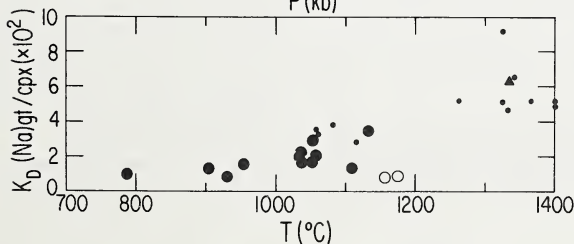


Fig. 2 K_D (Na for garnet/clinopyroxene vs. estimates of pressure and temperature from pyroxenes.



OXIDE AND SULFIDE MINERALS IN KIMBERLITE FROM GREEN MOUNTAIN, COLORADO

- N. Z. Boctor (Department of Geosciences, Purdue University, West Lafayette, IN 47907)
H. O. A. Meyer (Department of Geosciences, Purdue University, West Lafayette, IN 47907)

The opaque minerals in kimberlite from the Green Mountain, Colorado are represented by an assemblage of spinel solid solutions, ilmenite, rutile, perovskite, and minor sulfide minerals.

Spinel occurs as primary phases in the groundmass and as reaction mantles on ilmenite xenocrysts and rutile-ilmenite intergrowths. The groundmass spinels are characterized by their low Cr content and thus are different from the Cr rich spinels that are common in kimberlites (Haggerty, 1975; Mitchell and Clarke, 1976). They occur as euhedral crystals which are either zoned or unzoned. The cores of the zoned crystals are Ti and Mg rich (Table 1, Analysis 1), whereas the rims are more depleted in these elements and more enriched in Fe (Table 1, Analysis 2). Unzoned spinels are uniform in composition in the same specimen, and their chemical composition overlaps with that of the mantles in zoned crystals (Table 1, Analysis 3). Magnetite-ulvöspinel solid solution (Table 1, Analysis 4) and Ti poor magnetite are rarely present as groundmass spinels. Occasionally, magnetite-ilmenite intergrowths are also observed in the groundmass. The spinels in the Green Mountain kimberlite are solid solutions in the system $\text{Fe}_2\text{TiO}_4\text{-Mg}_2\text{TiO}_4\text{-MgAl}_2\text{O}_4\text{-MgFe}_2\text{O}_4\text{-Fe}_3\text{O}_4$. The spinels that are close in composition to the Ti rich spinels in kimberlite from the Green Mountain are those from Benfontein (Dawson and Hawthorne, 1973) and Lihobong (Haggerty, 1973).

Ilmenite is represented mainly by primary xenocrystic microilmenite (Table 1, Analysis 5), which commonly displays fine exsolution lamellae of spinel, and secondary microilmenite (Table 1, Analysis 6) in the groundmass and in reaction mantles on ilmenite xenocrysts. Secondary microilmenite is more enriched in Mg and Cr relative to the ilmenite xenocrysts. A Mn rich and Mg poor ilmenite occurs occasionally in the groundmass and as rims on rutile-ilmenite intergrowths (Table 1, Analysis 7).

Reaction mantles on ilmenite xenocrysts display different mineralogy in different specimens. In some cases, the ilmenite xenocryst is mantled by an inner zone of secondary microilmenite followed by a discontinuous rim of rutile-ilmenite intergrowth and an outermost zone of spinel. In general the spinel in these mantles is more enriched in Ti and FeO relative to the groundmass spinel (Table 1, Analysis 8) though its composition occasionally overlaps with that of the cores in zoned spinels. In some cases the Ti rich spinel mantles the ilmenite xenocryst followed by a discontinuous zone of secondary microilmenite and an outer zone of a second spinel that is more enriched in Fe_2O_3 and depleted in Ti (Table 1, Analysis 9) relative to the spinel of the inner zone. Occasionally the outermost spinel zone is a Ti poor magnetite (Table 1, Analysis 10). In some ilmenite xenocrysts a discontinuous rim of perovskite mantles an inner zone of secondary microilmenite or Ti rich spinel. Perovskite in the mantles and the groundmass has a low FeO content.

Rutile-ilmenite intergrowths have bulk compositions similar to armalcolite. They are commonly mantled by Ti rich spinel and/or Mn rich ilmenite. In rare instances the coexisting spinel and secondary microilmenite

in the reaction mantles are more enriched in Cr relative to the ilmenite and spinel in the groundmass or reaction mantle on ilmenite xenocrysts. The spinel contains up to 12 wt % Cr₂O₃ (Table 1, Analysis 11), while the secondary microilmenite contains up to 5.5 wt % Cr₂O₃.

The mineral assemblages observed in the reaction mantles on ilmenite xenocrysts and on rutile-ilmenite intergrowths in the Green Mountain diatreme suggest that fluctuations in fO₂ prevailed during their formation. Also large fluctuations in fO₂ are demonstrated by the presence in the same specimen of magnetite-ilmenite intergrowths produced by subsolidus oxidation together with ilmenite with magnetite lamellae produced by subsolidus reduction. The fluctuations in fO₂ are probably a reflection of the changes in CO/CO₂ and H₂/H₂O ratios during the progressive crystallization of the different phases in the reaction mantles.

The sulfide minerals are heazlwoodite, Ni bearing bornite, and covellite. They are associated with serpentine. Heazlwoodite (Table 2, Analyses 1,2,3) occurs as platelets oriented in two or more directions in serpentine; as veinlets in association with bornite; and as irregular masses. Bornite (Table 2, Analysis 4) is occasionally replaced by covellite. The mineralogy and textures displayed by the sulfide minerals in Green Mountain kimberlite are not suggestive of an origin by sulfide liquid immiscibility. More likely the sulfides were the products of sulfurization reactions during serpentinization.

References:

- Dawson, J. B. and Hawthorne, J. B. (1973), Magmatic sedimentation and carbonatitic differentiation in kimberlite sills at Benfontein, South Africa, *J. Geol. Soc. Lond.*, 129, 61-85.
- Haggerty, S. E. (1973), Spinels of unique composition associated with ilmenite reactions in the Lihobong kimberlite pipe, Lesotho. In: *Lesotho Kimberlites* (P. H. Nixon, editor), 350 pp, Lesotho National Development Corporation, Maseru.
- Haggerty, S. E. (1975), The chemistry and genesis of opaque minerals in kimberlites, *Phys. Chem. Earth*, 9, 295-307.
- Mitchell, R. H. and Clarke, D. B. (1976), Oxide and sulfide mineralogy of the Peuyuk kimberlite, Somerset Island, N. W. T., Canada, *Contrib. Mineral. Petrol.*, 56, 157-172.

Table 1. Chemical Compositions of Oxide Minerals in Green Mountain Kimberlite

	1	2	3	4	5	6	7	8	9	10	11
TiO ₂	22.82	19.04	19.77	5.55	54.39	56.40	52.33	33.25	9.85	0.99	23.66
FeO	15.79	19.97	21.15	33.46	25.78	10.39	42.28	31.75	12.67	30.85	27.09
Fe ₂ O ₃	24.68	30.69	28.91	53.87	5.57	6.60	---	11.93	52.73	66.85	12.33
MnO	0.82	0.55	1.01	1.66	0.25	0.64	4.96	0.97	0.91	0.28	2.19
MgO	24.45	19.97	18.90	0.69	12.86	22.63	0.66	19.43	17.80	1.65	19.57
CaO	0.08	0.02	0.03	0.88	0.04	0.04	0.07	0.01	0.05	0.02	0.12
Al ₂ O ₃	9.28	9.54	9.17	0.89	0.51	0.33	0.01	1.84	5.45	0.05	3.63
Cr ₂ O ₃	1.11	0.82	1.48	0.35	0.65	2.16	0.04	0.85	0.46	0.03	11.79
	99.06	100.60	100.42	99.35	100.05	99.19	100.35	100.03	99.03	100.72	100.38

Table 2. Chemical Compositions of Sulfide Minerals in Green Mountain Kimberlite

	1	2	3	4
S	26.71	26.86	26.97	25.55
Fe	1.04	1.10	1.22	11.34
Ni	72.58	71.85	72.22	1.28
Cu	<0.01	<0.01	<0.01	61.14
	100.33	99.80	100.41	99.30

METASOMATISM AND THE GENESIS OF KIMBERLITES AND ALKALI BASALTS

A.L. BOETTCHER (Department of Earth and Space Sciences and Institute of Geophysics and Planetary Physics, University of California, Los Angeles, Los Angeles, California 90024)

J.R.O'NEIL (U.S. Geological Survey, Menlo Park, California 94025)

K.E. WINDOM (IGPP, University of California, Los Angeles, Los Angeles, California)

D.C. STEWART (Pennsylvania State University, University Park, Pennsylvania 16802)

H.G. WILSHIRE (U.S Geological Survey, Menlo Park, California 94025)

Various lines of petrochemical evidence disclose that pervasive metasomatism of mantle lherzolite is precursory to or concomitant with anatexis in the production of many deep-seated alkaline basaltic magmas and kimberlites. For example, ultramafic mantle xenoliths in kimberlites and in alkali basalts, basanites and kindred rocks commonly exhibit evidence of metasomatic enrichment in TiO_2 , K_2O , total Fe, H_2O , etc. Evidence for this in many kimberlite xenoliths is abundantly manifest in the development of "secondary" phlogopite, i.e. phlogopite formed in the mantle, but subsequent to the crystallization of the primary mantle lherzolite. This process commonly converts the lherzolite to assemblages rich in clinopyroxene, amphibole, and other minerals in addition to the phlogopite (e.g. Lloyd and Bailey, 1975), which are abundant in kimberlites from many areas of the world (see Dawson and Smith, 1973).

We have selected for chemical and isotopic analysis a number of phlogopites that appear on the basis of textural evidence to be secondary, for comparison with those that have been classified by others as primary. The former occur as veins and overgrowths; the latter as discrete grains, such as the "primary" mica pictured by Dawson *et al.* (1970, plate 3) and Carswell (1975, Fig. 1-A). A facile examination of Table I discloses that the obviously secondary phlogopites are enriched in TiO_2 . Carswell previously pointed out that micas with high TiO_2 contents have textural relationships suggestive of being secondary, which is in chorus with our findings. Titaniferous phlogopites postulated as primary, such as in the garnet lherzolite xenolith (BD 738) from Lashaine Volcano (Dawson *et al.*, 1970) or the alkalic rocks from Jan Mayen (Flower, 1969) and West Kimberly (Prider, 1939), may be secondary.

The low- TiO_2 , high-Fe phlogopites in Table I, some of which are the cores for the high- TiO_2 phlogopite rims, themselves commonly appear to be secondary (e.g. Kb-9-5 and B-131). They exhibit reverse pleochroic schemes, previously reported in micas from kimberlites and alkalic ultramafic rocks (e.g. Wagner, 1914; Watson, 1955; Hogarth, 1964; Boettcher, 1967; Suwa and Aoki, 1975).

	Kb-5-1-b DeBeers core		Kb-9-5 Bulfontein core		Kb-8-3 Dutoitspan core		B-10-7 Roberts Selvage		Kb-5 Bulfontein		B-131 Libby Montana
	reverse	normal	reverse	normal	reverse	normal	reverse	normal	reverse	normal	reverse
SiO_2	41.72	39.15	42.73	40.96	41.23	40.33	38.91	42.92	41.97		
TiO_2	0.36	4.46	0.45	3.66	0.43	2.89	3.67	0.57	0.62		
Al_2O_3	10.55	13.95	9.86	12.28	9.48	11.33	14.62	10.24	9.83		
Cr_2O_3	0.14	1.23	0.10	0.24	0.07	0.13	0.17	0.30	0.03		
FeO^*	6.86	4.99	5.81	5.47	8.17	6.00	9.88	4.64	6.76		
MnO	0.02	0.04	0.03	0.01	0.04	0.04	0.05	0.01	0.09		
MgO	24.69	21.90	25.22	22.39	24.65	23.75	17.72	25.61	26.26		
CaO	0.26	0.14	0.00	0.00	0.15	0.16	0.07	0.12	0.15		
Na_2O	0.16	0.29	0.08	0.29	0.15	0.11	0.30	0.07	0.07		
K_2O	10.19	9.89	10.33	9.62	9.81	9.46	9.83	9.89	12.03		
Total	94.95	96.03	94.61	94.92	94.18	94.21	95.21	94.38	97.80		

Ecligite xenoliths also exhibit similar features. Some from the Roberts Victor Mine contain intergranular TiO_2 -rich phlogopite (Table I), potassic pargasite, analcime, augite, spinel, and plagioclase in an alkali-rich (K_2O+

$\text{Na}_2\text{O} > 12\%$), carbonate-bearing groundmass (Windom and Boettcher, 1977; Switzer and Melson, 1969). Again, fluids similar to those discussed above and not contamination by the kimberlite *per se* are responsible for the metasomatism.

Xenoliths of spinel lherzolite in alkali basalts and basanites also exhibit evidence of such metasomatic alteration. As much as 50% of these xenoliths from many areas in North America and elsewhere contain pargasitic or kaersutitic amphiboles that crystallized after the primary lherzolite assemblage but prior to incorporation of the xenoliths into the host magmas (e.g. Wilshire and Trask, 1971; Best, 1974; Francis, 1976; Stewart and Boettcher, 1977). The formation of this amphibole, commonly together with accompanying phlogopite, apatite, magnetite and other minor phases, is unrelated to contamination by the magma, and chemical and textural zonations of these and the primary lherzolite minerals are related to the emplacement of amphibolitic and pyroxenitic veins that pre-date incorporation of the lherzolite into the host magma. Chemical evidence reveals that pargasites in the spinel lherzolite have been metasomatized to kaersutitic amphiboles during emplacement of these veins, and the kaersutite and clinopyroxene (rarely orthopyroxene and spinel) megacrysts in the lavas are disaggregated remnants of the veins, as previously proposed by Wilshire and Trask (1971). For example, minerals in spinel lherzolite from Dish Hill, California show variations in the major elements as gradients strongly developed perpendicular to xenolith surfaces covered with rinds of amphibole (the rinds are remnants of veins); no gradients occur parallel to these surfaces. In traverses toward the rind from within the lherzolite, amphiboles exhibit a relative increase in TiO_2 (>250%), total Fe (>75%), and K_2O (>50%) and a decrease in Cr_2O_3 (>80%). Megacrysts of kaersutite in the host basanite have compositions equivalent to those of the rind extrapolated to a distance of >10 mm beyond the inner border of the rind.

$\delta^{18}\text{O}$, δD , and H_2O^+ of the amphiboles and phlogopites in the xenoliths and megacrysts were determined for kimberlites, alkali basalts, and basanites. The range of values of δD (relative to SMOW) for the micas is -60 to -73 ‰, which is consonant with the values of "primordial" H_2O obtained by Craig and Lupton (1976), Kuroda *et al.* (1977), and O'Neil (unpublished data). The narrowness of this range suggests that all H_2O is fractionated into the hydrous minerals with no vapor present. Values of δD for some amphiboles are lighter, ranging to -111 ‰. $\delta^{18}\text{O}$ for the micas and amphiboles ranges from 4.26 to 5.92, typical of deep-seated materials. The micas, and especially the amphiboles, are poor in OH and rich in F and Cl. For example, a Dish Hill kaersutite megacryst DH-IA contains 0.40% (wt) H_2O , 0.13% F, 0.1% Cl, and a large "oxyamphibole" component ($\text{Fe}_2\text{O}_3=13.76\%$; $\text{FeO}=0.29\%$). These data suggest that the $a_{\text{H}_2\text{O}}$ is considerably less than unity, although a discrete vapor may have coexisted with the hydrous minerals.

We interpret the above data as evidence that anatexis or mobilization of mantle lherzolite during the genesis of alkali basalts and kimberlites is subsequent to or concomitant with metasomatism by aqueous fluids rich in Ti, Fe, K, and other ions. Additional supportive evidence can be found in papers by Basu and Murthy (1977), Best (1975), Erlank (1976), Francis (1976), Frey and Green (1974), Lloyd and Bailey (1975), and Varne and Graham (1971). Primary alkali basalt and basanitic magmas unmodified by fractionation, such as those described from Australia (Kesson, 1973), Colorado Plateau (Best and Brimhall, 1974), Mauritius (Indian Ocean) (Baxter, 1976), and the Easter volcanic chain (Pacific Ocean) (Bonatti *et al.*, 1977), are enriched in elements including K, Ti, etc., as well as H_2O . Different degrees of partial melting of the mantle could account for the differences between some enriched primary magmas and others (Baxter, 1976), but marked heterogeneity of the source regions is sup-

ported by a plethora of geochemical data (Cox et al., 1976; Kesson, 1973; Sun and Hanson, 1975). The indifferences of the chemistry of alkali basalts to their environment of eruption, be it continental, oceanic, or island-arc, argues against crustal contamination as a viable explanation (see Schwarzer and Rogers, 1974). Migrating fluids associated with, say, mantle diapirism (Wilshire and Pike, 1975) or plumes (Bonatti et al., 1977) appear to have operated throughout much of the history of the mantle. Consequently, the chemistry of mantle samples has been altered by the very processes that have resulted in bringing them to the surface--Irving's (1976) Heisenberg uncertainty. The search for pristine mantle continues.

REFERENCES

- Baxter, A. N. (1976) Geol. Soc. Am. Bull. 87, 1028-34.
- Basu, A. R., and Murthy, V. M. (1977) Geology, 5, 365-8.
- Best, M. G. (1974) J. Geophys. Res. 79, 2107-13.
- Best, M. G., and Brimhall, W. H. (1974) Geol. Soc. Am. Bull. 85, 1677-90.
- Boettcher, A. L. (1967) J. Geol. 75, 526-53.
- Bonatti, E., Harrison, C. G. A., Fisher, D. E., Honnorez, J., Schilling, J. -G., Stipp, J. J., and Zentilli, M. (1977) J. Geophys. Res. 82, 2457-78.
- Carswell, D. A. (1975) Phys. Chem. Earth 9, 417-29.
- Cox, K. G., Hawkesworth, C. J., and O'Nions, R. K. (1976) Contrib. Mineral. Petrol. 56, 173-180.
- Craig, H., and Lupton, J. E. (1976) Earth Planet. Sci. Lett. 31, 369-85.
- Dawson, J. B., Powell, D. G., and Reid, A. M. (1970) J. Petrol. 11, 519-48.
- Dawson, J. B., and Smith, J. V. (1973) J. Petrol. 14, 113-31.
- Erlank, A. J. (1976) EOS, 57, 597.
- Flower, M. F. J. (1969) Earth Planet. Sci. Lett. 6, 461-6.
- Francis, D. M. (1976) Contrib. Mineral. Petrol. 58, 51-61.
- Frey, F. A., and Green, D. H. (1974) Geochim. Cosmochim. Acta 38, 1023-59.
- Hogarth, D. (1964) Canadian Mineral. 8, 136.
- Irving, A. J. (1976) Amer. Mineral. 61, 638-42.
- Kesson, S. E. (1973) Contrib. Mineral. Petrol. 42, 93-108.
- Kuroda, Y., Suzuoki, T., and Matsuo, S. (1977) Contrib. Mineral. Petrol. 60, 311-15.
- Lloyd, F. E., and Bailey, D. K. (1975) Phys. Chem. Earth 9, 389-416.
- Prider, R. T. (1939) Mineralog. Mag. 25, 373-87.
- Schwarzer, R. R., and Rogers, J. J. W. (1974) Earth Planet. Sci. Lett. 23, 286-96.
- Stewart, D. C., and Boettcher, A. L. (1977) Submitted to Geol. Soc. Amer.
- Sun, S. S., and Hanson, G. N. (1975) Geology 3, 297-302.
- Suwa, K., and Aoki, K. (1975) 1st Prelim. Rept. Afr. Studies, Nagoya Univ., 60-64.
- Switzer, G., and Melson, W. G. (1969) Contr. Earth Sci., no. 1, 1-9.
- Varne, R., and Graham, A. L. (1971) Earth Planet. Sci. Lett. 13, 11-18.
- Wagner, P. (1914) The Diamond Fields of Southern Africa. Transvaal Leader.
- Watson, K. D. (1955) Amer. Mineral. 40, 565-79.
- Wilshire, H. G., Calk, L. C., and Schwarzman, E. C. (1971) Earth Planet. Sci. Lett. 10, 281-84.
- Wilshire, H. G., and Pike, J. E. N. (1975) Geology 3, 467-70.
- Wilshire, H. G., and Trask, N. J. (1971) Amer. Mineral. 56, 240-55.
- Windom, K. E., and Boettcher, A. L. (1977) Submitted to Geol. Soc. Amer.

GEOPHYSICAL AND Rb-Sr STUDY OF THE ELLIOTT COUNTY, KENTUCKY AND PRAIRIE CREEK, ARKANSAS KIMBERLITES

Bolivar, S. L. and Brookins, D. G. (Department of Geology, University of New Mexico, Albuquerque, N. M. 87131)

General:

Rb-Sr systematics, uranium whole-rock analyses, whole-rock and mineral-separate chemical analyses have been determined for two areas of kimberlitic rocks: the Prairie Creek, Arkansas and Elliott County, Kentucky intrusions. In addition, petrologic data and detailed field investigations, completed as part of a joint University of NM-Purdue University study of mid-continental USA kimberlites allow the following interpretation to be made: The Prairie Creek intrusion is characterized by three rock types: micaceous peridotite, clearly distinguishable by magnetic data, and kimberlite breccia and associated tuff, not distinguishable by magnetic data. (1) Detailed mapping and geophysical data suggest the sequence of intrusion to be: kimberlite breccia, characterized by a 'typical' diatreme shape; peridotite, a shallow vertical intrusion of variable thickness; and scattered patches of tuff consisting of reworked breccia and peridotite. (2) Garnet, ilmenite, pyroxene, olivine and phlogopite megacrysts from the two study areas are similar in composition to those of kimberlites described elsewhere in the world.

Twenty Elliott County kimberlites yield $^{87}\text{Sr}/^{86}\text{Sr}$ ratios ranging from 0.7026 to 0.7102 with an arithmetic mean of 0.7065. Sixty five Prairie Creek analyses range from 0.7058 to 0.7132 with an arithmetic mean of 0.7094. Variability of $^{87}\text{Sr}/^{86}\text{Sr}$ and total Sr and Rb is attributed to both sample inhomogeneity and heterogeneous source regions. The rock are undateable by the Rb-Sr whole rock method.

Discussion:

In Elliott County at least two dikes several hundred feet long and one diatreme about 200 feet in diameter, Permian in age, crop out in poor exposure. The presence of megacrysts of pyrope garnet, magnesian-rich ilmenite, olivine, phlogopite and clinopyroxene in a panidiomorphic groundmass of euhedral olivine, primary carbonate and orthopyroxene indicates these rocks are properly classified as kimberlites, and compared to other U. S. kimberlites, these rocks are relatively fresh. Several xenoliths, including a very interesting metamorphic suite, were examined. These xenoliths suggest that a metamorphic suite of rocks may occur at the base of the crust in Eastern Kentucky.

The Prairie Creek intrusion, covering about 0.5 mi² consists of a micaceous peridotite (phenocrysts of subhedral, partially serpentinized olivine-Fo₉₂ in a groundmass of phlogopite, serpentine and diopside with minor amounts of perovskite, pyrite, amphibole and magnetite), a kimberlite breccia (serpentinized olivine phenocrysts in a groundmass of serpentinized olivine and phlogopite with minor amounts of spinel, perovskite, secondary biotite, chlorite, and secondary calcite) and associated tuff (containing fragments of breccia, peridotite and country rock). The lack of magnesian ilmenite, enstatite, and chrome diopside and the rarity of garnet suggest the kimberlite breccia may not be a true kimberlite rock in the "strictest sense"; however, the observed mineralogy is not believed to be representative of the original composition because of the extreme alteration of the breccia.

The sequence of intrusion, based on geophysical evidence is believed to be breccia, peridotite, then tuff. Analyses of magnetic and gravity data suggest qualitatively, that the peridotite intrusion is a shallow almost vertical intrusion of variable thickness which dips slightly to the south. The boundary of the kimberlite breccia was not clearly defined by geophysical data.

Garnet, ilmenite, pyroxene, olivine and phlogopite megacryst data from this study compare favorably with foreign and other U. S. analyses. Two suites of garnets occur, one high in Cr_2O_3 (0.5-4.0 wt. %), characteristic of kimberlites, and one low in Cr_2O_3 (less than 0.2 wt. %), characteristic of some other source (probably metamorphic). Compared to South African kimberlite data, Elliott County pyroxenes are equivalent in Al_2O_3 content but possess lower Ca/ Ca+Mg ratios. Most of the megacrysts in this study appear to be xenocrysts, as evidenced by petrographic data and composition similar to corresponding minerals in garnet lherzolites and garnet peridotites.

A Rb-Sr systematic study revealed extreme variations in $^{87}\text{Sr}/^{86}\text{Sr}$, total Sr and total Rb for both study areas. This variability is attributed predominantly to sample inhomogeneity, heterogeneous source regions and interactions with ground water. Extreme care in selecting "fresh" samples and tedious handpicking to remove xenoliths and megacrysts may (or may not) help to eliminate this scatter, consequently the data were not amenable to isochron treatment. An extensive leach program using dilute HCl was undertaken but did not resolve this problem. A histogram-frequency plot for Prairie Creek rocks is given in Figure 1.

An isochron plot of three Prairie Creek Montmorillonite rich samples yields preliminary data that is encouraging in that the age of intrusion may be successfully determined from clay isochrons in the near future.

References:

- Bolivar, S. L., 1977, Geochemistry of the Prairie Creek, Arkansas and Elliott County, Kentucky intrusions, Ph.D. dissertation, Dept. of Geology, University of New Mexico, Albuquerque, New Mexico.

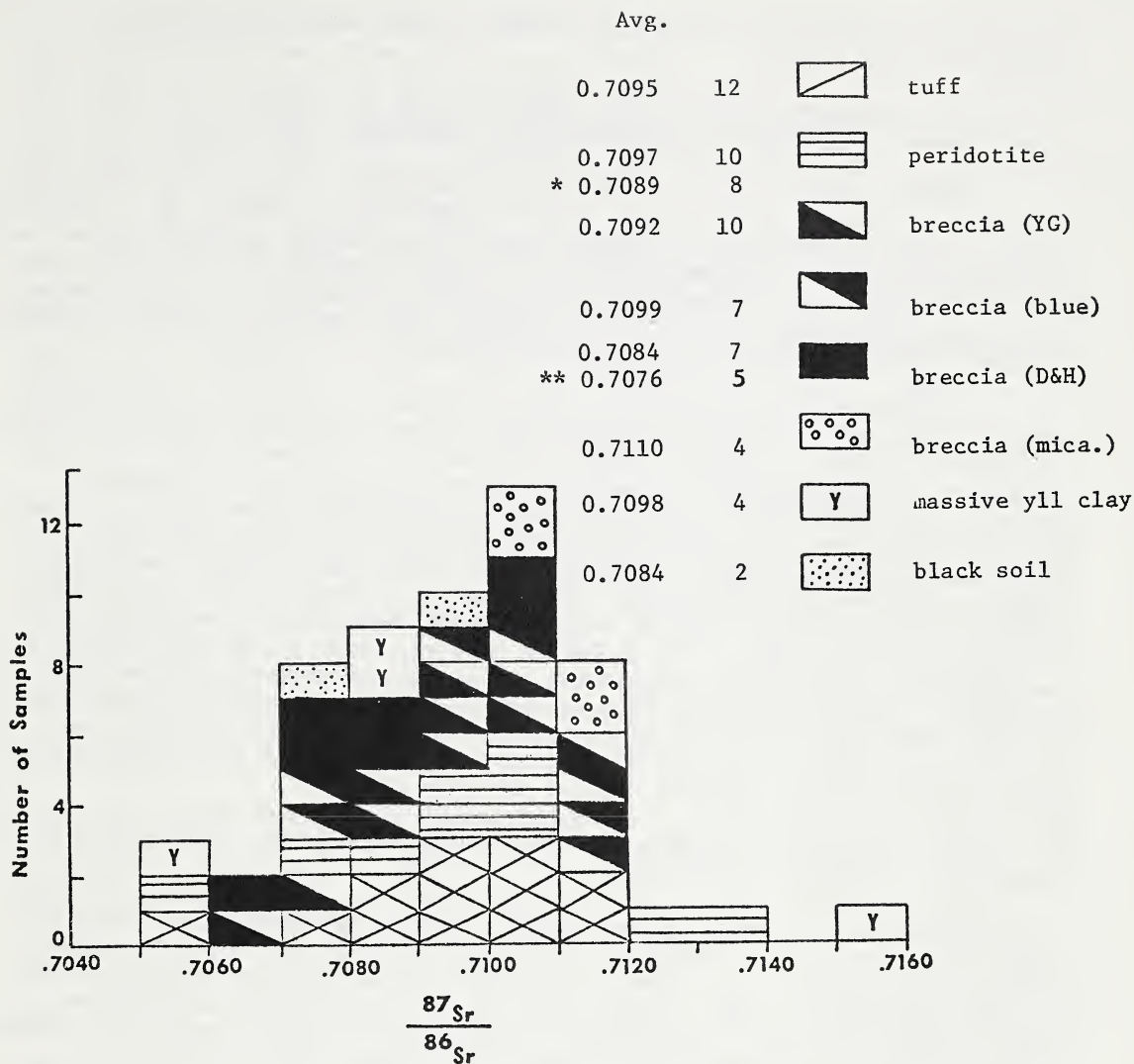


Figure 1. Histogram-frequence plot of $^{87}\text{Sr}/^{86}\text{Sr}$, from Prairie Creek rocks. The peridotite total for eight samples (*) does not include two weathered samples with 0.7120 and 0.7132 ratios. The D+H breccia total for five samples (**) does not include two weathered samples with 0.7102 and 0.7104 ratios. Weathered samples were not included in averages because of the presence of secondary minerals. Average for 52 samples (not including * and **) is 0.7094.

COMPOSITIONAL ZONING OF OLIVINES IN KIMBERLITE FROM THE DE BEERS MINE,
KIMBERLEY, SOUTH AFRICA

F. R. Boyd (Geophysical Laboratory, Washington, D. C., U.S.A.)

C. R. Clement (De Beers Consolidated Mines, Kimberley, South Africa)

Olivine, the most abundant mineral in the modes of most kimberlites, has long been recognized to be of more than one generation or origin (e.g., Wagner, 1914, p. 54). Coarse (>1 mm), rounded grains are commonly strained and may be xenocrysts derived from disaggregated wall rocks. Smaller (0.1-1 mm) olivines tend to be euhedral or subhedral and are commonly believed to be phenocrysts (e.g., Mitchell, 1973). Both types of olivine are present as remarkably fresh, unserpentinized crystals in the De Beers "Peripheral" kimberlite.

The "Peripheral" kimberlite, one of three major phases of kimberlite intrusion within the southeastern part of the De Beers pipe, is a dark gray rock containing abundant, commonly rounded and unaltered, yellowish green olivine megacrysts set in an aphanitic matrix. Scattered megacrysts of ilmenite, garnet, chrome diopside and rare flakes of phlogopite are also present. Near-vertical flow structures formed during emplacement are locally prominent. There are abundant subhedral to euhedral phenocrysts and microphenocrysts of olivine. The fine-grained groundmass is mainly monticellite and serpentine. Monticellite occurs as a closely packed granular aggregate of subhedral crystals ranging in size from about 0.008 to 0.04 mm. Much of the monticellite is unaltered, but deuteric replacement by calcite and serpentine is evident in places. Serpentine occurs as interstitial material between earlier crystallized components, as a deuteric mineral replacing other components, and as massive serpophite in irregular segregations where it is associated with much of the limited groundmass calcite and rare apatite.

The "Peripheral" kimberlite is diamondiferous but the grade is low--approximately 5 carats per 100 tons.

Idiomorphic olivines in the De Beers "Peripheral" kimberlite range in size mainly from 0.2 to 1 mm, but in the slide on which the electron microprobe analyses were made, there are two idiomorphic crystals that are 4-5 mm in maximum dimension. Most of the small (<1 mm) olivines in this specimen show the development of some crystal faces, although many are subhedral rather than euhedral. A few are near-perfect, doubly terminated crystals.

The ten idiomorphic olivines that were studied in detail have core compositions ranging from Fo₉₃ to Fo₈₇. There is no compositional distribution maximum in this range. Compositional scans made mainly across the short dimension of the euhedral olivines show complex zoning patterns that involve both normal and reverse trends (Fig. 1). The cores are usually homogeneous, and the zoning is confined to the outer 100-150 μ m. A number of the scans (Fig. 1) show Fe enrichment proceeding outward from the core, followed by a reversal of trend with Mg enrichment at the outermost margins. Although the zoning patterns are complex, the edges of these crystals tend to have Mg/(Mg + Fe) in the range 0.89-0.90. Crystals with cores more Mg-rich than this range (e.g., E2 and E9, Fig. 1) have predominantly normal zoning, whereas those with cores more Fe-rich than this range (e.g., E10 and E5, Fig. 1) have predominantly reverse zoning.

size less distinct of ol. 177.
* Dunks at Keweenaw - low Mg.

The large, rounded olivines vary in size up to a maximum dimension of 6 mm. Their shapes range from lobate to subangular. Seven of the ten rounded olivines that have been studied in detail are deformed with undulate extinction; some also have internal or adhering zones of mosaic-textured, recrystallized olivine. Values of $Mg/(Mg + Fe)$ for the homogeneous cores of these crystals are 0.840-0.934. This range is somewhat larger than that found for the euhedral olivines, although there is much overlap.

Electron microprobe scans across the margins of large, rounded olivines show that they are complexly zoned in patterns similar to those found for the small, euhedral olivines. Some crystals show restricted zoning, one has strong normal zoning and one has strong reverse zoning. The edges of these crystals tend to have $Mg/(Mg + Fe)$ of the order of 0.89-0.90 regardless of the core composition. This same tendency was noted above for the small, euhedral crystals, and it is concordant with the observations of Emelius and Andrews (1975), who stated that "Zoning converges on a compositional band around $Mg_{87-91} \dots$ "

Electron microprobe scans across shear zones of recrystallized, mosaic-textured olivine that adhere to the margins of some of the large, rounded crystals show that these zones have also been affected by the process that caused the zoning. Figure 2 shows four scans across the edges of a large, deformed olivine (R1). Scans A-A', B-B', and C-C' across edges where the olivine has not been recrystallized show a familiar (e.g., Fig. 1) zoning pattern in which an Mg-rich core is zoned normally in the outer 150 μm , but with a reversal in trend, toward more Mg-rich olivine, in the outermost 25 μm . Scan D-D' across the shear zone (Fig. 2) shows irregular zoning toward more Fe-rich compositions, but the zoning extends 350 μm in from the edge, almost the full width of the shear zone.

The compositional range for the euhedral olivine phenocrysts suggest that they crystallized from heterogeneous batches of magma of differing $Mg/(Mg + Fe)$ or differing temperature, or both, and were mixed during eruption. The more magnesian large, rounded xenocrysts are probably derived from peridotites, whereas the less abundant, more Fe-rich xenocrysts may have come from disaggregated dunites. The marginal zoning is believed to be metasomatic in origin rather than growth zoning because it affects patches of sheared and recrystallized olivine adhering to the edges of xenocrysts. Most of the xenocrysts have been rounded by abrasion or corrosion during eruption, and the marginal zoning has developed after the rounding. Whether the fluid that caused the metasomatism was a gas phase, residual magma, or a mixture of immiscible silicate and carbonate liquids (Clement, 1975) remains to be ascertained.

Clement, C. R., Phys. Chem. Earth, 9, 51-59, 1975.

Emelius, C. H., and J. R. Andrews, Phys. Chem. Earth, 9, 179-197, 1975.

Mitchell, R. H., Lithos, 6, 65-81, 1973.

Wagner, P. A., The Transvaal Leader, Johannesburg, 1914 (2nd impression C. Struik (PTY) Ltd., Cape Town, 1971).

Fig. 1. Compositional scans of euhedral olivines, mostly perpendicular to long axis. E1, 2 x 4 mm; E2, 5.5 mm, broken; E9, 790 μm ; E10, 795 μm . Reference values of $Mg/(Mg + Fe)$ are given for each scan. Crystal edges are indicated by short, vertical lines at one or both ends of each scan.

Fig. 2. Variation of $Mg/(Mg + Fe)$ across the margins of a deformed olivine crystal (R1) with an adhering, mosaic-textured, recrystallized zone. It has not been possible to show all the grain boundaries within the shear zone.

Mosses MS87

FIG. 1

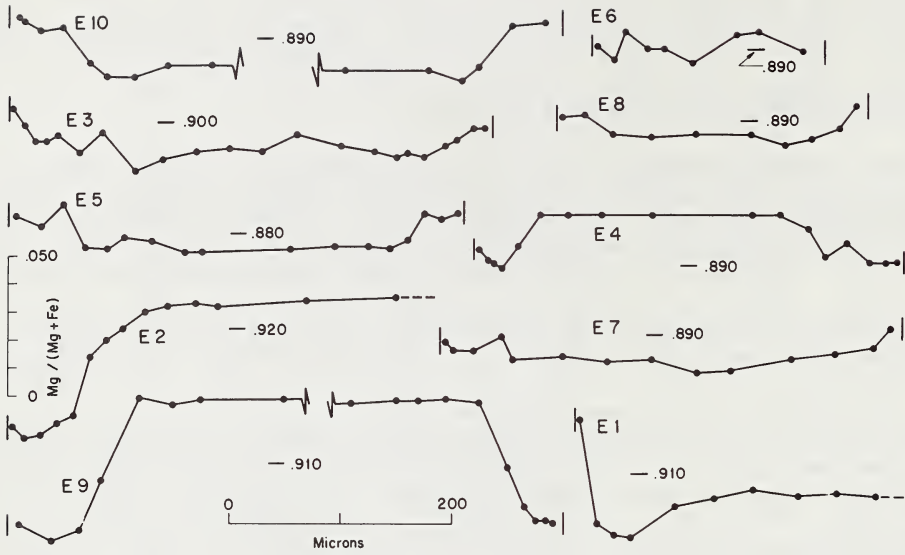
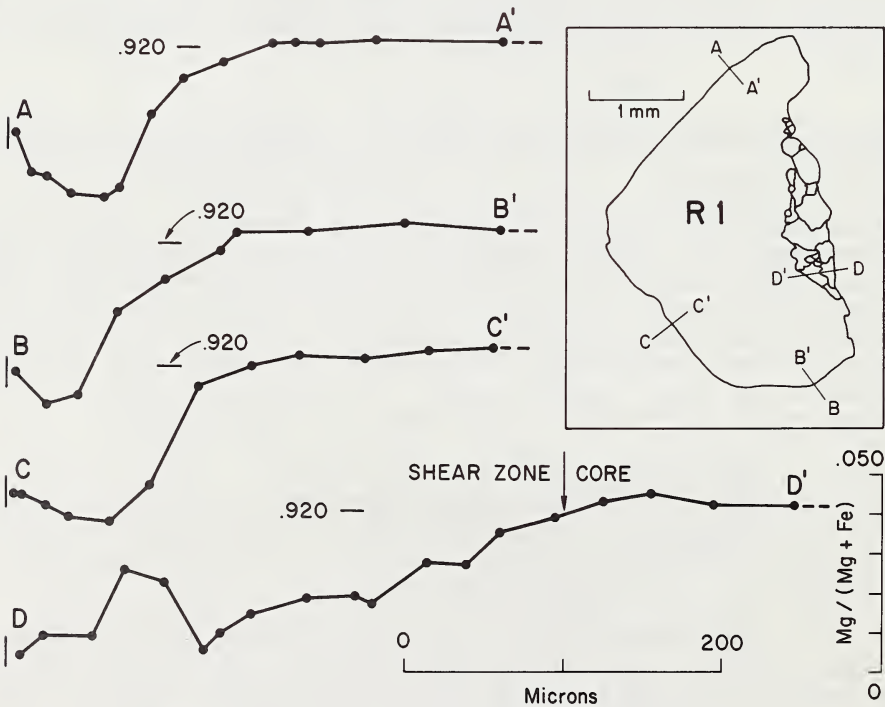


FIG. 2



PETROGENESIS OF OLIVINE MELILITE AND KIMBERLITE AND MELTING OF PERIDOTITE - C - O - H

G. Brey (Mineralogisches Institut der Technischen Universität, Welfengarten 1, D-3000 Hannover, Federal Republic of Germany)

D. H. Green (dept. of Geology, University of Tasmania, Box 252C, G.P.O., Hobart, Tasmania 7001, Australia)

Tasmania 27 kb 78A.0
6-8C2
SA paper

A survey of worldwide occurrences of olivine nephelinites, olivine melilitites and kimberlites reveals that primary mantle - derived magmas of each class can be identified (Brey, 1977) and systematic chemical differences between and within each class can be attributed to different conditions of origin. Olivine nephelinites and melilitites can be closely linked genetically by different degrees of partial melting of a peridotitic composition and/or varying $H_2O : CO_2$ in the source region. Olivine melilitites become increasingly undersaturated ($CaO + MgO/SiO_2$ increases) with increasing distance from a rift zone and if the W - coast of southern Africa is viewed as a part of a rifted zone then the olivine melilitites disappear at some distance from the rifted zone and are replaced by kimberlites. Kimberlites are chemically continuous to the olivine melilitites except for a much higher MgO/CaO . This may be attributed to increasing depth of magma segregation.

A systematic study of the liquidus phase relationships of a natural primary olivine melilitite + $H_2O + CO_2$ at 30 kb (and more limited studies at other pressures) has established liquidus fields for olivine, garnet, clinopyroxene and orthopyroxene and furthermore that the particular olivine melilitite is a possible partial melting product of a four phase garnet lherzolite at 27 kb, 1160 - 1180°C, if the melt contains 7 - 8 wt % H_2O and 6 - 7 wt % CO_2 in solution (Brey and Green, 1977). Limited experiments with a modified olivine melilitite (higher $CaO + MgO/SiO_2$), matching the most undersaturated melilitites show that these rocks are derived from greater depth (~ 34 kb) by lower degrees of partial melting and/or higher CO_2/H_2O in the source region. A kimberlitic composition (36 % SiO_2 , 35 % MgO , 8.7 % $CaO + 20$ % FeO , alkalis ...) with 15.3 % H_2O and 25 % CO_2 added has orthopyroxene and magnesite at its liquidus at 45 kb and 50 kb. Similar compositions may represent the melt near the solidus of carbonated peridotite at such high pressures. All these experiments were carried out under MH-buffered conditions which create oxygen fugacities probably too high for the actual conditions in the mantle. Oxygen fugacities in the region of the LVZ are more likely to be around or below those generated by a QFM buffer (Rosenhauer et al., this meeting ; Ryabchikov et al., in prep.). At these conditions carbon still shows high solubilities as carbonate ion in silicate melts (Ryabchikov et al., in prep.) and thus the above experiments are still applicable. Under these low oxygen fugacities however carbonates are not stable any longer under subsolidus conditions and graphite or diamond coexist with mantle silicate minerals (Ryabchikov et al., in prep. ; Rosenhauer et al., this meeting).

27 kb
Ng10

The oxidation state of carbon at subsolidus conditions has consequences on melting temperatures and the nature of first melts of peridotite - C - O - H. The melting of carbonated peridotite has found extensive coverage (e.g. Wyllie and Huang, 1976 and earlier papers ; Egglar, 1976 and earlier papers) and also is/was a matter of disagreement. CO_2

occurs in mantle peridotite at sufficiently high pressures and low temperatures in dolomite and at even higher pressures in magnesite. The composition of the first melts of carbonated peridotite (no H₂O present) is very Si - poor and especially CaO - rich and may be termed carbonatitic (Wyllie and Huang, 1976) Our own experiments with various mixes of olivine melilitite + increasing amounts of carbonate (CC₅₈MC₄₂) + CO₂ at 30 kb show that carbonates and silicates may be together at the liquidus for a composition somewhat Si - poorer than that found by Egger (1976). In the presence of excess H₂O, but high enough CO₂/H₂O, the first melt will also be carbonatitic (Wyllie, 1977), a conclusion supported by our experiments on olivine melilitite + CC₅₈MC₄₂ + CO₂ + H₂O. The melting temperatures increase with increasing CO₂/H₂O in the vapor phase (Wyllie, 1977), but note that with increasing CO₂/H₂O in the vapor phase, peridotite is carbonated and clinopyroxene and olivine are eliminated. Most interesting for nature is probably the case where all CO₂ and H₂O present can be accommodated in carbonates (dolomite and magnesite at higher pressures) and amphibole and phlogopite resp. The carbonated and hydrated peridotite will melt at lower (and for all CO₂/H₂O in the system constant) temperatures as compared to the systems with only carbonates or hydrous phases) and the composition of the first melt will also be the same for all CO₂/H₂O. Holloway and Egger (1976) investigated the melting in the stability field of phlogopite + dolomite and Brey (1976, unpublished Ph.D. thesis) for amphibole + dolomite at lower pressures. At present we attempt to establish the composition of the first melt at such conditions.

It is more likely that oxygen fugacities in the mantle are such that carbonates are not stable anymore and graphite or diamond are present at subsolidus conditions. For amounts of water in excess of what can be accommodated in hydrous phases a complex vapor phase consisting of H₂O, CO₂, CH₄ ... will coexist with graphite or diamond. The solidus temperature depends on the composition of this vapor phase. If all the water in the system is present in hydrous phases, esp. amphibole and/or phlogopite, the melting temperature will be determined by the stability of the hydrous phase, e.g. as in the case for amphibole in pyrolite + < .4 % H₂O (Green, 1973). Upon melting carbon will dissolve as the carbonate molecule in the resulting melts which still are highly undersaturated and probably resemble the most undersaturated olivine melilitites at lower pressures (~ 30 kb) and kimberlites (in the stability field of phlogopite) at higher pressures (> 30 kb, ~ 50 kb). The existence of the low - velocity zone is a consequence of interstitial melt of this type at depths beyond those at which amphibole is stable in peridotite compositions. Kimberlitic melts could, upon cooling at high enough pressures, precipitate diamonds.

References

- Brey, G., J. Volc. Geotherm. Res., in press
Brey, G. and Green, D.H., Contrib. Mineral. Petrol., 61, 1977
Egger, D. H., Geology, 4, 1976
Green, D.H., Earth Planet. Sci. Lett., 19, 1973
Holloway, J. R. and Egger, D. H., Ann. Rept. Dir. Geophys. Lab., Washington, 75, 1976
Rosenhauer et al., this meeting
Ryabchikov, I. D., Green, D. H., Brey, G., in prep.
Wyllie, P. J., J. Geol., 85, 1977
Wyllie, P. J. and Huang, Contrib. Mineral. Petrol., 54, 1976

SIGNIFICANCE OF URANIUM ABUNDANCE IN UNITED STATES KIMBERLITES

D. G. Brookins, R. S. Della Valle, S. L. Bolivar (Department of Geology,
University of New Mexico, Albuquerque, New Mexico 87131)

General:

The uranium content of some 150 kimberlite and other ultramafic rock samples from United States occurrences has been determined by delayed neutron activation analysis (DNAA). The kimberlites in particular are enriched in uranium relative to ultramafic rock with no apparent kimberlitic affinities. Further, there is usually a positive correlation between uranium content and the presence of carbonatitic material within kimberlites. Our data support Kresten's (1974) proposed positive correlation between perovskite content and uranium abundance only for those kimberlites with little or no carbonatitic calcite. When such carbonatitic material is present, then any contribution from perovskite is masked. High uranium abundances due to contamination from included material or from solution-deposited material from surrounding host rocks to the kimberlite are apparently of local importance only for the following reasons: (1) High uranium content commonly correlates with carbonatitic 87-Sr/86-Sr ratios (0.703 to 0.705). (2) The mean uranium content for many kimberlites is commonly significantly higher than the uranium content of the host rocks. (3) Where sedimentary (or other) contamination is obvious, uranium contents are lower than for uncontaminated parts of the kimberlites and more or less correlate with sedimentary carbonate 87-Sr/86-Sr ratios (0.708 ± 0.002).

Previous Work:

Kresten (1974) has reported on the uranium abundances in some 80 basaltic kimberlites (mean: 2.35 ppm) and 30 micaceous kimberlites (mean: 4.91 ppm) from locations outside the United States. For the basaltic kimberlites, he reported a positive correlation between uranium abundance and perovskite content and proposed that uranium substituted for calcium in the perovskite. No such correlation was apparent for the micaceous kimberlites. Brookins et al. (1976) reported on some United States kimberlites and showed that uranium commonly correlated with carbonatitic calcite for both basaltic and micaceous kimberlites; the amount of carbonatitic calcite was identified by petrography, distinctive trace element suites, or 87-Sr/86-Sr ratios in the range 0.703 - 0.705. Correlation of high total Sr content and low 87-Sr/86-Sr ratios was noted in only about 50 percent of the samples studied, however.

Both Kresten (1974) and Brookins et al. (1976) used DNAA for uranium determinations because this method is superior to uranium determinations by other methods. For limited thorium and potassium data wide variation for U/Th are noted and K contents do not correlate well with either U or Th although all three elements are higher than in ultramafic rocks not associated with kimberlites.

Discussion and Concluding Remarks:

Kresten (1974) and Brookins et al. (1976) point out that many ultramafic nodules from kimberlites are uranium-poor; values from 30 ppb to 1 ppm are common. Similarly, the uranium content of rocks without kimberlitic affinities is usually less than 1 ppm. Kresten (1974) further demonstrated that the uranium content of many basaltic kimberlites could be explained by perovskite content; for the present study this is only apparently the case in the absence of carbonatitic carbonates. The peridotites from Prairie

Creek, Arkansas and from inclusions in the Larimer County, Wyoming-Colorado occurrences are low in carbonatitic calcite and low in total uranium, and there is a crude correlation between uranium content and perovskite-rich mafic constituents.

When either high uranium contents or anomalous Th/U ratios are reported from kimberlitic rocks, contamination is commonly reported as the cause. For the present study we have attempted to monitor contamination effects by comparing strontium isotopic systematics of both kimberlitic silicate and carbonate fractions. Earlier work has shown that in many instances high total Sr and 87-Sr/86-Sr from 0.703 - 0.705 are typical of carbonatites whereas low total Sr and 87-Sr/86-Sr ratios near 0.708 are typical of sedimentary carbonate. The uranium content of sedimentary carbonates is variable, but usually lower than that of carbonatitic calcite. When sedimentary-derived Sr is mixed with kimberlitic-derived Sr (from silicates and carbonatitic material), extreme variations in uranium content, total Sr, and 87-Sr/86-Sr may result. If the kimberlites are poor in carbonatitic material, the 87-Sr/86-Sr ratios may be severely affected by the presence of sedimentary-derived material, and correlation of high uranium content with high 87-Sr/86-Sr and low total Sr may result. When carbonatitic material is present, such as at the Elk Creek, Riley County, Larimer County and some of the Prairie Creek localities (Table One); low 87-Sr/86-Sr, high total Sr, and high uranium are noted. Where data are available, carbon and oxygen isotopic data indicate mixing of deep-seated carbonatitic material with meteoric waters such that oxygen isotopic data range from + 5 to + 15 o/oo while carbon isotopic data fall near - 6 ± 0.5 o/oo. Due to the very different total Sr contents, 87-Sr/86-Sr ratios do not correlate with del 18-O nor del 13-C values; but uranium persistently correlates with carbonatic calcite content.

Micaceous kimberlites are of special interest. These (Table One) commonly possess high uranium, yet correlation with perovskite content (Kresten, 1974) or with Sr content difficult to establish. Typically, however, the calcite commonly associated with the micaceous kimberlites is of a deep-seated origin and correlates with uranium content.

Our data support Kresten's (1974) conclusion that uranium in kimberlites is probably due to mixing of carbonatitic fluid or vapors with kimberlitic silicate material at depth and not due to enrichment by partial melting. A partial melt hypothesis indicates that uranium should largely reflect variation in silicate rock types rather than presence of carbonatitic material, yet our study demonstrates the control by carbonatitic-derived uranium in the total kimberlite uranium budget.

References:

- Brookins, D. G., et al., 1976, EOS Trans. Am. Geophys. Un., v. 57 (762).
Kresten, P., 1974, Lithos, v. 7 (171).

The Present Study:

Our data plus earlier data are summarized below:

Table One: Uranium Content of Kimberlites

<u>Locality</u>	<u>U (ppm) Range</u>	<u>Mean</u>	<u>Number of Samples</u>	<u>Reference</u>
Elliott Co., Kentucky	1.5 - 3.1	2.33	11	This study.
Prairie Creek, Arkansas:				
a) mic. peridotite	1.6 - 2.8	2.35	14	This study.
b) kimb. breccia	0.9 - 2.3	1.97	75	This study.
c) tuff and kimb. soil	2.2 - 5.9	3.85	17	This study.
d) carb. kimb.	5.0 - 6.2	5.62	6	This study.
Norris Lake, Tennessee	2.0 - 2.9	2.52	4	This study.
Riley Co., Kansas	4.2 - 5.7	4.80	6	Brookins <u>et al.</u> (1976)
Larimer Co., Wyoming-Colorado				
a) inclusions	1.8 - 2.6	1.35	5	<u>ibid.</u>
b) kimberlite	2.6 - 8.0	5.25	11	<u>ibid.</u>
Elk Creek, Nebraska	5.1 -17.9	11.54	16	<u>ibid.</u>
Non-U. S.				
a) bas. kimb.	0.5 - 4.5	2.35	82	Kresten (1974)
b) mic. kimb.	2.5 -12.5	4.91	89	<u>ibid.</u>

THE GEOCHEMISTRY OF **ULTRAMAFIC** NODULES FROM PIPE 200 AND THEIR BEARING ON THE NATURE OF THE UPPER MANTLE BENEATH LESOTHO.

D.A. Carswell (Department of Geology, University of Sheffield, Sheffield, U.K).
D.B. Clarke (Department of Geology, Dalhousie University, Halifax, Canada).
R.H. Mitchell (Department of Geology, Lakehead University, Thunder Bay, Canada).

The following types have been recognised in a suite of 33 ultramafic nodules:

- A. Garnet Lherzolites (15 samples) - no primary spinel phase
- B. Garnet Chromite Lherzolites (8 samples) - primary chromite and garnet
- C. Chromite Lherzolites (4 samples) - garnet now absent but originally present.
- D. Chromite Harzburgites/Lherzolite (5 samples) - primary chromite only
- E. Spinel Harzburgite (1 sample) - primary aluminous spinel and enstatite.

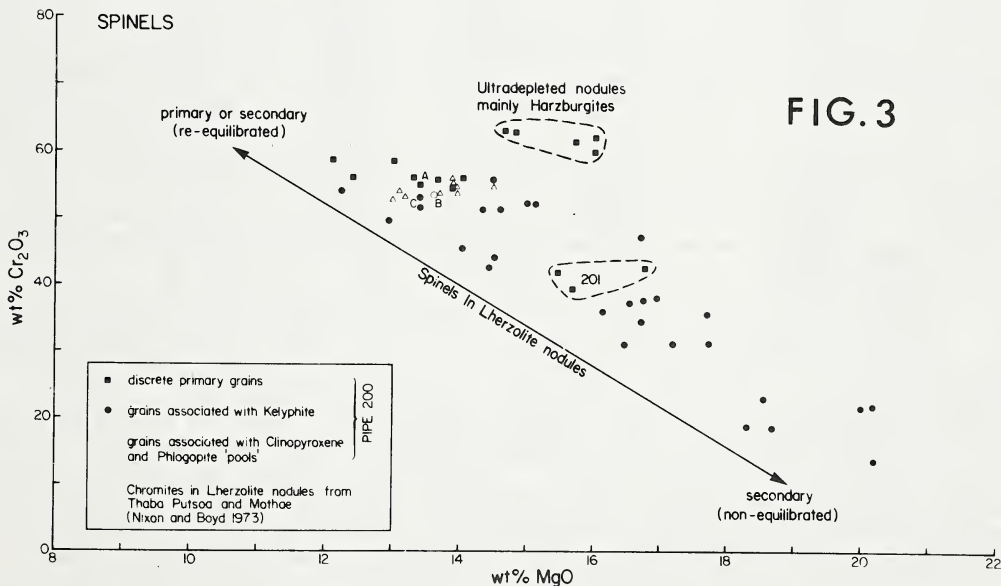
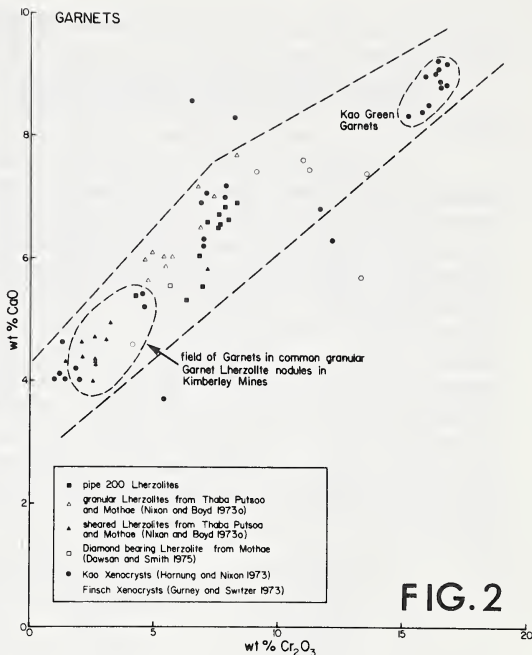
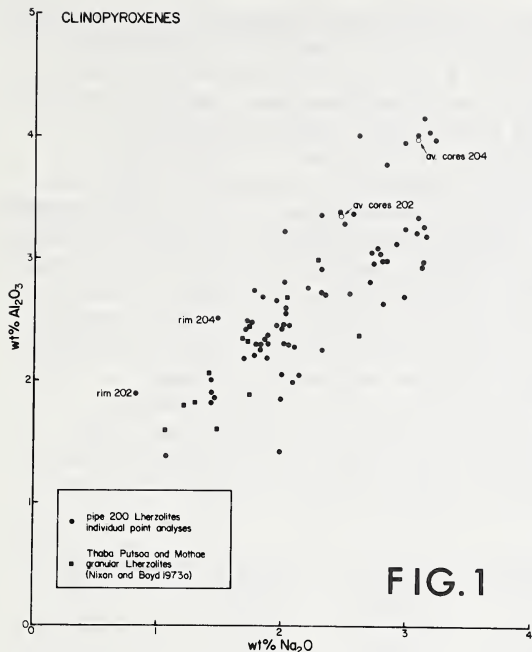
The majority of nodules are termed lherzolites, despite the fact that amounts of bright green chrome diopside are always small (<5 vol%, more typically only 1-2 vol%). When present purple chrome pyrope garnets and dark red brown chromites occur in similar small amounts. Garnets commonly have kelyphite alteration coronas and in some instances (Type C nodules) only kelyphite or coarser clusters of secondary spinels with phlogopites and clinopyroxenes remain to indicate the likely original presence of garnet.

Olivines are significantly more fosteritic (Fa 4.9-5.0) in the chromite harzburgites/lherzolite (Type D nodules) than in the lherzolite nodules (Fa 7.0-8.6) which contain or originally contained garnet (Types A, B and C). As in other aspects of its mineral chemistry, the spinel harzburgite (Type E) is exceptional in that it contains olivine Fa₇ yet lacks evidence to indicate that it ever contained garnet.

Orthopyroxenes in all nodules are enstatites but more magnesian in Type D nodules (Fs_{4.1-4.3}) than in Types A, B and C (Fs_{6.3-7.7}). In the latter nodule types they have mean values of 0.83 wt% Al₂O₃ (range 0.54-1.04), 0.45 wt% CaO (range 0.29-0.53) and 0.40 wt% Cr₂O₃ (range 0.18-0.50), in comparison with mean values of 0.65 Al₂O₃ (range 0.36-0.95), 0.25 wt% CaO (range 0.18-0.41) and 0.48 wt% Cr₂O₃ (range 0.23-0.76) in the Type D nodules. Orthopyroxene in the spinel harzburgite (Type E) has a significantly higher Al₂O₃ content (1.45 wt%).

Clinopyroxenes in all nodules have similar 100 Ca/(Ca+Mg) ratios (46.0-48.4) but quite variable contents of Al₂O₃ (1.64-3.99 wt%), Cr₂O₃ (1.59-4.25 wt%) and Na₂O (0.81-3.14 wt%). Al₂O₃ and Na₂O vary sympathetically (Fig.1) reflecting variable jadeite contents. In two nodules clinopyroxene grains have cloudy rims with lower jadeite than the clear cores. We attribute this jadeite depletion, and likewise the associated kelyphitic alteration of garnets, to the combined effects of metasomatism and decompression resulting from incorporation in kimberlite and subsequent diatreme emplacement. Nevertheless, much of the compositional variation between clinopyroxenes in different nodules, especially in Cr₂O₃, is thought to be a primary feature controlled by rock chemistry and the pressure/temperature conditions during equilibration.

Garnets in most nodules have higher Cr₂O₃ and CaO contents (14.3-18.6% uvarovite, 3.4-5.8% knorringite) than the garnets in the common lherzolite nodules in many other kimberlites and trend in composition towards the extreme chrome rich green garnets found as xenocrysts in the nearby Kao kimberlite (Fig.2).



Spinels of the primary type are low Al magnesiochromites, except in the spinel harzburgite (labelled 201) where they are aluminous chrome spinels with an appreciably lower $Cr/Cr+Al$ ratio. Primary spinels in Type D nodules have highest absolute Cr_2O_3 contents. Spinel associated with kelyphite show a wide range of compositions (Fig.3). Undoubted secondary spinels from the innermost parts of kelyphites are high Al chrome spinels. However, other spinel grains from the outer parts of kelyphites or occurring in 'pools' of phlogopite and clinopyroxene grains have compositions more akin to the primary spinels. Thus

if they do represent a secondary generation derived from garnet breakdown, it would appear that they have re-equilibrated with the lherzolite assemblage.

Average Whole Rock Compositions for the 5 ultramafic nodule types are given below. For comparative purposes the analyses have been recalculated to 100% on a H₂O and CO₂ free basis and with total iron expressed as FeO.

It is apparent that there are consistent differences in whole rock chemistry between the garnet only lherzolites (Type A), chromite lherzolites which either contain or originally contained garnet (Types B & C), and chromite only harzburgites/lherzolite (Type D). Mg/Mg+Fe and Cr/Cr+Al ratios increase and Al₂O₃, CaO and Na₂O contents decrease for the nodule types in that order reflecting their increasingly 'depleted' chemical nature in terms of their 'basalt' yielding potential. Thus primary mineralogical variations between these nodules seem likely to have been largely controlled by rock chemistry. However, such an explanation is inadequate in the case of the spinel harzburgite (Type E) which has a composition most comparable to nodule Types B and C. The absence of petrographic evidence to indicate it ever contained garnet, combined with the notably more aluminous character of its primary spinels and orthopyroxenes, point to lower pressure equilibration conditions for this particular nodule.

TYPE	A	B	C	D	E
SiO ₂	46.85	46.78	46.35	44.06	45.30
TiO ₂	00.06	0.12	0.09	0.18	0.17
Al ₂ O ₃	1.07	0.55	0.40	0.20	0.48
Cr ₂ O ₃	0.32	0.26	0.22	0.16	0.21
FeO	6.63	5.95	6.40	4.52	5.80
MnO	0.11	0.10	0.11	0.06	0.10
NiO	0.29	0.31	0.33	0.32	0.30
MgO	43.44	45.21	45.44	50.25	46.90
CaO	0.97	0.53	0.45	0.14	0.61
Na ₂ O	0.13	0.08	0.09	0.04	0.03
K ₂ O	0.09	0.06	0.08	0.03	0.07
P ₂ O ₅	0.04	0.04	0.04	0.22	0.02
100Mg/Mg+Fe	92. 1	93. 1	92. 7	95. 2	93. 5
100Cr/Cr+Al	17. 4	24. 1	28. 4	40. 0	22. 2

Calculated equilibration conditions for the garnet bearing lherzolites are 1025-1080°C, (Wood and Banno 1973) and 38-42kbs, (Wood 1974), implying derivation from a restricted depth zone some 120-130 kms down. With the obvious exception of the Type 3 spinel harzburgite, there is no evidence to indicate that the garnet free ultramafic nodules have been derived from substantially shallower mantle depths. Indeed those garnet free nodules with chrome diopside give similar Wood and Banno (1973) equilibration temperatures. The apparent rarity of nodules recognised as likely to have been derived from the uppermost 85-95 kms of the mantle beneath Lesotho may result either from their generally highly depleted chemical character which renders the employed geothermometers/geobarometers inapplicable or perhaps more likely from the inaccuracy of the latter over the appropriate pressure/temperature range.

Mineralogical and chemical comparison between the common Pipe 200 ultramafic nodules and those from other pipes in northern Lesotho and in the Kimberley area, as well as in the Lashaine volcano, indicates that the mantle beneath Pipe 200 and most of northern Lesotho is exceptionally depleted down to depths of the order of 130-150 kms.

COMPARISON OF ULTRAMAFIC AND MAFIC XENOLITHS FROM KILBOURNE HOLE AND POTRILLO MAAR, NEW MEXICO

James L. Carter (University of Texas at Dallas, P. O. Box 688, Richardson, Texas 75080)

A detailed mineralogical and chemical investigation of coexisting phases of ultramafic and mafic xenoliths from Kilbourne Hole and Potrillo Maar, New Mexico reveal major differences in the upper mantle and deep crust between these two localities which are only 15 kilometers apart. This is exemplified by Figure 1 which shows the relationship of nickel in olivines versus the fayalite content of olivines from various xenoliths from Kilbourne Hole and Potrillo. A preliminary investigation of the base surge deposits at Potrillo reveal at least seven major eruptive events (Figure 2) from probably three different vents within the main maar. Three of these major eruptive events are xenolith-bearing (Figure 2). Each event is characterized by a different xenolithic assemblage. The lowest xenolith-bearing assemblage consists primarily of basalt, small 4-phase (olivine, orthopyroxene, clinopyroxene and spinel) peridotites, and very rare 3-phase (clinopyroxene, spinel and olivine) pyroxenites. The middle xenolith-bearing assemblage consists of various types of volcanics in addition to rock types similar to the lowest assemblage. In addition, the average xenolith size of the peridotites has increased by at least a factor of two. The largest xenolith found was 40 centimeters in longest dimension. The upper xenolith-bearing assemblage is characterized by the presence of various types of greenschist facies metamorphic rocks and composite ultramafic-mafic xenoliths. Multiple xenolith-bearing eruptive events appear to have occurred also at the Kilbourne Hole maar but subsequent slumping, weathering, erosion and drifting sand has partially obscured the original relationships.

The composite xenoliths which are characteristic of the last xenolith-bearing eruptive event at Potrillo are less common at Kilbourne Hole. Detailed optical examination of these xenoliths reveal that they consist of 4-phase type mantle materials with metamorphic textures that were brecciated and the open cracks permeated by a liquid which partially reacted with the 4-phase assemblage, especially the pyroxenes. The resulting liquid crystallized to an average mixture of clinopyroxene (85 vol. %), spinel (10 vol. %) and olivine (5 vol. %).

As part of the continuing study of the nature and origin of the various types of xenoliths from these maars, an electron microprobe study of the coexisting phases was carried out to determine their detailed mineralogy and chemistry. This study reveals that the liquid represented by the 3-phase xenoliths equilibrated in the crust, whereas the 4-phase unreacted xenoliths equilibrated in the upper mantle. It is suggested from the estimated oxygen fugacity for the formation of the spinels from the various types of xenoliths that the spinels from the crystallized liquids and from the mafic xenoliths equilibrated over a relative range of oxygen fugacity of three orders of magnitude, possibly between 10^{-8} to 10^{-11} , whereas the spinels from the 4-phase xenoliths shows a relative range of oxygen fugacity of at least six orders of magnitude, possibly between 10^{-3} to 10^{-9} . This range of oxygen fugacity may reflect a large range in temperature, with the highest oxygen fugacity values indicating the highest relative temperature. A large range in temperature of formation is also suggested by distribution of K_D values for the Mg-Fe exchange reaction between spinel and olivine and spinel and pyroxenes (Figure 3). The slope of a line defines a K_D value. The large range of K_D values from approxi-

mately 1.2 to 4.1 suggest a large range in temperature of formation for the spinels. Since the most Cr-rich spinels have the largest K_D values and since very Cr-rich spinels generally have even higher K_D values, a continuous decrease in crystallization temperature from Cr-rich to Al-rich spinels is suggested. Applying the experimental data of James Dixon (personal communication, 1977) to the coexisting pyroxenes from the composite type xenoliths suggest temperatures from 1050 to 1350°C and pressures of 9 to 11 kilobars. These results are consistent with the physical process of a 4-phase mantle type xenolith being fractured and permeated with a hot liquid (3-phase xenolith) resulting in temperature and chemical reaction gradients at the same pressures.

A most unusual type of clinopyroxene xenolith is present at Kilbourne Hole but it has not been found at Potrillo. It consists of single crystals up to 15 centimeters in maximum dimension with olivine crystals in layers about 0.5 to 1 centimeter apart parallel to the basal plane, and triangular shaped spinel and rods and spherules of pyrrhotite are oriented in rows parallel to the c-axis. The clinopyroxene has a composition very similar to the clinopyroxene occurring in the 3-phase xenoliths and may have a similar mode of origin. The presence of the various inclusions parallel to crystallographic directions suggest the possibility of exsolution. Olivine in solid solution in clinopyroxene has been observed by Kushiro (1972) in the synthetic system Fo-Di-Si at 1 atmosphere. The undersaturated nature of the liquid represented by the 3-phase xenoliths may favor solid solution of olivine in clinopyroxene. On the otherhand, the olivine and spinel may represent trapped liquid that crystallized to this assemblage.

The subsurface differences between Kilbourne Hole and Potrillo as suggested by the ultramafic and mafic xenolithic suite is supported by the study of crustal xenoliths (Padovani, 1977; Padovani and Carter, 1977). This difference is demonstrated especially by the presence of an extensive suite of greenschist metamorphic grade rocks which are present at Potrillo but are absent at Kilbourne Hole, and by the presence of an extensive suite of garnet- and two-pyroxene-bearing granulites at Kilbourne Hole which are extremely rare at Potrillo. Only two examples of garnet-bearing granulites have been found at Potrillo and no example of a two-pyroxene-bearing granulite.

The almost total lack of mixing of the various xenolith-bearing horizons at Potrillo suggests that the present expression of the maar is close to the original maar limits. If this is correct, then the crater forming event was extremely energetic with very little fall back of the rubble into the crater. Energy calculations suggest that the Potrillo and Kilbourne Hole maar eruptive events fall within the top 5 to 10 most energetic volcanic events on earth. The relationship of the xenolith-bearing horizons is interesting in that the crustal-bearing assemblages were apparently the last to come up. This relationship suggest at least a two stage eruptive process, possibly with a long residence time for the magma within the upper mantle or lower crust.

REFERENCES:

- Kushiro, I. (1972) Determination of liquidus relations in synthetic silicate systems with electron probe analysis: The system forsterite-diopside-silica at 1 atmosphere, *The Am. Min.* Vol 57, nos 7-8, 1260-1271.
- Padovani, E. R. (1977) Granulite facies xenoliths from Kilbourne Hole maar and their bearing on deep crustal evolution, unpub. Ph.D. dissertation, Univ. of Texas at Dallas, Richardson, Texas.
- Padovani, E. R. and J. L. Carter (1977) Aspects of the deep crustal evolution beneath south central New Mexico, in *The Earth's Crust*, Geophys. Mongr. 20, Ed. J. G. Heacock, AGU, Wash., D. C., in press.

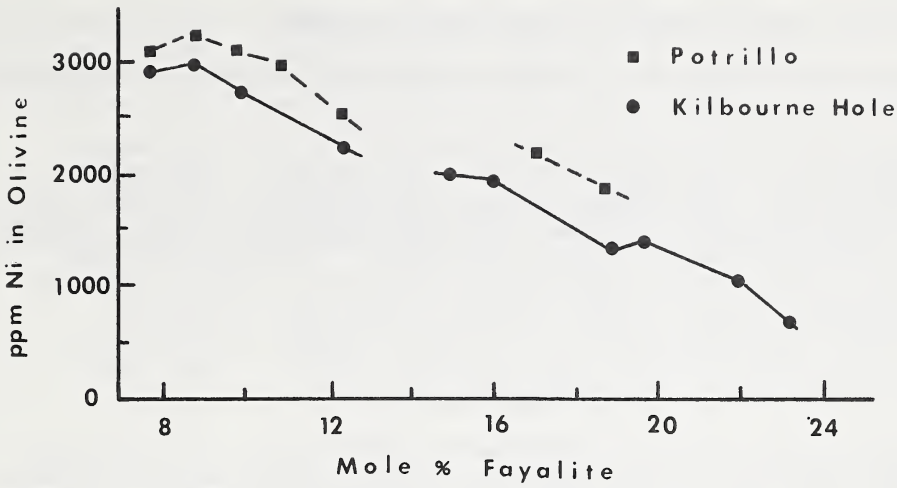


Fig. 1

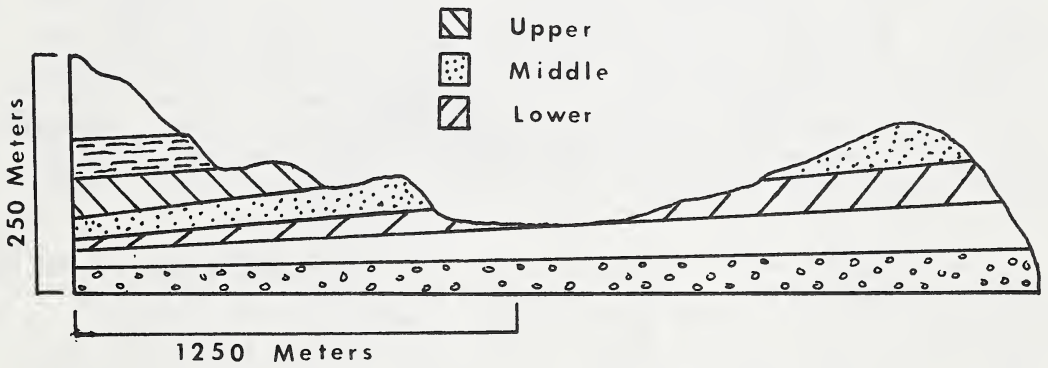


Fig. 2

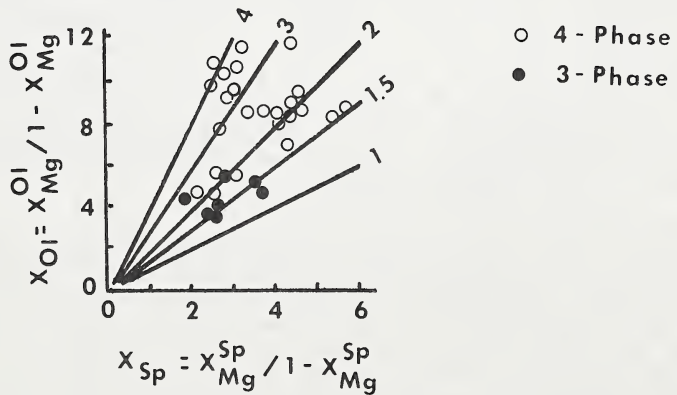


Fig. 3

SYNTHESIS OF THE K-Fe-Ni SULPHIDE FROM FRANK SMITH MINE

D.B. Clarke (Dept. of Geology, Dalhousie University, Halifax, N. S., Canada)

Potassium-iron-nickel sulphide has been found in a clinopyroxene-ilmenite intergrowth from Frank Smith Mine, Cape Province, South Africa (Clarke *et al.*, 1977). The mineral occurs principally in ovoid blebs with pyrrhotite and pentlandite, and these blebs are frequently in close spatial association with the ilmenite lamellae of the host. The blebs normally consist of a core of pyrrhotite-pentlandite and a rim of K-Fe-Ni sulphide. Discrete irregular grains of K-Fe-Ni sulphide also occur in minute fractures in the clinopyroxene host. A typical chemical analysis gives (wt. %): K 8.94, Fe 41.75, Ni 13.60, Cu 1.35, S 33.49, Cl 1.36, and a structural formula of $K_{6.1}(Fe,Ni,Cu)_{26.9}S_{28.0}Cl_{1.0}$.

Starting materials for the experimental work consisted of: potassium thioferrite ($K FeS_2$), Fe sponge, powdered Ni metal, synthetic FeS, synthetic NiS and KCl. Bulk compositions lying in the plane K-(Fe,Ni)S-Cl, roughly equal to the natural compositions plus excess potassium, were prepared. Losses of both K and Fe to the capsule walls occurred. Bulk compositions A, D and F had 100 Fe/Fe+Ni = 5 (atomic), whereas \bar{A} , \bar{D} and \bar{F} had 100 Fe/Fe+Ni = 50 (Fig. 1). The starting materials were loaded and welded in Au capsules in an Ar atmosphere, and then up to seven capsules were sealed in an evacuated silica glass tube. The tube was placed in a steel holder in a vertical resistance furnace with temperature control of $\pm 2^\circ C$. Care was taken not to overrun the desired run temperature during heating. All runs were at one atmosphere pressure. At the end of each run the silica tubes were lifted from the furnace and left to cool in air.

Preliminary results are given in Table 1. Bulk compositions A, D and F were contaminated with oxygen, the source of which was probably impure iron sponge, and as a result produced minor quantities of iron oxide. Nevertheless, the results on these runs are included here because of the additional information they provide on the degree of $Fe \rightleftharpoons Ni$ substitution in the potassic sulphide phase, namely 100 Fe/Fe+Ni = 99.27-92.51. The \bar{A} , \bar{D} and \bar{F} bulk compositions produced potassic sulphides with 100 Fe/Fe+Ni = 54.33 - 40.95. These synthetics bracket the natural compositions which have 100 Fe/Fe+Ni = 79.03 - 72.89. It is suggested that there is a continuous solid solution series from a pure iron end-member (${}^vK_6Fe_{27}S_{28}Cl_1$) to at least $K_6Fe_{13}Ni_{14}S_{28}Cl_1$, and probably extending to a pure nickel end-member (${}^vK_6Ni_{27}S_{28}Cl_1$). The potassic sulphide formed at temperatures from 356°C to at least 950°C, i.e. at temperatures both above and below the solidus in this sulphide system.

On the basis of textural relations in the natural sample, and phase relations in the system Fe-Ni-S, Clarke *et al.* (1977) favoured a mechanism of potassium metasomatism to generate K-Fe-Ni sulphide from the pre-existing sulphide blebs in the clinopyroxene-ilmenite nodule. The experimental work reported here demonstrates the feasibility of producing K-Fe-Ni sulphide below the solidus in the system K-Fe-Ni-S-Cl. Given that the original sulphides (pyrrhotite and pentlandite) have a well-developed flame-like exsolution texture, it seems most likely that the potassic sulphide has formed in the solid state at temperatures below 600°C., i.e.

after the diatrema had solidified. The source of the metasomatic fluid was probably the kimberlite, and the chemical constituents of the fluid included H_2O (which occurs in alteration products of the clinopyroxene host), and K, Cl and Cu (which have been added to the original Po-Pn intergrowths).

Clarke, D. B., Pe, G. G., MacKay, R. M., Gill, K. R., O'Hara, M. J. and Gard, J. A. A New Potassium-Iron-Nickel Sulphide from a Nodule in Kimberlite, *Earth Planet. Sci. Lett.* 35, 421-428, 1977.

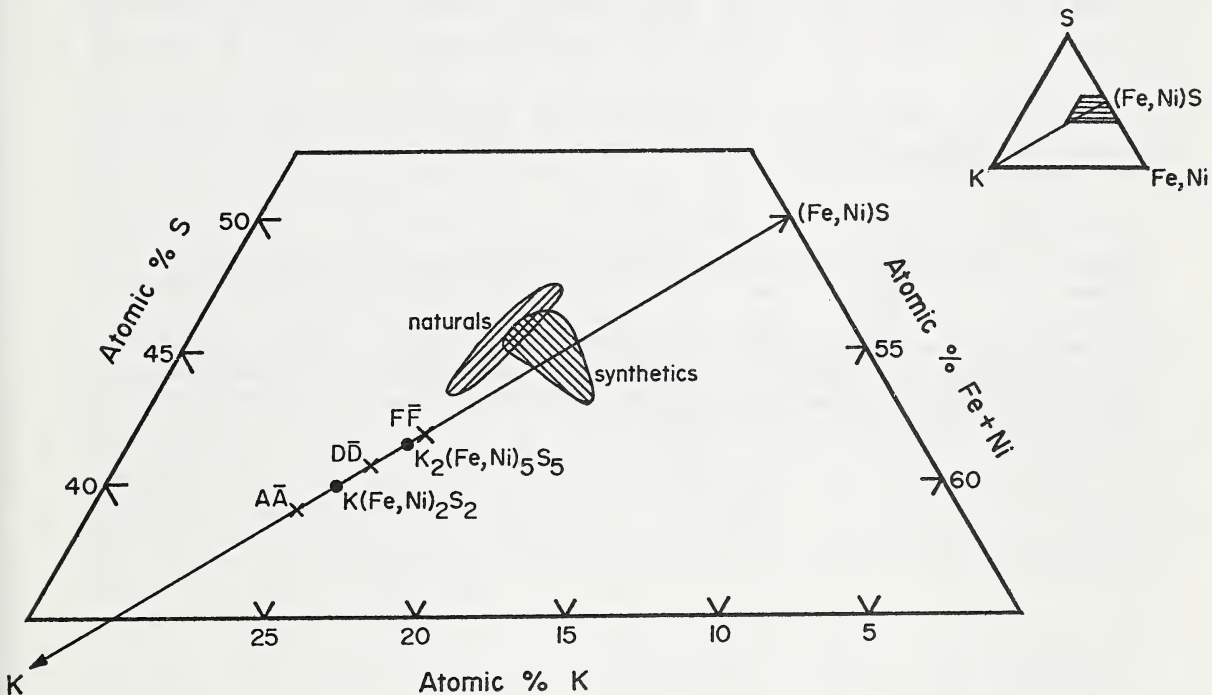


Fig. 1. Projection from chlorine into the plane $\underline{K-FeNi-S}$ showing the location of the bulk compositions ($\underline{A,A}; \underline{D,D}; \underline{F,F}$), the range of composition of the naturally occurring K-Fe-Ni sulphides at Frank Smith Mine, the range of composition of synthetic K-Fe-Ni sulphides and some hypothetical compounds $K(Fe,Ni)_2S_2$ ($\equiv KFeS_2 + Ni$) and $K_2(Fe,Ni)_5S_5$ ($\equiv 2KFeS_2 + 2Ni + FeS$).

		Bulk Compositions					
Temp (°C)	Time (hrs)	<u>A</u>	<u>Ā</u>	<u>D</u>	<u>D̄</u>	<u>F</u>	<u>F̄</u>
950	10	-	4	4	1,2,4	4,5	1,2,4
850	20	4,6	1,4	2,4,5,6	1,2,4	2,4,5,6	1,2,4
750	20	-	-	2,4,6	-	2,4,6	1,2,4
650	20	-	1,4	2,3,4,6	1,2,4	2,4,6	1,2,4
550	20	-	1,4	2,3,4	1,2,4	2,3	1,2,4
450	20	2,3	2,4	2,4	1,2,4	2,4,6	1,2,4

Table 1: Run products confirmed by electron microprobe analysis; other phases may be present in some of the runs but have not yet been identified. Phases are: 1 - heazlewoodite, 2 - K-Fe-Ni sulphide, 3 - metallic Ni-Fe 4 - monosulphide solid solution, normally containing 0.1 - 5.0% K, 5 - pyrrhotite, 6 - wüstite. In addition bulk compositions F and \bar{F} were run at four lower temperatures producing K-Fe-Ni sulphide at 425°, 400°, 356°C, but not 300°C.

PRECAMBRIAN ULTRAMAFIC DYKES WITH KIMBERLITE AFFINITIES IN THE KIMBERLEY AREA

C.R. Clement

E.M.W. Skinner (Geology Department, De Beers Consolidated Mines Limited,
J.B. Hawthorne P.O. Box 616, 8300 Kimberley, South Africa).

L. Kleinjan

INTRODUCTION: A suite of unusual ultramafic dykes has been located in underground mine workings near the Wesselton and De Beers kimberlite pipes. Five of these dykes contain abundant diopside and extremely altered olivine and are feldspar-free. Other petrographically similar dykes contain limited amounts of plagioclase (oligoclase to labradorite). The latter occurrences have not been studied in detail and are not discussed further in this paper although they may be genetically associated with the feldspar-free dykes.

FIELD RELATIONS: The dykes cut the granite-gneiss basement rocks and overlying Ventersdorp System lavas and quartzites. They trend in various directions ranging from northwest to due east. Dips vary between 50° and 80° . Dyke widths vary from a few centimetres to 1.5m. The widest dyke occurs in the wallrocks of Wesselton Mine. The other four occur near the De Beers kimberlite pipe. The Wesselton Mine occurrence was noted by Williams (1932) who classified it as a "serpentinized mica augite peridotite or a hardbank (kimberlite) dyke rock".

PETROGRAPHY: The dykes are tough, moderately hard, dark-grey, generally fine-grained rocks which exhibit varying textures. The wider dykes have prominent chilled margins. The textural variations are particularly well displayed by the Wesselton Mine dyke. Here a thin (1-3mm) vitrophyric selvage occurs at the contacts. This zone consists of altered olivine phenocrysts (1.0mm or smaller) set in a dark brown glassy base containing very small ($< 0.03\text{mm}$) opaque grains and scattered microlites of diopside. Olivine has been pseudomorphously replaced by talc together with subordinate serpentine and chlorite. The altered olivine phenocrysts commonly occur as skeletal hopper crystals and complex parallel growth forms.

Inwards from the vitrophyric margin the groundmass consists of very small acicular laths of diopside (up to 0.1 mm long) and similarly fine-grained phlogopite. Both minerals have been partly chloritized. Other minerals present are serpentine, chlorite, opaque oxides, rare calcite and unidentified clay material. Abundant hopper crystals and parallel growth aggregates of altered olivine, commonly measuring between 0.5 and 1.0mm, occur as phenocrysts in the extremely fine-grained groundmass. Talc remains the dominant alteration product of olivine.

The central panidiomorphic-granular parts of the dyke consist mainly of altered olivine and diopside which together make up approximately 60 vol.% of the rock. Diopside is generally slightly more abundant than olivine. Phlogopite, chlorite and serpentinous material are also relatively abundant. Accessory minerals include scattered opaque oxides, apatite, clay (sepiolite or hydromica) and calcite (rare).

As in the marginal areas of the dyke olivine is extensively altered and pseudomorphous replacement by talc and serpentine is widespread. Skeletal olivine is much less prominent but hopper crystals and parallel growth forms are present.

Most olivine grains are smaller than 1.0mm. Diopside occurs as well formed laths commonly between 0.5 and 1.5mm long. Steatization and chloritization of diopside is extensive.

Phlogopite occurs as laths up to 0.75 mm long and as an anhedral interstitial mineral between altered olivine and diopside crystals. This phlogopite displays prominent pleochroism ($\beta=\gamma$ brown, α pale yellow-brown). Apatite is a prominent accessory mineral. It occurs as highly acicular laths reaching 0.4mm in length. Opaque minerals occur in various forms including equant subhedral and euhedral crystals and acicular laths. Skeletal opaque grains are common.

The De Beers Mine dykes differ from the Wesselton occurrence in that phlogopite is rare or absent. In addition sulphides (mainly pyrite) are common accessory minerals and minor quartz is sometimes present within altered olivines.

HEAVY MINERALS: Microprobe analyses of heavy minerals, extracted from four dyke samples, indicate the presence of garnet and opaque oxide suites which fall within the compositional ranges of those commonly found in kimberlites, or within upper mantle peridotites and eclogites which occur as xenoliths in kimberlite. The grains are invariably small (most of those recovered lie between 100 and 28 mesh (Tyler) screen sizes) and are not abundant.

Opaque minerals include microilmenite, ilmenite, and a variety of spinels ranging from ulvospinel to high- Cr_2O_3 (64 wt.%) chromites. Four grains of an unusual Ti-oxide were found in a sample from one of the De Beers Mine dykes. Although the analyses do not include BaO and V_2O_5 their compositions are in all other respects virtually identical to a new mineral described by Haggerty (1975, p.305) from De Beers Mine kimberlite. Six minute fragmental diamonds were recovered from a 22kg. sample of the same dyke. The total weight of these diamonds is 2521×10^{-8} carats. Further sampling is being carried out to try and confirm the presence of this mineral in the dyke.

AGE OF THE DYKES: Field relations indicate that these dykes pre-date the Cretaceous (90m.y.) kimberlite pipes in the Kimberley area. Truncation of the dykes at the contacts of the pipes is evident at both De Beers and Wesselton mines. Furthermore the dykes do not cut Karroo System (Dwyka Series) shales which, together with dolerite sills, form the upper 130m of the geological succession. Field relations therefore indicate a post-Ventersdorp (2300m.y.) pre-Karoo age. In order to fix the age of the dykes more precisely radiometric dating of the Wesselton Mine dyke was carried out for the authors by Dr. H.L. Allsopp who reports as follows:

"Rb-Sr age determinations were made on one whole rock and four mica concentrates. Data for the E and A standard Sr, analysed by the same method, yielded a $^{87}\text{Sr}/^{86}\text{Sr}$ ratio of $.70795 \pm .00002$. Measurements on the NBS standard SRM 607 show that the Rb and Sr concentrations are accurate to within 1%. The data obtained are plotted on an isochron diagram (fig. 1) and have been regressed by the method of York (1966). Using a value of $1.42 \times 10^{-11}\text{yr}^{-1}$ for the decay constant of ^{87}Rb the computed results are:

Age = 1800 ± 40 m.y.
Initial $^{87}\text{Sr}/^{86}\text{Sr}$ = $.7068 \pm .0008$

where the uncertainties quoted are 1 sigma values. Noting that the Rb/Sr ratios of the four mica concentrates differed by a relatively small amount the data in effect define a whole rock-mineral pair and the result may reflect a minimum age."

RELATIONSHIP OF THE DYKES TO KIMBERLITE: Although these dykes are mineralogically similar to some kimberlites (Skinner and Clement, this volume) they do not conform with current definitions of kimberlite in certain important respects.

There is a complete absence in the dykes of anhedral, commonly rounded, megacrysts of olivine which, together with smaller euhedral phenocrysts, form the typical olivine assemblage in kimberlite. Similarly the previously described silicate and oxide heavy mineral suites, while clearly akin to those present in kimberlite, are unusual in that again none of the minerals occur as megacrysts. Furthermore textural features and the morphological characteristics of some minerals differ markedly from those reported from kimberlite. Notable in these respects are the panidiomorphic-granular textures of the major (central) parts of the dykes and the skeletal hopper olivines which have not been found in kimberlite. The abundance of parallel growth forms of olivine is also atypical of kimberlite olivine. An additional mineralogical difference is that diopside is commonly more abundant than olivine. No ultramafic nodules of any sort have been found in any of the dykes.

CONCLUSIONS: It is concluded that these ultramafic dykes were emplaced as hot liquids (relative to kimberlite) approximately 1800 m.y. ago. Textural features indicate that most of the minerals crystallized in situ. The abundance of hopper olivine crystals indicates rapid cooling and/or rapid olivine growth (Donaldson, 1976). Extremely rapid cooling at the margins of the dykes is indicated by prominent chill zones.

The garnet and opaque oxide minerals in the dykes indicate affinities with kimberlite as does the occurrence of the dykes in an area of intensive, albeit much later, kimberlite intrusion. In other respects the dykes differ considerably from kimberlites. Although a direct genetic association with the kimberlites cannot on available information be disproved, it seems unlikely in view of the long interval between the two periods of ultrabasic magmatism in the area. On the basis of heavy mineral chemistries it does, however, appear that the magma which gave rise to these dykes originated in the upper mantle within the depth zone postulated for the genesis of kimberlite (140+km.).

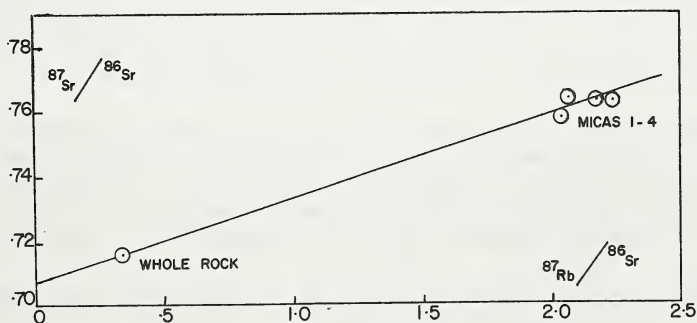


Fig. I: ISOCHRON DIAGRAM - WESSELTON MINE DYKE

KIMBERLITE REDEFINED

C.R.Clement (De Beers Consolidated Mines Limited, Box 616,
E.M.W. Skinner 8300 Kimberley, South Africa)

B.H. Scott (Anglo American Research Laboratories, Box 106, 2025 Crown Mines,
South Africa)

The term kimberlite was first proposed by Lewis (1887) when describing the "matrix of diamond" at its type locality - Kimberley, South Africa.

A number of authors have subsequently attempted to define kimberlite but we consider that none of these definitions has proved completely satisfactory, mainly because it is difficult to encompass in a single simple definition, the variety of rock types which are generally accepted as being kimberlites. Furthermore, although the mineralogical variability of kimberlite is widely recognized, most definitions fail to take into account the range of essential minerals that may be present in kimberlite. Other problems in defining kimberlite arise out of the presence of cryptogenic minerals (often but not always interpreted as xenocrysts), the frequent presence of abundant contaminatory xenolithic material, the presence of variable textures reflecting different near-surface emplacement processes and commonly extensive alteration. Some previous definitions have incorporated genetic implications (with regard to the origin of kimberlite or the minerals therein) which should not be included in a factual statement.

We therefore propose an alternative and, hopefully, more workable definition. In terms of general format this definition broadly follows that proposed by Dawson (1971) but differs in a number of important respects. We would welcome comments which may assist in improving this proposed definition before it is submitted for publication in a form which will incorporate details of its derivation:-

KIMBERLITE is a volatile-rich, potassic, ultrabasic, igneous rock which has a distinctively inequigranular texture resulting from the presence of macrocrysts set in an essentially microporphyritic matrix.

The matrix contains as prominent primary phenocrystal and/or groundmass constituents, olivine and several of the following minerals: phlogopite, calcite, serpentine, diopside, monticellite, apatite, spinels, perovskite and ilmenite. Other primary minerals may be present in accessory amounts.

The macrocrysts belong almost exclusively to a suite of anhedral, cryptogenic, ferromagnesian minerals which include olivine, phlogopite, picroilmenite, magnesian garnet, chromian diopside and enstatite. Olivine is extremely abundant relative to the other minerals which need not all be present. In addition to macrocrysts smaller grains belonging to the same suite also occur.

Kimberlite may contain diamond but only as a very rare constituent.

Kimberlite commonly contains rounded inclusions of a variety of ultramafic

rocks characterized by mantle-derived peridotites, eclogites and pyroxenites. Variable quantities of crustal xenoliths and xenocrysts may also be present.

Kimberlite is often altered mainly as a result of serpentinization and/or carbonatization.

EXPLANATORY NOTES:

Volatile-rich : High CO_2 and H_2O^+ contents relative to most other igneous rocks including other ultrabasic types.

Potassic : Refers to the high K/Na ratios of kimberlites and high K relative to most other ultrabasic rocks.

Cryptogenic : Implies an unknown or hidden origin.

Macrocryst : Crystals visible to the unaided eye and significantly larger than the surrounding matrix. The term megacryst could be reserved for even larger crystals which occur in kimberlite and are commonly termed discrete nodules.

Picroilmenite : Ilmenites with high MgO contents.

REFERENCES:

Lewis H.C. (1887), Geol. Mag., 3 iv: 22-24

Dawson J.B. (1971), Earth Sci. Rev., 7: 187-214

Analyse calc'd on vol-bas. bases are
hornite normative. - def - J. Miller -

PARTIAL MELTS IN UPPER MANTLE NODULES FROM LABRADOR KIMBERLITES

K. D. Collerson and J. Malpas (Memorial University of Newfoundland, St. John's, Newfoundland, Canada, A1C 5S7)

Recent mapping at Saglek, northern Labrador, has revealed the presence of several kimberlite dykes which cut early Achaean gneisses and contain rounded ultramafic inclusions up to 2 cm in diameter. The kimberlite is a dense melanocratic megacrystic rock. It consists predominantly of randomly distributed rounded to subangular megacrysts or glomeromegacrystic aggregates of olivine up to 4 mm diameter in a fine grained matrix with a pronounced fluidal texture resulting from aligned phlogopite crystals. The megacrysts range in composition from Fo_{87.5} to Fo₉₀ and are extremely homogeneous with less than 1 wt. % variation in MgO and a slight variation in NiO (0.16 to 0.11 wt.%) from core to rim. In contrast, the groundmass olivines are slightly more iron rich and display a range in composition from Fo_{86.5} to Fo_{87.7}. Both groundmass and megacrystic olivines have low concentrations of CaO, viz. 0.04 to 0.15 wt. % and 0.05 to 0.13 wt. % respectively. According to Simkin and Smith (1970) and Mitchell (1973) low calcium content in olivine implies a deep seated crystallisation environment. This is not surprising, despite the fact that the magma was moderately lime rich (Table 1) as the chemical potential of CaO in the liquid remained relatively high until late in the crystallisation history of the dyke when diopside, perovskite and calcite became solidus phases. The olivines display a similar range in composition to olivines from other kimberlites which display magmatic crystallisation textures. The slightly more forsteritic nature of the megacrysts relative to the matrix olivines in the Saglek kimberlites suggests that they are earlier crystallisation products from the kimberlite magma. The matrix also contains abundant Ti-phlogopite with TiO₂ contents ranging from 3.73 to 4.78 wt. % and Mg values between 81.95 and 85.9. The phlogopites are generally more titaniferous than micas reported previously from kimberlites, their higher values of TiO₂ being more typical of titaniferous phlogopites from glimmerite nodules. Other matrix minerals include Cr-poor diopside, spinel, magnesium rich ilmenite and melilite. Perovskite and nickeliferous pyrrhotite are also present.

The nodules can be classified mainly into two groups, micaceous dunites and glimmerites. In the dunite nodules, olivine is the major phase but phlogopite, magnetite, spinel and interstitial carbonate and glass are also present. Olivine, with rounded, resorbed or corroded outlines, forms a loose mosaic of relatively equidimensional grains and crystal outlines are enhanced by local magnetite coatings. The nature of the grain boundaries is probably a result of partial melting of original interstitial phases and selectively along olivine crystal phases. Although no major zoning patterns are recognised in the olivines, there is a tendency for iron enrichment and nickel depletion towards the rims of some. Core compositions vary from Fo_{85.5} to Fo_{88.4} in analysed samples, a 3% range comparable to that in the kimberlite megacrysts, although the overall composition is more comparable with the matrix olivines. Iron, calcium and aluminum contents are considerably higher in amounts than those found in most peridotite olivines. This suggests that the olivines have a cumulate rather than residual origin, and may be compared with olivines of the rare dunite nodules of Thaba Patsoa (Boyd and Nixon, 1975). The presence of the interstitial glass is direct evidence of the liquid phase produced by partial remelting of the cumulate dunite during mobilisation of

the kimberlite. The glass is of dunitic composition, depleted in the alkalis and calcium. The deficiency of these elements is explicable by assuming fractional crystallisation of phlogopite, clinopyroxene and potassic richterites. The association of phlogopite with areas of partial melting is quite clear and although clinopyroxene and potassic richterite have not yet been identified in association with the glass phase, they both occur as xenocrysts and in nodules within the kimberlites. Devitrification of the glass phase involves the formation of richteritic amphiboles poor in potassium as would be expected from glass composition.

It is thought that the origin of the glimmerite nodule suite lies in the fractionation of phlogopite from a liquid produced by partial melting at depth in the mantle and subsequent incorporation as xenoliths in the ascending kimberlite. The chemistry of the glimmerite phlogopites suggests that the original partial melt liquid was rich in Mg, Fe, Ti, K, OH and CO₂ but low in SiO₂ and Cr₂O₃.

Kimberlite genesis presumably took place at depths in excess of 150 km. However, the presence of glimmerite nodules and matrix melilite suggests emplacement at depths from 10-100 cm.

TABLE 1

wt %	1	2	3
SiO ₂	35.6	35.20	42.98
TiO ₂	3.06	1.28	0.08
Al ₂ O ₃	3.46	1.45	0.30
Fe ₂ O ₃	4.60	0.95	as FeO 6.26
FeO	8.71	10.83	
MnO	0.20	0.20	0.18
MgO	27.90	36.50	38.99
CaO	6.78	2.58	0.02
Na ₂ O	0.82	0.40	nd
K ₂ O	2.00	0.80	nd
P ₂ O ₅	0.40	0.14	nm
H ₂ O ⁵	3.72	insufficient sample	nm
CO ₂	2.42	1.47	nm
TOTAL	99.67	91.80	

ppm			
Zr	307	1)	Analysis of kimberlite dike, Saglek
Sr	726	2)	Partial analysis of micaceous dunitic nodule
Rb	72	3)	Partial analysis of glass in nodule.
Y	20		
Ni	1149		
Cu	73	nd	not detected
Ga	10	nm	not measured.

ULTRAMAFIC XENOLITHS FROM THE PREMIER KIMBERLITE PIPE

R.V. Danchin : Anglo American Research Laboratories
P.O. Box 106, Crown Mines, 2025, RSA

A varied suite of ultramafic xenoliths has recently been recovered from the Pre-Cambrian, Premier kimberlite pipe, South Africa. The suite includes garnet lherzolites, garnet harzburgites, garnet websterites, dunites, pyroxenites and eclogites, as well as chromite peridotites and harzburgites. Discrete nodules, predominantly of garnet, diopside, enstatite and ilmenite were also recovered. Major phase mineral compositions for 108 xenoliths, and bulk chemical compositions for 76 garnet lherzolites and harzburgites are discussed.

The garnet lherzolites can be subdivided into two groups that differ markedly in both texture and mineral chemistry (see Table 1). The first category consists of coarse-equant and coarse-tabular rocks which are believed to have originated at depths of 110 - 170 km. The second group is represented by deformed, extensively recrystallised, garnet-rich lherzolites whose textures vary from porphyroclastic to mosaic-porphyroclastic, that are believed to have been derived from depths of about 200 km. The garnets in the deformed nodules are reddish brown and characterised by unusually high TiO_2 contents (Ave. 1,5 wt%), whereas those in the coarse lherzolites are mauve and titanium-poor (Ave. 0,2 wt%). In the deformed lherzolites the co-existing diopsides, enstatites and olivines are, likewise, enriched in titanium relative to those in the coarse varieties as can be seen from Table 1. Mineralogically and texturally, the Premier garnet lherzolites are, therefore, extremely similar to those from many Late Cretaceous kimberlites in southern Africa, and more specifically to certain suites from northern Lesotho (Nixon and Boyd 1973; Boyd and Nixon 1975). Furthermore, a palaeogeotherm deduced from the Premier garnet lherzolites is very similar to the inflected Late Cretaceous geotherms determined for various pipes in southern Africa (see Boyd and Nixon 1977). A further similarity between the Premier xenoliths and those from northern Lesotho studied by Boyd and Nixon (notably Thaba Putsoa), is the restriction of primary phlogopite and chromite to the coarse (granular) rocks.

Garnet harzburgite inclusions from the Premier suite have been subdivided into three distinct groups on the basis of differences in mineral chemistry and texture (Danchin and Boyd 1977). Mineral data for these rocks are summarised in Table 1. Group I harzburgites have deformed textures and mineral compositions equivalent to those of the deformed garnet lherzolites. Group III harzburgites have coarse-equant textures comparable to the coarse garnet lherzolites. Group II harzburgites are intermediate between these two extremes, particularly with respect to $Mg/(Mg + Fe)$ of the component minerals, the $Ca/(Ca + Mg)$ of the enstatites, and the TiO_2 contents of the garnets and enstatites. Compared to the lherzolite and Group I garnets, those from Group II and III harzburgites are markedly enriched in chromium relative to calcium - several to such an extent that their compositions are equivalent to garnets included in diamond. Temperature-depth estimates for the garnet harzburgites suggest that the deformed Group I varieties equilibrated at depths of approximately 200 km in the mantle, whereas the Group II and Group III harzburgites appear to have equilibrated between 140 and 180 km in the range 1 000° - 1 200°C. The compositional similarities between the garnets in these harzburgites and the most common garnet found as inclusions in diamond suggest that the processes of formation of harzburgite and some diamonds in the mantle are related. The rocks of deepest origin now found as xenoliths in kimberlites are therefore not those in which diamond has most commonly formed.

Average bulk compositions for the Premier garnet lherzolites and harzburgites are given in Table 2 where they can be compared with analyses of equivalent rocks from northern Lesotho (Nixon and Boyd 1973). At Premier, relatively undepleted rocks corresponding in chemical composition to PHN 1611 from Thaba Putsoa, are rare, and the deformed garnet lherzolites show variable degrees of chemical depletion. On average the coarse-garnet lherzolites are more depleted than the deformed varieties, particularly with respect to their $\text{FeO}_t/\text{FeO}_t + \text{MgO}$ ratios (Table 2). Whereas in northern Lesotho, the two groups could be distinguished using their $\text{FeO}_t/\text{FeO}_t + \text{MgO}$ ratios, this is not the case for the Premier lherzolites where values for this ratio overlap markedly. The nature and extent of this overlap is illustrated in Fig. 1 which is a plot of bulk $\text{FeO}_t/\text{FeO}_t + \text{MgO}$ versus $\text{Mg}/\text{Mg} + \text{Fe}$ for each of the major lherzolite and harzburgite minerals. $\text{FeO}_t/\text{FeO}_t + \text{MgO}$ ranges from 13,9 to 20,5 in the deformed lherzolites, and from 12,0 to 17,2 in the coarse lherzolites. Also, it is clear that the harzburgites and lherzolites have equilibrated such that the most fertile, iron-rich garnet lherzolites contain the most iron-rich minerals, and vice versa. It is stressed that no modal combination of minerals from even the most iron-rich, coarse-garnet lherzolite could produce a composition equivalent to PHN 1611.

Bulk Al_2O_3 and CaO in the deformed and coarse-garnet lherzolites also display an overlap as shown in Figs. 2b and 2c, and in this context, it is noteworthy that modal analyses of 16 coarse-garnet lherzolites indicated average garnet and diopside contents of 8 and 6 volume percent respectively, compared to values of 4 and 5 percent for Thaba Putsoa (Nixon and Boyd 1973). It is therefore possible that the coarse Premier garnet lherzolites are somewhat less depleted, notably with respect to CaO , Al_2O_3 and $\text{FeO}_t/\text{FeO}_t + \text{MgO}$, than those from Cretaceous kimberlites in Lesotho, although additional data from the latter localities are required. The differences between the two localities are subtle, however, and the available data suggests that the depletion of the mantle beneath southern Africa was essentially complete 1 200 million years ago.

The distribution of titanium and potassium in these rocks is problematic. The unique levels of Ti enrichment in minerals comprising the deformed lherzolites and manifested in the bulk data, are shown in Fig. 2d, where a well-developed positive correlation with $\text{FeO}_t/\text{FeO}_t + \text{MgO}$ is illustrated. A similar, but less well-developed pattern of Ti enrichment in xenoliths from the substantially younger Frank Smith kimberlite has been attributed to metasomatic processes by Boyd (1975), however, the complex situation with regard to Ti and K in these rocks would require at least two, quite distinct metasomatic processes to have taken place.

REFERENCES

- Boyd, F.R. 1975. De Beers Kimberlite Symposium. Cambridge, U.K. Extended Abstracts.
- Boyd, F.R. & Nixon, P.H. 1975. Phys. Chem. Earth. Vol. 9. Pergamon. Eds. Ahrens et al. pp 431-454.
- Boyd, F.R. & Nixon, P.H. 1977. Carnegie Inst. Year Book 75. pp 544-545.
- Danchin, R.V.D. & Boyd, F.R. 1977. Carnegie Inst. Year Book 75. pp 531-537.
- Nixon, P.H. & Boyd, F.R. 1973. Lesotho kimberlites. Maseru, Lesotho National Devel. Corp. Ed. P.H. Nixon. pp 48-56.

Table 1 : SUMMARY OF MEAN COMPOSITIONS OF MINERALS FROM THE GARNET LHERZOLITES AND HARZBURGITES INCLUDED IN THE PREMIER KIMBERLITE

	Mg/(Mg+Fe) Mol. Fraction	TiO ₂ wt %	Cr ₂ O ₃ wt %	Na ₂ O wt %	CaO wt %	Al ₂ O ₃ wt %	K ppm
GARNETS							
A. Lherzolites							
Deformed (35)	0,845	1,15	3,89	0,09	4,86	19,47	-
Coarse (19)	0,846	0,23	4,16	0,04	5,16	20,82	-
B. Harzburgites							
Group I (20)	0,845	1,32	6,72	0,10	5,46	17,17	-
Group II (16)	0,872	0,20	6,73	< 0,03	4,32	18,57	-
Group III (2)	0,888	0,02	7,24	< 0,03	3,81	18,59	-
ENSTATITES							
A. Lherzolites							
Deformed	0,918	0,23	0,31	0,30	1,25	1,01	-
Coarse	0,932	0,05	0,34	0,14	0,43	0,97	-
B. Harzburgites							
Group I	0,924	0,17	0,47	0,31	1,22	0,96	-
Group II	0,936	< 0,03	0,40	0,11	0,80	0,85	-
Group III	0,950	< 0,03	0,54	0,12	0,44	0,90	-
OLIVINES							
A. Lherzolites							
Deformed	0,907	0,03	0,05	-	0,08	0,07	-
Coarse	0,921	< 0,03	0,02	-	0,03	0,03	-
B. Harzburgites							
Group I	0,913	< 0,03	0,07	-	0,05	0,04	-
Group II	0,926	< 0,03	0,06	-	< 0,03	0,04	-
Group III	0,943	< 0,03	0,05	-	< 0,03	0,03	-
DIOPSIDES							
A. Lherzolites							
Deformed	0,907	0,41	1,03	1,71	15,07	2,23	307
Coarse	0,931	0,15	1,85	2,31	19,27	2,94	99

* * * * *

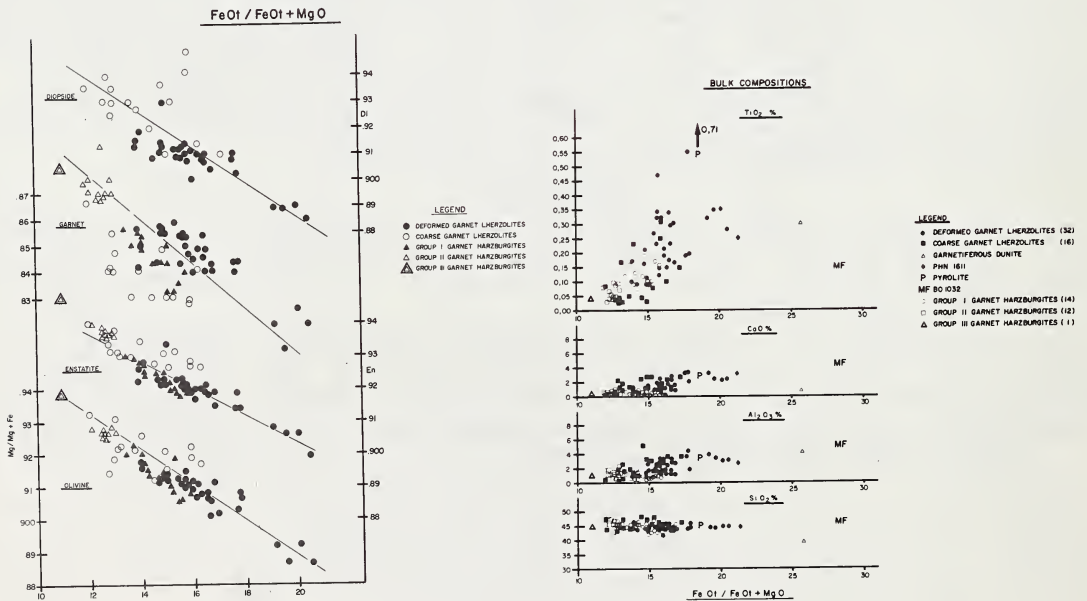


FIG. 1

FIG. 2

TABLE 2. BULK COMPOSITIONS OF GARNET LHERZOLITES AND HARZBURGITES FROM PERMIER, COMPARED TO GARNET LHERZOLITES FROM NORTHERN LESOTHO

	Premier "fertile" deformed garnet lherzolites (4)	PHN 1611 Thiba Putsoa	Premier depleted deformed garnet lherzolites (28)	N. Lesotho sheared garnet lherzolites* (5)	Premier coarse garnet lherzolites (16)	N. Lesotho granular garnet lherzolites (4)	Premier Group I harzburgites (16)	Premier Group II harzburgites (11)	Premier Group III harzburgites (11)
SiO ₂	44.31	44.60	44.95	43.72	45.83	45.80	44.21	45.55	44.69
TiO ₂	0.33	0.25	0.22	0.14	0.11	0.03	0.14	0.07	0.05
Al ₂ O ₃	3.40	2.80	1.98	1.65	2.12	0.50	0.87	1.14	1.22
Cr ₂ O ₃	0.34	0.28	0.30	0.21	0.36	0.21	0.25	0.25	0.18
FeO†	9.46	10.25	7.87	8.24	6.95	6.22	7.76	6.42	5.77
MnO	5.15	0.13	0.12	0.12	0.14	0.10	0.10	0.09	0.09
MgO	33.14	37.22	41.98	43.50	41.72	46.06	45.14	44.76	46.26
CaO	2.53	3.32	1.40	1.57	1.52	0.82	0.42	0.55	0.55
Na ₂ O	0.18	0.34	0.15	0.19	0.20	0.06	n.d.	0.07	n.d.
K ₂ O	0.18	0.14	0.08	0.03	0.35	0.04	0.02	0.05	0.10
NiO	0.22	n.d.	0.25	0.23	0.26	0.24	0.29	0.27	0.26
FeO/FeO _T + MgO	19.6	21.2	15.8	16.0	14.3	12.1	14.7	12.5	11.0

ALL ANALYSES WATER-FREE

* Excluding PHN 1611.

† Total iron expressed as FeO.

THE AGES AND URANIUM CONTENTS OF ZIRCONS FROM KIMBERLITES AND ASSOCIATED ROCKS

Gordon L. Davis (Geophysical Laboratory, 2801 Upton St., N.W., Washington, D. C. 20008)

Preliminary results (Davis, Krogh and Erlank, 1976) showed that zircons from kimberlites of the Kimberley area, South Africa, all had nearly the same age of 90 m.y. Additional age determinations have been made on zircons from pipes from South Africa, Lesotho, Botswana, Namibia, Zaire, Angola and Swaziland. Samples from Brazil and from Malaita in the Solomon Islands have also been analyzed. The ages and uranium contents of the zircons analyzed to date are given in the accompanying table.

Zircons are radioactive clocks, recording the time that has elapsed since the onset of accumulation of the Pb isotopes that are the products of the radioactive decay of U. Zircons are rare in kimberlites but are concentrated at the same time as diamonds because of their high density and X-ray fluorescence. They form rounded to sub-rounded crystals as large as 1 cm in diameter. They are considered to belong to the deep-seated suite of discrete nodules (Kresten, Fels and Berggren, 1975) and are believed to have originated in magmas which may have come from the low velocity zone (Boyd and Nixon, 1973). The occurrence of zircon as an inclusion in a diamond (Meyer and Svisero, 1973) provides additional evidence for a deep-seated origin. No matter how long ago the zircons crystallized, at the temperatures of 1100°C or more estimated for the pyroxene discrete nodules Pb would be lost by diffusion and could not accumulate to start the clock. The ages of the zircons mark the times of sudden lowering of temperature at eruption.

The zircons were decomposed by the low-contamination method of Krogh (1973). A mixed tracer of ^{205}Pb and ^{235}U was used (Krogh and Davis, 1975). Isotope ratios were measured at the Department of Terrestrial Magnetism on the automated 9-inch mass-spectrometer. The contents of Pb and U isotopes were calculated from the ratios after correction for a small laboratory blank (0.1 ng Pb, 0.05 ng U) and correction for the presence of common lead (from submicroscopic inclusions and fractures). The latter correction causes a large uncertainty in the ^{207}Pb concentration with the result that the ^{207}Pb - ^{235}U and the derived ^{207}Pb - ^{206}Pb ages have little significance for such young, low-U zircons. The ^{206}Pb - ^{238}U ages given in the table have an analytical error of $\pm 1.5\%$ that is independent of sample weight because of the use of a mixed tracer. The concentrations of U are dependent on the weights and may be in error by as much as $\pm 7\%$.

DISCUSSION OF RESULTS: Knowledge of the ages of emplacement of the kimberlites provides a better understanding of the sequence and types of tectonic activity in southern Africa. About 90 m.y. ago zircon-bearing pipes erupted through the Precambrian Transvaal Craton and its covering strata, having come from or penetrated a part of the mantle in which diamonds were stable. The zircon samples analyzed come from near the periphery of the craton, particularly in the southern part, with one sample from Botswana to the north. They are characterized by very low U concentrations. Outside of the craton in the Orange River Belt, the pipes are consistently younger, as young as 50 m.y. in Namaqualand. All of these young occurrences to the south of the craton are barren of diamonds--evidence that they may have originated in the mantle at depths above the diamond stability field. The Namaqualand zircons contain 10 to 20 times as much U as those from the Transvaal. Carbonatites and alkalic intrusives are found in this region.

Zircons were separated from two granulite xenoliths from Lesotho. These rocks appear to be fragments of Precambrian crustal wall rock that were picked up by the ascending kimberlite. The ages shown are extrapolated from the discordant U-Pb ages. In spite of having been entrained in the kimberlite, both of the zircon samples have retained a memory of Precambrian crystallization and therefore have not been subjected to very high temperature for long. A zircon from a peridotite nodule from Bultfontein was analyzed in hopes that its age might reflect a time of crystallization prior to eruption. Instead the age turned out to be close to but somewhat younger than the average for discrete zircons from the Kimberley area. Ambient temperatures in the mantle are higher than in the crustal basement: apparently the zircon from the mantle-derived peridotite was unable to retain any radiogenic Pb prior to or in the early stages of eruption. The 650 m.y. zircons from Dokolwayo, Swaziland, contain liquid inclusions, are high in U and generally appear to have originated in an upper level crustal pegmatite rather than in the mantle.

The zircons from Ramatseliso, Lesotho, have low U-contents in the range of kimberlitic zircons, but their older ages do not fit the South African age pattern as it has developed so far. The sample from Angola posed some analytical problems, possibly due to its low U-content. The suggested age of 134 m.y. is not in conflict with an Upper Jurassic stratigraphic age. At Muadui, Tanzania, where Cretaceous sediments occupy the crater of the diatrema, the age of the zircon is 189 m.y.

The ages of the zircons from Brazil range from 122 m.y. to 79 m.y., suggesting that Africa and South America, once parts of Gondwanaland, have similarities in their tectonic histories after separation. The ages of many Brazilian alkalic rocks (Herz, 1977) lend further support to this suggestion. Zircons from kimberlite pipes are often coated by soft chalky-white ZrO_2 , possibly the result of a desilication reaction with carbonates. A 1 cm zircon from a Brazilian kimberlite had such a coating, nearly 1 mm thick, in which were embedded many small brown crystals of baddeleyite, the monoclinic form of ZrO_2 that is stable below 1170°C. Upon analysis, the baddeleyite was found to have the same age as the zircon, but it contained 10 times the U, too much to have come from any reasonable volume of zircon. The chemical environment in the kimberlite at the time of desilication must have been very high in U, as suggested by Kresten (1974).

One zircon from the Solomon Islands with an age of 34 m.y. indicates that kimberlite-like eruptions took place as recently as Oligocene in this region of Melanesia.

REFERENCES:

- Boyd, F.R., and P.H. Nixon, Lesotho Kimberlites, 254, 1973
Davis, G.L., T.E. Krogh and A.J. Erlank, Carnegie Inst. Yr. Bk. 75, 821, 1976
Kresten, P., Lithos 7, 171, 1974
Kresten, P., P. Fels and G. Berggren, Mineral Deposita 10, 47, 1975
Krogh, T.E., and G.L. Davis, Carnegie Inst. Yr. Bk. 74, 417, 1975
Meyer, H.O.A., and D.P. Svisero, Phys. Chem. Earth 9, 785, 1975

Ages and uranium contents of zircons from kimberlites and associated rocks

	ppm U	m.y.	
<u>TRANSVAAL CRATON</u>			
Kimberley Pool, So. Africa	39.9	95.4	altered peridotite
Finsch, So. Africa	26.1	94.1	
Leicester, So. Africa	18.5	93.6	
Orapa, Botswana	14.4	93.1	
Roberts Victor, So. Africa	27.7	92.2	
De Beers, So. Africa	28.2	92.0	
Bultfontein, So. Africa	13.1	91.2	
Monastery, So. Africa	6.1	90.4	with ilmenite
Wesselton, So. Africa	18.6	90.3	
Mothae, Lesotho	8.6	87.1	
Kampfersdam, So. Africa	29.8	86.9	
Bultfontein, So. Africa	5.6	83.8	peridotite nodule
(duplicate)	6.0	81.7	
<u>AROUND THE CRATON</u>			
McKenzie's Post, So. Africa (1)	12.4	80.4	
McKenzie's Post, So. Africa (2)	129.4	79.7	
Rietfontein, Namibia	25.2	71.9	
(duplicate)	23.4	71.7	
Bokputs Camp, Namaqualand	197.1	67.9	
Lushof, Victoria West	64.9	67.7	
Platbakkies, Namaqualand	440.5	66.7	
Melkfontein, East Griqualand	109.4	63.4	carbonate tuff
Brakfontein, Namaqualand	338.1	54.1	
<u>FROM THE LITHOSPHERE</u>			
Kao, Lesotho	150.9	1500	altered granulite
Thaba Putsoa, Lesotho	61.9	1050	scapolite granulite
Dokolwayo, Swaziland	152.4	650	pegmatitic?
Ramatseliso, Lesotho (1)	17.9	150.8	
Ramatseliso, Lesotho (2)	12.0	148.6	
<u>OTHER KIMBERLITES</u>			
Val do Queve, Angola	3.1	(134?)	
Bakwanga, Zaire	38.0	71.3	
Nzega, Tanzania	6.3	53.2	
(duplicate)	6.7	52.2	
Mwadui, Tanzania	15.1	189.3	
<u>BRAZIL</u>			
Batovi 9 (1)	24.3	122.1	
Batovi 9 (2)	13.5	120.0	
Poco Verde, Minas Gerais	29.3	86.0	
Poco Verde, Minas Gerais	317.5	87.0	baddeleyite
Joana 5, Minas Gerais	17.1	80.1	
Joana 6	235.4	79.2	
Esperanca 1	47.5	79.6	
<u>MELANESIA</u>			
Malaita, Solomon Islands	4.8	33.9	

LATE-STAGE DIOPSIDES IN KIMBERLITE GROUNDMASS

J. B. Dawson, Dept. of Geology, University of St. Andrews, Scotland

J. V. Smith and R. L. Hervig, Dept. of the Geophysical Sciences, University of Chicago, Chicago, Illinois 60637, U.S.A.

Late-stage clinopyroxene, formerly regarded as a rare phase in kimberlite groundmass, has been identified in the groundmass of five micaceous kimberlites [Roberts Victor, New Elands, Zout en Zuur, Helam (Main and "Male" dykes)], in kimberlite stringers veining two MARID-suite nodules from the Wesselton and Bultfontein Mines, (Dawson and Smith, 1977), and in late-stage crystallizing patches (the overall mineralogy of which resembles that of kimberlite groundmass) in a pyroxene-ilmenite xenolith from the kimberlite of the Weltvreden Mine. These diopsidic pyroxenes are up to 1.5mm long (generally <0.5mm), are euhedral to subhedral, and vary morphologically from equant to acicular; they are usually optically zoned and larger crystals may be twinned. Together with titanian phlogopite (a ubiquitous, abundant, associated phase), the diopsides are randomly oriented in a matrix of various combinations of calcite, "serpentine" and calcite, the matrix varying from locality to locality. [The "serpentine" have been analysed chemically and smectite (var. saponite) has been identified in one specimen, but the others (often much richer in iron than published analyses of antigorite or chrysotile) await a detailed crystallographic study]. Microcrystalline opaque grains (chromite) occur as inclusions in all phases, except in the clear rims of diopside crystals, the cores of which often contain inclusions of phlogopite and opaques.

Chemically, the diopsides plot close to the diopside-hedenbergite join in the pyroxene quadrilateral; most are quite pure diopside but one is iron-rich (Fig. 1). They show very limited solid solution towards enstatite and most have insufficient Al to make up Si deficiency in tetrahedral sites, suggesting some of the iron is Fe^{3+} , implying the presence of acmite component. In analyzed zoned crystals the rims tend to be higher in TiO_2 , Al_2O_3 and CaO (higher Ca/(Ca+Mg) ratios), but lower in Na_2O and Cr_2O_3 than the cores. Core and rim analyses (in wt.%) for a zoned Roberts Victor kimberlite diopside are (rim analyses in brackets): SiO_2 54.6(54.2), TiO_2 0.44(0.70), Al_2O_3 0.19(0.36), Cr_2O_3 0.68(0.12), total iron as FeO 3.45(3.45), MgO 17.4(17.0), CaO 22.6(23.9), Na_2O 0.61(0.32), Ca/(Ca+Mg) 0.483(0.501).

Bulk analyses of host rocks show high K_2O (indicative of the high phlogopite) content and high CaO relative to CO_2 and P_2O_5 , indicating high diopside, e.g. BD 1089B, (New Elands Mine): SiO_2 36.12, TiO_2 1.46, Al_2O_3 4.38, Fe_2O_3 6.80, FeO 2.68, MnO 0.22, MgO 22.82, CaO 8.33, Na_2O 0.29, K_2O 5.04, H_2O^+ 4.89, H_2O^- 1.28, CO_2 3.80, P_2O_5 1.46, Σ 99.73, analyst - Joy R. Baldwin.

In simple synthetic systems, serpentine occurs only when the mole fraction of CO_2 in H_2O-CO_2 mixtures is less than ~0.05 (Kerrick, 1974, Fig. 13a), and serpentine + diopside is the low-T assemblage with respect to tremolite + forsterite + H_2O and ~400°C for 1 kbar pressure of H_2O (Winkler, 1974, Fig. 11-7). In the absence of direct phase equilibria relevant to the system diopside-phlogopite - "serpentine" - calcite, we tentatively suggest that the diopside-bearing late-stage assemblages may have crystallized at perhaps ~400-500°C with $X(CO_2) < 0.05$, and at low pressures (the last parameter based on estimate of overburden at the time of kimberlite emplacement). Even though the diopside-bearing assemblages are hydrous, there is no reason to expect crystallization of tremolite or richterite under these low P-T conditions.

References

Dawson and Smith (1977), *GCA* 41, 309.

Kerrick (1974), *Am. Mineral.* 59, 729.

Winkler (1974), *Petrogenesis of Metamorphic Rocks*, 3rd ed.

We thank NSF EAR 76-03604 and Materials Research Laboratory.

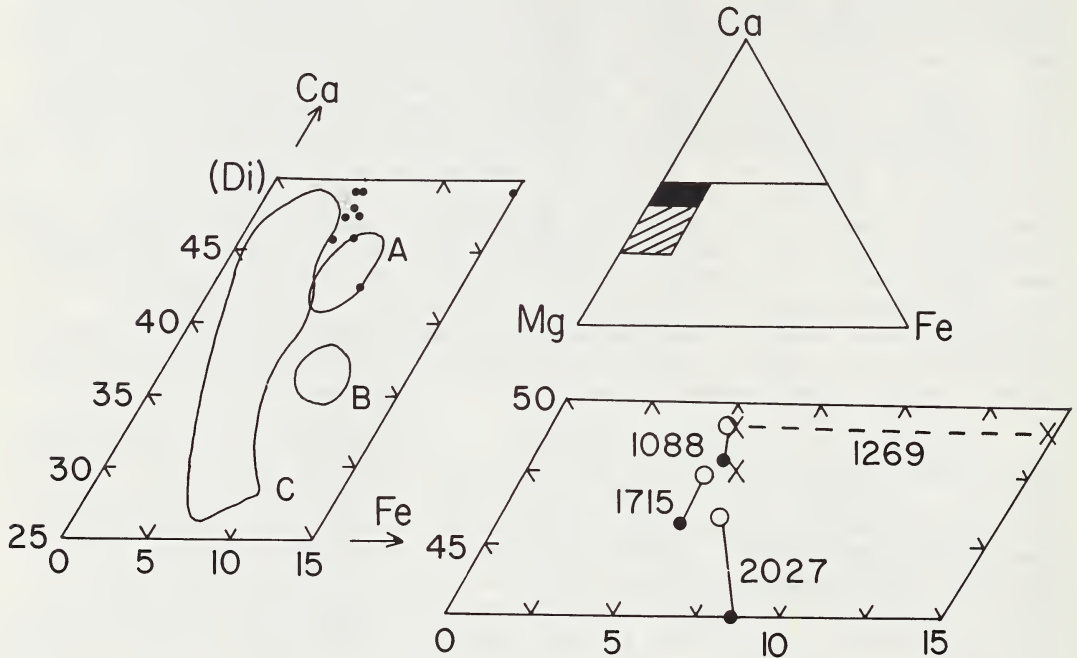


Fig. 1. Chemical composition of groundmass diopside. The left-hand and lower-right diagrams, respectively, are enlargements of the marked areas in the upper-right diagram. In the left-hand diagram, dots show the analyses listed in Table 2; in the lower-right diagram the analyses are distinguished by the following symbols: filled circle, core; open circle, rim; cross, other analyses. At the left, A shows the composition range for the MARID suite, B for clinopyroxene-ilmenite intergrowths, and C for lherzolite and websterite xenoliths.

GEOOTHERMOMETRY AND GEOBAROMETRY OF SYNTHETIC SPINEL LHERZOLITE IN THE SYSTEM $\text{CaO-MgO-Al}_2\text{O}_3\text{-SiO}_2$

James R. Dixon

Dean C. Presnall (both at Institute for Geosciences, University of Texas at Dallas, P. O. Box 688, Richardson, Texas 75080

The usefulness of the compositions of pyroxenes coexisting with spinel and forsterite (spinel-lherzolite) for geothermometry and geobarometry has been investigated experimentally in the system $\text{CaO-MgO-Al}_2\text{O}_3\text{-SiO}_2$. Experiments were performed on glass starting materials in welded (hydro-thermal) or folded (anhydrous) platinum capsules with piston-cylinder apparatus. W3Re/W25Re thermocouples were used and all experiments were of piston-out type with no pressure correction. Run durations were 24 to 141 hours. Phases were identified and analyzed with an electron microprobe. All runs consisted of forsterite + enstatite + diopside + spinel + liquid. Uncertainty in the Ca/Ca + Mg ratios of the diopside is less than or equal to 0.001, and the uncertainty of the Al_2O_3 content of the enstatite is a maximum of ± 0.4 weight percent.

Presnall (1976) suggested that the Al_2O_3 content of enstatite in synthetic spinel-lherzolite may be marginally sensitive to pressure, and thus useful as a geobarometer. In contrast, theoretical studies have indicated that Al_2O_3 isopleths in the spinel lherzolite field are nearly independent of pressure (for example, see Wood, 1975; Obata, 1976). The results of the present study support the conclusions of Presnall (1976). Figure 1 shows Al_2O_3 -isopleths of enstatite in equilibrium with diopside, forsterite, and spinel (spinel-lherzolite assemblage). Even considering the maximum uncertainty of the data, negatively sloping alumina isopleths are needed in order to fit the data. The exact position of the spinel- to garnet-lherzolite transition curve is uncertain (shown as a shaded zone between the limits of published determinations), but it is encouraging that the intersections of our Al_2O_3 -isopleths and the Al_2O_3 -isopleths of enstatite in the garnet-lherzolite field (Akella, 1976) occur in the region of the transition.

Because the isopleths are sloping in P-T space, determination of pressure from the alumina content of enstatite requires accurate knowledge of the temperature of equilibration. In the past, this temperature has usually been estimated by comparing the Ca/Ca + Mg ratio of diopside coexisting with enstatite to the pure end-member Di-En solvus. Al, Cr, Ti, and Na affect the Ca/Ca + Mg ratio of the diopside limb of the pyroxene solvus, but the magnitude of the changes has not previously been examined experimentally. We have determined the effect of aluminum saturation in pyroxenes, with respect to spinel (Figure 2). Compared to the 15 kbar solvus of Lindsley and S. A. Dixon (1976) without alumina, the amount of Di dissolved in the aluminous enstatite changes little or not at all. However, the Ca/Ca + Mg ratios of the alumina-saturated diopside are significantly higher than the two-component diopside. If the temperature of the run at 1275°C were to be determined from the pure end-member solvus, its temperature would be underestimated by approximately 100 degrees, an error so large that the aluminous enstatite geobarometer would be

completely useless. Within the uncertainty limits of our data, the alumina-saturated solvus is insensitive to pressure even though the Al_2O_3 content of diopside and enstatite may vary with fixed temperature. Thus, for essentially four-component spinel-lherzolite, the temperature of equilibration may be estimated from the alumina-saturated solvus using only the Ca/Ca + Mg ratio of diopside; no correction for Al^{+3} is necessary.

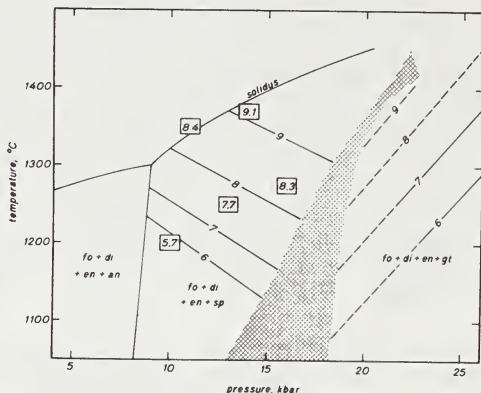


Figure 1. Stability fields of plagioclase-, spinel-, and garnet lherzolite in the system $CaO-MgO-Al_2O_3-SiO_2$ and Al_2O_3 -isopleths of enstatite. Size of rectangles represents maximum uncertainty of run conditions; number inside is wt. % Al_2O_3 in enstatite. Shaded region indicates limits of published transition curves between spinel- and garnet-lherzolite.

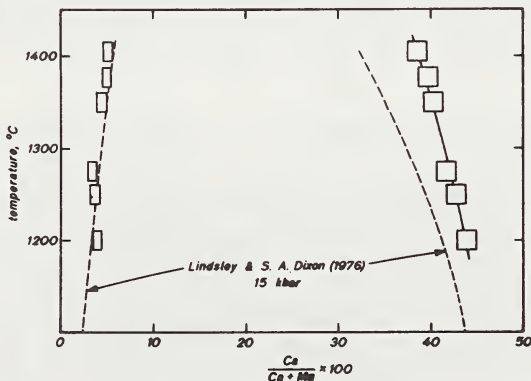


Figure 2. Aluminum-saturated pyroxene solvus compared to the 15 kbar Di-En solvus of Lindsley and S. A. Dixon (1976). Pressures of runs vary between 10 and 17.5 kbar. Size of rectangles represents maximum temperature and compositional uncertainty.

References

- Akella, J. (1976) Am. Mineral. 61, 589-598.
Lindsley, D. H. and Dixon, S. A. (1976) Am. J. Sci. 276, 1258-1301.
Obata, M. (1976) Am. Mineral. 61, 804-816.
Presnall, D. C. (1976) Am. Mineral. 61, 582-588.
Wood, B. J. (1975) Fortschr. Mineral. 52, 21-45.

Acknowledgment

This research was supported by the Earth Sciences Section, National Science Foundation, NSF Grant EAR74-22571-A01.

DISCRETE NODULE ASSEMBLAGES IN KIMBERLITES FROM NORTHERN COLORADO AND SOUTHERN WYOMING: EVIDENCE FOR A DIAPYRIC ORIGIN OF KIMBERLITE

David H. Egger (Geophysical Laboratory, Washington, D. C.)
M. E. McCallum (U. S. Geological Survey, Denver, Colorado and Dept. of Earth Resources, Colorado State University, Fort Collins, Colorado)
C. B. Smith (Colorado State University)

Two compositionally distinct groups of discrete nodules (megacrysts) from kimberlites of the Colorado-Wyoming State Line and Iron Mountain districts are described elsewhere in this volume (McCallum, Egger, and Smith). Both groups have orthopyroxene, clinopyroxene, olivine, garnet, and ilmenite megacrysts. Unaltered orthopyroxenes are found, however, only in one pipe, Sloan 2 from the State Line District. From those megacrysts, a paleogeotherm has been obtained that bears on the problem of kimberlite emplacement.

The ranges of chemical parameters of the Cr-rich and Cr-poor megacrysts in Sloan 2 in general adjoin but do not overlap (Fig. 1). The compositions of the Cr-rich megacrysts are similar to those of minerals of lherzolites and harzburgites believed to be residual (depleted) and are particularly distinctive in their high Cr₂O₃ content and tightly grouped, relatively high Mg/(Mg+Fe). The Cr-poor group shows a broader range in iron content and is less refractory in all elements; minerals of the Cr-poor suite have general similarities to discrete nodules from Lesotho (Boyd and Nixon, 1973).

Pressures and temperatures of equilibration of the enstatite megacrysts have been calculated on the assumption that every enstatite coexisted with clinopyroxene and garnet (re Boyd and Nixon, 1973). Methods have been described (Egger and McCallum, 1976). Pyroxenes are indeed found in a few cases as inclusions within each other or within other phases.

Five garnet lherzolite nodules and ten garnet websterite nodules from the Sloan pipes that were equilibrated at depths of 50-180 km fall along a shield geotherm (McCallum and Egger, 1976). The calculated equilibration conditions of the megacrysts, together with this geotherm, are plotted in Fig. 2. The majority of the megacryst points lie near the shield geotherm, but some lie about 100°C above the geotherm. This variability is far greater than can be accounted for by analytical error. Nor are the high-temperature megacrysts significantly different in composition from megacrysts on or near the geotherm. The array of points is interpreted as a partially disturbed geotherm. In contrast, the megacryst geotherms presented by Boyd and Nixon (1973) for the Lesotho pipes and by Boyd (1974) for the Frank Smith Mine, South Africa, are distinctly inflected to the high-temperature side at depths below about 150 km, while a geotherm from the Udachnaya pipe, USSR, is noninflected (Boyd *et al.*, 1976).

Nixon and Boyd (1973) suggested that the inflected limb of the Lesotho geotherm was caused by stress-heating in the low-velocity zone. This type of heating has been discounted by Green and Gueguen (1974) and Goetze (1975), and alternative models have been presented for heating by an upwelling diapir (Green and Gueguen, 1974) and by a mantle plume (Parmentier and Turcotte, 1974). Boyd (1976) now considers that a diapir associated with convective overturn is a possible explanation of the inflected limb.

In the model of Green and Gueguen (1974) it is assumed that peridotite of the diapir was less depleted than the mantle through which it flowed, that the top of the diapir was at the same temperature as the undisturbed mantle, that the diapir partially melted, and that there was no low-velocity zone

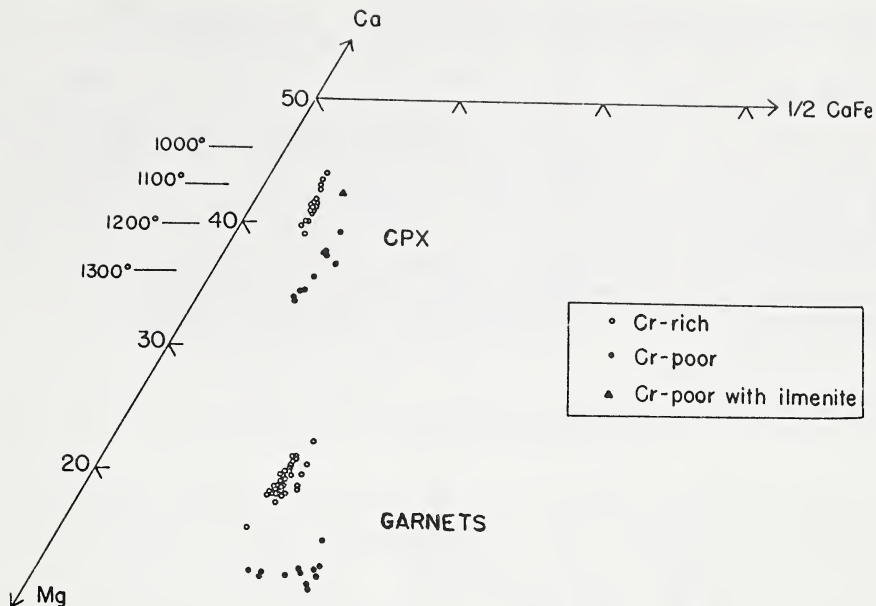


Fig. 1. Compositions of clinopyroxene and garnet megacrysts from the Sloan 2 kimberlite pipe, Colorado, plotted in mole % on a Ca-Mg-Fe projection. Temperatures are for points on the diopside solvus after Davis and Boyd (1966)

in that mantle region. This model adequately explains features of the Colorado megacryst-lherzolite suites if it is assumed that the diapir rose to a depth of about 160 km. Lherzolites at depths to 180 km would be above or very near the top of the diapir, and therefore equilibration temperatures could very well be undisturbed. Megacrysts, on the other hand, especially if they were part of the diapir, might be expected to show disturbed temperatures.

Megacrysts are here assumed to indeed have been part of the diapir and to have crystallized in a kimberlite magma. They are, in that sense, cognate. These observations support that interpretation: (1) The ultracoarse grain size and relative scarcity of mineral intergrowths suggest the megacrysts grew in a liquid, and the compositional trends of Cr-poor megacrysts can be most easily explained by liquid fractionation. Eggler and Wendlandt (this volume) show that the liquid produced by partial melting of peridotite can be kimberlitic. (2) The perturbed temperatures of megacrysts can be explained by association with a diapir. (3) Distinct groups of Cr-poor megacrysts are associated with particular pipes or groups of pipes, suggesting that the megacrysts are cognate (accidental inclusions should be found in more than one group) and that their chemical characteristics originated at the depth of kimberlite formation. (5) A few megacrysts contain carbonate inclusions.

The key to kimberlite formation is thought to be the coincidence of diapirs, rising through the asthenosphere, with a fracture system in the lithosphere. Kimberlite evolves by a combination of partial melting, liquid fractionation, and contamination. Little evidence is left of the original liquids save for the discrete nodules that grew in them. There is no need in this model for a low-velocity zone.

References

- Boyd, F. R., 1974, *Carnegie Inst. Wash. Yearb.* 73, 285-293.
Boyd, F.R., 1976, *Carnegie Inst. Wash. Yearb.* 75, 521-523.
Boyd, F. R., T. Fujii, and R. V. Danchin, 1976, *Carnegie Inst. Wash. Yearb.* 75, 523-531.
Boyd, F. R. and P. H. Nixon, 1973, in Lesotho Kimberlites, Nixon, ed., 254-268.
Davis, B. T. C. and F. R. Boyd, 1966, *J. Geophys. Res.* 71, 3567-3576.
Eggler, D. H. and M. E. McCallum, 1976, *Carnegie Inst. Wash. Yearb.* 75, 538-542.
Goetze, C., *Geology* 3, 172-173.
Green, H. W., II, and Y. Gueguen, *Nature (London)* 249, 617-620.
McCallum, M. E., and D. H. Eggler, 1976, *Science* 192, 253-256.
Parmentier, E. M., and D. L. Turcotte, 1974, *EPSL* 24, 209-212.

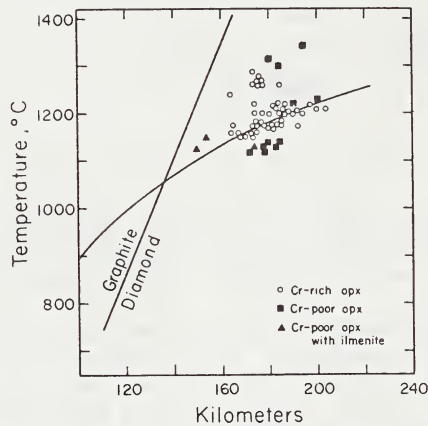


Fig. 2. Estimates of equilibration temperatures and depths for orthopyroxene megacrysts from the Sloan 2 kimberlite pipe, Colorado. The geotherm drawn is the shield geotherm of Clark and Ringwood (1964).

Research supported by the National Science Foundation, Earth Sciences Section, Grant DES 74-13098, and by the Carnegie Institution of Washington.

EXPERIMENTAL STUDIES ON THE RELATIONSHIP BETWEEN KIMBERLITE MAGMAS AND PARTIAL MELTING OF PERIDOTITE

David H. Egglar and Richard F. Wendlandt (Geophysical Laboratory, 2801 Upton St., N. W., Washington, D. C. 20008)

Theory. Theory of melting of peridotite in the presence of small amounts of volatiles has been developed (Egglar, 1977a,b) from simple systems (e.g., A-H₂O-CO₂). Subsolidus assemblages containing a carbonate or hydrous phase and the breakdown products of that phase can buffer the composition of a coexisting vapor, provided that sufficiently small amounts of volatiles are present that the buffer assemblage is not exhausted. Such an assemblage is called a zone of invariant vapor composition (ZIVC). All peridotite compositions with volatiles (CO₂/[CO₂+H₂O]) within a ZIVC melt at the same temperature (isobarically). In the presence of large amounts of volatiles, peridotite compositions with volatiles are not buffered and melt at different temperatures.

The system CaO-MgO-SiO₂-CO₂-H₂O. The upper limit of dolomite stability in the upper mantle, defined by the reaction En+Dol=Di+Fo+V, has been calculated by Egglar *et al.* (1976), and is shown in Fig. 1a. The CO₂/(CO₂+H₂O) contours have now been confirmed at 26 and 30 kbar by experiment. At 30 kbar, dolomite is stable in the melting range of peridotite, indicating that the CO₂/(CO₂+H₂O) contours on the decarbonation and solidus surfaces coincide along a ZIVC solidus (heavy line, Fig. 1a). This line defines a unique solidus for volatile contents within a certain range (i.e., at 30 kbar CO₂/(CO₂+H₂O) = 0.15-1.0 (mol) and total content of CO₂ < 5 wt %).

Natural peridotite. The same dolomite stability contours can be combined with solidi of natural peridotites to predict their ZIVC solidi (Figs. 1b and

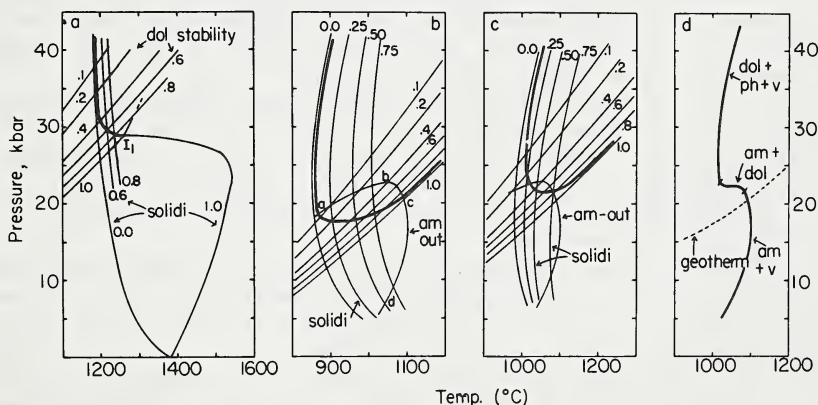


Fig. 1. ZIVC-type univariant reactions for peridotite compositions. (a) The system CaO-MgO-SiO₂-CO₂-H₂O. Numbers indicate vapor composition contours on the dolomite stability and solidus surfaces. Heavy line is the calculated ZIVC solidus. (b) ZIVC solidus, buffered by dolomite, calculated from the solidi of Mysen and Boettcher (1975), whose amphibole-out curve is also shown. (c) ZIVC solidus calculated from solidus of Kushiro *et al.*, 1968. (d) The preferred peridotite solidus for amphibole and dolomite-buffered vapor compositions. The solidus is applicable to volatile compositions with 0.02-0.37 wt% H₂O and < 5 wt% CO₂ in the range CO₂/(CO₂+H₂O)=0.15-0.85 (mol).

explosive

lc). Above 22 kbar, the subsolidus assemblage of a CO₂-H₂O-peridotite will be dolomite+phlogopite+opx+cpx+olivine+garnet (spinel). For realistic K contents (< 500 ppm), peridotite can contain no more than 0.02 wt% H₂O bound in phlogopite; therefore for peridotites containing more than 0.02 wt% H₂O, phlogopite cannot coexist with its breakdown products and cannot buffer the vapor composition. The vapor will be buffered entirely by dolomite (or, at higher pressure, magnesite; Kushiro et al., 1975), at fairly low CO₂/(CO₂+H₂O) (Figs. 1b and 1c).

Kimberlite. At pressures above 25 kbar, the subsolidus assemblage of kimberlite compositions is opx+cpx+olivine+gar+ph+carbonate, and therefore the principles developed above can also be applied to kimberlite. A composition was prepared (Table 1) nearly identical to the average Lesotho kimberlite of Gurney and Ebrahim (1973), with the exception that CoO was substituted for FeO to avoid iron loss to Pt capsules (Coons et al., 1976). This substitution principally results in somewhat higher solidus and liquidus temperatures. The 5.2% CO₂ in the natural kimberlite was considered to be a minimal value for the mantle-derived content, but the H₂O content of the natural (10.7%) was considered to be primarily meteoric water. For experiments, therefore, H₂O was added to the dry material (Table 1) in amounts shown in Figs. 2 and 3. Materials were sealed inside Pt capsules and run in talc-pyrex (30 kbar) and talc-boron nitride (55 kbar) assemblies in solid-media, high-pressure apparatus.

Table 1. Composition of kimberlite studied

SiO ₂	37.68
TiO ₂	2.16
Al ₂ O ₃	5.11
Cr ₂ O ₃	.23
CoO	11.27
MgO	25.85
CaO	10.62
Na ₂ O	.22
K ₂ O	.91
P ₂ O ₅	.74
CO ₂	5.22
	100.01

At both 30 and 55 kbar, melting behavior of the kimberlite is consistent with theory and prediction. At 30 kbar, the ZIVC assemblage (LHZ+dol+ph+V) melts at 1075°C, irrespective of the CO₂/(CO₂+H₂O). That temperature is only 30°C higher than the predicted temperature (Fig. 1d). The H₂O-deficient assemblage LHZ+dol+ph+ks+sa also melts invariantly at somewhat higher temperature (Fig. 2). Either dol or ph persists into the melting range, but garnet disappears near the solidus (Fig. 2).

At 55 kbar (Fig. 3), the pattern is similar, but garnet persists well into the melting range. These conclusions can be drawn from Fig. 3:

1. The kimberlite solidus temperature for volatile contents up to about 10% and for CO₂/(CO₂+H₂O) = 0.05-1.0 will be about 1225°C at 55 kbar. That would also be approximately the solidus of peridotite, because it would have the same phase assemblage.
2. Kimberlitic liquids (liquid somewhat more carbonatitic than the starting material [Table 1]) can coexist with 4-phase peridotite (+mag+ph) over a temperature interval of 200°-300°C, depending on volatile composition. Kimberlite, therefore, can be a primary magma.
3. The temperature range 1200°-1400°C at 55 kbar (175 km depth) is the range of equilibration temperatures and pressures from sheared lherzolites and discrete nodules from Lesotho (Nixon and Boyd, 1973). The coincidence with the range found in our experimental study strongly suggests that the mantle was partially molten, that the liquid was kimberlitic, and that the discrete nodules were phenocrysts in the liquid. The range of temperatures can be explained by a diapir model (Green and Gueguen, 1974).

Research supported by Earth Sciences Section, National Science Foundation, Grant DES 73-00266A01.

Kimberlite composition

References

- Coons, W. E., J. R. Holloway, and A. Navrotsky, 1976, *EPSL* 30, 303-308.
- Eggler, D. H., 1977a, *Carnegie Inst. Wash. Yearb.*, in press.
- Eggler, D. H., 1977b, *Amer. Jour. Science*, in press.
- Eggler, D. H., I. Kushiro, and J. H. Holloway, 1976, *Carnegie Inst. Wash. Yearb.* 75, 631-636.
- Green, H. W., II, and Y. Gueguen, 1974, *Nature (London)* 249, 618-620.
- Gurney, J. J. and S. Ebrahim, 1973, in *Lesotho Kimberlites*, Nixon, ed., 280-284.
- Kushiro, I., Y. Syono, and S. Akimoto, 1968, *J. Geophys. Res.* 73, 6023-6029.
- Kushiro, I., H. Satake, and S. Akimoto, 1975, *EPSL* 28, 116-120.
- Mysen, B. O., and A. L. Boettcher, 1975, *J. Petrology* 16, 520-548.
- Nixon, P. H., and F. R. Boyd, 1973, in *Lesotho Kimberlites*, Nixon, ed., 67-75.

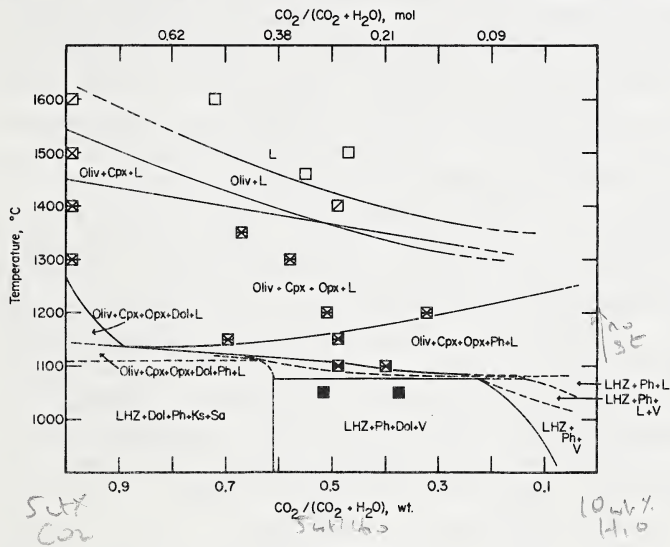


Fig. 2. Phase relations at 30 kbar of the kimberlite composition shown in Table 1, with various amounts of H₂O added. LHZ = oliv+opx+cpx+garnet Ph = phlogopite, Dol = dolomite, Ks = kalsilite, Sa = sanidine, L = liquid, V = vapor.

Handwritten notes: "no 35", "low temp in", "Carnegie Institution", "P = CO (approx)".

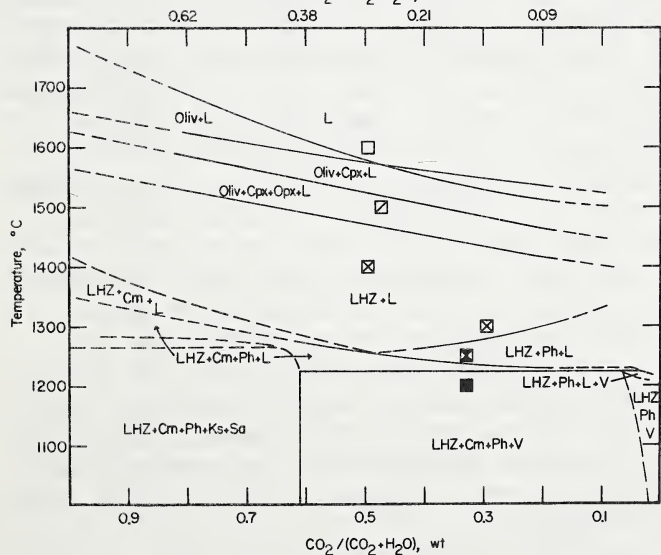


Fig. 3. Phase relations at 55 kbar of the kimberlite composition shown in Table 1, with various amounts of H₂O added. Abbreviations same as Fig. 2, except that Cm = magnesite.

Handwritten notes: "or possibly above 1000°C", "conclusion is", "pressure field".

THE WASHINGTON PASS VOLCANIC CENTER: EVOLUTION AND ERUPTION OF MINETTE MAGMAS OF THE NAVAJO VOLCANIC FIELD

S.N. Ehrenberg (Department of Earth and Space Sciences, University of California, Los Angeles, California 90024)

Minettes of the Navajo Volcanic Field are of interest because they formed at depths of at least 150 km and appear to be genetically related to kimberlite diatremes. Minettes and their extrusive equivalents (trachybasalts) at the 2 km diameter subsidence crater at Washington Pass were chosen for detailed study because of the relatively well-developed eruptive history displayed in the crater stratigraphy and the presence of contrasting mafic and trachytic lavas. Eruption began with ejection of voluminous pyroclastic deposits, including both tuff-breccias, composed predominantly of comminuted sediments with subordinate minette and crystalline basement fragments, and agglomerates, composed mainly of minette clasts. These deposits are thickest (>100 m) on the east and west sides of the crater, where they are exposed in cliffs produced by landsliding. On the west, tuff-breccias predominate and exhibit a remarkable alternation of coarse- and fine-grained beds 0.1 - 1 m thick, suggestive of rhythmic variation in the physical properties in the eruptive medium.

On the east, the pyroclastic materials are mostly agglomerates. Low-angle cross-bedding is common in all the pyroclastic beds, but in the eastern agglomerates this feature is accompanied by dune structures. Some of these formed by accretion on the lee side, while others display accretion on the side facing the crater. Asymmetrical bomb sags are also abundant in this area.

After the pyroclastic activity waned, thick trachybasalt flows covered the crater floor, and plugs of glassy to aphanitic minette were intruded in the crater center. These rocks consist of phenocrysts of phlogopite, diopside, and olivine (~Fo80) in a matrix of biotite, cpx, and Ti-magnetite microphenocrysts and interstitial sanidine, analcime, and chlorite. Xenoliths are uncommon in the mafic lavas. The eruption terminated with extrusion of a small volume of trachyte from vents cutting the plugs in the crater center. The trachyte is much lighter in color than the earlier flows and consists of biotite and diopside phenocrysts in a trachytic groundmass of sanidine laths and interstitial brown clay-like material. Intensely metasomatized xenoliths 1-5 cm in diameter of spinel lherzolite and websterite comprise ~5% of the volume of this flow. The trachyte is richer in Si, Al, Na, and K and lower in Fe, Ca, Ti, and P than the mafic rocks, but contains similar Mg and Ni (Table 1). A similar sequence of flows also occurs capping East Sonsela Butte, 15 km west of Washington Pass. The East Sonsela Butte trachybasalts and trachyte are very similar in both petrography and composition to their Washington Pass counterparts (Table 1).

Discussion. The basal pyroclastic beds at Washington Pass and other Chuska Mountains craters are the surface expression of diatreme formation; similar maar-like deposits probably capped the more deeply

eroded Navajo minette diatremes, such as Shiprock, Bennett Peak, and Agathla Peak. At all of the minette centers, eruption appears to have proceeded in a single cycle of (1) diatreme formation and (2) intrusion or effusion of minette magma, although the relative development of these two stages varies at different centers. The presence of common fragments of lower crustal and uppermost mantle rock types (garnet granulite, spinel lherzolite, and websterite) in the pyroclastic rocks and the substantial fraction (10-40%) of pumice in the agglomerate at Washington Pass indicate that the pyroclastic activity was not the result of near-surface groundwater/magma interaction, but probably reflects release of juvenile mantle volatiles. The characteristic cross-bedding, dunes, and accretion structures at Washington Pass, together with the asymmetrical bomb sags, suggest that the pyroclastic material was deposited by both base-surge and ballistic modes of transport.

The most intriguing problem at Washington Pass is the relationship between the contrasting mafic and trachytic lavas. This contrast is also observed at East Sonsela Butte, Buell Park, and just north of the Chuska Mountains where the felsic Mitten Rock neck stands equidistant between the mafic volcanic centers of Shiprock, the Thumb, and Beautiful Mountain. One way that mafic magmas may become more felsic is by removal of early-crystallizing minerals, and, indeed, phlogopite- and diopside-rich nodules which appear to be phenocryst segregations are common in the minettes. However, in contrast to other felsic minettes, the Washington Pass and East Sonsela Buttes trachytes have Mg and Ni contents similar to the associated mafic rocks. This pattern and the presence of altered lherzolite fragments throughout virtually every hand sample of the rock suggests that assimilation of peridotite contributed to the trachyte composition. Using a least-squares-fitting FORTRAN routine, an approximate fit to the composition of the trachytes may be obtained by removing 36% phenocrysts from the mafic composition and adding 9% peridotite (Table 1). The bimodal character of the Washington Pass and East Sonsela Butte magmas may thus be the result - at least in part - of fractional crystallization and assimilation of wall rock in an uppermost mantle magma chamber. Residuals for Al and especially K are large, however, indicating that this may not be the entire explanation. One problem may be that the trachyte contains relatively iron-rich biotite phenocrysts, whereas magnesian phlogopites typical of mafic minettes were used in the model.

The least-squares-fitting technique meets with variable success in relating diverse minette compositions from other localities in the volcanic field. The felsic Mitten Rock minette may be approximated by subtracting 25% phenocrysts from Shiprock minette. However, removal of assumed phenocryst compositions cannot have produced the Shiprock or Mitten Rock minettes from the more mafic Thumb composition, suggesting that the Thumb may represent a completely separate batch of primary magma. The inverse correlation of SiO_2 and REE in these three necks may be the result of either apatite fractionation or smaller percentages of melting for the more mafic liquids.

It seems probable that the compositional diversity of the Navajo minettes reflects the interplay of several different processes. Fractional crystallization and reaction with wall rocks are both likely to have influenced the compositions of these liquids during their ascent through very long and narrow conduits. In addition, the effects of these processes may have been superimposed upon primary compositional differences, relating to local variations in conditions of melting and bulk composition during the formation and extraction of a small percentage of melt from a large volume of possibly inhomogeneous and complex upper mantle. More significant than the compositional diversity, however, is the overall coherence of bulk compositions, mineral chemistry, and petrography exhibited by the Navajo volcanic centers. Compare, for example, columns 1, 4, and 8 in Table 1. The minette magmas represent the response of a single, K- and Rb-enriched region of the upper mantle to a relatively minor thermal or tectonic disturbance from a previous state of equilibrium. Evidence for the nature of this disturbance may be contained in the mantle xenoliths incorporated by the minette, as described in an accompanying abstract.

Table 1. Compositions of minettes and extrusive rocks from Navajo volcanic centers and computed best fits to higher silica compositions using combinations of phenocrysts, peridotite, and more mafic compositions.

	Ave. Washington Pass mafic (8)*	Ave. Washington Pass felsic (3)	Best least-squares fit to felsic composition	Ave. East Sonseala Butte mafic (5)	Ave. East Sonseala Butte felsic (3)	Best fit to felsic composition	Minette from the Thumb (A103THM)	Shiprock south dike (74-A07-SRM-W5B)**	Best fit to Shiprock using Thumb + phenocrysts	Mitten Rock (a072MTR)	Best fit to Mitten Rock using Shiprock + phenocrysts	Best fit to Mitten Rock using Thumb + phenocrysts
SiO ₂	52.4	57.3	56.7	51.4	59.2	57.6	47.3	52.2	52.5	57.8	56.6	57.5
TiO ₂	1.9	0.9	1.1	2.1	0.9	1.1	2.4	1.9	2.6	0.8	1.4	2.0
Al ₂ O ₃	11.0	11.8	12.3	10.8	12.0	12.6	9.2	11.2	11.4	12.4	12.6	12.7
FeO	6.6	4.1	4.0	6.6	4.0	3.8	7.6	6.5	6.4	4.5	4.3	4.3
MnO	0.09	0.06	0.09	0.10	0.06	0.13	0.14	0.11	0.18	0.07	0.12	0.24
MgO	9.0	9.0	8.9	9.5	8.4	8.1	13.3	8.0	8.0	5.5	5.2	5.3
CaO	7.1	4.4	4.4	7.6	3.8	3.6	8.8	7.4	7.3	6.3	6.4	5.8
Na ₂ O	2.0	2.3	2.6	1.5	2.1	2.1	1.2	2.0	1.8	2.6	2.5	2.4
K ₂ O	5.9	6.6	6.0	6.0	7.5	5.9	4.7	6.4	5.0	7.3	6.8	4.5
P ₂ O ₅	0.9	0.6	0.5	0.8	0.5	0.3	2.3	1.0	1.2	0.8	0.4	1.3
ig. loss	2.5	3.0	3.0	2.8	2.5	3.5	3.2	2.3	4.6	1.7	2.7	4.8
Ni	304	309		320	281		481	288		160		
Cr	407	324		478	341		631	296		123		
Sc	14	9		16	9		17	14		10		
Sr	1304	1541		1204	1192		1504	1295		1376		
Rb	155	183		189	239		132	159		159		
La	115	136		109	104		185	140		117		
Sm	15	17		15	14		28	20		15		
Yb	1.2	0.7		1.4	0.9		2.2	1.9		1.2		

Major elements (wt. %) and Sr by x-ray fluorescence. Trace elements (ppm) by I.N.A.A. (Prof. J.T. Wasson's Lab).

*Number of sample localities averaged for major element data. Trace element data are from fewer samples.

**Shiprock major element data are average of U.C.L.A. analysis and J.S.C. analysis courtesy of Dr. A.J. Irving.

GARNET PERIDOTITE XENOLITHS IN MINETTE FROM THE NAVAJO VOLCANIC FIELD

S.N. Ehrenberg (Department of Earth and Space Sciences, University of California, Los Angeles, California 90024)

Small and variably altered xenoliths of spinel and garnet peridotite are present in many of the minette/trachybasalt volcanic centers of the Four Corners area. Unaltered garnet peridotite xenoliths 1-30 cm in diameter, however, are relatively common at the Thumb, a small neck 21 km SW of Shiprock. Temperatures and pressures of equilibration were estimated for 47 of these rocks using pyroxene compositions and the experimental data of Mori & Green (1975) and Akella (1976). Pressures estimated are within the range 45-52 kb, indicating that only a very limited vertical interval was sampled by the eruption. Temperature estimates of 980-1385°C display little correlation with pressure, but have general correlations with xenolith chemical compositions and textures (Fig. 1). The most depleted rocks (CPX Ti/Cr ≤ 0.1) have protogranular to weakly porphyroclastic textures and equilibrated at the lowest temperatures - close to the continental geotherm calculated by Clark & Ringwood (1964). Less depleted rocks (CPX Ti/Cr between

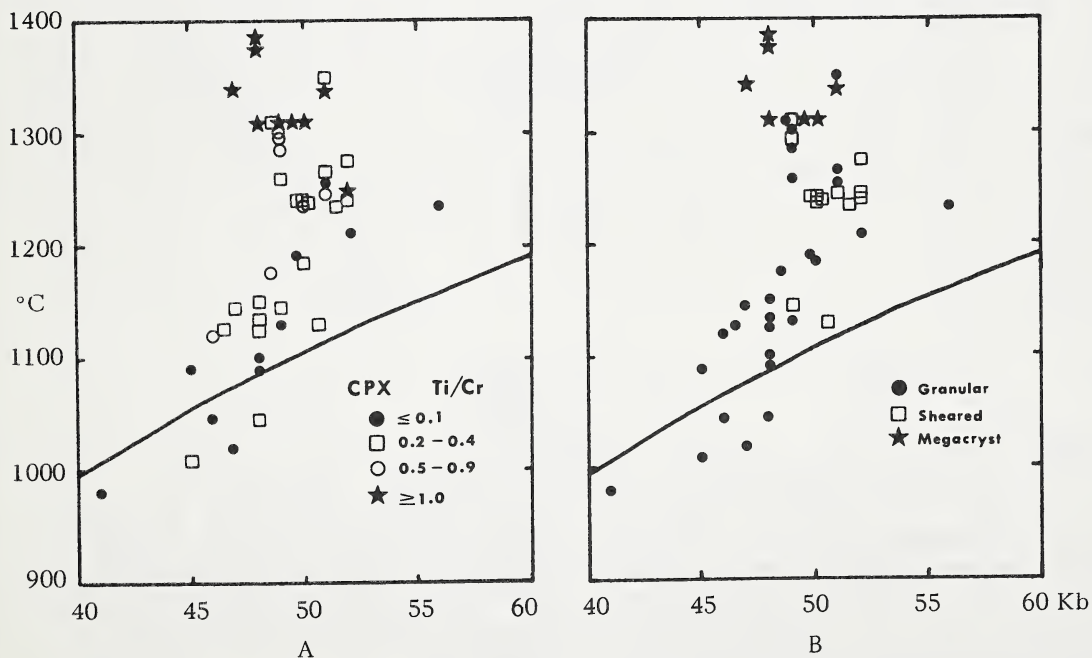


Fig.1 Relations of temperature and pressure estimates for garnet peridotite xenoliths from the Thumb to compositions of clinopyroxenes (A) and xenolith textures (B). Curved line represents continental shield geotherm.

0.1 and 1.0) yield temperatures mostly above this geotherm and have protogranular to mosaic textures. The least depleted rocks (CPX Ti/Cr ≥ 1.0) equilibrated at 1250-1385°C and include 2 mosaic texture lherzolites and 7 ultracoarse-grained (≤ 9 cm) nodules containing various assemblages of CPX, GA, OPX, OL, ILM, and Phlogopite. Following the model of Green and Gueguen (1974), it is proposed that these xenoliths are derived from the top of a mantle diapir which brought material from a warmer deeper part of the mantle into an overlying region which had previously been extensively depleted by partial melting.

Phlogopite is present in many of the lower temperature peridotites and in the high-temperature megacryst nodules. Texturally the phlogopite appears to be secondary in some peridotites, but plots of phlogopite vs. CPX Ti/Cr and Fe/Mg (Figs. 2 and 3) are roughly linear, indicating some chemical communication between phlogopite and the anhydrous phases.

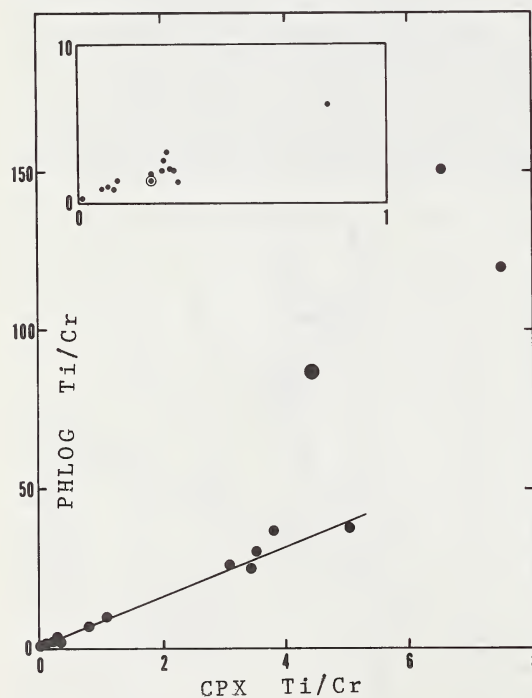


Fig.2 Phlogopite Ti/Cr vs. CPX Ti/Cr in garnet peridotite xenoliths (CPX Ti/Cr < 1.0) and megacryst xenoliths from the Thumb. Inset shows enlargement of peridotite values. Large symbol is average of Thumb phenocrysts. Circled point is garnet lherzolite from Shiprock (Baldrige, et al., 1975).

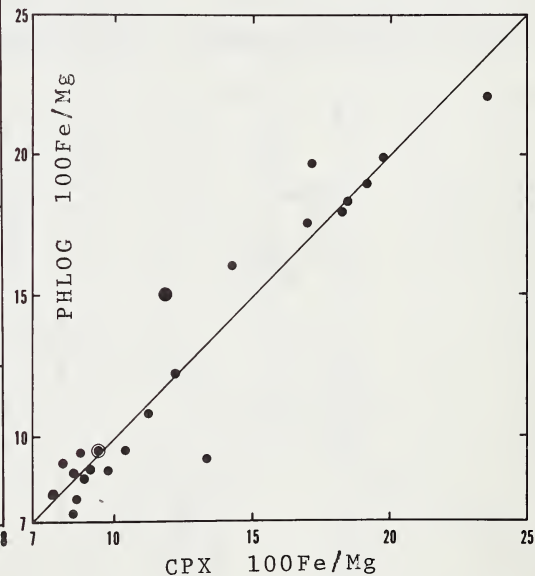


Fig.3 Phlogopite Fe/Mg vs. CPX Fe/Mg in garnet peridotite (CPX Fe/Mg < 0.14) and megacryst xenoliths from the Thumb and Shiprock.

Sr analyses of peridotite CPX (Fig. 4) indicate that the minette (with $87\text{Sr}/86\text{Sr} = 0.7056 - 0.7081$) did not equilibrate with its peridotite xenoliths, but must have originated at some greater depth. The megacryst clinopyroxenes have not been analyzed for Sr, but are similar in major and rare earth element composition to clinopyroxenes in the most iron-rich lherzolites and are thus probably related to these rocks rather than to the minettes. The correlation of Sr content with $87\text{Sr}/86\text{Sr}$ in the clinopyroxenes suggests that these rocks are related by a common geochemical history despite the wide variations in their other chemical parameters.

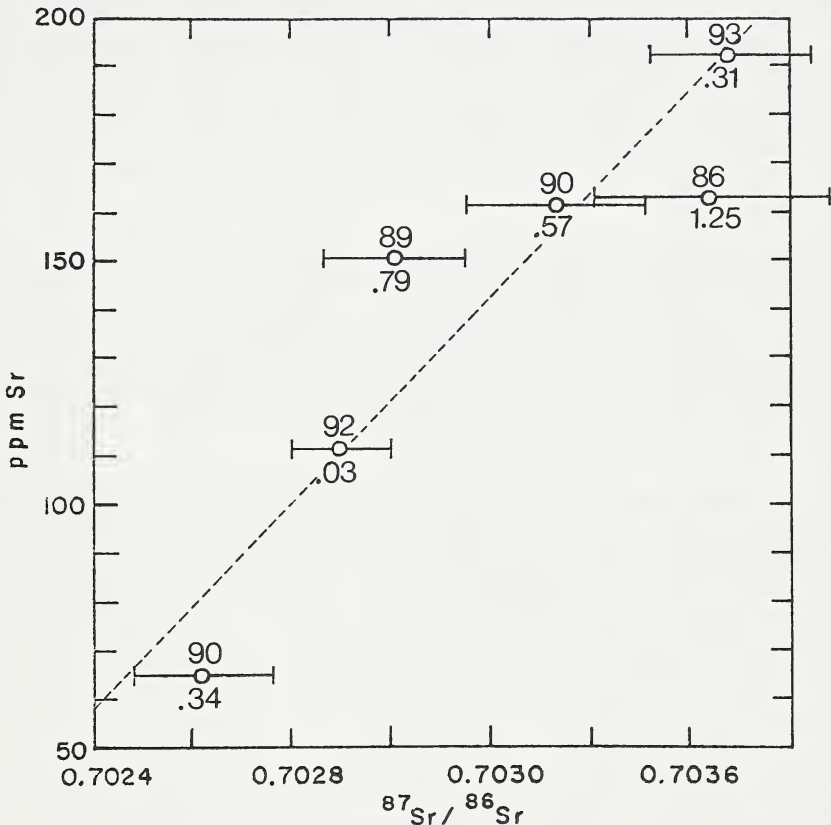


Fig. 4 $87\text{Sr}/86\text{Sr}$ vs. Sr concentrations in clinopyroxenes separated from six garnet peridotite xenoliths from the Thumb. Error bars represent two times standard error of the mean on each side of data points, based on counting statistics. Numbers above points give CPX 100Mg/(Mg+Fe). Numbers below points are CPX wt.% $\text{TiO}_2/\text{Cr}_2\text{O}_3$.

Akella, J., 1976, *Amer. Mineralogist*, **61**: 589-598.

Baldrige, W.S., S.N. Ehrenberg, and T.R. McGetchin, 1975, *EOS*, **56**: 464-465.

Clark, S.P., Jr., and A.E. Ringwood, 1964, *Rev. Geophys.*, **2**: 35-88.

Green, H.W., II, and Y. Gueguen, 1974, *Nature*, **249**: 617-619.

Mori, T., and D.H. Green, 1975, *Earth Planet. Sci. Lett.*, **26**: 277-286.

A MODEL OF PHASE RELATIONS IN THE SYSTEM $\text{MgO-SiO}_2\text{-H}_2\text{O-CO}_2$ AND PREDICTION OF THE COMPOSITIONS OF LIQUIDS COEXISTING WITH FORSTERITE AND ENSTATITE

David E. Ellis and Peter J. Wyllie, Dept. of Geophysical Sciences,
University of Chicago, Chicago, Illinois 60637

A P-T net, consistent with experimental studies of dehydration and melting reactions and with Schreinemaker's rules, has been derived for the system $\text{MgO-SiO}_2\text{-H}_2\text{O}$. Phase relations near the solidus of the system $\text{MgO-SiO}_2\text{-H}_2\text{O}$ are similar to those in the system $\text{MgO-SiO}_2\text{-CO}_2$. The positions of dehydration reactions which intersect the solidus in the system $\text{MgO-SiO}_2\text{-H}_2\text{O}$ are calculated on the basis of experimental studies at lower P and T, thermochemical data, and water fugacities predicted by the modified Redlich-Kwong equation of state. They occur at lower temperatures and higher pressures than the analogous decarbonation reactions in the system $\text{MgO-SiO}_2\text{-CO}_2$. The reaction $\text{Mg(OH)}_2 \rightarrow \text{MgO} + \text{H}_2\text{O}$ intersects the solidus at about 1250°C and 45 kbar, and the reaction $\text{Mg(OH)}_2 + \text{MgSiO}_3 \rightarrow \text{Mg}_2\text{SiO}_4 + \text{H}_2\text{O}$ intersects the solidus at about 1200°C and 90 kbar. Isobaric liquidus diagrams show that a large field for Mg(OH)_2 must exist not far above the pressure at which Mg(OH)_2 first becomes stable on the solidus.

A P-T net for the system $\text{MgO-SiO}_2\text{-H}_2\text{O-CO}_2$ has also been derived. Those reactions involving both forsterite and enstatite are shown in figure 1. A model mantle whose composition is equivalent to forsterite plus enstatite plus a small amount of volatiles may contain a vapor phase only in the P-T region enclosed by the reactions shown with heavy lines. P-T-X calculations indicate that at invariant point B, liquids coexisting with forsterite, enstatite, and vapor whose mole fraction of CO_2 is greater than 0.005 also coexist with magnesite.

The transition from vapor-present to vapor-absent melting in the upper mantle may be illustrated by a series of T-X sections through figure 1. Figure 2A shows that forsterite, enstatite, and liquid may coexist with a vapor phase having any mole fraction of CO_2 at 20 kbar. However, in figure 2B it may be seen that the assemblage forsterite plus enstatite plus liquid may not coexist with a vapor phase richer in CO_2 than that at the isobaric invariant point. The small amount of magnesite present in a volatile-poor model mantle would be completely reacted at that point. The mole fraction of CO_2 in the vapor at higher temperatures will then be controlled by the reaction $\text{Fo} + \text{En} + \text{V} \rightarrow \text{L}$. When the temperature maximum on that reaction is exceeded, all volatile must be dissolved in the liquid and any further melting will be vapor-absent. At pressures above about 90 kbar all H_2O and CO_2 are combined in brucite and magnesite. Melting takes place in the absence of a vapor phase, in the form of a simple eutectic shown in figure 2C.

The estimated composition of first liquids formed in a model mantle with an $\text{H}_2\text{O:CO}_2$ ratio of 3:1 at pressures of 20 kbar, 50 kbar, and 90 kbar is given in Table 1. In figure 3, the position of the plane of liquid compositions coexisting with forsterite and enstatite in the system $\text{MgO-SiO}_2\text{-H}_2\text{O-CO}_2$ is shown at 20 kbar and 90 kbar. At 20 kbar the first liquid is enstatite-quartz normative. However, at higher pressures the presence of magnesite on the solidus requires the composition of the first liquids to be highly silica-undersaturated. The appearance of the eutectic involving forsterite, enstatite, brucite, and magnesite at about 90 kbar requires the compositions of first liquids to be nearly constant as pressure is further increased. The

compositions of any first liquids formed at a pressure greater than 90 kbar must be periclase-forsterite normative.

Research was supported by the National Science Foundation through grant GA 76-20410 and the Materials Research Laboratory.

Table 1. The composition of first liquids coexisting with forsterite and enstatite in a model mantle with an H₂O:CO₂ ratio of 3:1. All compositions are given in mole percent.

<u>Pressure</u>	<u>MgO</u>	<u>SiO₂</u>	<u>H₂O</u>	<u>CO₂</u>	<u>Normative Minerals</u>
20 kbar	19.8	22.0	57.0	1.2	enstatite, quartz
50 kbar	37.6	9.6	24.3	28.5	forsterite, periclase
90 kbar	31.6	18.4	38.7	11.3	forsterite, periclase

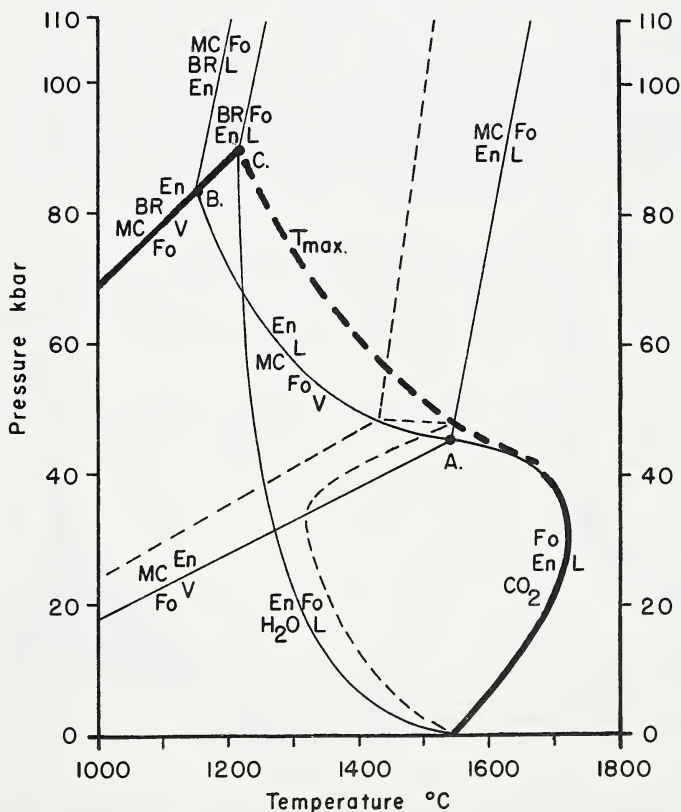


Figure 1. P-T projection of the system MgO-SiO₂-H₂O-CO₂ showing only reaction involving both forsterite and enstatite. The P-T range in which a model mantle could contain a vapor phase is bounded by heavy lines. The light dashed lines show a section through the system at X_{CO₂} = 0.2.

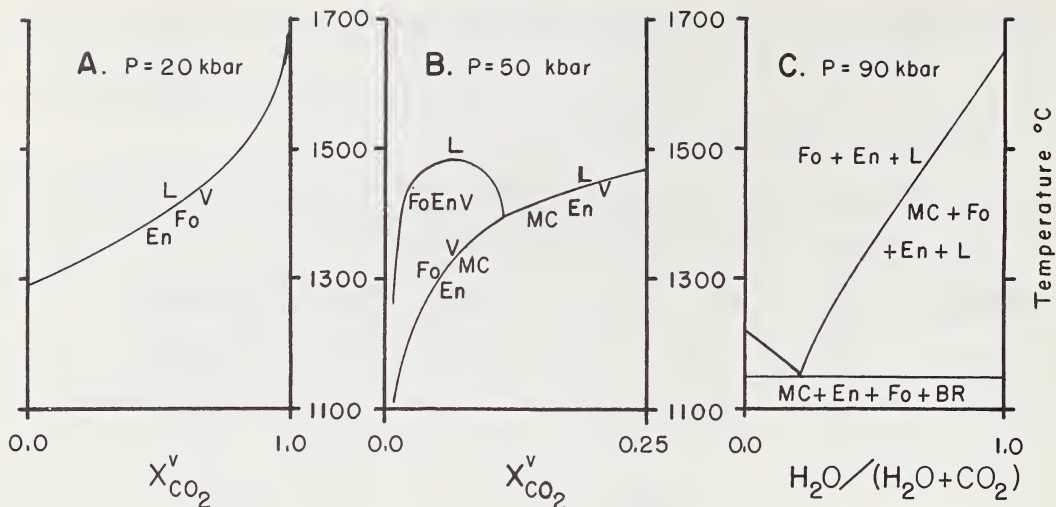


Figure 2. Sections through Figure 1 at 20, 50, and 90 kbar. The range of vapor compositions with which forsterite plus enstatite may coexist becomes smaller as pressure is increased, until at about 90 kbar they no longer coexist with vapor and the first melting takes the form of a eutectic.

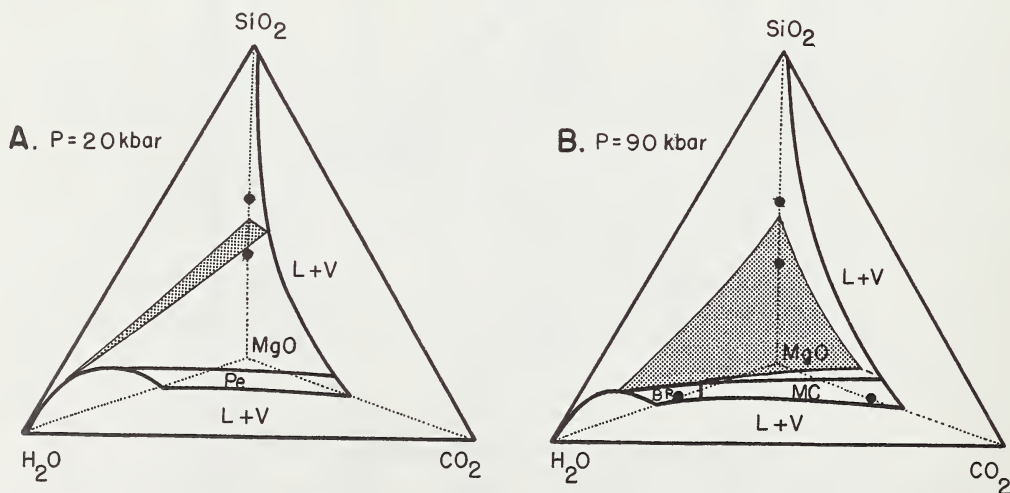


Figure 3. Partial isobaric liquidus diagrams for the system $\text{MgO-SiO}_2\text{-H}_2\text{O-CO}_2$ at 20 and 90 kbar. The plane of liquid compositions coexisting with forsterite plus enstatite is stippled. As pressure increases, the volatile-rich parts of that plane become increasingly silica-undersaturated. The compositions of stable binary compounds are shown by large black dots. All compositions are mole percent.

MINERAL CHEMISTRY OF THE PREMIER MINE KIMBERLITE

Don Elthon and W. Ian Ridley

Lamont-Doherty Geological Observatory of Columbia University

Palisades, New York 10964

The detailed crystallization history of kimberlite magmas still remains poorly understood compared to our knowledge of the xenoliths carried by these magmas. In the present study we have performed detailed microprobe analyses of oxide and silicate minerals occurring as phenocrysts, xenocrysts and matrix phases in a fresh kimberlite from the Premier Mine, South Africa.

The oxide minerals represent a complex yet systematic series of mineral assemblages. Picroilmenite (6-16% MgO) is the most distinctive kimberlite oxide mineral occurring as both inversely zoned and unzoned crystals. Typically, the inversely zoned crystals have MgO, TiO₂, MnO and CaO enriched rims with Fe₂O₃-rich cores, while Cr₂O₃, Al₂O₃ and FeO remain relatively constant from core to rim. However, in many instances, both FeO and Fe₂O₃ increase from rim to core with FeO/Fe₂O₃ remaining relatively constant. The larger picroilmenite grains may be chemically unzoned or erratically zoned with granoblastic textures. The picroilmenites are always mantled by perovskite and Ti, Mg, Cr, Al magnetites.

Textural evidence indicates that during the evolution of kimberlitic magmas picroilmenite undergoes a peritectic-like reaction with the liquid to produce these mantles of perovskite and Ti, Mg, Cr, Al magnetite. The perovskites comprising these mantles are slightly zoned with Cr-rich and Al-poor regions adjacent to picroilmenite and Cr-poor and Al-rich rims adjacent to the groundmass.

The presence of rutile in many mineralogical associations demonstrates its importance in the evolution of kimberlitic magmas. These rutile grains have ~ 1% Cr₂O₃, ~ 1% Fe₂O₃, ~ 1% MgO, and 0.5% Al₂O₃. Rutile is common as lensoidal intergrowths within both the perovskites mantling picroilmenite and the picroilmenite itself. Often it appears that rutile has resulted by exsolution from picroilmenite. The occurrence of armalcolite associated with rutile and picroilmenite in South African kimberlites (DuToitspan) has been reported by Haggerty (1975). In some instances that we have examined, rutile and picroilmenite intergrowths may have resulted from the breakdown of armalcolite. Rarely, rutile is found as a distinct crystal mantled by perovskite plus Ti, Mg, Cr magnetites. The other common occurrence of rutile is as inclusions within phlogopite crystals. Due to their encapsulation by phlogopite, these rutiles have not developed later crystallizing perovskite and Ti, Mg, Cr, Al magnetite reaction mantles.

Although some rutile grains may have been produced by exsolution from picroilmenite or decomposition of armalcolite into picroilmenite plus rutile, the rutiles associated with phlogopite crystals cannot be attributed to these processes. They are not associated with picroilmenite and must be crystallized directly from the kimberlitic magma.

Red chromium spinels are occasionally found in the groundmass or as inclusions within xenocrysts. Their chemical similarity to chromites from peridotite nodules as well as their mode of occurrence suggests a xenocrystic origin during ascent of the kimberlitic magma. When not enveloped by xenocrysts, the chromites are mantled by perovskite and Ti, Mg, Cr, Al magnetites.

The presence of opx, cpx, garnet, olivine and phlogopite megacrysts within the kimberlite matrix enables a comparison of xenocrystic and phenocrystic phases to be made. Diopside, opx and pyrope garnets are common in megacrysts but are not found as phenocrysts or groundmass minerals. However, both olivine and phlogopite are abundant as megacrysts and as groundmass minerals. It is possible to distinguish groundmass and phenocrystic phlogopites from xenocrystic phlogopites by higher Cr_2O_3 , Al_2O_3 , and lower FeO in the latter. It is also possible to distinguish two generations of olivines by microprobe analyses. Olivine megacrysts and xenocrysts (Fo_{94-92}) are distinct from the groundmass olivines which are more iron rich (Fo_{90-88}); the more fayalite rich rims of olivines have all been partially serpentinized. The groundmass is composed of serpentine, sulfide microphenocrysts, carbonate, perovskite and Ti, Mg, Cr, Al magnetite

During the early evolution of a kimberlitic magma at high pressure, minerals such as opx, cpx, olivine, garnet, phlogopite, and Mg-carbonates must be liquidus phases. Of these minerals, only olivine and phlogopite have extended crystallization intervals, continuing to crystallize at low pressure. Other minerals such as perovskite and Ti, Mg, Cr, Al magnetites are formed only during the groundmass crystallization of a kimberlitic magma; vast physiochemical changes must occur as evidenced by the changes in mineralogical associations.

Haggerty, S.E. (1975) The Chemistry and Genesis of Opaque Minerals in Kimberlite. Phys. Chem. Earth 9, 295-307.

POTASSIC RICHTERITE BEARING PERIDOTITES FROM KIMBERLITE AND THE EVIDENCE THEY PROVIDE FOR UPPER MANTLE METASOMATISM

A. J. Erlank and R.S. Rickard (Department of Geochemistry, University of Cape Town, Rondebosch, South Africa)

Introduction: The occurrence of the rare amphibole potassic richterite $\text{KNaCaMg}_5\text{Si}_8\text{O}_{22}(\text{OH},\text{F})_2$ in kimberlitic materials was described by Erlank (1973). The presence of this mineral has now been confirmed by microprobe analysis in 24 peridotite nodules including two samples described by Aoki (1976) and Dawson and Smith (1977), which have been made available by these authors for us to study. Apart from two samples from the De Beers and Monastery pipes all are from the Bultfontein pipe. Nodules from the latter locality have been the most intensively studied, and it is estimated that K-richterite bearing varieties comprise 5% of all nodules found at this locality. The ensuing discussion is directed to the Bultfontein nodules, unless otherwise indicated. Not all these nodules have been fully investigated, but available data indicate the following.

Bulk rock chemistry: In general, the K-richterite bearing nodules have major and minor element compositions similar to other nodules. The most obvious differences are that K-richterite bearing nodules have, on average, lower Al concentrations and higher contents of K, Na, Ti, Rb, Ba, Sr, Zr and Nb. Phlogopite bearing nodules which lack K-richterite are also somewhat enriched in the same elements but never reach the extremes of enrichment shown by those nodules containing K-richterite. Ranges found in K-richterite bearing nodules are: (%) Al_2O_3 , 0.1-1.6; TiO_2 , 0.04-0.4; Na_2O , 0.07-0.7; K_2O , 0.1-2.1; (ppm) Rb, 4-75; Ba, 26-149; Sr, 40-237; Zr, 12-162 ppm; Nb, 2-36.

Mineralogy: The dominant minerals in most K-richterite bearing nodules are olivine (Fo_{87-92}) and lesser amounts of enstatite (En_{90-93} , Al_2O_3 generally <0.1%) and phlogopite (2.6-5.3% FeO, 0.1-0.9% TiO_2 , 0.1-0.6% Cr_2O_3 , $\text{Mg}/\text{Mg}+\text{Fe} = 0.90-0.95$, $\text{Si}+\text{Al}$ usually <8). K-richterite varies widely in modal abundance within and between nodules; in some cases it may comprise a quarter of a thin section, in other cases it may be necessary to cut several thin sections from a nodule before its presence is revealed. Its chemistry is marked by high K and Na, low Al, and cation proportions of $\text{Si}+\text{Al}<8$ (Table 1). Diopside (generally 0.2-0.5% Al_2O_3 , $\text{Mg}/\text{Mg}+\text{Fe}=0.89-0.93$, $\text{Ca}/\text{Ca}+\text{Mg}=0.43-0.48$) is present in about half the samples studied; it is noteworthy that it is often absent in those samples which contain the most K-richterite. Varying amounts of opaque oxides are present; generally these are Al-poor chromites. Mg-rich ilmenites are subordinate, and possibly related to kimberlite contamination. Two nodules contain an unidentified opaque mineral similar to that described by Haggerty (1975) in phlogopite from the De Beers Kimberlite. Provisional analysis of this phase yields the following data (in wt.%): $\text{TiO}_2=52.5$, $\text{Cr}_2\text{O}_3=13.0$, $\text{FeO}=13.6$, $\text{MgO}=3.1$, $\text{BaO}=9.1$, $\text{ZrO}_2=7.4$, $\text{SrO}=2.4$, $\text{Nb}_2\text{O}_5 \sim 0.5$. Calcite is often present as lamellae in phlogopite, and in one sample is enclosed as euhedral grains in diopside. Garnet ($\text{Py}_{73}\text{Alm}_{15}\text{Gr}_{12}$) is present only in the nodule sample from Monastery, in the form of small rounded grains armoured in olivine. The K-richterite, enstatite and diopside in this nodule have the highest Al_2O_3 contents of those analysed (4.0, 0.9 and 1.6% respectively).

Individual phases within specific nodules show no compositional variability, except in two nodules which contain K-richterite rich veins where small corroded diopsides show appreciable variation in Cr, and possibly Na and Al. Another nodule, which is altered, shows appreciable variations in Na and K between different grains of K-richterite.

Textures: All but one of the nodules have a coarse or granular texture; the exception has a porphyroclastic texture and it is significant that both phlogopite and K-richterite in this sample have been deformed. Interpretation of the origin of the K-richterite is partly dependant on the textural relationship it

exhibits with the other minerals in the nodules under consideration. The K-richterite appears to be texturally equilibrated with the other minerals and in many nodules evidence for its origin is equivocal. However, the following features are important: (a) the K-richterite is clearly a late crystallizing phase because it often poikilolithically encloses the other minerals and is never itself enclosed. Several well formed K-richterite oikocrysts are of the order of 10mms in length (b) clear evidence for replacement is present in a few nodules with K-richterite corroding and embaying other minerals along grain boundaries, and enclosing optically continuous corroded grains of the same mineral (c) two nodules are traversed by more or less linear veins (one up to 3mms wide and 12 cms long) composed dominantly of K-richterite enclosing phlogopite and diopside. The K-richterite is not confined to the veins but is also present throughout these two nodules (d) there is a tendency for a close spatial association of phlogopite, diopside and K-richterite, with chromite often being enclosed in or associated with the phlogopite.

Origin of K-richterite: The bulk rock, mineralogical and textural evidence presented above, indicate that K-richterite is a late stage replacement mineral, and is probably the product of mantle metasomatism. This conclusion is in agreement with the preliminary reports by Erlank (1976) and Aoki (1976) which were based on studies of only a few nodules. The metasomatic process is dominated by the introduction of K (and Rb, Ba) with variable addition of Na, Ti, Sr, Zr and Nb, and occurred in or produced Al-deficient environments. Garnet (except armoured garnets as described in one nodule) or aluminous spinels could not have been present at the time of K-richterite formation, since the latter is not stable in the presence of garnet (Kushiro and Erlank, 1970). We infer that K-richterite is produced by reaction of olivine, enstatite, diopside and probably even phlogopite with a fluid phase containing K and other elements. Appropriate reactions may be written, except that we do not yet understand the role of the unidentified Ti-rich opaque minerals described above.

Mantle Metasomatism: We suggest that the K-richterite bearing nodules only represent the end product of the postulated upper mantle metasomatic process. A large proportion of the nodule suite at Bultfontein contains phlogopite, but no K-richterite. In these nodules there is also clear evidence of replacement textures with garnet being replaced by phlogopite and diopside. In garnet-free harzburgites enstatite is preferentially replaced by phlogopite, and in garnet-free lherzolites, diopside appears to be replaced by phlogopite. In all cases there is a strong association of phlogopite with chromite. Furthermore, these observations can be extended to nodules from Monastery and the other pipes from the Kimberley area. Thus we envisage that similar processes have produced both K-richterite and phlogopite indicating widespread upper mantle metasomatism. A generalized overall reaction could be: Olivine + Enstatite + Garnet + Diopside₁ + Fluid (K₂O etc, H₂O, CO₂) → Phlogopite + Diopside₂ + K-richterite + Calcite + chromite or other opaque minerals. The sequence of change (ignoring calcite and opaque minerals) would be lherzolite or harzburgite + garnet → lherzolite or harzburgite + garnet + phlogopite → lherzolite or harzburgite + phlogopite + K-richterite. Thus we believe that K-richterite is rare because normally either too much Al (garnet) is present in the original nodule or not enough K etc is supplied. In either case the resultant, and more common, assemblage would include phlogopite (+ garnet) rather than phlogopite and K-richterite. Sr-isotope studies (Erlank and Shimizu, this volume) indicate that the metasomatic event pre-dates kimberlite emplacement, is isotopically unrelated to the enclosing kimberlite, and is thus of upper mantle origin. The metasomatic process described above may be only one of a series of such processes that could occur in the upper mantle leading to lithospheric differentiation and enrichment, and it should be viewed in the context of the overall history of a kimberlite peridotite nodule as depicted in Fig. 1.

Table 1. Composition of K-richterites

	Weight %				Ionic Proportions (O=23,000)			
	1	2	3		1	2	3	
	Range		Ave.					
SiO ₂	53.6	56.0	54.4-56.3	55.4	Si	7470	7820	7782
TiO ₂	0.07	0.31	0.27-1.52	0.46	Ti	7	33	48
Al ₂ O ₃	4.01	0.99	0.47-1.70	0.99	Al	659	163	164
Cr ₂ O ₃	1.16	0.34	0.26-0.89	0.48	Cr	128	38	53
FeO	2.51	2.66	1.55-3.45	2.25	Fe	293	311	264
MgO	22.4	22.9	22.3-23.7	22.9	Mg	4653	4766	4797
CaO	6.98	6.83	5.09-7.65	6.74	Ca	1042	1022	1013
Na ₂ O	4.92	3.40	3.29-4.41	3.82	Na	1330	921	1040
K ₂ O	2.35	4.85	3.56-4.98	4.63	K	418	864	830
Total	98.0	98.3		97.7	Total	16,003	15,939	15,996

1 = Monastery JJG 41, 2 = De Beers 106, 3 = Bultfontein (22 samples).

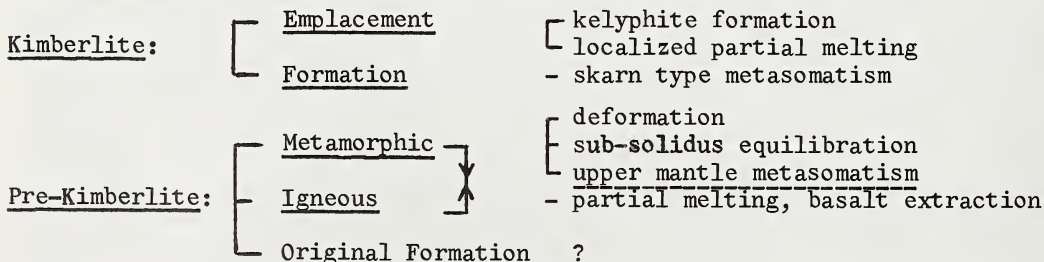
Acknowledgment: We are indebted to J.J. Gurney, J.B. Dawson and Ken-ichiro Aoki for allowing us access to their collections, and to J.J. Gurney for supplying us with unpublished whole rock data for five K-richterite nodules.

References:

- Aoki, K. (1976) Contrib. Mineral. Petrol. 53, 145.
 Dawson, J.B. and Smith, J.V. (1977) Geochim. Cosmochim. Acta 41, 309.
 Erlank, A.J. (1973) Extended Abstracts, 1st Int. Kimb. Conf., 103.
 Erlank, A.J. (1976) Eos 57, 597
 Haggerty, S.E. (1975) Phy. Chem. Earth 9, 295
 Kushiro, I. and Erlank, A.J. (1970) Carnegie Instit. Wash. Year Book 68, 231.

Fig. 1. Possible history of a kimberlite peridotite nodule.

Post Kimberlite: surface weathering, serpentinisation ?



COMPARATIVE CHEMICAL-MINERALOGIC INVESTIGATION OF FIVE WESTERN ALPINE LHERZOLITE COMPLEXES

W. G. Ernst (Department of Earth and Space Sciences; Institute of Geophysics
and Planetary Physics, University of California, Los Angeles, CA 90024)

Petrotectonic Setting:

The Alpine orogenic belt apparently marks the site of convergent lithospheric plate motion during Late Mesozoic and Early Cenozoic time. Prior to this complex event, Early Mesozoic rifting evidently resulted in generation of the Jurassic-Early Cretaceous Tethyan basin which separated the northern and western European plate from the more southeasterly South Alpine plate. The hypothesized onset of rapid convergence in Late Cretaceous time caused consumption of the intervening sea floor and mantle underpinnings along a southward and eastward dipping subduction zone (=Alpine Suture), and seems to have culminated in the collision of both northern and southern continental crust-capped sections and a partial subduction of the European sialic margin.

Ultramafic rocks of the Western Alps appear to reflect several different lithologic entities. (1) A first group represents pre-Jurassic mantle fragments which constitute an in situ portion of the terrane subjected to the multistage Alpine tectonic and metamorphic events. An example may be the Malenco complex; this mass exhibits the effects of Alpine deformation and metamorphism(s). (2) A second group consists of peridotites which lie structurally beneath the continental (locally oceanic) crust capping the Southern Alpine plate. The subcontinental Finero body, terminated on the northwest by the Insubric Line, is of this type inasmuch as it clearly occupies a basal portion of the southern continental crust-capped plate; its age of recrystallization appears to be pre-Mesozoic. Other peridotite massifs of unknown age may have formed beneath more oceanic portions of the South Alpine plate and were subsequently transported north and west during closure of Mesozoic Tethys. (3) A third ultramafic group is ophiolitic and is associated with the Mesozoic metasedimentary cover of the more southeasterly portions of the Tethyan-European plate. Typical examples include intensely serpentized peridotites of the Zermatt-Saas area east of the Dent Blanche nappe and the eclogite-bearing Voltri serpentinites of the Ligurian Alps. (4) Yet a fourth variety of ultramafic body in the Alps consists of peridotite derived from deep within the upper mantle and emplaced tectonically within the metamorphosed section of continental crust during or after most of the Alpine age recrystallization had occurred. Although its origin is still uncertain, the Alpe Arami garnet peridotite may belong to this group.

Rock and Mineral Chemistry:

Petrochemical study has been undertaken of five peridotite bodies exposed at Alpe Arami in southern Switzerland, and at Finero, Balmuccia, Baldissero and Lanzo in northwestern Italy. The Alpe Arami mass has been tectonically emplaced within the in part subducted, more northerly European-Tethyan lithospheric plate, whereas the other four ultramafic masses represent portions of the nonsubducted South Alpine plate.

The eighty samples examined are chiefly lherzolites, but a few are clinopyroxene-bearing harzburgites, olivine websterites or clinopyroxenite. Alpe Arami peridotites locally contain garnet; in contrast, the South Alpine lherzolites are spinel- ± plagioclase-bearing. All masses display strain

effects such as bent lamellae in pyroxenes, gradational or sectoral optical extinction, and minor recrystallization. Twenty-four bulk XRF analyses demonstrate that the investigated rocks closely match pyrolite composition, but are slightly impoverished in alumina. Normative olivines of all analyzed specimens have Fa contents ranging between 8 and 10 mole percent. Electron microprobe analyses for 26 olivines, 27 orthopyroxenes, 23 calcic pyroxenes, 3 garnets, 18 spinels, 3 plagioclases, 13 calcic amphiboles, 2 chlorites, and 2 phlogopites were performed. Phases in a particular sample are remarkably homogeneous, an observation consistent with an inferred close approach to chemical equilibrium.

Apparent temperatures of equilibration for opx + cpx-bearing peridotites were determined employing a variety of methods. Average values in °C and one standard deviation for each body are:

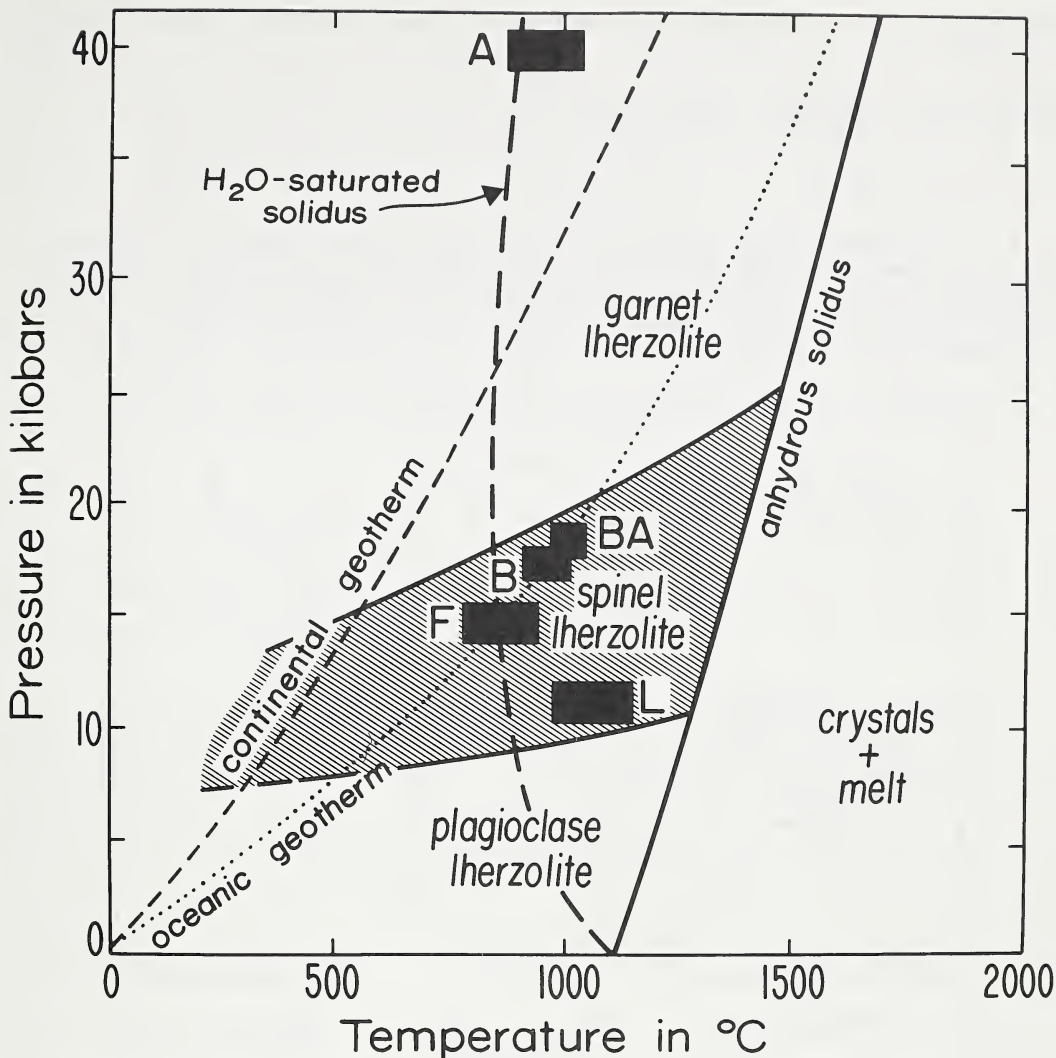
Area	Mysen (1976)	Lindsley & Dixon (1976)	Wood & Banno (1973)	Mysen & Boettcher (1975)	Grand Average
Alpe Arami	921 ± 58	1009 ± 87	1026 ± 44	908 ± 56	966 ± 78
Finero	848 ± 32	785 ± 50	966 ± 27	972 ± 81	893 ± 94
Balmuccia	966 ± 43	960 ± 75	971 ± 41	996 ± 44	973 ± 50
Baldissero	1002 ± 29	1026 ± 45	973 ± 25	1013 ± 32	1002 ± 37
Lanzo	1018 ± 56	1044 ± 88	1049 ± 43	1165 ± 72	1069 ± 85

Pressure estimates for the Alpe Arami mass depend critically on the method used, but cluster about 40 ± 10 kb; South Alpine lherzolites appear to have recrystallized within the range 5-20 kb. Apparent physical conditions of origin are shown in Fig. 1.

Interpretations:

Geologic and petrologic relationships demonstrate that, with the possible exception of the Finero complex, all the studied peridotites are bounded by faults or sheared contacts, hence were transported from elsewhere and tectonically emplaced in their present (deep) crustal surroundings. All five bodies exhibit mantle mineralogies and bulk rock chemistries. The phase assemblages indicate final apparent equilibration temperatures of about 900-1100°C, also reflecting a mantle origin. Pressure evaluation is more difficult, but clearly the Alpe Arami garnet lherzolite came from depths exceeding 70, and probably approaching 150 km. In contrast the four investigated spinel peridotites of the Southern Alpine plate appear to have equilibrated at shallow depths within the uppermost mantle.

Subsequent to their crystallization, transit towards the present crustal levels resulted in solid-state reequilibration; in some cases partial fusion accompanied this rise, producing mafic dikes and layers, especially in the Lanzo and Finero massifs, to a lesser extent in the Balmuccia complex, and perhaps only incipiently at Baldissero. If the grand average apparent temperature, $893 \pm 94^\circ\text{C}$, determined in the present study for two Finero samples closely approaches the true value, then partial melting of this largely recrystallized massif must have required at least a moderate activity of H₂O. In contrast, the P-T path followed by the ascending Alpe Arami body certainly did not intersect the peridotite solidus, as indicated by the lack of partial fusion phenomena. Hornblende may be part of the primary assemblage in some of the South Alpine peridotites, whereas it is definitely later than the garnet



lherzolitic phase compatibility at Alpe Arami. Judging from the calcic amphibole high-pressure stability limit of about 20-25 kb, even at $P_{\text{fluid}} = P_{\text{total}}$, the Southern Alpine peridotites must have crystallized at somewhat shallower depths than the Alpe Arami body.

Referring to Fig. 1, it seems likely that the garnet lherzolite now exposed at Alpe Arami was derived from a portion of the deep upper mantle characterized by a subcontinental geothermal gradient; the manner in which this small, dense mass was incorporated in the northern European plate is perplexing. The Southern Alpine spinel lherzolites, on the other hand, seem to have formed or recrystallized in much shallower, higher heat flow environments (i.e., typified by suboceanic geothermal gradients). Perhaps these latter peridotites represent fragments of mantle material derived from the northerly termination of the South Alpine lithospheric plate, where continental crust was thin--as at Finero--or nonexistent. Their high-temperature, low-pressure mineral assemblages seem to indicate a history which involved reequilibration under physical conditions more appropriate to an oceanic rather than a continental thermal regime, and to preclude an origin well within the continental crust-capped South Alpine plate.

PETROCHEMISTRY OF KIMBERLITIC ROCKS AND ASSOCIATED XENOLITHS OF SOUTH-EASTERN AUSTRALIA

John Ferguson (Bureau of Mineral Resources,
J.W. Sheraton P.O. Box 378, Canberra City, A.C.T. 2601, Australia)

Fourteen widely-separated areas of kimberlitic rocks have recently been discovered in south-eastern Australia in the States of South Australia, Tasmania, Victoria, and New South Wales (Fig. 1). (Locality details, structural relations and ages are given by Stracke et al., this volume). One of the occurrences exhibits an intimate spatial association with carbonatite.

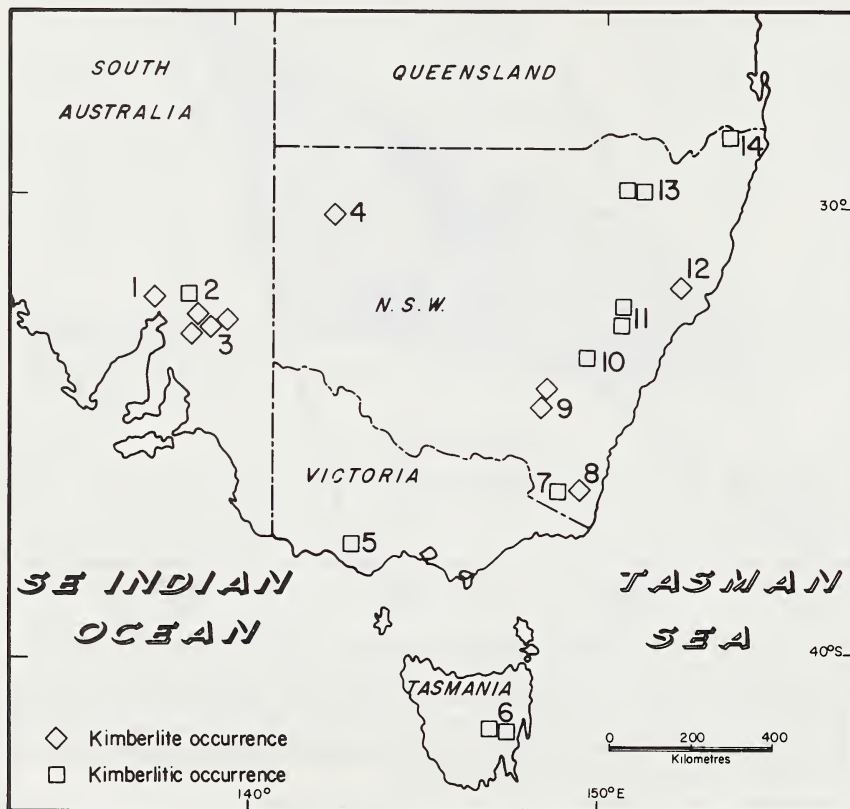


Fig. 1 Localities of kimberlite and kimberlitic occurrences in south-eastern Australia.

Areas: 1 = Pt. Augusta; 2 = Walloway; 3 = Terowie;
4 = White Cliffs; 5 = Bullenmerri; 6 = Oatlands; 7 = Delegate;
8 = Bombala; 9 = Jugiong; 10 = Abercrombie; 11 = Nulla Mountain;
12 = Gloucester; 13 = Bingara; 14 = Mt. Brown.

Analyses were carried out on mineral concentrates comprising one or more of the minerals clinopyroxene, garnet, and ilmenite, and were obtained from seven of the kimberlitic occurrences. Lherzolite nodules were obtained from two areas, and eclogite nodules from four areas. The garnet compositions are given in terms of the cluster group classification of Dawson and Stephens (1975) for garnets from kimberlites and associated xenoliths. By far the greatest proportion of garnets, including those from nodules and concentrates, fall into cluster 9. Cluster group 5 garnets also occur, but are confined to concentrates. Cluster group 3 garnets are found in concentrates and in some eclogites. With only minor exceptions, all cluster group 9 garnets from south-eastern Australian kimberlitic occurrences fall into the lherzolite field as defined by Boyd (1970) in terms of the ternary parameters Ca-Mg-(Fe²⁺ + Mn), and Cr-Fe³⁺ - Al. Similarly, they also fall within field II, as defined by Sobolev (1977), for the Russian occurrences of garnets from peridotite xenoliths. Over half the concentrate clinopyroxenes are chrome diopsides with Mg/Mg + Fe²⁺ ratios between 0.89 and 0.93, and Ca/Ca + Mg ratios of 0.45 to 0.50. Diopsides from lherzolite inclusions are virtually identical in composition to the concentrates from the same intrusions, which, together with similarities in garnet compositions suggest that the latter represent xenocrysts derived by fragmentation of similar nodular material. Ilmenite concentrates were recovered from five areas: in terms of the molecular proportions of ilmenite-geikielite-hematite those from two areas fall into the kimberlitic field; the remainder are Fe-enriched having chemical similarities to those found in alnoite (Frick, 1973; Mitchell, 1977).

The investigated kimberlitic rocks of south-eastern Australia may be divided into two chemically distinct groups, which define divergent trends within the CMAS tetrahedron. The South Australian kimberlites, notably those from the Walloway area, form part of the typical trend shown by kimberlites and related alkaline ultramafic rocks of southern Africa (Ferguson et al., 1975; McIver and Ferguson, this volume), and fall towards the more evolved end of this trend. Kimberlitic rocks of this type are considered to have been formed by small degrees of partial melting of phlogopite-bearing garnet lherzolite at depths exceeding 125 km. Olivine and orthopyroxene were the main fractionating phases during the early stages of kimberlite evolution, whereas the more evolved rocks may be explained on the basis of olivine-dominated fractionation; garnet and clinopyroxene do not appear to have been significant fractionating phases. The kimberlitic rocks of the Jugiong and Delegate areas have close chemical affinities with olivine nephelinites and related rocks, and appear to be unrelated to the 'normal' kimberlitic trend. Consideration of phase relationships in the CMAS tetrahedron (after O'Hara, 1968) indicate equilibrium pressures of about 20 kb, and the observed chemical variation may be explained on the basis of relatively minor olivine and possibly orthopyroxene fractionation. T-P conditions of 1240 ± 20°C and 22 ± 1 kb for these nodules are indicated by temperature estimates based on compositions of coexisting minerals in lherzolite and eclogite nodules (Mori, 1977; Råheim and Green, 1974), together with the occurrence of a unique garnet-spinel lherzolite inclusion containing an equilibrium assemblage falling on the quasi-univariant boundary between the spinel and garnet lherzolite fields (Ferguson et al., 1977). This is well supported by the data obtained for the host rocks. The very high geothermal gradient implied by these estimates suggests that kimberlitic magma could have been generated by small degrees of partial melting of garnet lherzolite at depths of about 70 km, and at temperatures of about 1300°C.

The abnormally high geothermal gradient present when the olivine nephelinite magmas of the Jugiong area were generated intersects the diamond/graphite inversion curve at much greater pressures and temperatures than those indicated by the nodules, so that it is highly unlikely that diamondiferous kimberlites of Cainozoic age occur in this part of New South Wales.

References

- Boyd, F.R. (1970). Garnet peridotites and the system $\text{CaSiO}_3\text{-MgSiO}_3\text{-Al}_2\text{O}_3$. Mineral. Soc. Amer. Spec. Pap. 3, 63-67.
- Dawson, J.B. and Stephens, W.E. (1975). Statistical classification of garnets from kimberlite and associated xenoliths. J. Geol. 83, 589-607.
- Ferguson, J., Martin, H., Nicolaysen, L.O. and Danchin, R.V. (1975). Gross Brukkaros: a kimberlite-carbonatite volcano. Phys. Chem. Earth 2, 219-234.
- Ferguson, John, Ellis, D.J. and England, R.N. (1977). Unique spinel-garnet lherzolite inclusion in kimberlite from Australia. Geology, 5, 278-280.
- Frick, C. (1973). Kimberlitic ilmenites. Trans. geol. Soc. S. Afr. 76, 85-94.
- Mitchell, R.H. (1977). Geochemistry of magnesian ilmenites from kimberlites in South Africa and Lesotho. Lithos 10, 29-38.
- Mori, T. (1977). Geothermometry of spinel lherzolites. Contr. Mineral. Petrol. 59, 261-279.
- O'Hara, M.J. (1968). The bearing of phase equilibria studies in synthetic and natural systems on the origin and evolution of basic and ultrabasic rocks. Earth Sci. Rev. 4, 69-133.
- Råheim, A., and Green, D.H. (1974). Experimental determination of the temperature and pressure dependence of the Fe-Mg partition coefficient for coexisting garnet and clinopyroxene. Contr. Mineral. Petrol. 48, 179-204.
- Sobolev, N.V. (1977). Deep-seated inclusions in kimberlites and the problem of the composition of the upper mantle (translated from Russian). American Geophysical Union, Washington, 279p.

MODE OF OCCURRENCE AND TECTONIC CONTROL OF THE KIMBERLITE-BODIES
IN EAST-KASAI (Zaïre).

C.L. Fieremans - Technical Manager - Soci t  Mini re de Bakwanga -
Mbujimayi - Zaïre.

Two main kimberlite fields are known in Zaïre :

- the Mbujimayi-kimberlite field in the East-Kasai province;
- the Kundelungu-kimberlite field in the province of Shaba.

Notwithstanding the fact that the Kundelungu-field is the oldest known (1908) it is only the Mbujimayi-field (where the first diamond was found in 1918 and kimberlite only in 1946) which proved workable.

The Mbujimayi-field is composed of :

- 1°) a northern group of pipes including ten "bodies" of a xeno-tuff-breccia kimberlite showing in places a "sedimentary" aspect and lying on a straight E-W line. Each "body" does not represent necessarily a "pipe";
- 2°) a southern group of 4 pipes, also of a tuff-breccia type.

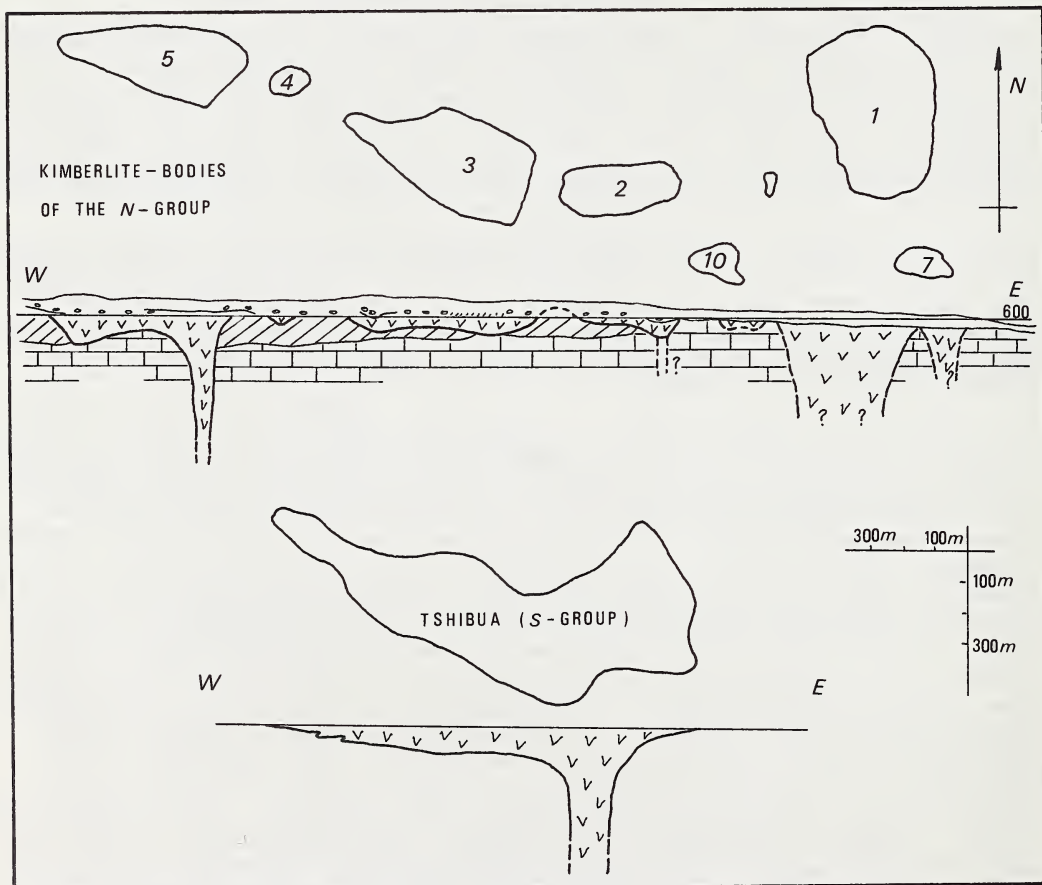
The kimberlite-"bodies" of the northern group exhibit an outstretched elliptical form and small "sacks" of kimberlite tuff occur between them. All lie on an E-W line, interpreted as a crustal fissure of minimum 10 km. length. A deep neck down these bodies is known with certainty in only one case but is suggested in three other cases. The other six bodies constitute tuffaceous material expelled by the four pipes. One body with N-S orientation probably constitutes a pipe situated on a fault perpendicular on the E-W crack.

There is no visible tectonic connection between this northern group of pipes and the southern group, but the biggest kimberlite body of this last cluster (the Tshibua-pipe) shows also a manifest E-W stretched elliptical form. The body is very flat and connected deeply with a neck or pipe of small diameter, intruded in a deep-seated E-W dyke of norite intrusive in the old precambrian gneissic basement.

As to the Russian nomenclature (cf. Dawson) the kimberlite formation can be described as a xeno-tuff-breccia, containing a large quantity of extraneous material : fragments, blocks and minute particles of the intruded formations (precambrian gneissic basement, dolomitic layers of the Mbujimayi-system, mesozoic sandstone layers). The kimberlitic formation also contains numerous fragments and nodules of a "primary kimberlite", of deep-metamorphic and of eclogitic rocks, besides numerous grains of chromiferous pyrope-garnets, magnesian ilmenites, chromiferous diopsides and green phlogopite. Characteristic are also the yellow zircons and the black-brown baddeleyite. The fragments of "primary kimberlite" are always very altered but one may recognize easily two generations of pseudomorphosed olivine-crystals, the biggest being rounded or sub-rounded. The pseudomorphic products comprise mainly serpentine-minerals, montmorillonite and calcite. The inclusions of deep-metamorphic rocks comprise plagioclase gneisses, with oligoclase, garnet, biotite, quartz and sometimes sillimanite. The eclogites comprise diopsidites, typical eclogites and plagioclase eclogites. Very interesting to note are the silicified nodules where the diopside-grains are completely replaced by quartz. Ultrabasic nodules seem very rare and were only mentioned in the Tshibua-pipe.

Diamonds are for somewhat 97 % of the industrial type, as well in the southern as in the northern group of kimberlites; 85 % is crushing-board. Characteristic are the dark green or brown cubes with rough surfaces and the very irregular "cindery" aggregates. As to their grade, the kimberlite-bodies of East-Kasai are the richest in the world.

Some authors have placed the East-Kasai pipes in a linear connection with the Angolan pipes situated at somewhat 400 km to the S.W. In particular some great graben-structure - the "Lucapa-graben" - would unite the two occurrences of pipes. As to our own observations however, as well in Zaïre as in Angola, there is nowhere any precise or definite indication of this graben-structure and the most typical tectonic structure in the basement-complex of the Kasai regions and also in Angola is the appr. E-W structure already mentioned. In Angola the most striking directions connecting the kimberlite intrusions are N. 75° - 85° E. and N. 20° W. These directions were also found back during aeromagnetic surveys and in the ultrabasic and basic dykes intrusive in the basement-complex of Kasai. Due to all this, we think that a relation graben-kimberlite does not exist.



References :

- L. Cahen - Géologie du Congo Belge.
- J.B. Dawson - A review of the geology of Kimberlite - 1967 -
In : Ultramafic and related Rocks - P.J. Wyllie.
- Y. de Magnée - Présence de Kimberlite dans la Zone Diamantifère de Bakwanga (Kasai, Congo Belge) - 1947 - Bull. Soc. B. de Géol. - T. LVI - fasc. 1-2 - 15.4.47.
- C. Fieremans - Les champs diamantifères de l'Angola - 1960 - (unpublished).
- C. Fieremans - Contribution à l'étude pétrographique de la Brèche kimberlitique de Bakwanga - 1966 - Mém. Inst. Géol. Univ. Louvain - T. XXIV - fasc. 1.
- Machado, F.J. de Sousa - The Volcanic Belt of Angola and its Carbonatites - C.C.T.A. - Assoc. Serv. Géol. Africains - Réunion conjointe - Léopoldville 1958 - Publication n° 44.
- C. Meyer de Stadelhofen - Les Brèches kimberlitiques du Territoire de Bakwanga (Congo) - 1963 - Archives des Sciences Soc. Phys. et Hist. Nat. de Genève.
- Fernando Real - Sur les Roches kimberlitiques de la Lunda (Angola) - 1958 - Boletim do Museo e Laboratorio Mineralogico e Geologico da Faculdade de Ciencias da Universidade de Lisboa - n° 26 - 7a Serie.
- B. Reis - Considerações sobre a Aplicação e Métodos de Prospecção Geofísica à Pesquisa de Estruturas Kimberlíticas, no Nordeste da Lunda (Angola) - 1966 - Bol. n° 14 - Serviços de Geologia e Minas - Luanda - Angola - Portugal.
- B. Reis - Preliminary Note on the Distribution and Tectonic Control of Kimberlites in Angola - 1972 - 24th International Geological Congress - Montreal.
- I. Wasilevsky - Note préliminaire sur les Gisements de Brèche kimberlitique de Bakwanga - 1950 - Elisabethville - C.R. du Congrès Scientifique - 50e anniv. du C.S.K. - Vol. II, T. II, pp. 291-332.

EXCHANGE OF Mn, Ca, Mg AND Al BETWEEN SYNTHETIC GARNET, ORTHOPYROXENE,
CLINOPYROXENE AND OLIVINE

Tony A. Finnerty (Geophysical Laboratory, 2801 Upton St., N.W., Washington,
D.C. 20008)

Fifteen exchange reactions among Fe-free garnet lherzolite minerals have been examined for pressure and temperature effects by experiments in the range 10 to 50 kbar and 1100° to 1400°C. Experiments were conducted on an oxide mixture of composition (wt%): MgO, 34.47; Al₂O₃, 8.80; SiO₂, 48.86; CaO, 7.26; MnO, 0.61, that crystallizes at high pressure and temperature to roughly equal proportions of olivine, ortho- and clinopyroxene, and garnet or spinel. The powder was loaded into graphite capsules, and sealed inside Pt in the presence of a (CO₂ + H₂O) - rich fluid, then run in a 1/2-inch diameter piston-cylinder high-pressure apparatus. Six grains of each mineral from each run were analyzed by electron microprobe. Backgrounds were analyzed at each spot for precise determination of Ca in olivine and Mn in all minerals. Standard deviations were less than 10% for Ca in olivine, less than 5% for all other oxides.

Concentrations of Ca in coexisting minerals at 30 kbar (open circles) and 40 kbar (closed circles) are presented in Fig. A. Components were calculated as CaMgSi₂O₆ (Di), Ca₃Al₂Si₃O₁₂ (Gr), and Ca₂SiO₄ (La). Al in pyroxene was combined with Mg as MgAl₂SiO₆ (Mgts). Pyroxene compositions from 30 kbar runs agree with the 20 kbar data of Lindsley and Dixon (1976) in Fig. A (bars represent their reversal brackets) within analytical uncertainty, suggesting attainment of equilibrium in these runs. The natural logarithms of the concentration ratios for several equilibria calculated as, for example, $K = (X_{Gr}/X_{Py})^{1/3} (X_{En}/X_{Di})$ for garnet-pyroxene Ca-Mg exchange, are plotted against inverse temperature in Fig. B through E (numbers beside data points refer to pressure in kbar).

To account for nonideality in Ca-Mg solid solutions, exchange data were fit by least squares techniques to equations of the form:

$$-RT \ln K = \Delta\bar{H}^\circ - T\Delta\bar{S}^\circ + P\Delta\bar{V}^\circ + \sum_q \nu_q \left(\sum_{i \neq q}^{n-1} X_i W_{iq} - \sum_{j=1}^n \sum_{k=j+1}^n X_j X_k W_{jk} \right) \quad (1)$$

($\Delta\bar{H}^\circ$, $\Delta\bar{S}^\circ$ and $\Delta\bar{V}^\circ$ are changes in molar enthalpy, entropy and volume, respectively, for exchange of one cation, q, i, j, k, and n are indices of components, the ν 's are stoichiometric coefficients in the exchange reaction, the X's are mole fractions, and the W's are Margules parameters for symmetric regular solutions). The fits for Ca-Mg and Al exchange were constrained by values (kcal gfw⁻¹) of Ca-Mg Margules parameters of 9.6 (garnet, 12 oxygens), 53.3 (olivine, 4 oxygens), and 5.9 and 25.5 (clino- and orthopyroxene, respectively, 6 oxygens), obtained by fitting data of Newton, et al. (1977), Warner and Luth (1973) and Lindsley and Dixon (1976), respectively, to binary symmetric regular solution models similar to Eqn. 1. Fits to data for exchange of Mn and Mg were unconstrained and, because of low Mn concentrations, an ideal solution model (all W's in Eqn. 1 set equal to zero) was assumed. Results are listed in the table ($\Delta\bar{H}^\circ$ in kcal gfw⁻¹, $\Delta\bar{S}^\circ$ in °K cal gfw⁻¹, $\Delta\bar{V}^\circ$ in cm³ gfw⁻¹, 1σ standard deviations in brackets).

Exchange reactions for Ca and Mg between garnet and orthopyroxene, between garnet and clinopyroxene, and between clinopyroxene and olivine, and for Mn and Mg between clino- and orthopyroxene and between clinopyroxene and olivine, are as temperature sensitive as the diopside-enstatite equilibrium. These may be useful as geothermometers.

The effect of pressure on the exchange equilibria is nearly as large for

Al in clinopyroxene coexisting with garnet as is the case for orthopyroxene. The Mn-Mg equilibria display pressure effects up to 15% as strong as for Al in pyroxenes. Simultaneous solution for pressure and temperature using two of these equilibria whose $\Delta\bar{V}^\circ$'s differ in sign may be useful as alternative barometers, about 30% as sensitive as Al in pyroxenes.

The apparent effects of pressure on Ca-Mg equilibria are strongly dependent upon Al content of the pyroxenes. For example, a fit to the data of Lindley and Dixon (1976) for Al-free diopside-enstatite yielded a value of $\Delta\bar{V}^\circ = -0.43 \pm 0.46 \text{ cm}^3 \text{ gfw}^{-1}$. More experiments are required to calibrate this effect.

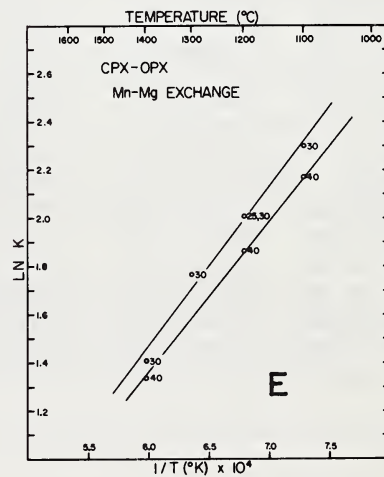
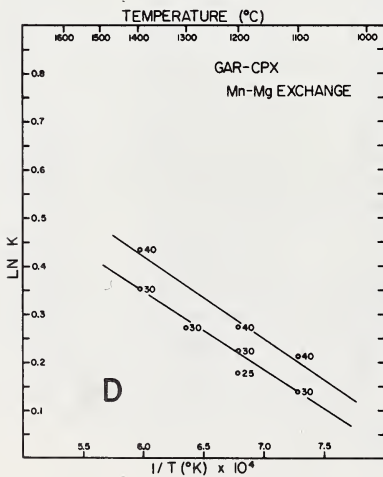
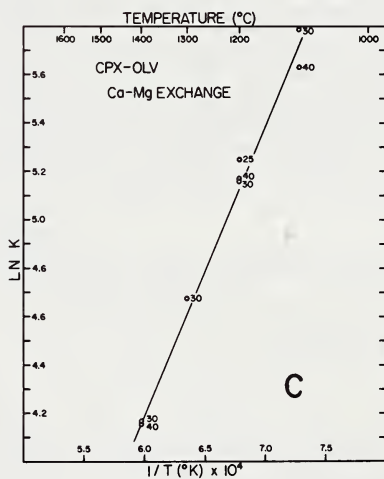
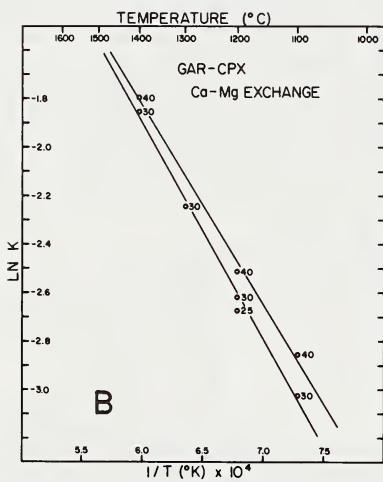
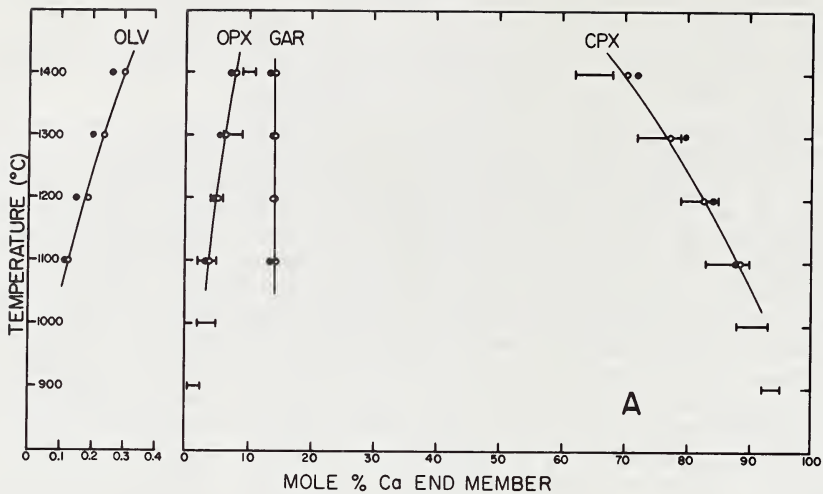
Di content of orthopyroxene coexisting with clinopyroxene in garnet lherzolite nodules used to construct the Lesotho geotherm of Boyd (1973) is lower than expected from experiments. Temperature estimates from Ca-Mg equilibria involving orthopyroxene are 100°-300°C lower than those of Boyd (1973). Strong preference of Fe for ortho- over clinopyroxene is probably responsible for this discrepancy. Simultaneous solution of equations for Mn-Mg exchange between garnet and olivine and between ortho- and clinopyroxene yields temperature estimates whose means are 60°C lower, and pressure estimates that average 1.9 kbar lower (sheared nodules) and 10.5 kbar higher (granular nodules) than the "Al₂O₃-Na₂O" estimates of Boyd (1973), owing most likely to the effect of Cr solution in garnet and clinopyroxene. Application of these exchange data to thermobarometry must await calibration of the effects of other components.

The concentration of CaO in olivine coexisting with ortho- and clinopyroxene decreases by about 0.002 wt% per kbar at fixed temperature, and may be useful as an empirical geobarometer with resolution of about ± 3 kbar. Pressures of equilibration estimated in this way for 14 garnet lherzolite nodules from the Lesotho geotherm (temperatures estimated from diopside compositions) agreed with the "Al₂O₃-Na₂O" estimates of Boyd (1973) to within 5 kbar.

References Cited

- Boyd, F.R., 1973, *Geochim. Cosmochim. Acta*, 37: 2533-2546.
 Lindsley, D.H., and S.A. Dixon, 1976, *Am. J. Sci.*, 276: 1235-1301.
 Newton, R.C., T.V. Charlu, and O.J. Kleppa, 1977, *Geochim. Cosmochim. Acta*, 41: 369-377.
 Warner, R.D., and W.C. Luth, 1973, *Am. Mineral.*, 58: 998-1008.

	$\Delta\bar{H}^\circ$	$\Delta\bar{S}^\circ$	$\Delta\bar{V}^\circ$	$\sigma(\text{fit})$
Gar/Cpx Ca-Mg	3.37(0.24)	0.82(0.14)	-1.36(0.12)	4.22%
Gar/Opx Ca-Mg	10.02(0.76)	5.72(0.46)	2.24(0.34)	1.20%
Gar/Olv Ca-Mg	19.00(0.30)	1.22(0.18)	-0.74(0.15)	0.34%
Cpx/Opx Ca-Mg	15.66(0.57)	4.91(0.34)	3.59(0.29)	0.75%
Cpx/Olv Ca-Mg	15.64(0.45)	0.40(0.28)	0.61(0.23)	0.56%
Opx/Olv Ca-Mg	-0.02(0.96)	-4.50(0.58)	-2.98(0.49)	4.14%
Gar/Cpx Al	10.0(1.6)	1.90(0.99)	5.28(0.83)	2.76%
Gar/Opx Al	1.95(0.90)	-2.01(0.55)	5.90(0.46)	1.79%
Cpx/Opx Al	-12.8(1.1)	-4.29(0.67)	1.26(0.56)	3.92%
Gar/Cpx Mn-Mg	4.09(0.22)	2.75(0.14)	-0.93(0.11)	5.26%
Gar/Opx Mn-Mg	-3.01(0.31)	0.25(0.18)	-0.21(0.15)	1.63%
Gar/Olv Mn-Mg	-3.26(0.31)	0.49(0.19)	-0.40(0.16)	1.36%
Cpx/Opx Mn-Mg	-7.25(0.29)	-2.52(0.18)	0.86(0.15)	2.01%
Cpx/Olv Mn-Mg	-7.35(0.32)	-2.25(0.20)	0.54(0.17)	1.76%
Opx/Olv Mn-Mg	-0.09(0.42)	0.27(0.25)	-0.32(0.21)	10.5%



PETROGENESIS OF SOUTH AFRICAN AND AUSTRALIAN KIMBERLITIC SUITES

F. A. Frey (Earth and Planet. Sci., MIT, Cambridge, Mass. 02139)
J. Ferguson (Bureau Mineral Resources, Canberra, ACT, Aust. 2601)
B. W. Chappell (Dept. of Geology, ANU, Canberra, ACT, Aust. 2600)

Kimberlites have unique geochemical and petrologic features that must reflect their mantle source and the fractionating processes occurring during ascent. In particular, the common occurrence of Mg-rich olivine (Fo₉₄, Mitchell, 1973) and characteristic very high abundances of compatible (e.g., Ni > 800 ppm) and incompatible trace elements (Dawson, 1962) are not features found in basalt suites. In order to determine the composition of their mantle source and to constrain petrogenetic models we are obtaining petrological and geochemical (major and trace element) data for kimberlitic and associated rock suites from South Africa and Australia. The study includes rock types, melilitites, carbonatites and peridotites so that we can evaluate the relationships of these rocks to kimberlite petrogenesis. Where possible kimberlite samples are autoliths which are believed to represent uncontaminated kimberlite (Ferguson et al., 1973; Danchin et al., 1975).

Ferguson et al. (1973) and Danchin et al. (1975) have shown that the major element composition of South African kimberlites and associated rocks can be used to form 7 cluster groups. When projected into a CMAS diagram (O'Hara, 1968) the trend defined by the cluster groups suggests that olivine and orthopyroxene are early fractionating phases in kimberlite magma evolution whereas the more evolved non-kimberlitic rocks lie on a simple olivine control line (Fig. 1 and 2). Ni and Cr abundances decrease systematically from kimberlites to the more evolved cluster groups; but heavy REE and Sc, elements sensitive to eclogite fractionation, increase in abundance by a factor of 2.

In terms of composition the eastern Australian kimberlites are similar to olivine nephelinites, and in the CMAS projections they are distinct from the South African cluster groups. However, as typical of kimberlites, they have high Ni and Cr contents (>800 ppm). When projected from diopside into the C₃A-M-S plane the eastern Australia kimberlites lie in the vicinity of the 20 kb pseudo-invariant point (consistent with an estimate of 22 kb equilibration pressure for a lherzolite inclusion, Ferguson et al., 1977) whereas the trend line of the cluster groups is unrelated to pseudo-invariant points at 20 and 30 kb (Fig. 2).

A well-established geochemical feature of all kimberlitic rocks is their enrichment in incompatible trace elements. For example, light REE typically range from 100 to 1000 x chondrites (Frey et al., 1971; Fesq et al., 1975; Mitchell and Brunfelt, 1975; Paul et al., 1975; and this work). Although there is a general trend of positive correlation among P, Sr, Ba, Th, U and light REE abundances (Fesq et al., 1975) there are distinct differences in trace element composition between different kimberlite

localities. Considering all kimberlites and associated rocks in terms of the cluster groups, there are only weak correlations of increasing incompatible element contents with increased major element differentiation. However, among our samples the olivine melilitite from Saltpetrekop has the highest REE concentrations (Fig. 3), and it also has the most evolved major element composition (Fig. 1 and 2). These South African olivine melilitites have much higher REE concentrations than Hawaiian nepheline and melilite-bearing basalts, but eastern Australian kimberlites have REE abundances similar to highly SiO_2 undersaturated Hawaiian basalts and a Tasmanian olivine melilitite (Fig. 4). Compared to African kimberlites the lower incompatible element abundances of the Australian kimberlites are consistent with an origin by higher degrees of melting and at relatively shallower depths (20-25 kb); for example, Frey et al. (1977) propose 5% melting for a Tasmanian melilite nephelinite.

There is a consensus (Gast, 1968; Frey et al., 1971; Fesq et al., 1975; Mitchell and Brunfelt, 1975; Paul et al., 1975) that the low Sc (<20 ppm) and Y contents and highly fractionated REE distributions of kimberlites reflect an origin by small degrees of melting of a garnet peridotite source. In order to obtain the very high incompatible element abundances it has been suggested that kimberlites derive from an incompatible element enriched source and are affected by zone refining processes. There is evidence that the upper mantle is light REE enriched (relative to chondrites) in some kimberlite areas (Fig. 5). Another popular model for some incompatible elements, such as REE, is that their abundances are strongly controlled by volatile transfer (e.g., Loubet et al., 1972; Mitchell and Bell, 1976). The very high REE abundances in carbonatites has been cited as strong evidence for the role of volatile transfer. However, in the Benfontein sill where Dawson and Hawthorne (1973) documented magmatic sedimentation structures with the formation of spinel-perovskite cumulates and calcite layers (classified as carbonatites), the calcite has relatively low REE concentrations (Fig. 6; also low Y, Zr, Nb and Th), very much unlike carbonatites. Even lower REE abundances were found in the Lashaine carbonatite (Ridley and Dawson, 1975).

As in South African kimberlites, eclogite inclusions occur in eastern Australia kimberlites, but our data do not require an extensive role for eclogite fractionation during kimberlite petrogenesis. For example, small amounts of melting of a moderately light REE enriched (relative to chondrites) garnet peridotite can adequately explain the large La/Yb ratio in kimberlites. However, we point out that the evaluation of eclogite fractionation in terms of REE geochemistry given by Mitchell and Brunfelt (Fig. 8, 1975) is incorrect. For their choice of partition coefficients less than 15% fractionation of eclogite (50% cpx, 50% gar) causes a La/Yb increase of 100 (Fig. 7). A more realistic choice of garnet partition coefficients for heavy REE (Yb garnet/liquid of 4) requires 70% fractionation for a similar La/Yb enrichment.

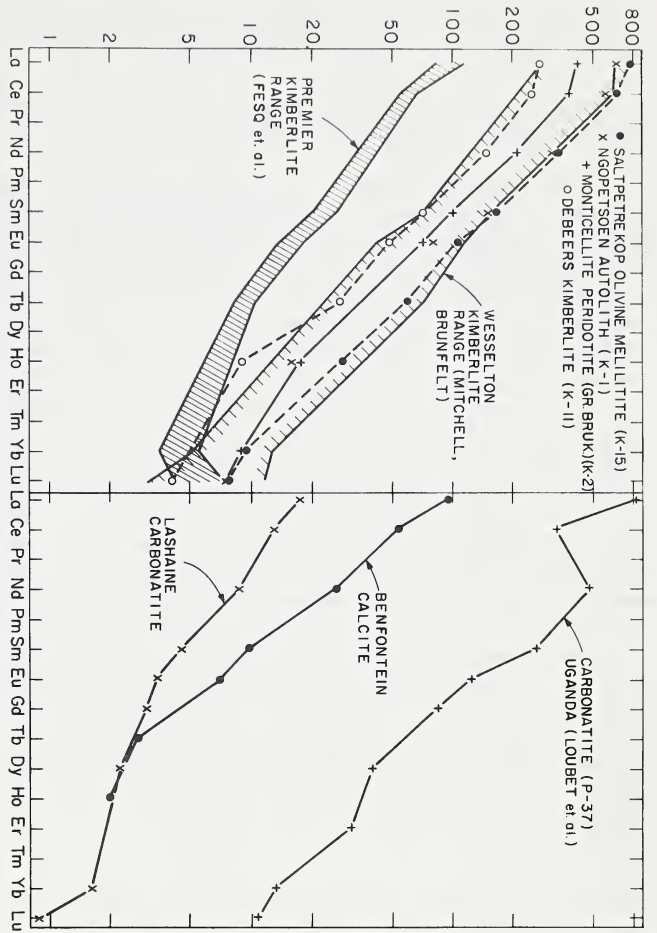


FIG. 3

FIG. 6

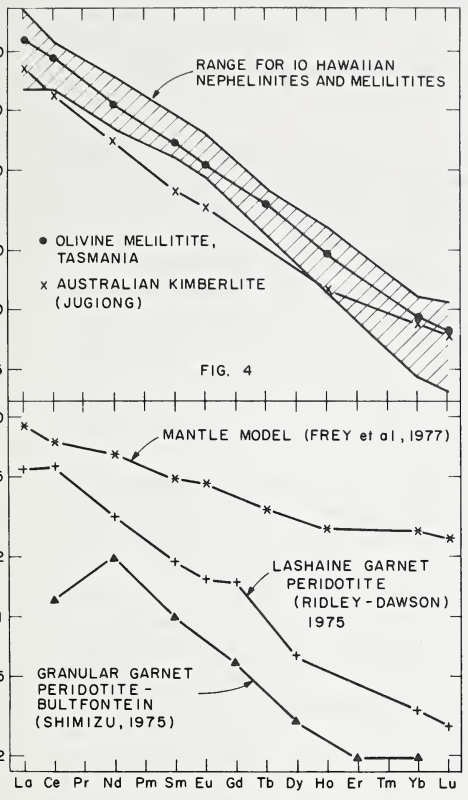


FIG. 4

FIG. 5

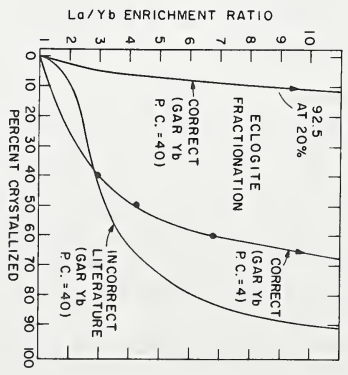


FIG. 7

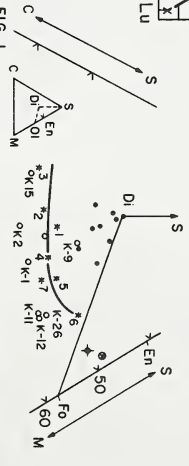


FIG. 1

+ GARNET-SPINEL LHERZOLITE (JUGIONG, AUST.)
 * GARNET LHERZOLITE (S AFRICA)
 • CLUSTER GROUPS
 • EASTERN AUSTRALIA "KIMBERLITES"
 o KIMBERLITES AND RELATED ROCKS (THIS PAPER)

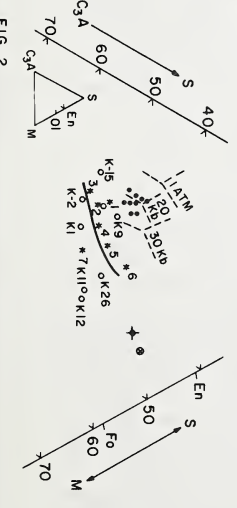


FIG. 2

BLUE SILLIMANITE AND THE ORIGIN OF CRUSTAL XENOLITHS AT KILBOURNE HOLE, NEW MEXICO, USA, AND BOURNAC, HAUTE-LOIRE, FRANCE

E. S. Grew (Department of Earth and Space Sciences, University of California, Los Angeles, California 90024 USA)

Crustal xenoliths of quartzo-feldspathic gneiss containing garnet and blue, colorless, or pale yellow sillimanite are found among the ejecta at Kilbourne Hole and Bournac. These xenoliths have been interpreted as fragments derived from granulite facies rocks at considerable depths in the earth's crust (Padovani and Carter, in press; Leyreloup, 1974). Similar quartzo-feldspathic gneisses containing only colorless or pale yellow sillimanite are common in granulite facies terrains exposed in deeply eroded metamorphic complexes. The aim of the present study is to compare the mineralogy and chemistry of sillimanite and ilmenite from these xenoliths with those from exposed granulite facies terrains. It is hoped that these relatively simple minerals will indicate: (1) differences in the physical conditions of formation of the two parageneses; and (2) the effect of the basaltic host on the xenoliths.

The granulite facies gneisses used for comparison are quartzo-feldspathic gneisses from the Precambrian shield of East Antarctica, most of which contain K-feldspar, plagioclase, garnet, biotite, sillimanite, and ilmenite. Some samples also contain cordierite, magnetite, spinel, rutile, or graphite.

Kilbourne Hole is located in the Rio Grande rift. The xenoliths form cores of basalt bombs in ejecta on bedded tuff overlying an alkaline olivine basalt flow in the Quaternary Afton Basalt (Hoffer, 1976). Depth to Precambrian basement is estimated to be about 6 km (Woodward et al., 1975). Precambrian rocks exposed 45 to 100 km distant include greenschist and amphibolite-facies metamorphic rocks and plutonic rocks, mostly granite (Denison and Hetherington, 1969). No granulite facies rocks have been reported from this area; but the basement in the down-dropped blocks of the rift itself has not been sampled near Kilbourne Hole.

At Bournac, the gneiss xenoliths are fragments in a tuff breccia resting on a gneissic basement and overlain by a "labradorite" (Boule, 1892). The "labradorite" is of alkali affinities (Brousse, 1971), and is one of the Miocene-Pliocene plateau basalts of east Velay, a volcano-tectonic horst (de Goer de Herve and Mergoil, 1971). The gneissic basement is an upper amphibolite facies terrain consisting of sillimanite-orthoclase gneisses, migmatites, and the Guéret-Velay granite containing biotite and cordierite (Chenevoy and Ravier, 1971).

The quartzo-feldspathic gneisses in the Kilbourne Hole and Bournac xenoliths are medium grained, friable, light-colored rocks; those at Kilbourne Hole have a sintered appearance. The gneisses at both localities contain the following minerals: quartz, perthitic K-feldspar (probably sanidine), plagioclase, garnet, prismatic sillimanite, ilmenite, rutile, biotite (Bournac only), and graphite. Glass, in places vesicular, is abundant in the Kilbourne Hole samples, generally as microveinlets or in pools surrounding garnet or orthopyroxene-spinel symplectite. Devitrified glass may be present in small amounts in some of the Bournac xenoliths. Garnet at Kilbourne Hole is partly replaced by the symplectite. Brown rutile is present at both localities; at Kilbourne Hole, some xenoliths also contain purple or blue rutile.

The xenolith ilmenite forms discrete grains free of hematite lamellae and contains 0.06 to 0.35 weight percent MnO, 0.96 to 2.90 weight percent MgO, 0.07 to 2.84 weight percent Al₂O₃, and 0 to 32 mole percent Fe₂O₃ (Figures 1 and 2). The xenolith ilmenites are richer in MgO than the granulite facies ilmenites

from Antarctica (Figure 1). Those from Kilbourne Hole, moreover, are also richer in Al_2O_3 . Sample 76-5-1 is richer in Fe_2O_3 than any of the granulite facies ilmenites.

Sillimanite in the xenoliths is pale yellow (sample 76-5-1 only), colorless, or blue. The pale yellow color is characteristic of iron-rich sillimanite in granulite facies rocks. Blue sillimanite, however, is reported from only 4 other localities in the world, and at none of these is information on the paragenesis available. The author has failed to obtain more information on Bank's (1974) report of blue sillimanite from Kenya, while the reported occurrence by Hattori (1967) in New Zealand appears to be blue kyanite misidentified as sillimanite. Blue sillimanite does occur as a detrital mineral in the gem gravels of Ceylon and Burma, but no information is available on the source rock.

The range in Fe_2O_3 contents for the Kilbourne Hole sillimanite (except for sample 76-5-1) is 0.35 to 0.99 weight percent, and, for Bournac, 0.17 to 0.87 weight percent, more or less within the ranges observed in granulite facies rocks from Antarctica (0.25 to 1.36 weight percent). The iron content of sillimanite in sample 76-5-1 (1.82 weight percent) is greater than that of any of the ilmenite-bearing rocks from Antarctica and is as great as that in sillimanite associated with hematite in granulite facies rocks. The iron content of blue sillimanite is less than that of the colorless. The upper limit for Kilbourne Hole is 0.94 weight percent. At Bournac, the upper limit is only 0.23 weight percent, and blue sillimanite is found only in graphite-bearing rocks.

The distribution of Fe_2O_3 between sillimanite and ilmenite is not regular. By comparison with granulite facies rocks, the xenolith ilmenites have a lower Fe_2O_3 content that would be expected from the composition of coexisting sillimanite (Figure 2).

The major mineralogical and chemical differences between the xenoliths and granulite facies rocks are the blue color of the sillimanite, structural state

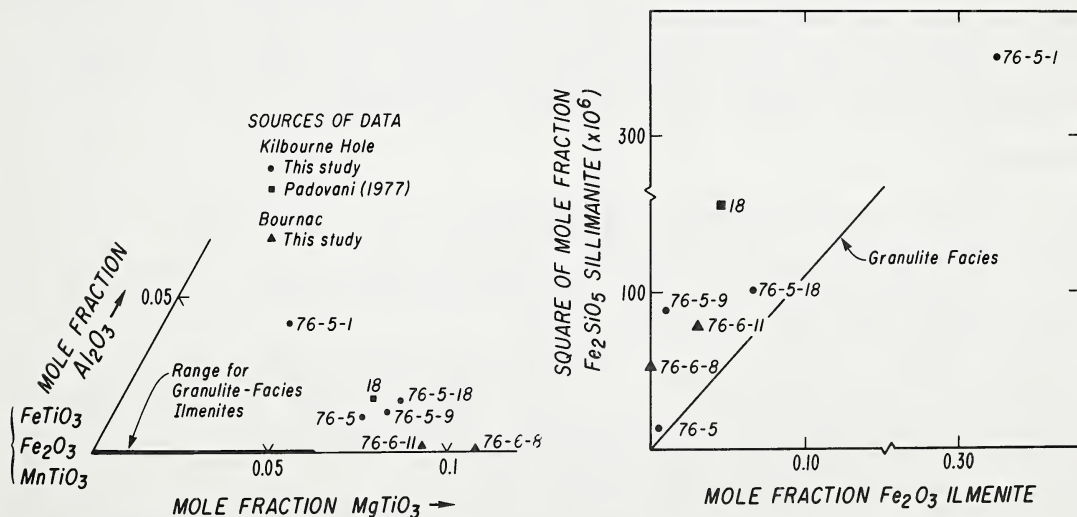
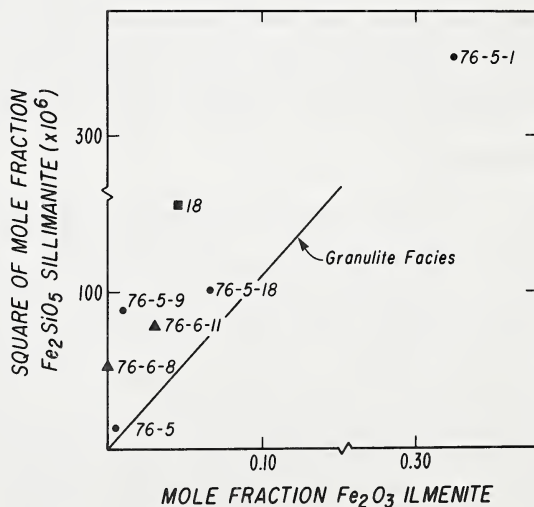


Figure 1. Compositions of ilmenite from crustal xenoliths and from Antarctic granulite facies gneisses.

Figure 2. Iron contents of associated ilmenite and sillimanite. Curve for granulite facies rocks based on 9 pairs from Antarctic granulite facies rocks, and one pair from an upper-amphibolite facies rock.



of the K-feldspar, and high MgO content in the ilmenite. The Kilbourne Hole samples, moreover, differ in the high Al_2O_3 content of ilmenite, replacement of garnet by symplectite, abundance of glass, and unusually high Fe_2O_3 content of some sillimanite and ilmenite. A few of these features in the xenoliths have been documented from rocks partially melted under high temperatures and low pressures. Examples are the conversion of microcline to sanidine (Butler, 1961) and partial melting of garnet to spinel, orthopyroxene, and liquid during shock-induced heating (Stähle, 1975). Thus the xenoliths must have been affected considerably by the heat treatment due to their incorporation into basalt. This heat treatment would alter the mineralogy and chemistry of the minerals, so that statements concerning the original source rock must be made with caution. For example, absence of biotite in the Kilbourne Hole xenoliths is probably no indication of its absence in the source rocks, for biotite breaks down early in the melting of rocks (Butler, 1961).

The composition of ilmenite probably was considerably changed by the heat treatment, although that of sillimanite may have remained relatively unaffected. Scatter in the distribution of Fe_2O_3 between associated sillimanite and ilmenite most likely is due to the heat treatment. The high Mg contents of the ilmenite in the xenoliths may be due to the high MgO/FeO ratio in the xenolith bulk composition. Differences in the Al_2O_3 content, however, probably reflect differences in the physical conditions of crystallization. As the high- Al_2O_3 ilmenites are found only in the Kilbourne Hole samples, the Al_2O_3 enrichment appears to be correlated with the intensity of the heat treatment and thus would not be due to unusual pressure-temperature conditions during the original metamorphism.

The greater extent of partial melting in the Kilbourne Hole samples is probably due to their having spent more time in the host basalt. Geologic evidence suggests that granulite facies source rocks were at greater depths at Kilbourne Hole than at Bournac.

The blue color in sillimanite is probably related to the heat treatment and quenching that occurred during the eruption that brought the xenoliths to the surface. Quenching may be critical in preserving the blue color; its absence in other metamorphic rocks may be explained by the fact that these rocks cooled sufficiently slowly for the color to be lost by annealing.

REFERENCES

- Bank, H., 1974, Zeits. deutschen Gemmologische Gesell., 23, 281-282.
Boule, M., 1892, Bull. Serv. Carte Géol. France, v. 4, no. 28, 259p.
Brousse, R., 1971, Symposium J. Jung: Géologie, géomorphologie et structure profonde du Massif Central français: Clermont-Ferrand, 377-478.
Butler, B.C.M., 1961, Min. Mag., 32, 866-897.
Chenevoy, M., and Ravier, J., 1971, Symposium J. Jung, op. cit. 109-132.
de Goer de Herve, A., and Mergoill, J., 1971, Ibid., 345-376.
Denison, R.E., and Hetherington, E.A., 1969, N.M. Bur. Mines Circ. 104, 1-16.
Hattori, H., 1967, N.Z. Jour. Geol. Geophys. 10, 269-299.
Hoffer, J.M., 1976, N.M. Bur. Mines Circ. 149, 30p.
Leyreloup, A., 1974, Contrib. Min. Petrol., 46, 17-27.
Padovani, E.R., 1977, Granulite facies xenoliths from Kilbourne Hole maar, New Mexico,...:Ph.D. Dissertation, University of Texas at Dallas, 158p.
Padovani, E.R., and Carter, J.L., in press, Amer. Geophys. Union Monograph 20.
Stähle, V., 1975, Earth and Plan. Sci. Letters, 25, 71-81.
Woodward et al., 1975, Map of the Rio Grande Region: New Mexico Geological Society.

LOWER CRUSTAL GRANULITES AND ECLOGITES FROM LESOTHO & SOUTH AFRICA

W.L. Griffin (Geologisk Museum, Oslo, Norway)

D.A. Carswell (Dept. of Geology, Univ. of Sheffield, England)

P.H. Nixon (Geol. Dept., Box 4820 University P.O., Papua New Guinea)

Nodules of granulites and "crustal" eclogites occur in many kimberlites around the edge of the Kaapvaal craton, but are apparently absent in pipes within the craton. In most Lesotho pipes this nodule suite is dominated by basic gnt + cpx + plag + opx granulites, with smaller numbers of eclogites, gnt pyroxenites and intermediate/acid granulites. Two-pyroxene granulites are common at Monastery Mine, and spinel peridotites occur at Lipelenang and Ngopetseu. The early Archean Kaapvaal craton is bordered by younger mobile belts, apparently formed by reworking of the older rocks. The garnet granulite suite may have formed in connection with the reworking process.

Major- and trace-element analyses of 22 nodules show that the basic granulites and eclogites are essentially olivine-basaltic in composition, with minor normative Ne or Hy (Table 1). The garnet pyroxenites, in contrast, are typically Hy-normative. The absence of modal plagioclase in the eclogites and gnt pyroxenites is controlled mainly by bulk composition; only rocks with >35% normative (An + Ab) and <45% normative ol + px contain modal plagioclase. The continuous variations in bulk chemistry and in the proportions of gnt + cpx + opx + plag within the suite strongly suggest that the rocks of the garnet granulite-eclogite-gnt pyroxenite suite have formed by metamorphism of related rocks under similar P-T conditions.

Microprobe data for > 50 rocks also demonstrate the consanguinity of the gnt granulite suite. Clinopyroxenes from all types of garnetiferous rocks generally have $Jd/Ts > \frac{1}{2}$, and thus are typically eclogitic (Fig. 1). $Jd/Jd+Ts$ is roughly proportional to $Ab/Ab+An$ in the coexisting plagioclase ($An=5-77\%$); Jd ranges up to 30%. The common difference in $Jd/Jd+Ts$ between cpx from eclogites and cpx from granulites collected in situ probably reflects cpx-plag reequilibration during normal uplift/cooling cycles. Garnets in all rock types fall in both the Class B (eclogites in gneiss) and Class C (eclogites in blueschist terranes) fields (Fig. 2). High-S ($3.5-6.8\% SO_2$) scapolite occurs in six samples.

The eclogites studied here are distinct in garnet composition (Fig. 2) and K_D (gnt/cpx) from the type "griquaite" (= mantle eclogites) of Roberts Victor Mine and similar rocks elsewhere, but resemble the gnt granulites in these and other respects. Published analyses of "griquaite" minerals from Kao and Sekameng suggest that these rocks are similar to ours and are probably of crustal origin. Distinction between crustal and mantle eclogites may thus be possible on the basis of mineral chemistry.

P and T were estimated by using empirical calibrations of element partitioning between gnt+cpx (Råheim & Green 1975), gnt+opx (Wood 1974) and cpx+plag (Currie & Curtis 1976) in samples where two or more of these pairs are present. Most suitable samples of the gnt granulite suite yield P-T estimates between 550-700°C and 5-13 Kb, implying an origin in the lower crust (Fig.

3). From seismic data on adjacent regions, measured densities of the nodules, and data on the relative abundances of nodule types, we estimate that the lower crust consists of 40-70% basic granulite + eclogite + pyroxenite, and 60-30% intermediate/acid granulite.

Seven Fe-rich gnt pyroxenites give P estimates in the range 20-35 Kb (Fig. 3), and may represent an important rock type in the uppermost mantle. However, the opx of the gnt pyroxenites shows a good inverse correlation of Al with FeO (up to 26%), so that P increases with FeO. There is thus a strong possibility that the high P values reflect an imperfect calibration of the opx/gnt geobarometer for Fe-rich compositions, and that the gnt pyroxenites are part of the crustal suite. T estimates (cpx/opx: Wood & Banno 1973) for three Monastery pyroxene granulites range from 795-885°C; estimates for three Lipelenang spinel lherzolites fall between 825-850°C. Cpx/opx temperatures for cpx+opx+gnt assemblages are higher than other T estimates for these rocks, casting doubt on the usefulness of the cpx/opx thermometer at low T.

A geotherm based on our crustal P-T estimates lies closer to an oceanic geotherm than to the "Shield" geotherm (Fig. 3), suggesting that the latter is only valid for the deeper parts of the upper mantle beneath Lesotho. The present-day heat flow in the Karroo basin is high, and is consistent with the elevated geotherm suggested by our data. The high T at lower-crustal depths during mid-Cretaceous time presumably was a consequence of the Karroo volcanic activity. The Monastery pyroxene granulites apparently crystallized at temperatures above our crustal geotherm. These rocks, and some garnet granulites giving anomalously high T estimates, may have equilibrated in the aureoles of Karroo-period gabbro plutons.

Table 1
Average Rock Compositions

	gnt granul. (10)	eclog. (2)	gnt pyroxen. (4)
SiO ₂	47.6	42.0	47.3
TiO ₂	1.0	1.4	1.1
Al ₂ O ₃	16.8	12.6	9.4
Fe ₂ O ₃	1.8	2.3	3.2
FeO	8.0	16.0	9.1
MnO	0.1	0.4	0.2
MgO	7.6	9.3	13.9
CaO	10.4	11.5	12.1
Na ₂ O	2.9	1.0	1.6
K ₂ O	0.9	0.4	0.1
P ₂ O ₅	0.2	0.1	0.2
H ₂ O	1.6	1.3	1.2

Fig. 1. Cpx chemistry. Short lines connect cores (symbols) with rims, where zoning is present.

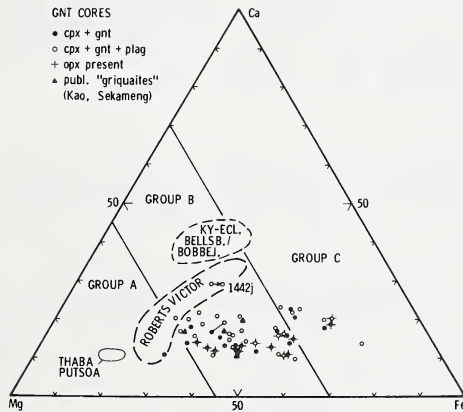
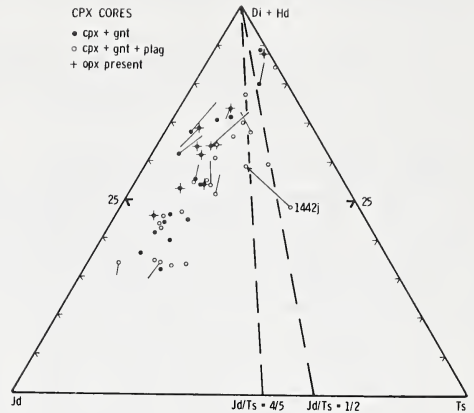
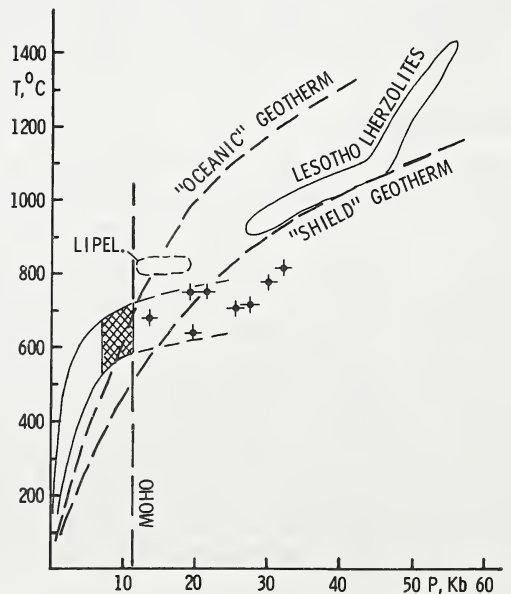


Fig. 2. Gnt chemistry.

Fig. 3. P-T estimates. Cross-hatched field contains 24 of 31 P-T estimates (cpx/gnt+cpx/plag) on rocks of the gnt granulite suite. Crossed dots are high-Fe, low-Al gnt pyroxenites.



EXPERIMENTAL STUDY ON TWO PICRITES WITH REFERENCE TO THE GENESIS OF KIMBERLITE

Alok K. Gupta and Kenzo Yagi (Department of Geology and Mineralogy, Hokkaido University, Sapporo, 060 Japan)

Introduction

The occurrence of eclogite xenoliths within kimberlites suggests the close genetic relationship between these two rocks. O'Hara and Yoder (1967) considered that separation of eclogite from a picritic magma at depth (25 kb or more) might produce a volatile-rich liquid similar in composition to kimberlite. According to Green and Ringwood (1967), however, a nephelinitic but not a kimberlitic magma is formed by the fractionation of a primary picritic melt. In order to find the genetic relationship between a picrite and a kimberlite, melting experiments on a nepheline-normative picritic dolerite from Nosappu Cape of the Nemuro Peninsula, Hokkaido and a hypersthene-normative picrite from Wakuike, Nagano Prefecture, Japan, have been made at various pressures and temperatures, up to 1300°C and 30 kb in presence of excess water.

Petrology of Picrites

The nepheline-normative picritic dolerite consists of plagioclase (An₅₇₋₆₄), orthoclase cryptoperthite, augite (Ca₄₁Mg₄₇Fe₁₂), olivine (Fo₇₀), biotite, Ti-magnetite and small amounts of ilmenite and apatite (Yagi, 1969).

The picritic basalt from Wakuike consists of plagioclase (An₉₂₋₈₇), olivine (Fo₆₈₋₇₁), augite (Ca₄₃Mg₄₂Fe₁₅-Ca₄₄Mg₃₉Fe₁₇) and magnetite phenocrysts in a groundmass of plagioclase, augite (Ca₄₁Mg₃₉Fe₂₀), pigeonitic augite (Ca₃₄Mg₄₂Fe₂₄), magnetite and slightly devitrified mesostasis. Presence of abundant megacrysts of anorthite (An₉₄) and olivine (Fo₈₁₋₈₂) is remarkable and can be distinguished from the other crystals of this rock by the absence of zonal structure (Takeshita, 1974, 1975). Chemical compositions of these two rocks are given in Table 1.

Experimentals

Results of investigation on these two picrites are summarized in Figs. 1 and 2. The subsolidus assemblage of the Nosappu picrite consists of clinopyroxene, plagioclase, amphibole, mica, magnetite and vapor at pressures, less than 22 kb, with the solidus at around 700°C. (Fig. 1). With increasing temperature amphibole disappears first, followed successively by plagioclase, mica, magnetite and clinopyroxene. The liquidus lies around 1200°C with clinopyroxene as the primary phase. At pressures, higher than 21-22 kb and temperatures lower than 1000°C, garnet is always present and there is a fairly wide field of clinopyroxene + garnet + mica + magnetite + liquid + vapor. It is worthy of note that mica (phlogopitic) has a large stability field compared to amphibole. This fact has already been noted by Yoder and Kushiro (1969) and Modreski and Boettcher (1970), suggesting that the phlogopitic mica may indeed be the source of potassium in the upper mantle.

EPMA analyses show that the garnet, appearing in the field of

Table 1

	Picritic dolerite, Nosappu	Picritic basalt, Wakuike	clinopyroxene + garnet + mica + magnetite + liquid + vapor is a solid solution of pyrope, almandine and grossularite and has a composition similar to that found in some eclogites in kimberlites. Coexisting clinopyroxenes contain up to 2.6 % Na ₂ O, 3.6 % Al ₂ O ₃ and 26% CaO, similar to omphacitic pyroxenes. Therefore the separation of these garnet and clino- pyroxene will result in the depletion of CaO, Al ₂ O ₃ , and Na ₂ O and rela- tive enrichment in K ₂ O and MgO in the residual liquid. Analysis of the glase form- ed immediately above the solidus at 25 kb showed it to be poor in SiO ₂ (34.5 %), Al ₂ O ₃ , Na ₂ O ₃ and CaO and rich in total iron, MgO and K ₂ O. These results thus substantiate the idea of derivation of a kimber- litic magma by the separa- tion of eclogite from a picritic magma at high pressures.
SiO ₂	46.07	47.47	
TiO ₂	1.98	0.71	
Al ₂ O ₃	11.06	17.09	
Fe ₂ O ₃	5.00	1.32	
FeO	5.44	7.31	
MnO	0.20	0.24	
MgO	9.97	11.31	
CaO	11.73	9.15	
Na ₂ O	2.59	1.51	
K ₂ O	2.01	0.60	
H ₂ O+	2.22	2.56	
H ₂ O-	1.78	0.64	
P ₂ O ₅	0.23	0.18	
Total	100.28	100.09	
Analyst	H.Onuki	H.Matsumoto	

The subsolidus assemblage of the Wakuike picrite is much simpler, consisting of plagioclase + amphibole + vapor with solidus around 700°C (Fig. 2). With increasing temperature, at about 800°C both clinopyroxene and magnetite appear, forming an assemblage of amphibole + plagioclase + clinopyroxene + magnetite + liquid + vapor. With further rise in temperature first amphibole and then plagioclase, magnetite and clinopyroxene disappear successively. The liquidus with clinopyroxene as the primary phase occurs at about 1250°C, slightly higher than that of the Nosappu picrite, because of higher MgO content. In this picrite garnet appears above 17-18 kb, about 5 kb below the lower stability limit of this phase in case of the Nosappu picrite which may be due to the higher concentrations of Al₂O₃ and CaO in the rock from Wakuike. Mica also does not appear in case of this rock (Fig. 2) because of vary low K₂O content.

EPMA analyses of the run products of the Wakuike picrite indicate that the garnet is a solid solution of almandine, pyrope and grossularite. The analysis of the H₂O-saturated glass, crystallized at 25 kb and 1000°C shows 42.5 % SiO₂, fairly high Al₂O₃ and CaO and very low MgO, Na₂O and K₂O contents. Therefore, although the hypersthene normative picrite produces silica undersaturated liquid at high pressures, its composition is quite different from that of kimberlite.

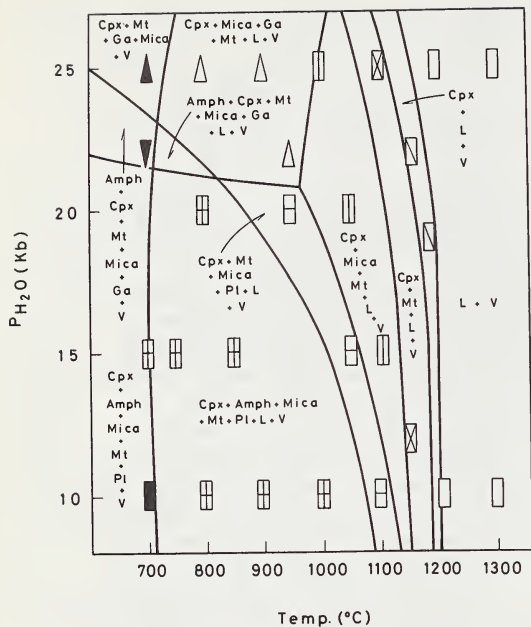


Fig. 1. P_{H_2O} -T diagram of picritic dolerite from Nosappu Cape.

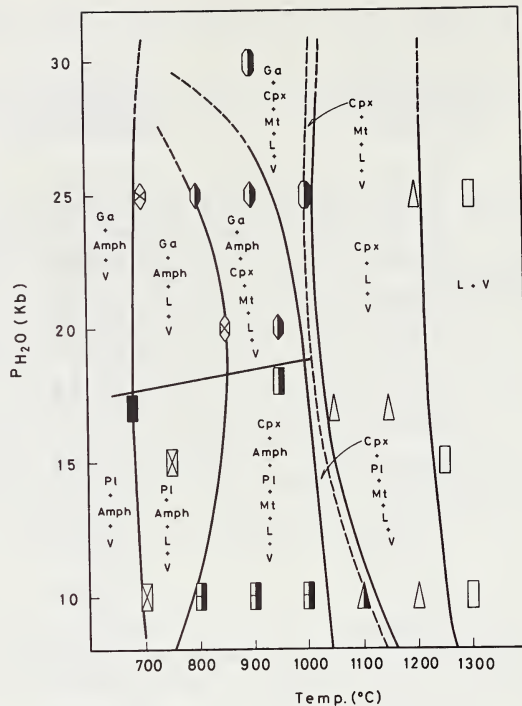


Fig. 2. P_{H_2O} -T diagram of picritic basalt from Wakuike

Conclusion

The present experimental study thus shows that partial melting of a nepheline-normative picrite at high pressures may produce a kimberlitic magma, by subtracting the eclogitic fractions. However, the partial melting of a hypersthene-normative picrite is not suitable for the formation of a kimberlitic magma.

The upper stability limit of amphibole in case of the Nosappu picrite indicates that the kimberlite-formation probably takes place at a depth of at least 23 kb (or 70 km) or possibly at or below 100 km under the condition of low geothermal gradient as amphiboles are usually absent in kimberlites.

References

- Green, D.H., and A.E. Ringwood, 1967, An experimental investigation of the gabbro to eclogite transformation and its petrological applications. *Geochim. Cosmochim. Acta*, 31, 767-833.
- O'Hara, M.J., and H.S. Yoder, Jr., 1967, Formation and fractionation of basic magmas at high pressures. *Scot. J. Geol.*, 3, 67-117.
- Takeshita, H., 1974, Petrological studies on the volcanic rocks of the northern Fossa Magna region, Central Japan (part 1). *Pacific Geology*, 7, 65-92.
- Takeshita, H., 1975, ditto (part 2). *Pacific Geology*, 10, 1-32.
- Yagi, K., 1969, Petrology of the alkalic dolerites of the Nemuro Peninsula, Japan. In *Igneous and Metamorphic Geology*; ed. L. Larsen. *Geol. Soc. Am. Mem.* 115, 103-147.

PERIDOTITES AND GARNET OLIVINE WEBSTERITES AT BULTFONTEIN MINE

J.J. Gurney (Dept. of Geochemistry, University of Cape Town, Rondebosch, R.S.A.)
P.J. Lawless (Anglo-American Research Labs., Crown Mines, Johannesburg, R.S.A.)
J.B. Dawson (Dept. of Geology, St. Andrews University, Scotland.)

The great majority of mantle xenoliths at Bultfontein are peridotites which would fall within the modal proportions which define the common peridotites (C.P.) at Matsoku, N. Lesotho. (Cox et al 1973) (i.e. garnet 0-11%; clinopyroxene 0-5%; orthopyroxene 20-50%; olivine 45-75%; olivine > orthopyroxene). Rare xenoliths fall outside this range because they contain more garnet and clinopyroxene and less olivine. In such rocks orthopyroxene is the major mineral. They are referred to here as garnet olivine websterites. The following features have been recorded:

1. The textures shown by the C.P. at Bultfontein vary from coarse to laminated and disrupted mosaic porphyroclastic rocks. Variable degrees of deformation have been noted in single xenoliths. (Dawson et al 1975).
2. The garnet olivine websterites have coarse textures.
3. The temperatures and pressures of equilibration of the C.P. and the garnet olivine websterites is restricted to a narrow range on the basis of the Ca/Ca+Mg ratios of the pyroxenes and the Al_2O_3 content of the orthopyroxenes. (Dawson et al 1975).
4. There is no correlation between the temperature of equilibration and degree of deformation. (Dawson et al 1975).
5. No sub-calcic diopsides have been found in the xenoliths.
6. Some xenoliths have phlogopite or potassic richterite present. These minerals have been interpreted to be of primary metasomatic origin. (Erlank and Rickard 1977). The phlogopite may be associated with rutile, ilmenite and sulphides.
7. The minerals in the C.P. have high Mg/Mg+Fe ratios.
8. The minerals with the lowest Mg/Mg+Fe ratios are found in garnet olivine websterites.
9. The titanium content of the minerals in the coarse unmetasomatised rocks shows a positive correlation with iron whilst chromium has a negative correlation. This is best shown by the garnets, in which these two elements are concentrated.
10. The highest titanium contents are found in the minerals of the metasomatised rocks, as are the highest bulk rock titanium and potassium values.
11. The full range of the observed variations in bulk chemistry for magnesium, iron, aluminium, calcium, chromium, sodium, manganese and nickel are found in the coarse xenoliths.
12. As a consequence of the changes in modal proportions and mineral chemistry the C.P. have high whole rock $\frac{Mg}{Mg+\sum Fe}$ ratios compared to the iron rich garnet olivine websterites. The richterite bearing rocks and most of the phlogopitic rocks have intermediate values.

In respect of the features listed the xenoliths described are very similar to the suite at the Matsoku Pipe, N. Lesotho described by Cox et al (1973), Harte et al (1975), Gurney et al (1975) and Harte and Gurney (1975). The Bultfontein xenoliths do differ in some respects, however. We draw attention to the facts that:

- (i) the most deformed rocks at Bultfontein are not found at Matsoku.
- (ii) the metasomatised rocks at Matsoku are fine grained, whilst those at Bultfontein may be coarse.

- (iii) potassic richterite is reported in metasomatised rocks at Bultfontein (Erlank and Rickard 1977) but has not been found at Matsoku.
- (iv) the range in bulk chemistry and in Mg/Mg+Fe ratio for the minerals at Bultfontein, whilst greater than that reported by Boyd and Nixon (1973) for both deformed and undeformed rocks at several localities in N. Lesotho, is less than that found at Matsoku.
- (v) some coarse garnet olivine websterites at Bultfontein do not show marked iron enrichment in the constituent minerals. At Matsoku the only pyroxenites which have similar chemistry are narrow pyroxene rich veins which are finer grained than the C.P. and appear to have re-equilibrated with adjacent peridotite. (Harte et al 1977).

Common Peridotites

The mineral and bulk rock compositions of the unmetasomatised C.P. at Bultfontein are very similar to the Matsoku coarse C.P. and for reasons advanced by Gurney et al (1975) are thought to most likely represent partly depleted mantle material. The trace elements Ba, Sr, Rb, Y, Zr, Nb, Zn, Cu and V are all very low in the unmetasomatised C.P. by comparison to the Stormberg volcanic rocks of Lesotho, whilst Ni and Cr and to a lesser extent Co are enriched, (Table 1) supporting this conclusion.

The most iron rich rock found at Bultfontein (JG1417) is similar to those coarse xenoliths interpreted to most probably be of cumulate origin at Matsoku, except that it contains minor (1%) phlogopite in textural equilibrium with the major minerals. The rock is a coarse garnet olivine websterite, with an olivine composition of Fo_{85.1} and an orthopyroxene of En₈₇. A similar rock is described by Williams (1932) (Wess 152). Wess 152 however has no olivine and is in that respect similar to LBM 18 (Cox et al 1973). O'Hara et al (1975) have described similar rocks from Matsoku (1031, 1032) and A17 from an unspecified locality in S. Africa. It has been suggested that the rocks represent either (i) Fertile mantle or (ii) Liquid compositions (komatiitic) or (iii) Cumulate minerals + intercumulus. (e.g. O'Hara et al 1975, Gurney et al 1975). As argued for Matsoku, we consider the latter to be the most probable of the three.

References

- K.G. Cox et al (1973). Chap. in Lesotho Kimberlites, Ed. P.H. Nixon. pp. 76-100
- J.B. Dawson et al (1975). Nature 257. pp. 299-300
- A.J. Erlank and R.S. Rickard (1977). This volume.
- J.J. Gurney et al (1975). Phys. Chem. Earth IX. pp. 507-524
- B. Harte et al (1975). Phys. Chem. Earth IX. pp. 477-506
- B. Harte and J.J. Gurney (1975). Ann. Rept. Geophys. Lab. Carnegie Inst. pp. 528-535
- B. Harte et al (1977). This volume.
- P.H. Nixon and F.R. Boyd (1973). Chap. in Lesotho Kimberlites. Ed. P.H. Nixon pp. 48-56
- M.J. O'Hara et al (1975). Phys. Chem. Earth IX. pp. 571-604
- A.F. Williams (1932). The Genesis of the Diamond. John Benn.

TABLE 1	3:1 Pyrolite II	Primary Lherzolite	HSS150	Stormberg Volcanics	PHN 1611	LBM 12	BD 2349	JJG 1417
SiO ₂	43.95	45.0	44.9	49.7	43.70	44.1	44.4	50.3
TiO ₂	0.57	0.36	0.28	1.00	0.25	0.11	0.01	0.11
Al ₂ O ₃	3.88	4.1	3.12	14.9	2.75	3.60	1.46	2.98
Fe ₂ O ₃	0.75		2.31		1.38	4.00	2.96	2.18
FeO	7.50	11.0*	11.53	11.4*	8.81	10.52	3.82	7.20
MnO	0.13	0.16	0.18	0.17	0.13	0.17	0.09	0.17
MgO	39.00	33.00	33.01	6.32	37.22	33.45	41.74	31.4
CaO	2.60	4.00	3.76	9.97	3.26	2.90	0.86	2.80
Na ₂ O	0.60		0.01	2.49	0.33	0.27	0.05	0.36
K ₂ O	0.22	0.68	0.01	1.11	0.14	0.03	0.03	0.09
P ₂ O ₅			0.03	0.23	tr.	0.01	0.01	0.07
S ²⁼⁵			0.04	0.04		0.29	0.02	0.01
LOI				2.73		0.81	4.20	1.38
H ₂ O ⁺				1.00	1.94		0.32	0.23
Ba			36	247		120	8	73
Sr			7	195		49	34	107
Rb			< 1	19		3	< 3	3
Y			7	24		< 3	< 3	6
Zr			21	101		14	7	32
Nb			< 1	5		< 3	< 3	5
Zn			80	81		102	32	70
Cu			36	102		17	< 3	< 3
Co			145	46		188	116	116
Ni	3222	2122	1745	75		2390	2250	1530
V			83	232		76	26	68
Cr	2669	2395	4370	204		5500	2300	5100
(FeO/MgO +FeO)	17.33	25.00	29.19	64.33	21.26	29.68	13.44	22.58

X 100

Total iron as FeO

Table 1: Footnote

The pyrolite II composition is that of Green and Ringwood (1967). Primary lherzolite is Pl from Kuno and Aoki (1970). The Stormberg data is an average from a Kao Mine borehole and for rocks from the Witsieshoek area in Lesotho, provided by J. Bristow (unpublished data). The rock HSS 150 is an aphyric peridotitic komatiite, and is thought to represent a magnesian liquid composition. (H.S. Smith).

SILICATE AND OXIDE INCLUSIONS IN DIAMONDS FROM THE FINSCH KIMBERLITE PIPE

J.J. Gurney (Dept. of Geochemistry, University of Cape Town, Rondebosch, S.A.)

J.W. Harris (Grant Institute of Geology, University of Edinburgh, Scotland)

R.S. Rickard (Dept. of Geochemistry, University of Cape Town, Rondebosch, S.A.)

Inclusions in diamonds from the Finsch Kimberlite Pipe, South Africa are predominantly peridotitic. (See Table 1.)

The Peridotitic Minerals

Apart from black inclusions many of which may be sulphide, olivine is by far the most abundant mineral followed by garnet, orthopyroxene and chromite in that order. Chrome diopside has not been found either in the initial inspection of 232,000 diamonds or in subsequent examinations of Finsch production.

The olivines are forsterites (See Fig.1) and do not have high Cr_2O_3 contents. The orthopyroxenes are also highly magnesian (See Fig.2) and are characterised by extremely low CaO (less than 0.3 wt.%) and Na_2O (less than 0.15 wt.%), Cr_2O_3 in the range 0.15 - 0.34 wt.% and by low but variable Al_2O_3 (0.26 - 0.66 wt.%). Garnet co-exists in the same diamond with both extremes of the alumina contents reported. The majority of the garnets are exceptionally low in CaO, have high Mg/Mg+Fe ratios and high Cr_2O_3 contents. (See Fig.3). The lowest calcium contents are largely outside both the previously reported range for garnets from diamond and the range for xenocryst garnets from Finsch (Gurney & Switzer, 1973). (See Fig.4 A and B). The chromites all have more than 61.5 wt.% Cr_2O_3 .

The Eclogitic Minerals

Rare eclogitic minerals found in Finsch diamonds included garnet and sulphide in the initial search, and subsequently clinopyroxene and kyanite. The garnets and pyroxenes are iron-rich. The garnets are very different from the peridotitic diamond inclusions at Finsch, not only with respect to Ca:Mg:Fe (See Fig.4) but also in their TiO_2 , Cr_2O_3 , MnO and Na_2O contents. A garnet clinopyroxene pair gives a temperature of equilibration of 1020°C at 40 Kb, using the Raheim & Green (1974) geothermometer and gives an intercept with the diamond graphite reaction curve at approximately 42 Kb and 1030°C .

Discussion

It is suggested that most of the Finsch diamonds may have crystallised from a partial melt which was derived from garnet lherzolite mantle and also contained water and CO_2 . This melt formed at depths where the temperatures and pressures defined by the ambient geothermal gradient were within the diamond stability field. Melting is considered to have occurred close to or on the normal geotherm probably at temperatures between 1000°C and 1130°C . This required high partial pressures of water to depress the peridotite solidus temperature. The CO_2 (probably present in the silicate melt as CO_3^{2-}) is considered to have captured most of the calcium in the melt from which low calcium garnet and orthopyroxene along with olivine, chromite, (and presumably sulphide) crystallised.

Coarse garnet lherzolite xenoliths have been found at Finsch giving equilibration temperatures on the diopside solvus (Davis & Boyd, 1966) of between 950°C and 1075°C .

The water and CO_2 rich melt in which it is suggested that most Finsch diamond forms, would be of Kimberlitic composition. It is possible that this melt subsequently broke through to the surface, sampling eclogite en route, capturing some diamonds from the disaggregated diamondiferous rock and finally forming the Finsch diatreme or a portion of it.

If such a model were to apply, the Precambrian Age obtained for at least one diamond inclusion from Finsch (Kramers; personal communication 1977) would have to be an eclogitic inclusion and if the majority of Finsch diamonds grew

in what is essentially the Kimberlite then such diamonds should not show plastic deformation. At present we cannot verify these aspects.

This proposed model for Finsch will not be directly applicable to other diamond inclusion suites but high Mg/Mg+Fe ratios for peridotitic minerals, low temperatures of equilibration, low calcium contents for most peridotitic garnets and orthopyroxenes and a great scarcity of chrome diopside in diamonds appear to be common features of diamond inclusions on a world wide basis. The model may therefore have more than simply local significance, and is similar to the ideas proposed by Wyllie & Huang (1975) on the basis of both their own experimental results and those of others.

TABLE 1

The relative abundance of inclusions in diamonds of sieve class -6+5^(a) from the Finsch Pipe, based on observation of the inclusions within the diamonds.

1. Peridotitic Paragenesis			2. Eclogite Paragenesis		
No	%		No	%	
Olivine (enstatite, other)	381	37.2	Orange garnet	8	0.8
Olivine + purple garnet	50	4.9	Orange garnet+sulphide	2	0.2
Purple garnet	63	6.2		10	1.0
Purple garnet+sulphide	3	0.3	3. Other Inclusions		
Chromite	4	0.4	Sulphides (b)	358	35.0
	501	49.0	Graphite	132	12.9
Totals (1+2+3)	1024	100.1	Clouds(dense particles)	23	2.2
				513	50.1

Estimated No. of carats inspected 14,500

Estimated No of stones 232,000

(a) Sieve class -6+5. Diameter in mm. of circular aperture = 1.829




Approximate average weight in carats/stone = 0.0427

(b) Sulphides occur with both peridotite paragenesis and eclogite paragenesis minerals. [The majority of silicates are olivine (i.e. peridotite paragenesis)]. * All essentially colourless inclusions are placed under this heading. > 70% are olivine. Most of the rest are orthopyroxene. Rare SiO₂ (coesite?) phases have been found.

References

- B.T.C. Davis and F.R. Boyd (1966): Jour. Geophys. Res. 71 3567 - 3576
 J.J. Gurney and G.S. Switzer (1973): Contr. Min. and Pet. 39 103 - 116
 H.O.A. Meyer and H.M. Tsai (1976): Min. Sci. and Eng. News 8 242 - 261
 A. Raheim and D.H. Green (1974): Contr. Min. and Pet. 48 179 - 208
 P.J. Wyllie and W.L. Huang (1975): Geology 3 621 - 624


Key to Figures 1 - 4

Fig.1(a) Olivines from Finsch:  in diamond;  in diamond and co-existing with garnet;  in garnet lherzolite xenoliths.

1(b) Other published analyses of olivines in diamond from Meyer & Tsai 1976.

Figs. 2(a) and (b) Orthopyroxenes. Symbols as for Fig. 1.

Fig.3 Chrome-garnet inclusions in diamond from Finsch, grouped according to calcium content.

Fig.4(a) and (b)  Garnet inclusions in Finsch diamonds.


 Xenocryst garnets from Finsch.

Fig.4(a) The unshaded field is for low calcium garnet inclusions in Finsch diamonds (44). The shaded field is for xenocryst garnets from Finsch.

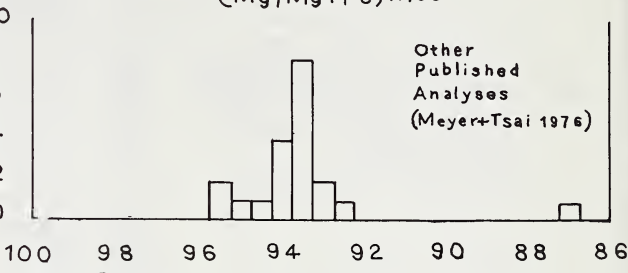
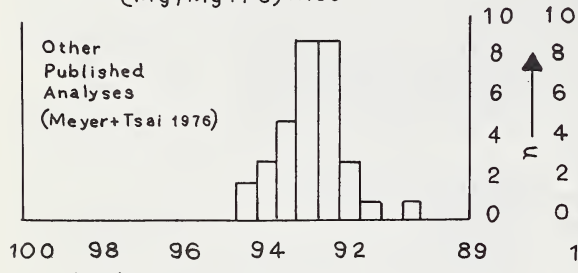
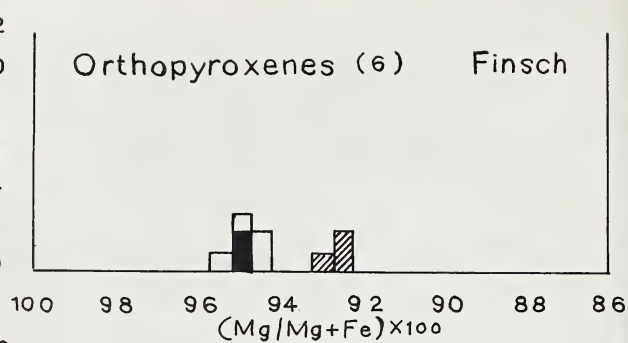
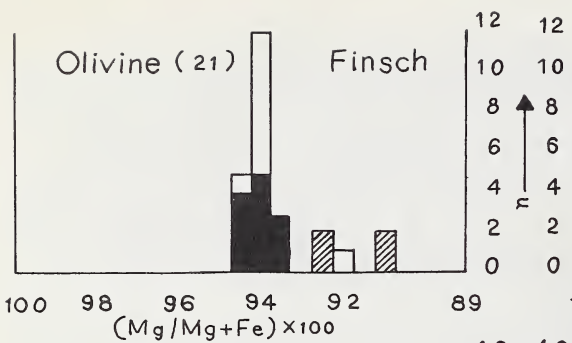


Fig 1

Fig 2

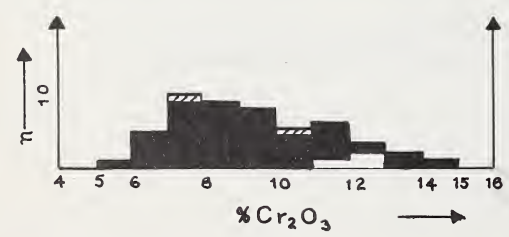
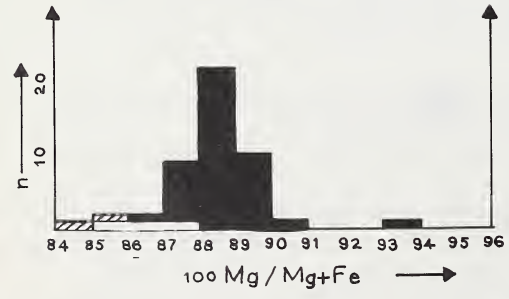
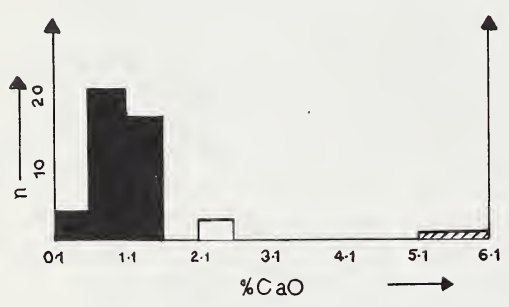


Fig 3

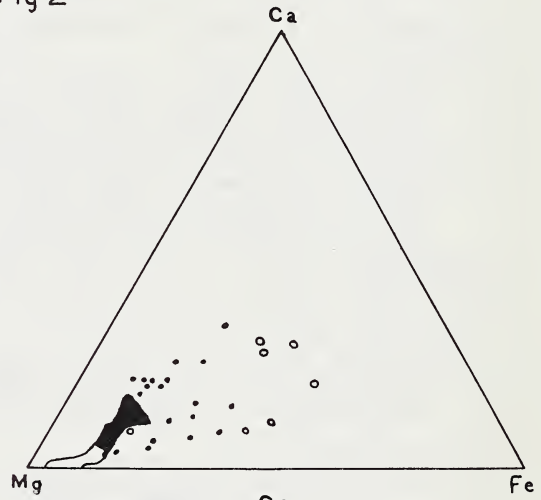


Fig 4(a)

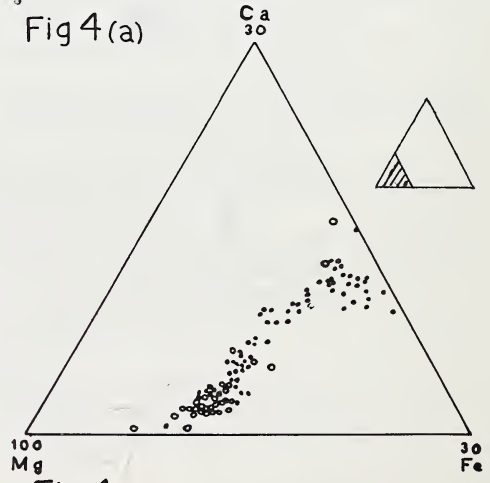


Fig 4(b)

Cumulus Jua pasand melle of ...
42 kb

MEGACRYSTS FROM THE MONASTERY MINE

J.J. Gurney (Department of Geochemistry, University of Cape Town, Rondebosch, 7700, Cape, South Africa.)
W.R.O. Jakob (Atomic Energy Board, Pelindaba, Pretoria, South Africa.)
J.B. Dawson (Geology Department, University of St. Andrews, Scotland.)

Megacryst minerals (> 2cm) are particularly common at the Monastery Kimberlite Pipe, O.F.S. They can exceed 20cm in longest dimension and garnet, clinopyroxene and orthopyroxene all occur both as large mono-mineralic single crystals and in association with ilmenite which is also a megacryst phase. The graphic intergrowths of ilmenite with clinopyroxene, and less commonly with orthopyroxene, are well known (e.g. Boyd & Nixon, 1973). Garnet when associated with ilmenite is found as small rounded grains in an ilmenite megacryst host. Olivine is a common megacryst but we can report only a single example of olivine/ilmenite. Large phlogopites are usually vermiculitised when exposed in the kimberlite. None of these minerals, not even the olivines nor the phlogopites, commonly show signs of deformation or recrystallisation.

The major element compositions of the megacryst phases (except for phlogopite) have been determined (~ 300 determinations). The variation in Ca, Mg and Fe (atomic proportions) of the clinopyroxenes, garnets, orthopyroxenes and olivines are shown in Fig.1.

The clinopyroxenes define a trend from high Mg, low Ca, low Fe (clinopyroxene megacrysts) to low Mg, high Ca and slightly increased Fe (clinopyroxene/ilmenite megacrysts). The garnets define a trend of changing Mg/Fe ratio from high magnesian megacrysts to iron rich garnet inclusions in ilmenite. The orthopyroxenes fall into two groups:-

- (A) Brown glassy homogeneous orthopyroxene megacrysts which can be associated with ilmenite and define a trend of increasing calcium with increasing magnesium and decreasing iron.
- (B) Opaque orthopyroxene megacrysts showing well developed cleavage and with small bright green chrome diopsides and sometimes chrome pyrope exsolution in the cleavage planes. These orthopyroxenes show constant and low calcium contents with changing Mg/Fe ratio and are all more magnesian than group (a).

The olivines fall into two groupings: $Fe_{84-88} NiO > 0.3\%$; $Fe_{78-82} NiO < 0.12\%$. The ilmenites show a wide range in compositions, particularly in iron and magnesium, but the ilmenites co-existing with clinopyroxene, orthopyroxene and garnet are all similar to each other and within the range for discrete ilmenite megacrysts.

Inclusions have been found in the megacrysts and two types are of particular interest:

- (1) Megacrysts occasionally contain small inclusions of another mineral in the megacryst suite. Tie-lines between such co-existing garnet and clinopyroxene are in excellent accord with theoretical tie-lines calculated on the basis of the results of experimental systems. (e.g. Davis & Boyd 1966, Akella & Boyd 1974).

Tie-lines between these phases above, and between garnet and orthopyroxene and garnet and olivine, suggest that the most sub-calcic clinopyroxenes, the most magnesian garnets, the most magnesian orthopyroxenes of group (A) and the most magnesian olivines have formed in equilibrium with each other, and that gently rotating concordant tie-lines may be drawn for successively more iron rich compositions, finally

linking the most iron rich garnets, clinopyroxenes and orthopyroxenes to the most iron rich high nickel olivines.

- (2) Tubular inclusions of kimberlite occur in some olivine crystals. They have only been found in the more magnesian high nickel olivines and are quite common. The first reported example was that described by Haggerty & Boyd, (1975). A small amount of material from one of these inclusions has a bulk composition very similar to that of the Monastery Mine kimberlite type called the "Quarry Kimberlite" (Gurney & Davids, 1973). Invasions of other megacryst phases by kimberlitic fluids has been found but is not as common as for olivine.

In broad agreement with the study of Boyd & Nixon (1973), it is suggested that all the megacrysts in Fig.1 represent a single differentiation sequence and are cumulate minerals which precipitated from a magma which formed in a mantle melting event. The earliest highest temperature ($> 1350^{\circ}\text{C}$) cumulus phase was orthopyroxene now represented by the group (B) orthopyroxenes which crystallised from a magma relatively poor in water content and containing CO_2 to account for the absence of olivine. The glassy homogeneous orthopyroxenes (group A), the magnesian olivines, the garnets and the clinopyroxenes then precipitated whilst the water content of the magma continuously increased. Ilmenite also became a liquidus phase at about 1230°C . Crystallisation of these co-existing phases was complete at $\sim 1130^{\circ}\text{C}$. Some fluid remained, however, and during subsequent cooling, ilmenite may have continued to crystallise, together with phlogopite. Possibly the iron rich low nickel olivines are formed as the temperature drops towards 950°C , in a CO_2 and water rich melt. The extremely wide range in temperature of crystallisation may be due to the increasing water content of the melt in an essentially closed system.

The highest temperature orthopyroxenes (group B) re-equilibrated at sub-solidus temperatures of 950°C or less by exsolution of diopside and garnet. The final very evolved liquid which had the composition of the Monastery Quarry Kimberlite, transported the megacrysts to the surface on emplacement.

The undeformed coarse garnet lherzolite which is the most common and widely distributed mantle xenolith in kimberlite, probably does not have a suitable composition to be parental material from which the postulated igneous event originated by partial melting. Such rocks do not have sufficient potassium, titanium, water or CO_2 . However, metasomatised peridotites, with amphibole, mica, ilmenite and sulphides are present at Monastery and metasomatised rocks have been widely reported from elsewhere (e.g. Harte & Gurney 1975, Lloyd & Bailey 1975, Erlank & Rickard 1977), thus providing strong evidence for the local concentration of potassium, titanium and hydrous phases in some mantle rocks.

The outlined model is applicable in detail only to the Monastery Pipe. The unusually high titanium and total iron contents of the Monastery Kimberlite and the extraordinary abundance of megacrysts with wide ranges in composition in it argue against the universal applicability of the proposed differentiation sequence to all kimberlites.

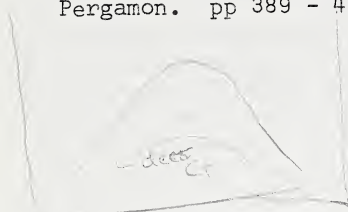
The temperatures given in the model are approximations only, based on various geothermometers and the assumption that these are applicable to the megacrysts.

References

- J. Akella and F.R. Boyd (1974) Ann. Report Geophys. Lab. Carneg. Inst. 73 pp269-273
F.R. Boyd and P.H. Nixon (1973) Ch. in Lesotho Kimberlites Ed. P.H. Nixon Cape & Tvl. pp 254 - 268
B.T.C. Davis and F.R. Boyd (1966) J. Geophys. Res. 71 3567 - 76

A.J. Erlank and R.S. Rickard (1977) This volume.
 J.J. Gurney and S. Davis (1973) Chap. in Lesotho Kimberlites. Ed. P.H. Nixon
 Cape & Tvl. pp 280 - 284
 S.E. Haggerty and F.R. Boyd (1975) Kimberlite Symposium, Cambridge pp 50 - 51
 B. Harte and J.J. Gurney (1975) Ann. Report Geophys. Lab. Carneg. Inst.
 74 pp 528 - 535
 F.E. Lloyd and D.K. Bailey (1975) Phys. Chem. Earth IX Ed. Ahrens et al.
 Pergamon. pp 389 - 417

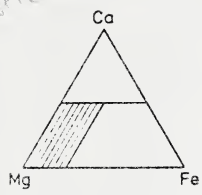
7.02



Cr ↑ decr.
 Ti ↑ decr
 st cox up

st in ilmenite

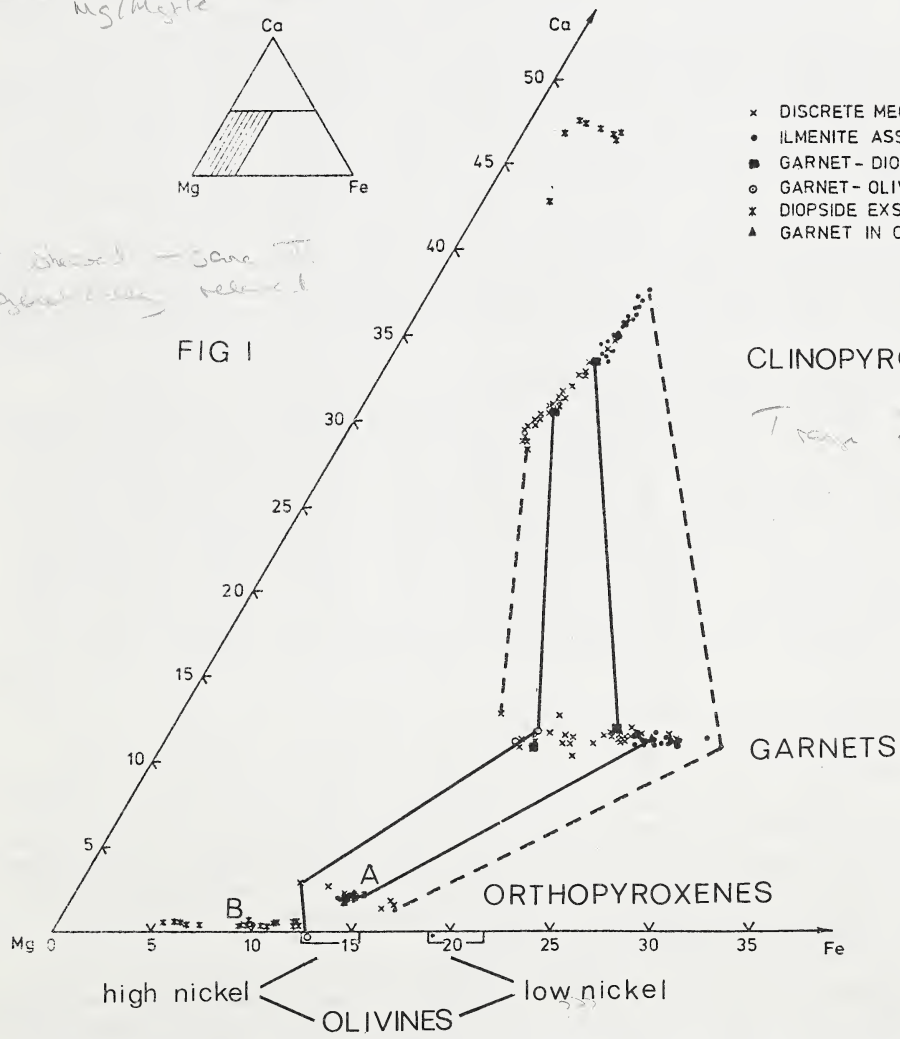
Mg/Mg+Fe



Mg & Mn - same Ti
 & garnet - olivine

FIG 1

- x DISCRETE MEGACRYSTS
- ILMENITE ASSOCIATION
- GARNET - DIOPSIDE
- GARNET - OLIVINE
- x DIOPSIDE EXSOLVED FROM OPX
- ▲ GARNET IN OPX - ILMENITE



Solid tie lines: coexisting phases Dashed tie lines: inferred coexisting phases

Thaba Pedra	1500	45%
Molten	1025	31
...	1050	27
Molten 1000	1000	22

Handwritten notes and scribbles at the bottom right of the page.

SPINELS AND ILMENITES IN HIGH PRESSURE REGIMES: AN EMPIRICAL ANALYSIS

S. E. Haggerty (Dept. of Geology, University of Massachusetts,
Amherst, Massachusetts 01003)

In an attempt to establish the nature of compositional variations among spinels and ilmenites in high pressure regimes a detailed analysis of mafic and ultramafic suites has yielded the following results:

(1) The distribution of spinel compositions are summarized in Fig. 1 and the following characteristic trends emerge: (a) an early enrichment of Cr and a later enrichment in Al is the typical kimberlite trend; (b) an early enrichment of Mg and a later enrichment of Fe^{2+} is the stratiform magmatic ore deposit trend; and (c) an early enrichment of Al and a later enrichment in Cr is exemplified by xenolith suites, and this is termed the peridotite trend. A preferred directional sweep towards the Fe-ternary is exhibited by all suites with the exception of kimberlitic spinels which continue to show relatively high MgO contents with increasingly higher concentrations of $\text{Fe}^{3+} + \text{Ti}$. In contrast, xenolith and peridotite suites are confined to the spinel prism base with little or no enrichment in either Fe^{3+} or Ti. The three basalt trends are for: (a) subaerially extruded tholeiitic suites; (b) island-arc volcanism; and (c) mid-oceanic ridge basalts. The latter trend is comparable to the trends exhibited by spinels in xenoliths and in peridotites and these basalts include the range from picrites with low Cr/Cr + Al, to olivine tholeiitic basalts with intermediate R^{3+} ratios, and to alkali olivine basalts with high Cr/Cr + Al ratios. Early enrichment trends are considered to be pressure and temperature dependent. Progressively later trends are a reflection of initial bulk rock chemistry, relative paragenetic relationships of co-precipitating Mg, Al and Fe-bearing silicates, and the degree of interstitial liquid interaction.

(2) The P-T lherzolite petrogenetic grid is broadly confirmed for spinel distributions in which the partitioning of Cr and Al among silicates and oxides results in: (a) a spinel absent field for high pressure garnet lherzolites (Cr is present in clinopyroxene + garnet); (b) a chromite, but Al-depleted, field in the region of low pressure plagioclase lherzolite stability (Al is present in plagioclase); and (c) a variable range in Cr/Cr + Al ratios for spinels which are stabilized between these two extremes in spinel lherzolites. This trend suggests that Cr/Cr + Al ratios should decrease with increasing pressure; however, the unresolved anomaly in this otherwise coherent pattern is that spinel inclusions in diamonds have an extremely high FeCr_2O_4 component which is supported, in part, by the overall trends displayed by kimberlitic spinels. A major and significant new result is that the Fe/Mg relationships of spinels are key to the spinel P-T grid and to the variations in Cr and Al. In a test of lunar intrusive rocks (gabbro, anorthosite, troctolite and dunite) the Fe/Mg variations of spinels fall along a smooth curve with the gabbro having the highest Fe value and the dunite the highest Mg content; the anorthosite and the troctolite occupy an intermediate range which is interpreted to be P-T dependent. The terrestrial test confirms this overall interpretation but is complicated by the fact that fractional crystallization and partial melting in particular, disrupt the inherent signature of the spinel.

(3) The distribution of ilmenite compositions for a variety of rock types is illustrated in Fig. 2 and from these the most significant component in the context of pressure regimes is the behavior of Mg as determined from diamond inclusion studies, from kimberlite studies, from autholith studies,

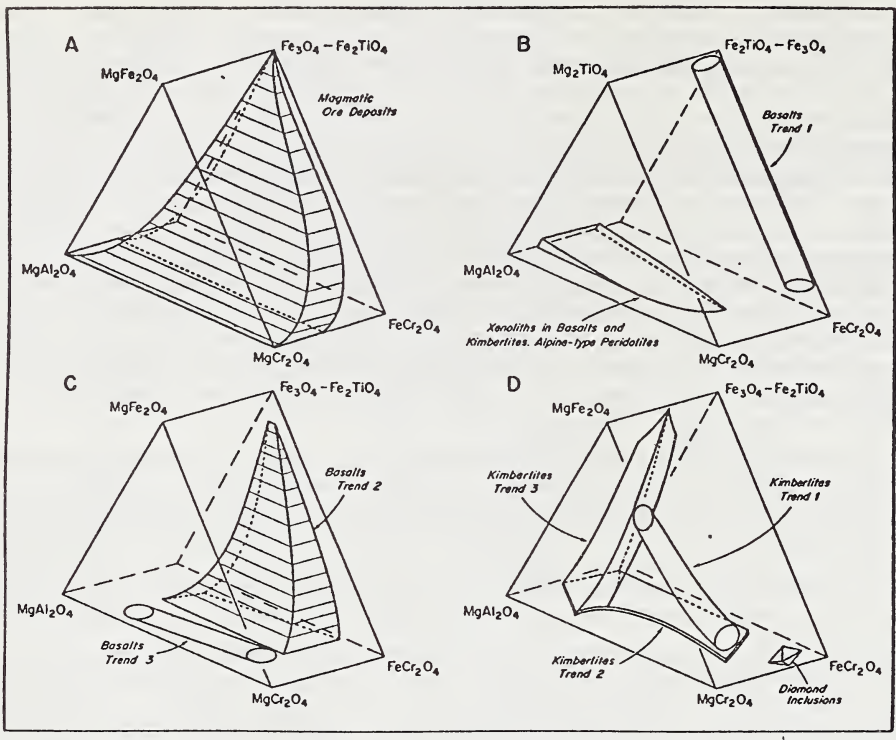
and from basaltic phenocrystal studies. The results of these data show: (a) phenocrystal ilmenites in kimberlites are commonly reversely zoned, with higher MgO contents at the margins and lower concentrations in the cores, a trend which is also observed in basaltic suites; (b) the MgO contents of ilmenites intergrown with diamonds are moderately high, in common with the encasements on autolith nuclei, the compositions of groundmass ilmenites, and the compositions of ilmenites in symplectic pyroxene intergrowths; (c) ilmenites included in diamonds have extremely low MgO contents and these are similar in composition to ilmenites in autolith nuclei. This suggests that an increase in pressure should lead to a decrease in the geikielite component, but this relationship is also clearly dependent on olivine precipitation. Early crystallization of olivine and magnesian chromites results in low MgO content ilmenites and this is reflected in all basic suites. The implied pressure dependency, however, is substantiated by volume changes associated with the reaction $Fo + Ilm \rightarrow Fa + Geik$ which is positive, and is indicative therefore of $Mg_{olivine} > Mg_{ilm}$ at high P.

(4) The high concentrations of Cr_2O_3 (1-8 wt%) in kimberlitic ilmenites is a unique property of this mineral in this setting. Low pressure experimental results demonstrate the instability of Cr in the ilmenite structure under high and very low f_{O_2} conditions, and the preferred partitioning of Cr between coexisting ilmenites and spinels is widely recognized with $Cr_{Sp} \gg Cr_{Ilm}$. An expected substitution of the form $Cr \rightarrow Fe^{3+}$ in the system $FeTiO_3$ - $MgTiO_3$ - Fe_2O_3 , which may be possible under mantle conditions, should result in chromian-stabilized members of the ilmenite-geikielite series. Hence, Cr-Mg relationships should correlate in some systematic manner but repeated tests yield a parabolic curve. Parabolic curves also result between Cr and Ti, Al, and Fe^{3+} .

In summary, this empirical analysis has identified three major aspects of spinel and ilmenite mineral chemistry in high pressure regimes: (a) that Al/Cr variations in spinel lherzolites are likely to result in a refinement of the P-T petrogenetic grid; (b) that Fe/Mg ratios are a sensitive and integral component of the P-T spinel grid; and (c) that the MgO contents of ilmenites are unequivocally related to pressure in kimberlitic suites. The outstanding problems which remain are: (a) that lherzolitic suites suggest a decrease in the Cr/Cr + Al ratio with increasing pressure, whereas kimberlites suggest the reverse; and (b) what is the role of Cr in kimberlitic ilmenite? For both, the concomitant effects of Fe/Fe + Mg variations in spinel and in coexisting silicates are considered to play a major role.

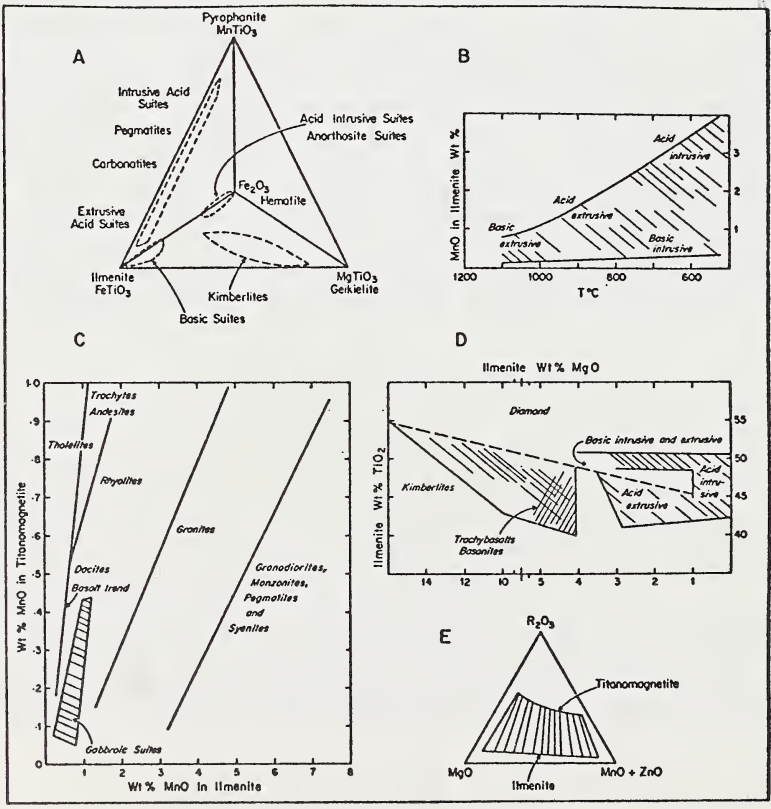
∇ - coexist low chromites but
 ∇ stability - Cr²⁺ at ~~high~~

see Ulmer & White
 C₂⁺ / C₃⁺ w. c.p.



high P
 Ti-Fe^{III}
 depleted.

base composition



low Mn - CO₂

Na⁺ in IV site
 Fe-Mg binary
 Fe / Basic / K / Mg
 - doesn't hold on

C₂/Al in $\frac{TiO_2}{SiO_2}$ site
 ↓ disp.
 K / read
 volc
 Al

THE MINERAL CHEMISTRY OF ILMENITE NODULE ASSOCIATIONS FROM THE MONASTERY
DIATREME.

S.E. Haggerty, R.B. Hardie III, and B. M. McMahon (Dept. of Geology, University of Massachusetts, Amherst, Ma. 01003)

A petrographic and electron microprobe study was performed on 163 ilmenite nodules from the heavy mineral concentrate of the Monastery Kimberlite pipe. We have classified these nodules into the following categories: (a) symplectic ilmenite-pyroxene intergrowths (57 nodules); (b) discrete ilmenite nodules (66 samples); and (c) ilmenite nodules encased in a closely adhering kimberlite matrix (40 nodules). This study was undertaken in an attempt to characterize these diverse associations and to evaluate the conditions and setting for ilmenite-pyroxene formation. The following new results have emerged.

- (1) Approximately 10% of the ilmenite-pyroxene assemblages contain orthopyroxene and the remainder are clinopyroxene.
- (2) The modal proportions of ilmenite to pyroxene vary enormously from a ratio of 1:1 to a ratio of at least 1:10; no preferred modal to compositional populations are apparent and no distinctions are present between Opx and Cpx hosts.
- (3) Reactions at Opx-ilmenite interfaces yield olivine + rutile + Ti-phlogopite, whereas interface reactions between Cpx and ilmenite result in perovskite + Fe-phlogopite + Opx.
- (4) Two of the pyroxene-ilmenite symplectites examined contain abundant sulfide-bearing tubes which are preferentially located at the terminal contacts of elongated ilmenite laths. The assemblage is pyrrhotite + pentlandite which is partially oxidized to magnetite + geothite.
- (5) Ilmenite compositions in Opx assemblages show little variation from those in Cpx assemblages and both form a tight cluster between 9-10 wt% MgO.
- (6) Oriented lamellae of magnesian-titanohematites in ilmenites are present in 76% of the symplectic assemblages. This mineral has lower MgO (~7.5 vs 9.0 wt%), lower FeO (~25.0 vs 28.0 wt%) and lower TiO₂ (~44.0 vs 49.0 wt%) contents, but higher Fe₂O₃ (~21.0 vs 12.0 wt%)² and Al₂O₃ (0.5-1.0 wt%) concentrations than those of the ilmenite host which forms the main body of the assemblage with pyroxene. An additional 20% of the nodules examined contain an aluminous-Cr spinel, and the remaining 4% are homogeneous.
- (7) The discrete nodule suite and nodules encased in kimberlite exhibit similar ranges in compositions and exsolution assemblages to those present in symplectic pyroxene intergrowths. The one major exception is that many of the nodules contain trapped ovoid inclusions of calcite + pyrrhotite + pentlandite. Reactions between these inclusions and the ilmenite result in a consistent sequence which is: (a) magnetite at the inclusion contact; (b) an intervening rind which is a strongly zoned titaniferous

magnetite (10-22 wt% TiO_2 , and 1-4 wt% MgO); and (c) a magnesian-depleted ilmenite which is also higher in Fe_2O_3 than the adjacent host ilmenite.

(8) Kimberlite-ilmenite reaction contacts are comparable to those previously reported and these are typically a Mn ilmenite + magnesian titanomagnetite + perovskite, or alternatively rutile + sphene + Fe phlogopite.

(9) Polycrystalline ilmenites with pronounced polyhedral textures characteristic of intense stress annealing are abundant in the discrete nodule suite and in the pyroxene-ilmenite intergrowths; 67% of the former and 47% of the latter display this feature.

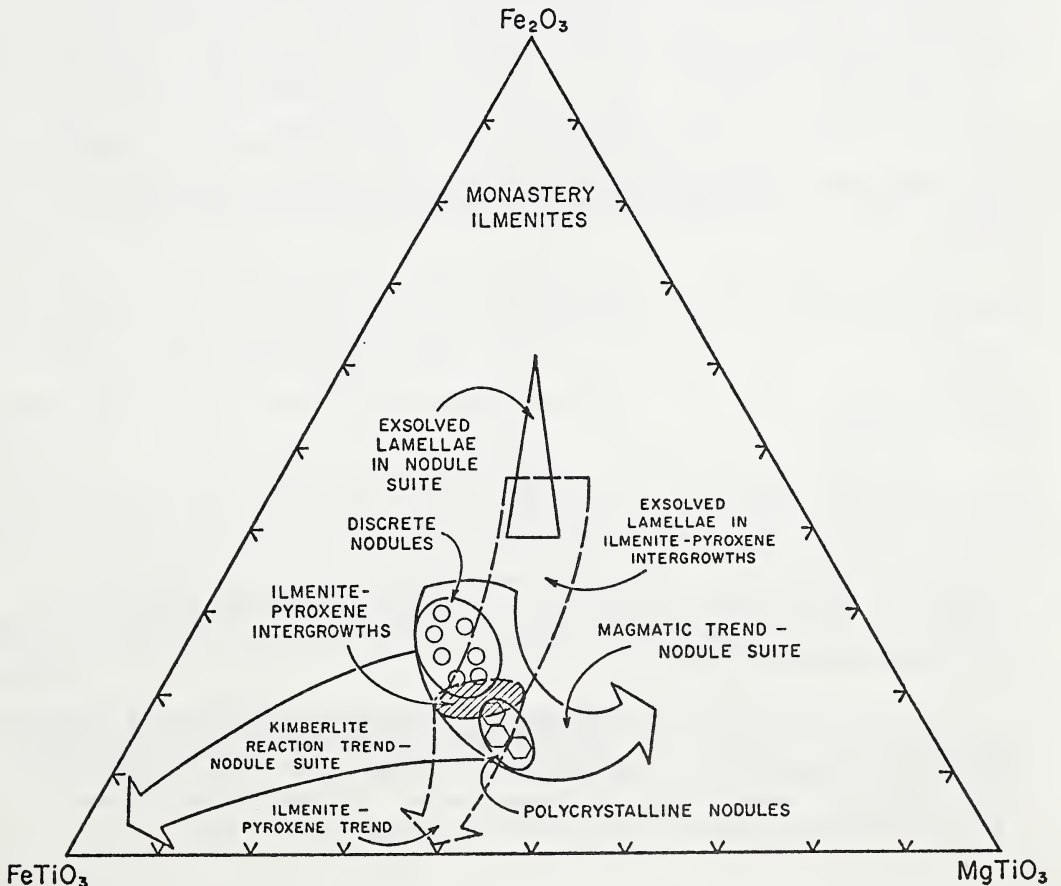
Two aspects of this study have received special attention. The first is a detailed analysis of ilmenite compositional variations among the nodule suites, and the second is related to "exsolution" intergrowths in ilmenite. Our data base consists of 792 electron microprobe analyses. These are summarized in Fig. 1 and the following conclusions may be drawn: (1) The cores of the discrete nodule suite form a tight cluster centered on $\text{Geik}_{30}\text{Ilm}_{55}\text{Hem}_{25}$; (2) Ilmenites in pyroxene intergrowths are lower in Fe_2O_3 contents than the discrete nodules and their core population reaches a maximum at $\text{Geik}_{35}\text{Ilm}_{45}\text{Hem}_{20}$; (3) The polycrystalline nodules have even lower Fe_2O_3 contents (15 mole % Geik) and FeTiO_3 contents are lower (Ilm_{40}); (4) Pronounced zoning is present in both the discrete nodules and in ilmenites in pyroxene intergrowths. The former is towards MgTiO_3 and the latter towards the join $\text{MgTiO}_3\text{-FeTiO}_3$; (5) Discrete nodules with closely adhering kimberlite have complex reaction mantles that include ilmenites whose compositions trend towards FeTiO_3 . Associated minerals are magnesian titaniferous magnetites and perovskite.

Our interpretation of these results suggests that there are at least four distinct events which can be identified: The first is the magmatic trend of the discrete nodule suite towards MgTiO_3 ; the second is the ilmenite-pyroxene trend towards $\text{FeTiO}_3\text{-MgTiO}_3$; the third is the kimberlite reaction trend towards FeTiO_3 ; and the fourth is an episode of exsolution in ilmenite. The magmatic nodule trend is a liquid-interaction trend and is most likely the result of a decrease in P_{total} with an accompanying decrease in f_{O_2} . The ilmenite-pyroxene trend is a reduction in the f_{O_2} path, and the kimberlite reaction trend marks the onset of nodule incorporation into the kimberlite. A small but marked displacement is apparent between the two compositional populations occupied by the cores of the discrete nodules and the cores of symplectic ilmenites and both have markedly different core-mantle reaction trends. These differences suggest one of two possible origins: (a) the discrete nodules and the symplectites are derived from different source regions with variable crystallization paths; or (b) the discrete nodules formed at high P_{total} followed by the symplectites at lower pressure. It is expected that continued growth of the discrete nodules, towards MgTiO_3 , would take place but that the pyroxene associated ilmenites would be protected because of their symplectic encasement. The latter origin is the preferred interpretation.

Lamellar intergrowths in ilmenite are of three types: (1) aluminous spinels; (2) magnesian-titanohematites; and (3) magnesian-titanomagnetites. All types are present in the discrete nodule suite but only the first two are observed in the symplectites. These minerals are lamellar in form and all have an exsolution-like appearance oriented along $\{0001\}$ planes in the host ilmenite. Mg-titanohematite and the Al-spinel are evenly distributed throughout single crystals of ilmenite, whereas the Mg-titanomagnetites are restricted to crystal margins and are frequently distorted. We interpret the Mg-titanohematites as

exsolution sensu stricto, suggest that the Al-spinel may be an exsolution-like process, and have demonstrated experimentally that the magnesian titanomagnetites can result as products of subsolidus reduction in the range $T=900-1200\text{C}$ and f_{O_2} 10^8 to 10^{14} atms. These experiments were performed on a Monastery ilmenite with $\text{MgO}=7.8$ wt% and runs in progress should yield a well defined $T-f_{\text{O}_2}$ grid for high MgO oxides.

In summary, we have identified two major ilmenite populations, one for the discrete nodule suite and one for those in pyroxene symplectites which we suggest are most likely derived from the same source region with the latter forming at slightly lower pressures. Although the reaction trends are drastically different, these can be accounted for by allowing progressive growth of the nodules under decreasing pressure and f_{O_2} , and by partial insulation of the pyroxene associated ilmenites in symplectic intergrowths. It is our contention, however, that none of the models proposed for pyroxene-ilmenite intergrowths (i.e. garnet decomposition; ilmenite or pyroxene replacement; eutectic crystallization; or exsolution) has adequately addressed (a) the variations in Opx and Cpx; (b) the modal variations of ilmenite and pyroxene; (c) the presence of associated sulfides; (d) the nature of reaction contacts between ilmenite and pyroxene; nor (e) provided an explanation for the abundance of exsolved ilmenite in the primary ilmenite constituent of pyroxene symplectic intergrowths.



REGIONAL AND LOCAL VARIATIONS IN THE CHARACTERISTICS OF DIAMONDS FROM SOME SOUTHERN AFRICAN KIMBERLITES

J.W. Harris (Grant Institute of Geology, West Mains Road, Edinburgh EH9 3JW, Scotland)

J.B. Hawthorne (Geology Department, De Beers Consolidated Mines Ltd., P.O. Box 616, Kimberley, S.A.)

M.M. Oosterveld (Computer Services Department, De Beers Consolidated Mines Ltd., P.O. Box 616, Kimberley, S.A.)

The diamond classification scheme (Harris et al 1975) has been used to obtain new data about diamond characteristics from several major kimberlite sources in southern Africa. Of the numerous relationships determined only the variation in crystal form and colour as a function of diamond size are considered in the following results because these relationships not only enable distinction to be made between the diamond sources studied, both on a local and regional basis, but also provide information about the environment of the diamond during and subsequent to its growth. The results are conveniently divided into four sections.

(1) Studies on diamonds from single kimberlite diatremes

a. Koffiefontein: The completion of the development levels at 244 m and 488 m at this mine has enabled crystal form and colour of diamond to be examined as a function of depth within the mine. The comparisons with surface productions indicate that crystal habit versus diamond size varies only slightly with depth. There is a steady increase in the proportion of octahedra from 5-20% with increasing diamond size, and this variation is not at the expense of the dodecahedra which contribute a fairly steady 20-25% to the diamond population. Macles and polycrystalline aggregates are also essentially constant through the size ranges at about 12% and 3% respectively. Broken and irregular diamonds constitute the remaining shape.

Colour variations are pronounced. With increasing depth over the common diamond size range, colourless diamonds decrease in proportion from about 60% to 40% and yellow and brown stones increase from 30% to 50%. A similarity of colour variation in each of the levels however is that yellow diamonds increase in proportion at the expense of browns as diamond size increases.

b. Finsch: At this mine, diamonds from the current production are compared with those from the new 348 level. Only minor variations of crystal habit with size are noted for both levels. Again there are very constant proportions of flattened dodecahedra (3%), macles (20%), irregulars (35%), and polycrystalline aggregates (2%) over the size ranges. Octahedra and dodecahedra account for the remaining 40% of the diamond population and with increasing size the octahedra steadily increase in proportion from 15-20%.

Colour variation between levels is dominated by the virtual disappearance of the transparent green-coated diamond on the 348 m level and this is accompanied by a complementary increase in the brown and colourless stones by some 10% and 5% respectively. At both levels yellow diamonds increase against brown with increasing diamond size.

c. Premier: From this mine diamond samples from two specific kimberlites on the 520 m level are characterised and compared with diamonds from the general production. At the 520 m level the brown and grey kimberlites respectively occupy one-fifth and four-fifths of the pipe area. Only very slight differences in morphology are observed from diamonds in the two specific kimberlites and the general production. With increasing diamond size octahedra and polycrystalline aggregates remain constantly low (<5%), the dodecahedra constitute about 15%, but macles steadily increase from 15-25%. The proportion of irregular diamonds is high, varying between 50-60%.

Differences of diamond colour between the two specific kimberlites are again marked. Relative to the brown kimberlite there is a 10% decrease in colourless diamonds, a 20-25% increase in yellows, an 8-10% increase in transparent green-coated diamonds, and a 30% increase in brown diamonds. Yellows also increase against browns as diamond size increase. Relative to diamond colour in the general production diamonds from the specific kimberlites show a 10% decrease in colourless stones.

(2) Studies on diamonds from a kimberlite dyke swarm at Zwartruggens

Classification of these diamonds showed them to be morphologically unique in comparison with other southern African sources in that the diamond population contained less than 2% macles; other sources have a macle content of at least 10%. Another prominent feature is the presence of between 5-10% of cubes; other sources so far studied have only 1%. Predominant amongst the several colours are between 2-5% of orange and amber stones compared to < 1% elsewhere. Multiply coloured diamonds (amber/colourless) are also a feature of this diamond source.

(3) Studies of diamonds from adjacent kimberlite diatremes

a. The Main and Satellite Pipe at Letsing-le-terai: A characteristic of the morphology of the diamonds from these diatremes is the very low octahedron content (<2%) coupled with a low macle content at about 10%. Differences in morphology between diamonds from the two mines appear slight, but there are colour differences, particularly in the proportion of brown and grey stones. An unusual colour feature for both mines is the absence of transparent green-coated diamonds.

b. Koffiefontein and Ebenhaezer diatremes: The only difference between the diamond morphology of these diatremes is that over the common size ranges there is a slightly higher proportion (3%) of flattened dodecahedra at Ebenhaezer. A diamond colour comparison shows that the proportion of specific colours varies, the diamond colours at Ebenhaezer being more similar to those of the 244 m or 488 m levels at Koffiefontein than with the surface production, (see before).

c. The Kimberley Group of Mines: Only preliminary data are available. The results show that the morphologies of the diamonds from Bultfontein, De Beers, Dutoitspan, and Wesselton are similar whilst colour differences are evident.

(4) Regional Variations of Diamond Morphology

On the basis of morphology the diamonds from the various sources can be

broadly divided into two groups which appear independent of kimberlite emplacement age. The first group comprises the Kimberley mines, Koffiefontein and Finsch and are characterised by the steady increase in the proportion of octahedra with increasing diamond size. There are also similar proportions of flattened dodecahedra, macles, and polycrystalline aggregates, although the proportion of irregular diamonds varies considerably between sources. Premier, Zwarttruggens, and Letsing-le-terai form the other group which has a much lower proportion of octahedra remaining essentially constant throughout the diamond size range studied. The diamonds from each of these mines however varies in proportion of dodecahedra, macles, cubes and irregulars. The particularly distinctive diamond characteristics from the kimberlite dykes at Zwarttruggens are not a function of the mode of kimberlite intrusion, as such characteristics are absent from other fissure mines such as those at Bellsbank.

Variation of Morphology and Colour

The principal primary morphologies of diamonds beneath southern Africa are the octahedron, macle, and their aggregates. Subsequent to their formation the diamond population from each of the kimberlites underwent modification. Resorption processes, possibly caused by the volatiles during kimberlite ascent, resulted in the formation of the dodecahedra and flattened dodecahedra. Most of the irregular or broken diamonds post-date the resorption event and fracturing probably occurred during kimberlite emplacement. The slight differences between the morphologies of the diamonds from the grey and brown kimberlites at Premier, or between diamonds from adjacent kimberlite diatremes can also be related to those late-stage processes.

The colourless, yellow, amber and brown colours noted in these studies are explained either by the way in which the impurity nitrogen became aggregated in, or combined with, carbon in the initial diamond growth environment, or by the extent to which the various established diamond populations subsequently underwent plastic deformation. The variations in the proportions of diamond colour with depth are not due to post-emplacement effects but are considered to be a consequence of the variation of the size distribution of diamonds within the kimberlite. Transparent green-coated diamonds result from α -particle irradiation by uranium or thorium atoms after kimberlite emplacement. The diamonds in unweathered kimberlite, as at Premier and Koffiefontein, are damaged according to the original distribution of radioactive elements in the kimberlite, but in weathered kimberlite, as until recently at Finsch, these elements have probably been mobilised in the groundwater and consequently a much higher proportion of the diamond population is affected.

References

- Harris, J.W., Hawthorne, J.B., Oosterveld, M.M. and Weymeyer, E. (1975). A Classification Scheme for diamond and a comparative study of South African Diamond Characteristics. In "Physics and Chemistry of the Earth" (Eds. Ahrens, L.H., Dawson, J.B., Duncan, A.R., and Erlank, A.J.) Vol. 9, p. 765-783 Pergamon Press, Oxford.

CLINOPYROXENE-RICH SHEETS IN GARNET-PERIDOTITE: XENOLITH SPECIMENS FROM THE MATSOKU KIMBERLITE PIPE, LESOTHO

B. Harte (Grant Institute of Geology, University of Edinburgh, Scotland)
J.J. Gurney (Dept. of Geochemistry, University of Cape Town, South Africa)
K.G. Cox (Dept. of Geology and Mineralogy, University of Oxford, England)

Introduction:

Examination of xenoliths collected from the Matsoku kimberlite pipe in 1973 has shown the existence of clinopyroxene-rich garnet-lherzolite sheets or dikes occurring within a peridotite host rock. The contacts of the sheets are extremely sharp and roughly planar, whilst the host rock is garnet-lherzolite of the type poor in clinopyroxene and garnet and referred to as common peridotite (CP) by Cox et al. (1973). The clinopyroxene-rich sheets range in thickness from approximately 3.5 to 16 cms. In some cases clinopyroxene is only abundant (35 to 45 modal %) in the marginal zones (1.2 to 3.5 cms thick) of the sheets, whilst their interiors are largely of orthopyroxene and olivine whose relative modal proportions vary considerably. In other cases clinopyroxene is abundant throughout the sheets, though some modal layering roughly parallel to the sheet margins may be present on scales varying from 0.2 to 0.5 cms.

Petrography of clinopyroxene-rich sheets:

In addition to olivine, orthopyroxene, clinopyroxene and garnet, the clinopyroxene-rich sheets may contain primary-metasomatic minerals (Harte and Gurney, 1975), especially ilmenite (locally exceeding 10 modal %). For the most part the olivine and pyroxenes form clear and relatively small grains (0.5 to 1.0 mm) with a mixture of moderately granoblastic-polygonal and rational grain boundaries. Clinopyroxene and more commonly orthopyroxene also occur in cloudy grains showing fine lamellae of included silicate and ilmenite which appear to be exsolution products. These cloudy grains often show irregular grain boundaries and a partly interstitial habit. In the relatively clinopyroxene-poor interiors of some sheets, large orthopyroxenes may occur showing clear cores surrounded by cloudy zones and sometimes with a clear outer selvage. The silicate lamellae in the cloudy orthopyroxenes are of clinopyroxene. Large orthopyroxenes are often accompanied by large olivine crystals with irregular grain boundaries.

The amount of garnet in the sheets is widely variable. A partial selvage (around 0.2 cms thick) of garnet is quite common at the contact of the sheets with the host CP, and a broader zone (up to 2.0 cms) of relatively high (up to 25%) modal garnet occurs at the margins of some sheets. In the clinopyroxene-poor interior of some sheets garnet forms <5.0 modal %, whilst in other cases 0.2 cm wide seams or stringers contain >50 modal % garnet. The garnet occurs principally in distinctive poikiloblastic grains, but also in "pools" (Cox et al. 1973) which might represent droplets of magmatic liquid.

Mineral and bulk-rock chemical compositions:

Pertinent aspects of these data are summarised in Figs. 1 and 2 and below:

(a) Olivine and orthopyroxene compositions are closely similar throughout any sheet and the adjacent host CP. This feature includes the orthopyroxene host of the cloudy orthopyroxenes, but not the bulk composition of such crystals which are enriched in clinopyroxene and ilmenite molecules.

(b) Clinopyroxene is often of nearly constant composition in the sheets and the adjacent host rock but a sharp change in Cr/Al ratio occurs across the contact in some xenoliths (Fig. 1a).

(c) Within the sheets garnet in both poikiloblastic and "pool" forms is of similar composition, but the host CP garnet varies in Cr/Al ratio and there is usually an abrupt change in this ratio across the contact (Fig. 1b).

(d) Compared with xenoliths of CP alone, the CP host of the sheets is enriched in Fe (Figs. 1 and 2) and all sheets and host CP have Mg/Fe ratios intermediate between those of CP xenoliths interpreted as depleted mantle and xenoliths interpreted as cumulates (Gurney et al. 1975).

(e) The compositions of homogenous pyroxenes indicate a common T and P similar to that of other Matsoku xenoliths (quoted as near 1050°C and 50 kbar by Gurney et al., 1975).

Discussion:

The structural and textural features of the sheets indicate a magmatic origin. The cloudy pyroxenes are related to this high temperature event, subsequent to which the minerals re-equilibrated to a common T. and P. Transfer of Fe and Mg between the sheets and their host rocks has occurred, but the movement of other elements, especially Cr, appears to have been restricted.

It is proposed that the large olivine and orthopyroxene crystals (rimmed by cloudy orthopyroxene) in the interiors of sheets represent residual crystals of a partial melt, whose progressive crystallisation formed the clinopyroxene-rich margins of sheets and eventually the garnet found concentrated near contacts and in thin seams. Such a sequence conforms with a crystallisation path along the clinopyroxene cotectic surface to the pseudoinvariant point where garnet commences crystallisation (O'Hara, 1970). The closely similar Cr/Al of garnet and clinopyroxene near the margin of all sheets supports this mode of evolution.

The high bulk CaO/Al₂O₃ of some clinopyroxene-rich margins (Fig. 2) have a cumulative aspect and some of the low melting fraction liquid may have been lost from the sheets. This is supported by the occurrence of garnet of the same composition as that of the sheets (Fig. 1b) in a garnet-rich vein in an orthopyroxenite (LBM 40). The mode of this vein as well as that of "pools" (Cox et al. 1970) suggest that the low melting fraction liquid may be very low in normative clinopyroxene.

The close association of primary-metasomatic minerals with some sheets, may indicate that this metasomatism is related to the magmatic event responsible for the clinopyroxene-rich sheets.

References:

- Cox, K.G., Gurney, J.J. and Harte, B., 1973; in 'Lesotho Kimberlites' (ed. P.H. Nixon) p. 76-100.
Gurney, J.J., Harte, B. and Cox, K.G., 1975; Physics Chem. Earth, 9, p. 507-523.
Harte, B. and Gurney, J.J., 1975; Carn. Inst. Wash. Yr. Bk. 75, p. 528-536.
O'Hara, M.J., 1970; Phys. Earth Planet Int., 3, p. 263-245.

Figure Captions:

- Fig. 1 Atomic ratios Cr/(Cr+Al) and Mg/(Mg+Fe) in: (a) clinopyroxene (b) garnet.
Fig. 2 Bulk rock weight percentages of: FeO* (total Fe as FeO), CaO, Al₂O₃ and Cr₂O₃ plotted against MgO/(MgO + FeO*).

In both figures the symbols indicate the following rock types: \diamond garnet-lherzolites of common peridotite (CP) type - interpreted as depleted mantle.
 \square garnet-lherzolites and garnet-pyroxenite - interpreted as cumulates.
 \blacktriangle clinopyroxene-rich margins of clinopyroxene-rich sheets. \blacklozenge common peridotites (CP) in contact with clinopyroxene-rich sheets. \triangle complete sections across clinopyroxene-rich sheets.

A DIAMOND GRAPHITE ECLOGITE FROM THE ROBERTS VICTOR MINE

C.J. Hatton & J.J. Gurney

(Geochemistry Department, University of Cape Town, Rondebosch 7700, South Africa)

HRV247, an eclogite from the Roberts Victor kimberlite pipe displays the primary assemblage garnet, clinopyroxene, graphite, diamond, pyrrhotite, rutile and possibly phlogopite. The rock is believed to have formed as a cumulate from partial melting of peridotite mantle. The well defined crystal shape of graphite is good evidence that this phase grew in a liquid medium.

Compositions of the garnet and clinopyroxene were determined (Table I). Garnet rims were found to be pyrope rich relative to cores. Garnets at one end (A) of the nodule were found to be pyrope rich relative to the other (F2), (Figure 1). Clinopyroxene rims were found to be diopside rich relative to cores and similarly clinopyroxenes in A were found to be diopside rich relative to F2. The nodule therefore evolves from jadeite-grossular compositions in F2 toward diopside-pyrope compositions in A. F2 is the bottom of the nodule, A the top.

The $\ln K_D$ for Fe/Mg distribution between garnet and coexisting clinopyroxene (Raheim and Green, 1974) of F2 is near to 1.4 while A has values close to 1.2.

Graphite is concentrated in F2 and diamond in A (Robinson, 1977). The carbon content of the nodule is approximately .15wt%.

The features outlined above may be explained if portion F2 formed at P,T within the graphite stability field while A formed at P,T within the diamond stability field. These conditions are illustrated in Figure 2 and indicate that a path of increasing pressure (and increasing temperature) must be followed. Pressure increase can be caused by a sinking magma (considered unlikely) or by increasing gas overpressure. This latter possibility cannot be discounted. However, the compositional variation in the silicates is described by a model of magma mixing, and the possible genesis of diamond will be incorporated into this model.

Magma mixing has been invoked to explain rapid compositional variations in several group II eclogites (e.g. HRV15, Hatton & Gurney, 1977a). It is envisaged that continued partial melting of garnet lherzolite produces successively more magnesian liquids at correspondingly higher temperatures (Mysen & Kushiro, 1976) and that these liquids are continuously intruded into and mixed in a magma chamber at higher levels. The compositional variation in HRV247 is on the scale of centimetres. In a large magma body hundreds of metres thick, magma compositional variation will be reflected over correspondingly large distances (metres) in the cumulates. The small scale of variation in HRV247 suggests that the coexisting magma was only metres thick.

Heat loss from a magma chamber is expected to be most rapid at the top wall. The warm cumulate crystal pile will ensure a slower rate of heat loss from the bottom of the magma chamber. Thus a heat profile through this body will reveal a cold upper portion, a hot centre and a warm lower portion.

A possible source of carbon is calcium carbonate. This consideration is prompted by the presence in a sulphide eclogite WM7, of small calcium carbonate (60wt%CaO) blebs on the margin of sulphide. On reaction with the silicate magma at least some dissociation of CaCO_3 will occur by reaction of the type $\text{CaCO}_3 = \text{Ca}^{++} + \text{O}^{--} + \text{CO}_2$. Some conversion of CO_2 to diamond or graphite might

occur depending on the fO_2 of the silicate magma. fO_2 of mantle material may be approximated by the iron wustite buffer (Sato pers. comm. to Huggins et al. 1976). P,T conditions under which fO_2 (IW) equals fO_2 defined by the graphite-CO-CO₂ buffer have been obtained by solution of equations given by Heubner (1971), and are diagrammatically represented in Figure 2. At pressures above this curve CO₂ is stable relative to graphite, if fO_2 is defined by the iron-wustite buffer. In the presence of H₂O, P_{CO_2} will usually be less than P total, and the curve fO_2 (IW) = fO_2 (G-C-CO₂)² will lie at higher temperature for a given pressure. Nevertheless, taking the equations at face value, at pressures below about 45kb carbon dioxide will be reduced to graphite, and to diamond at lower temperatures. If it is assumed that magma from which the diamond-graphite eclogite crystallises was initially at temperatures near 1100°C, and a pressure of 42kb then with heat loss diamond will crystallise adjacent to the cold upper wall (T 1020°C) while graphite will be stable near the warm bottom wall of the magma chamber. Garnet and clinopyroxene crystallise with diamond near the upper wall but on settling through the hot central portion are largely resorbed, while less reactive diamond shows only limited resorption. The small scale of the magma chamber allows significant concentrations of diamond to reach the bottom of the magma. Thus graphite settles first together with early low temperature cumulates, and diamond occurs together with later, higher temperature cumulates. Two zones of nucleation are proposed - the top and bottom walls of the magma chamber. The garnet inclusion in garnet 5 (table 1) may have crystallised at the upper wall of the magma chamber.

The model discussed above attempts to explain the coexistence of diamond and graphite in a particular eclogite, but if small volumes of magma are common in the mantle, the model may have wider application. Nucleation of graphite in the diamond stability field, rapid cooling of magma, the effects of other volatiles and of high gas overpressures are alternative processes which will allow coexistence of diamond and graphite in an eclogite nodule.

References

- Hatton, C.J. and Gurney, J.J. This volume (1977a)
 Heubner, J.S. in Ulmer, G.C. Springer-Verlag, Berlin, 123 (1971)
 Huggins, F.E., Rosenhauer, M. and Virgo, D. Eos, 57, 339 (1976)
 Raheim, A. and Green, D.H. Contrib. Mineral Petrology, 48, 179 (1974)
 Robinson, D.N. This volume (1977)

Figure Legends

- Fig. 1. Ca-Mg-Fe plot of clinopyroxenes (near Ca₅₀) and garnets in HRV247. Upper arrow indicates compositions in garnet 5. Lower arrow indicates garnet inclusion in garnet 5.
- Fig. 2. P,T plot with range in K_D ratios of rock; theoretical diamond-graphite equilibrium curve; curve in P,T space along which oxygen fugacity of the graphite, carbon monoxide, carbon dioxide buffer is equal to the oxygen fugacity defined by the iron-wustite buffer; and a possible P,T path followed during evolution of HRV247.

Table 1.

Garnet compositions in HRV247

	Portion A		Portion F		Garnet 5		Portion F		Portion A		Portion F	
	Centre	Edge	Centre	Edge	Centre	Garnet inclusion	Centre	Edge	Centre	Edge	Centre	Edge
SiO ₂	41.6	41.6	40.6	40.6	41.5	41.5	41.3	41.4	55.0	55.4	55.2	55.5
TiO ₂	.27	.22	.38	.32	.36	.36	.30	.27	.24	.26	.31	.29
Al ₂ O ₃	23.6	23.6	23.0	23.2	23.3	23.3	23.3	23.4	5.13	5.15	7.80	7.76
Cr ₂ O ₃	.06	.06	.05	.09	.10	.10	.05	.05	.07	.08	.07	.07
FeO	10.4	10.4	11.8	12.2	11.1	11.1	10.6	10.6	2.51	2.49	2.61	2.62
MnO	.26	.26	.22	.23	.33	.33	.22	.24	.03	.04	.05	.01
MgO	16.7	17.1	13.9	14.2	17.8	17.8	15.9	16.3	14.8	14.8	12.6	12.6
CaO	7.45	6.80	9.80	9.25	5.34	5.34	8.04	7.55	19.2	19.3	17.5	17.3
Na ₂ O	.09	.10	.11	.12	.06	.06	.09	.08	3.01	2.91	4.65	4.57
K ₂ O									.05	.06	.06	.06
Total	100.4	100.1	99.9	100.2	99.9	99.9	99.8	99.9	100.0	100.5	100.3	100.8

Clinopyroxene compositions

	Portion A		Portion F		Portion A		Portion F	
	Centre	Edge	Centre	Edge	Centre	Edge	Centre	Edge
SiO ₂	41.6	41.6	40.6	40.6	41.5	41.5	41.3	41.4
TiO ₂	.27	.22	.38	.32	.36	.36	.30	.27
Al ₂ O ₃	23.6	23.6	23.0	23.2	23.3	23.3	23.3	23.4
Cr ₂ O ₃	.06	.06	.05	.09	.10	.10	.05	.05
FeO	10.4	10.4	11.8	12.2	11.1	11.1	10.6	10.6
MnO	.26	.26	.22	.23	.33	.33	.22	.24
MgO	16.7	17.1	13.9	14.2	17.8	17.8	15.9	16.3
CaO	7.45	6.80	9.80	9.25	5.34	5.34	8.04	7.55
Na ₂ O	.09	.10	.11	.12	.06	.06	.09	.08
K ₂ O								
Total	100.4	100.1	99.9	100.2	99.9	99.9	99.8	99.9

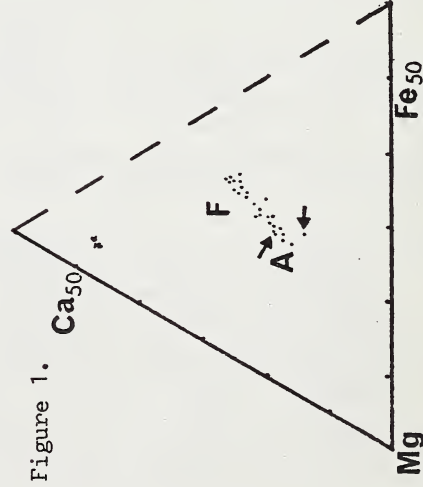


Figure 1.

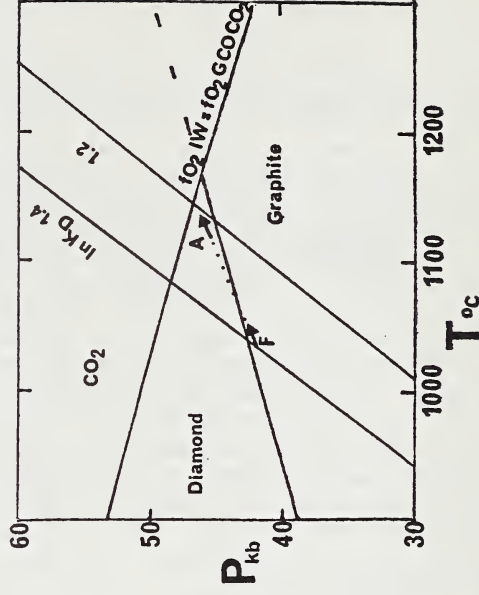


Figure 2.

KYANITE ECLOGITES FROM THE ROBERTS VICTOR MINE

C.J. Hatton & J.J. Gurney

(Geochemistry Department, University of Cape Town, Rondebosch 7700, South Africa)

Kyanite has been observed in both group I and group II (Hatton & Gurney, 1977a) Roberts Victor eclogites. Several different types of occurrence can be noted within each group.

Homogeneous kyanite eclogites in group I.

- (i) Trace amounts (less than 1%) of kyanite were observed in HRV26 (Figure 1,a), an eclogite of a composition very similar to the bulk of group I eclogites.
- (ii) Approximately five percent kyanite occurs in grossular rich members JJG4 and JJG30 of the group I eclogites (Figure 1,b).
- (iii) Abundant kyanite (greater than 10%) is present in kyanite eclogites PJJ17, JJG88 and RV390/4 (Figure 1,c).

No group I garnet compositions have been found to lie between b and c in figure 1.

Homogeneous kyanite eclogites in group II.

Kyanite occurs in two fresh group II eclogites HRV147 and HRV272 (d and e respectively in figure 1). Limited compositional variation is found in these specimens.

Grosspydites.

Homogeneous grosspydites (garnet > 50% grossular, clinopyroxene and disthene = kyanite) are rare at Roberts Victor, although kyanite eclogite blebs in the inhomogeneous kyanite eclogites are of grosspydite composition. A unique grosspydite containing coesite and sanidine as accessory phases has been found (Smyth & Hatton, 1976). Coesite grosspydites probably are present (Smyth, 1977).

Inhomogeneous kyanite eclogites in group I.

The majority of kyanite bearing eclogites are of this type. Kyanite occurs in a discrete bleb together with grossular garnet and jadeitic clinopyroxene. Examination of a number of samples indicates that the kyanite eclogite bleb is entirely surrounded by ordinary eclogite. The compositional variation of garnet between kyanite eclogite and eclogite is illustrated for JJG143 (Figure 1, line 3) and HRV17 (Figure 1, line 2 and Figure 2). The vertical variation in mineralogy and mineralogical composition of HRV17 illustrated in figure 2 may be considered as a type sequence. A is an ordinary eclogite layer with equal amounts of pyropic garnet and diopsidic omphacite typical of group I eclogites. Layer D contains kyanite, grossular garnet and jadeitic omphacite. The interface A - D is marked by sharp compositional variation as illustrated by the accompanying graph of CaO content of garnet. C is a kyanite free, grossular garnet, jadeitic omphacite layer, again grading sharply into the pyrope garnet rich band B₁. The upper part of layer B contains equal amounts of pyropic garnet and diopsidic omphacite. Garnet and clinopyroxene compositions in layers A and B are similar. Garnet cores in A and B are CaO poor relative to rims (Figure 2), except for garnet close to the interface A - D which contains a CaO rich core. A possible explanation of this feature is that the garnet nucleated in layer D, settled and

continued to grow in the CaO poor layer A. It is implied that D lay above A, and hence that the garnet rich layer lay above the kyanite eclogite bleb. The presence of the garnet rich layer above the kyanite eclogite bleb is consistent with the following interpretation of the geometry of HRV30 (Figure 3). K_D ratios (Raheim & Green, 1974) indicate that isobaric temperatures of equilibration were lower for the kyanite eclogite bleb than for surrounding eclogite. Incipient partial melting has been observed in kyanite eclogite (Switzer & Melson, 1969) but not, so far as is known, in ordinary eclogite. These latter two observations indicate that the solidus temperature of kyanite eclogite is lower than surrounding eclogite, hence the kyanite eclogite bleb may have been liquid while the garnet rich layer was in a semi-solid or plastic state. HRV30 consists of two discrete kyanite eclogite blebs in ordinary eclogite (Figure 3a) which coalesce within a distance of 10cm (Figure 3b). The coalesced kyanite bleb has a convex surface with the garnet rich layer which is thought to be caused by upward bulging of the liquid, and therefore less dense, kyanite eclogite bleb. The proposed orientation is consistent with that suggested for HRV17.

Inhomogeneous kyanite eclogites not related to group II or group I

Discrete kyanite eclogite blebs are found in medium grained (1.5mm compared to average group I grain size of 4mm) eclogites which are of similar geometry to group I inhomogeneous kyanite eclogites but which are more MgO rich in garnet eclogite compositions. Lateral variation in garnet composition in sample HRV116 (Figure 1, line 1) was found to follow a similar pattern to that observed for vertical variation in HRV17 (Figure 2). Garnet compositions in the kyanite blebs are similar to those in the group I inhomogeneous kyanite eclogites (Figure 1).

Conclusion

The discussion of the reverse zoning in garnets in HRV17 at interface A - D and of the geometry of HRV30 implied the coexistence of two liquids which are by definition, immiscible. The origin of kyanite eclogite blebs in Roberts Victor eclogites has been explained in other contexts (Lappin & Dawson, 1975; Chinner & Cornell, 1973; Cox, 1975) but the sharp interface between the grossular garnet, jadeitic clinopyroxene, kyanite bleb and surrounding eclogite; and the occurrence of kyanite eclogite in isolated blebs are consistent with the possibility that the inhomogeneous eclogites originated by processes of liquid immiscibility.

References

- Chinner, G.A. and Cornell, D.H. Contrib. Mineral. Petrol., 45, 153 (1974)
Cox, K.C. Volume of abstracts, Kimberlite Symposium, Cambridge (1975)
Hatton, C.J. and Gurney, J.J. This volume (1977a)
Lappin, M.A. and Dawson, J.B. Phys. Chem. Earth, 9, 351 (1975)
Raheim, A. and Green, D.H. Contrib. Mineral. Petrol., 48, 179 (1974)
Smyth, J.R. Amer. Mineral in press (1977)
Smyth, J.R. and Hatton, C.J. Earth Planet, Sci. Letters, 34, 284 (1976)
Switzer, G. and Melson, W.G. Smithsonian Contrib. Earth Sciences, 1,1 (1969)

Figure Legends

- Fig. 1. Ca-Mg-Fe plot of garnets. a,b,c (open circles) and d,e (filled squares) represent garnets in homogeneous kyanite eclogites. Lines 1,2,3 represent the range in garnet compositions in inhomogeneous kyanite eclogites.
Fig. 2. Explanation in text.
Fig. 3. Oblique lines - pyrope rich band. Dots - kyanite eclogite.

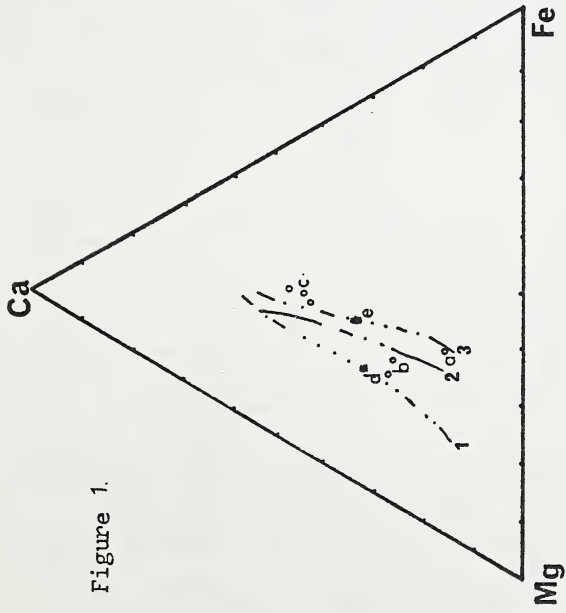


Figure 1.

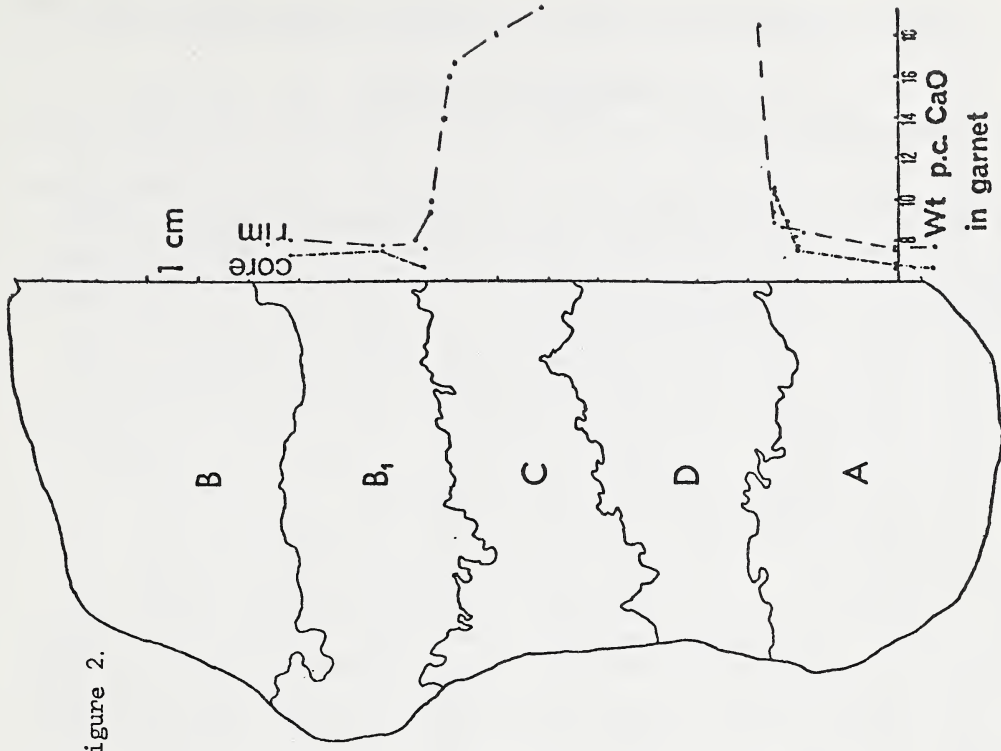


Figure 2.

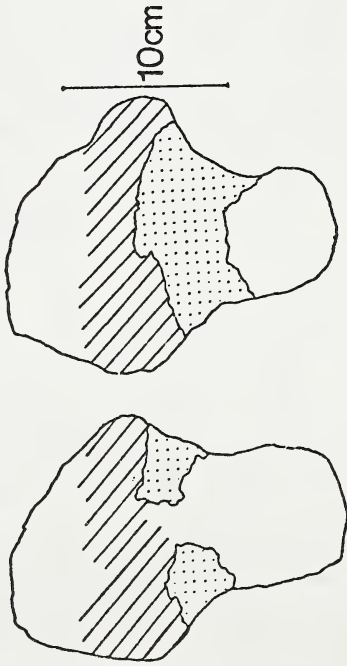


Figure 3. a b

IGNEOUS FRACTIONATION TRENDS IN ROBERTS VICTOR ECLOGITES

C.J. Hatton and J.J. Gurney

(Dept. of Geochemistry, University of Cape Town, Rondebosch 7700, South Africa)

A wide range in compositions has been revealed in general studies of the Roberts Victor eclogites (Kushiro & Aoki, 1968; MacGregor & Carter, 1970; Whitfield, 1971). MacGregor & Carter (1970) recognised two groups on textural grounds and identified the group I eclogites as cumulates and group II eclogites as the corresponding liquids. The higher K_2O in clinopyroxene of group I (Erlank, 1970) suggests that group II eclogites cannot be coexisting liquids. Data of the present study indicates that most, if not all of the eclogites are cumulates. The pervasive secondary alteration along grain boundaries by kimberlite has obscured the nature of the original intercumulus mineralogy. The possible effects of reequilibration of the cumulates with intercumulus material are therefore difficult to evaluate. Group I eclogites present a rather altered appearance, in contrast to the group II eclogites which are, by comparison fresh in appearance.

Several important points were noted during an examination of two hundred eclogite slabs. In certain eclogites kyanite was found to be confined to discrete zones of chemically distinctive character (Hatton & Gurney, 1977b). Clinopyroxene megacrysts were found entirely surrounded by biminerallitic eclogite (e.g. HRV77). Altered orthopyroxene was found to be present in a number of Mg-rich eclogites. High values of Cr_2O_3 (> 1wt%) in garnet and clinopyroxene of orthopyroxene bearing eclogites and certain other eclogites were found. In most cases the chrome rich eclogites exhibited considerable compositional inhomogeneity. Primary mica was identified in at least two eclogites. Na_2O contents of garnet and K_2O contents of clinopyroxene at levels greater than 0.10wt% were common in group I eclogites but are generally lower in group II. No genetic association of Na_2O in garnet or K_2O in clinopyroxene with diamond or graphite eclogites was discerned.

Representative analyses covering the range of composition in the thousand analyses carried out during this study are presented in table 1 and figure 1. In figure 1 clinopyroxene and garnet compositions lie at the upper and lower ends of the tie lines.

Analyses c, a and b are from a distinctly layered eclogite, HRV15 which contains hercynite spinel as a primary phase, and which was selected because the specimen illustrates the wide range in composition which may be found in a single group II eclogite nodule. Garnet and clinopyroxene of composition c lie 1cm from one end of the nodule. Compositions change toward those represented by analyses a lying 8cm from c. At the far end of the nodule compositions given by analyses b appear to be reverting toward those of c. A relatively rapid change in the magma toward more Mg, Cr compositions is indicated from c to a with a reversion toward Mg, Cr-poor compositions between a and b.

Garnet composition a is fairly typical of most type II garnets examined.

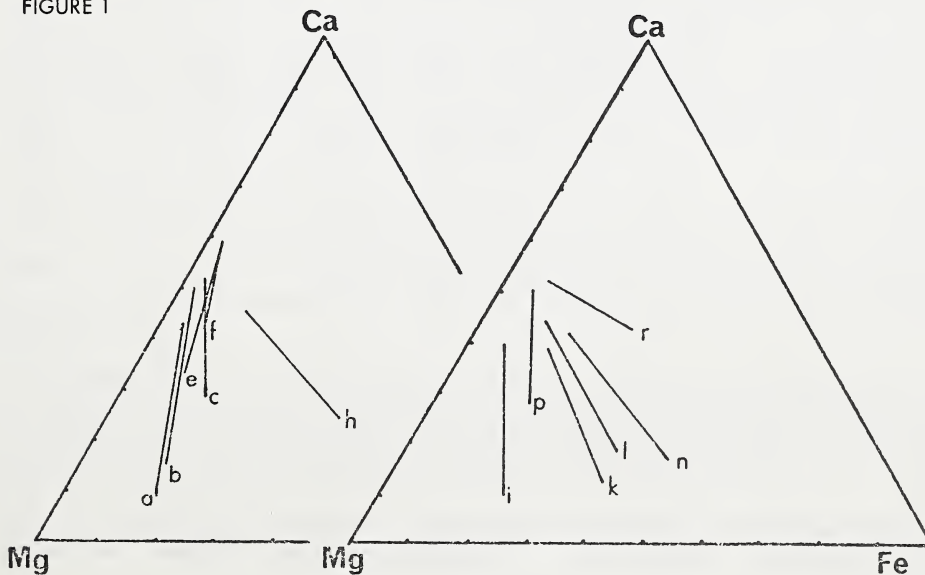
Core and rim analyses of a garnet and a clinopyroxene in a corundum eclogite RV372 of variable composition are tabulated as analyses e and f respectively. Iron rich members of the group II eclogites are represented by JJG6-h.

The most magnesian rich member of group I eclogites is HRV249-i. Most

TABLE 1

	Group II						Group I					
	c	a	b	e	f	h	i	k	l	n	p	r
	HRV15	HRV15	HRV15	RV372	RV372	JJG6	HRV249	HRV77	HRV77	XRV5	JJG30	PJL17
	Gt1	Gt5	Gt6	Gt1	Gt1	Gt	Gt	Gt3 in	Gt3 in	Gt	Gt	Gt
				Core	Rim			eclogite megact				
SiO ₂	41.9	42.1	42.5	41.5	41.1	39.7	42.4	39.9	39.8	39.6	40.7	39.7
TiO ₂	.12	.15	.17	.03	b.d.	.13	.42	.26	.27	.31	.25	.35
Al ₂ O ₃	24.0	23.6	24.1	24.0	23.7	22.4	23.8	22.7	22.7	22.2	23.2	22.7
Cr ₂ O ₃	.16	.83	.21	.11	.10	.09	.03	.17	.21	.09	.08	b.d.
FeO	7.55	8.21	7.62	7.21	6.52	19.1	11.0	18.0	17.5	21.7	11.4	13.0
MnO	.13	.23	.19	.12	.14	.34	.27	.43	.38	.37	.21	.23
HgO	16.1	21.2	20.1	14.5	12.5	9.54	19.7	13.7	12.2	9.89	14.2	8.29
CaO	11.6	3.56	6.02	12.9	16.0	9.06	3.74	4.47	6.93	6.10	10.5	16.0
Na ₂ O	b.d.	b.d.	.05	.05	b.d.	.07	.12			.16	.09	.11
Total	101.6	99.9	101.0	100.3	100.0	100.4	101.4	99.6	100.0	100.4	100.7	100.4
	c	a	b	e	f	h	i	k	l	n	p	r
	Cp1	Cp4	Cp7	Cp1	Cp1	Cp	Cp	Cp in	Cp in	Cp	Cp	Cp
				Core	Rim			eclogite megact				
SiO ₂	53.5	56.1	54.6	50.9	51.0	55.5	56.0	54.8	55.4	54.9	56.9	56.3
TiO ₂	.09	.17	.05	.03	b.d.	.15	.39	.30	.33	.37	.27	.29
Al ₂ O ₃	14.1	6.09	11.5	20.1	20.5	9.56	4.16	7.60	9.86	8.38	16.7	17.4
Cr ₂ O ₃	.16	.48	.18	.13	.13	.10	.05	.17	.19	.11		b.d.
FeO	1.33	2.12	1.25	1.01	.94	5.58	4.03	6.29	4.41	6.99	1.63	2.03
MnO	b.d.	.04	b.d.	b.d.	.03	.03	.08	.10	.04	.09		b.d.
MgO	10.3	14.8	11.4	7.09	6.94	9.47	16.7	11.5	10.2	10.2	6.91	6.06
CaO	15.8	16.9	16.6	15.3	15.0	14.4	17.2	13.1	13.7	13.9	10.9	10.7
Na ₂ O	4.95	3.65	4.76	5.68	6.11	5.86	2.68	5.37	5.89	5.22	7.32	7.51
K ₂ O	.05	.05	.06	b.d.	b.d.	b.d.	.11	.11	.13	.17	.10	.16
Total	101.3	100.4	100.4	100.2	100.6	100.6	101.4	99.3	100.1	100.3	100.7	101.0
lnK _D	1.29	.99	1.24	1.25	1.35	1.22	.84	.88	1.20	1.16	1.22	1.54
T(°C)	1058	1177	1077	1073	1037	1083	1248	1230	1093	1107	1083	971
at 40kb												

FIGURE 1



group I compositions lie near to HRV77 eclogite-k. HRV77 consists of a clinopyroxene megacryst surrounded by biminerallic eclogite. Garnet l is of the opposite edge of garnet k but lying within the large (10cm) clinopyroxene megacryst. XRV5-n is an iron rich end member of the group I eclogites which can be chemically distinguished from iron rich end members of group II eclogites by the lower CaO garnet and the presence of greater than 0.10wt% K₂O in clinopyroxene. Grossular garnet and jadeitic clinopyroxene end members are represented by kyanite eclogites JJG30-p and PJJ17-r.

Ages of a comprehensive suite of eclogites (Kramers, 1977) indicate that the eclogites originated during a single pre Cambrian thermal event. However the eclogites cannot be related by fractional crystallisation of a single magma. Multiple magma intrusion and magma mixing is indicated by samples HRV15, RV372, HRV77 and others. Small scale inhomogeneities are more common in group II eclogites which appear to have formed from relatively small volumes of magma, while the more homogeneous group I eclogites may have crystallised from larger batches of magma in which the effects of magma mixing will be less marked. The evolution of group II eclogites was dominated by partial melting processes while fractional crystallisation was more important in evolution of group I eclogites.

The presence of kyanite in JJG30 indicates that the coexisting magma lay on the SiO₂ rich side of the eclogite thermal divide (O'Hara & Yoder, 1967). The presence of H₂O during partial melting of garnet lherzolite can lead to the production of silica rich melts (Kushiro & Yoder, 1974). The relatively low temperatures of equilibration (Table 1) are consistent with presence of volatiles. The magma from which HRV15 crystallised lay on the MgO rich side of the eclogite thermal divide (MgAl₂O₄ present) hence if volatiles were present during melting the CO₂/H₂O ratio was probably high (Eggler, 1974).

References

- Eggler, D.H. Carnegie Inst. Wash. Yearbook, 73, 215 (1974)
Erlank, A.J. Carnegie Inst. Wash. Yearbook, 68, 433 (1970)
Hatton, C.J. and Gurney, J.J. This volume. (1977b)
Kramers, J.D. This volume. (1977)
Kushiro, I and Aoki, K. Amer. Mineral. 53, 1347 (1968)
Kushiro, I and Yoder, H.S. Carnegie Inst. Wash. Yearbook, 73, 266 (1974)
MacGregor, I.D. and Carter, J.L. Phys. Earth Planet. Interiors, 3, 391 (1970)
O'Hara, M.J. and Yoder, H.S. Scottish J. Geol., 3, 67 (1967)
Whitfield, G. M.Sc. Thesis, Rhodes University (1971).

GEOLOGY OF THE DOKOLWAYO KIMBERLITE AND ASSOCIATED PALAEO-ALLUVIAL DIAMOND DEPOSITS

J. B. Hawthorne
A. J. Carrington
C. R. Clement
E. M. W. Skinner

Geology Department, De Beers Consolidated Mines Limited,
P.O. Box 616, 8300 KIMBERLEY, RSA.

During 1973 exploration in northeastern Swaziland resulted in the discovery of diamond bearing grits and conglomerates of Red Beds (upper Triassic) age in the Karroo System sedimentary rocks of the Lebombo monocline. The richest and most extensive deposits occur in the Hlane Game Sanctuary. Palaeocurrent analysis of the diamond bearing beds indicate that they were deposited by an ancient river system flowing in a south-easterly direction. Further exploration carried out during 1975 in an upstream direction relative to the paleoslope resulted in the discovery of the Dokolwayo kimberlite diatreme some 30km. W.N.W. of the Hlane deposit. Despite intensive exploration no other diamondiferous kimberlites have been found in the area between Dokolwayo and the Hlane deposits.

In this paper the geology of the Hlane deposit is described and its possible relationship to the Dokolwayo diatreme is discussed. Results of the studies of the structure, petrography, xenoliths and mineral chemistry of the Dokolwayo kimberlite are presented; these studies are directed towards the elucidation of the age of formation of the diatreme, its mechanism of emplacement and the origin of the Hlane diamonds. So far no mica or zircon suitable for radiometric age determination of the kimberlite has been found.

THE HLANE DIAMOND DEPOSIT occurs near the top of the Karroo sedimentary sequence (Table I). These sediments dip at 10° - 12° E., are intruded by a swarm of dolerite dykes and are dislocated by numerous N.-S. trending faults downthrowing to the west. High diamond concentrations are found in two similar sedimentary units at the base of the Red Beds. The lower unit (0,5-2m.) occupies a system of broad irregular channels shallowly incised into underlying siltstones; the overlying unit (0,5-0,8m.) extends beyond the channel confines and laps onto the channel interfluves. Both units consist of cyclic deposits of carbonate cemented sediments fining upwards from carbonate and siltstone clast conglomerates set in a grit matrix, to muddy cross-bedded grits and ripple marked sandstones. Both units contain abundant kimberlitic garnet and less frequent Cr. spinel, Cr. diopside and diamond. The vectorial mean of 25 measurements of channel orientation and foreset azimuths of crossbeds was 106° from T.N. The high incidence of kimberlitic garnet relative to non kimberlitic garnet and the lack of Archaean clasts suggests that the source of the diamonds and kimberlite derived minerals lay within the Karroo basin at the time of deposition of the Red Beds.

THE DOKOLWAYO KIMBERLITE DIATREME is located on the Kaapvaal craton near its eastern margin and intrudes late Archaean granite gneisses. Drilling and pitting have shown that it is irregularly elongate in outline with steeply dipping walls. The surface area is 2,8 ha. increasing to 3,4 ha. at a depth of 50 m.

The central part of the diatreme is occupied by kimberlite characterised by a clastic texture and abundant xenogenic material. The xenogenic components range from

large (>1m.) blocks of country rock to microscopic xenocrysts. The most prominent feature in thin section is the abundance of quartz and felspar xenocrysts, the majority of which are <0,5mm. Also prominent are numerous altered olivine grains 2-3 mm. in diameter. The most common alteration products are a micaceous clay mineral, serpentine and calcite. Other microxenoliths consist of coal fragments, fine grained clastic kimberlite and porphyritic kimberlite. These mineral and rocks fragments are set in a mixture of finely comminuted quartz and felspar fragments, minute laths of mica, iron oxide, calcite and yellow clayey material. The larger wallrock blocks consist of granite gneiss and medium grained sandstones and grits, commonly associated with coals. The coals and sandstones are similar to those of the middle Ecca found elsewhere in Swaziland and it is concluded that they were incorporated in the kimberlite by downward slumping during emplacement of the diatreme from overlying Karroo horizons subsequently removed by erosion. Tuffisite veins containing up to 80% of quartz grains cut the central kimberlite and included xenoliths, disrupting and brecciating the latter.

The diatreme margins are occupied by a narrow zone of porphyritic kimberlite which contains numerous altered olivine insets and small wallrock xenoliths set in a grey-green aphanitic matrix. Phlogopite and serpentine are the most abundant groundmass minerals.

The clastic texture of the central kimberlite and the high proportion of xenogenic material are but two of the many features which suggest that the diatreme formed as a result of at least one major phase of gas-solid fluidized intrusion, probably preceded by an explosive breakthrough to a higher (now eroded) level. The abundance of tuffisite breccia suggests that this type of intrusive activity played a major role in filling and shaping the diatreme at higher (eroded) levels. The previously described irregularities in outline and the presence of marginally disposed porphyritic kimberlite suggest that processes such as magmatic stoping and inward spalling of country rock were responsible for shaping the diatreme walls at the present near surface levels.

Sedimentological studies indicate that the Hlane diamonds are possibly derived from the Dokolwayo diatreme but insufficient numbers of diamonds of comparable size are available for meaningful comparisons to be made. To test this hypothesis of origin comparison of the mineral chemistry of garnets and spinel from both sources was undertaken; virtually no ilmenite is found in either source. Roughly 1000 garnet grains in the 16-28 mesh (Tyler) range were selected from representative samples from each source and grouped into 7 colour categories. 22-52 Garnet grains selected at random from each colour category and 20-48 spinel grains in the same size range were analysed using an A.R.L. SEMQ automated electron microprobe. The mean chemical composition of grains analysed is shown in Table II. Comparison of the results strongly suggests that the grains analysed are from a common source.

If it is accepted that the Hlane diamonds are derived from the Dokolwayo diatreme it follows that the diatreme was emplaced in pre-upper to mid-Triassic times. Similarly if the coals found in the kimberlite are accepted as being derived from middle Ecca coal measures the diatreme must have been intruded during or after Permian times.

It is concluded that the Dokolwayo diatreme was intruded prior to the Stormberg volcanic event in Permo Triassic times; this represents a unique age of kimberlite emplacement in southern Africa.

<u>STAGE/SERIES</u>		<u>LITHOLOGY</u>	<u>THICKNESS</u>	<u>AGE</u>
Drakensberg Stage		Basalts, rhyolites agglomerates and stratified tuffs	>3000m	Triassic-Jurassic
Cave Sandstone Stage		Massive aeolianite	±70m	Upper-Mid Triassic
Red Beds Stage	Stormberg Series	Siltstones	±50m	Upper-Mid Triassic
<u>HLANE DIAMOND DEPOSIT</u>	<u>EMPLACEMENT OF DOKOLWAYO KIMBERLITE DIATREME</u>			
Molteno Stage		Fluvial sandstones and siltstones	±40m	Upper-Mid Triassic
Beaufort and Ecca Series		Sandstones, grits, shales and coals*	±800m	Permian
Dwyka Series		Tillite ~~~~~ Granite gneiss	±5m	Upper Car=boniferous Late Archaean

*The lowest coals are found in the Middle Ecca approximately 250m above the base of the Karroo succession.

TABLE II
ANALYSES OF GARNETS AND SPINEL FROM DOKOLWAYO(D) AND HLANE(H)
Mean Chemical Compositions

<u>GARNET</u>								No. of Grains Analysed
<u>Colour Group</u>		<u>Al₂O₃</u>	<u>FeO</u>	<u>TiO₂</u>	<u>CaO</u>	<u>Cr₂O₃</u>	<u>MgO</u>	
Mauve	D	17,6	6,4	0,1	6,2	7,3	19,4	49
	H	20,5	7,3	0,4	4,7	3,2	20,5	50
Cerise	D	20,5	7,3	0,4	4,7	3,2	20,5	48
	H	20,7	7,2	0,3	4,9	4,0	20,4	51
Pink	D	21,0	7,1	0,3	4,6	2,4	21,2	50
	H	21,1	7,1	0,3	4,6	3,1	21,1	28
Red	D	20,9	8,3	0,7	4,5	2,1	20,4	50
	H	21,1	8,2	0,7	4,6	2,4	20,8	50
Dark Orange	D	21,7	9,8	0,9	4,0	0,4	20,0	50
	H	22,1	10,0	0,9	4,2	0,5	19,7	51
Pale Orange	D	22,0	10,5	0,8	3,8	0,2	19,5	52
	H	22,9	11,4	0,3	4,5	0,1	18,2	50
Straw	D	22,9	11,5	0,3	4,5	0,3	18,5	22
	H	23,2	10,1	0,1	4,6	0,2	19,4	38
<u>SPINEL</u>	D	5,8	16,7	1,4	0	59,9	13,5	48
	H	5,3	17,5	1,3	0	59,8	12,8	20

Analyst: G. Hutchinson

TYPE A - TYPE C ECLOGITE TRANSITION IN A XENOLITH FROM THE MOSES ROCK DIATREME
- FURTHER EVIDENCE FOR THE PRESENCE OF METAMORPHOSED OPHIOLITES BENEATH THE
COLORADO PLATEAU

H. Helmstaedt and D.J. Schulze (Department of Geological Sciences, Queen's
University, Kingston, Ontario, Canada K7L 3N6)

A garnet clinopyroxenite xenolith from Moses Rock records the metamorphic transformation of the primary assemblage garnet ($Py_{73} Alm_{17} Gross_{17} Andr_{2} Spess_{1}$) and clinopyroxene ($Aug_{83} Jd_{11} Ac_{5}$) into the secondary assemblage² magnesian chlorite, garnet ($Py_{40} Alm_{30} Gross_{24} Andr_{3} Spess_{2}$), and omphacite ($Aug_{55} Jd_{40} Ac_{5}$). Large pyrope garnets are surrounded by haloes of magnesian chlorite which is intergrown with less pyrope, fine-grained euhedral garnet and omphacite. Omphacite also overgrows some of the anhedral clinopyroxenes of the original assemblage. Textures and mineral compositions indicate that the primary assemblage corresponds to that of a high P-high T Type A eclogite which was hydrated under high P but lower T to a chlorite-bearing eclogite of Type C affinities (Coleman et al., 1965). The presence of this unusual xenolith and a comparison of its subsolidus history with that of other ultramafic inclusions from the Four Corners kimberlites (Table 1) have several important implications for the Colorado Plateau.

Nature of uppermost mantle beneath the Colorado Plateau:

Although a Type A to Type C eclogite transition has not been documented previously in a single hand specimen, a similar reaction was inferred by Banno and Yoshino (1965) in the Bessi district of Japan where mantle-derived garnet-diopside eclogites (Type A) were transformed by high P-low T Sanbagawa metamorphism into hydrated garnet-omphacite rocks. Similar assemblages were produced by high P-low T metamorphism also in Alpine ophiolites (Moeckel, 1969). In the Sanbagawa Belt as well as in the Alps, retrograde Type A eclogites occur together with Type C eclogites formed by progressive metamorphism of basic igneous rocks. The Alpine meta-ophiolites contain titanoclinohumite found also at Moses Rock (McGetchin et al., 1970), Buell Park (Aoki et al., 1976), and Green Knobs (Smith, 1977a) and inferred by Smith (1977a) to be part of the hydrous alteration assemblage of peridotites. The fact that all hydration reactions recorded in the ultrabasic xenoliths from the Four Corners kimberlites are known also from metamorphosed ophiolites exposed at the earth's surface (Table 1) and the association of these retrogressed xenoliths with progressively metamorphosed Type C eclogites strongly suggest a derivation of this xenolith suite from metamorphosed ophiolitic rocks beneath the Colorado Plateau. This supports earlier proposals (Helmstaedt and Doig, 1975; Råheim and Green, 1975; Mercier, 1976) that these xenoliths represent fragments of oceanic lithosphere subducted and underplated beneath the Precambrian basement of the Plateau.

Feasibility of establishing paleogeotherms and upper mantle models for Plateau:

Using xenolith and xenocryst pyroxene compositions for calculations of pressures and temperatures of equilibration and assuming that differences in pressures represent differences in depth of derivation, paleogeotherms have been constructed for the Colorado Plateau (McGetchin and Silver, 1972; Mercier, 1976). As it is now well established that all types of ultrabasic xenoliths were modified by hydration reactions prior to the kimberlite eruptions, it becomes apparent that P-T assignments based on mineral compositions of metastably surviving protolith assemblages cannot be used to establish paleo-geo-

TABLE 1. BRIEF COMPARISON OF SUBSOLIDUS HISTORY OF ULTRAMAFIC XENOLITHS FROM FOUR CORNERS KIMBERLITES

Xenolith-type	Chlorite-garnet pyroxenite (this paper)	Chlorite-garnet peridotite (unpublished data)	Hydrated spinel websterite (unpublished data)	Serpentine schists (McGetchin & Silver, 1972). Various hydrated peridotites (Smith, 1977a). Foliated chlorite-serpentine schists (unpublished data)	Type C eclogites. Jadeite-clinopyroxenites (Helmstaedt & Doig, 1975; McGetchin & Silver, 1972)
Earliest recognizable protolith	Pyrope-diopside rock (Type A eclogite)	Garnet peridotite (Gavasci and Helmstaedt, 1969)	Spinel-pyroxenite	Spinel peridotite, possibly garnet peridotite (Smith, 1977b)	Basic to intermediate igneous rocks (Helmstaedt et al., 1972)
Pre-eruption subsolidus history	No signs of deformation in primary minerals	Some plastic strain	Pyroxene exsolution, deformation, recrystallization to spinel websterite	Pyroxene exsolution, deformation, recrystallization to spinel peridotite (Helmstaedt et al., 1972)	Metasomatic alteration, possibly spilitization. Synkinematic metamorphism to lawsonite-bearing Type C eclogite, K^*_{D} (mineral Cores) ~30 (Råheim & Green, 1975)
Post-eruption alteration	Formation of magnesian chlorite + less pyrope garnet + omphacite, $K^*_{D} = 8.3$	Alteration of garnet to magnesian chlorite (unpublished data)	Apparently static alteration to pargasite + chrome spinel + coronandum + chlorite + clinzoisite	Sequence of increasing hydration including formation of amphibole, chlorite, titanoclinohumite, and antigorite (Smith, 1977a). Static and synkinematic	Formation of atoll garnets, jadeite-rich rims on pyroxenes, more pyrope rims on garnets, $K^*_{D} = 8.5-10$ (Råheim & Green, 1975; unpublished data). Alteration of lawsonite to zoisite
Surface occurrence of similar rocks	Meta-ophiolites, Alps, Japan (Banno & Yoshino, 1965; Moeckel, 1969)	Meta-ophiolites, Alps (Moeckel, 1969)	Meta-ophiolites, France (Lashnier, 1976)	Common in meta-ophiolites. See Smith (1977b)	Type C eclogites (Coleman et al., 1965)

* $K^*_{D} = \frac{(\text{FeO}/\text{MgO})_{\text{Ga}}}{(\text{FeO}/\text{MgO})_{\text{Cpx}}}$

therms and upper mantle cross-sections for the Plateau. At best, it is possible to infer P-T conditions of metamorphism prior to eruption, but even these may not represent the conditions at the time of eruption. Iron-magnesium distribution coefficients of the garnet-omphacite pair from the metamorphosed Type A eclogite xenolith correspond to those determined for the rims of garnets and pyroxenes from the progressively metamorphosed Type C eclogites (Table 1) suggesting that, like in the mentioned surface occurrences, the two rock types may have existed at a similar structural level beneath the Plateau. The conditions for hydration of the other ultrabasic xenoliths (except for late serpentinization) are compatible with those required for the Type A-Type C transition. Although a certain depth range may have been sampled, compelling evidence to infer that the xenoliths were incorporated by the kimberlite at a depth much greater than indicated by the metamorphic assemblages does therefore not exist.

Mechanism and timing of uplift of the Colorado Plateau:

While their emplacement poses a formidable geotectonic problem, the presence of the partially hydrated ultrabasic rocks and eclogites under the Plateau at the time of the kimberlite eruptions may help to solve another problem, that of mechanism and timing of uplift of the Colorado Plateau. Hess (1955) mentioned the volume increase due to serpentinization as a possible reason for uplift. We propose that the volume increase caused by the hydration reactions preceding serpentinization is responsible for a significant part of this uplift. There is also the possibility of a link between the hydration of the underplated meta-ophiolites and the Laramide basement uplifts east of the Colorado Plateau.

References:

- Aoki, K., Fujino, K., and Akaogi, M., 1976, *Contrib. Mineral. Petrol.*, 56, 243-253.
- Banno, S. and Yoshino, G., 1965, *Upper Mantle Symp. New Dehli, 1964*, 150-160.
- Coleman, R.G., Lee, D.E., Beatty, L.B., and Brannock, W.W., 1965, *Geol. Soc. Am. Bull.*, 76, 483-508.
- Gavasci, A.T. and Helmstaedt, H., 1969, *J. Geophys. Res.*, 74, 6691-6695.
- Helmstaedt, H., Anderson, D.L. and Gavasci, A.T., 1972, *J. Geophys. Res.*, 77, 4350-4365.
- _____, and Doig, R., 1975, *Phys. Chem. Earth*, 9, 95-111.
- Hess, H.H., 1955, *Geol. Soc. America, Special Paper* 62, 391-408.
- Lasnier, B., 1976, *Bull. Soc. Geol. Mineral. Bretagne*, (C), IV, 2, 109-130.
- McGetchin, T.R., Silver, L.T., and Chodos, A.A., 1970, *J. Geophys. Res.*, 75, 255-259.
- _____, and Silver, L.T., 1972, *J. Geophys. Res.*, 77, 7022-7037.
- Mercier, J.C., 1976, *Amer. Mineral.*, 61, 603-615.
- Moeckel, J.R., 1969, *Leidse Geol. Meded.*, 42, 61-130.
- Råheim, A. and Green, D.H., 1975, *Lithos*, 8, 317-328.
- Smith, D., 1977a, *Contrib. Mineral. Petrol.*, 61, 213-215.
- _____, 1977b, *J. Geology*, 85, 476-482.

MINOR ELEMENT CONTENT OF OLIVINE AND ORTHOPYROXENE IN UPPER-MANTLE XENOLITHS.

R. L. Hervig and J. V. Smith, Dept. of the Geophysical Sciences, University of Chicago, Chicago, Illinois 60637, U.S.A.

J. B. Dawson, Dept. of Geology, University of St. Andrews, Scotland

Highly-sensitive electron microprobe analyses for Na,Al,Ca,Ti,Cr and Ni are reported for olivine and orthopyroxene from 10 lherzolite and 8 harzburgite xenoliths from Lashaine (Tanzania) and Bultfontein, Dutoitspan, Monastery and Newlands (S. Africa). [The term lherzolite is used if a Ca-rich clinopyroxene grain was found, irrespective of the modal abundance of cpx.] The harzburgites contain more modal orthopyroxene than the lherzolites. On the basis of trace elements we recognize 2 lherzolite groups. Group I (1 each from Bultfontein and Letseng) has minerals richer in Fe than those in Group II (7 from Lashaine, 1 from Mothae). The harzburgites also fall into 2 groups: Group III (2 from Bultfontein, 1 each from Dutoitspan and Newlands) with high-Ca orthopyroxene and Group IV (Bultfontein 2, Monastery 1 (with amphibole), Liqobong 1) with low-Ca opx.

Figs. 1-3. Group I olivines contain higher Al,Cr and Ca than II olivines, whose distinctive feature is higher Ti. Groups III and IV olivines have similar amounts of Al,Ca,Ti and Cr. Olivines from lherzolites contain 30-130ppmw Na₂O, while those from harzburgites have no detectable Na.

Figs. 4-6. Group I orthopyroxenes contain higher Ca,Na,Ni and Cr than II opx. The high-Ca III orthopyroxenes have more Na,Al,Cr than IV opx while Ni and Ti are similar. These high-Ca orthopyroxenes contain roughly twice as much Ca,Al and Cr as orthopyroxenes in "normal" Group I lherzolites.

Fig. 7. Ca is distributed nearly linearly between ol and opx, except for the high-Ca III harzburgites. If the lherzolites equilibrated at temperatures ranging over ~225°C and pressures ranging over ~10-20kb, as indicated by the pyroxene compositions, the Ca partitioning is essentially independent of these pressure and temperature variations.

Fig. 8. Cr partitioning between ol and opx is complex with no obvious pattern, though the harzburgites and lherzolites are separated. Lherzolite 1544 has clean opx grains with lower Cr than a remnant of an altered grain.

Fig. 9. $K_D Ni = Ni(ol)/Ni(opx)$ ranges as follows:

I lherzolite 3.6-4.1, II lherzolite 4.2 and 4.6, III harzburgite 4.4-5.9, IV harzburgite 4.6-5.3.

We draw attention to the Group III harzburgites whose high Al,Ca and Cr allow them to be described as "fertile harzburgites" because exsolution at high pressure and temperature would cause them to transform into garnet lherzolite [defined as containing gt,cpx,opx,ol without specification of the mode]. Such exsolution has been documented, e.g. Ext. Abstr. Int. Conf. Kimberlites, 1973, 81-82. O'Hara, Saunders and Mercy (Phys. Chem. Earth 9, 571, 1975) described a model of partial melting followed by solid-state exsolution which provides possible mechanisms for producing "fertile" and "barren" harzburgites; however, quantitative modeling of the trace-element distribution as a function of temperature, pressure and the bulk composition of coexisting partial melt will not be possible until appropriate experimental data are forthcoming on the distribution coefficients between individual minerals and melt.

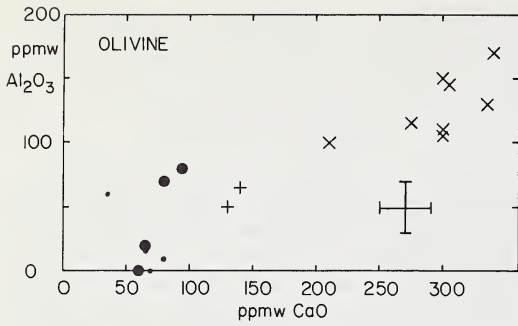


Fig. 1

Horizontal cross: group I lherzolite
 Inclined cross: group II lherzolite
 Large dot: group III harzburgite
 Small dot: group IV harzburgite

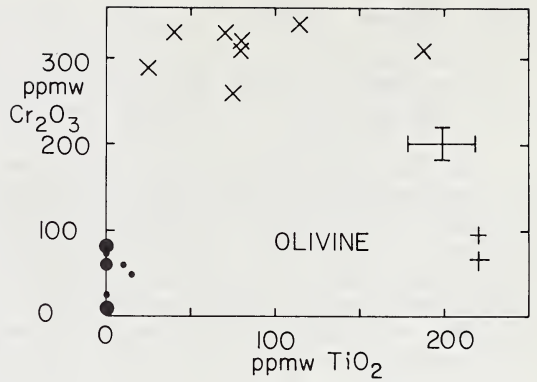


Fig. 2

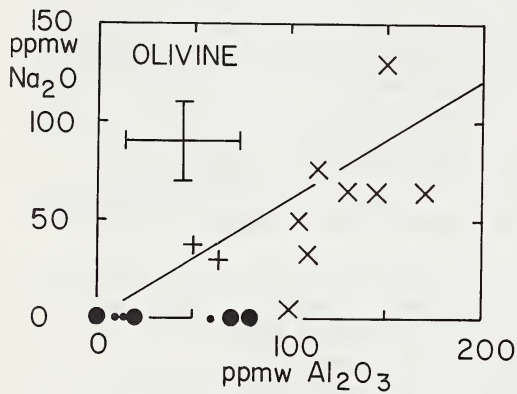


Fig. 3

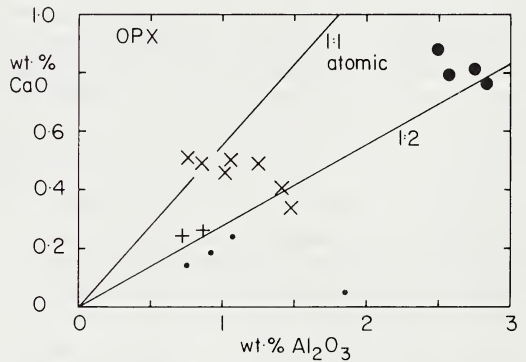


Fig. 4

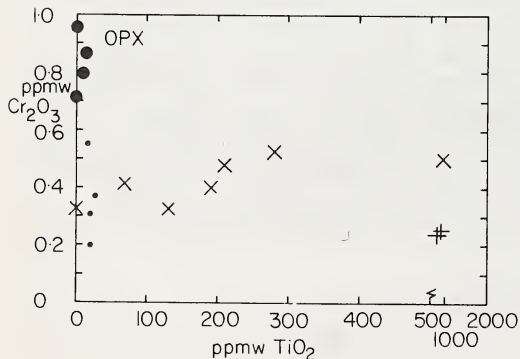


Fig. 5

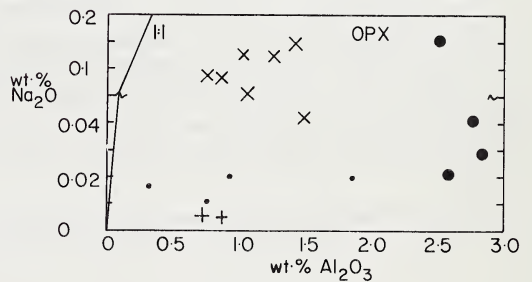


Fig. 6

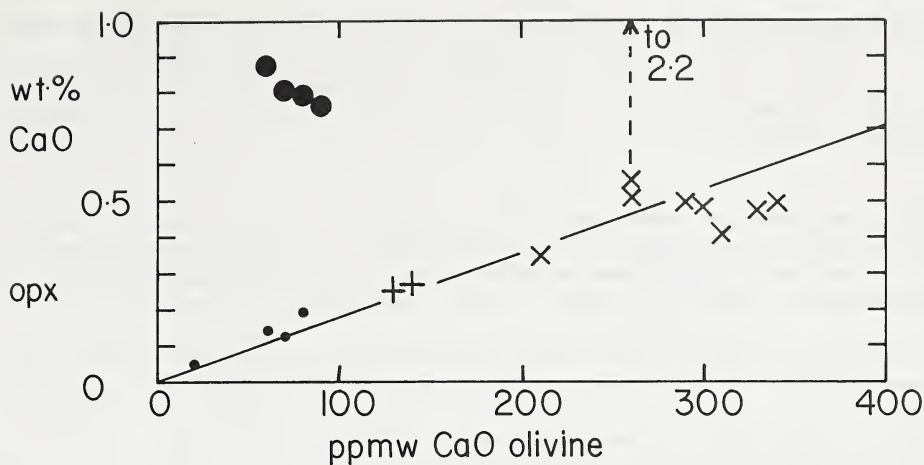


Fig. 7

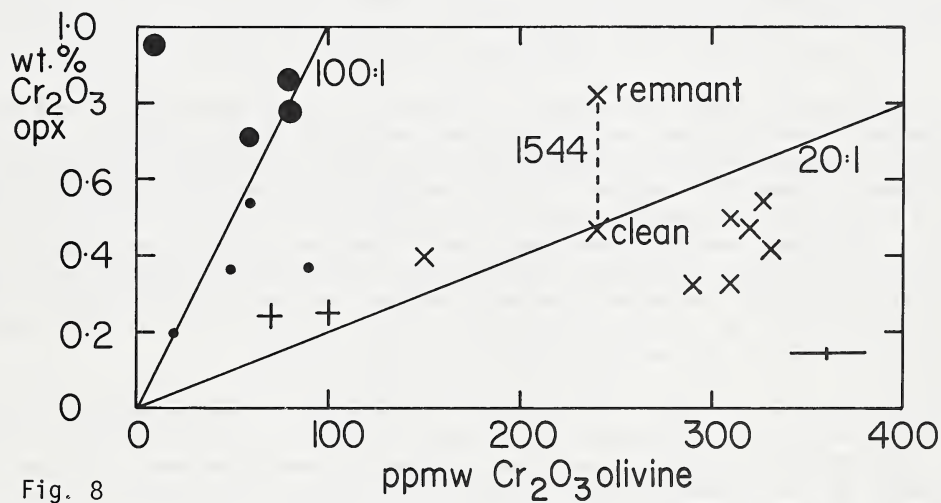


Fig. 8

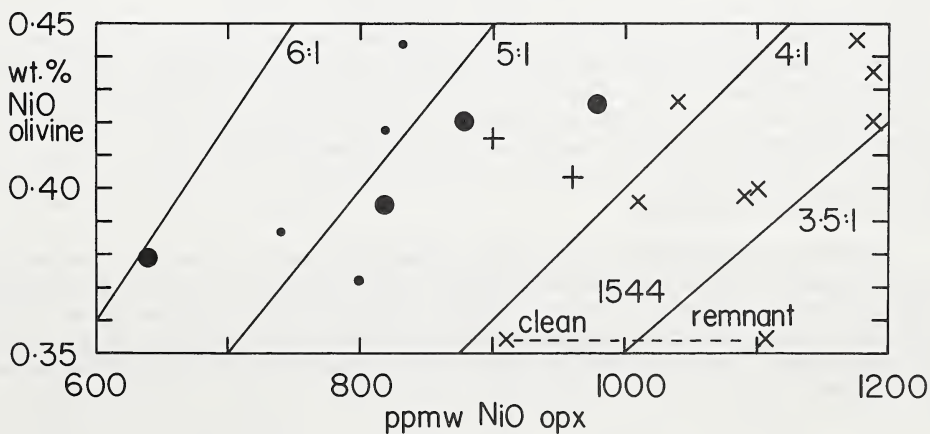


Fig. 9

THE ISOTOPIC COMPOSITION OF CARBONATE IN KIMBERLITE, MICA PERIDOTITE AND BASALT ALONG THE 38th PARALLEL LINEAMENT IN KENTUCKY AND VIRGINIA

Graham Hunt, Department of Geology, University of Louisville, Louisville, Kentucky, 40208

The close and intimate association between carbonatites, carbonatitic material, kimberlites, and alkaline rocks poses a number of problems and this study of isotope compositions is an attempt to better understand the genetic relationship and depth of origin of these carbonate-bearing rocks.

A differentiation of the carbonatitic material from the parent magma has been proposed for various mantle originated processes (Hyndman, 1972; Mitchell, 1970). Today there is much debate over the possible types of original compositions of the parent magma. O'Hara (1965) favors a process whereby fractional crystallization enriches the magma in volatiles, etc., to form kimberlite or carbonatite. In other cases, the carbonatite is thought to separate as immiscible liquid globules (Deines, 1970). Some workers (McGetchin and Silver, 1972) have suggested that the low velocity zone may have provided the constituents necessary for the carbonatitic material.

Analyses of fluid inclusions in peridotite minerals suggest that CO_2 is a dominant volatile species in the upper mantle (Roedder, 1965). Green (1972) preferred CO_2 dissolved in crystalline silicates, exsolving to form the fluid inclusions. Recently, Egger (1976) concluded that at depths of less than 90 km in suboceanic mantle, CO_2 may be present in carbonate minerals (or in vapor, depending upon the geotherm), but cannot be in solution in silicate peridotite minerals. However, beneath the continents he suggests that CO_2 will be present in carbonate minerals, and the mantle will not melt at least to depths of 120 km. Irving and Wyllie (1973) also pointed out that the carbonate minerals in the mantle may be the site of CO_2 .

Because of the abundant carbonate-bearing mafic alkalic igneous rocks including kimberlite and ultramafic intrusives that are distributed along the 38th Parallel Lineament and show a close agreement between the time of movement of the lineament and the time of intrusion, an attempt is undertaken to better understand these relationships (Hunt, 1976).

The spatial distribution of the igneous rocks within a local area is related to segments forming the Lineament but the occurrence of kimberlites of eastern Kentucky, the mica peridotites of western Kentucky, and the basalt of Virginia may be related in terms of an overall structural pattern involving possible ancient plate margins and chemical plumes.

Interpretation of Results

Figure 1 and Table 1 show the carbon and oxygen isotopic compositions of carbonate samples studied of kimberlite, carbonatite, mica peridotite, basalt, alnoite, marine limestone, and altered ore-rich limestone. The isotopic compositions are expressed in the standard delta notation as per mil deviations from the PDB standard for carbon and from the SMOW standard for oxygen.

The variation in isotope values may be due to a number of factors if some assumptions are taken. The dikes of western Kentucky and the kimberlites of eastern Kentucky may form a related petrographic province, in that they appear to have similar ages, are related to the 38th Parallel Lineament, same structural feature, and have similar silica contents. The chemical analyses taken from the literature (Koenig, 1956) for these rocks suggests a standard differentiation trend from a common parental source. The variation in chemical composition shows an increase in K and Na, and iron as a result of differentiation with time. There would be a preference of Mg over Fe in earlier formed minerals, and therefore, Fe becomes concentrated in the late fraction of the melt. If these rocks had a common source, the higher Mg content and lower Fe would represent an earlier and deeper source for the kimberlites of eastern Kentucky than the mica peridotites that are enriched in Fe and poorer in Mg than the kimberlites.

Therefore, the crystallization after differentiation of the primary calcite from the parent source the residual magma would be enriched in O^{18} and expressed in the late forming calcite of the mica peridotite. The main factors such as variations in depth of intrusion, temperature, PH_2O , PCO_2 will have an effect on the isotope ratios at the time of formation of the calcite.

The possibility of calcite as being a weathered product, the result of assimilation of rock fragments, a result of younger thermal solutions cannot be ignored. Even though samples came from drill cores beneath the surface, 270 to 329 feet depths, the carbonate of the Hutson dike represents ore carbonate replacement shown by the unusual isotope ratios. The oxygen isotope ratios in carbonates can be altered by post emplacement exchange with meteoric waters. It is possible to argue for the preservation of the ratios on the basis of observed textures, but in some cases there is evidence of cross-cutting alterations in the form of calcite recrystallization and veining in the Hutson dike.

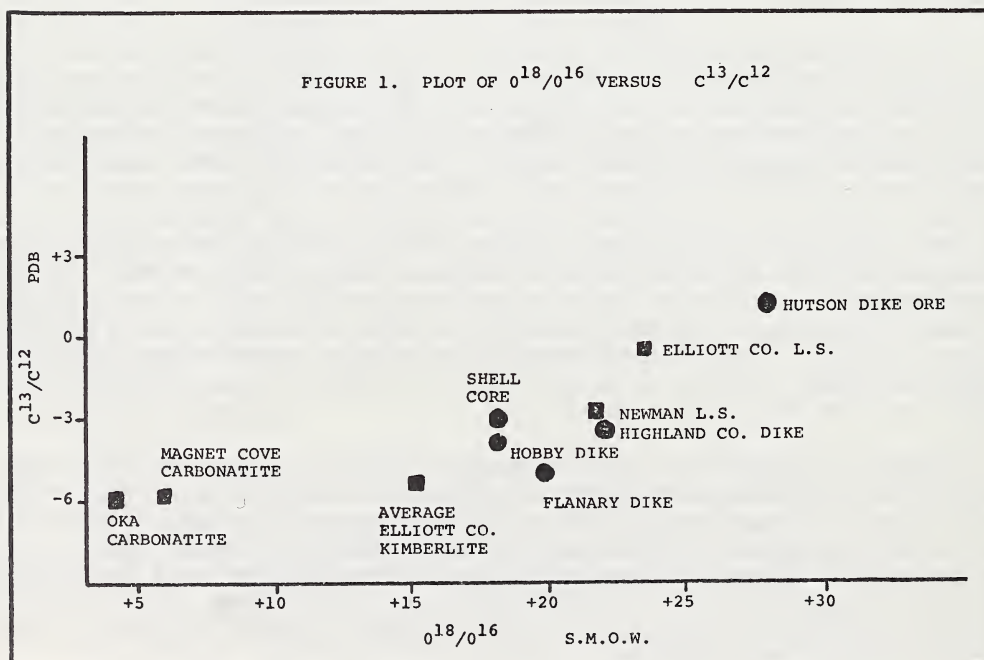
If the isotope ratios now observed in the rocks do represent the original ones, then it is possible to make some observations about conditions during and after the time the rocks were formed. The igneous rocks of eastern Kentucky are all relatively fresh, showing little or no obvious weathering. There are no subsequent thermal events in the area that would cause metamorphic decarbonation of the carbonates that would lower the isotope ratios in the residual carbonate as observed by Deines (1969) in the Montreal area of Quebec. If the isotope ratios represent changes during magmatic differentiation over a proposed chemical plume, then there may be a common source area of isotopically homogeneous material. The limited data suggests that differences do exist between comagmatic rock types; kimberlite, mica peridotite, and a basaltic dike. These rocks may represent different fractions of a parent magma which differentiates within the mantle, giving rise to a chemical plume (model of Anderson, 1975) followed by plate movement.

Carbon isotope ratios may be used as tracers of depth of origin for a particular tectonic grouping and in conjunction with the oxygen ratios they may be used to determine the effects of post-magmatic exchange. The calcite of the western Kentucky dikes and the eastern Kentucky kimberlites occurs as medium to fine-grained aggregates which is interpreted to be a late magmatic crystallizing mineral, but in some cases the calcite phenocrysts of the western Kentucky dikes is interpreted to be the original mineral composition formed at depths of about 90 to 120 km.

TABLE 1: Isotopic compositions of carbonate samples studied of kimberlite, limestone, carbonatite, mica peridotite, and basalt

Sample localities	Description (%)	C ¹³ PDB	O ¹⁸ SMOW
EL-100 Kimberlite from locality 1 Elliott County	14 calcite, 23 opa., 7 rock frag., 41 olivine, 12 serp.	-4.6	+11.6
EL-200 Kimberlite from locality 2 Elliott County	12 calcite, 22 opa., 2 rock frag., 45 olivine, 17 serp.	-3.7	+18.2
EL-304 Kimberlite from locality 3 Elliott County	9 calcite, 12 opa., 14 rock frag., 37 olivine, 21 serp.	-6.0	+14.2
EL-302 Rock frag. in kimberlite	27 calcite, 63 fine grain. (serp?) unidentified	-6.1	+15.9
NW-Y-71 Newman Ls. Stop 10 KGS conf. Grayson, Ky	62 calcite, 35 clay, 3 qtz.	-1.6	+21.5
EL-207 Limestone from locality 2 Elliott County	38 calcite, 60 clay	-0.3	+23.2
S-6c Carbonatite Oka Complex, Que.	90 calcite, 5 apatite, pyroxene, 5 biotite	-5.7	+4.1
Ark -K2 Carbonatite, Kimsey Quarry, Ark.	all calcite	-5.6	+5.8
HT-1 Hutson Dike Livingston County, Kentucky	57 calcite, 3 serp., 34 opa., perovskite, 6 mica, apatite, qtz.	+1.4	+27.8
HB-2 Hobby Dike Caldwell County, Kentucky	21 calcite, 41 serp., 23 mica, 7 opa., apatite, 8 sphene, clinozoisite, perovskite	-3.88	+17.95
F-5 Flanary Dike Crittenden County, Kentucky	42 calcite, 24 serp., 19 mica, 14 opa., apatite perovskite	-4.89	+19.68
SC-2 Shell Core Dike, Crittenden County, Kentucky	22 calcite, 38 serp., 27 mica, 11 opa., apatite, 2 clinozoisite, perovskite	-2.90	+19.02
Va-2 Basaltic Dike Highland County, Virginia	9 calcite, opa., 90 bio., plag., pyroxene	-3.3	+21.88

FIGURE 1. PLOT OF O^{18}/O^{16} VERSUS C^{13}/C^{12}



MANTLE PYROXENITIC "LIQUIDS" AND "CUMULATES": GEOCHEMISTRY OF COMPLEX XENOLITHS FROM SAN CARLOS, KILBOURNE'S HOLE AND EASTERN AUSTRALIA

Anthony J. Irving (The Lunar Science Institute, 3303 NASA Rd. 1, Houston, Texas 77058)

Mantle-derived xenoliths in alkalic basalts may be subdivided into several distinct series, the most common of which are the Cr-diopside spinel lherzolite series and the Al-Ti-augite series (eg. Wilshire and Shervais, 1975; Wass and Irving, 1976). Both series are mineralogically and texturally diverse. Rocks of both series commonly occur together, but nearly always as separate xenoliths showing no structural relationship to each other. At some localities, however, rare composite xenoliths are found which display the structural relationships among at least some members of each series.

Previous geochemical studies, especially trace element studies, of Al-Ti-augite series rocks have utilized discrete xenoliths (eg. Frey and Prinz, 1977; Irving, 1974). This paper is primarily concerned with the geochemistry of Al-Ti-augite-rich rocks which have an observable relationship to Cr-diopside spinel lherzolite or harzburgite. Most of the analyzed samples take the form of dikes or veins intruding or enclosing lherzolite or harzburgite. These structures imply that these particular Al-Ti-augite-rich rocks were mobile (probably liquid) at high pressures whereas adjacent lherzolite and harzburgite were more rigidly solid (cf. Wilshire and Shervais, 1975). Two discrete Al-Ti-augite series xenoliths showing poikilitic texture were also analyzed.

The following samples were studied:

Wehrlite SC74-1W and harzburgite SC74-1H, San Carlos, Arizona. A composite sample showing angular clasts of harzburgite enclosed and veined by black wehrlite to produce a "xenolith-in-xenolith" structure (see Fig. 1a).

Wehrlite dike SH76-2P and adjacent Cr-diopside spinel lherzolite SH76-2L, Sapphire Hill, north Queensland, Australia. An exceptionally large composite specimen showing a 6 cm wide dike of wehrlite with double contacts against spinel lherzolite (see Fig. 1b).

Wehrlite dike SC73-2 cutting spinel lherzolite, San Carlos. A 2 cm wide dike of wehrlite showing double contacts against spinel lherzolite.

Websterite dike KH73-1 cutting spinel lherzolite, Kilbourne's Hole, New Mexico. A 5 cm wide branched dike showing double contacts against fine grained, weakly foliated spinel lherzolite.

Wehrlite dike KH76-1 cutting more olivine-rich wehrlite, Kilbourne's Hole.

Part of a network of 3 cm wide dikes and 0.5 cm wide anastomosing veins cutting coarse grained more olivine-rich Al-Ti-augite-bearing wehrlite (see Fig. 1c).

Wehrlite SD72-1 enclosing spinel lherzolite, Mt. Shadwell, Victoria, Australia. A composite sample displaying "xenolith-in-xenolith" structure (see Fig. 1d).

The wehrlite contains areas of fine grained vesicular "basaltic" material which do not appear to be connected to the enclosing basalt.

Poikilitic wehrlites SC73-3 and SC73-6, San Carlos. Two similar samples (grainsize 5 mm) composed of olivine enclosed poikilitically by Al-Ti-augite and spinel. The textures are those of adcumulates. These samples are richer in olivine than any of the other analyzed wehrlites.

Major and trace element data (by XRF and INAA) for these materials are reported in Tables 1 and 2, and REE patterns are shown in Figs. 2 and 3. The pyroxene-rich "liquids" show a range in composition. 100 Mg/Mg+Fe ranges from 85 down to 75, but the largest variation is in Cr (44 to 3250 ppm). Chon-

drite-normalized REE patterns for most of these samples are characterized by depletion in light REE relative to Sm. Except for SH76-2P, they are also depleted in heavy REE relative to Sm. One sample (SD72-1) is light REE enriched. The two poikilitic wehrlites have similar REE patterns to the other wehrlites but at somewhat lower abundances. Spinel lherzolite SH76-2L is enriched in both light and heavy REE relative to Sm, Eu and Tb, like some examples from San Carlos and Victoria (Frey and Prinz, 1977; Frey and Green, 1974).

A popular interpretation of Al-Ti-augite-rich xenoliths is that they represent re-equilibrated cumulates from alkalic basaltic magmas at high pressures (10-20 kb). Most of the present samples were evidently entirely molten or crystal-liquid mushes at high pressures, yet their REE patterns are similar to those predicted for high pressure cumulates from magmas like their present hosts (Frey and Prinz, 1977). At mantle pressures, gravity crystal settling may be insignificant because of the difficulty of holding large magma chambers open. However, a process of flow crystallization within dikes like those described here could produce rocks chemically indistinguishable from settled cumulates. High-pressure fractionation of basanitic magmas to yield hawaiitic to phonolitic liquids (eg. Irving and Green, 1976) may well take place by such processes.

References

- Frey, F.A. and Green, D.H. (1974) The mineralogy, geochemistry and origin of lherzolite inclusions in Victorian basanites. Geochim. Cosmochim. Acta, **38**, 1023-1059.
- Frey, F.A. and Prinz, M. (1977) Ultramafic inclusions from San Carlos, Arizona: Petrologic and geochemical data bearing on their petrogenesis. Earth Planet. Sci. Lett. (in press).
- Irving, A.J. (1974) Pyroxene-rich ultramafic xenoliths in the Newer Basalts of Victoria, Australia. Neues Jb. Miner. Abh., **120**, 147-167.
- Irving, A.J. and Green, D.H. (1976) Geochemistry and petrogenesis of the Newer Basalts of Victoria and South Australia. J. Geol. Soc. Aust., **23**, 45-66.
- Wass, S.Y. and Irving, A.J. (1976) XENMEG: a catalogue of occurrences of xenoliths and megacrysts in basic volcanic rocks of Eastern Australia. Spec. Publ. Aust. Museum, 455 p.
- Wilshire, H.G. and Servais, J.W. (1975) Al-augite and Cr-diopside ultramafic xenoliths in basaltic rocks from western United States. Physics and Chemistry of the Earth, **9**, p. 257-272.

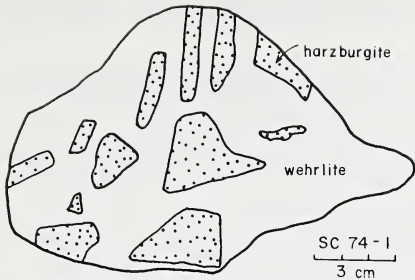


FIG. 1 (a)

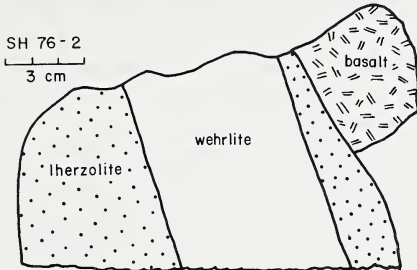


FIG. 1 (b)

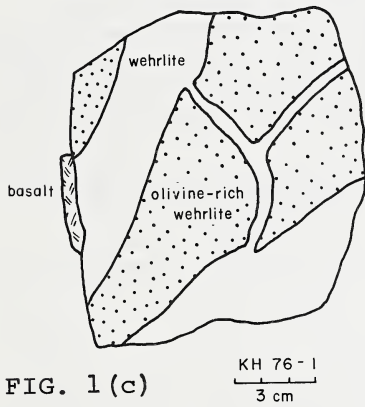


FIG. 1 (c)

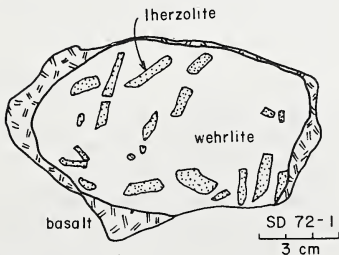


FIG. 1 (d)

Table 1. Major element data (by XRF, except * by IMAA)

	Wehrlite SC74-1W	Wehrlite SH76-2P	Wehrlite SC73-2	Wehsterite KH73-1	Wehrlite KH76-1	Wehrlite SC72-1	Harzburgite SC74-1H	Spinel Lherzolite SH76-2L	Poikilitic Wehrlite SC73-3	Poikilitic Wehrlite SC73-6
SiO ₂	52.07	47.29	43.03	42.26	42.31	47.89	42.33	44.28	40.15	41.90
TiO ₂	0.45	0.66	1.94	1.22	1.54	1.39	0.18	0.08	0.42	0.57
Al ₂ O ₃	4.83	10.12	13.33	15.45	13.53	6.48	1.83	2.88	3.84	3.32
Cr ₂ O ₃ *	0.47	0.34	0.10	0.006	0.016	0.19	0.35	0.36	0.16	0.16
FeO	9.27	6.17	6.62	6.51	9.11	7.49	13.56	9.03	15.16	14.09
MnO	0.20	0.16	0.18	0.17	0.20	0.18	0.21	0.17	0.26	0.25
MgO	28.01	20.21	16.92	15.36	15.45	17.10	40.06	40.09	33.01	30.87
NiO*	0.08	0.07	0.08	0.05	0.04	0.06	0.26	0.25	0.18	0.16
CaO	3.30	13.58	16.19	18.11	15.98	16.07	0.72	1.90	5.47	7.60
Na ₂ O*	0.290	0.67	1.11	0.82	1.12	1.37	0.089	0.102	0.387	0.409
K ₂ O	0.02	0.01	0.08	0.01	0.02	0.55	0.01	0.01	0.04	0.01
P ₂ O ₅	0.01	0.02	0.03	0.00	0.01	0.20	0.00	0.04	0.00	0.00
SUM	99.20	99.30	99.41	99.97	99.33	99.37	99.40	99.19	99.08	99.34
100 Mg										
Mg*Fe	84.3	85.4	82.0	80.8	75.1	79.8	84.0	88.8	79.5	79.6

Table 2. Trace element data (ppm)

	Wehrlite SC74-1W	Wehrlite SH76-2P	Wehrlite SC73-2	Wehsterite KH73-1	Wehrlite KH76-1	Wehrlite SC72-1	Harzburgite SC74-1H	Spinel Lherzolite SH76-2L	Poikilitic Wehrlite SC73-3	Poikilitic Wehrlite SC73-6
La	0.51	1.00	3.40	2.94	3.40	12.1	0.08	0.56	1.39	1.52
Ce	-	3.2	11.3	9.9	10.8	27.6	-	1.4	4.4	5.0
Sm	0.56	1.57	4.14	3.35	3.58	4.17	0.095	0.135	0.95	1.40
Eu	0.191	0.54	1.30	1.00	1.14	1.25	0.040	0.052	0.299	0.44
Tb	0.13	0.40	0.81	0.51	0.69	0.56	-	0.034	0.13	0.21
Yb	0.44	1.53	2.01	1.57	1.52	0.89	0.11	0.26	0.44	0.63
Zu	0.073	0.26	0.288	0.216	0.202	0.130	0.015	0.042	0.051	0.090
HF	0.35	0.99	2.47	1.78	2.08	2.40	0.05	0.06	0.54	0.94
Ta	0.21	0.23	0.57	0.40	0.40	1.23	0.39	0.19	0.46	0.27
Tb	2.2	1.8	3.0	2.6	2.6	3.5	1.3	1.4	1.7	0.18
Sc	22.2	51	50	59	49	35.5	7.05	12.0	20.7	29.4
Co	-	-	-	-	-	-	-	-	-	124
Cr	3250	2310	680	44	110	1320	2390	2430	1080	1070
Ni	660	550	640	630	290	480	2030	1970	1390	1220

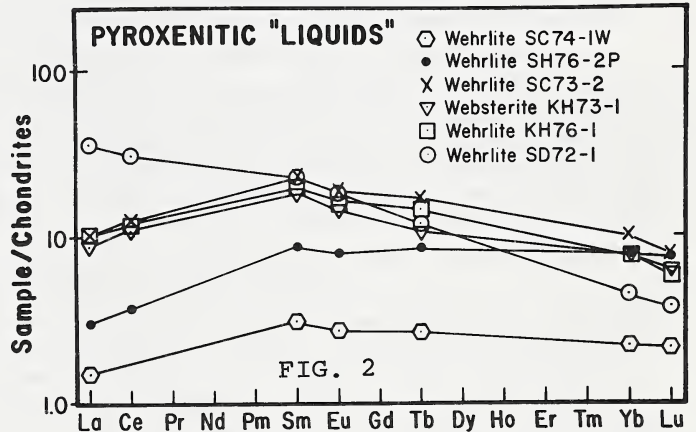


FIG. 2

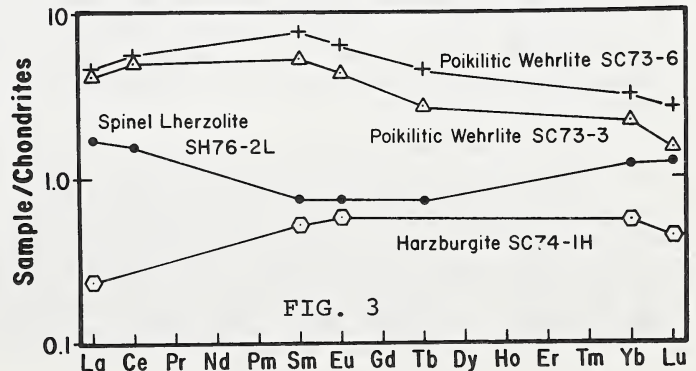


FIG. 3

THE NATURE AND CONDITIONS OF FORMATION OF GRANULITE FACIES XENOLITHS FROM THE MATSOKU KIMBERLITE PIPE, LESOTHO

P.M. Jackson (Grant Institute of Geology, Edinburgh University, West Mains Road, Edinburgh EH9 3JW, Scotland)

B. Harte (Grant Institute of Geology, Edinburgh University, West Mains Road, Edinburgh EH9 3JW, Scotland)

Introduction and Petrology

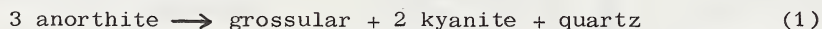
Granulite facies xenoliths in kimberlite provide information regarding the upper part of the lithosphere at the time of kimberlite eruption and their conditions of formation may be explored using various geothermometers and geobarometers.

The granulite facies xenoliths from the Matsoku kimberlite pipe show the assemblages:

- (a) garnet+clinopyroxene+rutile+amphibole+biotite+apatite
- (b) garnet+orthopyroxene+clinopyroxene+rutile
- (c) garnet+clinopyroxene+plagioclase/scapolite+rutile+quartz+biotite+amphibole
- (d) garnet+clinopyroxene+plagioclase/scapolite+rutile+quartz+kyanite+biotite
- (e) garnet+plagioclase/scapolite+kyanite+sphene
- (f) garnet+orthopyroxene+amphibole+biotite+rutile

The plagioclase is oligoclase to andesine in composition, scapolites are of mizzonitic composition, amphiboles are edenitic and pargasitic hornblends and biotite is dominantly phlogopitic. Coexisting garnets and pyroxenes are shown in the Ca-Mg-(Fe+Mn) projection in fig. 1. Clinopyroxenes have high molecular proportions of jadeite (10.00-32.9%) and relatively low molecular proportions of tschermakite (<12%). Al₂O₃ in orthopyroxenes ranges from 1.40 to 2.58 wt.%.

Average grain sizes range from 1 to 2 mm, textures appear granoblastic polygonal and are occasionally seriate. Mineral grains, which are largely unstrained, show some alteration along their boundaries and plagioclase is often completely altered. Where kyanite is present in rocks of assemblage (d) it typically occurs as needles which form radiating sheafs in association with quartz which are located at plagioclase-garnet grain boundaries. Assemblage (e) is found in only one xenolith in which kyanite predominantly occurs as stumpy prismatic crystals which are present as both inclusions in garnet and as independent matrix grains. In addition this assemblage shows some of the acicular sheaf-like kyanite noted for assemblage (d). The acicular kyanite found in these nodules forms a notable departure from the general characteristic of extreme textural equilibrium shown by the xenoliths and indicates the reaction



The nodules frequently show modal banding on a scale of up to 1 cm. In this gneissose structure the layers usually show diffuse margins but an extremely sharp contact separates orthopyroxene and plagioclase bearing layers in the one specimen where both minerals are present. This feature conforms with the lack of association of orthopyroxene and plagioclase in the xenoliths and indicates relatively high pressure granulite facies conditions

bracketed by orthopyroxene and plagioclase instability and the lower pressure limit of the eclogite facies.

Conditions of Formation

The distribution of Fe and Mg between adjacent garnet and clinopyroxene crystals for the assemblages (a) to (d) is plotted in fig. 2, and shows a very restricted range in Kd, around 4.13, which suggests closely similar temperatures of formation for all the specimens analysed. The formation of all the xenoliths under similar conditions is supported in fig. 1 by the generally compatible arrangement of tie lines.

Fig. 2 includes data from specimens displaying reaction (1) and implies that no major change in Fe/Mg distribution between garnet and clinopyroxene occurred in association with the kyanite reaction, although it is possible that the slight tendency for lower Kd values in rim rather than core compositions in fig. 2 is associated with this reaction. It must be noted that this reaction is more sensitive to pressure than to temperature (Hariya and Kennedy 1968). The pressures and temperatures of equilibration calculated for co-existing pyroxenes and garnet in assemblage (b) following Wood and Banno (1973) and Wood (1974) are 839°C and 32 kilobars for adjacent rim compositions. At these temperatures the pyroxene solvus is only slightly temperature sensitive and this in conjunction with the uncertainties in pressure estimates (Howells and O'Hara 1977) demands caution in accepting the above P-T values. Use of the Raheim and Green (1974) geothermometer in conjunction with the data of fig. 2 yields temperatures in the range 729-767°C at an assumed pressure of 10 kbar, and from 872-915°C for an assumed pressure of 30 kbar.

Another approach to the determination of pressure may be made by using reaction (1) assuming only minor changes from pre-reaction pressure values and a temperature based on Fe/Mg distribution between garnet and clinopyroxene rims. Employing a temperature of 839°C in conjunction with the method of Schmidt and Wood (1976) yields pressures of 21.5 kbar for two rocks containing assemblage (d). The same calculation performed using data wholly from Robie and Waldbaum (1968) yields pressures of 17 kbar. The result is clearly dependent on the exact entropy and enthalpy values adopted.

These data indicate that the Matsoku granulite suite may have equilibrated at a depth below the present day Moho in southern Africa which has been located at approximately 37 kilometers (Hales and Sacks 1959). The crust-mantle stratigraphic cross-section for Lesotho may have been similar to that envisaged by Brookins and Meyer (1974) for Kansas, USA where granulite facies xenoliths are believed to straddle the Moho. If the occurrence of granulites to depths of 70 kms is substantiated then the apparent gap in lithospheric stratigraphy between the Moho and the shallowest depths recorded by garnet lherzolite nodules in Lesotho kimberlites would be reduced. The presence of plagioclase granulites to such depths would also necessitate a recalculation of the geotherm for the Lesotho area.

References

- Brookins D.G. & Meyer H.O.A. (1974) *Geophys. Res. Lett.* 1, 269-272. Hales A.L. & Sacks I.S. (1959) *Geophys. J. Roy. Astron. Soc.* 2, 15-33. Hariya Y. & Kennedy G.C. (1968) *Amer. J. Sci.* 266, 193-203. Howells S. & O'Hara M.J. (1977) *Phil. Trans. R. Soc. Ser. B* (in press). Robie R.A. & Waldbaum D.R. (1968) *U.S. Geol. Surv. Bull.* 1259. Wood B.J. (1974) *Contr. Min. Pet.* 46, 1-15. Wood B.J. & Banno S. (1973) *Contr. Min. Pet.* 42, 109-124. Schmidt R. & Wood B.J. (1976) *Contr. Min. Pet.* 54, 255-279.

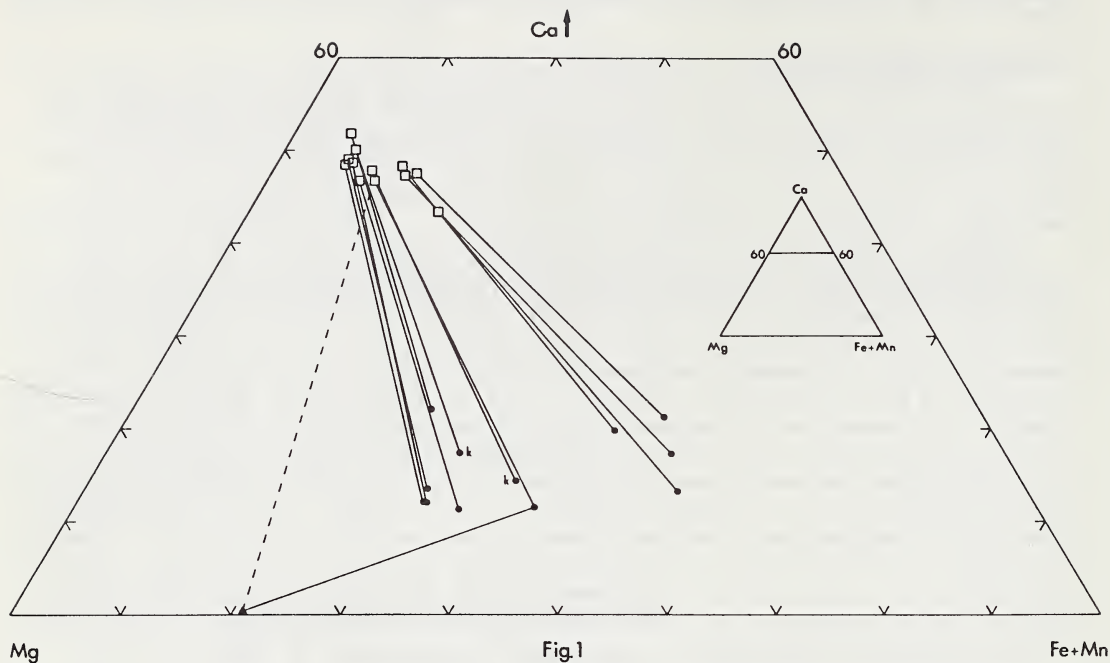


Fig. 1. Ca-Mg-(Fe+Mn) projection showing garnets (filled circles) clinopyroxenes (squares) and orthopyroxene (triangle). Coexisting phases for the same assemblage are connected by tie lines. Kyanite bearing assemblages marked k.

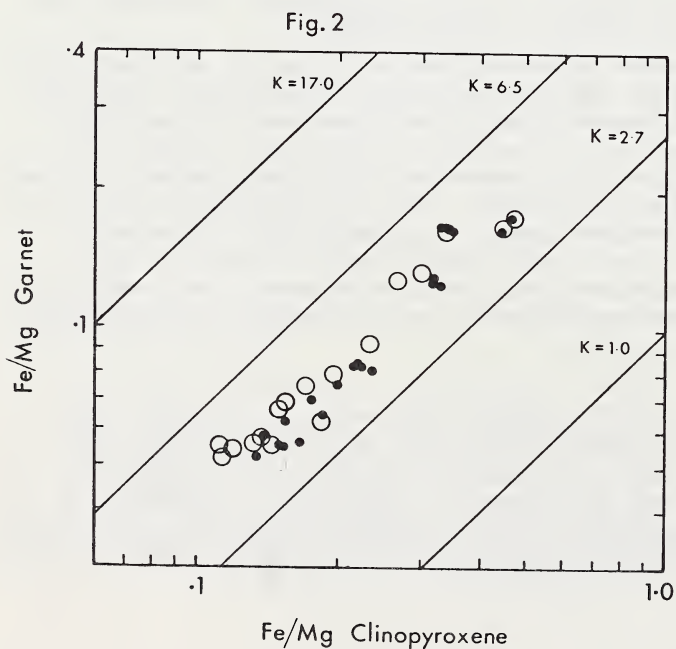


Fig. 2. $(Fe/Mg)_{gt}$ vs $(Fe/Mg)_{cpx}$ plotted for coexisting cores (filled circles) and rims (open circles).

AL-AUGIT AND CR-DIOPSIDE ULTRAMAFIC NODULES IN EUROPEAN ALKALI BASALTS.

E. Jagoutz, V. Lorenz* and H. Wänke

(Max-Planck-Institut für Chemie, Abteilung Kosmochemie, 65 Mainz, FRG)

(*Institut für Geowissenschaften der J.-Gutenberg-Universität, 65 Mainz, FRG)

Ultramafic nodules from West-Eifel/Germany, Massif Central/France and Kapfenstein/Austria were analyzed by micro-probe, X-ray fluorescence and instrumental neutron activation analysis.

To improve the relative accuracy of the micro-probe measurements we placed clinopyroxenes from different nodules and different locations in the same sample preparation.

The nodules of the pyroclastic deposit from the Dreiser Weiher Maar (West-Eifel/Germany) are in most cases unaltered. Two main classes of ultramafic nodules are found: wherlitic nodules (clinopyroxene, olivine and minor phases) and the more abundant lherzolitic nodules (clinopyroxene, orthopyroxene, olivine and spinell). The textures of the wherlitic nodules are granoplastic and of the Cr-diopside bearing lherzolitic nodules are metamorphic. In both cases the modal composition varies over a wide range. From the analyses of the bulk samples and of mineral separates it is shown that the major part of the REE resides in the clinopyroxene. The REE abundance pattern of the spinell shows a remarkable enrichment in light REE.

The temperature of equilibration is plotted in Fig. 1. Lherzolites from Massif Central are equilibrated at lower temperatures than the lherzolites from the Dreiser Weiher.

The clinopyroxenes from wherlitic nodules (from Dreiser Weiher) contain significantly more Fe than the clinopyroxenes from the lherzolites. The evolution of the wherlitic clinopyroxenes along the dashed lines resembles the evolution of the magma. This assumption is also supported by the trace element concentration.

Beside this trend the REE content of the Al-augit from wherlitic nodules is nearly constant (Fig. 2). The clinopyroxene concentrations of these nodules vary from 10 % to 90 %.

Nodules in which wherlite and lherzolite are in contact with each other were analyzed also. The Al-augit of the wherlitic portion has a wherlitic REE abundance. In the lherzolitic portion of these samples the lanthanum is enriched by a factor of 2.

From these investigations we favour a cumulate origin of the wherlitic nodules. All these cumulates are derived from the same magma. The evolution of this magma is demonstrated.

The lherzolitic nodules show a considerable variation in the REE content of their clinopyroxene within one location (Fig. 3).

From the Al-content of the co-existing orthopyroxene and the temperature the pressure is calculated (McGregor, 1974). From the REE content and the

P-T conditions the lherzolitic nodules can be divided in different groups.

In one group the pressure varies from 20 - 30 kb at nearly constant temperature (1100°C). Samples with less than 20 kb show a variation in temperature from 800° to 1100°C.

The first type seems to be derived from near the magma chamber with nearly constant temperature along its depth. The second type could be interpreted as the overlying country rock which was fragmented by the ascending magma.

The REE pattern of the clinopyroxene in these samples can be explained by partial melting and later contamination with strongly fractionated liquids (Frey and Green, 1974).

Comparing the clinopyroxenes from the lherzolitic nodules of different locations it can be shown that the major element chemistry is very similar. The sample with the highest Tschermak's component from the Dreiser Weiher/Eifel is not contaminated in light REE and is very similar to clinopyroxenes from the Massif Central/France and Kapfenstein/Austria (Fig. 4).

References:

- F. Frey, L. Haskin and M. Haskin (1971) *J. Geophys. Res.* 76, 2057-2070.
- F. Frey and D. Green (1974) *Geochim. Cosmochim. Acta* 38, 1023 - 1059.
- I. D. McGregor (1974) *American Mineralogist* 59, 110 - 119.

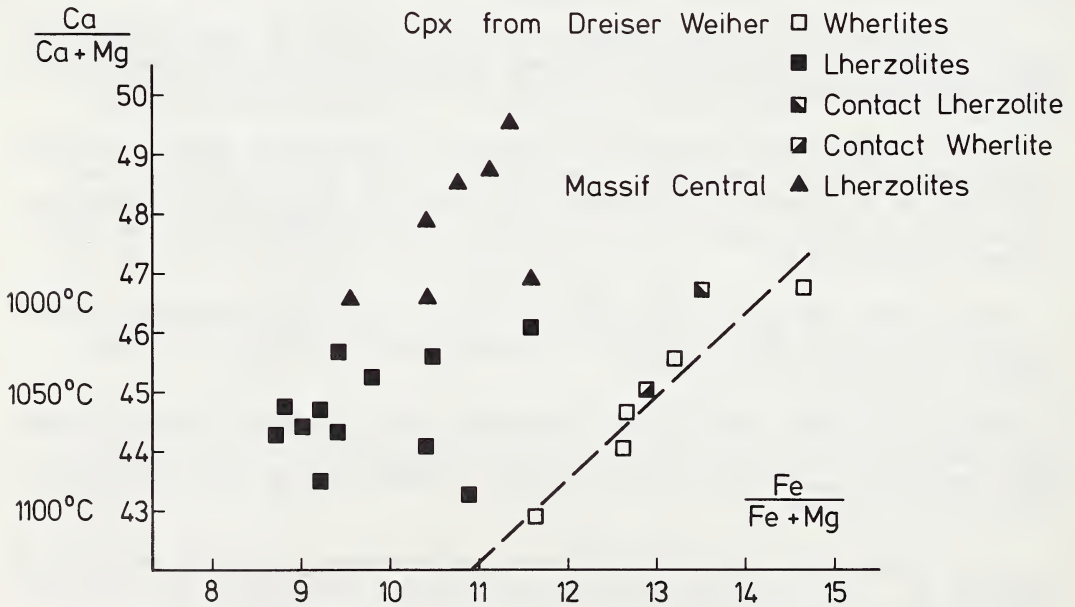
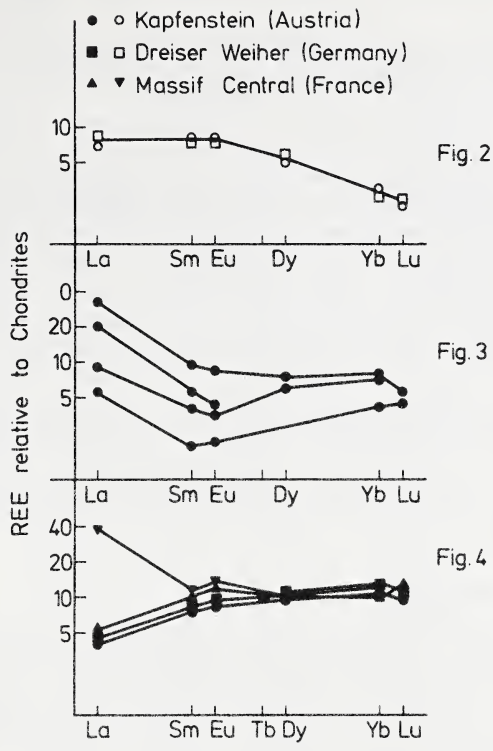


Fig. 1



HARZBURGITE NODULES FROM A LAMPROPHYRE NEAR WAWA,
ONTARIO, CANADA

A.J.A. Janse (Selco Mining Corporation Limited, 55 Yonge Street,
Toronto, Ontario M5E 1J4, Canada)

General

Composite lamprophyre dykes are exposed along highway 17 in a road cut 5 miles south of Wawa. There are three parallel dykes, two of which are approximately three feet wide and one is approximately nine feet wide. The dykes are intruded into a small stock of granodiorite and they have a vertical dip and a strike of N 240° E. The dyke rocks are rich in well preserved olivine and phlogopite phenocrysts which are embedded in a groundmass of serpentine, phlogopite and calcite, which also contains small, scattered, euhedral opaque crystals which are predominantly spinels of various composition. The widest dyke contains multiple intrusions of several varieties of lamprophyre rich in olivine phenocrysts or rich in mica. The olivine rich variety contains locally several fist-size harzburgite nodules.

Mineralogy of the nodules

The harzburgite nodules are composed of olivine with minor amounts of orthopyroxene and chromite. There is a beginning of serpentinization in the numerous cracks which penetrate the olivine crystals and there is little development of phlogopite. The orthopyroxene is slightly more altered than the olivine. The texture of the olivine is anhedral and granular with mortar texture and undulose extinction in places along the margin of the nodules. The forsterite content of the large unstrained olivines, the mortared olivine and the undulose olivines varies from 87.7 to 89.3 percent, while the enstatite content of the orthopyroxene varies from 88.3 to 90.0 percent. Electron probe analyses on several grains indicated that there is no iron enrichment in the olivines towards the margin of the nodules. The opaques consist of magnesian chromite (No. 3 Table 1).

Mineralogy of the lamprophyres

The olivine phenocrysts of the lamprophyre are euhedral to subhedral and they are more altered than the olivines in the nodules. Their forsterite content has a larger spread and varies from 63.0 to 80.2 percent. The phlogopites of the lamprophyre are of two types: one type consists of large poikilitic unzoned subhedral crystals, while the other type consists of euhedral zoned phenocrysts which contains amounts of up to 4% titania (No. 4 Table 1). The opaque minerals in the lamprophyre are predominantly chromium and titanium rich spinels of compositions varying between chrome spinel, titaniferous chrome-poor spinel, titaniferous chrome-rich spinel, ilmenite and titaniferous magnetite.

Concluding remarks

Because garnet has not been found in the lamprophyre and the magnesian content of the ilmenite is relatively low (approximately 3%) the lamprophyre cannot be classified as a kimberlitic rock. The lack of clinopyroxenes in the rock precludes the determination of its place on the temperature-depth curve, but the mineralogy of the nodules still indicates that the rock has a deep seated origin. The presence of harzburgite nodules in this lamprophyre indicates that the deep reaching fault and fracture system of the Kapuskasing Structure probably taps the Upper Mantle. Thus lamprophyres or other rocks containing nodules of deep seated origin may be found in other areas traversed by the Kapuskasing faults.

Table 1. Compositions of selected minerals from the Wawa dykes

Wt%	1	2	3	4	5	6	7	8
SiO ₂	41.81	57.96	0.74	38.17	40.30	0.46	0.25	0.46
TiO ₂	0.01	0.00	0.29	3.90	0.04	50.42	13.55	5.36
Al ₂ O ₃	0.02	1.26	1.51	15.04	0.07	0.05	5.13	10.79
Cr ₂ O ₃	0.02	0.12	64.35	0.03	0.11	0.02	2.87	33.50
FeO	6.68	4.33	20.99	7.48	12.61	41.15	70.90	38.35
MgO	50.97	35.73	10.61	20.93	46.15	2.83	5.17	10.21
CaO	0.03	0.21	0.09	0.00	0.23	0.43	0.16	0.05
MnO	0.08	0.10	0.47	0.11	0.19	2.24	0.94	0.31
Na ₂ O	0.05	0.11	0.01	0.45	0.01	0.11	0.00	0.18
K ₂ O	0.00	0.13	0.08	9.15	0.00	0.00	0.00	0.00
NiO	0.32	0.05	0.09	0.00	0.29	0.00	0.04	0.05
Total	99.99	100.00	99.24	95.27	100.00	97.72	99.01	99.25

Table 2. Structural formulae

	4 (0)	6 (0)	12 (0)	24 (0)	4 (0)	3 (0)	16 (0)	12 (0)
Si	1010	1946	78	5998	998	11	37	45
Ti	0	0	23	461	0	964	1607	417
Al	0	50	188	2784	1	1	954	1318
Cr	0	6	5313	0	1	0	356	2746
Fe	135	124	1832	982	263	875	9357	3327
Mg	1834	1818	1652	4900	1717	106	1213	1577
Ca	0	9	12	0	5	11	23	3
Mn	1	4	43	14	3	47	125	24
Na	3	7	0	133	0	5	0	33
K	0	6	12	1830	0	0	0	0
Ni	6	0	0	0	5	0	0	3
Total	2989	3970	9160	17102	2993	2021	13672	9493

Fo% 88

76

En% 89

Cr/Cr Al 0.96

0.27 0.67

Total iron as FeO

Probe analyses through Dr H.A.O. Meyer, Purdue University - 1: olivine from harzburgite, average of 10 analyses, calculated anhydrous, 2: orthopyroxene from harzburgite, average 6 analyses anhydrous, 3: chromite from harzburgite, 1 analyses, 4: phlogopite from lamprophyre, 1 analyses, 5: olivine from lamprophyre, average of 5 analyses, anhydrous, 6: ilmenite from lamprophyre, 1 analyses, 7: titaniferous magnetite, 1 analyses, 8: titaniferous chromespinel, 1 analyses.

GEOPHYSICAL AND GEOCHEMICAL CONSTRAINTS ON THE COMPOSITIONAL HETEROGENEITY OF THE UPPER MANTLE

T. H. Jordan (Geological Research Division, Scripps Institution of Oceanography, La Jolla, California 92093)

Constraints on the seismic velocity and thermal structure of the upper mantle indicate the existence of a root zone extending to a depth on the order of 400 km beneath the ancient shields which translates coherently with the continents in the course of plate motions. This root zone (tectosphere) is characterized by high seismic velocities, low temperatures and superadiabatic thermal gradients. Chemical gradients within the upper mantle are necessary to stabilize this zone against advective disruption. The nature of these chemical differences is indicated by peridotite xenoliths from kimberlite pipes, which suggest a strong depletion of the subcontinental mantle in the garnet forming components. Density calculations based on realistic mineralogies show that the inferred gradients in garnet depletion are in quantitative agreement with the geophysical model.

Root zone - no finite strength
depleted in volatiles
low Fe/Mg
lower T
low wet

near depletion of major elements
enrichment of minor elements

STRUCTURE AND PETROLOGY OF THE CONTINENTAL LITHOSPHERE:
METHODS AND INITIAL RESULTS FROM THE COCORP PROGRAM

S. Mahlburg Kay, J. Oliver, R. Kay, S. Kaufman, L. Brown
Department of Geological Sciences
Cornell University
Ithaca, New York 14853

B. Foster
Trumansburg, New York 14886

The study of xenolith suites from kimberlites and alkali basalts in conjunction with deep seismic reflection profiling is potentially a powerful method for exploration of the petrology and structure of the lower continental crust and mantle. The xenoliths provide information on the identity of rock units and the seismic profile provide information on the shape, distribution, and structure of rock bodies. Additional evidence can be obtained by direct observation of lower crustal sections such as the Ivrea zone (Berckhemer, 1969). Using these data in a fashion analogous to that of the seismic stratigraphers of the petroleum industry, it may be possible to piece together a regional picture of the lower crust and upper mantle. In this paper, we review the status of the COCORP deep seismic profiling program and describe the beginnings of our study of xenoliths from two localities near profiling sites.

Deep seismic reflection profiling of the lower crust and upper mantle is being carried out as an on-going project by the Consortium for Continental Reflection Profiling (COCORP). The COCORP program is funded by the National Science Foundation and is part of the United States Program for the International Geodynamics Project. State-of-the-art seismic reflection techniques are used to provide the high resolution of structure needed to study fundamental geologic problems of the continental crust and upper mantle. Field experiments were begun in Hardeman County, Texas where data were collected along three lines totalling a distance of 36.8 km using a 24-fold CDP stack. Information was obtained on intrabasement diffractors and reflectors to depths as great as about 45 kilometers. Reflectors in the upper part of the section are continuous over the length of the profile and give information on apparent(?) faulting and unconformities deep in the crust. Lower level reflectors are less continuous but zones and discontinuities may be distinguished on the basis of spatial density, length, and dip of reflectors. Zones of low reflector density may represent plutons and some hyperbolic events may indicate deep folded structures (see Oliver et al., 1976). The lower crust appears to be an area of great complexity of structure and rock types, much greater than indicated by other types of geophysical studies.

The second COCORP study was carried out across the Rio Grande Rift on the eastern margin of the Albuquerque Belen Basin in central New Mexico. This study was later extended so that a total of 165 kilometers of profiling has been completed from Abo Pass in the east to Sierra Lucero on the west. Preliminary study of the results indicates reflectors of generally limited lateral extent throughout the lower crust and possibly the mantle. Particularly impressive is a strong reflector at a depth of about 20 kilometers at Bernardo which dips to the north and corresponds with the top of the magma chamber proposed by Sanford et al. (1973). The rift margins are recognizable

in the profiles and show differences in record character. Considerable structural complexity is visible in the sediments.

A third study includes a profile 52.5 kilometers in length crossing a part of the Green River Basin and the Wind River Uplift in Wyoming. This line is currently being extended to the northwest. Preliminary analysis indicates a fairly continuous reflector exhibiting both apparent offsets and topography at a depth of 11 seconds (approximately 33 kilometers). This reflector may correspond to the Moho. Abundant evidence of radial and lateral structural complexities including apparent faulting and warping of reflectors can be seen on the profile throughout the crust and upper mantle.

Field data for profiles across the Great Valley of California and the San Andreas Fault are being processed at present. Sites to be profiled in the near future are located in the Michigan Basin, the Adirondacks, and the Appalachians.

Study of xenoliths from the Leucite Hills is being undertaken as this locality is close to the Wind River seismic profile. Xenolith types are being compared to surface exposures in the Wind River Uplift. In the Leucite Hills, crustal and possible mantle xenoliths are abundant in two localities and are present at several others. Types of xenoliths collected include gabbros, anorthosites, granites, and various sedimentary rocks as described by Carmichael (1967). In addition,* feldspathic gneisses, biotite-rich schists, mafic granulites, and pyroxenites have also been found to date. Further work may show some of these to be cognate xenoliths, but a large number are of foreign origin.

Field work is also underway to find xenoliths of crustal and mantle origin in the kimberlites of the Finger Lakes Region in New York. Small fragments of anorthosite kindred as well as numerous sedimentary xenoliths occur in the Poyer Orchard diatreme near Ithaca, New York. A syenite xenolith has been found in a small kimberlite dike in the same area. Although crystalline fragments are not common, this locality is one of the few areas in the eastern United States where xenoliths are found. Xenoliths from the Finger Lakes Region may tie in with seismic profiles in the Adirondacks or in the Appalachians.

References

- Berckhemer, H., 1969, Direct evidence for the composition of the lower crust and Moho, *Tectonophysics*, 8, 97-105.
- Carmichael, I.S.E., 1967, The mineralogy and petrology of the volcanic rocks from the Leucite Hills, Wyoming, *Contr. to Min. and Pet.*, 15, 24-66.
- Oliver, J., Dobrin, M., Kaufman, S., Meyer, R., and Phinney, R., 1976, Continuous seismic reflection profiling of the deep basement, Hardeman County, Texas, *Geol. Soc. Am. Bull.*, 87, 1537-1546.
- Sanford, A.R., Alptekin, O., and Topozada, T.R., 1973, Use of reflection phases on microearthquake seismograms to map an unusual discontinuity beneath the Rio Grande Rift, *Bull. of the Seismological Soc. of Am.*, 63, 2021-2034.

PARTITIONING OF Co AND Ni BETWEEN Fe-METAL AND OXIDE OR OLIVINE

S.E. Kesson (Research School of Earth Sciences, A.N.U., Canberra, A.C.T. 2600, Australia)

The siderophile element abundance patterns of the earth's mantle not only provide insight into the processes involved in core formation but also provide critical information concerning the question of core-mantle equilibrium. The partition behavior of Ni and Co are of particular interest in this context, since these elements appear to be uniformly distributed throughout the upper mantle and their abundances in upper mantle rocks and minerals are well established.

The partitioning of Ni and Co between oxides and Fe-metal, and between olivine and Fe-metal in both magnesian "model mantle" and Mg-free systems is currently being determined experimentally over temperatures ranging from 1000 to $\geq 1500^{\circ}\text{C}$ and pressures ranging from 0 to approximately 80 kbar.

The following equilibria have been studied: $\text{Ni}_2\text{SiO}_4 + 2\text{Fe} = \text{Fe}_2\text{SiO}_4 + 2\text{Ni}$; $\text{Co}_2\text{SiO}_4 + 2\text{Fe} = \text{Fe}_2\text{SiO}_4 + 2\text{Co}$; $5(\text{Mg}_{0.8}\text{Ni}_{0.2})_2\text{SiO}_4 + 2\text{Fe} = 5(\text{Mg}_{0.8}\text{Fe}_{0.2})_2\text{SiO}_4 + 2\text{Ni}$; $5(\text{Mg}_{0.8}\text{Co}_{0.2})_2\text{SiO}_4 + 2\text{Fe} = 5(\text{Mg}_{0.8}\text{Fe}_{0.2})_2\text{SiO}_4 + 2\text{Co}$; $\text{NiO} + \text{Fe} = \text{FeO} + \text{Ni}$; $\text{CoO} + \text{Fe} = \text{FeO} + \text{Co}$.

Experimental investigations of the following proved unsatisfactory due to kinetic problems: $5(\text{Mg}_{0.8}\text{Ni}_{0.2}\text{O}) + \text{Fe} = 5(\text{Mg}_{0.8}\text{Fe}_{0.2}\text{O}) + \text{Ni}$; $5(\text{Mg}_{0.8}\text{Co}_{0.2}\text{O}) + \text{Fe} = 5(\text{Mg}_{0.8}\text{Fe}_{0.2}\text{O}) + \text{Co}$. Experiments were carried out in evacuated SiO_2 -glass tubes and in piston-cylinder and "squeezer" high-pressure apparatus. Either Ni or Co together with Pt capsules were used. Minimal reaction was observed between the subsolidus charges and capsule materials below 1500°C . Experimental conditions and results are summarised in Tables 1 and 2.

The K values for the reaction $\text{CoO} + \text{Fe} = \text{FeO} + \text{Co}$ appear to decrease slightly with an increase in either temperature or pressure. A similar conclusion probably holds for the Ni-bearing system. These K values agree well with data from previous experimental studies, e.g. Schenk et al. (1968) and also with equilibrium constants derived from thermodynamic data, indicating essentially ideal behavior in metal and oxide solid solutions.

The K values for Co or Ni olivine-metal equilibria do not show a clear correlation with either temperature or pressure. The similarity between the K values for (CoFe) olivine and (CoFeMg) olivine equilibria indicate that there is only minor preferential distribution of cations in the olivine structure.

The K values for Ni-olivine equilibria are in accord with the experimental data of Irvine and Kushiro (1976) but differ significantly from K values for co-existing olivine and metal in lunar low-Ti mare basalts (Hewens and Goldstein, 1974) and in pallasites (Buseck and Goldstein, 1969). This suggests that site distribution phenomena are significant at high Ni concentration levels.

Olivine-metal and oxide-metal partition equilibria are particularly relevant to the question of core-mantle equilibrium, and will be evaluated in terms of the recent hypothesis of Ringwood (1977) that oxygen (as FeO) is an important light element in the earth's core.

Table 1. Co and Ni partitioning between metal and oxide in simple systems

P	T°C	K ¹	K	K _{mean}
		CoO+Fe ²	FeO+Co	
vacuum	1000	41	42	42
	1100	27	28	28
	1200	23	27	25
	1300	20	19	20
	1400	17	18	18
30 kbar	1200	17	19	18
	1300	16	16	16
	1400	—	13	13
75 kbar	1300	14	—	14
		NiO+Fe	FeO+Ni	
vacuum	1000	201	(83)	142
	1100	94	123	104
	1200	76	74	75
	1300	(98)	(102)	(100)
	1400	61	65	63
30 kbar	1200	—	69	69
	1300	61	61	61
	1400	78	—	(78)
60 kbar	1200	34	50	45

Dubious values in parentheses.

¹K is the equilibrium constant obtained using mole percent (n) values, e.g.

$$K = \frac{n_{\text{FeO}}^{\text{ox}}}{n_{\text{CoO}}^{\text{ox}}} \times \frac{n_{\text{Co}}^{\text{m}}}{n_{\text{Fe}}^{\text{m}}} \text{ where ox = oxide, m = metal.}$$

²Starting assemblage.

Table 2. Co and Ni partitioning between metal and olivine

P	T ^o C	K ¹		K _{mean}
		Co ₂ SiO ₄ +2Fe ²	Fe ₂ SiO ₄ +2Co	
30 kbar	1200	11	19	15
	1300	13	16	15
vacuum		5 (Mg _{0.8} Co _{0.2}) ₂ SiO ₄ +2Fe	5 (Mg _{0.8} Fe _{0.2}) ₂ SiO ₄ +2Co	
	1200	12	13	13
	1300	—	12	12
	1400	11	11	11
30 kbar	1200	did not equilibrate	10	10
	1300	"	8	8
	1400	"	7	7
	1500	"	10	10
30 kbar		Ni ₂ SiO ₄ +2Fe	Fe ₂ SiO ₄ +2Ni	
	1200	52	44	48
	1300	46	42	44
vacuum		5 (Mg _{0.8} Ni _{0.2}) ₂ SiO ₄ +2Fe	5 (Mg _{0.8} Fe _{0.2}) ₂ SiO ₄ +2Ni	
	1200	21	22	22
	1300	23	33	28
	1400	22	29	25
30 kbar	1200	—	46	—
	1300	15	42	—
	1400	14	37	—
	1500	19	36	—

$^1K = \frac{n_{FeO}^{ol}}{n_{NiO}^{ol}} \times \frac{n_{Ni}^m}{n_{Fe}^m}$; FeO + MgO + NiO in olivine = 100; n = mole percent; ol = olivine; m = metal.

²Starting assemblage.

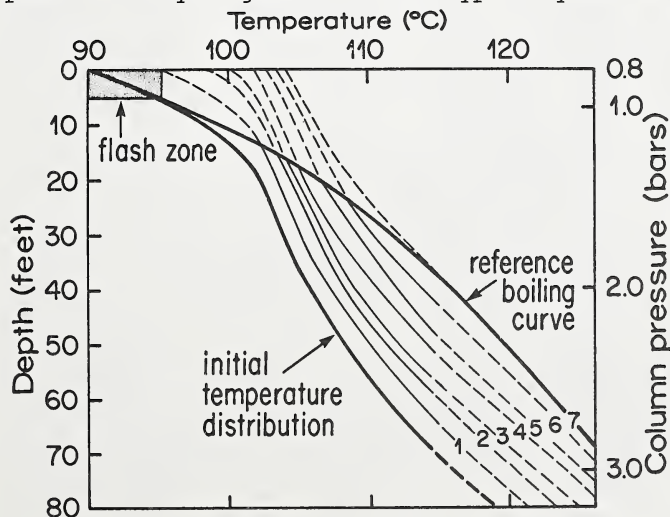
References

- Buseck P. R. and Goldstein J. I., 1969. Geol. Soc. Am. Bull. **80**, 2141.
Hewens R. H. and Goldstein J. I., 1974. Earth Planet. Sci. Letters **24**, 59.
Irvine T. N. and Kushiro I., 1976. Carnegie Inst. Ybk. Geophys. Lab. **668**.
Ringwood A. E., 1977. Geochem. J., in press.
Schenk H., Steinmetz E. and Grundmann R., 1968. Archiv für Eisenhüttenwesen, **B**, **914**, 895.

FLUID DYNAMICS DURING ERUPTION OF WATER-STEAM AND MAGMA-GAS SYSTEMS: GEYSERS, MAARS AND DIATREMES

Susan Werner Kieffer (Dept. of Earth and Space Sciences, University of California, Los Angeles, CA, U.S.A. 90024)

Expansion of a vapor phase in a multicomponent, multiphase system controls the fluid flow characteristics during eruption of geysers, maars and diatremes. In geyser eruptions the multiphase fluid is a water-steam or, rarely, a water-carbon dioxide mixture; in maars and diatremes the fluid may be as simple as a water-steam mixture, or may be a complex mixture of magma, water and/or carbon dioxide. Geysers are considered here as analogues of maars and diatremes because they are readily available for observation, because there are sufficient equation-of-state data on water that quantitative results and predictions can be obtained, and because geysers exhibit many patterns of eruption which should be common to thermodynamically similar mixtures erupted from greater depths. In this paper an analytic model of flow of two-phase systems (water-steam; water-carbon dioxide; and albite-water) is used to study eruption dynamics and to predict observed surface eruption patterns of geysers. In the eruption model, a liquid phase, initially undersaturated in volatiles at all depths except possibly near the top of the fluid column (Figure 1) is assumed to begin eruption instantaneously when the surface is unloaded (Figure 2), e.g., when surface fluid overflows or when a crack is propagated to the surface. The fluid flow equations of conservation of mass, momentum, and energy, supplemented by an equation of state for the fluid, are solved by the method of characteristics. The motions of the disturbance waves and the fluid surface are shown schematically in Figures 2 - 5. The initial unloading disturbance propagates down the fluid column as an unloading (rarefaction) wave ($R(-)$ in Figure 3) that accelerates the fluid out of the conduit; the motion of the fluid surface is shown as D_1 in Figure 3. The velocity of ejection of the fluid is proportional to the sound speed of the fluid which, in turn, depends on the composition, pressure, temperature, vapor fraction, bubble size, surface tension, and on whether or not thermal equilibrium is maintained between the liquid and gas phases during the eruption (Figure 6). The sound speed of a liquid-gas mixture is typically two to three orders of magnitude



lower than the sound speed of the pure liquid end member and one order of magnitude lower than the pure vapor end member; it is a few meters per second for water-steam mixtures at 100°C.

Figure 1. Initial temperature distribution in Old Faithful taken 15 seconds before eruption (Birch and Kennedy, 1972) compared to reference boiling curve at elevation of Yellowstone National Park. Curves 1-7 explained in text.

Figure 2.
Time: immediately prior to eruption

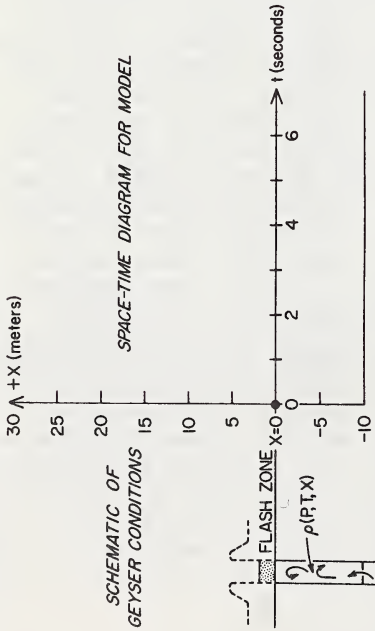


Figure 3.

Time: during ascent of column and descent of rarefaction into conduit

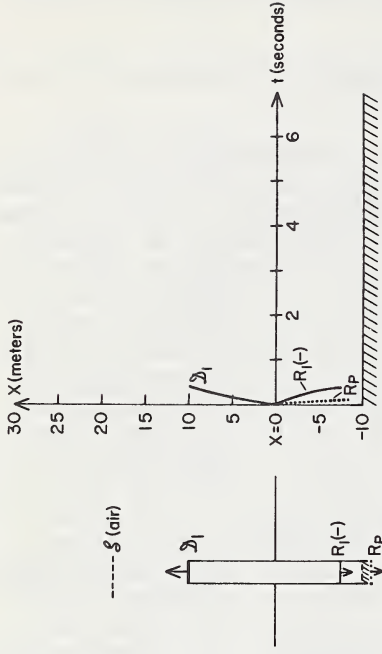


Figure 4.

Time: after column attains maximum height and begins descent

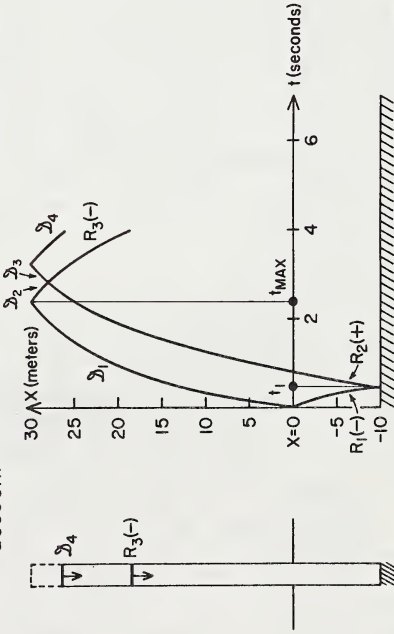
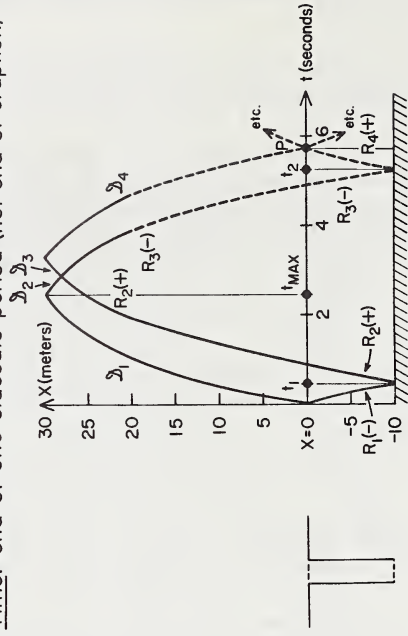


Figure 5.

Time: end of one staccato period (not end of eruption)



Figures 2,3,4,5. Schematic illustrations of propagation of initial unloading wave down a conduit containing a fluid which is initially below the reference boiling curve. In these drawings it is assumed that only 10 meters of the fluid can be brought to the boiling curve by the initial unloading disturbance; the bottom of this zone is modeled as a rigid wall--in reality it is the boundary between the two-phase zone developed by unloading and the single (liquid) phase at greater depths.

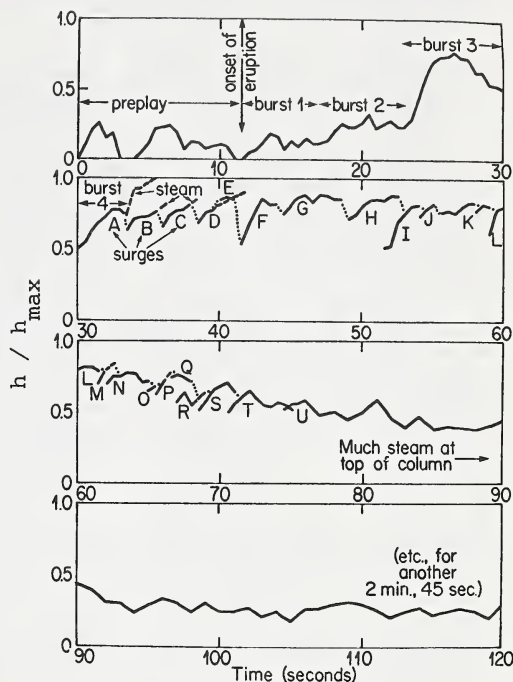
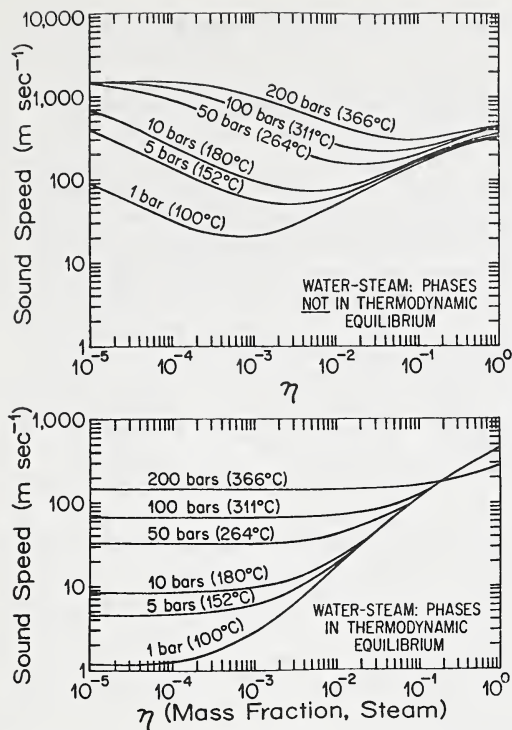


Figure 6 (left). Sound speed of water-steam mixture as a function of pressure and mass fraction steam. Figure 7 (right). The height of eruption of Old Faithful geyser normalized to the maximum height as a function of time. Nonsteady flow prevails from the onset of eruption through four bursts; steady flow prevails at later times.

The flow during an eruption is controlled by the sound speed of the fluid in the conduit as the rarefaction waves pass through it and is initially nonsteady flow which changes to steady flow only when the entire column of fluid has been brought to the saturation curve by a repeated series of staccato "bursts" of the kind shown in Figures 2-5. These bursts bring the column stepwise up to the boiling curve (see Figure 1 which shows seven such steps). The ejection velocity during nonsteady flow is characterized by these bursts which bring the eruption to its maximum height (Figure 7). The frequency of the bursts depends on the sound speed, on the depth of initial unloading, and on the temperature profile in the fluid at the onset of eruption. The duration of the nonsteady flow phase depends on the degree to which the initial temperature profile departs from the saturation curve: it is very short if the initial temperature profile lies near the saturation (or boiling) curve and long if it departs substantially from the saturation curve at depth. If the initial temperature profile is nearly isothermal at depth, steady state eruption conditions may never be reached and the entire eruption will be characterized by "bursts". The steady flow phase is characterized by relatively constant ejection velocities with small velocity variations which arise from organ pipe resonances (see Figure 7). In summary, the eruption of a two-phase system has a different character from the eruption of a single-phase system because the eruption dynamics are controlled by the kinetics and thermodynamics of expansion of a vapor phase within a multicomponent, multiphase system.

LEAD AND STRONTIUM ISOTOPES IN INCLUSIONS IN DIAMONDS AND IN MANTLE-DERIVED XENOLITHS FROM SOUTHERN AFRICA

J.D. Kramers (Bernard Price Institute of Geophysical Research, University of the Witwatersrand, Johannesburg, 2001, South Africa)

Batches of approximately one gram of diamonds with sulphide inclusions from three South African diamond mines were burned and the inclusions (and volatilised lead) recovered for analysis. The procedure was similar to that described by Welke et al.(1974), with however a reduced analytical blank for lead (1-1.6 nanogram). The samples were from the Premier mine (Transvaal), Finsch mine (Cape Province) and "Kimberley Pool", a plant which works kimberlite from the De Beers, Wesselton, Dutoitspan and Bultfontein pipes in Kimberley, Cape Province. The Finsch pipe and those in Kimberley are post-Karoo in age, whereas the Premier pipe is Precambrian (about 1250 m.y., Barrett and Allsopp, 1973). The results are listed in Table 1. Fig. 1 shows the results in the 207/204 vs. 206/204 diagram, in comparison with the lead isotopic compositions (initial) of the respective host kimberlites. Isotopic disequilibrium between the diamond inclusions and the host kimberlites is evident in each case, but is especially striking in the samples from Finsch and from the Kimberley Pool. Given the very primitive lead isotopic composition of the inclusions in these diamonds, it is inconceivable that they would have crystallised from liquids with the isotopic composition of the Finsch and Kimberley-Pool kimberlites. Observations of this kind have not yet been made on diamonds with other kinds of inclusions; nevertheless a xenocryst nature is indicated for some diamonds by the present data.

Lead and strontium isotope ratios of separated clinopyroxenes from three xenolith suites from cretaceous kimberlite occurrences are shown in Figs. 2, 3 and 4 and discussed below.

(1) Roberts Victor (Orange Free State). This pipe is 127 m.y. old (Allsopp and Barrett, 1975). It contains a large variety of eclogitic xenoliths, some of them banded, in which diamonds occasionally occur. These eclogites are considered products of fractional crystallisation (C.Hatton, personal communication). The spread in lead (Fig. 2) and strontium isotope ratios is very large. The lead data confirms the findings of Manton and Tatsumoto (1971) in that the slope of the data in the 207/204 vs. 206/204 diagram defines a deep Precambrian age (2500 m.y., excepting sample HRV 67). Apart from the evidence of this old age, the observation that rock units in the subcontinental mantle can retain very primitive lead isotopic compositions is important.

(2) Matsoku (Lesotho). This pipe is post-Karoo in age and is located in North-Eastern Lesotho. It contains a large variety of peridotitic xenoliths, recently described by Gurney, Harte and Cox (1975). On the basis of bulk chemistry (chiefly Mg/Fe ratio) these authors distinguish between residual mantle-material ("common peridotites") and products of fractional crystallisation ("cumulates") in this suite. Some xenoliths contain "veins" of fine-grained peridotite. Samples of three common peridotites, three cumulates and two vein rocks were analysed. The $^{87}\text{Sr}/^{86}\text{Sr}$ ratios are all between .703 and .704. The lead isotope ratios are plotted in Fig. 3. A fairly strong heterogeneity exists within the group of common peridotites, whereas the cumulates and vein rocks show relatively good homogeneity within their group. This data provides strong support for the abovementioned interpretations of rocks from this suite.

(3) Kimberley (Cape Province). The four pipes which make up the Kimberley Pool have yielded a large variety of xenoliths and xenocrysts. Six samples of separated diopsides from porphyroclastic and granular lherzolites from the De Beers and Bultfontein mines showed a large spread in lead and strontium isotope ratios (lead: see Fig. 4; strontium: .704-.713; Kramers, 1977), suggesting that they form part of a Precambrian rock province. Four clinopyroxene megacrysts from the four pipes on the other hand have lead isotope ratios very similar to each other (Fig. 4), as well as much more uniform $^{87}\text{Sr}/^{86}\text{Sr}$ ratios between .703 and .704. This data suggests that these megacrysts were produced in a more recent homogenisation event, possibly involving a magma chamber.

The data, considered together, allows the suggestion that the diamonds analysed might originally have been rock-forming minerals in a deep-Precambrian rock suite such as the one sampled by the Roberts Victor kimberlite. Furthermore the data shows that the occurrence of magmatic events which lead to fractional crystallisation in the subcontinental mantle need not obliterate older isotopic heterogeneity in their vicinity.

Table 1: Diamonds with sulphide inclusions.

Sample	206/204	207/204	208/204	206/204*	207/204*	208/204*
Premier	16.98 \pm .01	15.49 \pm .01	36.99 \pm .03	16.93	15.49	36.98
Finsch	14.48 \pm .06	14.93 \pm .06	35.05 \pm .14	13.72	14.81	34.20
Kimberley	15.16 \pm .17	14.93 \pm .12	35.05 \pm .30	age correction insignificant.		

*age correction. Premier: minimum (1250 m.y.; pipe age)
Finsch: maximum (2500 m.y.; "model age")

References

- H.L. Allsopp and D.R. Barrett (1975): Rb-Sr age determinations on South African kimberlite pipes. *Physics and Chemistry of the Earth*, 9 (Pergamon Press), pp 605-615.
- D.R. Barrett and H.L. Allsopp (1973): rubidium-strontium age determinations on South African kimberlite pipes. *First International Kimberlite Conference, extended abstract volume* (University of Cape Town), pp 23-25.
- J.J. Gurney, B. Harte and K.G. Cox (1975): Mantle xenoliths in the Matsoku kimberlite pipe. *Physics and Chemistry of the Earth*, 9 (Pergamon Press), pp 507-532.
- J.D. Kramers (1977): Lead and strontium isotopes in cretaceous kimberlites and mantle-derived xenoliths from Southern Africa. *Earth and Planetary Science Letters*, 34, pp 419-431.
- W.I. Manton and M. Tatsumoto (1971): Some Pb and Sr isotopic measurements on eclogites from the Roberts Victor mine, South Africa. *Earth and Planetary Science Letters*, 10, pp 217-226.
- H.J. Welke, H.L. Allsopp and J.W. Harris (1974): Measurements of K, Rb, U, Sr and Pb in diamonds containing inclusions. *Nature*, 252 No. 5478, pp 35-37.

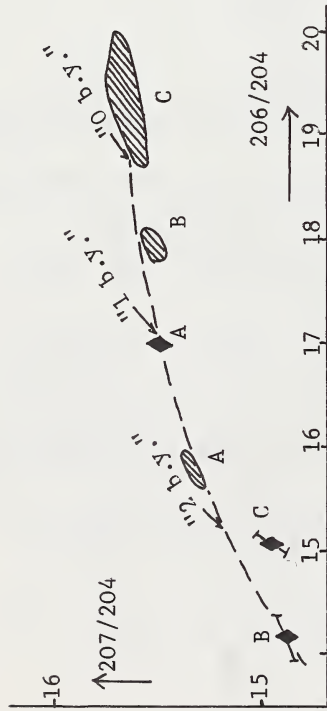



Fig. 1: Lead isotopes in diamond inclusions and host kimberlites. ◆ : inclusions in diamonds;  : host kimberlites, initial ratios. A: Premier, B: Finsch, C: Kimberley Pool. (Premier kimberlite: Kramers, unpubl.; Finsch, Kimberley kimberlites: Kramers, 1977).

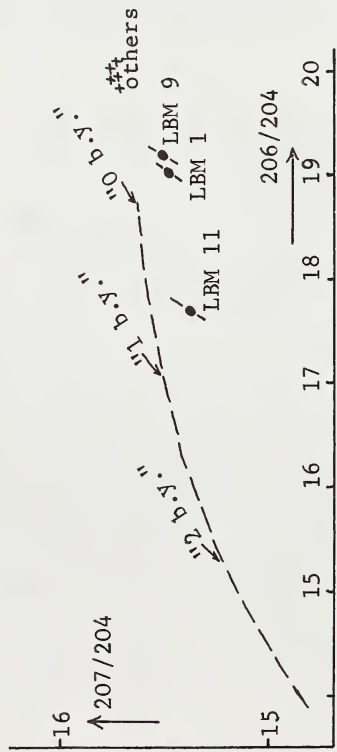


Fig. 3: Lead isotopes in separated clinopyroxenes from Matsoku peridotites. ● : "common peridotites"; + : "cumulates" (Kramers, 1977) and vein rocks (LBM 90 and 38B, this work)

NB: Growthcurve and "model ages" drawn in purely for orientation purposes.

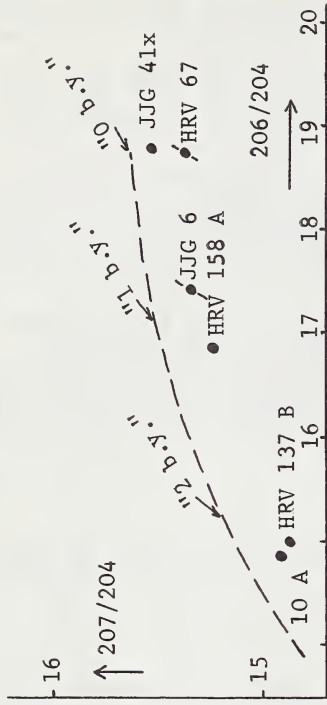


Fig. 2: Lead isotopes in separated clinopyroxenes from Roberts Victor eclogites. JGG 4lx: Kramers (1977); other samples this work. Slope (excepting HRV 67) defines age of 2.5 b.y..

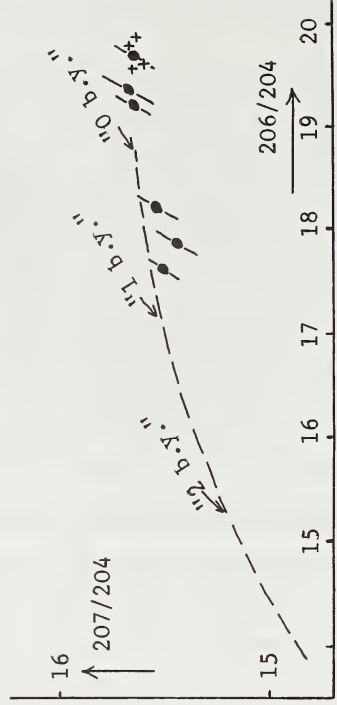


Fig. 4: Lead isotopes in separated clinopyroxenes from Kimberley peridotites (●, Kramers, 1977) and in clinopyroxene megacrysts (+, this work) from the four pipes of the Kimberley Pool.

POLYMICT PERIDOTITES FROM THE BULTFONTEIN AND DE BEERS MINES,
KIMBERLEY, SOUTH AFRICA

P.J. Lawless (Anglo-American Research Laboratory, P.O. Box 106, Crown Mines,
Transvaal, 2025, S. Africa)

J.J. Gurney (Dept. of Geochemistry, University of Cape Town, Private Bag,
Rondebosch, Cape, 7700, S. Africa)

J.B. Dawson (Dept. of Geology, Purdie Building, St. Andrews, Fife, Scotland
KY 16 9ST.)

Introduction

Six nodules have been found amongst the xenoliths of the Bultfontein and De Beers Mines. They have been termed polymict peridotites because they display gross disequilibrium features. The rocks are characterised by the presence of (a) Metasomatic minerals including ilmenite, phlogopite and sulphide phases, and (b) a wide variety of olivines, orthopyroxenes, garnets and clinopyroxenes sometimes as rock clasts. All appear to be of upper mantle origin. The mineral chemistry of four of the polymict nodules has been studied in some detail.

Description and Chemistry of Mineral Components

Olivine bearing clasts within two of the nodules are porphyroclastic, in one laminated disrupted porphyroclastic and in the other disrupted mosaic porphyroclastic using the terminology of Harte (1977). The rock clasts appear to be harzburgites, pyroxenites and lherzolites.

(i) Olivine. The most abundant silicate constituent occurs as phenocrysts and/or porphyroclasts, usually anhedral and displaying undulose extinction. Most grains are partially serpentinised and may have recrystallized to variable extent to produce neoblasts or tabular crystals. Olivine compositions vary from Fe_{86} to Fe_{96} . The higher iron varieties are generally the recrystallized, neoblastic or tabular crystals.

(ii) Orthopyroxene is found as (a) phenocrysts and/or porphyroclasts and as (b) small grains partially or completely enclosing clinopyroxene grains or megacrysts. (a) Clear porphyroclasts seldom exceed 5 mm, are usually anhedral, show good cleavage and straight extinction. Some porphyroclasts are "cloudy" and have been deformed and partially recrystallized. Rare examples have been disrupted and show kink bands. The range of compositions is given in Table 1, which shows the variation in unaltered porphyroclasts and the maximum value for edges of porphyroclasts or for recrystallized grains where either exceeds the unaltered range.

TABLE 1.

Rock No.	JJG 513		BD 2394		BD 2666		JJG 1414	
	Unaltered	Alt.	Unaltered	Alt.	Unaltered	Alt.	Unaltered	Alt.
Mg/Mg+Fe	86.8-94.2		88.0-94.0		85.0-95.4		88.3-96.0	
Al ₂ O ₃ wt%	<.01- .91	2.97	.02 -.79	3.21	<.01-.90	1.91	.05 -2.40	2.45
CaO wt%	.02- .62	1.33	.22 -.91	1.21	.25-.70	1.00	.42 -1.69	
Cr ₂ O ₃ wt%	.05- .59	.96	.06 -.58	1.24	.05-.67	1.06	.17 -1.46	
TiO ₂ wt%	<.01- .29	.36	.01 -.30	.36	<.01-.29	0.32	.01 - .30	.32

(b) Orthopyroxene around clinopyroxene grains and or within clinopyroxene megacrysts varies in shape, size, orientation and appearance. It is usually associated with phlogopite and finely disseminated opaque minerals, and the manner of its association with clinopyroxene has not been observed in any other clinopyroxenes we have seen. In one small clast in BD 2666, the orthopyroxene forms an optically continuous rim around the clinopyroxene grains but in the other cases the orthopyroxene is randomly oriented in these clasts and megacrysts. The compositions of the orthopyroxenes are extraordinarily variable.

The maximum range for any clast in a particular nodule is given in Table 2.

TABLE 2.

Rock No.	JJG 513	BD 2394	BD 2666	JJG 1414
Mg/Mg+Fe	88.5 -92.3	86.9 -90.6	86.5 -94.2	90.6 -92.3
Al ₂ O ₃ wt%	0.54- 2.85	0.33- 3.35	0.37- 2.01	0.73- 4.23
CaO wt%	0.33- 1.63	0.57- 1.76	0.27- 2.49	0.59- 1.51
Cr ₂ O ₃ wt%	0.27- 1.68	0.18- 0.71	0.08- 1.50	0.45- 1.88
TiO ₂ wt%	<.01- .35	0.13- 0.40	0.01- 0.36	0.12- 0.37

(iii) Garnet. Yellow, orange, red and mauve garnets (occasionally alexandritic) are present in all four specimens and show kelyphitic borders. They are never euhedral and invariably cracked. Most are <5 mm in longest dimension but a garnet in JJG 1414 is approximately 20 mm in diameter. Some garnets are disrupted. The garnets can be broadly classified into three groups: (a) chromian garnets similar to those found as inclusions in diamond and having <3 wt% CaO; (b) harzburgite-lherzolite-websterite chromian garnets with >3 wt% CaO including rare high calcium-high chromium varieties; (c) eclogitic garnets having <1 wt% Cr₂O₃. One low calcium garnet is zoned with respect to CaO, TiO₂ and Cr₂O₃ and some of the lherzolite group garnets are zoned particularly with respect to TiO₂ (from <0.01 to 1.15 wt% on some edges).

(iv) Clinopyroxene occurs in altered megacrysts and small altered clasts in JJG 513 and BD 2394 but only as small clasts in BD 2666 and JJG 1414. It is also found as inclusions in garnets, and olivines and in lherzolite or pyroxenite rock clasts. Orthopyroxene is always associated with the clinopyroxenes in the megacrysts and small clasts.

The compositions of the clinopyroxenes vary both within single clasts and between clasts. Table 3 shows maximum variations for any single clast in a particular nodule.

TABLE 3.

Rock	JJG 513	BD 2394	BD 2666	JJG 1414
Ca/Ca+Mg	41.3 -46.9	46.6 -47.5	44.0 -45.5	43.6 -45.4
Al ₂ O ₃ wt%	0.51- 2.93	0.94- 1.07	1.77- 2.11	1.64- 2.63
Cr ₂ O ₃ wt%	0.44- 2.16	0.50- 0.65	1.08- 1.23	2.46- 2.70
TiO ₂ wt%	0.17- 0.49	0.19- 0.21	0.20- 0.34	0.27- 0.44
Na ₂ O wt%	0.91- 2.35	1.36- 1.51	1.65- 2.23	2.43- 2.77

(v) Phlogopite is associated with ilmenite veins; as relatively undeformed phenocrysts; as inclusions in ilmenite blebs and also in fine grained mixtures with ilmenite and as alteration products in and around garnets in all four rocks. It also occurs along grain boundaries and around rock clasts. Phlogopite compositions vary considerably with respect to TiO₂ and Cr₂O₃.

(vi) Ilmenite occurs as either blebs (4x3 cm) or as veins (ranging up to 8 x 1.5 cm). The large compositional differences of the ilmenite veins and blebs are illustrated by the variations in chrome content. In BD 2666 Cr₂O₃ ranges from 1 to 4.4 wt% in separate veins and may vary from 2.5 to 3.5 wt% across a vein. In BD 2394 Cr₂O₃ varies from 3.9 to 7.0 wt%. Ilmenites in JJG 1414 show even larger variations in individual veins (1.2 to 7.0 wt% Cr₂O₃). Ilmenite in the orthopyroxene-clinopyroxene association occurs as tiny grains of variable composition. Cr₂O₃ content ranges from 5.3 to 7.7 wt% and in what appears to be a rutile-ilmenite mixture may be as high as 11.2 wt% Cr₂O₃.

(vii) Rutile occurs as rims to ilmenite veins and blebs; as blebs or veins; in an intimate mixture with ilmenite in BD 2394; as tiny orientated platelets in rare orthopyroxene crystals; and associated with serpentine veins and phlogopite; and in the orthopyroxene-clinopyroxene clasts. The Cr₂O₃ content of the rutile rims on ilmenite veins varies from 1.8 to 3.5 wt% with Fe₂O₃

contents of approximately 0.5 wt%. Rutilcs in the orthopyroxene-clinopyroxene associations have between 3 and 4 wt% Cr₂O₃ and 0.3 and 1.5 wt% Fe₂O₃, whereas rutilcs associated with serpentine have <3% Cr₂O₃ and <0.27 % Fe₂O₃.

(viii) Chromites have been found as inclusions in olivine, garnet, in a clinopyroxenite rock clast and in the orthopyroxene-clinopyroxene clasts. The different compositions of these chromites is given in Table 4 and a range for those in one of the orthopyroxene-clinopyroxene clasts.

TABLE 4.

		Inclusion in	In Rock	Inclusion	In opx-cpx
			clast	in Garnet	clasts
Cr ₂ O ₃	wt%	54.5	>62.	29.5	44.8-54.0
Al ₂ O ₃	wt%	10.5	<1.5	36.4	5.5-10.2
TiO ₂	wt%	<0.6	2.0	<0.1	2.51-5.85

(ix) Sulphide phases are associated with ilmenite veins and phlogopites in BD 2666 but in the other rocks are rare and appear to be confined to serpentine veins and around silicate grain boundaries. Pyrrhotite, chalcopyrite, pyrite and pentlandite have been tentatively identified.

(x) Zircon has been found in BD 2666 giving a lead uranium age of 84.5 million years (Davis, 1977).

(xi) Calcite is extremely rare in these nodules and is found in association with serpentine veins and phlogopite.

Conclusions

(a) The compositions of the silicate and metasomatic minerals indicate that they are all probably of upper mantle origin. The ranges of Mg/(Mg+Fe) for olivines and orthopyroxenes suggest that pieces of a wide variety of mantle rocks have been incorporated into these nodules.

(b) The clinopyroxene megacrysts appear to have unmixed on cooling and are considered to have been formed at depth and to have been transported to a lower pressure/temperature environment in the magmatic event mentioned under (d).

(c) The zoning of the peridotitic minerals suggests that they partially re-equilibrated at least with respect to temperature and pressure and to their TiO₂ contents prior to sampling.

(d) The presence of ilmenite and phlogopite and their compositions together with mantle rocks of diverse origin suggests that the event in which the rock formed was a magmatic event crystallizing ilmenite, phlogopite and sulphides and that it was a precursor to the event which finally transported the nodule to surface.

(e) These nodules possibly represent the remnant decarbonated conduit filling related to a kimberlitic event in the upper mantle.

Harte, B. (1977) Rock nomenclature with particular relation to deformation and recrystallization textures in olivine-bearing xenoliths. J. Geol. (in press).

MANTLE XENOLITHS FROM SOUTHEASTERN NEW ENGLAND

B.D. LEAVY (Department of Geology, University of Rhode Island, Kingston, Rhode Island, 02881).

O.D. HERMES (Department of Geology, University of Rhode Island, Kingston, Rhode Island, 02881).

We have identified a suite of ultramafic nodules that are enclosed in mafic dikes that intrude granites near Westerly, Rhode Island. Xenoliths include lherzolites, harzburgites, and wehrlites, all of which are rock types that are believed to represent accidental samples of the upper mantle. In addition, there are megacrysts of olivine, pyroxenes, and several types of presumed crustal fragments. To our knowledge, this is the first documented occurrence of such rocks in southeastern New England.

The dikes dip vertically and appear to follow a prominent regional joint trend (N25E). They cross-cut both the Narragansett Pier and Westerly Granites, both generally accepted to be of late Paleozoic Age. Xenolith abundance appears to be controlled both by dike width and by position within the dikes; they are sparse at dike margins and in constricted areas, but where dike width is greatest they may comprise up to 70 percent of the rock.

Alteration of the host dikes is common. Relict primary phases include titaniferous augite, kaersutitic amphibole, biotite, and opaque minerals (Table 1). The presence of the secondary minerals serpentine, calcite, and chlorite makes it difficult to determine the primary chemical composition. However, whole-rock and mineral compositions (Table 1) indicate affinities to alkalic basaltic rocks, lamprophyres, monchiquites, or even kimberlites. The titaniferous augite and kaersutitic amphibole present in the Westerly dikes is similar to that common to alkalic basalts or basanites (MacDonald and Katsura, 1964).

The ultramafic xenoliths enclosed in these dikes are subrounded, and up to 8 cm. in longest dimension. At least two major textural varieties are present; 1) a coarse granular type, and 2) a tectonite type. Both varieties display foliation similar to the metamorphic textures common to xenolith suites of presumed mantle origin (Pike and Schwarzman, 1977).

The granular types include spinel lherzolites and spinel harzburgites; major minerals include olivine, orthopyroxene, clinopyroxene, and a Cr-rich spinel (Table 1). Pargasitic amphibole is also present, but not common. The tectonite types are wehrlites, composed of large porphyroclasts of olivine and clinopyroxene surrounded by a fine-grained recrystallized matrix of the same minerals. Spinel grains are elongated, but appear to have resisted recrystallization. A red-stain, probably iddingsite, coats grain margins in the wehrlites.

Bulk chemistry of these nodules (Table 1) is comparable with that of mantle xenoliths worldwide, and the range of nodule types contained in the Westerly suite is likewise similar to that reported for other localities. A $MgO/\Sigma Fe = FeO$ of 5.20 is within the range (6.57 - 2.28) reported for most peridotite nodules from basalts (Kuno and Aoki, 1970); this ratio is somewhat lower than that for continental peridotites, but is comparable to nodule suites from oceanic rocks (Suwa, *et al.*, 1975).

Representative microprobe analyses of minerals from the lherzolite nodules are shown in Table 1. Mineral chemistry is similar to published data for comparable peridotite xenoliths from other regions. Compositions are relatively homogeneous from nodule to nodule, grain to grain, and

within grains, as well as between rock types. Only spinel displays significant chemical variation (Cr_2O_3 , 11-35%, Al_2O_3 , 20-35%). Based on the chemistry of coexistent pyroxenes, preliminary estimates of temperatures and pressures of final equilibration are within the range 1000-1200 °C, 15-20 kb. This places them slightly above the estimated P-T conditions for an oceanic geotherm (Mercier and Carter, 1975), and may reflect the disturbance of such a gradient by a period of epeirogenic doming following a tectonic episode, such as the Allegheny orogeny. Dikes similar to the host rocks are associated with major granitic intrusions elsewhere, such as the Appinite-Hewer Granites association of Northern Ireland and Scotland (Carmichael, et al., 1974); this sort of cogenetic relationship may exist between the Westerly dikes and the Narragansett Pier Granite.

The possible relationship of these dikes with a major tectonic episode is also suggested by the coincidence of the trend of the dikes with that of regional jointing and faulting, and that of the Mesozoic diabase dikes which are common in this part of New England. The trend of these diabase dikes has been attributed to a stress field associated with the last opening of the Atlantic Ocean (May, 1971). It is possible that such a deep-seated stress field could have mobilized upper mantle as represented by the nodule suite.

REFERENCES CITED:

- Carmichael, I.S.E., Turner, F.J., and Verhoogen, J., (1974), Igneous Petrology, Mc-Graw Hill, N.Y.
- Kuno, H. and Aoki, K., (1970), Chemistry of ultramafic nodules and their bearing on the origin of basaltic magmas: Phys. Earth. Planet. Int., v. 3, p. 273-301.
- May, P.R., (1971), Pattern of Triassic-Jurassic diabase dikes around the North Atlantic in the context of pre-drift position of the continents: Geol. Soc. Amer. Bull., v. 82, p. 1285-1292.
- MacDonald, G.A. and Katsura, T., (1964), Chemical composition of Hawaiian Lavas: Jour. Petrol., v. 5, p. 82-113.
- Mercier, T.C. and Carter, N.L., (1975), Pyroxene geotherms: Jour. Geophys. Res., v. 80, p. 3349-3362.
- Pike, J.E.N. and Schwarzman, E.C., (1977), Classification of textures in ultramafic xenoliths: Jour. Geol. v. 85, p. 49-61
- Suwa, K, Yusa, and Kishida, N., (1975), Petrology of peridotite nodules from Ndonyou Olchoro, Samburn District, Central Kenya: Phys. and Chem. Earth, v.9, p. 273-286.

TABLE 1: REPRESENTATIVE CHEMICAL ANALYSES OF ROCKS AND MINERALS FROM THE WESTERLY DIKES.

Wt. %	1	2	3	4	5	6	7	8	9	10
SiO ₂	37.99	43.45	41.11	39.30	37.94	40.49	55.64	52.44	0.00	42.07
TiO ₂	1.90	0.03	0.00	6.98	7.50	0.03	0.07	0.30	0.18	2.17
Al ₂ O ₃	4.67	1.66	0.00	11.50	13.86	0.03	3.46	5.46	47.83	12.71
Cr ₂ O ₃	0.11	0.11	0.00	0.01	0.01	0.03	0.29	0.89	20.35	7.22
Fe ₂ O ₃	5.44	1.37	*	*	*	*	*	*	*	*
FeO	8.05	6.44	7.43	8.07	10.65	8.89	5.48	2.99	11.99	3.56
MnO	0.19	0.13	0.09	0.10	0.20	0.16	0.12	0.11	0.18	0.21
MgO	28.91	42.27	50.70	9.96	12.20	50.01	34.16	15.78	18.93	18.07
CaO	5.75	1.75	0.02	23.04	12.12	0.04	0.63	20.37	0.02	11.20
Na ₂ O	1.15	0.33	0.01	0.61	2.08	0.02	0.07	1.54	0.04	3.65
K ₂ O	0.46	0.11	0.00	0.07	1.68	0.32	0.00	0.00	0.00	0.14
NiO	0.18	0.38	0.00	0.00	0.00	0.27	n.d.	n.d.	0.29	n.d.
H ₂ O+	3.69	0.39	n.d.	n.d.	n.d.	n.d.	n.d.	n.d.	n.d.	n.d.
H ₂ O-	0.52	0.05	n.d.	n.d.	n.d.	n.d.	n.d.	n.d.	n.d.	n.d.
P ₂ O ₅	0.30	0.01	n.d.	n.d.	n.d.	n.d.	n.d.	n.d.	n.d.	n.d.
CO ₂	0.57	1.36	n.d.	n.d.	n.d.	n.d.	n.d.	n.d.	n.d.	n.d.
TOTAL	99.89	99.84	99.36	99.64	98.24	100.19	99.96	99.93	99.81	96.00
ΣFe=FeO	12.06	8.13	7.43	8.07	10.65	8.39	5.48	2.99	11.99	3.56
MgO/ΣFeO	2.48	5.20	6.82	1.23	1.20	5.63	6.23	5.23	1.58	5.08

1.) Representative bulk composition of dike groundmass

2.) Representative bulk composition of ultramafic xenoliths

3.) Representative mineral microprobe analysis, groundmass olivine megacryst

4.) " " groundmass clinopyroxene

5.) " " groundmass amphibole

6.) " " nodule olivine

7.) " " nodule orthopyroxene

8.) " " nodule clinopyroxene

9.) " " nodule spinel

10.) " " nodule amphibole

*ΣFe = FeO

DIAMOND-BEARING KIMBERLITE OF PRAIRIE CREEK, MURFREESBORO,
ARKANSAS

Richard D. Lewis

Henry O.A. Meyer: Dept. of Geosciences, Purdue University
West Lafayette, Ind. 47907

Until recently the Prairie Creek kimberlite was unique in that it was the only known occurrence of diamondiferous kimberlite in North America. It is also unique in being the only kimberlite in the U.S. that has been commercially exploited for diamond. However, in spite of these two features little modern petrological and mineralogical study has been undertaken and the most significant geological report on this locality is by Miser and Ross (1923). In this report we are concerned with the mineralogy and petrology of the pipe; subsequently we intend to examine the mineral inclusions from the authenticated diamonds from this pipe.

The total surface extent of the pipe is about 73 acres and within this area three distinct lithological types of rock can be identified: breccia, tuff and peridotite. In contrast to Miser and Ross (1923) it is believed the order of intrusion is breccia, peridotite and tuff. Based on geological evidence the pipe is believed to be early Late Cretaceous in age (Glenn, 1912). In close proximity to this large diatreme are 3 smaller satellite pipes. These have not been extensively investigated other than by Gregory (1969) who examined the geochemistry of soils overlying the pipes.

The breccia is believed to be the first intrusion and based on color and lithology can be subdivided into at least three events. In chronological order these are DH breccia, BGY breccia and "breccia dikes" (Lewis, 1977; Bolivar, 1977). Most of these breccias are very friable and consist of serpentine, chlorite and mica. In the DH breccia mica, perovskite and Mg-Cr spinels are present.

The tuff is blue-grey in color and contains altered breccias, mica, detrital quartz and other sedimentary fragments. Bedding is clearly evident and it is likely this material represents sub-aerial reworking of breccias that formed the original crater rim. Diamonds are usually found in the breccias, rarely in the tuff and appear to be absent from the peridotite.

The peridotite, micaceous in nature, is the freshest rock at Prairie Creek. In some respects it resembles the hardbank of South African kimberlites. Fresh olivine phenocrysts are common, plus smaller crystals of phlogopite. Minor diopside and chromite occur. Phlogopite often poikilitically encloses perovskite, chromite and small diopside crystals. Potassic richterite is also present and in this and other respects the rock appears comparable to a hypabyssal peridotite in Best's Mine, Barkly West (Erlank, 1973).

Mineralogically the tuffs and breccias are of limited nature although as noted above these two rock types are diamondiferous. Garnets have been reported in the peridotite but during the present study have only been obtained from the breccia and tuff. Two distinct garnet suites are noted. One group is kimberlitic in character (Table 1) whereas the other is most likely crustal in origin. These latter garnets contain numerous inclusions of apatite, ilmenite and magnetite.

The peridotite appears to contain two distinct groups of diopside (Table 4) but texturally there is no evidence to indicate the chemical disparity. During the present study no mantle xenoliths have been found in the peridotite, breccia or tuff.

Although diamonds were not studied as part of this initial investigation it is worth noting that approximately 40 cts per year are found by tourists mining the pipe at leisure. Unfortunately, the original mining records are sufficiently vague that it is not possible to properly assess the total production and quality. However, in the years following the 1939-45 period one stone of 40 cts (Star of Arkansas) was found and more recently a 16 ct stone was discovered.

References

- Bolivar (1977) Ph.D. Thesis. Univ. of New Mexico.
Erlank (1973) (Abs.) Int. Kimb. Conf., Cape Town.
Glenn (1912)(Abs.) Geol. Soc. Amer. Bull., 23, 726.
Gregory (1969) Ph.D. Thesis. Imperial Coll. London.
Lewis (1977) M.S. Thesis. Purdue University.
Miser and Ross (1923) U.S. Geol. Surv. Bull, 735, 279-322.

Table 1. Representative Analyses of Minerals
(except garnet) from Hypabyssal peridotite.

	Garnet	Diopside	Diopside	Olivine	Phlogopite	Richterite	Spinel	Perovskite
SiO ₂	42.5	54.2	54.8	41.5	42.5	55.3	-	-
TiO ₂	0.09	0.47	0.13	0.01	3.30	2.44	2.40	53.7
Al ₂ O ₃	22.5	0.02	1.88	<0.01	4.96	0.29	0.48	0.04
Cr ₂ O ₃	1.80	0.16	2.34	0.15	0.10	<0.01	0.91	0.65
FeO	7.51	2.52	2.56	8.14	7.70	3.88	82.5	0.72
MgO	20.5	17.6	17.8	50.3	22.9	20.8	2.85	0.30
CaO	5.09	24.6	18.7	0.04	2.60	6.01	0.20	38.9
MnO	-	0.11	0.15	0.16	0.07	0.09	0.46	0.02
NiO	<0.01	-	-	0.38	0.10	0.02	<0.01	<0.01
Na ₂ O	<0.01	0.38	1.51	<0.01	1.16	4.47	-	0.57
K ₂ O	-	0.02	0.09	<0.01	9.51	5.14	-	-
Nb ₂ O	-	-	-	-	-	-	-	0.38
	100.1	100.1	100.0	100.7	(95.0)	(98.4)	(89.8)	(95.3)

THE MELILITE NEPHELINITE DIATREMES OF THE SWABIAN ALB/GERMANY AND THE FORMATION OF AUTOLITHS

Volker Lorenz (Institut für Geowissenschaften, Joh. Gutenberg-Universität, 6500 Mainz, FRG)

The melilite nephelinite diatremes of the Swabian Alb, well-known since Cloos's careful analysis (1941), have frequently been compared with kimberlite diatremes and vice versa. Recent studies allow a new interpretation in respect to the cause of their formation and a phreatomagmatic origin is suggested. Consequently the formation of autoliths, typically developed in the Swabian diatremes, is discussed from this point of view.

The 350 diatreme structures of the Swabian Alb formed in Upper Miocene time soon after the sea had covered the southern half of the Swabian Alb and deposited the Upper Marine Molasse. Retreat of the sea was followed by the deposition of the Upper Freshwater Molasse during which most of the diatremes were emplaced immediately north a few also south of the previous coastline. Strong uplift and erosion affected the Swabian Alb only in Pliocene/Pleistocene time and, therefore, the landsurface of the diatreme area was near the sea-level.

The diatremes as such extend downwards for about 1.5 km to the boundary between the basement and its sedimentary cover. The latter consists of Permian clastic rocks including coarse grained conglomerates and rather undeformed Triassic and Jurassic clastic and carbonate rocks. The well-jointed Upper Jurassic limestones display karst phenomena initiated at least in Eocene time.

Judging from the internal structure and fresh-water lake deposits in the upper parts of the larger diatremes the diatremes must have ended at the original surface in maars which were cut into the Upper Jurassic limestones. Evidence of subsidence of the floors of the fresh-water lakes as for instance slump structures and large blocks of Upper Jurassic limestone embedded in the lake deposits points to accumulation of groundwater within these maars immediately after the diatremes stopped erupting. The slightly younger Ries and Steinheim meteorite impact craters east of the diatremes also show evidence of deep fresh-water lakes.

In all probability these data suggest the existance of copious amounts of groundwater and a rather free groundwater table within the sedimentary cover of the basement near the original landsurface during the time of diatreme emplacement. It seems for the respective magma to have been rather inevitable to contact groundwater during its rise through the sedimentary cover of the dense basement and consequently to get involved in phreatomagmatic eruption processes. Internal structures of the diatremes are very similar in a number of

aspects to those from other diatremes for which a phreatomagmatic origin has already been suggested (Lorenz 1973, 1974).

Within some 20 diatremes melilite nephelinite magma was able to rise at the end of the eruptive activity towards high levels, in a few cases up to levels of only several tens of meters below the original surface or possibly even less. As the original land surface has been lowered by erosion no original surface deposits of the diatremes are preserved and, therefore, it cannot be judged if the magma of the respective intrusive rocks had actually reached the surface and formed cinder cones and lava flows. The high level intrusive rocks, however, are not highly vesicular at their chilled margins which points out that the previously dissolved gasphase had neither very much nor very rapidly exsolved at the time of intrusion. It may not have been very high amounts of gas dissolved in the magma at all.

The juvenile fraction of the pyroclastic rocks of the Swabian diatremes occurs mostly as spherical ash grains or lapilli, i.e. autoliths. Larger juvenile particles are mostly angular. Typically both the small and large juvenile particles contain hardly any vesicles despite the fact that they represent chilled magma droplets. The core of the spherical autoliths consists either of a phenocryst or of a xenolith derived from the Mesozoic sediments. As formation of the spherical particles points to spraying of a liquid into a free space and action of surface tension formation of these autoliths must have taken place within the diatremes themselves, i.e. above their respective feeder dikes.

Up to now autoliths have been assumed to be the result of rapid fragmentation of the magma owing to explosive exsolution of the contained very large amounts of gases. On the other hand a number of features point to rapid chilling of the pyroclastic rocks as well which is widely accepted. This poses the question of how rapid exsolution of the gasphase, consequent disintegration of the magma into droplets, and rapid chilling can take place near-simultaneously without the particles showing any evidence of such an exsolution of the gasphase. At the surface such a process leads to formation of cinders or pumice with the vesicles largely preserved owing to chilling by air. As the Swabian diatremes are suggested to have been of phreatomagmatic origin, the autoliths representing the major part of the juvenile fraction of these diatremes should be of phreatomagmatic origin as well. Most phreatomagmatic eruptions, however, give rise to production of angular fragments their vesicle content indicating the state of vesiculation at the time of magma/water contact. The vesicle content may thus vary between nearly nil and values found in pumice depending on the depth at which the contact takes place. In diatremes of appreciable depth, e.g. the Saar-Nahe diatremes/SW Germany the vesicle content and size is in fact small and negligible. Judging from the literature autoliths are only found in diatremes from SiO₂ undersaturated basic to ultrabasic magmas. This suggests influence of the

chemistry and thus of the viscosity and surface tension on their formation. Experiments on water vapour explosions owing to metallic liquids getting into contact with water show that production of droplets can take place when the liquid metal is sprayed into an open space as a result of the explosion (Fröhlich pers. communication 1977). It is therefore suggested that the autoliths of the Swabian diatremes formed when the respective magma, the most SiO₂ undersaturated of central Europe (35% SiO₂), contacted copious amounts of groundwater available in the sedimentary cover of the basement. During the consequent water vapour explosions the magma disintegrated into fragments which were sprayed into the space surrounding the explosion foci. The surface tension of the liquid enabled formation of droplets even around xenoliths derived from the wall-rocks. The cool temperatures of the water vapour and the remaining water caused rapid chilling and thus preservation of the autoliths in their original shape. The assumption of water vapour explosions as a result of magma/water contact would explain the lack of vesicles in the juvenile fraction of the pyroclastic rocks as at the depth of contact the juvenile gasphase need not have exsolved yet to any great extent.

At some cinder cones in the West Eifel/Germany it can be shown that external water intermittantly got into contact with the rising magma. This caused phreatomagmatic eruptions and typical phreatomagmatic eruptionproducts including cauliflower bombs and autoliths.

References:

- Cloos, H.(1941) Geol.Rundschau 32, 705-800.
Lorenz, V.(1973) Bull.Volcanologique 37, 183-204.
Lorenz, V.(1975) Physics and Chemistry of the Earth 9, 17-27.

MAFIC AND ULTRAMAFIC XENOLITHS FROM THE KAO KIMBERLITE PIPE, LESOTHO

Ian D. MacGregor (Dept. of Geology, University of California, Davis, Ca., 95616)

Mantle xenoliths from the Kao kimberlite pipe include both spinel and garnet harzburgites and lherzolites, eclogites and a suite of discrete nodules which resemble the phase assemblages characteristic of xenoliths from many other South African kimberlite pipes (Rolfe, 1973; Nixon and Boyd, 1973; Boyd and Nixon, 1975; MacGregor, 1975). Similarly, the range of textures observed in the ultramafic xenoliths are comparable to those described by Boullier and Nicolas (1975).

Estimates of the temperatures and pressures of equilibration of the ultramafic xenoliths using the experimentally defined diopside-enstatite solvus (Mori and Green, 1976), and the Al_2O_3 solubility in enstatite (MacGregor, 1974) yield the following. The coarse grained granular, tabular and porphyroclastic textured samples form a roughly linear array of data points that is comparable to estimates of shield geothermal gradients and similar to gradients derived for other Lesotho xenolith suites. In general the granular textured samples are more deformed with increasing temperature and pressure. The most highly deformed, or mosaic textured, xenoliths have equilibrated at the highest temperatures ($>1200^\circ C$) but do not form part of the linear array illustrated by the less deformed suite. Rather they form a separate population that cluster over a range of pressures (53 Kb to 80 Kb) in the temperature range from $1200^\circ C$ to $1450^\circ C$. Discrete pyroxene xenoliths indicate minimum equilibration temperatures of $1400^\circ C$, and although no pressure estimates are available they are presumed to be comparable to that for the mosaic textured suite. The partition of Mg and Fe between coexisting clinopyroxene and garnet in eclogites suggest equilibration over a wide range of temperatures and pressures (Räheim and Green, 1974).

The mineral chemistry of the highly sheared, mosaic textured suite is distinctly different from the granular textured samples. The minerals from the mosaic textured xenoliths have lower Mg/Mg+Fe ratios and the pyroxenes and garnets have higher TiO_2 , Na_2O and Al_2O_3 , and lower Cr_2O_3 contents. Similarly the orthopyroxenes have higher and the clinopyroxene lower CaO contents reflecting their higher temperatures of equilibration. Comparable to other studies (Boyd and Nixon, 1975; MacGregor, 1975) the mosaic textured suite appears to be enriched in those components normally concentrated in basaltic liquids during partial melting of ultramafic compositions.

Mantle xenoliths from the Kao kimberlite pipe are very similar to other suites from northern Lesotho kimberlites. Of prime importance to further interpretive analysis is the observation that regionally two main populations of xenoliths are found. The first composed of essentially underformed samples, whose chemistry indicates that they are refractory residues after, at least, one period of partial melting and which have equilibrated to the conditions defined by the ambient geothermal gradient. These xenoliths are truly 'accidental' and have a passive role with respect to the origin of kimberlites. The second population of xenoliths are highly deformed and may well have been in the process of deformation at the time of eruption (Kohlstedt and Goetze, 1974). Their chemistry indicates that they represent a portion of

the mantle richer in the fusible components and hence are more 'primitive'. They have formed at higher temperatures and pressures and are associated with an 'inflection' or 'perturbation' of the anticipated geothermal gradient. The sheared xenoliths appear to be dynamically associated with kimberlite formation.

References:

- BOULLIER, A. M., and NICOLAS, A., 1975, Classification of textures and fabrics of peridotite xenoliths from South African kimberlites; Phys. Chem. Earth, v. 9, p. 467-476.
- BOYD, F. R., and NIXON, P. H., 1975, Origins of ultramafic nodules from some kimberlites of northern Lesotho and the Monastery Mine, South Africa; Phys. Chem. Earth, v. 9, p. 431-454.
- KOHLSTEDT, D. L., and GOETZE, C., 1974, Low-stress high temperature creep in olivine single crystals; Jour. Geophys. Res., v. 79, p. 2045-2057.
- MACGREGOR, I. D., 1974, The system $MgO-Al_2O_3-SiO_2$: Solubility of Al_2O_3 in enstatite for spinel and garnet peridotite compositions; Amer. Mineral. v. 59, p. 110-119.
- MACGREGOR, I. D., 1975, Petrologic and thermal structure of the upper mantle beneath South Africa in the Cretaceous; Phys. Chem. Earth, v. 9, p. 455-466.
- NIXON, P. H. and BOYD, F. R., 1973, Deep seated nodules; in 'Lesotho Kimberlites', ed. P. H. Nixon, p. 106-110.
- MORI, T., and GREEN, D. H., 1976, Subsolvus equilibria between pyroxenes in the $CaO-MgO-SiO_2$ system at high pressures and temperatures; Amer. Mineral., v. 61, p. 616-625.
- RÄHEIM, A., and GREEN, D. H., 1974, Experimental determination of the temperature and pressure dependence of the Fe-Mg partitioning coefficient for coexisting garnet and clinopyroxene, Contrib. Mineral. Petrol., v. 48, p. 179-203.
- ROLFE, D. G., 1973, The geology of the Kao kimberlite pipes; in 'Lesotho Kimberlites' ed. P. H. Nixon, p. 101-106.

EVALUATION OF P-T CONDITIONS OF DIAMOND FORMATION WITH REFERENCE TO CHROME-BEARING GARNET STABILITY

I.Yu.Malinovsky, A.M.Doroshev (Institute of Geology and Geophysics, Siberian Branch of the USSR Academy of Sciences, Novosibirsk, U.S.S.R.)

Among minerals included in diamond crystals chrome-bearing garnets are of special interest (Nixon et al., 1963, Sobolev, Sobolev, 1967, Meyer, Boyd, 1972, Sobolev, 1974, Sobolev et al. 1976) The experimental studies of the system: pyrope (Py)-grossularite (Gros)-knorringite (Kn)-uvarovite (Uv) at $T=1200^{\circ}\text{C}$, $P=30$ kbar (Malinovsky et al., 1974) showed that the stability field of garnets is confined to the region of Py-Gros-Uv (Fig.1). The effect of $T=1000-1500^{\circ}\text{C}$ and $P=25-50$ kbar on chrome-garnet stability has been studied at the Py-Kn section (Malinovsky et al. 1975). When $T=1200^{\circ}\text{C}$ the limiting Kn-component contents in garnets gradually increases from 3-4 mol % at $P=25$ kbar to 23-25 mol % at $P=50$ kbar. With rising temperature the solubility of Kn-component increases by 1-2 mol % for each 100°C . According to the preliminary experimental data obtained in the cubic apparatus (Ran, Malinovsky, 1975) the limiting Kn-component contents in the garnets increases to 70-72 mol % at $P=100$ kbar and $T=1300-1400^{\circ}\text{C}$ ($a_0=11.5602(6)\text{\AA}$, $N=1.800(5)$, violet colour), while enstatite and Cr_2O_3 are formed instead of pure knorringite. Coesite and stishovite are present in the products of pyrophyllite decomposition enclosing the heating device from outside. At $T=1000-1200^{\circ}\text{C}$ knorringite has not formed even at $P>150-160$ kbar, which was controlled by the calibration point of ZnS (Yagi, Akimoto, 1976). However, it is not unprobable that the stability field of knorringite is situated in higher-temperature regions.

The stability of chrome-garnets contained in peridotite parageneses has been studied on harzburgite assemblage as an example $\text{Ga}_{\text{ss}} + \text{En}_{\text{ss}} + \text{Spl}_{\text{ss}} + \text{Fo}$ in the system: $\text{MgO}-\text{Al}_2\text{O}_3-\text{Cr}_2\text{O}_3 - \text{SiO}_2$ (Malinovsky, Doroshev, 1975). The Kn-component contents in garnets from this assemblage is by 1-2 mol % below compared to

the limiting garnets at equal T and P. The Cr-component of spinels increases with rising P but unlike in garnets it decreases with falling T (Fig. 2).

The experimental data provide a possibility to evaluate the P-T conditions of the diamond formation by composition of garnets and spinels included in diamond crystals. The Kn-component content in those garnets is usually within 15-50 mol % (Sobolev, 1974, Sobolev et al., 1976). The harzburgite assemblage with garnet $Py_{85}Kn_{15}$ together with diamond becomes stable beginning with 45 kbar (Fig. 2). The admixtures of additional components up to 15-20% does not seem to affect significantly the stability of chrome-garnets. Therefore it may be concluded that the lower pressure limits of natural diamond crystallization do not usually drop lower than 45 kbar. The pressure above 75-80 kbar is required for Kn-richest garnets (40-50 mol %) to form at $T=1200-1300^{\circ}C$. Thus the diamonds are formed in a very wide range of pressures $\Delta P=30-40$ kbar. The spinels included in diamonds contain usually 80-90 mol % of Cr-component, which according to the plot of Fig. 2 corresponds to $T=900-1100^{\circ}C$ at $P=40-80$ kbar. These estimates, however, do not take into account the possible effect of Fe-component, whose contents in natural spinels sometimes attain 30-50 mol %.

REFERENCES

1. Malinovsky I.Yu., Doroshev A.M., Godovikov A.A. Experimental studies in mineralogy (1972-1973), Novosibirsk 73 (1974).
2. Malinovsky I.Yu., Doroshev A.M., Ran E.N. Experimental studies in mineralogy (1974-1975); Novosibirsk 110 (1975).
3. Malinovsky I.Yu., Doroshev A.M. Experimental studies in mineralogy (1974-1975), Novosibirsk 121 (1975).
4. Meyer H.O.A., Boyd F.R. Geochim.Cosmochim. Acta, 36, 1255 (1972).
5. Nixon P.H., Knorring O., von Rooke J.M. Amer.Mineral., 48, 1090 (1963).
6. Ran E.N., Malinovsky I.Yu. Experimental studies in mineralogy (1974-1975); Novosibirsk 149 (1975).
7. Sobolev N.V. Deep-seated inclusions in kimberlites and the problem of the composition of the Upper Mantle, Novosibirsk, Nauka Press; 1974.
8. Sobolev V.S., Sobolev N.V. Geology of Ore Deposits, N2, 10 (1967).
9. Sobolev N.V. Botkunov A.I., Lavrent'ev Yu.G., Usova L.V. Geologia i geofiz. N12, 3 (1976).
10. Yagi T., Akimoto S.I. J.Appl. Phys. 47, 3350 (1976).

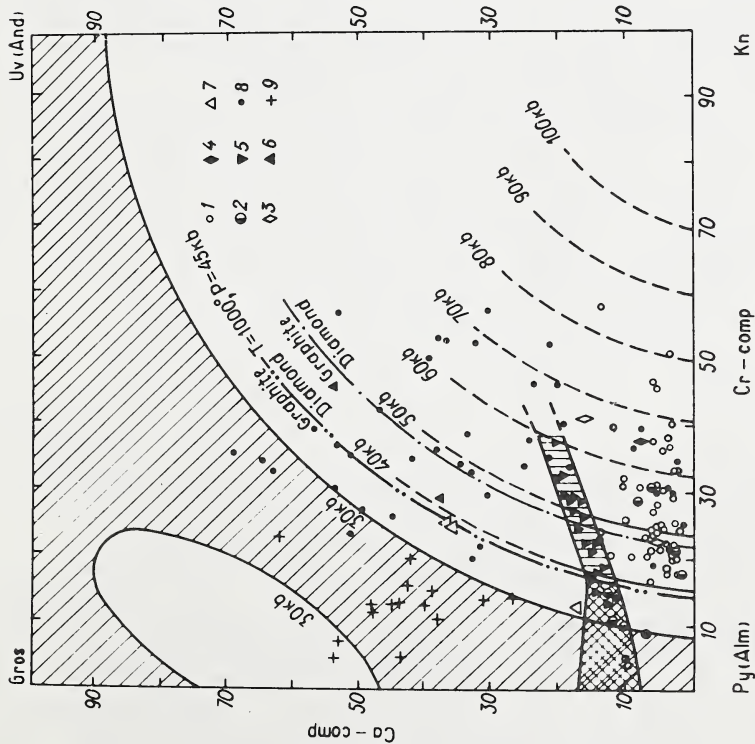


Fig. 2. Effect of P and T on garnet and spinel compositions from harzburgite assemblage $Ga_{55} + En + Spl_{55} + Fo$ of the systems $MgO-Al_2O_3-Cr_2O_3-SiO_2$. The numerator stands for khorringite contents in garnets, the denominator stands for chrome content in spinel.

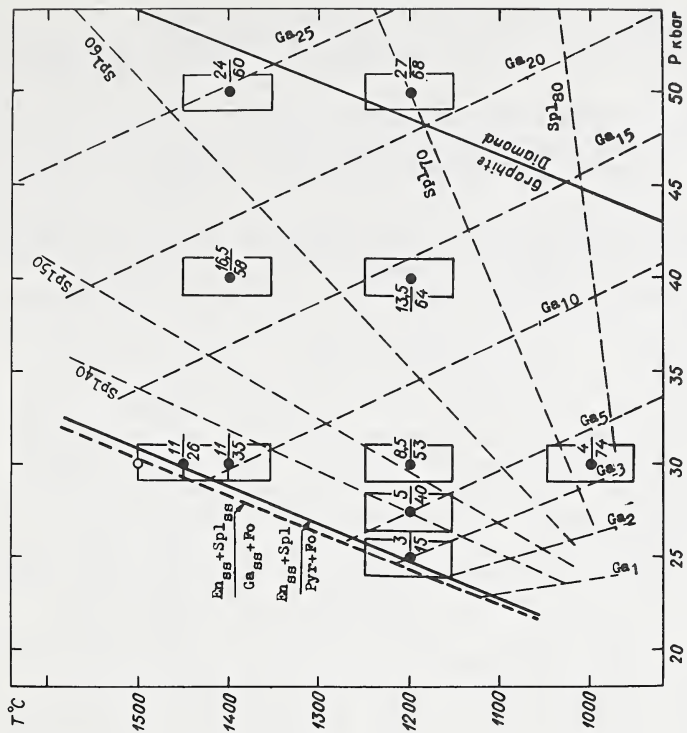


Fig. 1. Compositions of chrome-bearing garnets from the kimberlitic pipes (after Sobolev, 1974, 1976) and isobar position in the system: pyrope-grossularite-khorringite-uvarovite at $T=1200^{\circ}C$. Garnets from: 1, 7- diamonds; 2, 3- intergrowths with diamonds; 4, 5, 6- peridotites; 8- kimberlitic concentrate, 9- grosspydrites and kyanitic eclogites.

THERMAL HISTORY AND EXOLUTION MICROSTRUCTURES OF TWO
CLINOPYROXENES FROM THE THABA PUTSOA KIMBERLITE PIPE, LESOTHO

Robert H. McCallister: Department of Geosciences
Henry O.A. Meyer: Purdue University
Ricardo Aragon: West Lafayette, Indiana 47907

Two specimens of clinopyroxene from sheared and discrete lherzolites from the Thaba Putsoa Kimberlite pipe, Lesotho, have been examined by means of transmission electron microscopy. (Both were collected by P.H. Nixon and analyzed by F.R. Boyd, who kindly provided them.) The clinopyroxene in the sheared lherzolite (PHN 1611) has a Ca/Ca+Mg of 0.315, whereas the ratio is equal to 0.320 in the discrete lherzolite (PHN 1600E4). Crushed grain mounts of each sample were prepared and observed on a Siemens Elmiskop I, operating at 100kV. For each bright field image that contained lamellae, a corresponding diffraction pattern was taken in order to correct the apparent lamellae thicknesses, and calibration of the magnification was done by imaging and photographing a carbon replica of a waffle grating with spacing equal to $0.50 \pm 0.01 \mu$. In both specimens the lamellae appear to be parallel to (001) with the "exsolved" phase being pigeonite. The average of at least 4 measurements yields values of lamellae thicknesses of $187 \pm 8 \text{ \AA}$ for PHN 1600E4 and $192 \pm 12 \text{ \AA}$ for PHN 1611. The appearance of reflections corresponding to pigeonite in both x-ray single-crystal and electron diffraction photographs is evidence for exsolution. However, the scale of the exsolution microstructures or wavelength indicates that the process occurred rapidly.

From the recent experimental results of McCallister and Yund (in press) on exsolution mechanisms and microstructures in iron-free pyroxenes, it is possible to delineate the (001) coherent spinodal for diopside solid solutions with Ca/Ca+Mg > 0.27. For a Ca/Ca+Mg = 0.317 the (001) coherent spinodal is at 1275°C (see Fig. 1). Above this temperature, although well within the solvus, no exsolution occurred in the experimental runs; below 1275°C , exsolution occurred by spinodal decomposition with a resulting exsolution microstructure remarkably similar to that observed in the natural clinopyroxenes. In an attempt to arrive at a thermal history of the latter specimens, a continuous cooling experiment was made on a synthetic diopside solid solution (Ca/Ca+Mg = 0.317) with a rate of cooling equivalent to 40°C/hr over the temperature range of 1275°C to 1000°C . It is obvious from a recent study by McCallister (in press) that the rate constants associated with the coarsening of a fine-scale exsolution microstructure below 1000°C are sufficiently small, such as to contribute little to the final microstructure. The wavelength of the 40°C/hr experiment is $181 \pm 15 \text{ \AA}$, which is to be compared with the average of the two natural clinopyroxenes: $190 \pm 10 \text{ \AA}$. While the similarity in wavelength is apparent, the amplitude of the fluctuations or composition difference as reflected in the respective electron diffrac-

tion patterns appears greater for the natural samples, which indicates either a slightly slower cooling rate and/or a difference in kinetics associated with the presences of small amounts of ferrosilite and jadeite molecules in the natural clinopyroxenes. The former of these is currently being investigated; however, assuming that the 40°C/hr run does reflect a value close to the true rate, the samples cooled from 1275°C-1000°C and the microstructure was developed in excess of 7 hours.

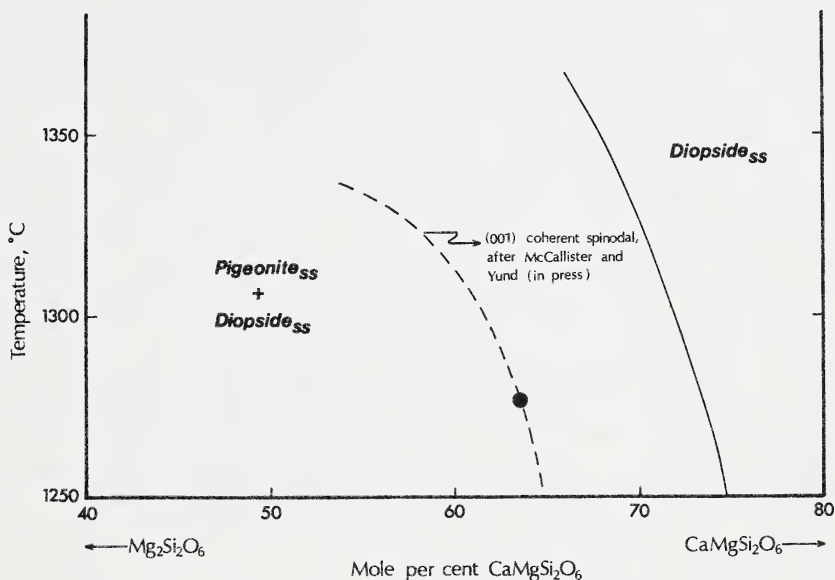


Figure 1. The diopside solid solution solvus on the $\text{CaMgSi}_2\text{O}_6$ - $\text{Mg}_2\text{Si}_2\text{O}_6$ join above 1250°C (Kushiro, 1972). The solid dot: on the coherent spinodal at 1275°C represents the point at which spinodal decomposition is initiated for a clinopyroxene of relatively low ferrosilite content and a $\text{Ca}/(\text{Ca}+\text{Mg})$ of 0.317.

References

- Kushiro, I, 1972. Determination of the liquidus relations in synthetic silicate systems with electron probe analysis. The system forsterite-diopside-silica at 1 atmosphere. Am. Mineral., 57, 1260-1271.
- McCallister, R.H., in press. The kinetics of exsolution microstructure coarsening in a Mg-rich diopside. Contrib. Mineral. Petrol.
- McCallister, R.H. and Yund, R.A., in press. Coherent exsolution in iron-free clinopyroxenes. Am. Mineral.

DISCRETE NODULE ASSEMBLAGES IN KIMBERLITE FROM NORTHERN COLORADO AND SOUTHERN WYOMING

M. E. McCallum (Colorado State University, Fort Collins, Colorado 80523)*
D. H. Egger (Geophysical Laboratory, 2801 Upton St., N. W., Washington, D. C. 20008)
C. B. Smith (Colorado State University, Fort Collins, Colorado 80523)

Two compositionally distinct groups of discrete nodule megacrysts (more than 1 cm in diameter) occur in kimberlite of the Colorado-Wyoming State Line and Iron Mountain districts. The megacrysts are characterized by Cr-rich and Cr-poor assemblages and include garnet, clinopyroxene, orthopyroxene, olivine (rare), ilmenite and clinopyroxene-ilmenite intergrowths. The latter three types are essentially restricted to the Cr-poor group. Most Cr-rich nodules have relatively high Mg/Mg + Fe and CaO and are quite similar chemically to comparable minerals from peridotite nodules (Fig. 1). Some of the Cr-rich megacrysts could be peridotite disaggregation products; however, their coarse grain size is atypical of the peridotite fabric. The Cr-poor megacrysts differ from the Cr-rich discrete nodules in their relatively more subcalcic nature, higher TiO₂, and higher, more variable contents of iron, along with lower Cr₂O₃ (Fig. 2). Many megacrysts of both groups contain mineral inclusions of one or more members of that group. The megacryst assemblages are characterized by distinctive color variations between Cr-rich and Cr-poor members. Most Cr-rich garnet megacrysts (more than 6 percent Cr₂O₃) are lavender to deep purple whereas Cr-poor garnets (less than 4 percent Cr₂O₃) are typically reddish brown. Cr-rich vs. Cr-poor clinopyroxene (more than 1 percent vs. less than 1 percent Cr₂O₃) are emerald green and bluish gray to gray green respectively. Cr-rich orthopyroxene megacrysts (more than .4 percent Cr₂O₃) are bright to pale green; Cr-poor varieties (less than .3 percent Cr₂O₃) are gray green to gray brown.

Cr-poor megacrysts are quite similar to discrete nodules described by Nixon and Boyd (1973) and Boyd and Nixon (1975) from Lesotho and the Monastery Mine, South Africa (Fig. 1). However, the Colorado-Wyoming samples are more enriched in Cr₂O₃, have slightly higher Mg/Mg + Fe, and no high temperature (greater than 1300°C) orthopyroxene megacrysts have been found. Cr-rich megacrysts are not reported from the Lesotho and Monastery kimberlites.

Megacrysts from the Iron Mountain, Wyoming kimberlite district are almost exclusively of the Cr-poor assemblage, and show a prominent enrichment in iron relative to State Line district nodules. Chemical trends in ilmenite are especially pronounced. In addition to significantly higher average iron contents, a MgO vs. Cr₂O₃ plot (Fig. 3) shows a parabolic relationship similar to that reported by Haggarty (1975) for African ilmenites; most of the Iron Mountain samples fall on the bottom and left side (low MgO side) of the parabola. Chemical variations also occur in ilmenite from kimberlite within the State Line district. Megacrysts from the Schaffer, Ferris and Moen pipes are more enriched in iron than those from the Sloan and Nix pipes, but they do not show the degree of enrichment or extreme variation of iron as in the Iron Mountain ilmenite megacrysts. Similar chemical trends occur in garnet and clinopyroxene megacrysts. Clinopyroxene-ilmenite intergrowths are found primarily at Iron Mountain and contain the most magnesian ilmenite and Fe-rich clinopyroxene in that district. However, Mg concentrations in intergrowth ilmenites are appreciably lower than those in most State Line ilmenite megacrysts (Fig. 3).

Rare earth element concentrations determined for representative Cr-rich and Cr-poor diopside and garnet megacrysts suggest small but distinct

differences in abundance and chondrite normalized fractionation patterns between the two groups. Cr-rich garnet and diopside are slightly enriched in the light and intermediate REE (La to Gd) and depleted in the heavy REE (Dy to Yb) relative to Cr-poor minerals. The patterns are strikingly similar to those of garnet and clinopyroxene mineral separates from Lesotho granular and sheared garnet lherzolite (Shimizu, 1974). REE fractionation patterns and abundances of the Cr-rich megacrysts correspond closely to granular (depleted) lherzolite minerals, whereas the Cr-poor megacrysts are more similar to the sheared lherzolite minerals studied by Shimizu (1974).

Pressure and temperature equilibration data for orthopyroxene megacrysts indicate depths of approximately 150–200 km and temperatures of 1110^o–1300^oC. Clinopyroxene megacrysts have a range of equilibration temperatures of approximately 1050^o–1350^oC; Cr-rich diopsides range to 1210^oC, whereas Cr-poor diopsides exceed 1210^oC. All diopsides may be considered to have been derived from depths of less than 200 km if pressure values for the higher temperature nodules are calculated from the inflected or disturbed portion of the geotherm established from State Line megacrysts (Eggler and McCallum, 1976). Equilibration temperatures for clinopyroxene-ilmenite intergrowths are confined to the narrow range of approximately 1220^o–1240^oC as determined from the diopside solvus after Davis and Boyd (1966), and would correspond to depths of about 170–175 km if pressures are determined from the inflected geotherm. Similar depth figures were established previously utilizing the uninflected geotherm and assuming that the intergrowths crystallized in equilibrium with ilmenite bearing orthopyroxene megacrysts at 1150^o–1160^oC (Smith et. al., 1976).

Chemical and physical properties suggest that both Cr-poor and Cr-rich suites crystallized in the presence of a liquid. Compositional trends of Cr-poor megacrysts, in particular ilmenite and garnet, are interpreted to reflect liquid fractionation trends. Most silicate phases crystallized before ilmenite; the clinopyroxene-ilmenite intergrowths represent a transition from silicate to oxide crystallization. Recent experimental work by Wyatt (1977) in which clinopyroxene-ilmenite intergrowths were formed at 38 kb pressure, strongly supports the contention that the megacryst suites crystallized in the presence of a melt. The liquid in which megacrysts crystallized may have been a primitive kimberlitic partial melt generated by the intrusion of mantle diapirs.

References

- Boyd, F. R., and Nixon, P. H., 1975, *Phys. Chem. Earth*, 9, p. 431–454.
Davis, B. T. C., and Boyd, F. R., 1966, *J. Geophys. Res.*, 71, p. 3567–3576.
Eggler, D. H., and McCallum, M. E., 1976, *Carn. Inst. Wash. Year Book* 75, p. 538–541.
Haggarty, S. E., 1975, *Phys. Chem. Earth*, 9, p.295–308.
Nixon, P. H., and Boyd, F. R., 1973, in Lesotho Kimberlites, P. H. Nixon, ed., Lesotho Natl. Development Corp., Maseru, Lesotho, p. 67–75.
Shimizu, N., 1974, *Carn. Inst. Wash. Year Book* 73, p. 954–961.
Smith, C. B., McCallum, M. E., and Eggler, D. H., 1976, *Carn. Inst. Wash. Year Book* 75, p. 542–544.
Wyatt, B. A., 1977, Contrib. Mineral. Petrol., 61, p. 1–9.

*Also with U. S. Geological Survey, Denver, Colorado

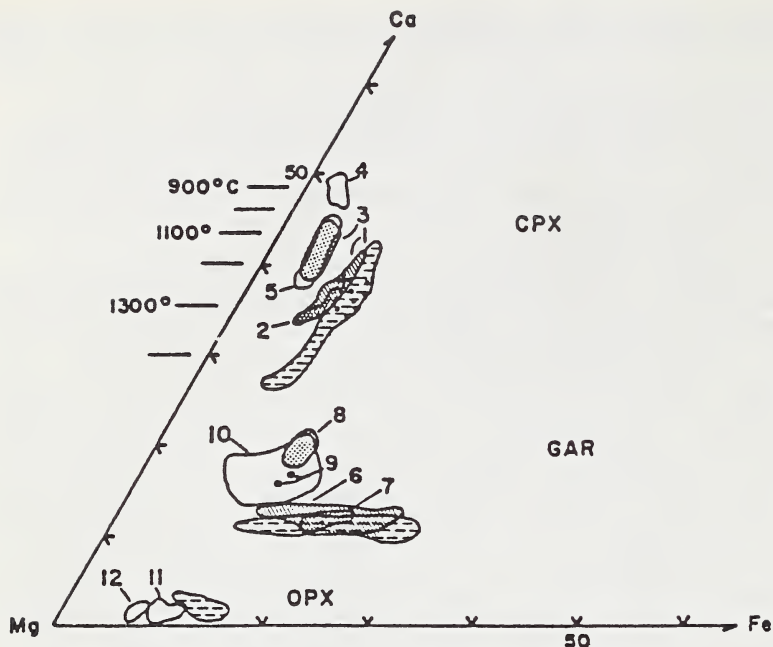


Figure 1. Compositions of megacryst minerals

1) Iron Mountain Cr-poor diops. 2) State line Cr-poor diops.
 3) State Line Cr-rich diops. 4) depleted spinel peridotite diops.
 5) depleted garnet peridotite diops. 6) Iron Mountain Cr-poor gar.
 7) State Line Cr-poor gar. 8) State Line Cr-rich gar.
 9) Iron Mountain Cr-rich gar. 10) depleted peridotite gar.
 11) State Line Cr-poor enstatite 12) State Line Cr-rich enstatite
 Fields with horizontal dashed lines define compositional ranges of megacrysts from South Africa and Lesotho. Cpx-ilmenite intergrowth diopsides are shown as cross (Iron Mountain) and points (South Africa). Cr-rich cpx and opx megacrysts have not been found at Iron Mountain.

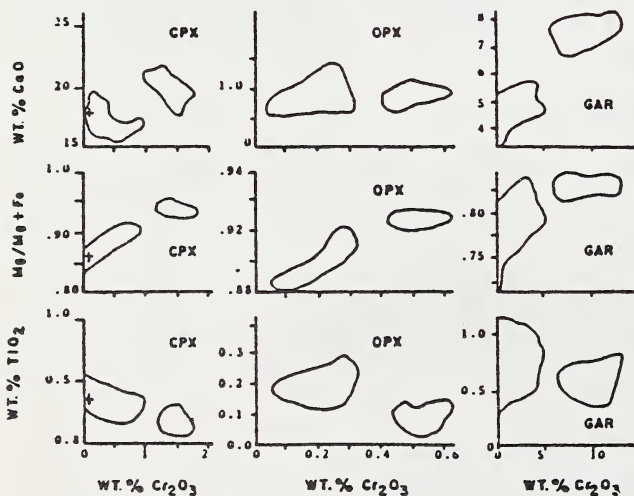


Figure 2. Compositional fields of Cr-rich and Cr-poor megacrysts. cross = cpx from cpx-ilm intergrowth.

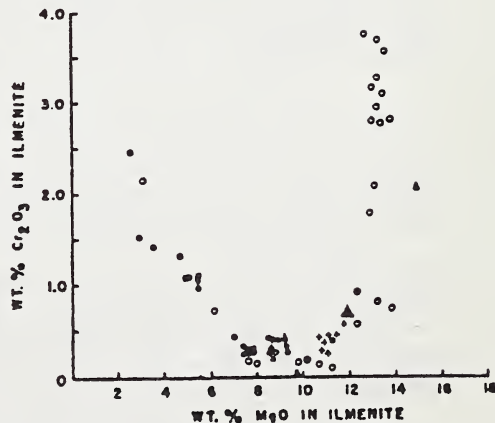


Figure 3. Ilmenite megacryst compositions. solid points = Iron Mountain; open points = State Line; crosses = cpx-ilm intergrowths; triangles = peridotite ilmenite.

DIAMONDS FROM KIMBERLITE IN THE COLORADO-WYOMING STATE LINE DISTRICT

M. E. McCallum, C. D. Mabarak, and H. G. Coopersmith (Colorado State University, Fort Collins, Colorado 80523)

Seventy-eight diamonds recovered from weathered kimberlite from diametres in the Colorado-Wyoming State Line district are described in terms of size, weight, morphology, color, fluorescence and inclusions. The diamonds range from approximately 0.2 mm to 2.0 mm in average diameter and less than 0.5 mg to 11.8 mg in weight (McCallum and Mabarak, 1976a and b). The stones are subdivided into two groups: 1) "microdiamonds", those greater than approximately 1 mm and 1 mg (24), and 2) "minimicrodiamonds", those less than 1 mm and 1 mg (54) (Table 1). The total weight of the 78 diamonds is about 84 mg or approximately 0.42 carat. "Microdiamonds" comprise nearly 64 mg (0.32 carat) of the total whereas "minimicrodiamonds" account for the remaining 20 mg (0.10 carat) (Table 2, Fig. 1).

Morphological descriptions are based on the six-fold classification of Whitelock (1973) that categorizes diamonds as octahedra, rhombic dodecahedra, flattened dodecahedra, macles, aggregates and irregular shapes (formless and fragments), plus a seventh category of rounded crystals transitional between octahedra and dodecahedra. Aggregate types and octahedra predominate (27 and 18 respectively - Table 1, Fig. 2); most aggregates are comprised of octahedral forms and complex interpenetrations of octahedra. There is a progression between planar, laminated and distorted octahedra through rounded transitional octahedral-dodecahedral forms to rhombic dodecahedra to flattened dodecahedra. Octahedra are more abundant in the "minimicrodiamond" fraction and octahedra/dodecahedra ratios show a general decrease with size ("minimicrodiamond": $O/D = 6.0$, $O/D^+ = 1.09$; "microdiamond": $O/D = 1.2$, $O/D^+ = 0.67$) (Table 1, Fig. 2). Five flats (flattened dodecahedra) were found and three of these are in the larger size category; seven of the eight macles recovered fall into the smaller size category.

Many octahedral forms show a well developed lamellar buildup and presence of abundant triangular growth platelets and terraces on 111 surfaces. Triangular shaped, pyramidal or flat bottomed depressions (trigons) commonly occur on octahedral surfaces, and both regular and irregular shaped etch pits have been observed on many surfaces.

The diamonds are predominantly colorless to glassy although a few range from white to grayish white to pale brown, pale orange or pale yellow, and a few inclusion-rich crystals are nearly black (Table 3). The largest proportion of colorless crystals are in the macle and octahedral groups, along with aggregates that predominate in octahedral forms. Colored stones show a moderately even distribution among crystal types except for macles that are characteristically uncolored. Pale yellow coloration is restricted to stones having octahedral forms (chiefly in the transitional octahedra-dodecahedra group). There is a general tendency for the number of colored stones to increase with crystal size (Table 4). Colored crystals comprise approximately 15 percent of the lowest two size fractions (less than 0.5 mm), but increase to nearly 40 percent of the four larger size categories (0.5 - more than 2.0 mm).

Many of the diamonds show a pronounced fluorescence in ultraviolet light: pale to bright yellow colors predominate, although blue white and pale orange colors were also observed. More than half of the crystals (40), especially those in the "minimicrodiamond" category, are non-fluorescent (Table 5). Yellow shades of fluorescence are most predominant in octahedral forms (octahedra, transitional octahedra-dodecahedra, and intergrown octahedra in aggregate

crystals). Blue white colors are confined to transitional octahedra-dodecahedra and dodecahedra, whereas pale orange fluorescence occurs primarily in aggregates. Macles are consistently non-fluorescent, as are two-thirds of the untwinned octahedra.

Minute inclusions are abundant in many of the diamonds, and although definitive analytical work has not yet been completed, garnet, olivine and pyroxene have been tentatively identified. Small black platelets of graphite occur along cleavage planes in some crystals. The graphite inclusions all appear to be concentrated near the surface of crystals and are probably the result of graphitization of diamond along planes of weakness (stress planes). Numerous clear fluid inclusions are also present.

Most State Line district diamonds apparently formed originally as octahedra, many of which were later modified to dodecahedral forms. Macles also are considered to be primary forms.

References

- McCallum, M. E., and Mabarak, C. D., 1976a, *Geology*, 4, p. 467-469.
 _____, 1976b, *Wyo. Geol. Surv. Rept. Invest. no. 12*, 36 p.
 Whitelock, T. K., 1973, in *Lesotho Kimberlites*, P. H. Nixon, ed., Lesotho Development Corp., Maseru, Lesotho, p. 128-140.

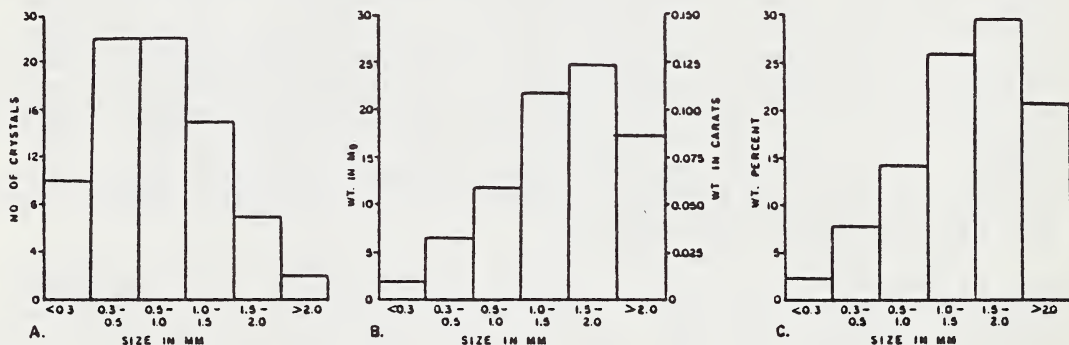


Figure 1. Size distribution of State line diamonds. A. Number of crystals per size interval. B. Weight per size interval. C. Weight percent of total per size interval.

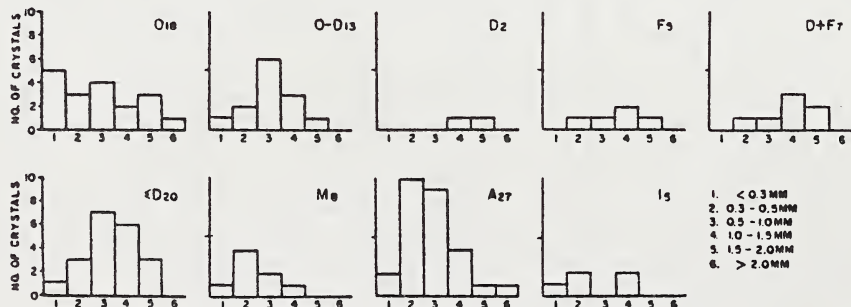


Figure 2. Crystal form as a function of size. Form symbols same as in Table 1 with the addition of D+F = dodecahedra and flats, and $\leq D$ = total dodecahedral forms. Subscripts on form symbols indicate number of crystals of that type.

Table 3. Color as a function of crystal form (form symbols same as in Table 1).

Color	O	O-D	D	F	M	A	I	Total
colorless to glassy	13	8	1	3	6	16	3	50
white	2	0	0	0	1	2	0	5
gray to gray white	0	0	0	0	1	5	0	6
pale brown	0	1	0	1	0	2	2	6
pale orange to orange brown	1	1	1	1	0	0	0	4
pale yellow	1	3	0	0	0	1	0	5
dark gray to black	1	0	0	0	0	1	0	2

Table 4. Color as a function of crystal size.

Size mm	colorless to glassy	white	gray to white	pale gray to brown	pale orange to brown	pale yellow to black	Dark Gray to black
0.3	12	1	0	0	0	0	0
0.3-0.5	13	1	3	2	0	0	0
0.5-1.0	10	3	1	1	2	4	1
1.0-1.5	0	0	2	1	1	1	1
1.5-2.0	5	0	0	2	1	0	0
2.0	2	0	0	0	0	0	0
Total	50	5	6	6	4	5	2

Table 5. Fluorescence as a function of crystal form (form symbols same as in Table 1).

Color	O	O-D	D	F	M	A	I	Total
yellow to bright yellow	3	2	0	1	0	5	2	13
pale yellow	3	6	0	2	0	3	1	15
blue white	0	2	1	0	0	0	0	3
pale orange	0	1	0	0	0	6	0	7
non-fluorescent*	12	2	1	2	8	13	2	40

* Most of the "microdiamonds" are non-fluorescent or very weakly fluorescent.

Table 1. Morphological classification of State line diamonds as a function of size. O = octahedra, O-D = transitional octahedra-dodecahedra, D = dodecahedra, F = flattened dodecahedra, M = macles, A = aggregates, I = irregular shapes, O/D = ratio of octahedra to dodecahedra, O/D³ = ratio of octahedra to dodecahedra including O-D group with dodecahedra.

Size mm*	O	O-D	D	F	M	A	I	Total	O/D	O/D ³
0.3	5	1	0	0	1	2	1	10	---	5.0
0.3-0.5	3	2	0	1	4	10	2	22	3.0	1.9
0.5-1.0	4	6	0	1	2	9	0	22	4.0	0.57
Totals (ave.)	12	9	0	2	7	21	3	54	(6.0)	(1.09)
1.0-1.5	2	3	1	2	1	4	2	15	0.67	0.33
1.5-2.0	3	1	1	1	0	1	0	7	1.5	1.0
2.0	1	0	0	0	0	1	0	2	---	---
Totals (ave.)	6	4	2	3	1	6	2	24	(1.2)	(0.67)
Overall Totals (ave.)	18	13	2	5	8	27	5	78	(2.57)	(0.90)

* Categorized according to largest dimension.

Table 2. Weight as a function of size

Size mm	no. of crystals	average weight		total weight	
		mg.	carat	mg.	carat
<0.3	10	~0.2	~0.001	~2.0	~0.010
0.3-0.5	22	~0.3	~0.0015	~6.6	~0.033
0.5-1.0	22	~0.54	~0.0027	~11.85	~0.059
Totals (ave.)	54	(~0.38)	(~0.0018)	(~20.45)	(~0.102)
1.0-1.5	15	1.55	0.0078	21.65	0.108
1.5-2.0	7	3.09	0.0155	24.72	0.1236
>2.0	2	8.72	0.0436	17.43	0.0872
Totals (ave.)	24	(2.60)	(0.013)	(63.80)	(0.3188)
Overall Totals (ave.)	78	(~2.37)	(~0.012)	(~84.25)	(~0.421)

KIMBERLITES ON MARS

T. R. McGetchin (Lunar Science Institute, Houston, Texas)

J. R. Smyth (Geological Research Group, Los Alamos Scientific Laboratory, Los Alamos, New Mexico 87545)

Observation of surface features, geophysical data, surface chemistry, and theoretical models of solar system cosmology are consistent with the inference that kimberlite-like ultrabasic ash may be a very abundant constituent of Martian soil and that kimberlitic volcanism may be an important process on Mars.

The density of the Martian mantle is estimated to be about 3.55 gm/cc, significantly greater than that of the Earth. This higher density has been taken to imply a greater abundance of FeO. Model mineral assemblages have been calculated for a variety of chemical compositions at 30 kb using a high pressure norm scheme. For the simplest models, FeO was added to Pyrolite III and the densities of the resulting mineral assemblages calculated. The model yielding a density of 3.55 is not a garnet lherzolite, but rather is an assemblage of 2% oxide, 11% garnet, 73% olivine (Fo₆₇) and 12% clinopyroxene. Such an oxide-garnet wherlite is a rather different assemblage than any calculated for Earth, and may be unique among the terrestrial planets. Partial melting of such an assemblage would be likely to yield iron-rich ultrabasic lavas of extremely low viscosity. Model partial melts, assuming quaternary eutectic melting (at ol₁₇gar₄₂cpx₄₃oxide₈) yield an ultrabasic picritic alkali-olivine basaltic melt, with a computed viscosity of 12 poises at 1200°C.

There is evidence for abundant lava flow and flood volcanism on Mars. On the earth, pyroclastics associated with basaltic volcanism on the earth are minor. However, kimberlites reflect the accumulation of deep-seated volatiles which are blown through the lithosphere in violent gas-dynamic eruptions. Hence, if volatiles are abundant in the interior of Mars, ultrabasic pyroclastics may be common. Current models for early solar system evolution (Lewis, 1972; Cameron, 1963, 1973) suggest that Mars formed at cooler temperatures than the Earth, and therefore may have accreted five to six times the abundance of volatile material per unit mass. If this is correct, Mars may have (or have had) an extremely volatile-rich interior. The rift features suggest global extension of the lithosphere, and thermal evolution models also imply global expansion, at least throughout most of Martian history. A tensional stress state in the lithosphere would promote eruption of internally generated melt and gas.

If the mantle of Mars is indeed richer in FeO and volatiles than that of the Earth, there are a number of geological implications which follow that appear to be compatible with results of Mariner and Viking experiments and observations. (1) Copious ultrabasic flood volcanism may account for some of the massive flood and erosional features commonly ascribed to water erosion on Mars. (2) The Viking 1 and 2 XRF inorganic chemistry experiments may be measuring compositions of such lavas. (3) A number of unusual Martian mantle mineralogies, and therefore unusual magma types, are possible which depend largely on the activity of volatile substances--S, O, C, H. (4) A relatively small amount of ferro-granite might be produced by liquid immiscibility. (5) Ultrabasic (ferro-kimberlitic) ash may be a very important constituent of the Martian soil--especially if cosmological models concerning accretion of volatile material within Mars are correct. Thus, kimberlitic volcanism may have been a major process on Mars.

KIMBERLITIC, MELILITIC, TRACHYTIC AND CARBONATITIC ERUPTIVES AT SALTPETRE KOP, SUTHERLAND, SOUTH AFRICA

J.R. McIver (University of the Witwatersrand, Johannesburg, South Africa)
John Ferguson (Bureau of Mineral Resources, Canberra, Australia)

In the western portion of southern Africa a large number of post Karroo alkaline eruptive centres occur in a zone parallel to the coast. One of these, the Saltpetre Kop volcano near Sutherland, Cape Province, is characterised by the association of kimberlitic rock, olivine melilitite, trachyte and carbonatite which are present in some twenty relatively small volcanic necks and vents situated in the immediate vicinity of the main Saltpetre Kop crater. The latter forms the centre of a regular circular updomed region within the otherwise near flat lying Karroo sediments with dips of up to 60° being present in the vicinity of the throat of the volcano.

The main vent occupies an area of some 1000 x 1500 m and is filled with lithic pyroclasts which in the vicinity of carbonatite intrusions have a carbonate cement. Pyroclastic rocks having a strong macroscopic resemblance to certain types of kimberlite comprise the least abundant of the satellite eruptives. In these rocks inclusions and groundmass for the most part comprise equal volumes; crustal rocks are volumetrically dominant but are accompanied by ilmenite grains up to 2.5 cm across, brown amphiboles up to 3 cm across, augite crystals measuring 0.5 cm and prominent biotite flakes. The groundmass is dominated by carbonate and perovskite but ghost outlines of pre-existing crystals possibly represent original olivine grains. Analysis of the ilmenite present revealed it to be low in MgO and TiO_2 compared to kimberlitic ilmenites (Frick, 1973). Olivine melilitites represent the most widespread intrusives being recorded up to 20 km from Saltpetre Kop. These rocks are invariably porphyritic or microporphyritic containing an abundance of olivine and minor magnetite set in matrices containing variable proportions of melilitite, augite, phlogopite, olivine, perovskite, apatite, zeolites, magnetite and rare monticellite and nepheline. A feature of many of these rocks is the presence of well developed reaction rims and internal areas around and within olivine phenocrysts where olivine-liquid reaction has produced assemblages of phlogopite, melilitite, magnetite, perovskite and minor monticellite. Trachytic rocks, in part nepheline bearing, comprise the most abundant of the eruptives and frequently contain an abundance of crustal rock fragments. Both sövitic and ankeritic varieties of carbonatite are present and some outcrops contain an abundance of amphibole, biotite and ilmenite megacrysts.

Danchin *et al.* (1975) and Ferguson *et al.* (1975) have established seven major cluster Groups based on statistical comparison of 126 analyses of kimberlites and associated ultrabasic rocks. The distribution of these within the CMAS tetrahedron (O'Hara, 1968) was determined and Fig.1a shows the projection of these points into the CMS plane where they define a linear olivine dominated trend from magnesian (kimberlitic) compositions (Groups 5, 6 and 7) to less magnesian (melilitic, alnöitic) compositions (Groups 1, 2 and 3); Group 4 contains both kimberlitic and non-kimberlitic compositions. The average analysis of Saltpetre Kop and other olivine melilitites from south western South Africa define an additional point on this trend. Also shown in Fig.1a is the trend of the ultrabasic komatiite - tholeiite sequence of the Onverwacht eruptives of the Barberton Mountain Land (McIver and Lenthall, 1974). Both trends are largely linearly away from the olivine point indicat-

ing the importance of olivine fractionation in both series and represent compositional loci of evolving magmas providing natural parallels to the two trends predicted by Boettcher et al. (1975) shown in Fig. 1b.

Eggler (1974) has shown that under CO_2 saturated conditions the minimum melting point in the assemblage Di-Fo-En moves to the larnite normative side of the Di-Fo join between 15 and 30 kb. At higher pressures contraction of the olivine volume is likely to occur and the kimberlite - olivine melilitite trend of Fig. 1a possibly mimics the movement of the minimum melting point at higher pressures. Mixing calculations show that both olivine and orthopyroxene subtraction is required to permit derivation of compositions such as Groups 4, 5 and 7 from Group 6; subtraction of olivine alone from Group 4 was, however, sufficient to yield compositions akin to Groups 1, 2 and 3.

The foregoing, together with the data of Fig. 1a, strongly suggest the evolution of magma compositions such as the Saltpetre Kop olivine melilitites by polybaric fractionation initially of orthopyroxene and olivine and then olivine alone from kimberlitic magma. The olivine-liquid reaction phenomena preserved in the olivine melilitites would appear to provide the natural analogue of the forsterite - liquid reaction in the system Ne-La-Fo- SiO_2 (Schairer and Yoder, 1964). This reaction would be constrained to low pressure regimes (<6 kb) by the stability of melilitite in the presence of CO_2 (Yoder 1975). The Ne-La-Fo- SiO_2 system has been shown to fractionate to a wollastonite, diopside, nepheline, feldspar assemblage which Platt and Edgar (1972) suggest may simulate phonolite; in the natural system this end product is likely to be represented by the trachytic rocks of Saltpetre Kop. At Saltpetre Kop kimberlitic eruptives are characterised by the presence of amphibole megacrysts and iron-rich ilmenite and in terms of the evolutionary model suggested by Fig. 1a probably represent kimberlite equilibrated at and erupted from shallower depths (\pm 60 km) than many other kimberlites.

Based on the foregoing, the following sequence of events is envisaged as being involved in the formation of Saltpetre Kop: 1. Kimberlitic magma with dissolved H_2O and CO_2 was generated by melting of hydrous carbonate-bearing garnet lherzolite at depths probably between 100 - 200 km; 2. Initial slow uprise of this magma accompanied by olivine and orthopyroxene fractionation; 3. Arrest of a portion of the magma in a pressure regime where amphibole was the stable phase followed by rapid transport to surface to give rise to the kimberlitic pyroclastic rocks; 4. Further slow uprise accompanied by olivine fractionation and arrest of the remaining magma at depths of less than 18 km and the onset of the olivine-liquid reaction; 5. Possibly concomitant with 4 the separation of a carbonatite phase (Wyllie and Huang, 1976) accompanied by increasing volatile pressure which culminated in the formation of the central vent at Saltpetre Kop; 6. Exploitation of fractures in the vicinity of the vent by olivine, melilitite and carbonatite; 7. Continued fractionation of olivine melilitite magma in a crustal regime to beyond the limit of melilitite stability to produce a potassium-rich feldspar system.

REFERENCES

- BOETTCHER, A.L., MYSEN, B.O. and MODRESKI, P.J. (1975). Melting in the mantle: phase relationships in natural and synthetic peridotite- H_2O and peridotite- $\text{H}_2\text{O}-\text{CO}_2$ systems at high pressures. *Physics and Chemistry of the Earth* 9, 855-868.
- DANCHIN, R.V., FERGUSON, J., McIVER, J.R. and NIXON, P.H. (1975). The composition of late stage kimberlitic liquids. *Physics and Chemistry of the Earth*, 9, 235-245.

- EGGLER, D.H. (1974). Effect of CO₂ on the melting of peridotite. *Carnegie Inst. Yearbk.*, 73, 215-224.
- FERGUSON, J., MARTIN, H., NICOLAYSEN, L.O. and DANCHIN, R.V. (1975). Gross Brukkaros: a Kimberlite-Carbonatite Volcano. *Physics and Chemistry of the Earth*, 9, 219-234.
- FRICK, C. (1973). Kimberlitic ilmenites. *Trans. geol. Soc. S. Afr.*, 76, 85-94.
- McIVER, J.R. and LENTHALL, D.H. (1974). Mafic and ultramafic extrusives of the Barberton Mountain Land in terms of the CMAS system. *Precamb. Res.*, 1, 327-343.
- O'HARA, M.J. (1968). The bearing of phase equilibria studies in synthetic and natural systems on the origin and evolution of basic and ultrabasic rocks. *Earth Sci. Rev.*, 4, 69-133.
- PLATT, R.G. and EDGAR, A.D. (1972). The system nepheline-diopside-sanidine and its significance to the genesis of melilite- and olivine-bearing alkaline rocks. *J. Geol.*, 80, 224-236.
- SCHAIRER, J.F. and YODER, H.S. (1964). Crystal and liquid trends in simplified alkali basalts. *Carnegie Inst. Yearbk.*, 63, 64-74.
- WYLLIE, P.J. and HUANG, W.L. (1976). Carbonation and melting reactions in the system CaO-MgO-SiO₂ at mantle pressures with geophysical and petrological applications. *Contrib. Mineral. Petrol.*, 54, 79-107.
- YODER, H.S. (1975). Relationship of melilite-bearing rocks to kimberlite. A preliminary report on the system akermanite-CO₂. *Physics and Chemistry of the Earth*, 9, 883-894.

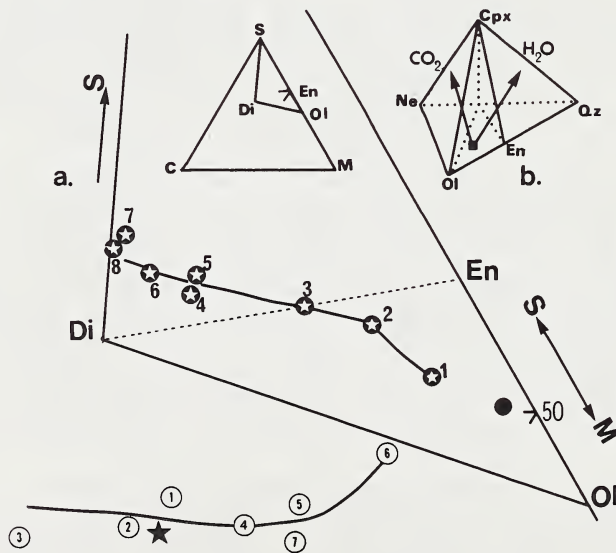


Fig. 1a. Projection from A into the C-S-M plane. Circled figures - average CO₂-free cluster Group analyses; solid star - average olivine melilitite; circled stars - Onverwacht eruptives, 1 and 2, high magnesia peridotitic komatiites, 3, 4, 5, Geluk, Badplaas and Barberton basaltic komatiites, 6, 7, 8, tholeiitic eruptives. Circle - Garnet lherzolite in kimberlite (O'Hara, 1968).

1b. Inferred magmatic trends occasioned by mantle melting in the presence of H₂O and CO₂, after Boettcher, et al., 1975.

THE OKA CARBONATITE COMPLEX: MAGNETITE COMPOSITIONS AND THE ROLE OF IMMISCIBLE SILICATE LIQUIDS

B.M. McMahon and S.E. Haggerty (Dept. of Geology, University of Massachusetts, Amherst, MA 01003)

A detailed microprobe study has been undertaken to characterize the variations in magnetite compositions between carbonatite assemblages and the associated alkaline igneous rocks of the Oka carbonatite complex. Within the context of an immiscible liquid and/or mechanical unmixing hypothesis for the generation of a carbonatite magma, the data indicate that the probable segregated silicate counterpart to these carbonatites is a melteigite-ijolite of the nephelinite series. These new data are consistent with the experimental work in synthetic "carbonatite"-silicate systems (Koster Van Groos and Wyllie, 1966, 1968). $^{87}\text{Sr}/^{86}\text{Sr}$ ratios, and oxygen and carbon isotope data (Taylor, 1967) also substantiate this "next of kin" relationship.

The carbonatitic magnetites in general are jacobsite-magnetite_{SS}. MnO ranges from 1.5 to 13.5 wt%, averaging about 10 wt%. Manganese depletion is generally indicated from crystal core to mantle. Late TiO₂ enrichment (3-8 wt%) accompanies MnO depletion in those magnetites with less than 5 wt% MnO. MgO and Al₂O₃ are virtually constant ranging from 1-4 and 0-3 wt% respectively, (excluding mantle reaction relations, which are generally present). Late MgO-Al₂O₃ depletion may be present, but pleonaste exsolution contributes to this uncertainty. The carbonatite ilmenites are ilmenite-pyrophanite solid solutions ranging from 25-75 mole % pyrophanite. They appear as discrete phases or as exsolution in low MnO (approximately 3%) magnetite. These also exhibit disequilibrium/reaction relationships with the calcite matrix (producing a Mn-siderite). Clean pyrophanite survives only as an exsolved phase or if crystals are wedged between magnetite grains, partially insulated from calcite. The reaction rim texture of the magnetites in the sovite matrix suggests the possibility that they may have been transported in a mobile carbonate liquid upon encountering a silicate-carbonate immiscibility field.

The associated alkaline ultrabasic rocks in their relative order of emplacement are the jacupirangite-okaite series (titanaugite pyroxenites-melilitites), the melteigite-urtite series of the nephelinites (aegerine-augite + nepheline rocks), and the alnoite-kimberlite diatremes. The magnetites of the jacupirangite-okaite series contain significant MnO (5.5 wt%) on the okaite to Ne-okaite end of the series tapering down toward the jacupirangitic value of 3.5 wt% (refer to figure). TiO₂ ranges from 1.5 to 5.5 wt% with a minimum in Ne-okaite and a maximum in jacupirangite. MgO remains relatively uniform at 3.5 wt% throughout the series, whereas Al₂O₃ reaches a maximum of 3.3 wt% in Ne-okaite and a minimum of 2.5 wt% in jacupirangite.

The magnetite in alnoites are low in MnO (0.5-2.0 wt%), high in TiO₂ (8.5 wt%) and MgO (7.5 wt%), and have intermediate values of Al₂O₃ (2-4 wt%). The magnetites in the Isle Bizard kimberlite have the lowest MnO content of any of the associated rocks (less than 0.25 wt%). TiO₂ is a steady 5.5 wt%, Al₂O₃ less than 1 wt%, and MgO increases from 3.5 to 4.5 wt% from core to mantle (clearly very distant from the type of compositions seen in any of the carbonatites).

The magnetites of the nephelinite series (melteigite-urtite) are only abundant in the intermediate member, ijolite (aegerine-augite/nepheline = 1:1), in which MnO reaches a maximum for the alkaline silicate rocks at 8.5 wt%; TiO₂, Al₂O₃, and MgO average 4.5, 2.2, and 2.8 wt% respectively. These

values are an extremely close approximation to those of magnetites in the aegerine pyroxene-bearing carbonatite (MnO-7.5 wt%, TiO₂-3.5-4.0 wt%, Al₂O₃ less than 1 wt%, MgO-1.5 wt%). The extreme compositional similarity in magnetite suggests a comagmatic relationship. Although it is widely recognized that magnetite is compositionally responsive to minor environmental changes, the close similarity is unexpected because: (1) the response of component activities anticipated to accompany any form of segregation process should be much greater than that observed; and (2) equilibrium across an immiscible surface may be expected if surface to volume ratios are small, a situation which is clearly not the case at Oka. Further support for immiscibility is provided by oxidation trends in sovite and in ijolite magnetites and these trends are consistent with an increase in CO₂ activity and a concomitant decrease in a_{SiO_2} .

Experimental data in the plane NaAlSi₃O₈-Na₂CO₃-H₂O through the quinary system Na₂O-Al₂O₃-SiO₂-CO₂-H₂O (Koster Van Groos and Wyllie, 1968) indicate that fluid immiscibility relations, which are synthetically analogous to co-existing nepheline or ijolite magmas, carbonatite melts, and fenitizing solutions, vary relative to the proportions and partial pressures of CO₂ and H₂O as well as P_{total}. Our data indicate that an ijolitic magma is the closest approximation to an equilibrium situation with respect to carbonatitic magnetite stability.

It is emphasized, that considering the extreme range of a_{SiO_2} indicated in sovite mineralogy, that carbonate-silicate immiscibility is a_{SiO_2} not independent of fractional crystallization and should not be considered as a singular event, but more probably as part of an ongoing periodic decarbonation-carbonation process (eg. as alkalis become locally concentrated in response to fractional crystallization).

The following points emphasize the apparent non-singularity of carbonatitic segregation as a process, and contrast the Oka complex with other carbonatitic segregation environments:

-Magnesian carbonatite segregation and subsequent small scale diapiric structures have been observed in the Benfontein kimberlite sills near Kimberley, S. Africa (Dawson and Hawthorne, 1973). Segregation bubbles were shown to need not result from immiscibility in the classical sense, but from density and viscosity contrast, within a rapidly cooling sill.

-Natrocarbonatite lava has been observed by Dawson (1962) in eruption at Oldoinyo Lengai in Tanzania.

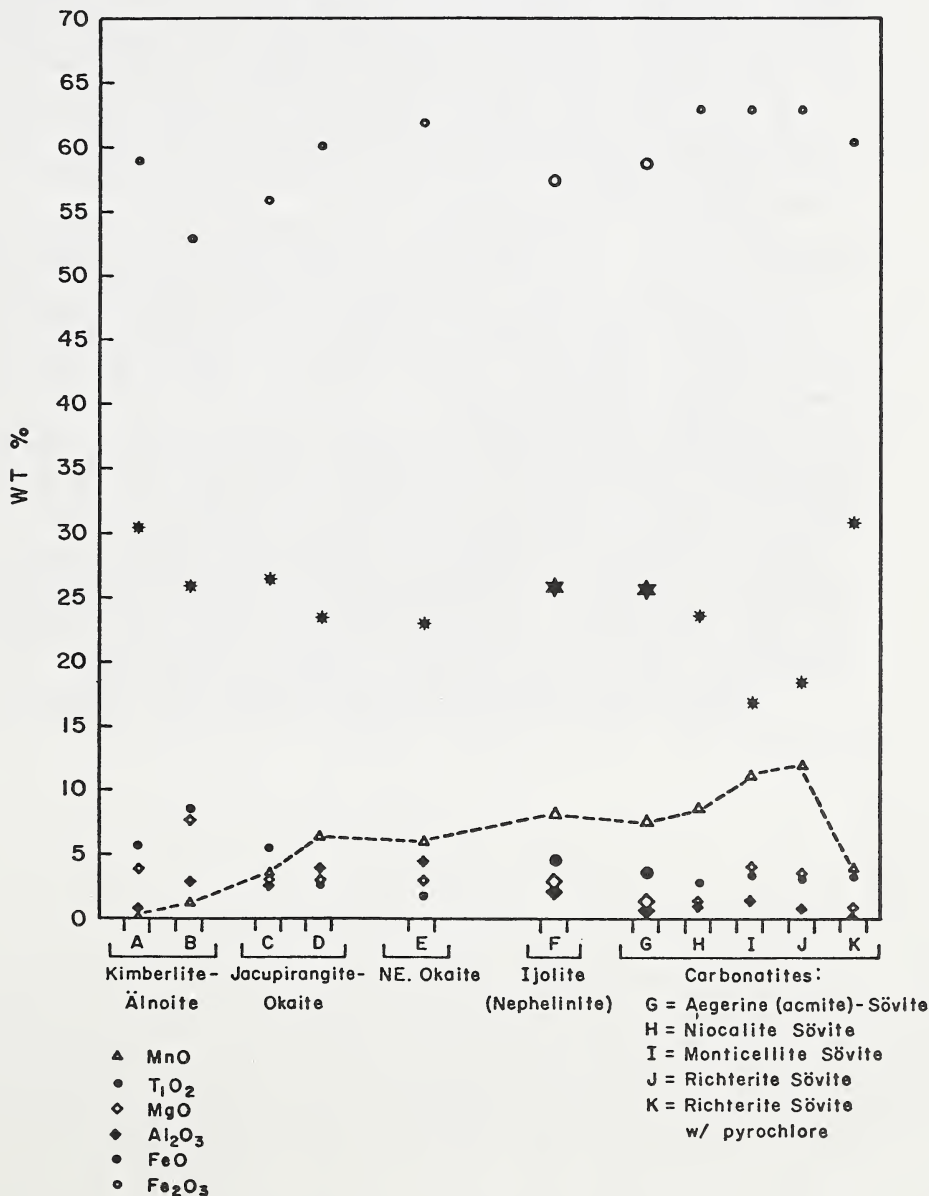
-The Oka Carbonatite Complex (Quebec, Canada), has eroded to ring-dike and cone sheet level. The carbonatite is typically neither highly magnesian nor highly sodic. The carbonatite igneous textures vary from phaneritic to porphyritic, and silicates, oxides and immiscible sulfides are present in a calcitic matrix of highly variable matrix to phenocryst ratio, which is typically >0.8. These rocks are also strongly flow-foliated, consistent with the overall ring-dike structure and mode of emplacement.

In summary, although no new model for carbonatite genesis is proposed in this paper, additional support is offered for deep-seated "kimberlitic" devolatilization as a source of CO₂ which is apparently largely responsible for higher level fractionation and immiscibility/segregation processes in upper mantle-low crustal continental rocks. This paper does not establish a detailed genealogy of alkalic-carbonatitic associations, but does identify the carbonate-silicate assemblage which most closely approximates an equilibrium situation. This assemblage is ijolite and aegerine carbonatite. A final and noteworthy comment is that carbonatitic opaque mineral oxides are charac-

terized by high MnO contents, a feature which is also apparent in numerous late stage kimberlitic constituents where high CO₂ activity is apparent.

References: Dawson (1962). *Nature*, 195, 1075; Dawson and Hawthorne (1973). *J. Geol. Soc. Lon.* 129, 61; Taylor et al., (1967). *Geochim. et Cosmochim. Acta* 31, 407; Koster Van Groos and Wyllie (1966). *Am. Jour. Sci.* 264, 234; Koster Van Groos and Wyllie (1968). *Am. Jour. Sci.* 266, 932.

Magnetite Compositional Averages for OKA Carbonatites and Associated Alkaline Igneous Rocks:



THE UPPER MANTLE BENEATH THE SOUTHWESTERN UNITED STATES.

Jean-Claude C. Mercier, Dept Earth & Space Sciences, S.U.N.Y.
at Stony Brook, NY 11794

Systematic field study of tens of thousands of xenoliths from 15 major Quaternary volcanic fields of the Southwestern United States and neighboring Mexico, completed by detail structural and chemical study of hundreds of selected samples, show mappable patterns in the distribution of textures, petrological and chemical parameters and related physical mantle conditions. The upper mantle appears laterally homogeneous over large regions which correspond to major tectonic provinces, but composition and physical properties vary with depth within such cells, the latter being limited by sharp boundaries of deep extension. Common ultramafic cumulates are genetically related to the overlain metamorphic mantle. Xenoliths from older volcanics indicate petrologic variability throughout time and the following recent (<30 m.yr.) evolution and present state of the upper mantle can be inferred:

- Colorado Plateau and Sierra Nevada (Moho at 45-48 km): formerly intracratonic-type depleted mantle, chemically and texturally modified some 20 m.yr. ago through impregnation by tholeiitic liquids;

- Central Nevada (Moho at \leq 16 km): Cr-rich peridotites with large (5-10 cm) poikiloblastic olivines ($\sigma \sim 20$ bars) typical of a late stage of continental rifting, indicate a zone of present mantle upwelling and crust thinning;

- Basin-and-Range (excluding Nevada; Moho at ~ 32 km): fine-grained homogeneous lherzolites passing down to coarse (8-10 mm) harzburgites with websteritic banding (diffusion?); 60-to-70 km-deep peridotite-xenolith-bearing neo-websteritic batholiths imply a residual coarser highly-depleted (melting) deeper facies;

- Baja California: homogeneous lherzolites; this province escaped the late (10 m.yr.?) differentiation processes illustrated by the last two provinces. Sheared facies ($\sigma \sim 800$ bars) would be related to reactivation of major lithospheric fault/shear zones immediately prior to the eruption it probably triggered.

General petrogenetic and rheological models derived yield new constraints for the tectonic history of the Southwestern United States.

PERIDOTITE XENOLITHS AND THE DYNAMICS OF KIMBERLITE INTRUSION.

Jean-Claude C. Mercier, Dept Earth & Space Sciences, S.U.N.Y.
at Stony Brook, NY 11794.

Mean olivine subgrain-sizes and grain-sizes resulting respectively from syntectonic (dynamic) recovery and recrystallization are inverse functions of the differential stress applied during deformation. During primary annealing recrystallization, tablet-shaped olivine neoblasts are characterized by a constant growth-rate proportional to the annealing temperature (pyroxene geothermometry) and to the strain energy stored in the paleoblasts, this energy being itself proportional to the stress immediately prior to annealing. The time for the xenoliths to reach the surface and the kimberlite average intrusion velocity (depth from pyroxene geobarometry) are then derived from the growth-rate for annealing calculated on the basis of experimental data and from maximum annealed olivine-tablet sizes in blastogranular peridotites, with some corrections for heating by the kimberlite and supercooling at shallow depths and, eventually, for the distance of the sample studied from the xenolith surface.

Experimentally determined flow laws for dry olivine are used to derive strain-rates from the stress and temperature data. Rough estimates of the late-deformation duration are then obtained whenever strain can be appreciated from internal deformation of olivine (blastolaminar samples) or recrystallized enstatite laminae (PHN-1611-type textures). As these estimates range from a few hours to a few tens of years, the deformations cannot be related to major tectonic phenomena such as the ascent of large diapirs or convection-related flow, a conclusion in accord with the unrealistic velocity estimates (3 to 30 km/yr) implied by such models. These deformations are therefore ascribed to kimberlite-conduit formation and the longest times are regarded as artifacts possibly due to superplastic behavior of the deepest samples. Strain-rates prior to sampling and velocities of intrusion are ultimately combined for estimating the diameter of the zone mechanically perturbed by the kimberlite ascent, the initial force which initiated the intrusion and the related energy involved.

THE HILLS POND PERIDOTITE, WOODSON COUNTY, KANSAS: A RICHTERITE-BEARING CRETACEOUS INTRUSIVE WITH KIMBERLITIC AFFINITIES

R. B. Merrill (Lunar Science Institute, 3303 NASA Rd. 1, Houston, TX 77058)

M. E. Bickford (Department of Geology, University of Kansas, Lawrence, KS 66045)

A. J. Irving (Lunar Science Institute, 3303 NASA Rd. 1, Houston, TX 77058)

Geologic Relationships

The Hills Pond Peridotite (e.g. Wagner, 1954) is the larger of two micaeous peridotites exposed in Woodson County, Kansas (Fig. 1); others are known from drilling. The body is located on the Hill farm in southern Belmont township, and intrudes sedimentary rocks of Pennsylvanian Age. The age of the body is about 90 m.y., as determined by K-Ar and Rb-Sr measurements on phlogopite (Zartman *et al.*, 1967). The Hills Pond Peridotite and the nearby peridotite intrusive at Rose Dome (Franks *et al.*, 1971) are on the westward extension of the Thirty-eighth Parallel Lineament of Heyl (1968).

Surface mapping and drilling have established that the peridotite body is an elongate, plug-like mass about 1.7 km long and about 300 m wide, with several sill-like extensions to the south. The emplacement of the igneous material has caused gentle doming of the sedimentary rocks, forming the Silver City Dome. A contact metamorphic aureole extends outward from the main plug for about 300 m; principal metamorphic effects are the conversion of sandstone to quartzite and the development of chlorite, but local development of epidote, tremolite-actinolite, hornblende, and chert is observed in limestone and calcareous shale (Wagner, 1954).

The exposed rock is deeply weathered to a mass of clay still containing abundant phlogopite. Fortunately, the body has been drilled extensively. The following petrographic and chemical data are based upon 18 samples from a core that penetrated the main plug to a depth of about 180 m.

Petrography

The peridotite is strikingly porphyritic. The phenocrysts include titanphlogopite, serpentine pseudomorphous after olivine, potassic richterite, and titanite, all in a fine-grained groundmass of serpentine. Accessory minerals include perovskite, apatite, and chrome spinel. Olivine pseudomorphs are large (about 1.5 mm ave. dia.), typically rounded, and are characterized by curved veins of chrysotile in more homogeneous lizardite or antigorite that is commonly coarser than the serpentine of the matrix. Phlogopite phenocrysts are also large (1.5 mm ave. dia.), are only slightly pleochroic, and many are subhedral, but most are intergrown optically with earlier olivine and titanite; much phlogopite is bent and deformed. Richterite occurs in fan-shaped bladed aggregates and less commonly as bladed crystals about 0.5 mm long. It is colorless in plane light and faintly pleochroic in shades of pale pink. Optically, richterite is negative with $2V$ of about 60° , and typically is zoned showing undulose extinction with angles increasing from edges of grains inward.

Apatite occurs typically as tiny, prismatic crystals enclosed in phlogopite. Perovskite occurs as brownish opaque crystals with square outlines or as irregular masses. Chrome spinel occurs as crystals of square to rounded and irregular outlines. It is reddish in both transmitted and reflected light, and is not completely isotropic.

Modal data for three samples are given in Table 1. The ratio of phenocrysts to matrix decreases with increasing depth, while richterite increases and titanite decreases in abundance relative to other phenocryst species.

Chemistry

Major element analyses of the peridotite are listed in Table 2. REE and other trace element contents are reported in Table 3. In general, the chemical characteristics of this peridotite are very similar to those of "typical" kimberlite (cf Dawson, 1967), but potassium content is significantly higher. The chondrite-normalized REE plot (Fig. 2) shows that La abundance is 500 times chondrites and that La/Yb = 111, suggesting that the peridotite equilibrated with garnet at some point in its history.

Major element mineral analyses also are listed in Table 2. The titanaugites (Ca/Ca + Mg = 0.51) are similar chemically to groundmass pyroxenes in some kimberlites, and except for unusually high TiO₂, fall within Group 3 of Stephens and Dawson (1977). The titanphlogopite is similar in composition to specimens which coexist with richterite in nodules from South African kimberlites (Aoki, 1974) but is richer in TiO₂ and lower in Al₂O₃ than most kimberlite phlogopites thought to be "primary". The potassic richterite is very rich in TiO₂ relative to richterites in South African kimberlites, which implies that the Kansas richterites have equilibrated at shallower depths. This is consistent with the absence of garnet from the Hills Pond phenocryst assemblage.

Comparison with Kimberlites

Although the chemical data suggest kimberlitic affinities, in some respects the Hills Pond Peridotite is quite different from "typical" kimberlite and also differs from the mica peridotites of western Kentucky and southern Illinois (Watson, 1967). These differences are summarized below:

1. The Hills Pond Peridotite contains no garnet, whereas kimberlites characteristically contain pyrope-almandine.
2. No inclusions of eclogite or of garnet peridotite have been found in the Hills Pond body, although these commonly are found in kimberlite. The similar peridotite at Rose Dome, about 8 km to the northeast, contains large inclusions of Precambrian granite, but these are not present in the Hills Pond body.
3. Typical kimberlites contain Mg-bearing ilmenite. The Hills Pond body contains only perovskite and chrome spinel as oxide phases.
4. Clinopyroxene is relatively abundant in the Hills Pond body, but is rare in the micaceous peridotites of western Kentucky and southern Illinois.
5. Petrographic relations (ophitically intergrown phlogopite) and the occurrence of peridotite as thin sills suggest that the Hills Pond body was emplaced primarily as a liquid and not explosively. Kimberlites commonly are microbreccias and appear to have been emplaced explosively.

Six kimberlites are known in Riley County, Kansas (Fig. 1; Meyer, 1976). These are believed to be Cretaceous in age, but their relation to the Woodson County bodies is unknown. Marked differences in mode of emplacement and in major element chemistries suggest that any connection is remote. The Hills Pond and Rose Dome Peridotites are more similar to the bodies in western Kentucky, southern Illinois, and Missouri, suggesting a relationship with the Cretaceous rifting in the Mississippi Embayment region.

Conclusions

Field relations suggest that the Hills Pond Peridotite was emplaced as a largely-liquid magma. REE evidence indicates that this magma equilibrated with garnet at some time in its history, presumably within a mantle source region. We infer that the magma was a partial melt of primitive material or the result of limited crystal fractionation. The exceptionally high potassium content may not be a primary feature, but rather a result of crustal contamination.

REFERENCES

Dawson, J.B. (1967) In *Ultramafic and related rocks* (P.J. Wyllie, ed.), p.269. John Wiley and Sons, New York.

Franks, P.C., Bickford, M.E., and Wagner, H.C. (1971) *Geol. Soc. Amer. Bull.*, v. 82, p.2869.

Heyl, A.V. (1968) *Econ. Geol.*, v. 63, p.585.

Meyer, H.O.A. (1976) *J. Geol.*, v. 84, p.377.

Stephens, W.E., and Dawson, J.B. (1977) *J. Geol.*, v. 85, p.433.

Wagner, H.C. (1954) U.S. Geol. Surv. Map CQ49.

Watson, K.D. (1967) In *Ultramafic and related rocks* (P.J. Wyllie, ed.), p.312. John Wiley and Sons, New York.

Zartman, R.E., Brock, M.R., Heyl, A.V., and Thomas, H.H. (1967) *Amer. J. Sci.*, v. 265, p.848.

TABLE 1 -- MODAL DATA

Sample	Depth (meters)	Phlogopite	Serp. Psdmp. Olivine	Titanaugite	Richterite	Perovskite	Chromepinel	Apatite	Serp. Matrix
SCP70	23	24.9	14.1	4.8	3.9	0.5	0.2	0.2	51.4
SCP290	97	21.8	11.2	2.6	5.9	0.5	0.2	0.1	57.7
SCP427	142	19.7	11.0	0.3	7.6	1.0	0.6	Trace	59.7

TABLE 2 Major element data for peridotites (by XRF, except * by INAA) and constituent minerals (by microprobe).

	Peridotites				Minerals		
	1	2	3	4	5	6	7
SiO ₂	44.62	45.55	47.34	45.76	53.3	41.2	51.1
TiO ₂	2.68	2.85	2.97	2.45	1.4	5.0	5.5
Al ₂ O ₃	5.00	4.96	5.06	6.31	0.0	5.7	0.1
Cr ₂ O ₃ *	0.19	0.18	0.17		0.3	0.1	0.1
ΣFeO	6.82	6.74	6.78	7.49	2.6	8.8	3.3
MnO	0.10	0.14	0.16				
MgO	20.40	18.65	17.29	22.31	17.1	22.9	20.7
NiO*	0.11	0.10	0.09				
CaO	3.51	3.67	2.88	1.56	24.4	0.0	6.3
Na ₂ O*	0.340	0.49	0.66	1.52	0.5	0.1	3.4
K ₂ O	4.31	5.18	5.71	6.30	0.0	10.1	5.6
P ₂ O ₅	0.72	0.78	1.00	0.28			
S	0.31	0.24	0.10	0.04			
Loss				4.38			
SUM	89.11	89.53	90.21	98.40	99.6	93.9	96.1
100 Mg	84.2	83.1	82.0	84.1	92.1	82.3	91.8
Mg+ΣFe							

1. SCP60; 2. SCP270; 3. SCP510; 4. Material from depth of 59.3 feet. Analysis from Franks et al. (1971); 5. Titanaugite in SCP70; 6. Titanphlogopite in SCP70; 7. Potassic richterite in SCP70.

Table 3. Trace element data (ppm)

	SCP60	SCP270	SCP510
La	167	172	184
Ce	341	356	374
Sm	14.1	14.6	15.5
Eu	3.93	4.20	4.36
Tb	1.15	1.35	1.17
Yb	1.50	1.52	1.60
Lu	0.21	0.19	0.23
Hf	17.2	18.6	18.8
Th	10.5	11.2	12.6
Ta	4.1	4.3	4.5
Sc	12.2	13.6	13.3
Co	56	53	51
Cr	1290	1260	1170
Ni	870	770	730

INAA

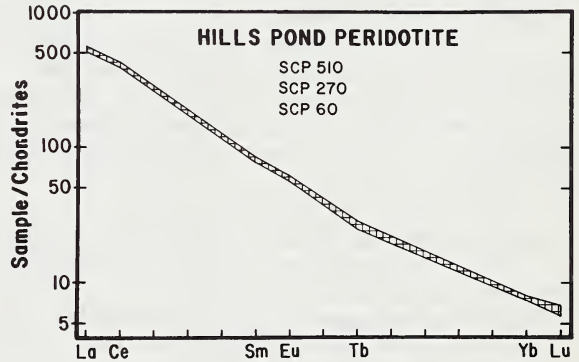


Fig. 2. Chondrite-normalized plot of REE data from Table 3.



Fig. 1. Distribution of kimberlites and alnöite in eastern North America (from Watson, 1967). Star marks Hills Pond Peridotite.

GREEN MOUNTAIN KIMBERLITE, COLORADO: MINERALOGY AND PETROLOGY.

Henry O.A. Meyer: Dept. of Geosciences, Purdue Univ.
West Lafayette, Indiana 47907
Stephen J. Kridelbaugh: Dept. of Earth Sciences, Lower
Columbia College, Longview, Wash. 98632

The Green Mountain diatreme, near Boulder, Colorado, is presently the most southerly occurrence of kimberlite in the Colorado-Wyoming region. It is approximately 100 miles south of the main field of diamond-bearing kimberlites described by McCallum et al. (1975). Tectonically it is similar in position to the northerly kimberlites in that it has intruded pre-cambrian Boulder granite. However, the original geometry of the intrusion has been modified subsequently by the Laramide orogeny. An attempt to date the intrusion using palaeomagnetic data proved ambiguous (Kridelbaugh et al., 1972) and it is most likely that this kimberlite is comparable in age with those of the State Line region which are supposedly Devonian.

The rock comprising the diatremes was first described by Whitaker (1902) who referred to it as an olivinite dike. Whitaker believed similar rocks occurred in a line 7 miles to the west and thus the idea of a dike was instituted. However, up to the present time no other occurrences of kimberlite have been verified to the west and the Green Mountain diatreme appears to be a single isolated body. It is relatively small, about 100 ft. in diameter and is completely enclosed by Boulder granite. The rock is dark in color and relatively hard, although some variations in petrographic type are obvious. Generally, the rock is characterized by large (<5cm) xenocrysts of emerald green diopside, as well as coal-black Mg-ilmenite and smaller xenocrysts of red-purple garnets (Table 1). The kimberlite varies from fine grained with few inclusions to coarser grained varieties containing phenocrysts of olivine and enstatite. These phenocrysts are partly serpentinized as are also the similar minerals of the groundmass, which includes mica, carbonate and opaque phases (Boctor and Meyer, 1977). Xenoliths of Boulder granite are common as well as samples of biotite gneiss, garnet granulites and related rock types. Presumably, these xenoliths represent basement sub-crustal rocks beneath the Boulder granite. Evidence for mantle xenoliths is not conclusive but possible altered fragments of eclogite and garnet-peridotite may have been observed.

The major silicate phase is olivine, often serpentinized, and this mineral occurs both as large phenocrysts and smaller ground mass crystals. Generally, the phenocrysts are more Mg-rich than those in the ground mass (Fo_{92} versus Fo_{84})

(Table 1). Pyroxenes occur as both clino- and orthopyroxene types. The orthopyroxene is usually comparable and associated with olivine in size and occurrence, and is enstatite (En_{91}). Hypersthene (En_{60}) has been recognized in samples of the granulite xenoliths. The clinopyroxene in the kimberlite is emerald green and appears as large xenocrysts having a relatively restricted compositional range (Mg_5 ; $Ca_{41}Fe_4$) and $Ca/(Ca+Mg)$ of about 0.43. Cr_2O_3 is present up to 1.6 wt% and is approximately equal to Al_2O_3 in content. Na_2O amounts to about 1.5 wt%. If these diopside xenocrysts are assumed to coexist with enstatite and garnet and to have equilibrated in the presence of these two phases then from the diopside-enstatite solvus one obtains a temperature of equilibration of about $1100^{\circ}C$.

Ilmenite occurs as large xenocrysts and also as smaller crystals in the ground mass. The xenocrystic ilmenites are Mg-rich with up to 13 wt% MgO. Chromium contents of these ilmenites are generally low, averaging about 0.4 wt% Cr_2O_3 (Table 1). Phlogopite mica is present and may occur as large crystals or be also scattered throughout the matrix. The mica appears to be characterized by containing up to 6 wt% TiO_2 (Table 1). Some biotite is also present but it is likely this is from diaggregated Boulder granite and from biotite gneiss xenoliths.

Garnets that occur in the Green Mountain kimberlite are either purple-red in color or dark orange. As in most kimberlites this feature is related to varying contents of Cr, Fe and Ca. However, all xenocryst garnets analyzed are typical of kimberlitic garnets. Other garnets analyzed during this study include samples from the garnet granulites as well as garnet in association with ilmenite. In this latter case the garnet is much more almandine-rich and the ilmenite is poor in Mg. Whether this assemblage is part of a xenolith is unknown.

References

1. Boctor, N.Z. and Meyer, H.O.A. (1977). These Abstracts.
2. Kridelbaugh, S.J.; Hobbitt, R.; Kellogg, K. and Larson, E. (1972). *Abst. Geol. Soc. Am. Program with Abst.*, 4, p. 386.
3. McCallum, M.E.; Eggler, D.H., and Burns, L.K. (1975). *Phys. Chem. Earth*, 9, 149-162.
4. Whitaker, M.C. (1902). *Colorado Sci. Soc., Proc.* 6, 104-118.

Table 1. Representative analyses of minerals from the Green Mountain diatrema, Boulder, Colorado.

Oxide	Olivine	Enstatite	Diopside	Ilmenite	Garnet	Garnet	Phlogopite
SiO ₂	42.6	56.9	54.0	-	41.1	42.4	36.2
TiO ₂	0.04	0.12	0.23	53.2	0.02	0.69	5.50
Al ₂ O ₃	0.02	0.65	1.63	0.49	18.2	21.0	15.0
Cr ₂ O ₃	0.02	0.21	1.43	0.43	5.6	1.08	<0.01
FeO	7.62	5.51	2.78	31.9	7.39	11.2	14.6
MnO	0.14	0.14	0.11	0.28	0.44	0.39	<0.01
MgO	51.2	35.3	18.5	12.4	19.9	19.6	14.5
CaO	0.01	0.89	19.3	0.02	5.97	4.18	<0.01
Na ₂ O	-	0.12	1.63	<0.01	<0.01	<0.01	0.11
K ₂ O	-	-	0.03	-	-	-	9.41
Total	101.6	99.8	99.6	98.7	98.6	100.5	95.3 (+OH)

ENSTATITE XENOCRYST CONTAINING COEXISTING Cr-POOR AND Cr-RICH GARNET, WELTEVREDEN FLOORS, SOUTH AFRICA.

Henry O.A. Meyer: Dept. of Geosciences, Purdue University,
Hsiao-ming Tsai: West Lafayette, Ind. 47907
John J. Gurney: Dept. of Geochemistry, University of Cape
Town, Rondebosch, South Africa

The genesis and depth of origin of the large xenocrysts of garnet, ilmenite, diopside and enstatite that occur in kimberlite is still a major problem with respect to petrologic models of the upper mantle. The relation of these xenocrysts to other kimberlitic minerals and the constituents of the ultramafic xenoliths is unknown. Of particular interest in this context was the discovery of a large (~20 cm) single crystal of enstatite (En_{88}) containing abundant Mg-ilmenite ($MgO \sim 12$ wt.%) and rarer polyphase garnet inclusions. This xenocryst was obtained from Weltevredden Floors near the present Frank Smith Mine, South Africa.

The polyphase garnet inclusions are unique in that they consist of two chemically distinct suites of minerals - one Cr-rich and one Cr-poor. The major garnet phase is orange in color and is predominantly pyrope-almandine ($Py_{71}Al_{21}Gr_8$) (Table 1,4) whereas inside this garnet is a second one that is pink and Cr-rich ($CrPy_{33}Py_{28}Al_{19}Gr_{20}$) (Table, 5). This inner chrome-pyrope garnet itself contains Cr-diopside, (Table 1,6) chromite (Table 1,9) and ilmenite. The enclosing orange almandine-pyrope contains rounded Mg-ilmenites (Table 1,3) at the boundary with the Cr-pyrope as well as elongated strings of both olivine (Fo_{86}) (Table 1,8) and another diopside (Table 1,7). The assemblage described above is shown diagrammatically in fig. 1. Within the enstatite host and in close association with polyphase garnet assemblage are calcite, Ti-phlogopite, and serpentine. These three phases are considered to be later than the original formation of the enstatite host.

The compositions of the host enstatite (Table 1,1) and the major ilmenite inclusions (Table 1,2) are comparable with similar minerals from xenocrysts at Frank Smith Mine (1). Interestingly, the association of this ilmenite with the host enstatite varies from irregularly dispersed blobs to crystallographically controlled lamellar intergrowths (2). Enstatite/ilmenite ratio is about 73:25 with polyphase garnet accounting for the remaining 2%. Using these values plus chemical composition and X-ray cell parameters (3) the density of this specimen is 3.61 ± 0.09 gm/cm³. This is important in as much as a value exceeds that of the ultramafic and eclogitic xenoliths and will have important geophysical implications with respect to seismic velocities. Furthermore, the relatively widespread occurrence of ilmenite-silicate xenocrysts should be now contrasted with the occurrences of eclogite in kimberlite.

Most of the minerals in the polyphase garnet inclusions can be matched compositionally with other minerals either from Frank Smith or other localities. Of interest, however, is the resemblance of the Cr-pyrope garnet and Cr-diopside with some mineral inclusions in diamond. This resemblance adds credence to the idea that diamond did not form in kimberlite as presently known but in an igneous process associated with some precursor of kimberlite whose chemistry is uncertain. It must be stressed that we are not here concerned with the eclogitic environment in which some diamonds are known to have formed.

Although it is likely the Cr-rich garnet and related suite represent the remnant of an earlier pre-existing rock that underwent considerable partial melting it must also be considered that the outer orange garnet may be metamorphic. However, irrespective of the origin, based on orthopyroxene geothermometry (1) and Al_2O_3 content (4) possible pressure and temperature of equilibration are in the region of 60 kb and 1200°C.

References

1. Boyd and Nixon (1973). "Lesotho Kimberlites", p. 254-268.
2. McCallister, Meyer and Brookins (1975). Phys. Chem. Earth, 9, 287-293.
3. Boyd and McCallister (1976). Geophys. Res. Letts., 3, 509-512.
4. MacGregor (1974). Am. Mineral., 59, 110-119.

Table 1. Average analyses of minerals in enstatite xenocryst, Weltevreden Floors (See text for numbers)

	1	2	3	4	5	6	7	8	9
SiO ₂	56.7	0.15	0.29	41.8	40.7	54.5	55.4	39.7	0.34
TiO ₂	0.23	53.5	49.8	0.96	0.71	0.33	0.40	0.05	7.70
Al ₂ O ₃	0.82	0.32	1.07	21.5	15.5	2.13	1.84	0.04	10.7
Cr ₂ O ₃	0.02	0.19	1.89	0.33	9.96	2.50	0.36	0.06	35.5
FeO	8.09	33.5	35.1	10.6	7.72	3.20	4.39	13.1	30.5
MnO	0.16	0.35	0.28	0.32	0.38	0.08	0.11	0.12	0.38
MgO	33.2	12.4	10.8	20.2	17.3	17.0	17.4	47.5	13.4
CaO	0.93	0.06	0.09	4.05	8.36	17.8	18.2	0.05	0.09
NiO	0.02	-	<0.01	<0.01	<0.01	0.06	0.02	0.07	<0.01
Na ₂ O	0.16	-	<0.01	0.12	0.10	2.06	1.82	0.03	<0.01
K ₂ O	0.01	-	<0.01	<0.01	<0.01	0.05	0.06	<0.01	<0.01
	100.3	100.4	99.3	99.9	100.6	99.7	100.0	100.7	98.6

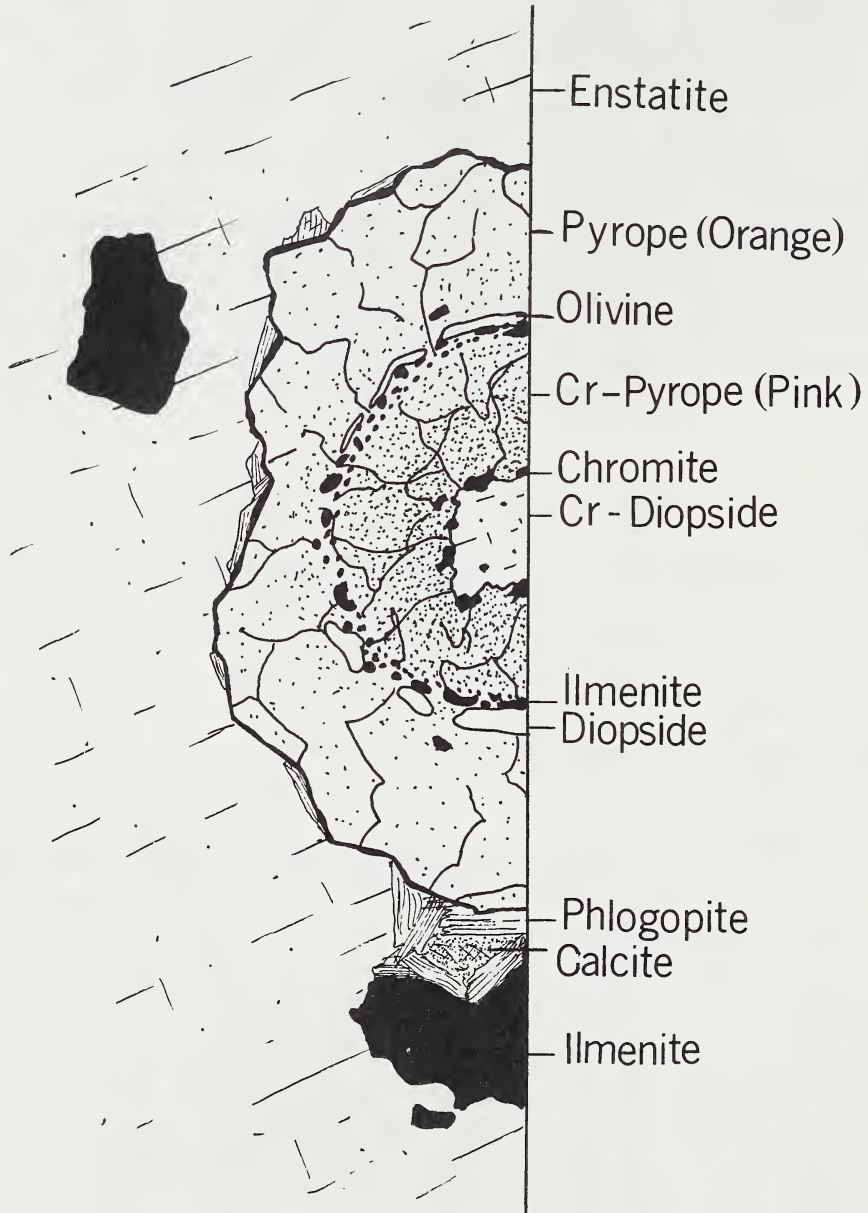


Figure 1. Garnet polyphase assemblage in enstatite xenocryst, Weltevreden Floors.

MINERAL INCLUSIONS IN DIAMOND: PREMIER, JAGERSFONTEIN AND
FINSCH KIMBERLITES, SOUTH AFRICA, AND WILLIAMSON MINE, TANZANIA

Henry O.A. Meyer (Dept. of Geosciences, Purdue University,
Hsiao-ming Tsai West Lafayette, Ind. 47907)

Jules Moreau (Lab. de Mineral., 3 Place L. Pasteur, Univ.
Catholique de Louvain, 1348 Louvain-la-Neuve, Belgium)

H. Judith Milledge (Dept. of Chemistry, University College
London, Gower St., London)

A major consideration with regard to inclusion research is the possibility of overall variation in inclusion type and mineralogy between different diamond-bearing localities. The answer to this and other questions related to inclusions should reveal the petro-chemical link between host kimberlite, associated xenoliths, and transported diamond.

We have undertaken a reconnaissance study of diamonds from four known localities: Premier, Jagersfontein, Finsch kimberlites, South Africa; and Williamson Mine, Tanzania. These localities were chosen because of availability of diamonds, difference in geographic locality and divergent differences in geologic age. Premier kimberlite is known to have been intruded in pre-cambrian times whereas the other kimberlites are phanerozoic. Also this was the first opportunity to sample inclusions from East African diamonds.

Overall the chemistry of inclusions from all four localities are similar to previously reported inclusions (1,2,3). For example, olivine, enstatite, garnet, clinopyroxene and spinel are all present (Table 1). However, as noted earlier (4) the inclusions may be subdivided into two distinct suites. One suite contains minerals that resemble the mineral assemblages in ultramafic xenoliths, whereas the other contains minerals comparable to those occurring in eclogite (Fig. 1).

Based on our limited sampling the Williamson Mine in particular is characterized by inclusions of the ultramafic suite. In contrast the diamonds from the Premier Mine contain fairly abundant pyrope-almandine and omphacitic diopside that are characteristic of eclogite. It appears that such minerals are more common in Premier diamonds than from any other locality. Whether this is due to the Pre-cambrian age of the pipe or otherwise is unknown. However, other diamonds which reached the earth's crust in Pre-cambrian times do not show this trait.

Of interest is the occurrence of two unusual pyrope garnets from Jagersfontein diamonds. These garnets appear transitional between the Cr-pyrope and eclogitic types and thus support the contention (5) of a sub-group of garnet inclusions. These garnets are much more akin to those from garnet lherzolite xenoliths. This could possibly indicate not two, but three chemical environments for diamond genesis.

With regard to this last point it should be noted that in general most unequivocal pre- or syngenetic inclusions do not resemble the present constituent minerals of kimberlite. The evidence at present, based on undeniable primary inclusions in that diamond does not form in kimberlite as presently defined but in some other preexisting chemical environments.

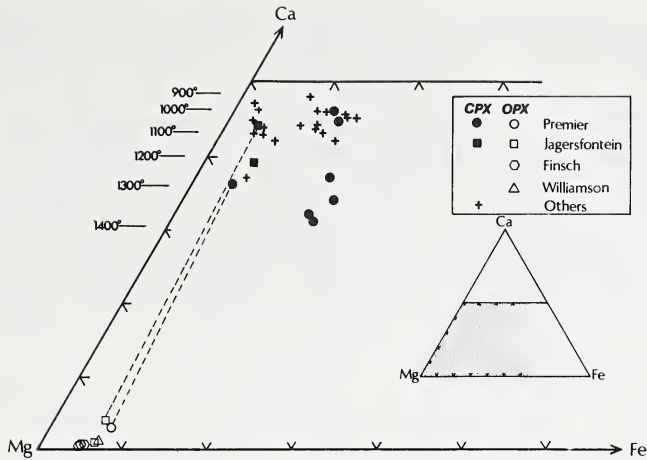
References

1. Meyer and Boyd (1972) *Geochim. Cosmochim. Acta*, 36, 1255-1273.
2. Sobolev, Botkunov, Lavrent'yev and Pospelova (1971) *Zap. Vses. Mineral. Obshch.*, 106, 558-564.
3. Meyer and Tsai (1976) *Mins. Sci. Engng.*, 8,
4. Meyer and Boyd (1968) *Carnegie Inst. Wash. Yrbk.*, 67, 130-135.
5. Harris and Gurney (1976) "Properties of Diamond". *Oxford Univ. Press.*, Oxford.

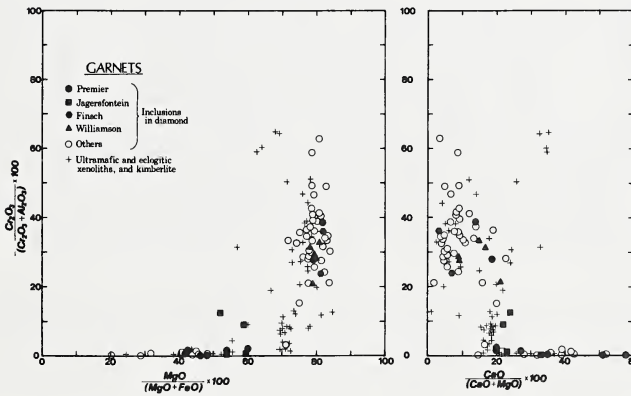
Table I. Representative analyses of inclusions in diamonds from Premier (P), Finsch (F), Jagersfontein (J) and Williamson (W) kimberlites.

Oxide	<u>Garnet</u>			<u>Clinopyroxene</u>			<u>Orthopy-</u>	<u>Chro-</u>	
	F	J	P	J	P	P	roxene	Olivine	mite
							F	W	F
SiO ₂	42.3	41.3	41.3	55.3	54.3	54.8	58.2	40.6	0.16
TiO ₂	0.04	0.71	0.31	0.04	0.94	1.23	<0.01	0.01	0.48
Al ₂ O ₃	16.7	19.4	22.4	2.39	7.43	0.89	0.46	<0.01	7.16
Cr ₂ O ₃	9.61	1.27	0.11	2.01	0.09	0.12	0.37	0.02	63.9
FeO*	5.46	12.8	14.7	1.95	8.18	9.21	3.64	7.24	10.7
MgO	25.2	18.2	13.5	16.2	12.5	16.6	37.0	51.6	14.7
CaO	0.69	5.28	7.35	19.2	12.1	14.0	0.24	0.04	0.05
NiO	<0.01	<0.01	<0.01	0.05	0.05	0.05	0.10	0.40	0.11
Na ₂ O	0.10	0.07	0.35	2.17	4.34	2.64	0.06	0.04	<0.01
K ₂ O	0.01	<0.01	<0.01	0.24	0.09	0.05	0.02	<0.01	<0.01
Total	100.2	99.0	100.0	99.5	100.0	99.6	100.1	100.0	97.3

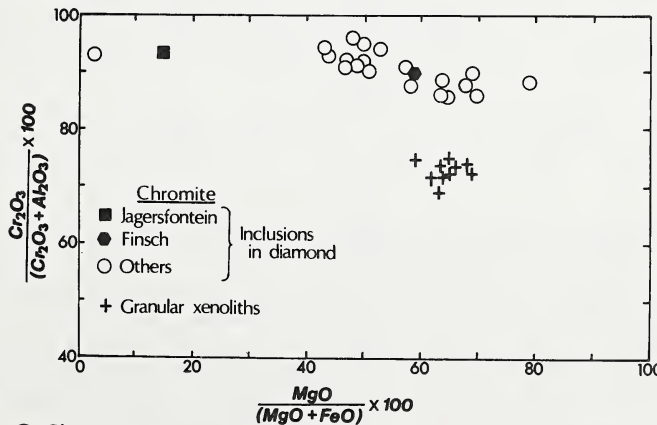
* All Fe reported as FeO



A. Pyroxenes



B. Garnets



C. Chromites

Fig.1. Mineral inclusions in diamonds from Premier, Jagersfontein, Finsch and Williamson mines.

Ol margin Fogg.

13 rutile + 2% Nb.

MINERALOGY OF THE TUNRAQ KIMBERLITE, SOMERSET ISLAND, N.W.T., CANADA
Roger H. Mitchell, Department of Geology, Lakehead University, Thunder Bay,
Ontario, Canada

The Tunraq kimberlite is the only occurrence of micaceous kimberlite within the Somerset Island kimberlite province (Mitchell, 1976). The diatreme is composed dominantly of kimberlite, this being cut by a composite dike of massive and fissile micaceous kimberlites. Megacrysts common to all phases of the intrusion are rutile, ilmenite and garnet. Rutile is a niobian ($0.18-2.0\% \text{Nb}_2\text{O}_5$), chromian ($0-4\% \text{Cr}_2\text{O}_3$) variety unlike the low Nb and low Cr rutiles found in diamonds and eclogites. Ilmenites are magnesian ($8.4-17.5\% \text{MgO}$), the most magnesian types occurring as mantles upon rutile. Individual megacrysts are moderately ($2\% \text{MgO}$) to weakly ($0.2\% \text{MgO}$) zoned in an irregular fashion. Compositional trends are interpreted to be from high to low MgO with increasing Fe_2O_3 . No correlation of Cr_2O_3 with MgO ($r=0.3$) is evident and no "parabolic relationship" between these elements as described by Haggerty (1975) is present. Garnets occur as rounded megacrysts up to 1 mm., in diameter and fall into 3 compositional groups using the statistical classification of Dawson and Stephens (1975) i.e. group 1 (34%), group 2 (3%), group 9 (63%). Group 9 is bimodal and contains a group of high Cr_2O_3 ($>2.5\%$) garnets derived by fragmentation of ultrabasic xenoliths, all other garnets are considered to be true phenocrysts. Groups 1 and 2 garnets are a characteristic phenocryst in other kimberlites e.g. Frank Smith, Artur de Paiva, Sloan. Similar garnets in the nearby Elwin Bay monticellite-kimberlite are dominantly group 2 garnets. Garnet compositions indicate that subtle differences are present in the nature of the garnet suites between individual diatremes in the same kimberlite province, and that they are unlikely to be xenocrysts.

Mica is present only as phenocrysts, of prefluidization origin. No compositional differences exist between micas in the different facies and little range ($0.87-0.92$) in the Mg/Mg+Fe ratio occurs. High ($>2\%$) TiO_2 contents are characteristic. The evolutionary trend is considered to be towards decreasing TiO_2 and Cr_2O_3 . $\text{TiO}_2 < 6\%$ but 1. non serjor.

Olivine occurs, as in other kimberlites, in two generations. Early prefluidization phenocrysts are essentially homogeneous, $\text{Fo}_{92}-\text{Fo}_{90}$ with thin iron enriched margins ($\text{Fo}_{90}-\text{Fo}_{88}$). Groundmass olivines are weakly zoned from $\text{Fo}_{92}-\text{Fo}_{87}$. Reverse zoning rarely occurs (Fo_{86} to Fo_{88}). No difference in olivine compositions in the different facies is evident. Olivines are extensively replaced by iron rich ($10\% \text{FeO}$) serpentine.

Spinel is all post-fluidization euhedral groundmass spinels. Each facies of the diatreme has a distinct spinel assemblage. Spinel crystallization in the kimberlite commenced with relatively uncommon Al_2O_3 poor aluminous magnesian chromites (AMC; $11-14\% \text{Al}_2\text{O}_3$, $<1\% \text{TiO}_2$) and evolved to rare titaniferous-magnesian-aluminous chromite (TIMAC, $2-3\% \text{TiO}_2$; $10-11\% \text{Al}_2\text{O}_3$) to abundant titaniferous magnesian chromite (TMC, $2-8\% \text{Al}_2\text{O}_3$; $1-15\% \text{TiO}_2$) and eventually to magnesian ulvospinel-ulvospinel-magnetite (MUM; $16-20\% \text{TiO}_2$). The compositional trend is one of increasing Fe^{3+} and Ti at approximately constant Fe/Fe+Mg as illustrated in figure 1.

Massive micaceous kimberlite initially crystallized TMC identical to the

early spinels of the kimberlite but the trend towards Ti enrichment at constant Fe/Fe+Mg does not exceed 3% TiO₂, therefore members of the MUM spinel series are not developed. Spinel richest in TiO₂ (6-7%) are unusual in being Al and Mg poor titaniferous chromites with Fe/Fe+Mg > 0.8. The most abundant spinel is a Ti-free magnetite. The titaniferous chromite and lack of MUM indicate that in this facies spinels were rapidly depleted in Al and Mg, a trend along the axis of the spinel prism (figure 1).

The fissile micaceous kimberlite initially crystallized TMC with greater than 7% TiO₂ which evolved into members of the MUM series. The trend is identical to that of the kimberlite, and Ti-free magnetite is absent (except pseudomorphing olivine) as a primary spinel phase in both of these facies.

Spinel compositional trends are in general similar to those determined for other kimberlites (Haggerty, 1975; Mitchell and Clarke, 1976) as illustrated in figure 1 where the Tunraq spinel trend is compared with that of the Peuyuk kimberlite and a preliminary trend for the Kirkland Lake, (Ontario) micaceous kimberlite.

The mineralogy and petrology of the Tunraq kimberlite indicates that the phases which are common to all three facies and which crystallized in the mantle are rutile, ilmenite, pyrope and olivine. With decreasing pressure as the magma ascends pyrope and ilmenite cease to crystallize and phlogopite replaced garnet as the aluminous liquidus phase in the lower crust and uppermost parts of the mantle. This crystallization sequence is very different to that deduced for the Elwin Bay and Peuyuk kimberlites (Mitchell and Clarke, 1976, Mitchell, 1978) in which AMC and TIMAC spinels are abundant, ilmenite is absent or insignificant and in which only minor phlogopite is formed. The studies of the Somerset Island kimberlites demonstrate that each diatreme exhibits both subtle and gross differences in its pre and post-fluidization history and that the observed evolutionary trends are established in the mantle, those trends being merely emphasized in the lower crust and post-fluidization history. The trends must reflect different degrees of partial melting and/or high pressure differentiation. Although the Tunraq facies which is poor in modal mica is referred to here as kimberlite, the Al₂O₃ deficiency in the spinels and lack of AMC and TIMAC indicates that even this facies should be termed "micaceous kimberlite".

REFERENCES

- Dawson, J.B. and Stephens, W.E. (1975): Statistical classification of garnets from kimberlite and associated xenoliths. *Journal of Geology* 83, 589-607.
- Haggerty, S.E. (1975): The chemistry and genesis of opaque minerals in kimberlite. *Physics and Chemistry of the Earth*, 9, 295-307.
- Mitchell, R.H. (1976): Kimberlites of Somerset Island, District of Franklin. *Geological Survey of Canada Paper* 76-1A, 501-502.
- Mitchell, R.H. (1978): Mineralogy of the Elwin Bay kimberlite Somerset Island, N.W.T., Canada. Submitted to *American Mineralogist*.
- Mitchell, R.H. and Clarke, D.B. (1976): Oxide and sulphide mineralogy of the Peuyuk kimberlite, Somerset Island, N.W.T., Canada. *Contribution to Mineralogy and Petrology*, 56, 157-172.

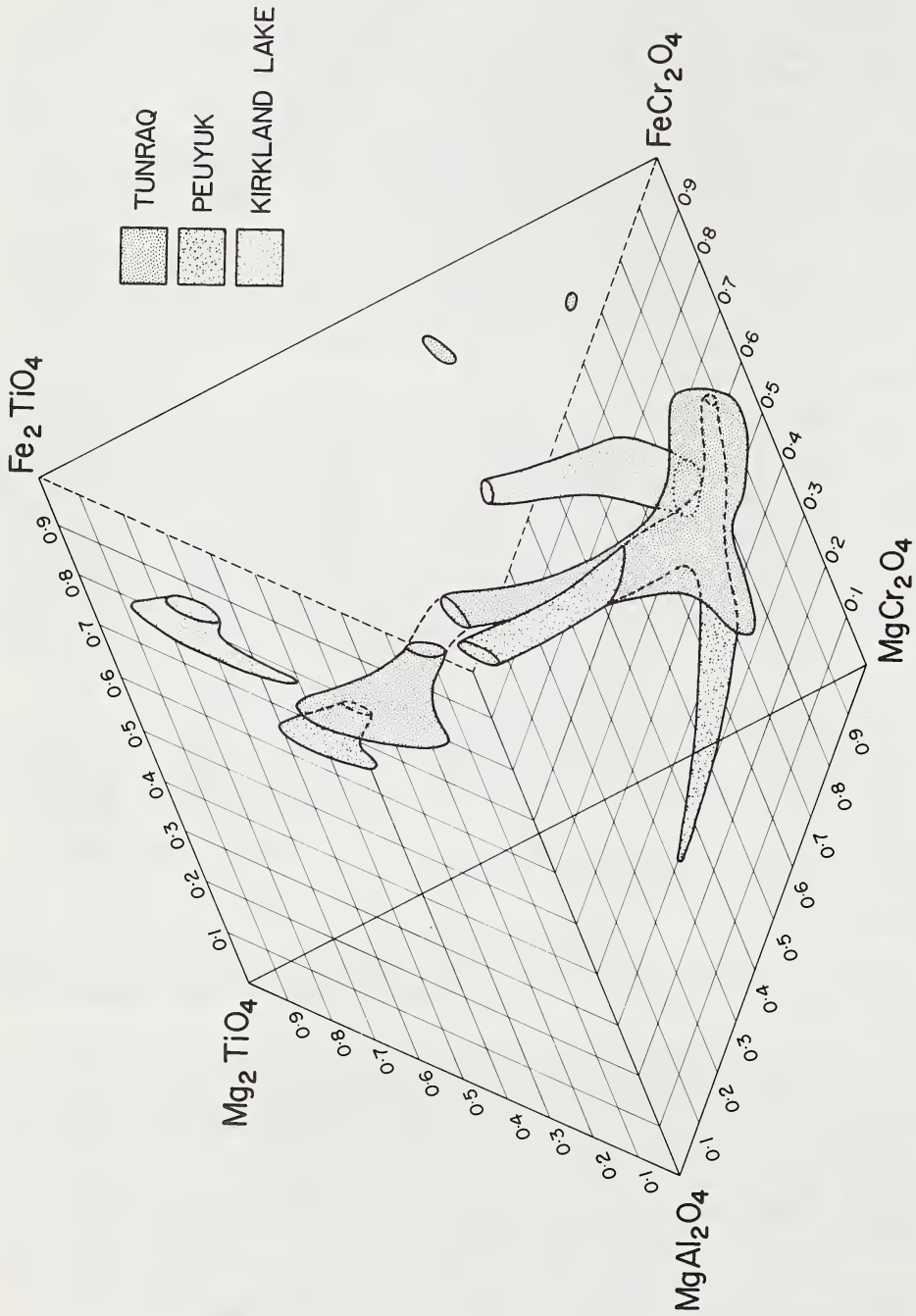


Figure 1. Composition of kimberlite spinels plotted in a reduced iron spinel prism.

OLIVINE COMPOSITIONAL COMPLEXITY IN OLIVINE MELILITITES FROM NAMAQUALAND, SOUTH AFRICA, AND ITS BEARING ON KIMBERLITE GENESIS.

A.E. Moore, Dept. of Geology, University of the Western Cape, Bellville, S.A.

A.J. Erlank, Dept. of Geochemistry, University of Cape Town, Rondebosch, S.A.

A microprobe investigation of the olivines in a suite of olivine melilitites from Namaqualand, South Africa (previously described by Moore, 1973) reveals a complex and unusual pattern of chemical variation. Fig. 1 illustrates $Mg/(Mg + Fe^{2+}) - Ni$ relations defined by olivines from three thin sections cut from one rock specimen (Dik-9, 12.6% MgO). Petrographic and chemical criteria make it possible to distinguish three distinct olivine sub-populations in this and other samples studied:

(a) The first suite consists of the dominant (95% of all olivines) population of euhedral (and sometimes skeletal) olivines that will be termed "hoppers" as they bear a striking resemblance to the growth forms described by Donaldson (1976), with sharply defined crystal edges and corners in contrast to the rounding that would be expected from resorption processes. Some of the olivines enclose groundmass minerals that have apparently crystallized from trapped liquids, which would seem most likely to have been included during rapid crystal growth. Hopper morphology is best developed in the Mg-poor volcanics, possibly reflecting compositional control on growth forms. The interiors of the hoppers define a compositional trend of decreasing Mg/Fe with decreasing Ni, while the olivine margins are characterized by a narrow (100 μ m) rind that shows continued Ni depletion, but strong reversed zoning with respect to Mg/Fe together with marked Ca-enrichment. The margin compositions correspond to those of late-crystallizing olivine microphenocrysts, and apparently reflect equilibration of the hopper margin in response to late-stage changes in the magma composition or conditions of crystallization. Although the hoppers dominate the phenocryst population in all samples studied, major and trace element variations in bulk-rock compositions cannot be explained by crystal fractionation of hopper type olivines. (Moore, Ph.D. thesis (in preparation).

(b) The second suite consists of ragged anhedral with undulose extinction and compositions (Fo_{91} , 0.40%NiO), that fall within the range found for presumed mantle olivines. Such individuals are only common in one of the pipes studied, and this pipe is unusual in having numerous ultrabasic inclusions - mainly dunites (Fo_{92} , 0.40%NiO), but also rare garnet lherzolites which appear to have equilibrated at 38Kb and 960°C. (Moore, 1973). This second olivine groups is excluded from further discussion since we believe that they are probably of exotic origin.

(c) The third suite consists of rare anhedral or subhedral olivines that are enriched in Fe and Mn (>1%MnO in some individuals) and markedly depleted in Ni relative to the remaining olivines in the same rock specimen. We have given these the name of high iron, low nickel (HILN) olivines. Marginal zonation analogous to that displayed by the hoppers results in HILN edges being enriched in Mg and Ni relative to the cores. (Note that the hoppers have margins relatively enriched in Mg but depleted in Ni.) Representatives of the HILN suite can be distinguished petrographically by their relatively large size, absence of marked undulose extinction and by the presence of fluid inclusions about their margins and in trains (presumably representing annealed fractures) that traverse the olivine interiors. Data from a range of specimens indicates that $Mg/(Mg + Fe^{2+})$ of the HILN olivines varies sympathetically with that of the bulk rock, which, together with the subhedral outline of some of the HILN olivines would indicate that they are true phenocrysts and not accidental inclusions.

Since we believe that both HILN and hopper olivines are phenocrysts from the same magma we must suggest appropriate processes to explain their radically different compositions.

On the basis of their morphology and restricted occurrence we have made the assumption that the HILN olivines crystallized before the hopper olivines, and thus that they crystallized from a magma which did not have unusually low Mg or Ni content (in view of the hopper compositions). It is also unlikely that the HILN composition results from low Ni^{++} distribution coefficients since the high temperatures (Leeman, 1974) or high MgO contents (Hart, 1976) necessary to achieve this would result in the crystallization of a more magnesian olivine. We therefore suggest that the peculiar compositional characteristics of the HILN olivines reflect crystallization at low oxygen activities, significantly below the Ni/NiO buffer but above the Fe/FeO buffer. Crystallization of these olivines at low fO_2 would result in high Fe^{2+}/Fe^{3+} , Mn^{2+}/Mn^{3+} and Ni^0/Ni^{2+} ratios in the magma thus producing high Fe and Mn combined with low Ni in the olivines crystallizing in equilibrium with such a liquid.

The crystallization of hopper olivines could take place at higher fO_2 (above Ni/NiO) giving rise to substantially higher Mg/Fe ratios and higher Ni contents in the olivines crystallizing under these conditions. The Mg and Ni enriched rims surrounding the HILN olivines may reflect partial re-equilibration under the new fO_2 conditions, or may be overgrowths under these conditions.

The trend of decreasing Mg/Fe ratio and decreasing Ni content in the cores of the hopper olivines is seen as a response to falling temperature and the progressive removal of Ni by Rayleigh-type crystallization. The reversed-zoned hopper margins may reflect extensive crystallization of Fe-Ti oxide phases or extreme late-stage oxidation of the magma.

Having suggested major changes in fO_2 during the crystallization of the olivine melilitite magma, let us now consider a possible explanation for this crystallization path. Recent experimental studies, for instance Brey and Green (1977) have stressed the importance of CO_2 in the generation of olivine melilitites. It therefore seems plausible that a gas buffer involving CO_2 may have initially maintained the olivine melilitite magma at low oxygen fugacities close to or on the carbon saturation surface. Equations summarized by Heubner (1971) indicate that the carbon - gas buffer will be below the wustite - magnetite buffer, and thus well below the Ni/NiO buffer at high pressures and temperatures (10 - 50Kb, 1000 - 1300°C). Under such conditions, a_{NiO} in the liquid will be held at low values and metallic Ni will be formed, while Fe^{3+}/Fe^{2+} and hence Mg/Fe²⁺ ratios will be relatively low. These conditions of low oxygen activity are considered responsible for the compositional characteristics of the HILN olivines. Ilmenite is a rare phase in the olivine melilitites and may similarly have crystallized from such a strongly reduced magma.

Reduction in pressure and loss of volatiles during magma ascent would be expected to lead to a dramatic increase in oxygen activities and hence in Ni^{2+}/Ni^0 , Fe^{3+}/Fe^{2+} and Mg/Fe²⁺ ratios in the melt. Furthermore, liquidus temperatures would increase, and we suggest that the result would be the rapid crystallization of the relatively Mg and Ni enriched hopper olivines and HILN rims. The marginal fluid inclusions in the HILN olivines may reflect the onset of volatile loss.

Various authors (e.g. Taljaard, 1936; Yoder, 1975) have implied a close genetic relationship between olivine melilitites and kimberlites, and it is therefore possible that kimberlite mineralogy may reflect the effects of exterior oxygen fugacity control. Low fO_2 in kimberlite magmas would strongly affect Cr^{2+}/Cr^{3+} ratios which could account for the crystallization of phases such as chromium-rich ilmenite. In addition, Haggerty (1975) has described some reversed-zoned ilmenites with complex reaction rims which he ascribed to changing fO_2 conditions, and Gurney, Jakob and Dawson (this volume) describe discrete megacrysts from the Monastery Kimberlite, some of which may well prove to be the equivalents of our HILN olivines.

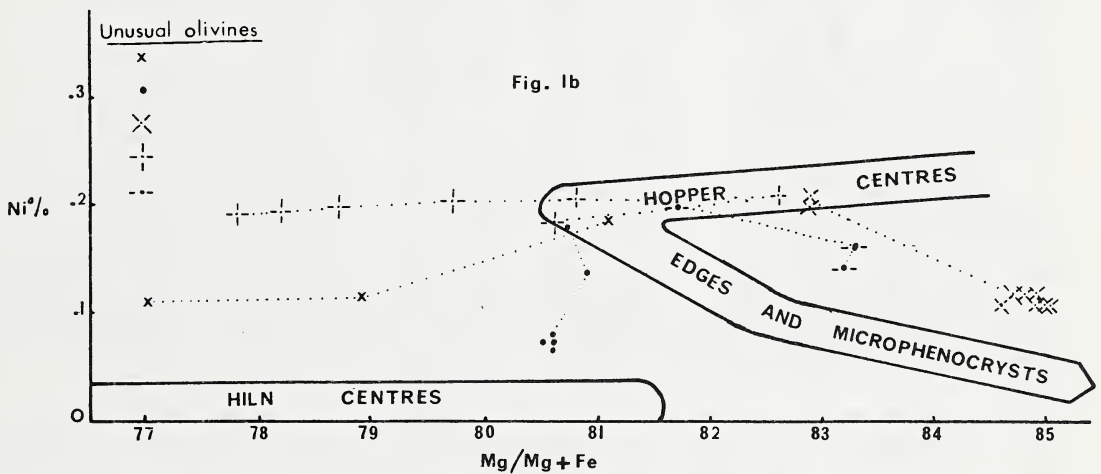
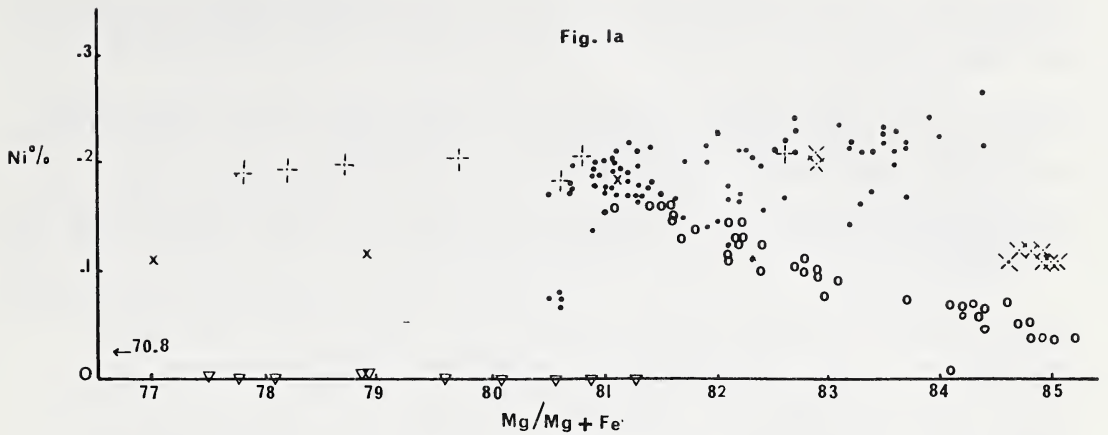


Fig 1 (a) Plot of all olivine analyses from sample DiK-9. Inverted triangles: HILN olivines; Solid dots: Hopper interiors; Open circles: edges and microphenocrysts. Remaining symbols are traverses across three olivines with unusual compositional zonation.

Fig 1 (b) Diagrammatic representation of the fields for HILN, hopper and groundmass olivines. Dotted lines connect points from traverses across olivines with unusual zonation towards hopper centres and edge compositions.

- Brey, G. and Green, D.H. (1977) *Contrib. Min. and Pet.* 61, p. 141.
 Donaldson, C.H. (1976) *Contrib. Min. and Pet.* 57, p. 187.
 Gurney, J.J., Jakob, W.R.O. and Dawson, J.B. (this volume).
 Haggerty, S.E. (1975) *Phys. and Chem. of the Earth*, vol. 9, p. 295.
 Hart, S.R., Davis, K.E., Kushiro, I. and Watson, B.E. *G.S.A. Abs.* 8 (6) p.906.
 Heubner, J.S. (1971) In Ulmer, G.C. (ed.) *Research techniques for high pressures and high temperatures*, p. 123 (Springer Verlag).
 Leeman, W.P. (1973) *Trans. Am. Geoph. Union* 54, p. 1222.
 Moore, A.E. (1973) *Extended Abstracts, 1st Int. Kimberlite Conf.*, Cape Town.
 Taljaard, M.S. (1936) *Trans. Geol. Soc. S.A.* 39, p. 281.
 Yoder, H.S. (1975) *Phys. and Chem. of the Earth*, vol. 9, p. 883.

EXPERIMENTAL STUDIES OF DIFFUSION OF WATER IN CRYSTALLINE PERIDOTITE AND PARTITIONING OF SOME TRACE ELEMENTS BETWEEN WATER-RICH VAPOR AND CRYSTALS IN THE UPPER MANTLE

Bjørn O. Mysen (Geophysical Laboratory, Carnegie Institution of Washington, 2801 Upton Street, N. W., Washington, D. C. 20008)

Ikuo Kushiro (Geological Institute, University of Tokyo, Hongo, Tokyo 113, Japan)

Toshitsugu Fujii (Geological Institute, University of Tokyo, Hongo, Tokyo 113, Japan)

Striking features of peridotite nodules sampled by kimberlite are porphyroblasts of phlogopite and richterite (e.g., Aoki, 1974) and large enrichments of light REE. Chondrite-normalized heavy REE contents are frequently less than unity (Shimizu, 1974). The enrichment of incompatible trace elements is particularly striking in light of the depletion of low-temperature fusible components in many of these nodules (Nixon and Boyd, 1973). These observations point to the possibility that metasomatism is a viable process in the segments of the upper mantle that are associated with formation and evolution of kimberlite. Experiments have been conducted, therefore, to determine diffusion rates of volatiles and the distribution of certain trace elements between such volatiles and crystalline peridotite.

Water was chosen as a first approximation to the composition of a volatile phase in the mantle. The diffusion rate of H₂O was determined by spiking H₂O with some ³H (activity ~1 mCi/mg). This H₂O was stored in synthetic serpentine which was loaded in the bottom of 1 cm long Au capsules and run in 3/4"-diameter furnace assemblies in a solid-media, high-pressure apparatus (Kushiro, 1976). The serpentine was overlain by powdered, dried garnet peridotite of about 100 μm grain size. The samples were annealed at 400°-425°C and desired pressure for a time period sufficient so that the diffusion rate was independent of the annealing time. During this time period, some serpentine broke down. The H₂O thus released migrated through the peridotite and coated the olivine grains in the peridotite with serpentine. About 1-2% serpentine was formed in the peridotite during this time period. At the temperatures of the experiments (650°-850°C) most of the serpentine broke down, and a front of water-rich vapor moved through the slightly serpentinized peridotite making amphibole in the process. The distance traveled by the tritiated water was determined with the help of beta-track mapping (Mysen and Seitz, 1975) by measuring the distance (on K-2 nuclear emulsions supplied by the Ilford Co.) from the serpentine-peridotite interface to the level in the experimental charge beyond which only the original serpentine was found. The latter interface is sharp (<0.01 mm wide) making such measurements rather accurate. Results of replicate experiments and measurements indicate about 10% relative uncertainty.

Experiments with different run lengths at given temperature and pressure reveal that diffusion rate of H₂O is independent of run time thus suggesting that the water is moving by infiltration. Experiments were carried out in the pressure range 15-30 kbar. The results show that the diffusion rate depends strongly on pressure, and is a nearly linear function of f_{H_2O} (Fig. 1). It is also evident that the diffusion rate is on the order of several mm/hr under the pressure and temperature conditions of the upper mantle.

Partition coefficients, $K^{\text{vapor/crystal}}$, were determined for cpx and ga in equilibrium with H₂O-rich vapor at 20 kbar at 1100°C using 4 day run durations and determining Sm and Tm contents of the crystalline phase with ¹⁵¹Sm and ¹⁷¹Tm as source of beta particles. Initial experiments were conducted with crystals together with vapor that contained radioactive tracer. A split of crystals after such an experiment was then run together with a vapor containing no radioactive isotope. The trace element content of the vapor was determined with mass balance calculations. Reversal experiments agreed within 10-20%. Average values of partition coefficients from reversal runs were used. Partition coefficients involving light REE and other peridotite phases were calculated from the data of Mysen (1977). Results are shown in Table 1.

TABLE 1. Partition coefficients

	Cerium	Samarium	Thulium
Garnet	120 ± 30	2.5 ± 0.6	0.9 ± 0.2
Clinopyroxene	27 ± 6	13 ± 3	21 ± 5
Orthopyroxene	160 ± 40	160 ± 40	120 ± 30
Olivine	380 ± 90	360 ± 80	320 ± 70
Pargasite	220 ± 50	110 ± 20	140 ± 30

It is evident from the data in Table 1 that a water-rich vapor in equilibrium with garnet peridotite minerals will be enriched in light REE relative to the peridotite. Furthermore, REE partition strongly into the H₂O-rich vapor relative to the crystals.

The experimental data reported here show that metasomatism in the mantle is a possible mechanism for redistribution of trace elements. The data therefore support an hypothesis that such a mechanism plays a role in determining the mode of formation and evolution of kimberlite.

References

- Aoki, K., 1974, *Contr. Mineral. Petrol.*, 48, 1-7.
 Kushiro, I., 1976, *Carnegie Instn. Washington, Year Book* 75, 832-833.
 Mysen, B. O., 1977, *Ibid.*, 76. In Press.
 Mysen, B. O., and Seitz, M. G., *J. Geophys. Res.*, 80, 2627-2635.
 Nixon, P. H., and Boyd, F. R., 1973, p. 48-56 in *Lesotho Kimberlites* (ed.: P. H. Nixon). Cape and Transvaal Printers Ltd., Cape Town, South Africa. 350 pp.
 Shimizu, N., 1974, *Carnegie Instn. Washington, Year Book* 73, 954-961.

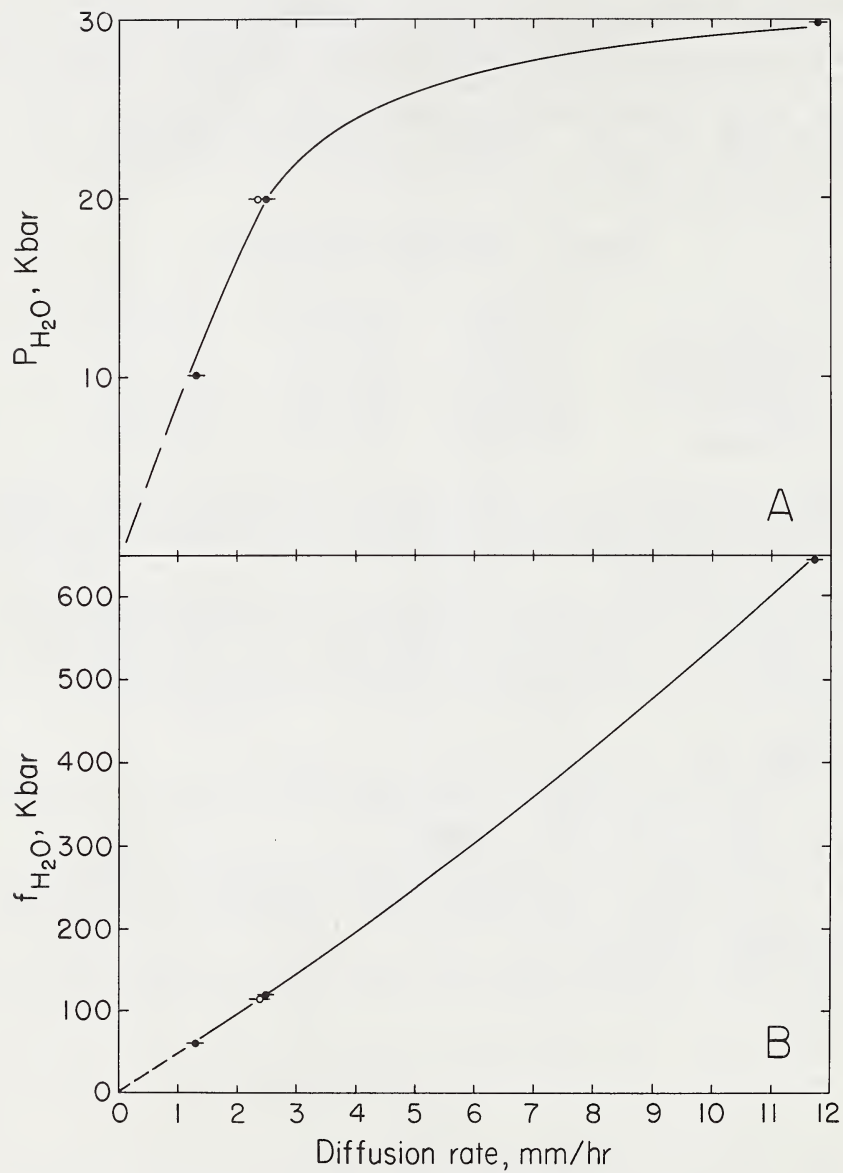


Figure 1. Diffusion rate of H_2O as function of P_{H_2O} and f_{H_2O} .
 Closed symbols - $850^\circ C$.
 Open symbols - $650^\circ C$.

FISSION-TRACK DATING OF KIMBERLITIC ZIRCONS

- C. W. Naeser (U.S. Geological Survey, Box 25046, Denver Federal Center, Denver, Colorado)
M. E. McCallum (Colorado State Univ., Fort Collins, Colorado and U.S. Geological Survey, Denver, Colorado)

Zircons separated from the matrix of kimberlite pipes can be dated by the fission-track method. The zircon fission-track age represents the last time the zircon cooled below approximately 200°C. In the case of a rapidly cooling kimberlite, it should date the time of emplacement, provided it was emplaced high in the crust where the temperature was less than 200°C.

Zircons from six kimberlite pipes have been dated with the fission-track method. One sample is from the Schaffer 3 pipe in Wyoming, and the other five are from African kimberlites (table 1).

Six small (0.1-mm) zircons from the Schaffer-3 pipe have an average age of 377 ± 9 m.y. ($\pm \sigma$). This age is compatible with the post-Silurian and pre-Pennsylvanian age estimated on geologic grounds for the Colorado-Wyoming kimberlites.

The zircons from the five African localities are splits of large crystals that were dated by the U-Pb method (G. L. Davis, written commun., 1977). Zircons from these five pipes have the following fission-track ages: Bultfontein (57.7 ± 7 m.y.), Monastary (60.9 ± 7 m.y.), Platbakkies (59.0 ± 2 m.y.), and Finsch (71.1 ± 4 m.y.), all in South Africa, and Nzega (54.3 ± 7 m.y.), in Tanzania. Four of these fission-track ages are considerably younger (about 30%) than the U-Pb ages, whereas at Platbakkies the fission-track age is only 12% younger than the U-Pb age.

At the present this discordance is unexplained. It could be the result of thermal track fading, or possibly some pre-emplacement history recorded in the U-Pb system.

Table 1. Fission-Track Data for Six Kimberlitic Zircon Samples

Sample	$\rho_s \frac{1/}{\times 10^6}$ t/cm ²	$\rho_i \frac{2/}{\times 10^6}$ t/cm ²	$\frac{3/}{\emptyset}$ $\times 10^{15}$ n/cm ²	T $\times 10^6$ yr	$\frac{+2\sigma}{\bar{x} \times 10^6}$ yr	U ppm
Schaffer 3 (Wyo.)	30.4	8.95	1.86	377	19	150
Bultfontein (S. Africa)	.271	1.094	3.82	57.7	11	8.7
Monastery (S. Africa)	.344	1.30	3.77	60.9	7.7	10
Finsch (S. Africa)	1.51	4.99	3.85	71.1	3.7	39
Platbakkies (S. Africa)	11.16	12.02	1.04	59.0	2.7	350
Nzega (Tanz.)	.149	.635	3.80	54.3	8.7	5.1

$$\lambda_F = 6.85 \times 10^{-17} \text{yr}^{-1}$$

$\frac{1/}{P_s}$ = number of fossil track per cm²

$\frac{2/}{P_i}$ = number of induced track per cm²

$\frac{3/}{\emptyset}$ = neutrons/cm²

LHERZOLITE-BEARING LAVAS AND THE NATURE OF THE UPPER MANTLE BENEATH BRITISH COLUMBIA, CANADA

J. Nicholls (Dept. of Geology, University of Calgary, Calgary, Canada T2N 1N4)
M.Z. Stout (Dept. of Geology, University of Calgary, Calgary, Canada T2N 1N4)

Quaternary volcanic activity has produced scattered cinder cones and lava flows between the Snake River Plain, U.S.A. and the British Columbia-Yukon border; a region 2000 km long and 500 km wide (Fig. 1). The rock types are alkali olivine basalts, basanites, trachybasalts, ankaramites, nephelinites and iron-rich lavas lacking pyroxene. The basalts and trachybasalts are strikingly similar in chemistry to rocks from the mid-Atlantic islands (Fig. 2). Associated with the lavas are xenoliths of lherzolite and gabbro and xenocrysts of plagioclase, olivine, and augite. The lherzolites are confined to the basalts, basanites, and nephelinites, indicating that these rocks represent melts which have come from the mantle with little or no modification.

Geophysical data provide an estimate of 30 to 50 km for the crustal thickness beneath the region (Fig. 1) with the low velocity zone near the Moho. These data indicate a minimum pressure of 15 to 25 Kb in the source region of the magmas.

The lherzolite xenoliths are remarkably uniform in mode, mineral chemistry (e.g. Fo 90 - Fo 92; see also Fig. 3) and texture across the entire region. In contrast the mantle-derived lavas show a range in chemistry which is reflected in the diversity of rock types (Fig. 2 and 4). One interpretation of these data is that the lherzolite xenoliths represent samples from a uniform layer or lid to the mantle whereas the lavas represent melts from the slightly deeper low velocity zone; the diversity in composition of the lavas being the result of either different degrees of partial melting of a uniform source or the result of melting of source materials of different compositions.

Given a source of uniform composition (e.g. pyrolite) the maximum amount of partial melting can be calculated (Fig. 5). The residua from these postulated melting episodes can then be recalculated as equilibrium lherzolite mineral assemblages. Finally, the P-T conditions for equilibrium between melt and residual mineral assemblage can be calculated. With pyrolite as the postulated source material, the results of the calculations are: 1) Maximum amounts of partial melting range between 4% and 20%; 2) The residua from the partial melting episodes would be non-uniform in composition; and 3) The melts, with rare exceptions, could not have been in equilibrium with these residua at the pressures prevailing near the top of the mantle.

Given a pressure and temperature, the composition of the olivine that would be in equilibrium with each melt can be calculated. With pressures estimated from the geophysical data and assuming a temperature of 1400°C, the calculated range in residual olivine compositions is Fo 77 to Fo 91 (Fig. 6); a range much greater than that of the xenolith olivines. One interpretation of these calculations is that the source materials for the lavas were not uniform in composition in the mantle beneath British Columbia.



Fig. 1: Recent volcanic centres studied and depths to the Moho in British Columbia and adjacent U.S.A. Circles are studied volcanic centres and squares are locations of Moho depth determinations in km. Present plate boundaries shown for reference.

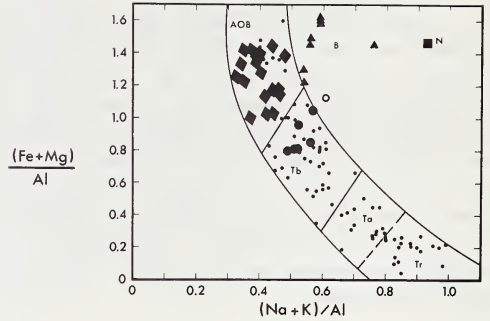


Fig. 2: Molecular $(Fe + Mg)/Al$ versus $(Na + K)/Al$ for rocks from North America and Atlantic Islands. Small dots are the Tristan da Cunha and Gough Island basalt-trachyte series. Large symbols this study: Filled diamonds-alkali olivine basalt; filled circles-trachybasalts; filled triangles-basanites; filled square-nephelinite; and open circle-iron-rich alkali olivine basalt.

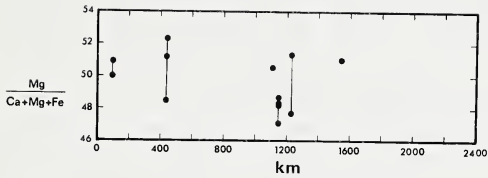


Fig. 3: Mg/(Mg+Ca+Fe) in clinopyroxenes from spinel lherzolites. Location of occurrences projected into a NW-SE section from NW British Columbia to SE Idaho. Distance along section in km.

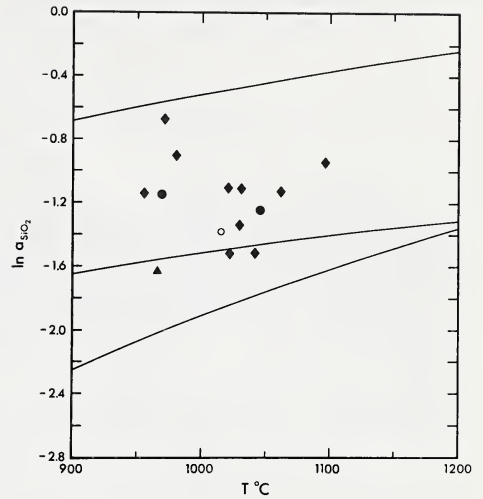


Fig. 4: Natural logarithm of silica activity versus temperature. Curves are defined by the reaction relations: Upper curve—forsterite, enstatite; Middle curve—albite, nepheline; Lower curve—sphene, perovskite. Tholeiites and associates plot above forsterite-enstatite; Alkali olivine basalts and associates below. Nepheline-bearing rocks fall near and below the middle curve. Feldspar-free rocks below lower curve. Symbols as in Fig. 2.

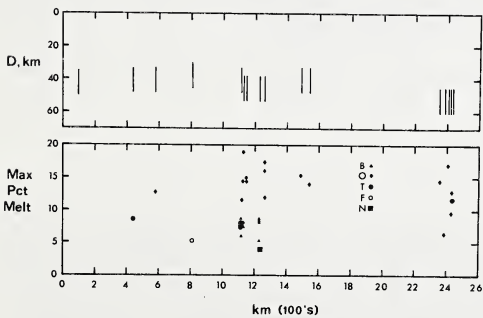


Fig. 5: Upper diagram. Depths to Moho and estimated minimum depths to low velocity zone (lower end of lines). Lower diagram. Maximum amounts of partial melting of a uniform pyrolite source which can produce magmas of the same composition as the rock types in this study. Locations projected onto section as in Fig. 3.

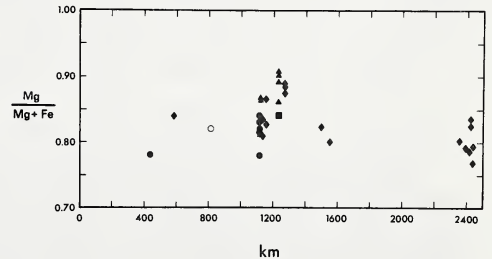


Fig. 6: Calculated compositions of olivines in equilibrium with the magmas at Moho pressures + 10 kb and 1400°C. Same projection of locations as Fig. 3.

ESTIMATES OF STRESS AND RECOVERY CONDITIONS IN VARIOUS TYPES OF
MANTLE PERIDOTITES.

A. NICOLAS and D. RICOULT

Laboratoire de Tectonophysique, NANTES - France.

Structural studies in mantle peridotites have been hitherto essentially devoted to describing the geometry of the deformation and to understanding the mechanisms and kinematics of flow. A wide consensus is now obtained on the idea that the elementary mechanism is the motion of dislocation in nearly all the studied peridotites, like it is in metals. This achievement makes it possible to use for investigating the flow dynamics, after the appropriate experimental calibration, the empirical relations established in metals between the dislocation microstructure and the deviatoric stress. RALEIGH and KIRBY (1970) and GOETZE (1975) have been the first authors to apply these relations to olivine from mantle peridotites. Since, both the experimental record and the data on naturally obtained microstructures have increased and it is possible to make some comparisons between the stress-recovery histories of the various mantle peridotites, namely peridotites from kimberlite and basalt nodules and peridotites from lherzolite and harzburgite massifs. The results can also be compared with the stress estimated for asthenospheric flow by other methods. Prior to presenting these results the different kinds of "structural geopiezometers" will be critically assessed, summarizing a more complete discussion already presented (NICOLAS, in press).

The relations between dislocation microstructure and stress have been experimentally established for olivine which is the dominant mineral in peridotites, largely controlling their flowage. The empirical relations tie with the stress, the dislocation curvature and density, the subgrain size and the dynamically recrystallized grain (neoblast) size (NICOLAS and POIRIER, 1976, p.137). From the above mentioned discussion, it has been concluded that the last relation is the most reliable when estimating the stress applied during the presumably steady state flow. Three calibrations have been made :

$$\sigma = 11 \times d^{-0.5} \quad (\text{GOETZE, 1975}) \quad (\sigma = \text{Kb}; d = \mu\text{m})$$

$$\sigma = 19 \times d^{-0.67} \quad (\text{POST, 1973})$$

$$\sigma = 40 \times d^{-0.81} \quad (\text{MERCIER, 1976})$$

The subgrain size consists usually for olivine in the measurement of the (100) subboundary spacing. Here the question of the scale of observation is important. With the TEM or the decoration technique all the subgrains are deciphered whereas with the optical microscope at low magnification in crossed nicols only the subgrains misoriented by more than 1° are visible. Our preliminary studies on recovery suggest that the latter subgrains are fairly stable either to a recovery or to a stress pulse (strain < 2%, DURHAM et al, in press). Therefore their (100) spacing can be used in a comparable way to the neoblast size: for instance in the Lanzo massif a good linear relation has been found between this (100) spacing and the neoblast size with $d_{(100)} = 0.44 d_{\text{neobl}}$. (BOUDIER and NICOLAS, in press).

With the decoration technique at a x 1000 magnification all the subbound-

daries are decorated. The (100) spacing is now one order of magnitude narrower than above, due to the fact that most subboundaries are misoriented by less than one degree. The relations with the stress are :

$$\sigma = 17 \times d^{-1} \quad (\text{GOETZE, 1975}) \quad (\sigma = \text{Kb}; d = \mu\text{m})$$

$$\sigma = 10 \times d^{-1} \quad (\text{DURHAM et al, in press}).$$

The low angle subboundaries are thought to be very sensitive to a recovery or to a stress pulse. Therefore this piezometer can be used to decipher these phenomena from the stress operating during the steady state flow. The same conclusion applies to the stress estimated from the density of dislocations but here appears the further difficulty of obtaining a correct estimation of the dislocation density (GUEGUEN, 1977).

The first systematic data on stress oriented studies of dislocation microstructures in mantle peridotites are those by GUEGUEN (1977) for kimberlite and basalt nodules, COISY (1977) for the Massif Central basalt nodules, MERCIER (1976) for the U.S. basalt nodules and the Newfoundland ophiolite peridotites and BOUDIER and NICOLAS (in press) from the Lanzo lherzolite massif.

In the porphyroclastic and mosaic textured nodules from kimberlites, the average size of the dynamically recrystallized olivine grains ($75 \mu\text{m}$) suggests a stress in the range of 1 Kb. However, these nodules display evidence of subsequent recovery and annealing with static recrystallization of olivine in tablets and stress relaxation down to 400 bars estimated from a mean density of free dislocations of $2 \cdot 10^7 \text{ cm}^{-2}$. On the basis of the kinetics of growth of the olivine tablets, MERCIER (1976) has evaluated to a few hours, during the eruption, the annealing time.

In the case of basalt nodules, the stress corresponding to the main flow is comprised between 100 and 600 bars, based on the neoblast grain size and on the (100) subboundary spacing observable with crossed nicols. This is mainly valid for the protogranular and equigranular textures, with a clear tendency from the stress to be higher in the latter textures. In the porphyroclastic textures from some areas (Massif Central, Western U.S.) these structural piezometers record stresses in the range 500-1000 bars. The free dislocation density is uniformly in the range of $10^6 - 10^7 \text{ cm}^{-2}$ suggesting during the eruption process a moderate recovery sometimes obscured by a late stress pulse.

In peridotite massifs a distinction has been made between those associated with ophiolites in which the flow structures are believed to reflect the oceanic mantle flow and others like the Lanzo lherzolite massif, which could represent mantle intrusions into the crust, at plate margins. The only extensive data concern the Lanzo massif where the stress associated with the intrusion at solidus conditions has been estimated at 200 - 400 bars (neoblast size : $500 - 700 \mu\text{m}$). Further flowage into the crust led to an heterogeneous distribution of stress and strain whose values continuously increased at the margins of the massif and inside bands dividing it. The ultimate deformation yields mylonites with stresses of a few Kb.

If the intrusion model for Lanzo is correct the flow at solidus conditions should be representative of the asthenosphere as occurring at strain rates in the $10^{-14} \text{ sec}^{-1}$ range (BOUDIER and NICOLAS, in press). This raises the problem of the corresponding stress (200 - 400 bars) which is found to be one order of magnitude greater than that derived from models on the rheology of the mantle. Stress values in the same range have been reported above for the protogranular

and equigranular textures in peridotite nodules from basalt. As discussed in a former paper (NICOLAS, in press), the discrepancy between these different stress estimates could be due to the analytical uncertainties which are still important in both approaches. Thus the flow structures observed in these peridotites and associated with apparent stresses of a few hundred bars could indeed represent the asthenospheric flow. On the other hand, the porphyroclastic and mosaic textures in kimberlite nodules and the high stress porphyroclastic textures locally observed in basalt nodules correspond to stresses and strain rates too high for an asthenospheric flow and certainly represent some local tectonic instabilities. COISY (1977) has attributed such porphyroclastic textures in basalt nodules to narrow shear zones (one kilometer thick) developing during the last stage of an asthenosphere upwelling, a situation recalling what has been described in the Lanzo massif.

REFERENCES :

BOUDIER, F. and NICOLAS, A. - Stress and strain estimates in the Lanzo Peridotite massif (Western Alps). C.N.R.S. Colloque Inter., in press.

COISY, P., 1977 - Thesis, Nantes, 115p.

DURHAM, W.B., GOETZE, C. and BLAKE, B. - Plastic flow of oriented single crystals of olivine part II : observations and interpretations of the dislocation structures. Jour. Geophys. Res., in press.

GOETZE, C., 1975 - Eos Trans. AGU, 56, 6.

GOETZE, C., 1975 - Geology, 172-173.

GUEGUEN, Y., 1977 - Tectonophysics, 39, 231-251.

MERCIER, J.C., 1976 - Ph. D., S.U.N.Y. at Stony Brook.

NICOLAS, A. - Stress estimates from structural studies in some mantle peridotites. Phil. Trans. R. Soc. Lond., in press.

NICOLAS, A. and POIRIER, J.P., 1976 - J. Wiley, London Publ., 444p.

POST, R., 1973 - Ph. D., U.C. at Los Angeles.

RALEIGH, C.B. and KIRBY, S.M., 1970 - Mineral. Soc. Amer. Spec. Pap. 3, 113-121.

GARNET BEARING ULTRABASIC AND DISCRETE NODULE SUITES FROM MALAITA, SOLOMON ISLANDS, S.W. PACIFIC, AND THEIR BEARING ON AN OCEANIC GEOTHERM

Peter H. Nixon, Dept. of Geology, P.O. Box 4820, University Papua, New Guinea
 F. R. Boyd, Geophysical Laboratory, Carnegie Institution, 2801 Upton Street,
 N. W., Washington, D. C. 20008

A volcanic rock previously described only from limited samples (Allen and Deans, 1965) from Babaru'u, Northern Malaita, Solomon Islands, contains a wide variety of deep seated inclusions that resemble those found in kimberlites. Shallow inclusions of country rock mudstone, limestone and basalt show metasomatic (and possibly fenitic) alteration. The rock is close to alnoite composition and consists of olivine microphenocrysts, melilite and some augite and phlogopite in a fine grained matrix of magnetite, perovskite and spinel with glass, carbonate and/or gonnardite cement. Textures indicative of a vent (pipe) origin include lapilli and autoliths. Varieties which are brecciated, rich in phlogopite, and carbonate but deficient in melilite appear as "yellow ground" and "hardebank," and are indistinguishable from kimberlite. This is unusual in an oceanic environment (outer melanesian arc) but nevertheless suggests a relationship with the few other circum-Pacific deep-seated volcanic occurrences at Kakanui, Kamchatka and SE Kalimantan.

The ultrabasic nodules have coarse grained to tabular textures and are lherzolites and pyroxenites with spinel and/or garnet. Olivine is largely altered but opx, cpx and garnet have similar ranges in chemistry to those found in other mantle suites: (numbers of electron microprobe analyses given in parentheses).

Wt %	<u>orthopyroxene (15)</u>	<u>clinopyroxene (14)</u>	<u>garnet (7)</u>
TiO ₂	0.00 - 0.16	0.00 - 0.51	0.00 - 0.14
Cr ₂ O ₃	0.25 - 0.86	0.53 - 1.40	0.65 - 5.46
Na ₂ O	0.01 - 0.10	0.28 - 1.80	0.00 - 0.02
Mg/(Mg + Fe)%	89.4 - 92.3	91.2 - 93.2	79.2 - 85.8

A notable feature is the presence in many nodules of aluminous spinel. Six out of eight analyses clustered close to Al: Cr: Fe³, 85:11:4 and Mg(Mg+Fe²)% = 82%. All have TiO₂ < 0.25 wt %. Brown amphibole was noted in one small nodule.

The discrete nodule (megacryst) suite is richer in Ti and Fe but poorer in Cr than that of the ultrabasic nodules and is thus similar to the Lesotho nodules (Nixon and Boyd, 1973). However there is a two-fold subdivision which is especially noticeable in the clinopyroxenes and which can be detected by slight colour differences and chemically, as shown by the ranges in the following table:

Wt %	<u>Subcalcic Diopsides (7)</u>	<u>Augites (5)</u>
TiO ₂	0.59 - 1.02	0.82 - 0.92
Cr ₂ O ₃	0.03 - 0.29	0.02 - 0.03
Na ₂ O	1.70 - 2.41	3.43 - 3.86
Mg/(Mg + Fe)%	80.0 - 85.6	69.8 - 72.6

Since some of the parameters overlap and because peripheral augitic alteration of diopside xenocrysts has been seen in thin section it is tentatively concluded that the augites are a shallower equilibration product of the sub-calcic diopsides brought about by changing magma conditions.

A two-fold chemical division of discrete nodule (megacryst) clinopyroxenes from kimberlites at Sloan, Colorado (Eggler and McCallum, 1976) and Kamfersdam and Jagersfontein, S. Africa (unpublished data) may have a similar explanation. A clinopyroxene from an ilmenite lamellar intergrowth from Malaita has intermediate properties of the two groups.

The five bronzite nodules analyzed probably equilibrated with the subcalcic diopsides (see below). Four chromium poor samples are chemically similar as shown by the following ranges in wt %; a fifth sample with more chromium is indicated in parentheses: TiO_2 , 0.30-0.34 (0.29); Cr_2O_3 , 0.03-0.07 (0.16); Na_2O , 0.28-0.29 (0.29) $\text{Mg}/(\text{Mg} + \text{Fe})\% = 84.8-85.9$ (87.3).

The garnets are rounded, fractured, reddish brown discrete nodules which attain a large size (megacrysts!)-up to 8.2 kg. They are Cr-poor ($\text{Cr}_2\text{O}_3 = 0.08-0.17$ wt %) but richer in Ti ($\text{TiO}_2 = 0.54-0.59$ wt %) and contain detectable amounts of Na (up to 0.05 wt %).

Six analyses of ilmenite from gravels, including two lamellar intergrowths have geikielite (15.6-34.4%), haematite (8.3-9.6%) and unusually low amounts (for kimberlitic rocks) of Si and Cr which were not detected by the probe. Other minerals noted in the gravels include zircon, (?) kaersutite, and abundant phlogopite. Garnet-spinel (alkremite) and garnet-clinopyroxene (griquaite) chips were observed in the breccia.

A geotherm calculated from garnet bearing ultrabasic nodule data (Boyd, 1973) suggests that for equivalent temperatures, sampling of the mantle has taken place at unusually shallow depths compared with previously calculated continental geotherms e.g. Lesotho. The geotherm is considered to be more typical of non-shield or oceanic regions of the earth but, nevertheless, the proximity of Malaita to the Ontong Java Plateau--a thickened portion of the SW Pacific Plate--suggests that even this gradient defines a "minimum." Although data on "hot" garnet bearing nodules from oceanic regions are sparse, original equilibration chemistry of exsolved pyroxenes in nodules from Hawaii (Beeson and Jackson, 1970) points to a steeper oceanic geotherm.

The discrete subcalcic diopside nodules appear to have equilibrated at higher temperatures than any of the ultrabasic nodules and the discrete bronzites are calculated to have equilibrated within the same range (using a $\text{Ca}/(\text{Ca} + \text{Mg})$ calibration curve derived from co-existing pyroxenes in the ultrabasic nodules). These bronzites define an inflected limb of the geotherm. It is concluded that all crystallization phenomena associated with the nodules took place within PT conditions of the graphite stability field and that the Malaita pipe is unlikely to contain diamonds.

References

- Allen, J. B. and Deans, T., 1965, Mineral Mag., 34, 16-34.
Beeson, M. H. and Jackson, E. D., 1970, Mineral. Soc. Amer. Spec. Pap. 3, 95-112.
Boyd, F. R., 1973, Geochem. Cosmochem. Acta, 37, 2533-46.
Eggler, D. H. and McCallum, M. E., 1976, Carnegie Institution Yr. Bk. 75, 538-541.
Kennedy, C. S. and Kennedy, G. C., 1976, Jl. Geophys. Res. 81, 2470-70.
Nixon, P. H. and Boyd, F. R., 1973, Lesotho Kimberlites (ed. P. H. Nixon) 67-75.

GRANULITE FACIES XENOLITHS FROM KILBOURNE HOLE MAAR, NEW MEXICO MAAR, NEW MEXICO, AND THEIR BEARING ON DEEP CRUSTAL EVOLUTION

Elaine R. Padovani (Department of Earth and Planetary Sciences, Massachusetts Institute of Technology, Cambridge, Massachusetts 02139)

James L. Carter (Program for Geosciences, University of Texas at Dallas, Richardson, Texas 75080)

Introduction. Abundant quartzofeldspathic and mafic granulite facies xenoliths occur in the ejecta blanket at Kilbourne Hole maar, Dona Ana County, New Mexico. No rocks of such high metamorphic grade occur either in outcrop or in wells drilled into the Precambrian basement of the area (Denison *et al.*, 1970). These xenoliths were incorporated into ascending magmas during the explosive volcanic eruptions that formed the maar and provide an opportunity to study samples of the earth's deep crust.

Xenolith Mineralogy. Anhydrous, sillimanite-bearing and orthopyroxene-bearing garnet granulites, charnockites, two-pyroxene granulites and anorthosite are the principal rock types represented in the deep crustal xenolith population. Garnet-bearing granulites have two distinct mineralogies: group 1 contains almandine-pyrope garnet, perthitic potassium feldspar (sanidine), quartz, + plagioclase + sillimanite, with ilmenite, rutile, zircon and graphite as accessories; group 2 contains almandine pyrope garnet, plagioclase, + orthopyroxene + quartz, with ilmenite and/or hercynite as accessories. Charnockites contain two pyroxenes, perthitic potassium feldspar (sanidine), plagioclase and ilmenite. Two-pyroxene granulites contain plagioclase and ilmenite in addition to pyroxenes. Anorthosite is the least abundant rock type and contains less than 2% orthopyroxene. The detailed chemistry of the xenoliths is given in Padovani (1977) and Padovani and Carter, (1977).

Variable amounts of partial fusion, due to heating and decompression during transport to the surface, produced melts which are now seen as inhomogeneous interstitial glasses or symplectites of either orthopyroxene-spinel-glass around garnet, or olivine-glass around orthopyroxene. The fusion occurred rapidly enough to have had little effect on the homogeneity of major phases and to have prevented mixing of melts on a microscale.

Discussion. The phases present in the garnet granulites, their chemistry and especially the absence of the hydrous phase, biotite, require that these granulites formed at temperatures greater than those necessary for the breakdown of biotite, and at pressures greater than those necessary for the breakdown of cordierite (Holdaway and Lee, 1977). This suggests minimum equilibrium P-T conditions of 5.4 kilobars and 700°C. Equilibrium temperatures of 750°C to 1000°C are indicated from feldspar geothermometry (Stormer, 1975; Padovani, 1977; Padovani and Carter, 1977). Modal analyses of the percent rock melted indicate that there appears to be no direct relationship between visible melt and calculated temperature (Figure 1). Application of geobarometry to the garnet-plagioclase equilibria yields a pressure range corresponding to depths of 22 to 28 kilometers (Ghent, 1976; Padovani, 1977; Padovani and Carter, 1977). This is equivalent to a geothermal gradient of about 30°C/km beneath the southern Rio Grande Rift (Figure 2).

Similar application of feldspar and pyroxene geothermometry and geobarometry to the more mafic charnockites and two-pyroxene granulites support equilibration in a temperature-pressure regime similar to that of the garnet granulites (Stormer, 1975; Irving, 1974; Ross and Huebner, 1975; Padovani and Carter, 1977).

Conclusions. The garnet granulite xenoliths plot along the geotherm derived from heat flow and gravity measurements in the southern Rio Grande Rift implying that the mineral assemblages reflect the ambient geothermal gradient in the deep crust (Figure 2) (Decker and Smithson, 1975). The estimated range of P-T conditions for the mafic granulites agrees with that of the garnet granulites. Anhydrous, garnet-bearing granulite facies rocks may be constituents of the deep crust in tectonic environments similar to that of the southern Rio Grande Rift. The garnet granulites are probably residues after partial melting and extraction of felsic magmas in the lower crust. Such magmas would be rich in volatiles and would probably crystallize before reaching the earth's surface, enriching the intermediate crust in water and volatiles.

Acknowledgments. This work was supported by NSF grant DES 74-14532. Contribution No. 342 of the Program for Geosciences at the University of Texas at Dallas.

References

- Decker, E. R. and S. B. Smithson, Heat flow and gravity interpretation across the Rio Grande Rift in southern New Mexico and west Texas, *J. Geophys. Res.*, 80, p. 2542-2552, 1975.
- Denison, R. E., W. H. Burke, Jr., E. A. Hetherington and J. B. Otto, Basement framework of parts of Texas, southern New Mexico and northern Mexico, in: Symposium in honor of Ronald K. DeFord, West Texas Geological Society, p. 3-14, 1970.
- Ghent, E. D., Plagioclase-garnet- Al_2SiO_5 -quartz: a potential geobarometer-geothermometer, *Am. Mineral.*, 61, p. 710-714, 1976.
- Holdaway, M. J., Stability of andalusite and the aluminum silicate phase diagram, *Amer. J. Sci.*, 271, p. 97-131, 1971.
- Holdaway, M. J. and S. M. Lee, Significance of Fe-Mg cordierite stability relations on temperature, pressure and water pressure in cordierite granulites, in: *The Earth's Crust*, Geophys. Monogr. Ser., 20, AGU, Washington, D. C., ed. J. G. Heacock, in press, 1977.
- Irving, A. J., Geochemical and high pressure experimental studies of garnet pyroxenite and pyroxene granulite xenoliths from the Delegate basaltic pipes, Australia, *J. Petrol.*, 15, p. 1-40, 1974.
- Kerrick, D. M., Experimental determination of muscovite and quartz stability with P_{H_2O} P_{total} , *Amer. J. Sci.*, 272, p. 946-958, 1972.
- Luth, W. C., The influence of pressure on the composition of eutectic liquids in the binary systems sanidine-silica and albite-silica, *Carnegie Inst. Wash. Yearbk.*, 66, p. 480-484, 1968.
- Padovani, E. R., Granulite facies xenoliths from Kilbourne Hole maar and their bearing on deep crustal evolution, PhD dissertation, Univ. of Texas at Dallas, Richardson, Texas, 1977.
- Padovani, E. R. and J. L. Carter, Aspects of the deep crustal evolution beneath south central New Mexico, in: *The Earth's Crust*, Geophys. Monogr. Ser., 20, AGU, Washington, D. C., ed. J. G. Heacock, in press, 1977.
- Ross, M. and J. S. Huebner, A pyroxene geothermometer based on composition-temperature relationships of naturally occurring orthopyroxene, pigeonite and augite, in: *Extended Abstracts*, International Conference on Geothermometry and Geobarometry, 1975.
- Stormer, J. C., A practical two-feldspar geothermometer, *Amer. Mineral.*, 60, p. 667-674, 1975.

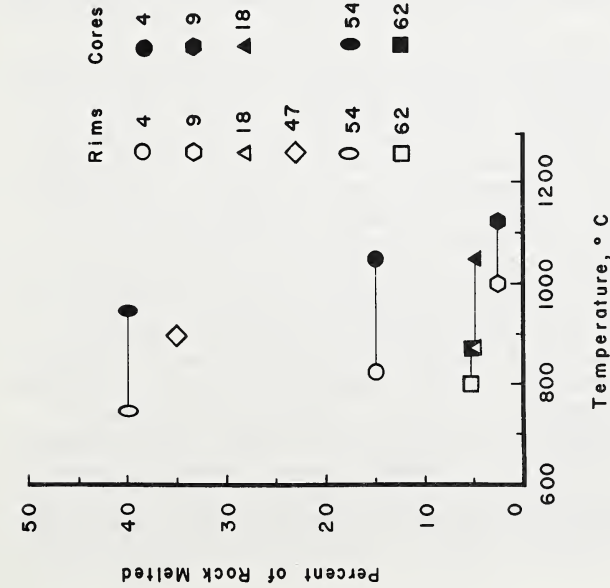


Figure 1. Percent of rock melted versus its temperature range calculated using the method of Stormer(1975). Open and closed symbols, respectively, represent temperatures calculated from electron microprobe analyses of the rims and cores of potassium feldspar (Padovani and Carter, 1977).

and Lee(1977); (4) & (5) = dry melting of sanidine-rims of southern Rio Grande Rift(Decker and Smithson, 1975); (7) & (8) = the range of temperatures as a function of depth for surface fluxes(q_s) of 2.4 HFU for the southern Rio Grande Rift and of 2.0 HFU for the Basin and Range Province, respectively(Decker and Smithson, 1975). Temperatures were calculated from perthite-free sanidine rims.

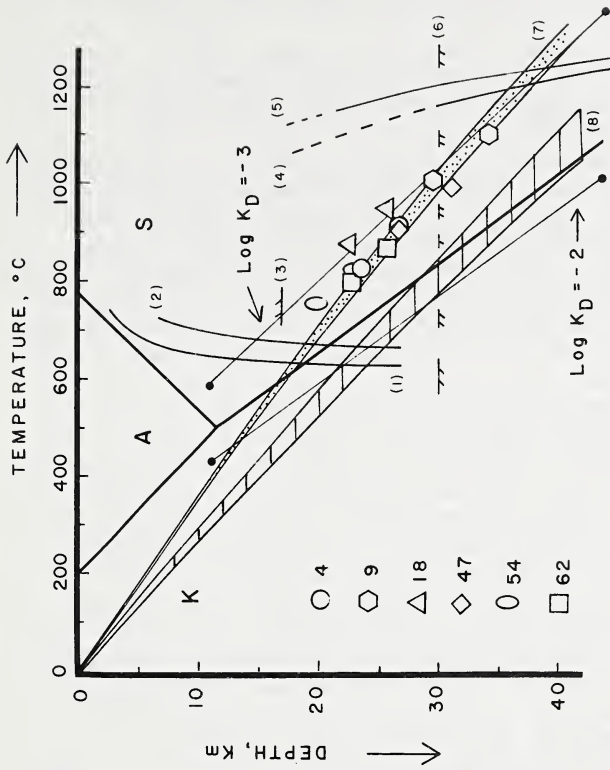


Figure 2. Temperature-depth plot showing the Al_2SiO_5 stability field(Holdaway, 1971) with respect to hypothetical K_D values for coexisting garnet and plagioclase according to Ghent(1976). The positions of garnet granulites were calculated using the methods of Ghent(1976) and Stormer(1975). Curves (1) & (2) = melting of granite at $P_{H_2O} = 1$ P_{total} and $P_{H_2O} = 0.5$ P_{total} , respectively; (3) = minimum p-T conditions predicted by the data of Holdaway and albite-silica(Luth, 1968); (6) = base of crust in southern Rio Grande Rift and of 2.0 HFU for the Basin and Range Province, respectively(Decker and Smithson, 1975). Temperatures were calculated from perthite-free sanidine rims.

THE ILMENITE ASSOCIATION FROM THE FRANK SMITH KIMBERLITE, SOUTH AFRICA

J. D. Pasteris (Dept. Geology, Yale Univ., New Haven, Conn. 06520, U.S.A.)
F. R. Boyd (Geophysical Laboratory, 2801 Upton St., N. W., Wash., D.C. 20008)
P. H. Nixon (Dept. Geology, The University, Port Moresby, New Guinea)

The relationship between common ilmenite discrete nodules in kimberlites and less-common intergrowths of ilmenite with silicates has been a subject of both interest and controversy (e.g. Mitchell, 1977, Haggerty *et al.*, this volume). The abundance of ilmenite nodules and ilmenite-silicate intergrowths at Frank Smith encouraged a detailed study in which over sixty mineral analyses of ilmenites and coexisting silicates have been obtained. Ilmenite nodules in coarse concentrate from Frank Smith range up to 4-5 cm; also studied were two enstatite megacrysts with intergrown ilmenite and other phases that have maximum dimensions of 15-20 cm.

Virtually all the ilmenite discrete nodules from Frank Smith are polygranular with a grain size that ranges widely from 0.2-25 mm. Pitting on polished surfaces is the most distinctive optical feature of the ilmenite discrete nodules; similar pitting has been observed in kimberlitic ilmenites from other pipes (e.g. Dawson, 1962). Some pits are round, others triangular or elongate. SEM pictures of the pits show them to be internally irregular. Individual nodules often contain both pitted and non-pitted grains. Pits may cover an entire grain, but coarser pits often delineate grain boundaries. Pitted boundaries usually define an optically continuous grain; more rarely the region delineated by pits consists of two grains with an interface recognizable only by differences in pleochroism and/or anisotropism. Pitted grain boundaries show neither greater nor lesser degrees of textural equilibrium than do non-pitted boundaries. Detailed electron microprobe study of a nodule containing both pitted and non-pitted grains showed no significant chemical differences or inhomogeneities associated with pitting. Vickers' hardness tests on adjacent pitted and smooth grains gave variable, overlapping values, suggesting the absence of physical inhomogeneities. The pitting is possibly an alteration feature because it is enhanced at grain boundaries and shows crystallographic control.

Most of the ilmenites contain fine ($\sim 1\mu$ wide), rod-like, black spinels, often appearing as a freckling within the ilmenite grains. These spinels are too fine-grained for microprobe analysis. Spinel lamellae within a single ilmenite grain have a common orientation. Sometimes the rods of spinel are concentrated along continuous, curved trends which simulate grain boundaries. Configurations of these trends define domains that are as variable in shape as are true grains. A few specimens contain two kinds of spinel with the same orientation. Grayish tan spinel (probably ulvöspinel solid-solution) forms long lamellae with more abundant, black spinel (possibly pleonaste) forming short colinear rods that are sometimes included in the ulvöspinel lamellae. There is no relationship between pitting and spinel exsolution. Black spinels are most abundant in those ilmenite nodules which are richest in the geikielite component. Exsolution of spinel probably results from subsolidus reduction of ilmenite. Alignment of rods of exsolved spinel in curved trends may result from concentration of exsolution along dislocations in ilmenite, similar to hematite lamellae in ilmenite (S. E. Haggerty, personal communication).

Grain boundary textures and their degree of definition vary widely, even within one ilmenite nodule (e.g. Mitchell, 1973). Kimberlitic ilmenites have

few deformation lamellae, in contrast to other igneous ilmenites. There are various features, however, that indicate partial or total recrystallization: (1) twin lamellae are occasionally present near the edges of a nodule; (2) equilibrium grain boundary intersections are common; (3) bands of fine mosaic ilmenite sometimes traverse coarse grains; (4) there are occasionally bands or long, tapering wedges within grains that have a slightly different extinction position from the host; (5) spinel lamellae appear to lie along dislocations; (6) a few specimens show a foliation due to alignment of elongated, highly sutured grains.

Twenty nodules in which ilmenite is intergrown with silicates include nine lamellar intergrowths, four ilmenite discrete nodules with garnet or pyroxene inclusions, five enstatite discrete nodules with inclusions of ilmenite and two polygranular nodules in which the ilmenite has an interstitial texture that may be metasomatic. A number of the lamellar intergrowths and enstatite nodules are deformed, as noted by Frick (1973). Severe deformation destroys the lamellar texture, causing recrystallization of the ilmenite as irregular blebs. It is impossible to judge whether the primary textures in some sheared enstatite-ilmenite nodules were lamellar or host-inclusion configurations.

The ilmenite discrete nodules show a substantial range in $Mg/(Mg + Fe)$ (Figs. 1A and B; see also Mitchell, 1977). There is a tendency for Fe_2O_3 to increase with $FeTiO_3$ in the ilmenites (Fig. 1A). Cr_2O_3 in the ilmenite discrete nodules varies erratically with $Mg/(Mg + Fe)$ in the range $< 0.05-1.00$ wt % Cr_2O_3 (Fig. 1B). The two ilmenites with highest Cr_2O_3 (~3 wt %, Fig. 1B) come from nodules with textures suggesting the possibility of metasomatic introduction of ilmenite. Ilmenites from the lamellar intergrowths show a very restricted range in $Mg/(Mg + Fe)$ (Figs. 1A and B), that is overlapped by the more magnesian discrete ilmenites.

Host-inclusion relations appear to establish a consanguinity between the discrete ilmenites and discrete garnets and pyroxenes (e.g. Boyd and Nixon, 1973). $Mg/(Mg + Fe)$ shows the range 0.750-0.838 for twelve garnet discrete nodules from Frank Smith and the range 0.876-0.921 for twenty-five enstatite discrete nodules. These ranges in $Mg/(Mg + Fe)$ for the discrete ilmenites, garnets, and pyroxenes are most reasonably interpreted as due to igneous fractionation prior to kimberlite eruption.

Ilmenites from the lamellar intergrowths cannot be distinguished on the basis of chemical parameters from ilmenites forming discrete nodules. Moreover, applications of pyroxene thermometry and barometry suggest that the discrete nodules and lamellar intergrowths have come from overlapping depth ranges (Boyd and Nixon, 1975). A related origin therefore seems probable. Equilibration temperatures for enstatites and diopsides from the Frank Smith lamellar intergrowths fall in the range $1175^\circ-1275^\circ C$. This restricted range together with the restricted range in $Mg/(Mg + Fe)$ for ilmenites from the lamellar intergrowths suggest that the chemical and possibly the physical conditions under which these intergrowths nucleated and crystallized were more constrained than for the ilmenite discrete nodules as a whole.

Boyd, F. R. and P. H. Nixon (1975): *Phys. and Chem. of the Earth*, 9, 431-454.

Boyd, F. R. and P. H. Nixon (1973): *Lesotho Kimberlites*, P. H. Nixon ed. 254-268.

Dawson, J. B. (1962): *Bull. Geol. Soc. Amer.*, 73, 545-560.

Frick, C. (1973): *Trans. Geol. Soc. South Africa*, 76, 195-200.

Mitchell, R. H. (1977): *Lithos*, 10, 25-37.

Mitchell, R. H. (1973): *Jour. Geol.*, 81, 301-311.

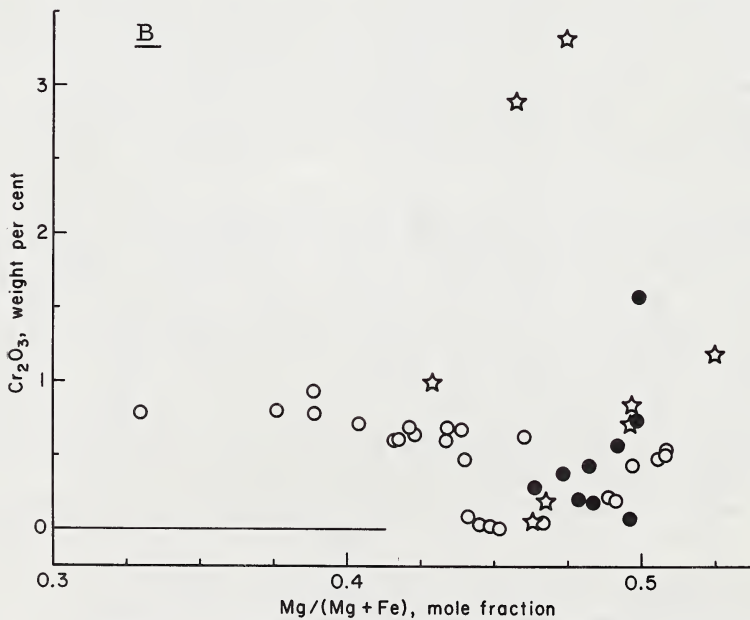
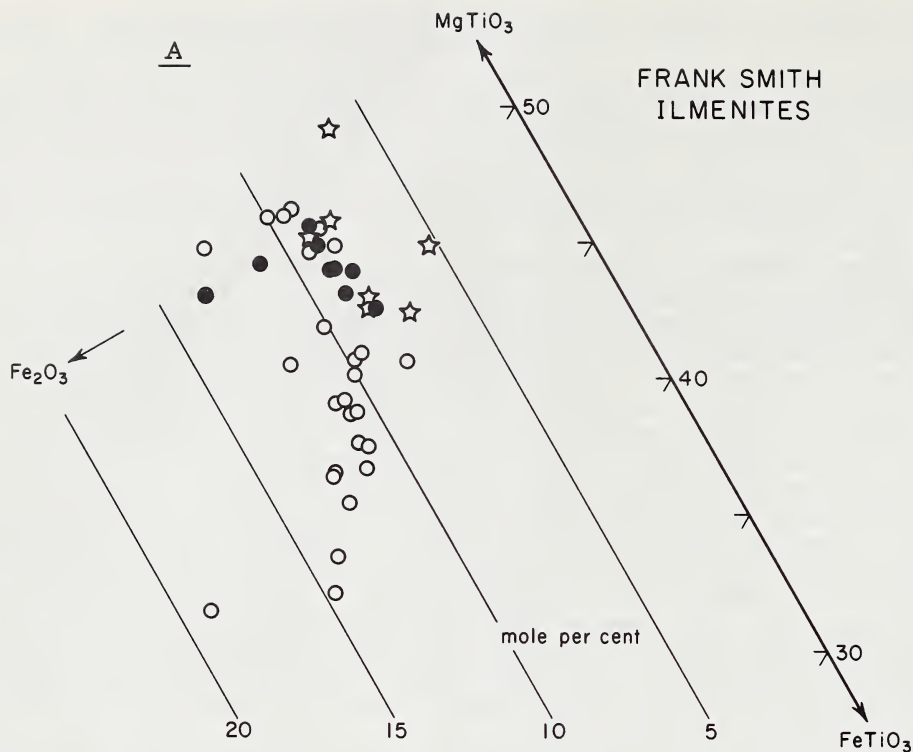


Fig. 1: Chemical variations in ilmenite discrete nodules and intergrowths from the Frank Smith mine. Open circles: discrete nodules; solid points: lamellar intergrowths; stars: other ilmenite-silicate intergrowths.

ABUNDANCES OF PALLADIUM, IRIDIUM AND GOLD IN KIMBERLITES AND ASSOCIATED NODULES

D. K. Paul (Geochronology Division, Geological Survey of India, Calcutta 16, India)

J. H. Crocket (Dept. Geology, McMaster University, Hamilton, Ontario, Canada)

P.H. Nixon (Dept. Geology, University Papua New Guinea, Port Moresby, New Guinea)

INTRODUCTION

Garnet peridotite nodules found in kimberlites are accepted as direct samples of the mantle and have been studied extensively. Abundances of the noble metals in kimberlites and associated nodules are, however, poorly known. This study reports neutron activation data for Pd, Ir and Au in twenty-two kimberlites and associated nodules from India and Southern Africa (Fig. 1). The data are compared with mafic and ultramafic rocks and Type I carbonaceous chondrites in Table 1. Fig. 2 is a plot of Pd, Ir and Au proportions in kimberlites and nodules.

DISCUSSION

Geochemical properties

From Table 1 and Fig. 2 the following generalizations are drawn:

- 1) The average Ir content of the nodules is six times higher than that of the kimberlites; the reverse is true for Pd and Au which are lower by a factor of two in the nodules (omitting PHN 2829).
- 2) The Pd/Ir ratios of the kimberlites average 2.7 ± 1.4 and are more consistent than those of the nodules which average 0.56 ± 0.85 . The kimberlite average is three times chondritic. It is similar to alpine peridotite although lower than that of komatiitic peridotites. The average Pd/Ir ratio of the nodules is unusual as sulfur-poor silicate rocks with Pd/Ir < 1 are rare.
- 3) Ratios of Pd or Ir with respect to gold are highly variable due to the great range in gold contents of both nodules and kimberlites.
- 4) The Ir contents of the nodules are high by comparison with sulfur-poor mafic or ultramafic rocks.
- 5) Systematic geographic variation in noble metal content is absent at the sampling density employed. An exception is the gold content of the Indian kimberlites which is three times that of the Southern African kimberlites.

Contamination

Nodules may be contaminated by alkalis, uranium and thorium from the host kimberlites (Gurney *et al.*, 1966). The distribution pattern of the noble metals, however, indicates that contamination of the nodules by host kimberlite would not affect the abundances of Ir and Au in the former.

Lateral and vertical variability of mantle with respect to iridium

Textural and mineralogical data indicate that the nodules are samples of the mantle from depths of up to 200 km. Iridium, a refractory element, is apparently concentrated in the residua when liquid is extracted from the mantle. The iridium content in the nodules should be inversely related to the degree of partial melting provided their source region was initially of uniform Ir content. If the nodules are samples of a heterogeneous mantle, a simple relationship would not exist. The Ir content of the nodules do not correlate with the abundances of easily extractable elements (unpublished data, P. H. Nixon) suggesting that the Ir content in the mantle source region was variable. Further, there is no systematic variation in Ir (or Au) content of the nodules with respect to depth of origin as qualitatively inferred from texture and content of fusible constituents (Fig. 2).

Partition of noble metals in partial melting of peridotite nodules

Recent studies indicate that kimberlites are products of small amounts

of partial melting in the mantle (Paul et al., 1975). Rozhkov et al. (1973) found that Au content in the major mantle minerals was equal to that in the whole rock. Ir and Pd contents of mantle minerals are unknown but the partition coefficients of Ir in some relevant minerals can be calculated from available data (Gijbels et al., 1976; Crocket et al., 1976; Gottfried and Greenland, 1972). The abundance levels of Ir in a hypothetical melt derived by partial melting of a garnet peridotite mantle containing 15 ppb Ir in the major silicate and oxide phases would range from 2.6 ppb (1% melt) to 6.3 ppb (10% melt), a range similar to that found in the kimberlites.

The possibility that minor phases are carriers of noble metals cannot be excluded as Fe-Ni-Cu sulfides and metallic Fe, Ni-Fe and Cu are common in kimberlitic ultramafic nodules (Bishop et al., 1975; Haggerty, 1975). These phases should be significant contributors to early partial melts. A preferential partition of Pd and Au into kimberlite relative to the nodules would result if these metals were hosted in such early melting phases. However, the same partition trend would also be expected of Ir, as opposed to that actually observed. This suggests that part of the Ir is hosted by a relatively refractory phase.

Noble metal fractionation during kimberlite emplacement

Noble metals in the kimberlites are not correlated with Ni, Fe, P, Ti or the Fe/Mg index. Apparently they have not been fractionated during emplacement.

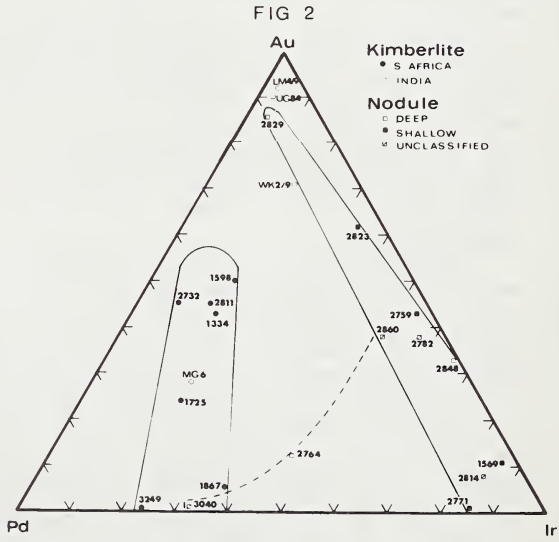
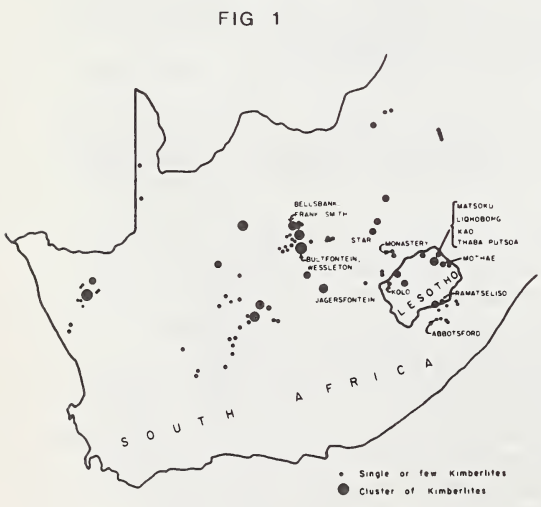


Table 1 -- Pd, Ir and Au contents in kimberlites and associated nodules

Sample No.	Locality	Pd	in ppb		Pd/Ir
			Ir	Au	
<u>Kimberlite</u>					
UG	Majhgawan, Central India	4.1	5.9	24	0.7
MG 6	Majhgawan, Central India	4.3	1.5	2.3	2.9
LM 4/9	Lattavaram, South India	2.3	1.5	43	1.5
WK 2/9	Wajraharur, South India	1.3	0.49	17	2.7
PHN 1598	Thaba Putsoa, Lesotho	7.7	3.5	11	2.2
PHN 1334	Kolo, Lesotho	5.0	2.0	5.2	2.5
PHN 1725	Ramatseleiso, Lesotho	15	5.0	6.4	3.0
PHN 1867	Monastery, South Africa	3.5	2.2	0.34	1.6
PHN 3249	Frank Smith, South Africa	19	5.9	0.14	3.3
PHN 2811	Jagersfontein, South Africa	8.9	2.6	10	3.4
PHN 2732	Wessleton, South Africa	18	2.8	16	6.4
<u>Nodules</u>					
PHN 2848	Thaba Putsoa, Lesotho	0.27	33	16	0.008
PHN 1569	Thaba Putsoa, Lesotho	1.0	32	4.1	0.03
PHN 2823	Liqhobong, Lesotho	1.0	6.3	12	0.16
PHN 2860	Matsoku, Lesotho	1.3	5.5	4.1	0.24
PHN 2829	Kao No. 2, Lesotho	11	4.9	103	2.3
PHN 2771	Monastery, South Africa	3.4	21	0.28	0.16
PHN 2782	Frank Smith, South Africa	1.2	13.5	8.9	0.09
PHN 2814	Jagersfontein, South Africa	4.6	53	5.3	0.09
PHN 2759	Bultfontein, South Africa	0.7	12	9.6	0.06
PHN 2764	Bultfontein, South Africa	7.1	7.8	2.0	0.9
PHN 3040	Abbotsford, South Africa	9.3	4.5	0.16	2.1
<u>Averages</u>					
All kimberlites		8.1	3.0	12	2.7
Indian kimberlites		3.0	2.3	22	2.0
S. African kimberlites		11	3.4	7.0	3.2
Ultramafic nodules		3.8	18	15	0.56
<u>Comparison with other mafic and ultramafic rocks and meteorites</u>					
Komatiitic peridotite, S. Africa (Au) and Munro Twp., Ont. (Pd & Ir)		8.3	1.1	1.1	7.5
Alpine peridotite-dunite, Mt. Albert, Que.		7.9	2.4	1.1	3.3
Sea-floor basalt, MAR, Leg 37		<0.7	<0.025	2.8	--
Intra-plate and mid-ocean ridge basalt		2.0	0.33	2.1	6.1
Continental plateau-building basalt		5.5	0.10	3.3	5.5
Type I Carbonaceous chondrites		570	510	140	1.1

REFERENCES

- Bishop, F., Smith, J. and Dawson, J. (1975). Physics and Chemistry of the Earth, 9, 323.
 Crocket, J., Teruta, Y. and Garth, J. (1976). Econ. Geol., 71, 1308.
 Gijbels, R., Henderson, P. and Zels, J. (1976). Econ. Geol., 71, 1364.
 Gottfried, D. and Greenland, L. (1972). XXIV Intl. Geol. Congress, 10, 135.
 Gurney, J., Berg, G. and Ahrens, L. (1966). Nature, 210, 1025.
 Haggerty, S. (1975). Physics and Chemistry of the Earth, 9, 295.
 Paul, D., Potts, P., Gibson, I. and Harris, P. (1975). E.P.S.L., 25, 151.
 Rozhkov, I., Kaminskiy, F. and Frantsesson, Ye, V. (1973). Geochem. International, 10, p. 1385.

PETROCHEMICAL AND THERMODYNAMIC EVIDENCE OF THE ORIGIN OF KIMBERLITES

L. L. Perchuk, V. I. Vaganov, J. P. Ilupin (Institute of Experimental Mineralogy, Academy of Sciences, Moscow, USSR).

The petrochemistry of kimberlites from Yakutia and Lesotho has been studied on a silicate melt model with the SiO_2 , CO_2 and H_2O derivatives as the main anions.

The dissolution of H_2O in an ultramafic melt results in orthosilicates, ($\text{H}_2\text{SiO}_4^{2-}$, H_2SiO_4 , H_4SiO_4 etc.) rather than metasilicates, while the dissolution of CO_2 produces additional hydrocarbonate complexes. At

high $P_{\text{CO}_2}^{\text{fl}}$, and where the orthosilicic calcium salt clusters are present in the magma, the kimberlite melt can break down into carbonate and silicate liquids. Therefore, the composition of kimberlite magma will be determined by the $\text{H}_2\text{O}/\text{CO}_2$ ratio under the relatively constant fluid pressure. This can be seen from the distinct "fluid" trend in the $\text{H}_2\text{O}-\text{CO}_2-\text{SiO}_2$ diagram for the Yakutia and Lesotho Palaeozoic kimberlites. The $\text{H}_2\text{O}/\text{CO}_2$ ratio changes with the liquidus temperature along this trend (Perchuk a. Vaganov, 1977) which suggests that the liquation process predominates over the simple CO_2 solubility in the melts of kimberlite composition. The well-known Boyd's diagrams for the equilibrium PT-conditions in peridotites have been applied to natural Cpx and Opx, and the PT-parameters were correlated for peridotite inclusions in kimberlite pipes in Yakutia and Lesotho.

The liquidus temperatures for the extrapolated area of these correlations gave depths (pressures) at which kimberlite magmas are formed (200-250km).

The hypothesis on SiO_2 partitioning between the melt and the fluid was used to calculate the average composition of the dry initial kimberlite, which characterised the average mantle composition: SiO_2 - 45,12; TiO_2 - 2,49; Al_2O_3 - 3,58; Cr_2O_3 - 0,12; FeO - 9,32; MnO - 0,16; CoO - 0,11; MgO - 23,47; CaO - 13,44; Na_2O - 0,20; K_2O - 1,12; P_2O_5 - 0,69; S - 0,18; sum - 100 wt. %. This kimberlite is close to verlite in composition.

LASHAINE, TANZANIA XENOLITHS: A NEW COLLECTION

JANE E. N. PIKE (Department of Earth Sciences, California State University,
Hayward, California, 94542)

C. E. MEYER
H. G. WILSHIRE (U. S. Geological Survey, Menlo Park, California, 94025)

A previously-unstudied collection of xenoliths from Lashaine, Tanzania consists predominantly of peridotites and pyroxenites, and includes a few samples of mica- and amphibole-rich rocks. The dominant rock type is non-garnetiferous peridotite (lherzolite and wehrlite), with spinel clinopyroxenite and garnet wehrlite subordinate. Spinel-websterite and garnet-clinopyroxenite are less abundant. Two samples are nearly all phlogopite (87%), and one other rock is kaersutite peridotite.

Among the lherzolites, either clino- or orthopyroxene is dominant in the mode. The dominant phase usually forms large grains that appear to have exsolved the subordinate phase, which occurs as small, marginal grains. Occasionally, the exsolved phase may still be enclosed by the dominant phase. One analysed garnet-lherzolite contains 5 phases: orthopyroxene (En₉₃) is the dominant pyroxene, the garnets are pyrope; in addition to olivine (Fo₉₀) and minor clinopyroxene, there is chromite and secondary Mg-Al spinel. Of the 20 thin sections studied, 3 evidently contained garnets, which now are cloudy patches of alteration minerals including clays, serpentines, and secondary spinels. Few of the non-garnetiferous peridotites actually contain spinel; the opaque phase probably is titan-magnetite, and in some samples ilmenite and magnetite are partially exsolved.

Among pyroxenites, several of the spinel-bearing varieties contain a pink-to-green pleochroic (hypersthene?) pyroxene, and one garnet-pyroxenite contains plagioclase, in probable melt areas. One rock of especial interest is composite, comprising dunite-wehrlite-websterite zones. In this rock the olivines are chemically zoned, while pyroxenes are zoned in some other peridotites and pyroxenites.

About 90% of all the rocks in the collection contain micas (phlogopite), either as selvages and veins or as interstitial flakes or clusters of flakes. Notably, none of the garnet-rich rock types studied in thin section contain micas of either habit.

The textures of these rocks are dominantly allotriomorphic-granular, with fewer porphyroclastic and rare mosaic types. Allotriomorphic-granular textures frequently are overprinted by porphyroclastic texture; the mosaic-textured rocks contain a few relic porphyroclasts.

Nearly all rocks, whether strained or not, are modified by a later partial melt episode that generally is confined to interstitial areas, and is especially well-developed at the edges of clinopyroxenes. In all observed cases, interstitial micas did not form as a result of the melt event, but were melted by it. However, several sections contain red-brown phlogopite as thin rims around grains of opaque minerals (?Ti-magnetite or spinel). This is obviously due to reaction, and may be related to melting, but in all other rocks studied the genetic relation between micas and other phases is unclear. The phlogopites frequently are overgrown by darker phlogopite rims. In rocks with porphyroclastic overprinting, interstitial mica grains are often bent and have migratory extinction. In veins, very coarse mica grains (up to 10 mm) appear to have recrystallized in a process of strain recovery.

Phlogopite compositions generally are similar to those reported by Dawson and Smith (1973): 3-5 wt. % TiO₂, 13-15% Al₂O₃, 18% MgO, 9% FeO and 8-9% K₂O. The darker overgrowths probably contain higher Mg and Ti, in accord with results reported by Boettcher, et al. (this symposium). This is contrary to the hypothesis of Reid, et al. (1975), that their single phlogopite with very high Ti represents a primary mica.

Bulk analyses were performed on fifteen samples, and electron microprobe analyses were carried out for all phases in four selected sections. According to the bulk analyses, this collection has greater chemical variability than that studied by Dawson and colleagues. Figure 1 compares several chemical parameters of the new collection to those of Rhodes and Dawson's (1975) peridotites. Lashaine nodules can be classified into two main peridotite categories: 1. a group comprising garnetiferous and non-garnetiferous types characterized by a narrow range of Mg-Fe ratio (Mg/Mg+Fe .92-.94) and low K₂O (0.0-0.07 wt. %). with large variability in other oxides, especially SiO₂, Al₂O₃, CaO and Na₂O. This group may be subdivided on the basis of Al₂O₃ content (Figure 1b), 2. the group of higher-Fe peridotite (Mg/Mg+Fe .71-.85) that is also characterized by higher K₂O (0.09-0.38%) and smaller variations in the content of other oxides (SiO₂, Al₂O₃ and Na₂O); CaO is highly variable (0.06-3.3%), reflecting a broad range of pyroxene contents in these predominantly clinopyroxene-rich peridotites.

Figure 1a includes pyroxenites of the new collection; their Al₂O₃ contents range from 2.71% to 4.90%, K₂O 0.08-0.36% and CaO 5-17%. The single sample of kaersutite-peridotite corresponds to an Fe-rich peridotite, low in SiO₂ but rich in Al₂O₃ (6.1%, not plotted). In thin section, this rock exhibits textures that strongly suggest conversion of clinopyroxene to amphibole.

The single composite sample is not a simple layered rock. A fragment of pyroxenite is detached from the main mass and surrounded by dunite. The texture of the dunite contrasts with that in the websterite. Olivines in the (cpx-bearing) dunite are strongly zoned: cores Fo₇₄₋₇₆, rim₈₀₋₈₄. There is a marked Fe gradient across the wehrlite into the websterite, where olivines are Fo₇₀. Analogous phase-chemical changes characterize the clinopyroxenes: Mg/Mg+Fe in dunite is .69-.75, in wehrlite .65, and in websterite .63-.66; there are marked gradients at the dunite-wehrlite and wehrlite-websterite contacts. The orthopyroxenes of the websterite are iron-rich: Mg/Mg+Fe = .59. These rock types are all characteristic of the Al-augite ultramafic group (Wilshire and Shervais, 1975), and the structural, textural and chemical relations suggest that the websterite was intrusive into the dunite; the wehrlite is intermediate chemically and texturally between dunite and websterite, and may represent a zone of mobile components.

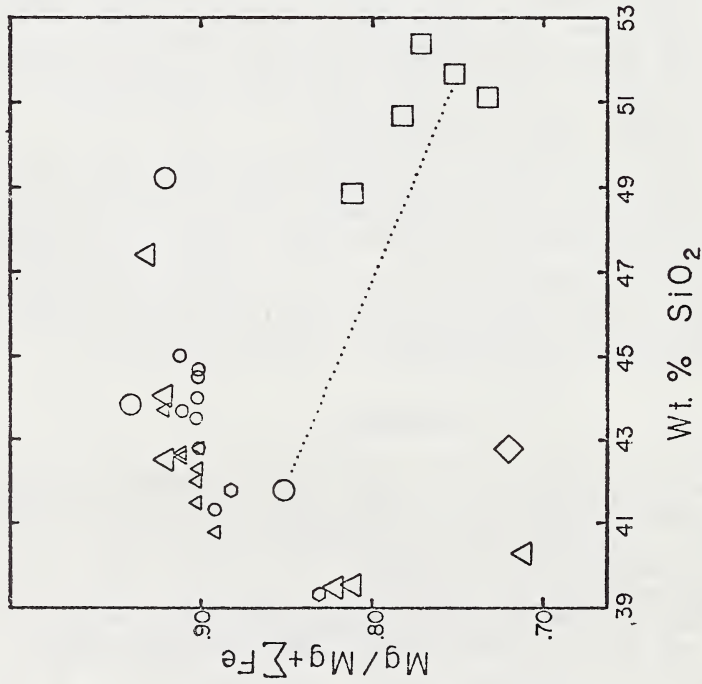
The chemical and petrographic data accumulated from this collection point to metasomatism and local intrusion as important influences in the formation of these rocks. Minerals with clearly secondary chemical and textural characteristics can be found in most rock types. At one or many stages in the formation of these samples the environment seems to have been open to mobile chemical components, possibly resulting in large variations in Fe and Al₂O₃ among the peridotites. The Lashaine rocks seem to be evidence of the chemical activity within the mantle, rather than representatives of "primary" or "residual" mantle.

REFERENCES

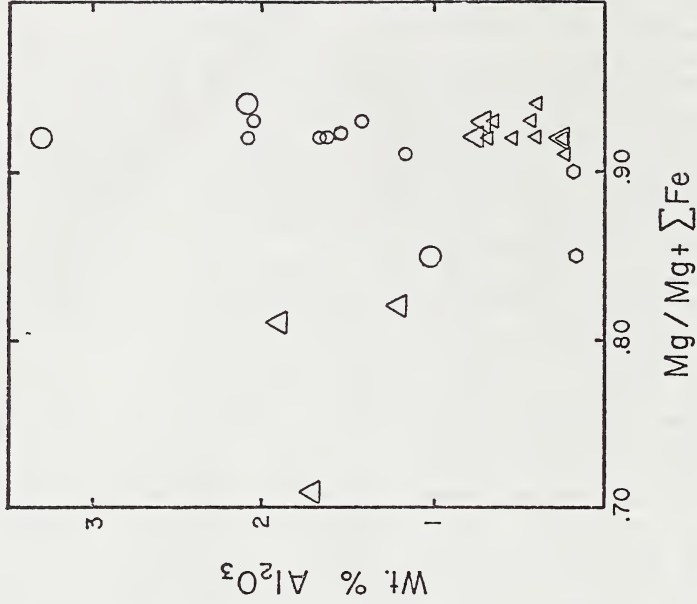
- Boettcher, A. L., J. R. O'Neil, K. E. Windom, D. C. Stewart and H. G. Wilshire, (1977) Abstract submitted to the 2nd Int'l. Kimberlite Conference.
- Dawson, J. B. and J. V. Smith (1973) J. Petrol. 14, 113-131.
- Reid, A. M., C. H. Donaldson, R. W. Brown, W. I. Ridley and J. B. Dawson (1975) Physics and Chem. Earth 9, 525-543.
- Rhodes, J. M. and J. B. Dawson (1975) Physics and Chem. Earth 9, 545-557.
- Wilshire, H. G. and J. W. Shervais (1975) Physics and Chem. Earth 9, 257-272.

FIGURE 1

a. SiO_2 vs Mg-Fe ratio, includes all analysed Lashaine rocks.



b. Al_2O_3 vs Mg-Fe ratio, Lashaine peridotites



Small symbols are analyzed samples of Rhodes and Dawson, 1975; large symbols are analyses from this report: circles, garnet peridotite; triangles, garnet-free and spinel peridotite; hexagons, 'interned, Fe' peridotite (Rhodes and Dawson, 1975); diamond, kaersutite peridotite; squares, pyroxenite.

XENOLITHS OF DIAMONDIFEROUS ULTRAMAFIC ROCKS FROM YAKUTIAN KIMBERLITES

N.P. Pokhilenko, N.V. Sobolev and Yu.G. Lavrent'ev (Institute of Geology and Geophysics, Siberian Branch of the USSR Academy of Sciences, Novosibirsk, USSR)

Sixteen xenoliths of diamondiferous ultramafic rocks were found to occur in "Udachnaya" and "Aikhal" kimberlite pipes in Yakutia. Four xenoliths were found to occur in "Aikhal" pipe (2 - Sobolev et al., 1969; 1 - Sobolev, 1974; 1 - a new sample of the authors), 12 - from "Udachnaya" pipe (1 - by I.P. Ilupin, personal communication; 1 - Pokhilenko et al., 1976; 10 - newly collected samples of the authors). The size of xenoliths varies between 1.4 and 14.3 cm. The xenoliths from "Aikhal" pipe belong to serpentinite containing Cr-pyropes and sometimes chromite (two samples). The xenoliths from "Udachnaya" pipe are of varied mineral composition. The rocks containing these xenoliths belong to the following mineral parageneses: 1) olivine-garnet-diamond (3 samples), 2) olivine-chromite-diamond (1 sample), 3) olivine-garnet-chromite-diamond (6 samples); olivine-garnet-enstatite-chromite-diamond (1 sample); olivine-enstatite-garnet-diopside-ilmenite-diamond (1 sample). All the xenoliths except ilmenite-bearing lherzolite contain more than 90% of olivine as fragments of the deep-seated extremely coarse-grained rocks, in which olivine grains sometimes attain 10 cm in diameter. It is merely xenoliths of ilmenite-bearing lherzolite that is composed of common granular texture with traces of deformations (Pokhilenko et al., 1976).

The electron probe technique was applied to studying the composition of minerals of these xenoliths. The minerals from 15 samples have similar compositions with those included in diamonds (Meyer, Boyd, 1972), (Sobolev, 1974), see Table 1. The lack of diopside from these samples along with low CaO content in the garnets indicates their relation to harzburgite-dunite paragenesis, which predominates in the ultramafic associations with diamond (Sobolev, 1974). No analogues are, however, known among several hundred of crystalline inclusions in diamonds of the mineral compositions of xenoliths of diamondiferous pyrope lherzolite, which contains ilmenite (Table 2).

Extremely interesting structures were found in one of xenoliths characterized by regular strongly altered enstatite and chromite lamellar intergrowths. It is quite probable that these structures had formed as decomposition products of knorringite-rich garnet (70-80 mol %) after the following pattern:



On analysing the obtained data based on experimental investigation of knorringite component entering in Mg-garnets (Malinovsky et al., 1976) it may be concluded that the studied associations containing knorringite-richest garnets had been formed

at pressured not lower than 60 kbar.

REFERENCES

- Malinovsky I.Yu., Godovikov A.A., Doroshev A.M., Ran E.N., 1976. Physico-chemical conditions of mineral-forming processes in the light of experimental data. pp. 135-146.
- Meyer H.O.A., Boyd F.R., 1972. *Geochim. Cosmochim. Acta*, 36, pp. 1255-1274.
- Pokhilenko N.P., Sobolev N.V., Sobolev V.S. and Lavrent'ev Yu.G. 1976. *Dokl. Akad. Nauk SSSR*, 231, pp. 438-441.
- Sobolev N.V., 1974. Deep-seated inclusions in kimberlites and the problem of the composition of the Upper Mantle. *Nauka*, 264 p.
- Sobolev V.S., Nai B.S., Sobolev N.V., Lavrent'ev Yu.G. and Pospelova L.N., 1969. *Dokl. Akad. Nauk SSSR*, 188, pp. 1141-1143.

Table 1

Chemical composition of minerals composing typical xenoliths of diamondiferous ultramafic rocks from Yakutian kimberlite pipes

Min	Olivine			Garnet			Chromite			
	Uv- -823	Uv- 69/76	Uv- -406	Uv- -823	Uv- 69/76	Uv- -406	Uv- -404	Uv- -823	Uv- 69/76	Uv- 406
SiO ₂	41.4	40.7	40.7	41.2	41.9	41.7	42.8	0.00	0.00	0.17
TiO ₂	0.0	0.0	0.0	0.06	0.05	0.02	0.04	0.24	0.17	0.07
Al ₂ O ₃	0.0	0.0	0.0	15.0	14.4	16.2	18.9	4.45	4.08	5.79
Cr ₂ O ₃	0.05	0.04	0.03	12.7	12.4	9.95	7.10	64.5	65.3	63.0
FeO	6.15	6.96	6.44	6.74	7.36	6.88	6.56	17.9	18.2	20.5
MnO	-	-	-	0.39	0.40	0.36	0.30	0.25	0.23	0.36
MgO	52.0	51.2	51.5	20.0	21.4	22.8	22.8	12.0	11.8	11.0
CaO	0.02	0.01	0.01	4.99	3.05	1.71	1.52			
Na ₂ O					0.0	0.02				
NiO	0.28	0.27	0.27							
Total	99.9	99.2	99.0	101.1	101.0	99.6	100.0	99.3	99.8	100.9
f	6.2	7.1	6.6	15.8	16.2	14.3	13.3	45.6	46.5	46.9
Kn				23.2	30.6	26.5	17.1			

Table 2

Chemical composition of minerals composing xenolith of
ilmenite-pyrope diamondiferous lherzolite and pyrope
harzburgite xenolith

Sp.	Uv-255/75					Uv-198/76			
	Ol	Ga	En	Di	Il	Ol	Ga	En	Chr
SiO ₂	41.0	40.6	57.4	55.3	0.01	41.7	41.1	57.0	0.01
TiO ₂	0.01	1.91	0.12	0.36	56.0	0.01	0.14	0.03	0.50
Al ₂ O ₃	0.02	16.9	0.67	2.16	0.54	0.01	14.7	0.41	4.74
Cr ₂ O ₃	0.09	5.99	0.41	1.97	5.45	0.06	11.6	0.50	61.7
FeO	8.74	7.22	5.12	3.16	21.8	6.76	6.85	4.08	19.4
MnO	0.09	0.24	0.09	0.09	0.25	0.01	0.36	0.12	0.22
MgO	50.4	20.5	34.3	17.8	15.6	51.5	21.3	36.2	11.4
CaO	0.03	5.41	0.86	15.9	0.01	0.01	3.72	0.22	0.01
Na ₂ O	-	0.19	0.30	2.37	-	-	0.03	0.13	
NiO	0.28	-	-	0.03		0.26			
Total	100.7	98.9	99.3	99.1	99.7	100.3	99.8	98.7	98.0
f	8.8	16.4	7.7	9.1	43.9	6.8	15.3	5.9	48.8

Table 3

Peculiarities in the Mineral Composition of Xenoliths of
Diamondiferous Ultramafic Rocks (Harzburgite-dunite para-
genesis) from Yakutian Kimberlites

N	f	Cr ₂ O ₃		TiO ₂		CaO			
		min-max	x	min-max	x	min-max	x		
Ol	10	6.2-8.1	6.9	0.03-0.09	0.05	0.01-0.02	0.01	0.01-0.06	0.02
Ga	13	12.3-16.1	14.7	7.1-14.1	10.8	0.02-0.19	0.07	1.52-6.24	3.07
Chr	7	44.6-48.8	46.6	61.7-65.4	64.0	0.07-0.50	0.21		

ZIRCON-OXIDE REACTIONS IN DIAMOND-BEARING KIMBERLITES

E. Raber and S. E. Haggerty (Dept. of Geology, University of Massachusetts, Amherst, Massachusetts 01003)

Zircons ($ZrSiO_4$) and ilmenites ($FeTiO_3$) in kimberlites have widely contrasting distributions: the former are as rare or rarer than diamonds, whereas the latter are characteristic constituents. Our working hypothesis is that zircons and diamonds may be genetically related, and that ilmenites which are commonly associated with zircons provide the best estimate of ilmenite compositions which are likely to form during diamond nucleation. Although ilmenites are widely used as a placer prospecting guide to kimberlites, because they are finger-printed by having high MgO contents, low to intermediate Fe_2O_3 contents and the presence of Cr_2O_3 , no data to our knowledge are available on distinguishing barren kimberlites, from diamondiferous kimberlites based on associated mineralogy. Zircons are important from another aspect inasmuch as they provide among the most reliable age dates for kimberlites.

The objectives of this study are four fold: (1) to determine the compositions of ilmenites associated with zircons; (2) to determine the differences between rutile-zircon and ilmenite-zircon assemblages; (3) to characterize the reactions at rutile-zircon and ilmenite-zircon interfaces; and (4) to compare the inclusions in zircons with those present in diamonds.

In a petrographic and electron microprobe study of discrete zircons, and of zircons associated with ilmenite and rutile from the kimberley pipes, the Monastery mine, and the Mothae pipe, Lesotho we have established:

- (1) The compositions of ilmenites associated with zircons have a narrow range in MgO (8-10 wt %) and in Cr_2O_3 contents (0.02 - 0.85 wt %).
- (2) Subsolidus reactions, along the zircon-ilmenite interfaces, yield an exotic mineral assemblage consisting of zirconolite ($CaZrTi_2O_7$), Ti-rich baddeleyite ($[TiZr]O_2$), and diopside ($CaMgSi_2O_6$) in association with minor calcite ($CaCO_3$).
- (3) Rutile-zircon interface assemblages consist of zirconium-bearing armalcolite ($FeMg$) Ti_2O_5 , zirconolite, baddeleyite, sphene ($CaSiTiO_5$), calcite and diopside.
- (4) The most abundant inclusion in zircon is pyrrhotite, followed by pentlandite. Native Cu, diopside, rutile and ilmenite have also been identified. The overwhelming abundance of sulfides correlates with those of diamond inclusion studies.

Kimberlitic ilmenites exhibit an unexplained parabolic relationship for Mg vs Cr which reaches a minima at values of MgO between 6 and 10 wt % (Haggerty 1975). This minima is characterized by a relatively small number of data points, with the exception of Monastery, which we now propose reflects those ilmenites which formed in association with zircons. These ilmenite compositions may be indicative of a characteristic P-T regime which is not only suitable for zircon formation, but the probability exists also that it is within the diamond stability field.

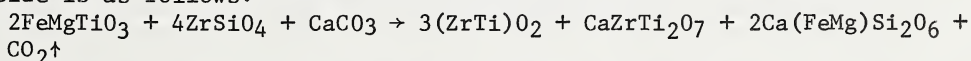
This is the first reported occurrence of zirconolite in a kimberlite and the Mothae locality is the second to contain armalcolite. Both minerals are rare in lunar, meteoritic, and terrestrial rocks and their common association has been identified in only one lunar highland anorthosite (Haggerty, 1973). The ZrO_2 contents of kimberlitic zirconolites vary between 41.9 and 71.3 wt %;

those from the Arbarastkh and the Afrikanda massifs vary between 33.0 and 33.5 wt%; and the lunar examples have ZrO_2 contents between 29.8 - 41.3 wt%. For TiO_2 , the variations from these localities are 16.7 - 40.5 wt%, 30.4 - 31.6 wt% and 26.6 - 35.8 wt% respectively. The kimberlitic examples have ZrO_2 contents which are substantially higher than those from other sources, whereas TiO_2 is both higher and lower. Although we have yet to undertake a detailed REE study of the kimberlitic zirconolites, preliminary data do suggest that these are in low abundances in contrast to the USSR and to the lunar examples which are in the range 3.5 - 21.7 wt%. The divalent cations are relatively constant for all zirconolites, and these are in the range 14 - 18 wt%. The Ti/Zr ratios are of particular interest because of the data by Wark et al., (1973) who show that this ratio may be temperature sensitive. These authors estimate $T=1400 - 1450^\circ C$ for lunar zirconolites, which have Ti/Zr ratios between 1.07 - 1.52, based on experimental data which yields Ti/Zr at $1500^\circ C = 1.31$ and at $1300^\circ C = 2.75$. The kimberlitic zirconolites have average Ti:Zr ratios of 1.49, 0.94 and 0.41 which yields $T = 1450^\circ, 1550^\circ$ and $1625^\circ C$ respectively; these temperatures seem extraordinarily high but the Ti:Zr ratio may also be pressure sensitive.

Of the occurrences of armalcolite, which was first recognized in the lunar samples, those from the Apollo 16 site and one of the rutile-zircon assemblages from Mothae are the only known varieties which are Zr-bearing. Our analytical totals for the latter yield 95-97 wt% and we have tentatively ascribed the deficiency to REE. For all major and minor elements the Mothae example differs in one way or another from lunar Zr-armalcolites and one major distinction is that for values of $ZrO_2 \approx 6wt\%$ all lunar armalcolites are both Ca and Cr enriched ($CaO = 3.0 - 3.5 wt\%$; $Cr_2O_3 = 4.3 - 11.5 wt\%$); the Mothae sample has $CaO = 1.5 wt\%$ and $Cr_2O_3 < 1\%$. High pressure experimental data (Lindsley et al., 1974; Friel et al., 1977) show that armalcolite is stable as a single phase at $1200^\circ C$ and 10kb, but decomposes to a more magnesian armalcolite plus $Geik-Ilm_{SS}$ plus rutile ($dT/dP = 20^\circ C/kb$); at 14 kb and $1200^\circ C$ this three phase assemblage is replaced by rutile plus $Geik-Ilm_{SS}$ ($dT/dP = 30^\circ C/kb$). With the addition of Zr, decomposition is 1-2 kb less than that of Zr-free armalcolite; but with the addition of Mg the end member $MgTi_2O_5$ is stable to at least 20 kb. It is significant that all three of the rutile-zircon assemblages we have examined contain abundant sigmoidal lenses of ilmenite (7-9 wt% MgO) and this is most likely the result of primary armalcolite decomposition (Haggerty 1975). The interface Zr-armalcolite must clearly have formed at $P < 12 kb$.

A comparison of kimberlitic reaction baddeleyites with baddeleyites that are present in association with lunar zirconolite show that there are both minor differences and similarities in oxide concentrations. The outstanding feature is that both types are titaniferous (3.68 - 7.93 wt% TiO_2), a property which is not displayed by primary baddeleyite in gabbros which have TiO_2 concentrations $\sim 0.5 wt\%$ (Keil and Fricker, 1974).

Other minerals which are present in the interface reaction zone are diopside, calcite and sphene. Because these minerals and zirconolite are all Ca-bearing we consider that the mechanism which triggered the reaction was most likely that of a carbonatitic liquid, because all other components necessary for the formation of these minerals are already present in ilmenite and in zircon. One possible reaction to yield zirconolite + baddeleyite + diopside is as follows:



Analytical data on zircons show, on average, that these are close to

stoichiometric $ZrSiO_4$ with minor concentrations of other elements. Although the associated interface baddeleyites are titanian-rich, an evaluation of the P-T conditions of zircon and baddeleyite can be made from available thermodynamic data on coexisting zircon and baddeleyite at high pressures (Nicholls et al., 1971), from the experimental system ZrO_2-SiO_2 at 1 atm. (Butterman and Foster, 1967), the system $CaO - ZrO_2 - TiO_2$ at 1 atm and $T = 1450 - 1550^\circ C$ (Coughanour et al., 1955), and from the occurrences of zircon decomposition to baddeleyite and SiO_2 in impact glasses (El Goresy, 1965; Kleinmann, 1969). From these data we note: (1) Zircon + baddeleyite can coexist in the diamond stability field at $T = 1327^\circ C$, $P = 55.7$ kb; (2) Zircon is stable at $T < 1676^\circ C$ in association with tetragonal ZrO_2 , and at $T < 1170^\circ C$ in association with monoclinic ZrO_2 (baddeleyite), (3) Two of the three zirconolite-bearing assemblages plot within the correct two phase region zirconolite + baddeleyite, whereas the third plots in the one phase titanian-baddeleyite_{ss} field in the system $CaO - ZrO_2 - TiO_2$. If the Ti/Zr ratios of the zirconolites are considered as being $T^\circ C$ -dependent, then those assemblages in the two phase region are compatible with $T = 1450 - 1550^\circ C$. For the third assemblage, Ti/Zr yields $1625^\circ C$ and this too may be compatible but is beyond the limit of available experimental data; and (4) Impactite studies suggest that temperatures $> 1676^\circ C$ and $P \approx 7$ kb are required for the reaction zircon \rightarrow baddeleyite + cristobalite.

From the available pressure and temperature estimates on zirconolite, armalcolite, and baddeleyite we conclude that the formation of these minerals at rutile-zircon and ilmenite-zircon interfaces took place at $P < 12$ kb (based on armalcolite) and $T < 1200^\circ C$ (based on, but unconfirmed, monoclinic baddeleyite, Kresten and Fels, 1975); higher temperatures are also likely $1450 - 1650^\circ C$ (based on zirconolite) in which case tetragonal ZrO_2 should be present. Because CaO is a major component of the interface assemblages we consider the availability of a carbonatitic liquid an essential constituent to promote intercrystalline reaction between zircon and either ilmenite or rutile. A broader conclusion from this study is that the compositions of ilmenites associated with zircons are in a critical range of Mg and Cr; this range may well be constrained by a P-T relationship which is compatible with that of diamond stability.

References: Butterman and Foster (1967). Amer. Min. 52, 880; Coughanour et al., (1955). J. Res. Nat. Bur. Stds. 54, 191; El Goresy (1965). J. Geophys. Res. 70, 3453; Friel et al., (1977). Geochim. Cosmochim. Acta 41, 403; Haggerty (1973) *ibid.* Suppl 4, 777; Haggerty (1975). Phys. Chem. Earth, 9, 295; Keil and Fricker (1974). Amer. Min. 59, 249; Kleinmann (1969). EPSL 5, 497; Kresten and Fels (1975). Mineral. Deposita. 10, 47; Nicholls et al., (1971). Contrib. Min. Pet. 33, 1; Wark et al., (1973). Proc. L. S. C. IV. Houston 764.

A QUENCH ORTHOPYROXENE-ILMENITE XENOLITH FROM KIMBERLITE - EVIDENCE FOR
TI-RICH LIQUID IN THE UPPER MANTLE

Penelope J. Rawlinson and J.B.Dawson, Department of Geology, University of
St. Andrews, Scotland.

Textural, mineralogical and experimental studies have been made on a currently unique non-equilibrated, pyroxene-ilmenite nodule (BD 2027) from the kimberlite of the Weltvreden Mine, S. Africa. The xenolith comprises mainly acicular high-Ti bronzite (terminology of Stephens and Dawson, 1977) irregularly intergrown with magnesian ilmenite in macro-spherulites and comb-layered units; some macrospherulites are nucleated upon larger equidimensional crystals of high-Ti bronzite. These phases are compositionally similar to phases in orthopyroxene/ilmenite nodules from Monastery (Boyd, 1971; this work) and Frank Smith (Frick, 1973) except for slightly higher Al_2O_3 , Cr_2O_3 and $Mg/(Mg+Fe)$; the main difference is in the acicular morphology of the opx in the Weltvreden specimen. Representative analyses are given in Table 1. Relatively coarse, much less abundant clinopyroxene in regular intergrowths with ilmenite occur only in the vicinity of late-stage pegmatitic patches; compared with previously reported analyses of clinopyroxene in lamellar clinopyroxene/ilmenite intergrowths (summary by Gurney et al. 1973), the pyroxene is more calcic, lower in Cr_2O_3 , Al_2O_3 , and Na_2O , and most closely resemble clinopyroxenes in MARID-suite nodules (Dawson and Smith, 1977). The nodule is cut by a 0.5cm vein of more iron-rich magnesium ilmenite. Other phases are rare high-Ti pyrope and titanian phlogopite, the latter occupying interstices between acicular orthopyroxene, but also occurring most abundantly as larger bent crystals in the pegmatitic patches, together with coarse serpentinized olivines, calcite, apatite and ilmenite. Also present are small patches of very fine-grained calcite, serpentine, ilmenite phlogopite and diopside, (together resembling a kimberlite groundmass assemblage (Dawson et al. 1978)), which are interpreted as the final products of essentially "closed" crystallization of the presumed high-titanium liquid. We propose a complex cooling history for the rock. Initial crystallization of garnet and orthopyroxene, was followed by rapid simultaneous crystallization of ilmenite and acicular high Ti-bronzite. The phases in the pegmatitic and kimberlitic patches were the last to crystallize under high fH_2O and fCO_2 conditions. Pyroxene-ilmenite geothermometry (F.C. Bishop pers. comm.) suggests temperatures of $1020 \pm 40^\circ$ for opx-il intergrowths, and $910 \pm 30^\circ C$ (at 30 kbars) for cpx-ilmenite intergrowths, thereby confirming the textural evidence for at least two stages of crystallization.

Experimental work on the bulk rock, (containing the pegmatitic calcite, serpentine and phlogopite areas, in addition to the highly refractory px-il areas), attempted to establish the crystallization sequence and to simulate the unusual texture of the opx-il intergrowths. The solidus at 20 kb was $1200^\circ C$, rising to $1230^\circ C$ at 30 kb. Olivine was the liquidus phase from 5-30 kb, and the ilmenite-out curve coincided with the beginning of melting. Olivine reacted with liquid to give enstatite. The range of simultaneous crystallisation of enstatite and ilmenite increased from $180^\circ C$ at 20 kb to $260^\circ C$ at 30 kbars. Bulk-rock

melted at 20 kb and held at the solidus temperature for 10 minutes before quenching produced fine acicular intergrowths of opx and ilmenite, strongly resembling the texture of the original rock.

The acicular opx-ilmenite crystallization stage of the natural rock is interpreted as due to rapid co-precipitation of opx and ilmenite from an undercooled, supersaturated Ti-rich liquid in an upper mantle vein or dyke. Coarser intergrowths described previously are possibly derived from upper-mantle pegmatites - the textural differences perhaps being a reflection of the volatile content at the time of injection. These conclusions are in agreement with theories that pyroxene-ilmenite intergrowths result from cooling of Ti-rich liquids (e.g. Wyatt, 1977) rather than by exsolution from earlier high-pressure phases.

References

Boyd (1971) Carn. Inst. Wash. Yk. 70, 134. Dawson & Smith (1977) GCA 41, 309. Dawson, Smith & Hervig (1978) Neu. Jahrb. Min.. Frick (1973) Trans. G. Soc. S. Afr. 76, 195. Gurney, Fesq & Kable (1973) in Lesotho Kimberlites, Nixon ed., Lesotho Dev. Corp., 238. Stephens & Dawson (1977) J. Geol. 85, 433. Wyatt (1977) Contr. Min. Pet. 61, 1.

Table 1. Representative analyses of phases in BD 2027

	1	2	3	4	5	6	7
SiO ₂	56.16	0	51.94	0.15	0	41.74	40.11
TiO ₂	0.37	53.00	2.66	54.05	48.52	1.62	5.14
Al ₂ O ₃	1.57	0.37	1.32	0.05	0.60	21.70	11.65
Cr ₂ O ₃	0.12	0.72	-	0.36	0.89	0.08	0.15
FeO	7.96	33.72	3.70	34.72	41.24	11.00	6.58
MnO	0.19	0.27	0.07	0.59	0.20	0.27	0.05
MgO	32.00	11.08	15.89	9.19	10.20	20.56	20.41
NiO	0.20	0.07	-	-	-	-	0.04
CaO	1.07	-	23.48	0.1	-	3.22	-
Na ₂ O	0.27	-	0.62	-	-	0.12	0.26
K ₂ O	n.d.	-	-	-	-	-	9.73
Total	99.9	99.3	99.7	99.3	101.7	100.7	94.1

1 Opx; 2 Ilm intergrown with 1; 3 Cpx; 4 Ilm intergrown with 3; 5 Ilm in vein; 6 Garnet; 7 Ti-phlogopite in pegmatitic patch.

THE DETAILED CHEMISTRY OF THE REACTION $SP + PX = GT + OL$ IN PYROXENITE INCLUSIONS FROM SALT LAKE CRATER, HAWAII

J.B. Reid, Jr. (School of Natural Science, Hampshire College, Amherst, MA, 01002 and G-6, LASL, Los Alamos, NM, 87545)
 Margaret Eggleton (School of Natural Sciences, Hampshire College, Amherst, MA, 01002).

In most of the garnet pyroxenite inclusions at Salt Lake Crater, Hawaii, garnet is not a primary mineral but rather has formed during the cooling of an assemblage of aluminous pyroxene(s) and spinel (Green, 1966). The garnet occurs mainly as reaction rims between spinel and clinopyroxene; it may also occur as directly exsolved blebs in certain occasional grains of clinopyroxene. The goal of this study has been to reconstruct the modal proportions and chemical compositions of the pre-garnet mineralogy in these rocks, and thereby identify the components of the initial pyroxenes and spinels which have contributed to the formation of the garnet and olivine in the rock. For each major element determined by microprobe analysis in the phases of a given rock, a mass-balance equation can be written:

$$a [e_i]_{SPI} + b [e_i]_{CPXI} + c [e_i]_{OPXI} = d [e_i]_{GTII} + e [e_i]_{OLVII} + f [e_i]_{OPXII} + g [e_i]_{CPXII} + h [e_i]_{SPII}$$

(where I refers to the initial, pre-garnet rock and II refers to the present analysed rock. a through h are modal proportions (wt.%) and e_i refers to one of the eight analysed elements. All of the terms on the right side of the equation are known, leaving a system of eight equations and at the outset, 27 unknowns.)

A number of additional compositional and textural constraints exist. Even in a single rock, spinels are surrounded by garnet coronas of differing relative size, and show a systematic linear variation in composition as a function of the degree to which the garnet-forming reaction has proceeded. (As the reaction progresses the remnant spinel becomes richer in Cr, Fe, Ti, and Mn and poorer in Al and Mg.) Although the reasons for this variation are unclear, one can extrapolate these trends to $GT/SP = 0$, and closely fix the composition of the pre-garnet spinel (SPI). The modal proportion of SPI is determined by knowing the compositions of SPI and SPII, the modal proportion of SPII, and by the observation that to a first order approximation the initial spinel's Cr budget simply becomes concentrated in the eventual, smaller, garnet-rimmed spinel. (In such rock studied in detail, SLC8, Cr_2O_3SP/Cr_2O_3GT ranges from 10 for low Cr spinels (2.3% Cr_2O_3) to 22 for spinels with about 9% Cr_2O_3 ; Cr_2O_3SP/Cr_2O_3CPX ranges from 18 to 47 over the same range).

The combined composition and modal proportion of CPXI plus OPXI are thus determined, allowing a balanced relation, for SLC8, to be written:

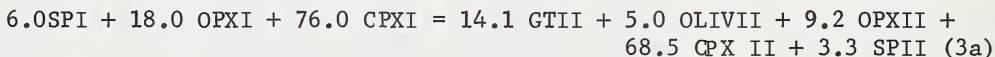


or equivalently



where SPR and PXR refer to the components contributed to the reaction by the initial spinel and combined pyroxene. If just prior to garnet formation, the rock had simply consisted of SPI + a single subcalcic pyroxene (combination of OPXI + CPXI), PXR would be the actual contribution from that pyroxene. Textures indicate however that such a single pyroxene, if it ever existed, had exsolved to discrete grains of opx and cpx prior to garnet formation.

An approximate composition for CPXI is obtained by the recombination of CPXII and GTII, in those isolated clinopyroxenes showing exsolved garnet. This composition (particularly its Al_2O_3) is very sensitive to the proportions of CPXII and GTII used in the vicinity of the modally determined values. The best values for the compositions and modal abundances for both CPXI and hence for OPXI are obtained by choosing a CPXII/GTII ratio which allows the ratio $\text{Al}_2\text{O}_3\text{CPXI}/\text{Al}_2\text{O}_3\text{OPXI}$ to be 1.5, a value consistently found in aluminous spinel lherzolites at Salt Lake Crater and Kilbourne Hole. (See table I for compositional data.) Equations (2a) and (2b) can now be rewritten:



and



Two interesting geophysical results follow from these data. (1) As predicted by MacGregor's experimental study of the effects of Cr content on the P-T position of the spinel-garnet boundary (MacGregor, 1970), the increasing Cr content of the garnet-rimmed spinels as the reaction proceeds indicates that spinel and garnet should coexist over a certain range of pressures for any given bulk composition, and that even if the upper mantle were regionally homogeneous with respect to $\text{Cr}/(\text{Cr} + \text{Al})$, one would not expect a sharp boundary or density contrast to exist at any depth. (2) It should be noted that the dominant contribution of CPXI to the garnet forming process is high in Mg (23.20%) and low in Ca (9.78%). This suggests that caution is needed when comparing apparent equilibration temperatures for garnet-bearing and garnet-free rocks using the simple En-Di solvus for clinopyroxene temperatures.

Table I

	SPI	SPII	SPR	CPXI	CPXII	CPXR
SiO ₂	.00	.00	.00	50.71	51.97	42.86
TiO ₂	.30	.23	.38	.74	.88	.00
Al ₂ O ₃	64.00	62.90	65.31	7.36	6.80	13.04
Cr ₂ O ₃	1.50	2.75	.00	.17	.16	.27
FeO	12.10	12.50	11.62	4.39	3.74	10.68
MnO	.10	.09	.11	.14	.10	.51
MgO	21.70	21.32	22.15	15.54	14.83	23.20
CaO	.00	.00	.00	18.60	19.71	9.78
Na ₂ O	<u>.00</u>	<u>.00</u>	<u>.00</u>	<u>1.59</u>	<u>1.74</u>	<u>.34</u>
	99.70	99.84	99.57	99.24	99.95	100.68
	OPXI	OPXII	OPXR	GTII	OLIVII	
SiO ₂	54.38	55.30	53.33	41.87	40.78	
TiO ₂	.34	.17	.51	.14	.00	
Al ₂ O ₃	5.42	4.30	6.59	23.70	.00	
Cr ₂ O ₃	.09	.10	.08	.16	.00	
FeO	7.24	6.80	7.70	8.93	11.18	
MnO	.12	.11	.14	.33	.14	
MgO	31.52	31.99	30.99	19.81	47.72	
CaO	.67	.66	.66	4.91	.08	
Na ₂ O	<u>.06</u>	<u>.11</u>	<u>.12</u>	<u>.00</u>	<u>.00</u>	
	99.84	99.55	100.12	99.91	99.97	

References:

- (1) Green, D.H. (1966) The Origin of the "eclogites" from Salt Lake Crater, Hawaii, EPSL, 1, 414-420.
- (2) MacGregor, I. (1970) The effect of CaO, Cr₂O₃, Fe₂O₃ and Al₂O₃ on the stability of spinel and garnet periodites, Phys. Earth Planet. Interiors, 3, 372-377.

MINERAL CHEMISTRY AS AN INDICATOR OF CRYSTALLIZATION PATHS IN CARBONATE-BEARING MAGMAS

W. I. Ridley (Lamont-Doherty Geological Observatory, Columbia University, Palisades, New York 10964)

D. Elthon (Department of Geological Sciences, Columbia University, Palisades, New York 10964)

There are several localities at which carbonatites are intimately associated with other carbonated rocks showing a range of carbonate/silicate ratios, e.g., kimberlites, alnoites, damkjernites, mica lamprophyres, carbonated nepheline syenites, ijolites etc. Usually these associations are sufficiently intimate to suggest genetic relationships which may throw some light on the ultimate origin of both kimberlitic and carbonatitic magmas. Presently, little comprehensive data are available that document variations in crystal chemistry, stability limitations and reaction relationships in such rock associations. We are currently examining the detailed mineral chemistry of suites of samples from the Oka Complex, Monteregeian Hills; Magnet Cove Complex, Arkansas; Beemersville Complex, New Jersey; and the Fen District of Norway. Initial studies have focussed on the nature of the spinel phases. The Oka carbonatites are unique in containing abundant magnetite showing a considerable solid solution of magnesioferrite, hercynite and jacobsite. For instance, MnO is rarely < 2.5% and commonly 9-10%, MgO 1-9% and Al₂O₃ 1-13%. These rocks also contain spinels which are hercynite-spinel (s.s) solutions but also contain ~ 3% MnO. Similar spinels occur in the Magnet Cove carbonatites but with negligible MnO contents; the magnetites are similar to the Oka type, but again are lower in MnO.

In contrast, the Beemersville carbonatite contains a magnetite-ulvospinel solid solution phase with only minor MnO, Al₂O₃, MgO. In all these localities there is clear evidence for perovskite rimming magnetite, as well as perovskite occurring as a separate, groundmass phase. Preliminary data indicates that the more silicate-rich rocks associated with the carbonatites have spinels with much more restricted compositions.

SYNTHESIS OF PYROPE-KNORRINGITE GARNET AND THE ORIGIN OF DIAMONDS OF PERIDOTITE PARAGENESIS

A. E. Ringwood (Research School of Earth Sciences, Australian National University, Canberra, A.C.T. 2600, Australia)

S. E. Kesson (Research School of Earth Sciences, Australian National University, Canberra, A.C.T. 2600, Australia)

The garnet solid solution series between pyrope ($Mg_3Al_2Si_3O_{12}$) and knorringite ($Mg_3Cr_2Si_3O_{12}$) was synthesised from oxide mixtures at 60-80 kbar and 1400-1500°C using Bridgman anvils. Lattice parameters and refractive indices were found to vary linearly with composition (Table 1 and Figure 1). Pure knorringite, synthesised for the first time, has a lattice parameter of 11.600 Å and a refractive index of 1.83. Synthesis of pure chromium kyanite Cr_2SiO_5 proved unsuccessful, however, Cr-rich kyanites ($Al_{0.5}Cr_{1.5}SiO_5$) were synthesised at 70 kbar, 1500°C. Refractive index data indicate complete solid solution from Al_2SiO_5 to at least $Al_{0.5}Cr_{1.5}SiO_5$.

The common occurrence of knorringite-rich garnets as inclusions in natural diamonds may provide a key to diamond genesis. Most diamonds occur in one of two major mineral parageneses (i) eclogitic, and (ii) peridotitic. The latter, either in close association with diamond or as inclusions within diamond, typically consists of olivine, enstatite and knorringite-rich garnet. Calcic pyroxene is absent and, moreover, the very low CaO content of the orthopyroxene would appear to preclude any prior coexistence of calcic pyroxene (Sobolev et al., 1973). These assemblages differ from normal mantle-derived garnet peridotites not only by lower CaO contents (and hence an absence of calcic pyroxene) but also in the much higher Cr_2O_3 contents exhibited by garnet and higher 100 Mg/(Mg + Fe) ratios in all phases.

The above chemical and mineralogical characteristics are inconsistent with the hypothesis that diamonds crystallised directly from kimberlite parent magmas (e.g. Williams, 1932), and point towards a more complex petrogenesis. It is suggested that the magnesian olivine + enstatite + knorringite-rich garnet paragenesis ultimately may have been derived from olivine + orthopyroxene + Cr-spinel cumulates (with minor sulfides) precipitated within the oceanic crust, and subsequently recycled into the mantle by subduction. Low-grade alteration may have introduced minor amounts of carbonates and hydrated phases (e.g. serpentine) into the cumulate assemblage. During subduction, partial melting is believed to have occurred, accompanied by metamorphic re-equilibration of the magnesian residual mineralogy to Cr-rich, Ca-poor garnet and orthopyroxene plus Fe-rich olivine. The lower redox state imposed by the low Fe^{3+}/Fe^{2+} of the original cumulates (compared to their parental magma) together with the presence of minor sulfides, resulted in the breakdown of carbonate phases and CO_2 -bearing fluids in fluid inclusions, and precipitation of diamond within its P,T stability field. The wide range of carbon isotope compositions observed in natural diamonds (Sheppard and Dawson, 1975) appears to be compatible with this hypothesis. Moreover, the conclusions of Fesq et al. (1975) that some diamonds crystallised in the presence of a H_2O and CO_2 -rich picritic magma (the partial melt produced during subduction) and an immiscible sulfide phase, is consistent with the above hypothesis for diamond genesis.

References

- Fesq H., Bibby D., Erasmus C., Kable E. and Sellschop J. (1975) Phys. Chem. Earth 9, 817.
 Sheppard S. and Dawson J. (1975) Phys. Chem. Earth 9, 747.
 Sobolev N. V., Lavrent'ev Y., Pokhilenko N. and Usova L. (1973) Contrib. Mineral. Petrol. 40, 39.
 Williams A. F. (1932) The Genesis of the Diamond (Ben, Ltd., London).

Table 1. Lattice parameters and refractive indices of pyrope-knorringite solid solutions

Composition	Lattice parameter \AA	Refractive Index
$\text{Mg}_3\text{Al}_2\text{Si}_3\text{O}_{12}$	11.460 ± 0.001	1.714
$\text{Mg}_3\text{AlCrSi}_3\text{O}_{12}$	11.537 ± 0.002	1.768 ± 0.005
$\text{Mg}_3\text{Al}_{0.5}\text{Cr}_{1.5}\text{Si}_3\text{O}_{12}$	11.571 ± 0.002	1.795 ± 0.005
$\text{Mg}_3\text{Al}_{0.2}\text{Cr}_{1.8}\text{Si}_3\text{O}_{12}$	11.586 ± 0.002	1.82 ± 0.01
$\text{Mg}_3\text{Cr}_2\text{Si}_3\text{O}_{12}$	11.600 ± 0.001	1.83 ± 0.01 (extrap)

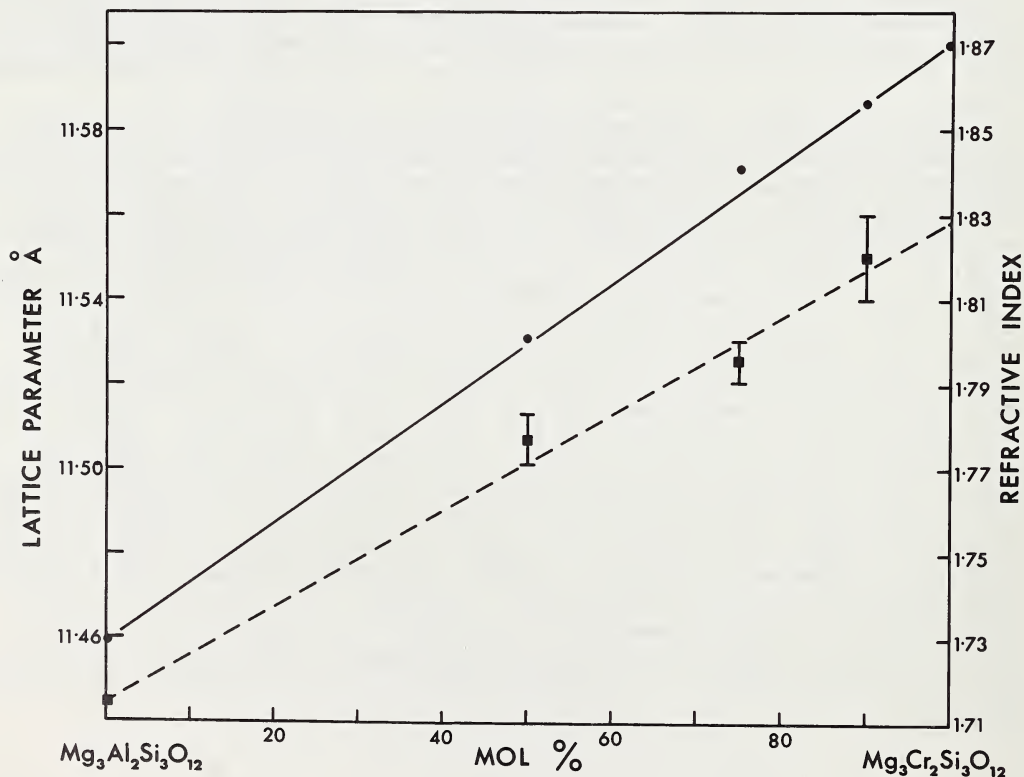


Figure 1.

DIAMOND AND GRAPHITE IN ECLOGITE XENOLITHS FROM KIMBERLITE

D.N. Robinson, Anglo American Research Laboratories, P.O. Box 106,
Crown Mines, 2025. Republic of South Africa.

Some characteristics of nine diamond eclogite xenoliths, five diamond-graphite eclogite xenoliths and ten graphite eclogite xenoliths are summarised below.

SPECIMEN	KIMBERLITE LOCALITY	MASS, g	+ MODAL COMP.				NO. OF DIAMONDS	LARGEST, ± carat	NO. OF GRAPHITE XLS.
			cpx	ga	ky	cor			
AK1/9	Orapa	7,4	60	40			14 ^x	0,06	
AK1/10	"	14,7	60	40			2 ^x	0,2	
DB/1	Doornkloof	15,2	50	50			1 ^x	5	
DB/2	"	13,3	30	70			1 ^x	1,8	
DB/3	"	3,1	30	70			1 ^x	0,15	
DB/4	Bobbejaan	9,1	60	40			1 ^x	1	
DB/5	Jagersfont.	1,5	65	35			5 ^x	0,01	
DB/6	Excelsior	24,2	75	20	5		1 ^x	1	
DB/7	"	10,8	50	45	5		1 ^x	4	
HRV 247	Rob.Victor	943,0	30	70			49	0,2	+ 200
XRV 22	"	248,1	70	30			119	0,006	+ 200
PJL/18	"	115,7	25	25			3	0,002	6
JJG 531	Jagersfont.	13,1	85	15			5	0,3	+ 150
AK1/25	Orapa	12,0	55	45			1	0,003	16
AK1/13	"	8,5	30	70					3
AK1/24	"	8,4	50	50					25
AK1/26	"	2,1	65	35					3 ^x
AK1/28	"	1,8	80	20					28 ^x
AK1/29	"	8,8	20	80					11
AK1/30	"	8,5	15	85					11
AK1/31	"	24,4	35	65					3 ^x
AK1/12	"	11,6	60	30	10				3
AK1/27	"	4,9	50	50	tr				5
AK1/34	"	21,2	60	35		5			2 ^x

^x exposed at xenolith surface only.

The xenoliths are from both kimberlite pipes and dykes and kyanite - and corundum-bearing varieties are represented. In some cases diamond and graphite were recovered by dissolving the eclogite but in other cases only exposed portions of these minerals were examined.

DIAMOND

Diamond-bearing xenoliths contain either a single, fairly large diamond or a number of small diamonds. Crystals as small as 3×10^{-6} carat were recovered (eg. XRV 22) and much of the range in diamond size found in kimberlite is represented in the xenoliths. In all diamond-bearing xenoliths diamond is considerably more common than in kimberlite, e.g. in AK1/9, HRV 247 and JJG 531 diamond is more than 10 000 times as abundant, by mass, as in host kimberlite and in XRV 22 and PJL/18 it is more than 1 000 times as abundant. In some small xenoliths diamond constitutes a few per cent of the specimen. Only a very small proportion (i.e. a few hundred ppm) of disaggregated diamond-bearing eclogite can, therefore, account for all of the diamond in some kimberlite.

Primary growth forms of diamond are the octahedron and cube, with the latter forming at relatively low temperatures (Giardini and Tydings, 1962), while the dodecahedron is a dissolution form (Seal, 1962; Moore and Lang, 1974). Dodecahedral diamond examined in situ in HRV 247 was seen to be directly in contact with clinopyroxene and garnet (and phlogopite) indicating that partial dissolution of diamond occurred before crystallisation of the eclogite. A variety of diamond crystal forms is represented in the xenoliths, including octahedra, cubes, dodecahedra and, most commonly, combined forms. In individual diamond eclogite specimens, all diamond crystals are similar in habit, e.g. the diamonds in AK1/9 are all octahedral-dodecahedral combined forms. In diamond-graphite eclogite specimens, however, an assortment of diamond crystal forms can be present. eg. in HRV 247, XRV 22 and JYG 531 the dodecahedral form is strongly developed among the larger crystals while the smallest are octahedra. This suggests that either two populations of diamond, of which one experienced little or no dissolution, are represented or the smallest crystals were protected from dissolution, in some diamond-graphite eclogite. Diamond cubes are also present in HRV 247 and XRV 22, suggesting that some of their diamond crystallised at relatively low temperature. Contact- and interpenetrantly-twinned crystals are common in some xenoliths and many diamonds are broken. In XRV 22 some crystals are hopped at one side as if their growth was impeded.

Surface textures, such as trigons on octahedral surfaces, which are common features of diamonds from kimberlite and are indicative (Phaal, 1965) of etching at temperatures above about 1000°C, are developed on most of the diamonds. The diamonds of two xenoliths (DB/7 and JYG 531) exhibit black surface coatings, however, beneath which irregular and hexagonal pits, the latter of which suggests (Phaal, 1965) etching at 900-1000°C, are developed in diamond.

GRAPHITE

Graphite in both diamond-graphite eclogite and graphite eclogite occurs as discrete crystals, up to 2,5 mm in diameter, which are predominantly tabular hexagonal prisms with slightly rounded edges. Embayed and irregular graphite crystals, which can be interpreted either to have grown in a confined space or to have experienced partial dissolution, are also present in some specimens (eg. AK1/25, AK1/13, AK1/30 and AK1/27). Excepting for the black coatings noted on diamonds of two specimens, nothing suggests that graphite is not a primary mineral in the xenoliths.

Because of the low density of graphite (even at very high pressure if temperature is high; see Berman, 1965), graphite-bearing eclogite is unlikely to be igneous crystal cumulate.

DIAMOND-GRAPHITE RELATIONSHIPS

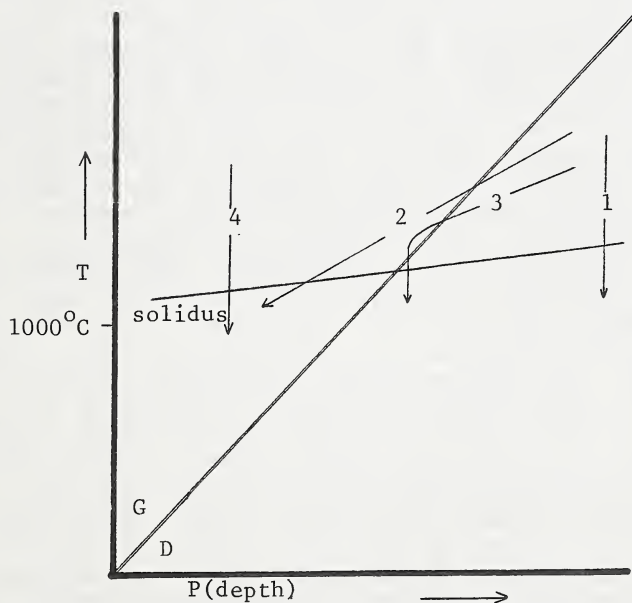
In diamond-graphite eclogite xenoliths, diamond and graphite crystals can be either interspersed (eg. JYG 531) or each concentrated in a portion of the specimen (eg. HRV 247 and XRV 22). Xenoliths consisting of a diamond-rich and a graphite-rich portion can only have crystallised from liquid, and are likely to be samples of common, very small volumes of carbon-bearing eclogite rather than of diamondiferous-graphitic interfaces in large bodies of carbon-bearing eclogite. In eclogite in which diamond and graphite are interspersed, carbon must have crystallised late if from magma.

PETROGENESIS

Evidence that partial dissolution of diamond pre-dated eclogite crystallisation, and the association of diamond-rich and graphite-rich eclogite in some xenoliths suggest an igneous origin for the rocks. At graphite-stable conditions, diamond will dissolve in liquid while graphite may crystallise, so partially resorbed diamond crystals (ie. exhibiting dodecahedral surfaces) may indicate that diamond-stable conditions were followed by graphite-stable conditions. Such a change can be explained either by diminishing pressure or increasing temperature, so that more than one type of crystallisation path can be invoked to explain some types of carbon-bearing eclogite. Likely crystallisation paths are, however, illustrated in the accompanying figure.

REFERENCES

- Berman, R. 1965. Physical Properties of Diamond. Ed. Berman, R. p371-393.
Giardini, A.A. and Tydings, J.E. 1962. Amer. Mineral., 47, p1393-1421.
Moore, M. and Lang, A.R. 1974. J. Crystal Growth, 26, p133-139.
Phaal, C. 1965. Ind. Diam. Rev., 26, p97-100.
Seal, M. 1962. First Int. Conf. on Diamonds in Ind., Paris, p361-375.



P(depth) - T paths for magma crystallising various types of carbon-bearing eclogite. 1. Diamond eclogite in which diamonds are sharp-edged octahedra. 2. Diamond eclogite in which diamonds are partly resorbed and graphite floated off to subsequently form graphite eclogite, or diamond-graphite eclogite in which carbon crystallisation either late or from very small volume of magma only and unresorbed diamond crystals were protected. 3. Diamond-graphite eclogite with more than one generation of diamond. 4. Graphite eclogite.

FIELD GEOLOGY AND PETROLOGY OF THE MINETTE DIATREME AT BUELL PARK, APACHE COUNTY, ARIZONA

M.F. Roden¹ (Department of Geological Sciences, University of Texas, Austin, Texas 78712)

Field relations and rock and mineral chemistry were investigated to understand the volcanology of the minette diatreme, the relationship between minette and kimberlite, and the genesis of minette varieties at Buell Park, Arizona. The compositional variation of the minettes there encompasses the range of compositions found in minettes throughout the Navajo volcanic field. "Minette" is used for a group of intrusive and extrusive rocks which are linked by their potassic nature (3-7.5% K₂O) and mineralogy (phenocrysts of diopside + phlogopite + olivine in a groundmass of alkali feldspar + diopside + oxides + mica + analcime + quartz + amphibole). Previously kimberlite and minette were known to occur together at Outlet Neck and Buell Park within the Navajo field, but two new occurrences have been found: The Beast, a minette neck 5 km east of Buell Park, contains a block of kimberlite, and a small unnamed kimberlite pipe 8 km east of Buell Park is bisected by a minette dike. Furthermore, at Buell Park where a minette diatreme is nested within a kimberlite diatreme, evidence indicates an overlap in time of minette and kimberlite eruptions: the upper 75 m of the layered kimberlite contains subrounded, altered minette clasts (analysis BP-69, Table 1), and two small kimberlitic breccia pipes (Fig. 1) occur along the margins of two late minette intrusions. In addition to xenocrysts derived from minette, the kimberlitic breccia pipes contain xenocrysts of kinked olivine (Fo₈₉₋₉₁), chrome-rich spinel (39.5% Cr₂O₃, 25.1% Al₂O₃), chrome-rich diopside (TiO₂ < 0.04%, 0.5% Cr₂O₃), and enstatite (Wo_{0.5}En₉₂Fs₇). The bulk of the kimberlite, however, was erupted before the minette.

The Buell Park minette diatreme occupies the southern third of Buell Mountain (Fig. 1); the northern two thirds consist of layered kimberlite lapilli tuff capped and intruded by minette. As at other minette centers explosive eruptions preceded extrusion and intrusion of massive minette. The floor of the maar could not have been more than 100 m above the presently exposed tuff-breccias; more likely, the tuff-breccias were just below the crater floor. Two types of tuff-breccia crop out: a light-colored variety, unsorted and unbedded, containing subangular nonvesicular glassy minette clasts up to a meter across, and a crudely bedded, more coherent dark-colored tuff-breccia containing both subangular minette clasts and flattened bombs. The light-colored tuff-breccia probably is a vent filling akin to the tuff-breccias that form Shiprock, while the dark-colored tuff-

1. Present address: Department of Earth and Planetary Sciences, Massachusetts Institute of Technology, Cambridge, Massachusetts 02139.

TABLE 1

Chemical Analyses of Buell Park minettes

	BPR-6	BPR-5	BP-69	BP-37	BP-41	BP-35.
SiO ₂	49.13	48.94	55.46	56.23	58.88	59.50
TiO ₂	2.02	2.03	0.91	1.08	0.87	0.89
Al ₂ O ₃	10.51	10.11	10.65	12.14	13.38	12.93
Fe ₂ O ₃	3.82	4.47	3.68	4.38	3.77	3.02
FeO	4.30	3.60	1.08	1.36	1.17	1.46
MnO	0.12	0.12	0.05	0.08	0.06	0.06
MgO	9.87	10.03	9.17	6.63	4.31	4.90
CaO	9.06	8.98	4.34	6.37	6.12	5.30
Na ₂ O	2.06	1.28	1.42	2.60	2.87	2.53
K ₂ O	4.86	5.22	6.98	6.76	7.20	7.21
H ₂ O+	2.38	2.92	2.09	0.94	0.36	0.54
H ₂ O-	0.38	0.80	2.71	0.36	0.08	0.60
P ₂ O ₅	0.97	1.08	0.63	0.77	0.74	0.64
CO ₂	0.00	0.01	0.00	0.02	0.06	0.10
Total	99.48	99.59	99.17	99.62	99.87	99.68

BPR-6 = olivine-bearing minette, western end of the ring dike, Buell Park; BPR-5 = olivine-bearing minette, central portion of the ring dike, Buell Park; BP-69 = minette clast, layered kimberlite lavilla tuff, Buell Mountain; BP-37 = minette clast, minette tuff-breccia, Buell Mountain; BP-41 = felsic minette, northern end, Buell Mountain; BP-35 = quartz-bearing felsic minette plug, southern end, Buell Mountain (Analyst for all samples: G. Karl Hoops).

breccia formed from material plastered on the vent walls. The tuff-breccias and layered kimberlites were later intruded by numerous minette dikes and sills and a late quartz-bearing plug (Fig. 1).

Six K-Ar ages have been obtained on phlogopite from minettes: three from Buell Park, and one each from Fluted Rock, Black Rock (Ft. Defiance), and The Beast. Five of the six agree within experimental error and average 25.4 m.y., about 5 m.y. younger than previously reported ages (for example, Naeser,

1971; Armstrong, 1969). One clast from a tuff-breccia dike(?) at Buell Park was dated at 33 m.y. although field evidence conclusively demonstrates that it must be the same age as the other samples.

The felsic minettes of Buell Mountain contrast sharply with the mafic minette of a ring dike located within Buell Park less than 2 km to the south. The ring dike minettes are characterized by lower SiO₂, lower total alkalis, and higher total Fe, TiO₂, MgO, and CaO (Table 1) than the Buell Mountain minettes. The ring dike minette also differs from the felsic minettes in containing titaniferous phlogopite (7.5-11% TiO₂, Mg/Fe = 3.6-2), olivine phenocrysts (Fo₆₆-Fo₇₈, core to rim), groundmass analcime, and in the rarity of xenoliths. The felsic minettes of Buell Mountain lack olivine and analcime, many contain interstitial quartz, all contain abundant xenoliths (5% volume), including numerous spinel lherzolites and websterites, and the phlogopites are less titaniferous (TiO₂ <6%, Mg/Fe = 3-6). The diopsides from all the minettes are similar, typically Ca₄₆Mg₄₅-50Fe₄₋₉. The spatial association suggests that the mafic minettes might be related to the felsic minettes by fractionation of olivine, diopside, and phlogopite, but the phenocryst compositions cannot be combined with the daughter composition (analysis BP-37), a clast from the tuff-breccias on Buell Mountain, to yield a satisfactory ring dike composition. Moreover, the presence of dense inclusions argues against crystal settling being effective above their original location, presumably the upper mantle. More likely, primary mafic and felsic minettes arose by partial melting of a heterogeneous, enriched portion of the mantle



Fig. 1. Geologic map of Buell Mountain. Units from youngest to oldest are: Q, Quaternary alluvial and colluvial deposits, undifferentiated; Qc, soil and talus; Ql, landslide masses; Qn, stream deposits currently being dissected; Tkb, kimberlitic breccia; Tmfp, quartz-bearing, felsic minette plug; Tmfa, altered felsic minette; Tmf, felsic minette, undifferentiated; Tmf4, quartz-bearing, felsic minette plug(?); Tmf3, platy-cleaved, diopside-rich minette; Tmf2, oxidized felsic minette; Tmf1, phlogopite-rich, schistose minette; Ttl, layered minette lapilli tuff; Ttbd, dark-colored minette tuff-breccia; Ttbl, light-colored minette tuff-breccia; Tkgl, layered kimberlite lapilli tuff; Pdc, De Chelly Sandstone.

consisting of garnet + phlogopite + diopside + apatite ± olivine + ilmenite. The more felsic minettes (analyses BP-35, BP-41, Table 1) may be related by fractionation of diopside, phlogopite, and magnetite from a magma similar in composition to minette clasts in the tuff-breccias (analysis BP-37, Table 1), although magnetite appears to be restricted to the groundmass.

Distinctive, sparse green salite cores occur in diopside phenocrysts throughout the Navajo field (for example, Shiprock, Roof Butte, Church Rock, Twin Buttes, and Zildlitloi field). These cores rich in Na_2O (0.6-1.8%) and Al_2O_3 (2-4.8%) but notably poor in Cr_2O_3 ($\leq 0.10\%$). In contrast, normal diopside cores commonly have Cr_2O_3 contents greater than 0.15%. The low Cr_2O_3 contents of the green cores militates against a genetic relationship with the minette magmas; more likely, the cores are xenocrysts from a widespread rock type in the upper mantle or lower crust. S.N. Ehrenberg (written communication) has also concluded that similar salite cores at The Thumb are xenocrysts.

Armstrong, R.L., 1969, Geol. Soc. Amer. Bull. 80: 2087-2090
 Naeser, C.W., 1971, Jour. Geophys. Research, 76: 4978-4985

THE STABILITY OF GRAPHITE AND DIAMOND AS A FUNCTION OF THE OXYGEN
FUGACITY IN THE MANTLE.

Rosenhauer, M. (Frankfurt), Woermann, E., Knecht, B. (Aachen)
and Ulmer, C.G. (Philadelphia).

Since graphite as well as diamond are found in kimberlitic material, equation (4) of the preceding abstract :

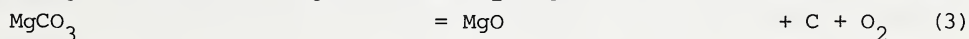
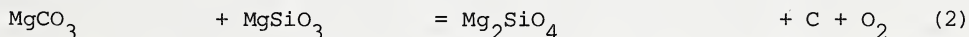
$$\log f_{O_2} = 2.74 - \frac{19559}{T} + \frac{0.13 (P-1)}{T} \quad \text{for bar and K}$$

is directly applicable for the evaluation of limiting oxygen fugacities as a function of temperature and pressure in the earth's mantle. Strictly speaking this equation is valid only as long as graphite coexists with a pure fluid carbon oxide phase.

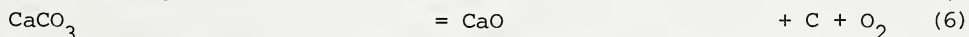
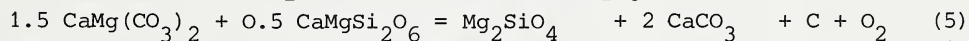
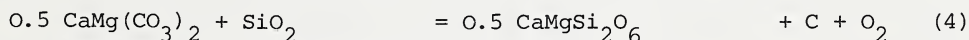
Extensive work has been performed on the model mantle system CaO-MgO-SiO₂-CO₂ by P.J. Wyllie and coworkers and by D.H. Eggler and coworkers. In this system CO₂ occurs either uncombined as a fluid carbon oxide phase, or in the combined form as a carbonate phase. The addition of carbon as a further component adds another degree of freedom to this system, requiring the definition of equilibrium oxygen fugacities.

Reduction leads to several characteristic reactions in this system :

1.) Carbonates are reduced in several separate steps according to :



and



- 2.) Each of the above reactions constitutes in itself an oxygen buffer.
- 3.) From figure 1 it is evident that the highest oxygen fugacity for stable existence of elementary carbon is given by the CCO buffer surface.
- 4.) Below the CCO surface graphite or diamond coexist with carbonate phases.
- 5.) The lower limit of stability of carbonates is given by the CaCO₃-CaO-C and MgCO₃-MgO-C divariant surfaces.
- 6.) Subsolidus equilibria among silicates and carbonates are shifted to lower temperatures upon reduction.
- 7.) At the same time, since CO₂ is ultimately replaced by the inert graphite or diamond, the solidus temperatures will be raised to the solidus of the "volatile absent" system CaO-MgO-SiO₂. (According to Wyllie (1976) this effect will be much less pronounced in natural systems containing small amounts of water).

For the genesis of diamond the P-T-fO₂ relations in the mantle are relevant :

Estimates of prevailing pressures and temperatures are taken from Boyd's (1975) Lesotho Geotherm.

The oxygen fugacity in a model mantle material will be controlled by a sliding buffer assemblage olivine + orthopyroxene + clinopyroxene + spinel or, at greater depths, olivine + orthopyroxene + clinopyroxene + garnet, which will be quantitatively dominant with respect to a possible carbon-carbonate oxygen buffer as defined above in a kimberlitic material. Thus an oxygen fugacity slightly below QFM may be assumed for mantle conditions, which is in agreement with observations and deductions made by other investigators, applying widely different methods. (Mitchell(1973), Ulmer et al.(1976), Ryabchikov et al.(in prep.), Brey (personal communication)

The oxygen fugacity of the CCO equilibrium has been calculated from the above equation for temperatures and pressures of the Lesotho Geotherm and plotted in figure 2. It is compared with the oxygen fugacities of the QFM and WM buffers respectively. It is evident that the QFM surface intersects the CCO surface on the geotherm at about T = 950°C, P = 39 kbar and log fO₂ = -9.1. At temperatures above 950°C and correspondingly greater depths elementary carbon will thus be unstable with respect to a carbon oxide phase or carbonates in a QFM buffered environment.

The hatched area in figure 2 outlines a range of oxygen fugacities slightly below QFM, according to the deductions of natural oxygen fugacities. Here the stability of carbon is extended to higher temperatures and pressures. But still a lower limit for diamond in the earth's mantle is demonstrated. On the other hand an upper limit is defined by the graphite-diamond equilibrium. Thus it may be concluded that the stability range of diamond ("diamond facies") is a restricted zone in the mantle.

From figure 2 it can be concluded that any transgression of carbon bearing and oxygen buffered mantle material across the CCO surface will lead to a redox reaction of the carbon bearing phase : Transgression towards higher temperatures and pressures results in exothermic oxidation of diamond (~ 400 KJ.mol⁻¹), while transgression towards lower P-T-ranges leads to endothermic reduction of carbonates or a carbon oxide fluid phase to diamond.

Pressure oscillations across the CCO boundary will thus lead to repeated production of heat on the high pressure side, while a corresponding enthalpy is consumed on the low pressure side. This process will eventually lead to a distortion of the temperature profile of the geotherm.

This deduction may help to provide a new hypothesis for the origin of the Boyd Inflection in the Lesotho Geotherm. It requires : Diamonds may be present in lherzolite nodules from the shallower part of the mantle, as reported from various localities, while diamonds must be absent from sheared lherzolites (Boyd(1976)) from locations on the geotherm beyond the Boyd Inflection.

References :

- Boyd, F.R. and Finger, L.W.: Ann.Rep.Geophys.Lab. 74, (1975), 519-525.
Brey, G.: personal communication.
Danchin, R.V. and Boyd, F.R.: Ann.Rep.Geophys.Lab. 75, (1976), 531-538.
Eggler, D.H. et al.: Ann.Rep.Geophys.Lab. 75, (1976), 631-636.
Kubaschewski, O. et al.: Metallurgical Thermochemistry, Pergamon Press, 1967.

Mitchell, R.H. : *Lithos* 6, (1973), 65-81.
 Ryabchikov, I.D. et al. : in preparation.
 Ulmer, G.C. et al. : *Amer.Min.* 61, (1976), 653-660.
 Wyllie, P.G. : *Journ.Geol.* 85, (1976), 187-207.

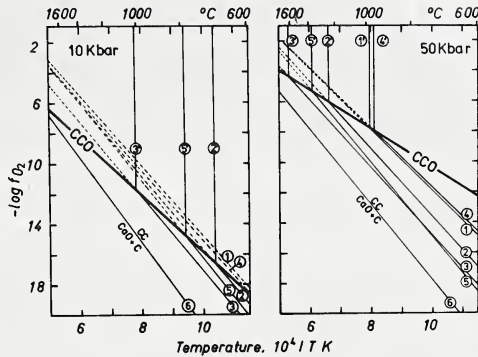


Figure 1.

Isobaric sections in the P-T- f_{O_2} space of the CCO buffer and of various carbon-carbonate buffers, calculated from thermodynamic data (Kubaschewski et al. (1967), Eggler et al. (1976)). Numbers refer to reactions (1)-(6) in the text. Stippled lines in the range above the CCO curve represent meta-stable extensions of the above reactions. (1')-(6') are decarbonation reactions resulting from Schreinemakers analysis.

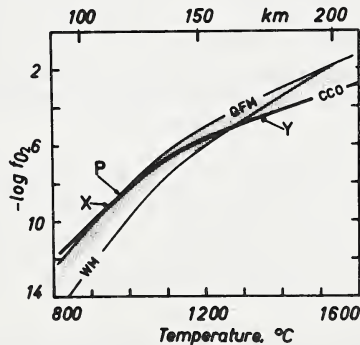


Figure 2.

Oxygen fugacities of the CCO, QFM and WM buffers at temperatures and corresponding pressures along the Lesotho Geotherm (Boyd and Finger, (1975)). P = equilibrium point graphite + diamond + CO_2 on the geotherm. In a QFM buffered environment graphite will be oxidized to CO_2 at $T = 950^\circ C$, $P = 39$ kbar and $\log f_{O_2} = -9.1$; (point "X"). At an oxygen fugacity one log unit below QFM diamond will be oxidized to CO_2 at $T = 1350^\circ C$, $P = 59.5$ kbar and $\log f_{O_2} = -4.5$; (point "Y") The distance P - Y corresponds to the width of the "diamond facies" = 55 km.

CO₂-RICH FLUID INCLUSIONS IN THE POLYMETAMORPHIC BASEMENT ROCKS OF THE VREDEFORT STRUCTURE, SOUTH AFRICA, AND THEIR POSSIBLE BEARING ON ITS ORIGIN

W. Schreyer¹⁾, O₂ Medenbach¹⁾, K. Abraham¹⁾, and L.O. Nicolaysen²⁾

The ring-like Vredefort Structure consists of a collar of steeply dipping overturned Witwatersrand metasediments and a 50 km diameter core of Archean basement in a similar tectonic position. The border between the Archean and the collar is marked by a sedimentary unconformity. Thus the whole structure represents a section through most the continental crust (Slawson 1976).

Within the collar metamorphism increases inward changing the nearly unaffected peripheral slates into hornfelses with andalusite, cordierite etc. On the basis of the mineral assemblages reported by Bisschoff (1969) maximum temperatures of about 500°-600°C may be estimated for this static metamorphism. Petrologic studies of the Archean basement rocks reveal, however, that this type of metamorphism continues and increases further towards the center of the structure, where it is superimposed on the previous dynamic metamorphism of the Archean and where it may affect possibly unmetamorphosed granites and other intrusives. Metamorphic conditions could be deduced for two polymetamorphic sediments:

1. A former regional metamorphic granulite located about midway between collar and center exhibits breakdown of its former garnet in the presence of quartz into a symplectite of cordierite, hypersthene, and a different garnet. Microprobe analyses yield the following M-values (Mg/(Mg+Fe)) of the new minerals:
cordierite: 0.60; hypersthene: 0.41; garnet: 0.19.

Based on the experimental results of Hensen and Green (1973) who studied this multivariant breakdown reaction some 750° and 5 kb can be estimated.

2. In an iron formation occurring at the center of the ring ferropigeonite (En₇₀Fs₁₇Wo₁₃) had formed which requires minimum temperatures of some 800°-850°C (Simmons et al. 1974). Upon cooling this pyroxene did not invert but exsolved into clinoeuilite and ferroaugite (Schreyer et al. 1977).

Many quartz crystals occurring in polymetamorphic basement rocks from various localities within the ring contain two-phase fluid inclusions which, on the basis of their freezing temperature near -56°C, consist of virtually pure CO₂. In some

-
- 1) Institut für Mineralogie der Ruhr-Universität, Universitätsstr. 150, D-4630 Bochum, West Germany
 - 2) Bernard Price Institute of Geophysical Research, University of Witwatersrand, 1 Jan Smuts Avenue, Johannesburg 2001, South Africa

rocks near the unconformity three-phase inclusions with some additional H₂O were found. Although CO₂-rich inclusions are well known from deep-seated granulites elsewhere (Touret 1971), the ones observed here are of particular genetic significance: In rocks of the outer portion of the core they form decorations of quartz lamellae which are regarded by some investigators as indications for meteorite impact (e.g. Carter 1968).

Kink bands in biotites and the appearance of pseudotachylites and shatter cones both in the outer core as well as in the collar are further testimonies of a high-strain-rate deformation which has been attributed to shock metamorphism. Since this deformation is clearly younger than the static metamorphism, the impact hypothesis meets with the difficulty in explaining why a meteorite should have hit the very spot in Southern Africa where this localized static metamorphism had occurred.

Comparison of quartz lamellae and other deformational features of Vredefort with the shock features observed in basement rocks of the Ries crater indicate that similarities only exist with the very lowest grades of shock metamorphism of the Ries. Contrary to the Ries the quartz lamellae of Vredefort exhibit all stages of a recrystallization which increases in intensity from the outer core to the center of the structure. Thus, whereas in rocks close to the unconformity SEM investigations show parallel open fractures, these are healed by finely recrystallized quartz closer to the center. In the central portion of the structure the quartz grains form excellent polygonal annealing textures with 120° triple points. Nevertheless, in many cases the CO₂ inclusions can be found to follow parallel planes that are continuous beyond the grain boundaries of the annealing fabric. Since the arrangement of these planes is directly comparable to that of the decorated quartz lamellae of the outer core, this observation must be considered as evidence that high-strain-rate deformation has also produced quartz lamellae in the center of the structure prior to annealing. In the course of the complete recrystallization of quartz the CO₂ inclusions have partly coalesced into larger but fewer inclusions which are notably rarer in zones close to the new grain boundaries of quartz.

Heating-stage measurements of CO₂ inclusions in six rocks of various portions of the core revealed a remarkably consistent behavior: In all cases the inclusions homogenized to form liquid at temperatures ranging from 22°-28°C which indicates specific densities of 0.7-0.8 gr/cm³. Using the extrapolated PVT data for CO₂ of Kennedy (1954) in conjunction with the metamorphic temperatures derived mineralogically the following ranges of partial pressures of CO₂ can be estimated: At 750°C 2.9-3.9 kb, at 850°C 3.3-4.4 kb.

The spatial arrangement of CO₂-rich inclusions along the lamellae in quartz suggests that the gas was incorporated either concomitantly with or subsequently to a rock deformation characterized by very high strain rates. Similar fluid inclusions

decorating quartz lamellae in rocks of the Charlevoix structure, Quebec, were found by Pagel and Poty (1975) to consist of H₂O. The lack of CO₂ is used by those authors as a strong argument for meteorite origin of that structure. Following their reasoning and keeping in mind that no higher-grade features of shock metamorphism were found at Vredefort, a meteorite impact is unlikely to have caused the Vredefort structure but an endogenous origin must be sought: The time of CO₂ incorporation is, like that of the high-strain-rate deformation, subsequent to the first period of static metamorphism, but it precedes a second period of static metamorphism (annealing) which is confined to the central area of the core. Thus all these events must be seen as episodes in a long history of thermal and structural development of the Vredefort dome. As already suspected by Nicolaysen (1972) for other cryptoexplosion structures high fluid pressures and their explosive release seem to be the dominant reason for the high-strain-rate deformation at Vredefort. The source of both the CO₂ and the enormous heat flow causing static metamorphism with a vertical extent of more than 25 km over a limited area can best be seen in a mantle-derived magma diapir that cooled near the base of the continental crust.

References

- Bisschoff, A.A.: D.Sc.Thesis, Univ. of Pretoria, 234 pp., 1969
- Carter, N.L.: In: Shock Metamorphism of Natural Materials, Mono Book Corp., Baltimore, 453-475, 1968
- Hensen, B.J. and Green, D.H.: Contr.Mineral.Petrol. 38, 151-166, 1973
- Kennedy, G.C.: Am.Journ.Sci. 252, 225-241, 1954
- Nicolaysen, L.O.: Geol.Soc.Am.Mem. 132, 605-120, 1972
- Pagel, M. and Poty, B.: Fortschr.Mineral. 52, 479-489, 1975
- Schreyer, W., Stepto, D., Abraham, K. and Müller, W.F.: Manuscr.for Contr.Mineral.Petrol., 1977
- Simmons, E.C., Lindsley, D.H. and Papike, J.J.: Journ.Petrol. 15, 539-565, 1974
- Slawson, W.F.: Geochim.Cosmoch.Acta 40, 117-121, 1976
- Touret, J.: Lithos 4, 423-436, 1971

GARNET PYROXENITES AND PARTIALLY MELTED ECLOGITES FROM THE SULLIVAN BUTTES
LATITE XENOLITH SUITE, PRESCOTT, ARIZONA

Daniel J. Schulze and Herwart Helmstaedt (Department of Geological Sciences,
Queen's University, Kingston, Ontario, Canada K7L 3N6)

Tertiary latite plugs and flows (the Sullivan Buttes Latite) on the margin of the Colorado Plateau near Prescott, Arizona contain numerous garnet-bearing ultramafic xenoliths. Highly altered metamorphic eclogites dominate, though locally garnet pyroxenites and garnet amphibolites may abound. Neither olivine-bearing nor primary plagioclase-bearing xenoliths have been found.

The garnet pyroxenite group is the texturally most spectacular. Well preserved pyroxene porphyroclasts contain exsolution lamellae of garnet and an Fe-Ti oxide (referred to as "ilmenite", though actually consisting of two finely intergrown phases, probably ilmenite and magnetite). The primary (pre-exsolution) assemblage consisted of three coexisting aluminous pyroxenes (calcic clinopyroxene, subcalcic clinopyroxene, orthopyroxene) and possibly garnet and "ilmenite". Porphyroclasts of the calcic cpx (approx. $Wo_{45}En_{45}Fs_{10}$) and opx (approx. $En_{80}Fs_{20}$) contain lamellae of both "ilmenite" and garnet. The subcalcic cpx (preserved as granules of intergrown cpx-opx lamellae, in various proportions) also exsolved garnet, seen as poorly preserved garnet lamellae in the areas of the cpx-opx intergrowths, and may also have exsolved "ilmenite", though only granular "ilmenite" is found associated with the subcalcic cpx. In the opx and calcic cpx all stages between lamellae-bearing porphyroclasts and complete recrystallization of the grains are preserved.

The garnets are variable in composition from one xenolith to another, ranging from approx. $Py_{50}Gr_{15}Alm_{35}$ to $Py_{35}Gr_{15}Alm_{50}$, the Ca content remaining constant. Xenoliths with high-pyrope garnets sometimes contain rutile and not "ilmenite". Within a single xenolith the garnet compositions are constant.

Late stage (though pre-eruption) amphibole replaces some of the pyroxenes, especially in the fine-grained lamellar cpx-opx domains. These xenoliths appear to have reacted little with the latite.

The eclogites, some of which have metamorphic fabrics are in general highly altered, and except for xenoliths from one plug, garnets are not preserved. Prior to late stage amphibolitization which also altered the pyroxenites, these rocks consisted of almandine-rich garnet + omphacite + rutile + sodic amphibole + apatite + quartz (in garnet cores). Phlogopite may be primary or secondary.

The garnets are more variable in composition than those in the pyroxenites ranging within the following limits: $Py_{15-35}Gr_{15-30}Alm_{35-65}$. On a Mg-Ca-Fe diagram, no overlap between the two groups exists.

The primary pyroxene is omphacite, which contains up to approx. 15 mole % jadeite. The primary amphiboles (barroisite?) are highly altered, but contain up to 4 wt % Na_2O .

Though the extent of alteration varies in the eclogites, garnet is

rarely preserved. Most often it is completely pseudomorphed by a very finely intergrown symplectite of plagioclase, orthopyroxene, magnetite and (?) olivine that is nearly opaque due to dispersed magnetite. This symplectite displays a feathery texture caused by dendritic growth of these minerals from radial expansion fractures (formed upon incorporation into the magma) towards unaltered garnet.

Where the clinopyroxenes are incompletely altered, they consist of "porous" rims surrounding clear unaltered cores, commonly in optical continuity. Some pyroxenes show marked dispersion and are optically zoned even where unaltered. Plagioclase is present interstitial to, and within these altered rims.

The amphiboles and phlogopite are usually highly altered as well, and the rutile is commonly surrounded or completely replaced by pseudobrookite.

The rims of the omphacite are jadeite-poor relative to the cores (Fig. 1). They are similar in jadeite content to the diopside phenocrysts in equilibrium with the magma. The core and rim texture is likely due to partial melting of the omphacite to a jadeite-rich liquid + diopside, the liquid having later crystallized as plagioclase (+ nepheline, which may have reacted with free silica to form more plagioclase). The secondary assemblage plagioclase + orthopyroxene + magnetite + diopside + olivine is compatible with partial melting of the omphacite and subsolidus re-equilibration of the garnet upon heating in the latite magma, and subsequent transport to the surface.

Fe-Mg distribution coefficients between garnet and clinopyroxene for both the eclogites and garnet pyroxenites suggest relatively low temperatures of equilibration (600-700°C at 10-20 kb) before incorporation into the latite magma. The sodium-bearing eclogite xenoliths were apparently less stable at high temperatures than were the garnet pyroxenites and could not survive in the latite.

Although metamorphic eclogites have been found in the Four Corners kimberlite diatremes, they are not known from the xenolith suites of basalts in the western United States. Basalts are probably too hot to preserve such eclogites whereas the kimberlites were not. The Prescott eclogites may only have survived because the latite magma was sufficiently cooler than the basalts to allow their partial preservation.

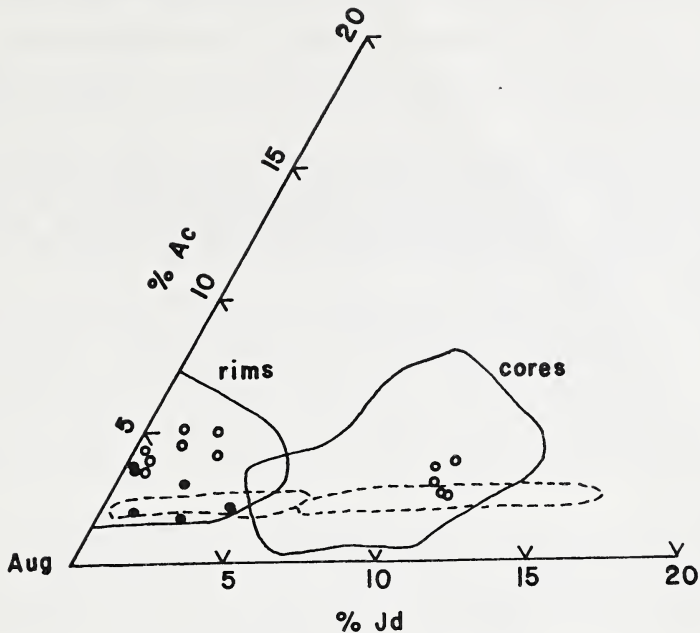


FIGURE 1. Clinopyroxene compositions (mole %) of Prescott and South African xenoliths. Solid lines enclose core and rim pyroxenes from six Prescott eclogite xenoliths, dotted lines enclose core and rim pyroxenes from five South African garnet lherzolite xenoliths (D.A. Carswell, 1975, *Phys. Chem. Earth*, v. 9, pp. 417-429), open circles represent core and rim pyroxenes from Roberts Victor eclogite SA 11-2, filled circles represent diopside phenocrysts in Prescott latite.

PETROGENESIS OF KIMBERLITES AND ASSOCIATED POTASSIC LAMPROPHYRES FROM WEST GREENLAND.

B.H. Scott, Grant Institute of Geology, University of Edinburgh, West Mains Road, Edinburgh 9, Scotland,.

Present Address: Anglo American Research Laboratories, P.O. Box 106, Crown Mines, 2025, Transvaal, R.S.A.

A suite of post-tectonic dykes, which occur in the region south of Holsteinsborg in Central West Greenland, were formed by numerous injections of magma. These dykes include both kimberlites and unusual potassic lamprophyres, most of which are extremely fresh and therefore particularly suitable for a whole-rock geochemical study.

The kimberlites contain rounded macrocrysts of olivine, phlogopite, picroilmenite and rare pyropic garnet in a matrix which contains often euhedral crystals of olivine, phlogopite, diopside, perovskite, spinel, apatite and both primary calcite and serpentine. They can be classified as diopside-phlogopite kimberlites (after Skinner and Clement, this volume). The kimberlite dykes sometimes contain abundant rounded ultrabasic inclusions dominated by dunites, which is unusual in comparison with inclusion suites known from other kimberlites.

The non-kimberlite dykes of the Holsteinsborg suite are referred to as potassic lamprophyres (despite the occurrence of felsic macrocrysts in some dykes). They contain macrocrysts of anhedral olivines with distinct reaction rims, euhedral pseudoleucite, phlogopite and diopside set in a finer grained groundmass which may include phlogopite, diopside, potassic richterite, potassium feldspar and both primary calcite and serpentine.

93 whole-rock analyses of samples from the Holsteinsborg dykes demonstrate an overall wide range of compositions, particularly in MgO and K₂O, while as can be seen from Fig. 1, the dykes form two compositionally distinct groups. The kimberlites have all the characteristics of micaceous kimberlites except for lower H₂O and Fe⁺⁺⁺/Fe⁺⁺ values. The lamprophyres are characterised by high K₂O contents (up to 10 wt %) and are distinguished from the kimberlites by higher SiO₂, K₂O, Al₂O₃, Na₂O, P₂O₅, Rb, Sr, Y, Zr, Ba, Ce and La but lower MgO, FeO, Fe₂O₃, CaO, MnO, H₂O⁺, Cr, Ni and Cu. All the dykes are rich in volatiles, especially CO₂.

The extreme K₂O contents together with certain mineralogical features of the potassic lamprophyres indicate a similarity with the rare ultrapotassic volcanic rocks, such as lamproites, from the Leucite Hills, Wyoming and West Kimberley, Australia.

The close association of kimberlites and potassic lamprophyres near Holsteinsborg lends itself to speculation about possible genetic relationships between these rock types. One petrogenetic model is put forward here which suggests that the potassic lamprophyres were derived from a parental kimberlitic magma by a simple fractionation process.

For a discussion about the petrogenesis of such rock types to be meaningful the analyses should be considered on a volatile-free basis. Although the CO₂ and H₂O⁺ are considered to be primary, some attempt must be made to account for the random loss of either volatiles or an immiscible carbonatitic fluid during emplacement. The concentration of the remaining oxides (recalculated to 100%), relative to each other, then becomes significant.

The whole-rock analyses of the Holsteinsborg dykes are summarised on oxide versus oxide variation diagrams (Fig. 1). In these plots the potassic lamprophyre dykes tend to plot on a continuation of the kimberlite dyke trends.

The variation in chemistry within each group of dykes can be explained largely by olivine fractionation or enrichment. The kimberlites trend away from an olivine with the composition, Mg_{85} , of the euhedral crystals found in the kimberlite dykes. The lamprophyres trend away from an olivine, with a composition, $Mg_{91.5}$, the mean composition of the olivines in the lamprophyres. The lamprophyre trend, in detail, is more accurately explained by extracting relatively minor amounts of clinopyroxene and phlogopite together with olivine.

Since most of the rocks considered in this study are porphyritic, it is difficult to distinguish between that part of the trend due to liquid evolution and that part of the trend which might be the result of phenocryst and/or xenocryst accumulation in the liquid. The MgO contents of the rocks do correlate with the modal content of olivine. The wide range of Mg/Mg + Fe ratios found in the olivine, particularly in the kimberlites (Mg_{79-93}), however, implies olivine fractionation. For the kimberlite dykes, the abundant dunite inclusions may represent cumulates from this fractionation. Both the kimberlite and potassic lamprophyre dykes, therefore, may have resulted from the pulsatory eruption from a magma system in which olivine was able to fractionate.

Any discussion of the possibility of a genetic relationship between the two groups requires an estimate of the composition of the initial liquids from which the two groups of dykes evolved. The average composition of each group was taken to represent these initial liquid compositions. For the lamprophyres this choice was reasonable since the average composition is similar to the most magnesian aphyric sample analysed. For kimberlites, however, it is impossible to be certain of any liquid composition. These average compositions (recalculated) are plotted on Figure 1.

Considering all the Holsteinsborg dykes as one group the trends observed (see Fig. 1) lie close to an overall olivine control line. It is clear, however, that the chemistry of the group as a whole cannot be explained solely by olivine fractionation. In the plot MgO vs TiO_2 (Fig. 1), for example, the evolution from a kimberlitic parental magma to a lamprophyre magma with a similar TiO_2 content cannot be explained by the fractionation of a TiO_2 -free phase such as olivine. To explain the deviations from an olivine control line requires the crystallisation of a Fe-Ti phase together with olivine. The most abundant Ti-rich phase in the kimberlites, apart from perovskite, is titanomagnetite of fairly constant composition (also plotted on Fig. 1). The suggested olivine (Mg_{92}) plus spinel (titanomagnetite) fractionation trends are illustrated in Fig. 1. It can be seen that the evolution of the initial lamprophyric liquid from a parental kimberlitic magma is consistent with the fractionation of approximately 75% olivine (Mg_{92}) and 25% spinel. It should be noted that some modification to the estimated liquid compositions, within the range of observed compositions, does not alter the principal conclusions of this discussion.

In summary this model proposes

- (1) the evolution of part of a kimberlitic parental magma by olivine fractionation which was then intruded to form the kimberlite dykes
- (2) the evolution of the initial lamprophyric magma from a parental kimberlitic magma by the fractionation of olivine plus spinel
- (3) further evolution of the lamprophyric magma by olivine plus clinopyroxene plus phlogopite (+ pseudoleucite) fractionation before intrusion.

Interpretation of the data is a variety of different ways including molar ratio comparisons, extract calculations and plots in FMA and CMAS all support this fractionation model deduced from the simple oxide versus oxide variation diagrams.

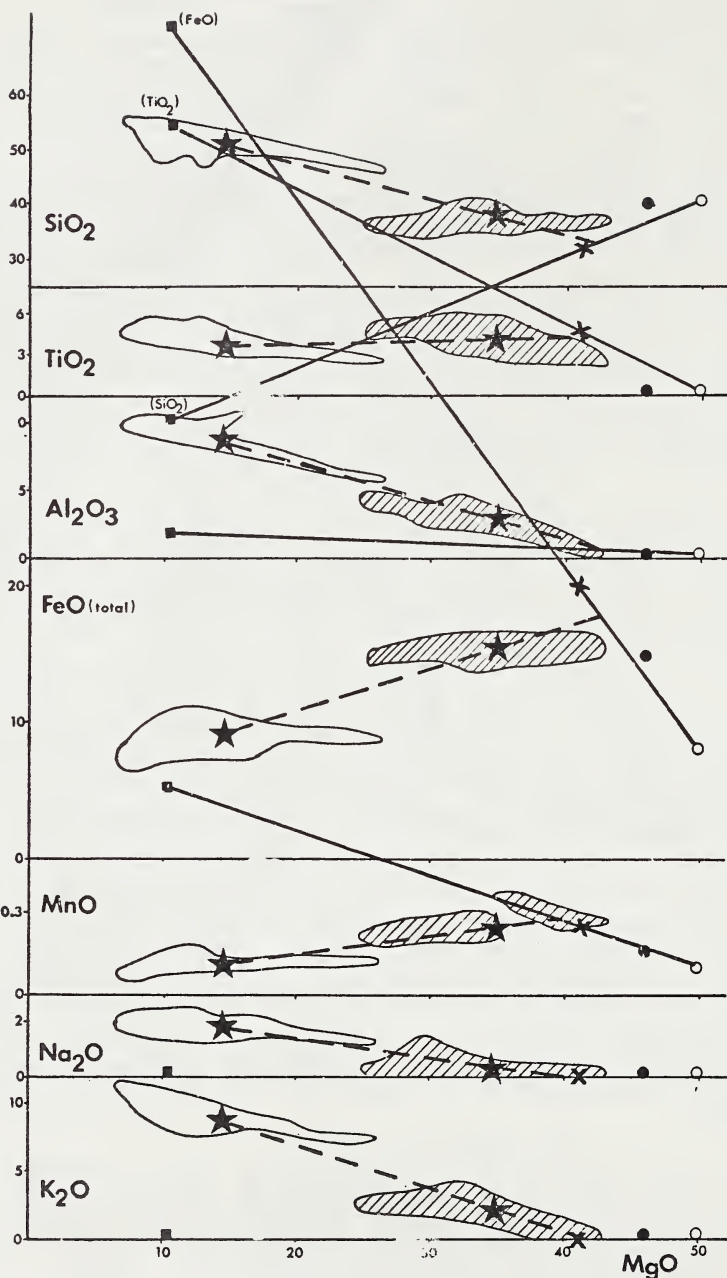


FIGURE 1

Compositional fields of the Holsteinsborg kimberlite (shaded) and potassic lamprophyre (white) dykes plotted on oxide versus oxide (wt %) variation diagrams using $\text{Ca}(\text{Mg})\text{CO}_3$ - and H_2O^+ -free analyses (recalculated to 100%).

Legend

stars = average compositions of each group of dykes

solid circles = olivine Mg_{35}

open circles = olivine $\text{Mg}_{91.5}$

solid squares = spinel (titanomagnetite)

dashed lines = possible fractionation paths

solid lines = olivine ($\text{Mg}_{91.5}$)-spinel join where the cross marks 22.5% spinel

ELECTRICAL CONDUCTIVITY AND VELOCITY ANOMALIES IN PARTIAL MELTS

T. J. Shankland (Geological Research Group, Los Alamos Scientific Laboratory,
Los Alamos, New Mexico 87545)

It is possible to use the theories of aggregates to predict physical properties of partial melts and to interpret high conductivity or low velocity anomalies in the mantle. Electrically a partial melt is regarded as an aggregate of a good conductor, the melt, in a relatively insulating crystalline matrix. Elastically the partial melt is a mixture of low velocity basaltic liquid intermixed with a high velocity crystal phase. Lines of constant conductivity or velocity can be plotted on a graph of temperature vs. melt fractions; when combined with plots of temperature vs. degree of partial melting from experimental petrology, these results can be used to estimate both temperatures and melt fractions in mantle zones having anomalous conductivity or velocity. The results are applicable to a range of tectonic and geothermal features such as Yellowstone or oceanic ridges.

Figure 1 illustrates an application of this approach to the oceanic low-velocity zone (LVZ). Figure 1a depicts the electrical conductivity of a partial melt which is about 0.1 S/m at 100 km depth (Shankland and Waff, 1977). The conductivity data can be satisfied along the approximately hyperbolic curve of possible temperature and melt fractions. The addition of a petrological curve of partial melting (Wyllie, 1971, Fig. 8-20) constrains the permissible temperature range and allows the estimation of the melt fraction. In Figure 1b is a similar plot of a constant shear velocity V_S of the LVZ normalized to V_{S0} of the unmelted material according to the saturated crack model of O'Connell and Budiansky (1974). A representative V_S/V_{S0} is 0.9. The aspect ratio of crack thickness to diameter has been adjusted to give the same temperature and melt fraction. In this case the data are satisfied by a dominant aspect ratio of .038 at a melt fraction of .034.

While other elastic and electrical models (and eventually experimental data) could have been used, the important point is that plots of temperature vs. melt fraction for a given physical property permit us to obtain information about the temperature, amount, and configuration of existing regions of partial melting. The results can be applied to problems of magma genesis or regional geothermal exploration.

REFERENCES

- O'Connell, R. J., and B. Budiansky, 1974, "Seismic Velocities in Dry and Saturated Cracked Solids," J. Geophys. Res., 79, 5412-5426.
- Shankland, T. J., and H. S. Waff, 1977, "Partial Melting and Electrical Conductivity Anomalies in the Upper Mantle," J. Geophys. Res., 82, in press.

Yyllie, P. J., 1971, The Dynamic Earth: Textbook in Geosciences, Wiley, New York.

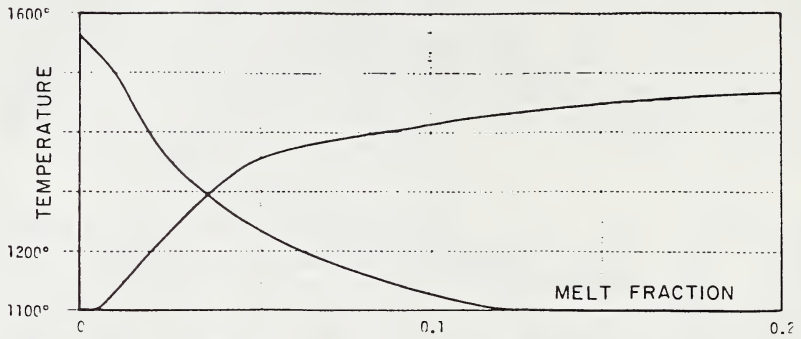


Fig. 1(a). Plots of temperature vs. melt fraction for an effective conductivity of 0.1 S/r and of Yyllie's (1971) peridotite melting curve.

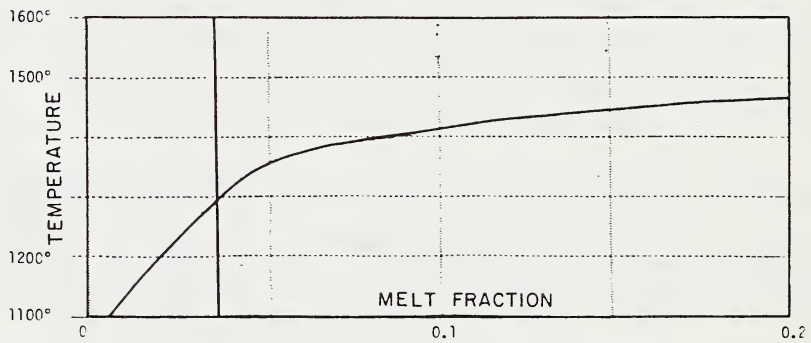


Fig. 1(b). Plots of temperature vs. melt fraction for shear velocity ratio $V_S/V_{S0} = 0.9$ and of the same peridotite melting curve as in 1(a).

THE MINERALOGY OF XENOLITHS FROM ORAPA, BOTSWANA

S.R. Shee and J.J. Gurney

Introduction

The main Orapa pipe (AK1) is one of some 23 pipes in north eastern Botswana. It is 1550m. X 950m. at surface. The near-surface filling of the pipe is sedimentary (epiclastic) kimberlite which indicates that the pipe has been only slightly eroded since emplacement (Hawthorne, 1973). Serpentinized primary kimberlite is intersected in borehole cores below 90m (Baldock et al, 1973). The pipe is a major diamond producer.

Small samples (1½ - 5cm longest dimension) of mantle material are recovered during the mining process. We have found abundant eclogite and garnet, clinopyroxene and ilmenite megacrysts (> 1½cm) but no olivine bearing rocks (peridotites or olivine websterites).

Eclogites

Garnet and clinopyroxene are dominant in the eclogites. Variants with minor orthopyroxene, chromite, amphibole, rutile, kyanite, corundum, graphite and diamond have been found. The wide range in mineral chemistry is illustrated for the garnet compositions (Fig.1) and by the plot of the coexisting clinopyroxenes (Fig.2). In Fig.1 there are two main trends, both starting at magnesian garnet compositions, but in the one case showing major enrichment in iron and minor enrichment in calcium and in the second showing the reverse.

Garnets in the orthopyroxene, chromite and chrome rich eclogites have the most magnesian compositions and have the highest chrome contents for eclogite garnets at Orapa. Coexisting clinopyroxenes are calcic, have high Mg/Mg+Fe ratios and also have significant chromium and low sodium contents compared to other Orapa clinopyroxenes. Chromites have 52.1 to 57 wt.% Cr₂O₃. The orthopyroxenes have ~ 0.75 wt.% Al₂O₃ and Mg/Mg+Fe at ~ 0.93 and are similar to enstatites in mantle garnet lherzölitites.

The garnet compositions of the amphibole eclogites show a range of compositions. The amphibole which poikilitically encloses garnet and clinopyroxene may be a replacement mineral. Analysed examples have subcalcic edenite (1), edenite (3), and pargasitic hornblende (1) compositions (Leake, 1968). Kyanite and corundum bearing rocks have high grossular garnets (Fig.1) with high Na₂O contents (0.07 - 0.17 wt.% Na₂O) and low Cr₂O₃. Corundum eclogite garnets are less iron rich than the kyanite eclogite garnets (Fig.1). The pyroxenes are diopsidic jadeites with 4.46 - 8.75 wt.% Na₂O and 15 - 18 wt.% Al₂O₃. Corundum eclogite pyroxenes tend to be more jadeitic than the kyanite eclogite pyroxenes.

Diamond has been found in four eclogites and one diamond/garnet rock. Graphite has been found in a number of eclogites including kyanite and corundum bearing types. Twelve graphite eclogites have been analysed. The garnets and pyroxenes in these rocks show wide ranges in compositions (see Figs.1 and 2). Sodium was detected in all the diamond eclogite garnets (0.08 - 0.19 wt.% Na₂O) and in nine graphite eclogite garnets (0.06 - 0.15 wt.% Na₂O). Potassium was detected in all the diamond eclogite clinopyroxenes (0.03 - 0.13 wt.% K₂O) and in five of the graphite eclogite clinopyroxenes (0.05 - 0.17 wt.% K₂O).

Use of the geothermometer developed by Raheim and Green (1974) combined with consideration of the diamond - graphite reaction curve (Kennedy and Kennedy, 1976) suggests that the minimum temperature and pressure of equilibration ranges from 1120^o - 1330^oC and 47 - 53 Kb for the diamondiferous rocks. If graphite cannot form in the diamond stability field then the maximum equilibration conditions for graphitic rocks ranges from 910^oC - 1180^oC and from

42 - 49 Kb. This implies a minimum total range of equilibration conditions of 11 Kb and 420°C. Graphite, however, can possibly crystallise within the diamond stability field.

In addition to the eclogites already described there are abundant xenoliths of kyanite and almandine garnet (~29 wt.% FeO); kyanite, almandine and plagioclase; and almandine and plagioclase which define a separate compositional field and are interpreted as being of deep crustal metamorphic origin.

Megacrysts

Only garnet, clinopyroxene and ilmenite have been found. The garnets which have high titanium contents, show increasing Fe/Mg with constant calcium and are similar to garnets found at Monastery Mine (Jakob, 1977) and to the low chrome megacrysts from Colorado/Wyoming (Eggler and McCallum, 1974). Sodium is detected in all megacryst garnets (0.07 - 0.17 wt.% Na₂O).

The clinopyroxene megacrysts fall into two groups similar to the high chrome calcic and the low chrome subcalcic megacrysts from the Colorado/Wyoming kimberlites. Calcic clinopyroxenes have Ca/Ca+Mg ratios between 0.347 and 0.469 whilst subcalcic clinopyroxenes (2) show ratios of 0.347 and 0.363.

Garnet Xenocrysts

Garnets (<0.5cm) from the concentrate of heavy minerals obtained during diamond recovery have been analysed. A considerable proportion appear to have been derived from disaggregated eclogitic xenoliths and some appear to be fragments of the discrete garnets. The rest are low titanium chrome pyropes which do not match garnet compositions in the xenoliths or the megacrysts.

References

- Baldock, J.W., Hepworth, J.V. and Marengwa, B.S. (1976). *Economic Geology* 71, No1, pp 139 - 156
- Eggler, D.H. and McCallum, M.E. (1973). *Carnegie Inst. Yearbook* 73 pp 294-300
- Hawthorne, J.B., (1973). *Physics and chemistry of the Earth* Vol.9 (Pergamon Press) pp 1 - 15
- Jakob, R (1977) MSc. Thesis. Geochemistry Dept. University of Cape Town.
- Kennedy, C.S. and Kennedy, G.C. (1976) *Jour. Geophys. Res.* 81, No 14, pp2467 - 2470
- Leake, B.E. (1968) *Geol. Soc. America Spec. Paper* 98 210p
- Raheim, A and Green, D.H. (1974) *Contrib. Min. and Pet.* 48, pp 179 - 283

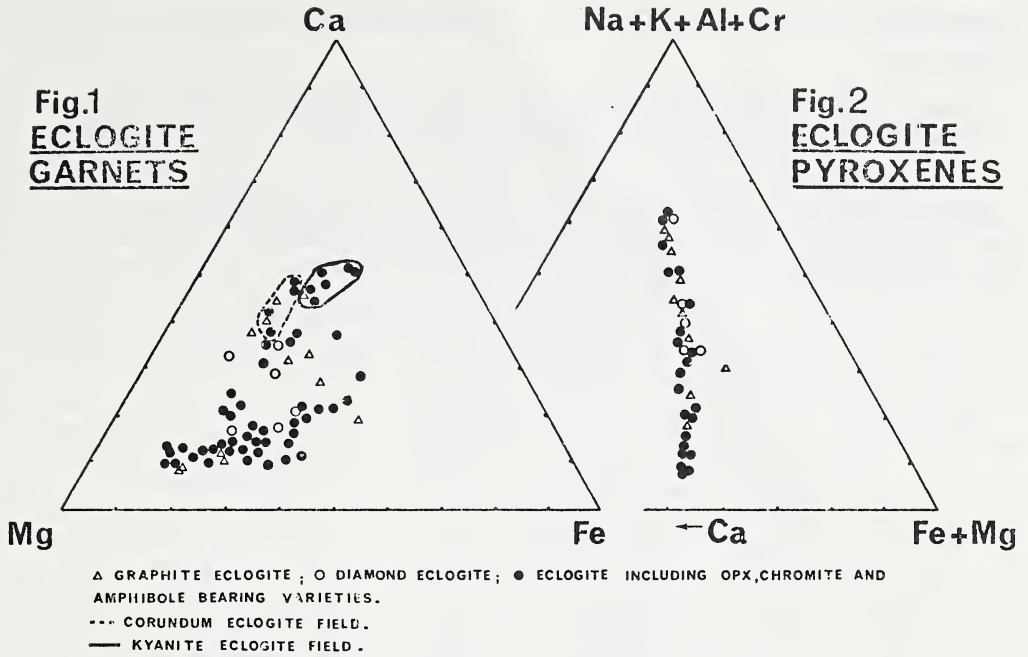


Fig.1 Atomic proportions of Ca, Mg, Fe for analysed eclogite garnets from Orapa.

Fig.2 Atomic proportions of Na + K + Al + Cr, Ca, Fe + Mg for eclogite clinopyroxenes from Orapa.

GEOCHEMISTRY OF TRANSITION ELEMENTS IN GARNET LHERZOLITE NODULES IN KIMBERLITES.

N. Shimizu and C. J. Allègre (Laboratoire de Géochimie et Cosmochimie, Institut de Physique du Globe, Université de Paris 6, Paris, France)

Introduction- The purpose of the study is to describe distributions of transition elements among major phases of garnet lherzolite nodules in kimberlites in order to obtain information on upper mantle chemical processes and to assess possible use of the partitioning of trace transition elements among phases as geothermometric-geobarometric indicators. The lherzolite nodules analyzed here (all from Lesotho and South Africa) include garnet lherzolites with sheared (or mosaic) texture, granular garnet lherzolites and lherzolites with K-richterite and/or phlogopite.

Procedures- The secondary ion mass spectrometry (SIMS) techniques were applied for quantitative analyses of minerals for Na, Mg, Al, Si, K, Ca, Sc, Ti, V, Cr, Mn, Co, Ni, Sr and Zr on spots of approximately 30x50µm using a Cameca IMS 300 ion-microprobe. Interferences of molecular ion species (oxide ions, for example) were practically eliminated by suppressing their intensities relative to those of single-atom ions with the energy filtering technique based on the difference in the kinetic energy distributions between single-atom and molecular ion species (Shimizu et al. 1977). The single-atom ions have significantly higher initial kinetic energy acquired during sputtering-ionization process compared with molecular ions, so that by counting secondary ions in a population with high energy (150 eV higher than the energy due to acceleration), contributions from molecular ions on a single nominal mass number could be practically eliminated. The interference-free intensities of major elements relative to Si measured in samples were then converted to atomic ratios (against Si) using empirical relationships between relative intensities and atomic ratios established separately for each group of minerals with well-analyzed standard samples. The major element compositions were calculated as cation atomic percentage by normalizing the total to 100%. The precision of the major element analysis is within 2-3% and the accuracy (relative to the electron probe data) is within 2-3%. The trace element concentrations were obtained from the empirical relationships between relative intensity (against Si) and concentration established for standard samples. Those standard samples were checked for their homogeneity with the ion-microprobe and analyzed with isotope dilution and neutron activation techniques. The analytical uncertainties for trace elements are determined essentially by the counting statistics and range, for clinopyroxene for example, from +14% (2σ) for Co to less than +2% for Mn.

Distribution of elements- homogeneity of minerals is critical to usefulness of trace element partitioning data. The individual mineral grains were found to be homogeneous with respect to all the elements analyzed, suggesting that equilibrium was closely approached. However, significant inter-grain variations were observed in some of the nodules as shown by Boyd and Finger (1975). For example, clinopyroxene grains in a sheared garnet lherzolite PHN 1611 show variations of Cr from 2000 to 2600 ppm (individual grains being homogeneous) and of Sc from 12 to 16 ppm, high Cr being associated with high Sc. In contrast, other transition elements do not show variations. The high Cr-Sc grains appear to be more abundant than the low Cr-Sc ones and there appear to be no peculiarities in Cr and

Sc contents of orthopyroxene and olivine grains surrounding the low Cr-Sc clinopyroxene grain.

An attempt was made to compare partitioning of transition elements between mineral pairs and P-T values estimated from the major element compositions of pyroxenes. For clinopyroxene-garnet pairs, for example, the partition coefficient of Sc ($K_{Sc} = (Sc/Al)_{cpx} / (Sc/Al)_{gar}$) was found to be constant (0.17±0.02) for the ranges of P (40-60 kb) and T (1370-970°C). Significant variations of the partition coefficients were observed for Mn ($K_{Mn} = (Mn/Mg)_{cpx} / (Mn/Mg)_{gar}$) ranging from 0.49 to 0.17 (high values being associated with high P and T) and for V ($K_V = (V/Al)_{cpx} / (V/Al)_{gar}$) ranging from 0.80 to 0.35 (low values being associated with high P and T). Ti, Cr, Co do not show definite correlations with P and/or T.

Chemistry of nodules- Chemical classification of nodules is a useful basis for considering genetic relationships among the nodules and for discussing chemical processes in the mantle. Erlank and Rickard (1977) suggest a metasomatic process for deriving peridotites containing phlogopite and K-richterite. The results of Erlank and Shimizu (1977) suggest that Sr content of clinopyroxene could be a good indicator of metasomatism as it is high (higher than 500 ppm) in lherzolites affected by metasomatism. Zr in clinopyroxenes was found to be consistent with Sr, being high (by more than a factor of 2) in metasomatized lherzolites. Combination of Sr, Zr, Sc, Ti and Cr contents of minerals, notably those of clinopyroxene and garnet allows a classification of the lherzolite nodules into three groups. Group I: relatively undepleted, high Fe/Fe+Mg, typically high P and T. Clinopyroxenes are characterized by low Sr (around 100 ppm), low Zr (10-20 ppm), low Sc (16 ppm), low Cr (typically below 4200 ppm) and high Ti (1300-1800 ppm); Group II: depleted, low Fe/Fe+Mg, typically low P and T. Clinopyroxenes characterized by intermediate Sr (200-250 ppm), low Zr (10-35 ppm), intermediate Sc (17-21 ppm), high Cr (6200 ppm-1.4%) and low Ti (typically around 250 ppm); Group III: metasomatic, low Fe/Fe+Mg, low P and T. Clinopyroxenes characterized by high Sr (500-970 ppm), high Zr (70-120 ppm), high Sc (27-90 ppm), high Cr (higher than 1.1%) and intermediate Ti (up to 920 ppm). All three types exist as garnet lherzolites and only Group III rocks contain phlogopite and/or K-richterite. The depleted nature of the Group II garnet lherzolites suggests that they could be residua of partial melting of relatively undepleted Group I rocks.

References

- Boyd, F. R. and Finger, L. W. (1975) Carnegie Inst. Wash. Yb, 74, 519.
Erlank, A. J. and Rickard, R. S. (1977) This volume.
Erlank, A. J. and Shimizu, N. (1977) This volume.
Shimizu, N., Semet, M. P. and Allègre, C. J. (1977) In preparation.

MINERALOGICAL CLASSIFICATION OF SOUTHERN AFRICAN KIMBERLITES

E.M.W. Skinner (De Beers Consolidated Mines Limited, Box 616,
C.R. Clement 8300 Kimberley, South Africa)

A fundamental requirement for the mineralogical classification of any suite of rocks is the delineation of valid petrographic limits. For this classification we consider that such limits are embodied in the definition of kimberlite proposed by Clement et al. (this volume). The salient points of this definition are:

- i) Kimberlite is a volatile-rich, potassic, ultrabasic, igneous rock which has a distinctively inequigranular texture resulting from the presence of macrocrysts set in an essentially microporphyritic matrix.
- ii) The matrix contains as prominent primary phenocrystal and/or groundmass constituents, olivine and several of the following minerals; phlogopite, calcite, serpentine, diopside, monticellite, apatite, spinels, perovskite and ilmenite. Other primary minerals may be present in accessory amounts.
- iii) The macrocrysts belong almost exclusively to a suite of anhedral, cryptogenic, ferromagnesian minerals which include olivine, phlogopite, picroilmenite, magnesian garnet, chromian diopside and enstatite. Olivine is extremely abundant relative to the other minerals which need not all be present. In addition to macrocrysts smaller grains belonging to the same suite also occur.

Early classifications of Southern African occurrences subdivided kimberlites into two main types, namely, "basaltic" kimberlite and "lamprophyric" or "mica-ceous" kimberlite. These terms have become widely accepted and this subdivision still forms the basis of most recent classifications (eg. Milashev, cited by Frantsesson, 1970). A different approach is used by Mitchell (1970) who subdivides kimberlites according to the relative abundances of olivine, phlogopite and carbonate minerals.

We consider that previous classifications are inadequate principally for one or more of the following reasons:

- i) Usage of incorrect or misleading terminology.
- ii) Failure to take into account the range of essential minerals that may be present in kimberlites.
- iii) Failure to discriminate adequately between xenogenic, cryptogenic, metasomatic and primary minerals.

All previous subdivisions have in some respect utilized the presence of olivine in kimberlite. This is not surprising as olivine is often the most abundant mineral present. Its abundance is, however, largely independent of the variation in abundance and type of other constituents. Furthermore much of the olivine in kimberlites may have a xenogenic origin and adequate distinction between this olivine and undoubtedly primary olivine cannot be made. Conse=

quently olivine is of limited use for classification purposes.

The classification presented here is based on the examination of more than 200 Southern African kimberlites. Modal analyses indicate that, in addition to olivine, any one of five other primary minerals may be a major constituent of kimberlite. These minerals are PHLOGOPITE, CALCITE, SERPENTINE, DIOPSIDE and MONTICELLITE. Accordingly we propose the recognition of five basic subdivisions of kimberlite, named after whichever one of these five minerals is volumetrically most abundant (eg. diopside kimberlite, monticellite kimberlite, etc.) Further subdivision can be made if one (or more) of these minerals is present in sufficient abundance to qualify as a characterizing accessory or modifier (eg. diopside-phlogopite kimberlite). We accept the possibility that, in addition to the five minerals listed above, some other mineral may occur as a major constituent of kimberlite. In this event our primary subdivision could be extended.

In the kimberlites examined only one other mineral has been found to occasionally occur in sufficient abundance to qualify as a modifier. This mineral is apatite. A problem exists with respect to opaque oxides which are sometimes volumetrically abundant in kimberlites. Since individual opaque minerals cannot be identified during point counting in transmitted light the use of opaque oxides for classification purposes is limited. However, kimberlites containing abundant opaque oxides could be referred to as opaque-oxide-rich. Modal analyses of 12 kimberlites are presented in table I. These analyses have been selected to illustrate the application of the proposed classification to kimberlites exhibiting variable mineralogies.

Any mineralogical classification of kimberlites will often be hindered by alteration. This alteration reflects deuteric and/or metasomatic processes which cannot always be distinguished from each other. The effects of deuteric alteration are evident to some degree in many kimberlites but for the most part do not cause serious problems with respect to classification. Extensive metasomatic alteration introduces a subjective element into classification as interpretive assessment of the nature of the original minerals, based on relict mineralogy and texture, becomes necessary. Extreme alteration such as that commonly reflected by highly metasomatized and weathered kimberlites (the latter containing considerable clay material) can render reliable classification impossible. In such cases we suggest that altered kimberlites be named according to the dominant alteration process as indicated by the alteration products present (eg. carbonatized kimberlite).

We consider that, as it is based on quantitative modal analyses, our proposed classification provides a practical basis for subdividing kimberlites in terms of mineral content. Hopefully it will provide a broader base for comparing kimberlites of divergent and like mineralogy and for comparing kimberlites with other rock types.

REFERENCES:

- Frantsson E.V. (1970), *The Petrology of the Kimberlites*. Trans. by D.A. Brown. Aust. Nat. Univ., Canberra.
- Mitchell R.H., (1970), *Jour. Geol.* 78, 686-704.

TABLE I MODAL ANALYSES OF SELECTED SOUTHERN AFRICAN KIMBERLITES

SOURCE	1		2		3		4		5		6		7		8		9		10		11		12		
	A	B	A	B	A	B	A	B	A	B	A	B	A	B	A	B	A	B	A	B	A	B	A	B	
Matrix Minerals																									
Phlogopite	44	67	28	38	43	73	45	55	<1	1	13	23	13	23	14	32	7	10	22	34	16	29	1	2	
Calcite	8	12	<1	1	tr	tr	7	8	29	50	14	18	10	18	32	47	<1	2	tr	tr	7	14	tr	tr	
Serpentine	4	6	25	35	7	12	10	12	11	19	12	22	18	32	21	21	20	28	16	25	7	25	6	13	
Diopside			18	25													35	49	26	40					
Monticel= lite											6	11													
Apatite	1	1	tr	tr	7	12	18	22	5	9	1	2	4	7	3	7	tr	tr	tr	tr	22	41	26	58	
Opaque Oxides	6	9	<1	1	1	2	1	2	11	19	7	13	8	15	6	14	7	8	1	1	1	2	tr	tr	
Perovskite	3	5			<1	1	<1	1	1	2	2	4	3	5	tr	tr	2	3	3	3	4	8	4	9	
Olivine (Total)	34		28		41		18		42		45		44		56		28		34		46		55		

A Volume percentage recalculated to exclude all xenogenic and cryptogenic constituents except olivine.

B Column A recalculated to exclude all olivine.

- | | | |
|----|--|------------------------------|
| 1 | Phlogopite kimberlite | |
| 2 | Serpentine - phlogopite kimberlite | Sydney On Vaal dyke |
| 3 | Phlogopite kimberlite - (olivine-rich) | Finsch pipe |
| 4 | Phlogopite kimberlite - (olivine-poor) | De Beers pipe |
| 5 | Calcite kimberlite | Steyn dyke, Star |
| 6 | Serpentine - phlogopite - calcite kimberlite | De Beers dyke |
| 7 | Phlogopite - serpentine kimberlite | Wesselton pipe |
| 8 | Calcite - serpentine kimberlite | Frank Smith pipe |
| 9 | Diopside kimberlite | Dutoitspan dyke |
| 10 | Phlogopite - diopside kimberlite | Beit Bridge dyke |
| 11 | Phlogopite - monticellite kimberlite | Intermediate dyke, Bellsbank |
| 12 | Monticellite kimberlite | Wesselton pipe |
| | | De Beers pipe |

PETROGRAPHY, PETROLOGY AND CHEMISTRY OF KIMBERLITE FROM THE COLORADO-WYOMING STATE LINE AND IRON MOUNTAIN, WYOMING DISTRICTS

C. B. Smith, M. E. McCallum,* and H. G. Coopersmith (Colorado State University, Fort Collins, Colorado 80523)

D. H. Eggler (Geophysical Laboratory, 2801 Upton St., N. W., Washington, D. C. 20008)

Kimberlite of probable Devonian age is intrusive into Precambrian granitic rocks along the Front Range of northern Colorado and southern Wyoming (McCallum et al., 1975). Known occurrences are confined predominantly to two areas that have been designated as the State Line district and the Iron Mountain, Wyoming district 70 km to the north. Kimberlite occurs in a variety of intrusive forms including dikes, sills, small plugs, blind diatremes and diatremes. Emplacement was localized along fault and joint planes, and at various intersections thereof.

The kimberlite is compositionally and texturally heterogeneous and four transitional varieties have been recognized: massive to porphyritic, carbonate-rich massive to porphyritic, breccia and carbonate-rich breccia. Massive to porphyritic kimberlite occurs in dikes, sills and small plugs and, as such, reflects more deeply eroded levels of the intrusive systems. Brecciated kimberlite is restricted to diatremes and blows. Carbonate-rich phases appear to be closely related to pipe structures, the massive to porphyritic varieties occurring in associated dikes and sills.

Massive to porphyritic kimberlite consists essentially of phenocrysts and/or xenocrysts of rounded olivine and enstatite (both usually serpentized), Cr-rich and Cr-poor diopside and pyrope, magnesian ilmenite, phlogopite and chromite set in a fine grained groundmass of serpentine, calcite, dolomite, phlogopite, magnetite, perovskite, apatite, rutile, hematite, zircon, and locally, chlorite and talc. Diamond is present in several of the State Line pipes but has not been found at Iron Mountain. Most kimberlite is distinctly porphyritic, but where phenocrysts or xenocrysts are absent or sparse a massive texture is imparted to the rock. Serpentine occurs as fibrous pseudomorphs after olivine and enstatite, and as very fine grained, nearly isotropic patches (serpophite) within the matrix. The latter variety is interpreted as being a primary crystallization product of the kimberlite magma. Carbonate (mostly calcite) comprises up to 30 percent of the matrix, and in some samples is distributed with serpophite in an emulsion-like texture. Contacts between serpophite and calcite patches are generally sharp and irregular, and calcite may be poikilitic. The textural relationships indicate that, at least locally, carbonate and silicate fluid phases were immiscible during the final stages of emplacement.

Massive to porphyritic carbonate-rich kimberlite is texturally similar to the more serpentine-rich variety described above but contains greater amounts of calcite and dolomite. Phenocrysts and xenocrysts may be suspended in a matrix composed primarily of carbonate with minor amounts of chaotically distributed serpentine, phlogopite, apatite and secondary hematite and leucocoxene after magnetite and perovskite. In some phases phenocrysts, xenocrysts and serpentinous matrix material may be completely carbonatized, resulting in a rock that may contain as much as 80 percent carbonate (abundant only at Iron Mountain).

Kimberlite breccia and carbonate-rich breccia are similar in composition to the massive to porphyritic varieties except that matrix serpentine and

carbonate contents are more widely variable within any one exposure, and greater amounts of xenolithic material are present. Rock clasts include Lower Paleozoic sedimentary rocks, upper and lower crustal Precambrian crystalline rocks (granite, gneiss, schist, basalt, pyroxenite and granulite), and upper mantle nodules of spinel and garnet peridotite, garnet clinopyroxenite and websterite, dunite, eclogite and carbonatite. Kimberlite breccia fragments and/or autoliths are locally abundant. Breccia phases are generally structureless; flow structures defined by alignment, layering and/or size sorting of phenocrysts that are locally present in massive to porphyritic kimberlite dike facies are absent in the breccias.

Preliminary chemical analyses reveal no pronounced differences in major or trace element chemistry relative to kimberlite in other parts of the world (Fig. 1, Table 1). Most low carbonate rocks have high MgO and relatively low Al_2O_3 , K_2O , CaO and CO_2 contents which, coupled with low phlogopite and calcite contents, indicate a "basaltic" affinity (Dawson, 1967). High rare earth element (REE) abundances and highly fractionated chondrite normalized patterns ($La/Yb = 75$ to 377) are similar to other kimberlites (Fig. 2). Major variations in chemistry of the Colorado-Wyoming kimberlite appear to be directly related to the highly variable carbonate content; carbonatized samples have the highest CaO, CO_2 , La, Ce, Nd, Cs, Ba, Be, Pb, Sr and Zn contents. However, even the most carbonate-rich samples that petrographically display intense carbonatization do not differ markedly in chemistry from average kimberlite. This similarity apparently results from the presence of dolomite and the tendency for high carbonate kimberlite to contain greater amounts of foreign SiO_2 in the form of granitic fragments and silicified groundmass constituents. The carbonate-rich kimberlite is chemically dissimilar to carbonatitic-kimberlite dikes reported from the Saguenay River valley, Quebec, Canada (Gittins et. al., 1975) in having substantially higher SiO_2 and MgO contents.

Petrographic and field evidence in the Colorado-Wyoming districts indicates that kimberlite magma containing immiscible silicate and carbonate fluid phases in various degrees of segregation was emplaced into hypabyssal dike systems. Diatreme formation by fluidization and explosive boring, and attendant carbonatization, apparently was initiated in portions of the dike systems where the carbonate-rich fluid phase was most concentrated, and where fluid pressures exceeded load pressures.

References

- Cornelissen, A. K., and Verwoerd, W. J., 1975, Phys. Chem. Earth, 9, p. 71-94.
Dawson, J. B., 1967, in Ultramafic and Related Rocks, P. J. Wyllie, ed., John Wiley & Sons, Inc., New York, p. 269-278.
Gittins, J., Hewins, Roger H., and Laurin, Andre F., 1975, Phys. Chem. Earth, 9, p. 137-148.
McCallum, M. E., Eggler, D. H., and Burns, L. K., 1975, Phys. Chem. Earth 9, p. 149-161.

*Also with U.S. Geological Survey, Denver, Colorado

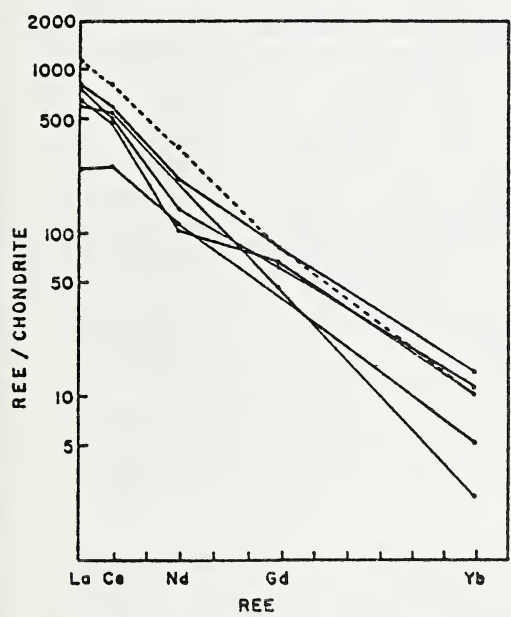
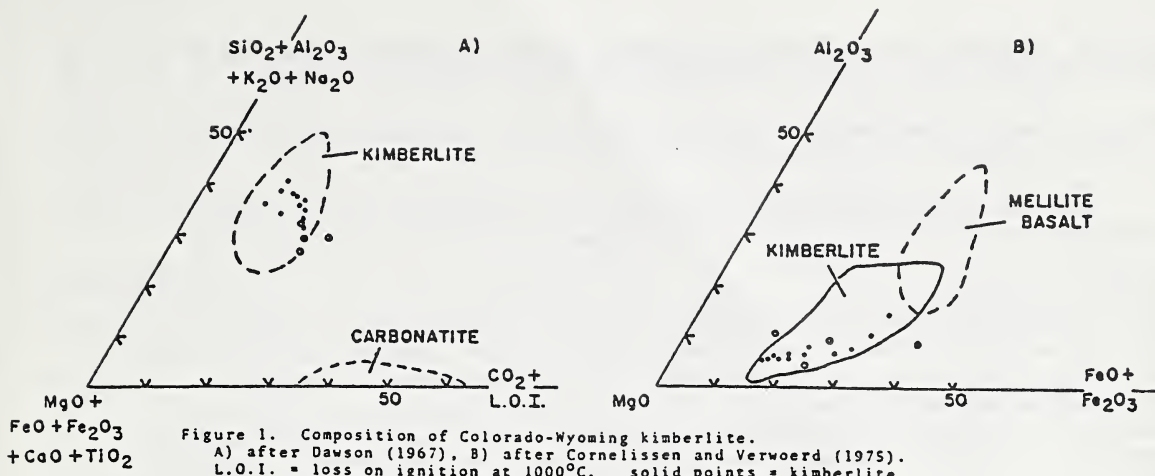


Table 1. Chemical analyses of representative samples

	SD1-86	IM16-5	NX4-10	NX3s-1	IM1-8
SiO ₂	30.4	33.6	34.2	24.8	25.7
Al ₂ O ₃	1.9	2.8	2.4	3.1	2.1
Fe ₂ O ₃	4.0	7.7	4.7	7.0	8.7
FeO	2.0	3.8	2.1	1.3	0.87
MgO	25.9	20.4	31.2	22.2	12.6
CaO	14.8	5.1	7.9	16.2	19.9
Na ₂ O	0.04	0.05	0.07	0.07	0.05
K ₂ O	0.29	1.4	1.1	0.16	1.0
TiO ₂	0.90	3.0	0.75	1.4	2.6
MnO	0.13	0.18	0.13	0.15	0.16
P ₂ O ₅	0.35	0.35	0.15	1.4	0.35
CO ₂	8.9	1.7	3.5	10.5	20
L.O.I.	10.2	11.2	12.0	10.0	5
total	99.81	99.20	100.2	98.20	99.03

Figure 2. Rare earth normalized patterns for Colorado-Wyoming kimberlite
 solid curves = kimberlite
 dashed curve = carbonate rich kimberlite

SD1-86 = kimberlite breccia; IM16-5, NX4-10 = porphyritic kimberlite; NX3s-1, IM1-8 = carbonate rich porphyritic kimberlite.
 L.O.I. = loss on ignition at 1000°C

HYDROUS MINERALS AND CARBONATES IN PERIDOTITE INCLUSIONS FROM THE GREEN KNOBS AND BUELL PARK KIMBERLITIC DIATREMES ON THE COLORADO PLATEAU.

Douglas Smith (Department of Geological Sciences, University of Texas at Austin, Austin, Texas 78712)

Over 90% of the peridotite inclusions in kimberlitic tuff at these diatremes contain hydrous phases which appear to have formed before the inclusions were incorporated in the erupting kimberlite, and a few percent contain carbonate of similar origin. Such "primary" phases are distinguished from "secondary" phases formed during or after incorporation in kimberlite by the following criteria: primary phases were deformed together with anhydrous silicates, they occur locally in relatively large crystals in apparent equilibrium metamorphic textures, and they show systematic compositional variations together with anhydrous silicates. The "primary" hydrous phases -- amphibole, chlorite, titanoclinohumite, and probably antigorite -- comprise from trace amounts to 90% of the hydrated inclusions. Antigorite also formed as a late "secondary" phase, and many antigorite textures cannot be interpreted unambiguously.

Mineral compositions in Table 1 are from three rocks (N53, N23, N51) with relatively homogeneous hydrous phases; the rocks are arranged in order of increasing abundance of hydrous minerals (N51 most hydrated). Amphiboles and pyroxenes become less aluminous, and orthopyroxene becomes less calcic with increased rock hydration. Textures, compositional differences between grains, and zoning indicate chemical disequilibrium: in an extreme example, one rock contains amphibole with a range of over 8% Al₂O₃. Several assemblages (e.g. ol-opx-cpx-sp-amph; ol-cpx-antig) may represent local equilibrium, as judged from experimental data and assemblages in ultramafic rocks metamorphosed in the crust (e.g. Evans, 1977). Neither talc nor anthophyllite is present, and orthopyroxene occurs together with antigorite in many rocks. This pair most likely indicates disequilibrium even on a local scale; high water pressure and high Al plus Cr may relatively stabilize antigorite, however (e.g. Hemley and others, 1977), and equilibrium in the uppermost mantle is conceivable. Titanoclinohumite is likely stabilized by Ti; it has very similar compositions in different assemblages (Table 1). Magnesite, a likely "primary" carbonate, has been analyzed in five inclusions and has a systematic Fe/Mg partition with associated olivine. Dolomite, of debatable origin, is a rare phase, and late, secondary calcite is common.

The solid-fluid reactions may have occurred over ranges of temperature and water fugacity. Magnesite and recrystallized diopside occur in near contact but may not have been in equilibrium; the lower-pressure pair dolomite-enstatite was not observed. Consideration of the phases present and the study of anhydrous reactions of Smith and Levy (1976) suggest reactions at less than 700°C and less than 18 kb. Fe is partitioned into relict and recrystallized olivine as hydrous phases with lower Fe/Mg ratios are formed; observed olivine zoning (Fig. 1) is most compatible with some hydration preceding kimberlite eruption by less than tens of millions of years.

Peridotite hydration may be directly related to the genesis of kimberlite and associated rocks. The Defiance uplift has been a persistent Phanerozoic high (Hunt, 1956). Hydration may have begun along zones of weakness in the mantle associated with the high even before Laramide monocline formation. Three analyzed peridotite inclusions with possible primary antigorite contain

$\leq 0.03\%$ Na₂O, while 5 inclusions without "primary" antigorite contain 0.18 - 0.49%. Na may have been released during hydration in the stability field of antigorite, and it may have contributed to the formation of the unusually sodic Plateau eclogites found primarily in kimberlite diatremes to the north. Subsequent intrusion of minette magma into the hydrated peridotite may have caused dehydration reactions and provided the volatiles for disaggregation and eruption of non-magmatic Plateau kimberlite.

References

- Evans, B. W., 1977, Metamorphism of alpine peridotite and serpentine: Ann. Rev. Earth Planet. Sci., v. 5, p. 397-447.
- Hemley, J. J., Montoya, J. W., Shaw, D. R., and Luce, R. W., 1977, Mineral equilibria in the MgO-SiO₂-H₂O system: II Talc-antigorite-forsterite-anthophyllite-enstatite stability relations and some geologic implications in the system: Amer. Jour. Sci., v. 277, p. 353-383.
- Hunt, C. B., 1956, Cenozoic geology of the Colorado Plateau: U. S. Geol. Surv. Prof. Pap., v. 279, 99 p.
- Smith, D., and Levy, S., 1976, Petrology of the Green Knobs diatreme and implications for the upper mantle below the Colorado Plateau: Earth Planet. Sci. Letters, v. 29, p. 107-125.

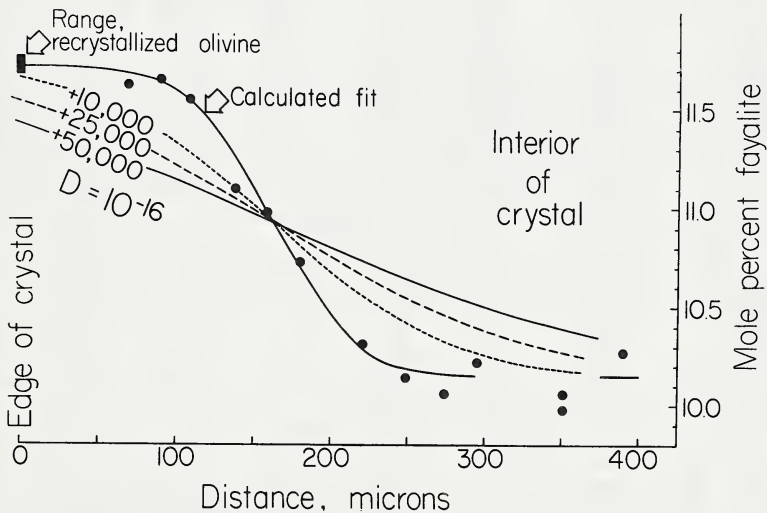


Figure 1: Observed compositional profile in olivine. The recrystallized olivine is in Fe/Mg exchange equilibrium with amphibole, chlorite, and titanoclinohumite: the crystal interior is typical of rock olivine before hydration. D , the diffusion coefficient, is an estimate for 700°C. Times for the calculated fit to decay are in years. A decrease in D by any factor results in an increase in time by the same factor.

Table 1: Mineral compositions in peridotites with increasing amounts of hydration (N51 most hydrated).

<u>Rock N53</u>							
	Opx	Cpx	Ol	Amph	Spinel		
SiO2	54.3	52.6	na	42.6	nd		
TiO2	.08	.22	na	.28	nd		
Al2O3	5.22	6.40	na	15.7	56.9		
Cr2O3	.47	.87	na	.80	11.9		
Fe as FeO	6.07	2.20	9.45	3.91	12.2		
MnO	.16	.10	na	.06	.13		
MgO	32.8	15.9	50.4	18.3	19.1		
CaO	.77	20.2	.01	12.0	.02		
Na2O	.07	1.67	na	3.49	nd		
K2O	nd	nd	na	.03	nd		
	<hr/>	<hr/>		<hr/>	<hr/>		
	100.0	100.2		97.2	100.2		
<u>Rock N23</u>							
	Opx	Cpx	Ol	Amph	Chlor	Clinoh	Magnesite
SiO2	57.3	54.7	40.4	55.6	31.8	35.6	na
TiO2	.06	.08	.01	.05	nd	5.55	na
Al2O3	1.47	1.73	.00	1.64	12.4	.00	na
Cr2O3	.29	1.24	.00	.18	2.05	.02	na
Fe as FeO	6.24	2.03	11.6	2.85	4.28	11.7	5.28
MnO	.12	.06	.20	.08	.01	.18	na
MgO	35.6	16.8	49.1	23.2	34.2	46.2	42.0
CaO	.24	22.6	.00	9.23	na	.01	.17
Na2O	nd	1.19	.00	3.83	na	na	na
K2O	na	na	na	.84	na	na	na
	<hr/>	<hr/>	<hr/>	<hr/>	<hr/>	<hr/>	<hr/>
	101.3	100.4	101.2	97.4	84.8	99.2	
<u>Rock N51</u>							
	Opx	Cpx	Ol	Antig	Chlor	Clinoh	
SiO2	57.2	54.8	42.1	41.1	32.9	36.3	
TiO2	.03	.02	nd	.03	.02	5.57	
Al2O3	1.09	.33	nd	2.82	12.3	nd	
Cr2O3	na	.18	na	.79	1.95	na	
Fe as FeO	5.81	1.94	9.26	3.64	3.47	9.20	
MnO	na	.08	.18	.04	nd	.19	
MgO	35.1	17.4	49.1	37.5	34.9	46.5	
CaO	.11	24.4	nd	.03	.04	.03	
Na2O	na	.59	na	na	na	na	
NiO	na	na	.36	.16	.19	.29	
	<hr/>	<hr/>	<hr/>	<hr/>	<hr/>	<hr/>	
	99.3	99.8	101.1	86.2	85.7	98.1	

GARNET-PYROXENE GROWTH IN ECLOGITE INCLUSIONS FROM THE GARNET RIDGE
KIMBERLITIC DIATREME, ARIZONA.

Douglas Smith, Department of Geological Sciences, The University of Texas
at Austin, Austin, Texas 78712

Michael Zientek¹, Department of Geological Sciences, The University of Texas
at Austin, Austin, Texas 78712

Petrographic studies and electron probe analyses of compositional zoning have been made to evaluate hypotheses for the origins of Garnet Ridge eclogites. The rock investigated in most detail is a sodic (8.00% Na₂O) garnet-poor eclogite containing clinopyroxene, garnet, phengite, rutile, lawsonite, and pyrite. Garnets and pyroxenes are primarily Py-Alm-Gross and Jd-Di-Ac solid solutions, respectively. Generalized sequences of garnet and pyroxene zoning are shown below and in Figs. 1 and 2. Phengite is unzoned with the following 7-cation formula: $K_{.94}Al_{1.32}Fe_{.12}Mg_{.62}Si_{3.74}Al_{.26}$.

Garnet:	Alm	Gross	Py	Clinopyroxene:	Jd	Ac	Di-Hd
	69	21	10	<u>CORE</u>	58	12	30
	65	26	9				
discontinuity	-			discontinuity	-		
	66	14	20		75	9	16
	60	11	29				
	61	13	26	<u>RIM</u>	57	8	35

More detailed electron probe traverses show that the major discontinuities in Ca-Mg zoning in garnet shown in Fig. 1 are abrupt; they occur over a maximum distance of several microns. Oscillatory Fe-Mg zoning (variations up to 6% Py) occurs on a 15 micron scale in some garnet cores. Jadeite is highest in an intermediate zone in pyroxene crystals (Figs. 2, 3). Oscillatory Di-Jd zoning is pronounced on a 10-15 micron scale with variations up to 15% Jd (Figs. 2, 3). Rim compositions vary widely within single crystals, partly as a function of the contacting phases. Phengite was a late-crystallizing phase, and pyroxene in contact with phengite has relatively jadeite-poor compositions.

Models proposed elsewhere suggest that mineral zoning in a Garnet Ridge eclogite reflects equilibrium crystallization at increasing P and T (Raheim and Green, 1975), and that these eclogites represent ocean floor subducted off the west coast of North America (Helmstaedt and Doig, 1975). Ryburn and others (1976) noted the difficulty of calculating ferrous-ferric ratios from probe analyses of jadeite-rich pyroxene, and the problem precludes meaningful calculations of temperature based on gt-cpx Kd's for the data presented here. An analysis of error propagation in calculation of ferric iron, together with an assumption of a 1% relative error in electron probe data, can be used to calculate uncertainties in derived temperatures. Such error analysis indicates that the core and rim temperatures calculated by Ryburn and others (1976) for pyroxene and garnet in a Garnet Ridge eclogite are well within an uncertainty interval of two

¹ Current address: Department of Geology, Stanford University, Stanford, California 94305

standard deviations. No pressure differences between core and rim crystallization may be inferred from available data.

Textures indicate that some garnets in many of the eclogites began growth as hollow, skeletal crystals which subsequently filled. The textures and oscillatory zoning are unusual for metamorphic rocks, and they suggest a model of disequilibrium crystallization after overstepping of reaction boundaries. Such crystallization might be a consequence of garnet-pyroxene growth during cooling at constant pressure in the lower crust or uppermost mantle with the low geothermal gradient typical of some shield areas. Eclogite inclusions are associated with hydrated peridotite inclusions at Garnet Ridge; some of the hydrated peridotite inclusions in a similar kimberlitic diatreme, Green Knobs, are very low in sodium (Smith, this volume), and peridotite may have released sodium to recrystallizing eclogites as hydration occurred. The results here do not preclude other origins for the eclogites, such as subduction zone metamorphism. Textures and mineral zoning do indicate the probable importance of disequilibrium crystallization.

References

- Helmstaedt, H., and Doig, R., 1975, Eclogite nodules from kimberlite pipes of the Colorado Plateau--samples of subducted Franciscan--type oceanic lithosphere: *Phys. Chem. Earth*, v. 9, p. 95-111.
- Raheim, A., and Green, D. H., 1975, P, T paths of natural eclogites during metamorphism--a record of subduction: *Lithos*, v. 8, p. 317-328.
- Ryburn, R. J., Raheim, A., and Green, D. H., 1976, Determination of the P, T paths of natural eclogites during metamorphism--record of subduction. A correction to a paper by Raheim and Green (1975). *Lithos*, v. 9, p. 161-164.

Figures (next page)

- Figure 1: Results of an electron probe traverse across a typical zoned garnet crystal. Points are at 10-micron intervals.
- Figure 2: Results of an electron probe traverse across the center of a zoned pyroxene crystal. Points are at 10-micron intervals. The asymmetrical zoning is typical. Note the high jadeite content in intermediate zones.
- Figure 3: Results of an electron probe traverse from rim to core of a different part of the same pyroxene crystal as that of Fig. 2. Points are at 3-micron intervals. Note the oscillatory jadeite-diopside zoning. Oscillations appear to follow growth boundaries and do not reflect exsolution.

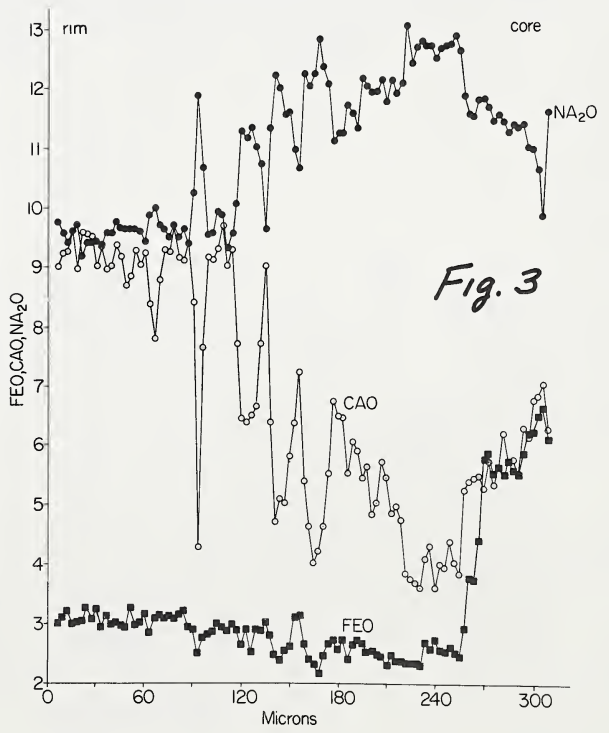
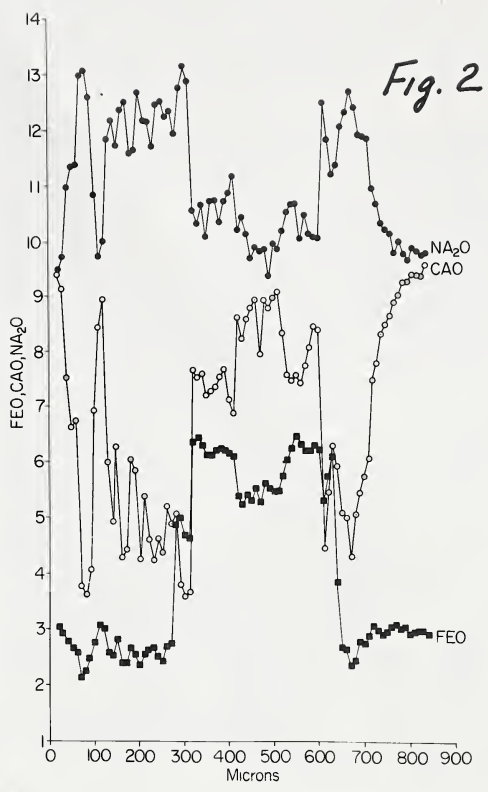
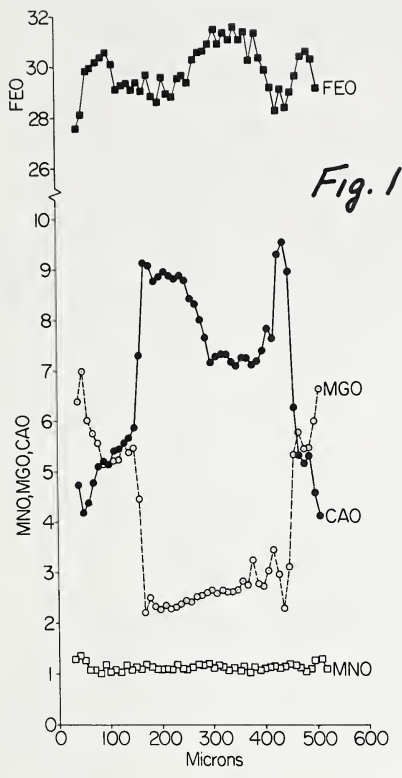


Figure explanations on previous page.

LATE-STAGE MICAS IN KIMBERLITE GROUNDMASS.

J. V. Smith and R. Brennesholtz, Department of the Geophysical Sciences,
The University of Chicago, Chicago, Illinois 60637 U.S.A.

J. B. Dawson, Department of Geology, University of St. Andrews, Scotland

Micaceous kimberlites from South Africa contain two types of groundmass mica <1mm across. Very rare Type I micas are relatively iron-rich with \underline{mg} [= $Mg/(Mg+Fe)$] 0.45-0.65, TiO_2 3-6 wt.%, low Cr_2O_3 , Al_2O_3 14-16 wt.%, no Fe^{3+} required in tetrahedral sites, low NiO (~0.02 wt.%), and relatively high \underline{na} [$Na_2O/(Na_2O+K_2O)$] 0.02-0.03. The much more abundant Type II micas are variable in composition, but relative to Type I micas are more magnesian (\underline{mg} 0.80-0.93), lower in TiO_2 (0.7-4.0 wt.%) and Al_2O_3 (6.8-14.2 wt.%), have substantial Fe^{3+} in tetrahedral sites, and have relatively low \underline{na} and variable Cr_2O_3 . Inter-grain variations in composition of Type II micas may result from establishment of local reservoirs on a mm scale, with competition of other phases for minor elements (e.g. chromite for Cr, serpentine for Ni). Associated phases in the groundmass, varying from one kimberlite to another, are combinations of Fe-rich serpentines, Fe-rich talc, calcite, dolomite, diopside, chromite, Mg-ilmenite, perovskite, barite, pyrite, pentlandite, millerite?, heazlewoodite?, quartz.

Type I micas may result from an intrusive precursor (carbonatitic?) to kimberlite, perhaps genetically related, which was incorporated into a later pulse of kimberlite from which the Type II micas crystallized.

NSF EAR 76-03604 and Materials Research Laboratory.

Figs. 1-4. Type I mica-hexagon. Type II mica-circle->0.5mm² area, dot - 0.05-0.5mm², cross-<0.05mm². Triangle-high- Fe^{3+} rims on 1097A Type II mica, square Type II rim on Type I core. $\Delta T = 8-Al-Si$ in structural formula based on 22 oxygens (H_2O -free; microprobe data). Localities - 1084 Saltpeterpan dyke, 1088 Zout en Zuur dyke, 1089 New Elands Mine, 1097 Star Mine, 1268 Main dyke, Helam Mine, 1978 Lovedale Mine.

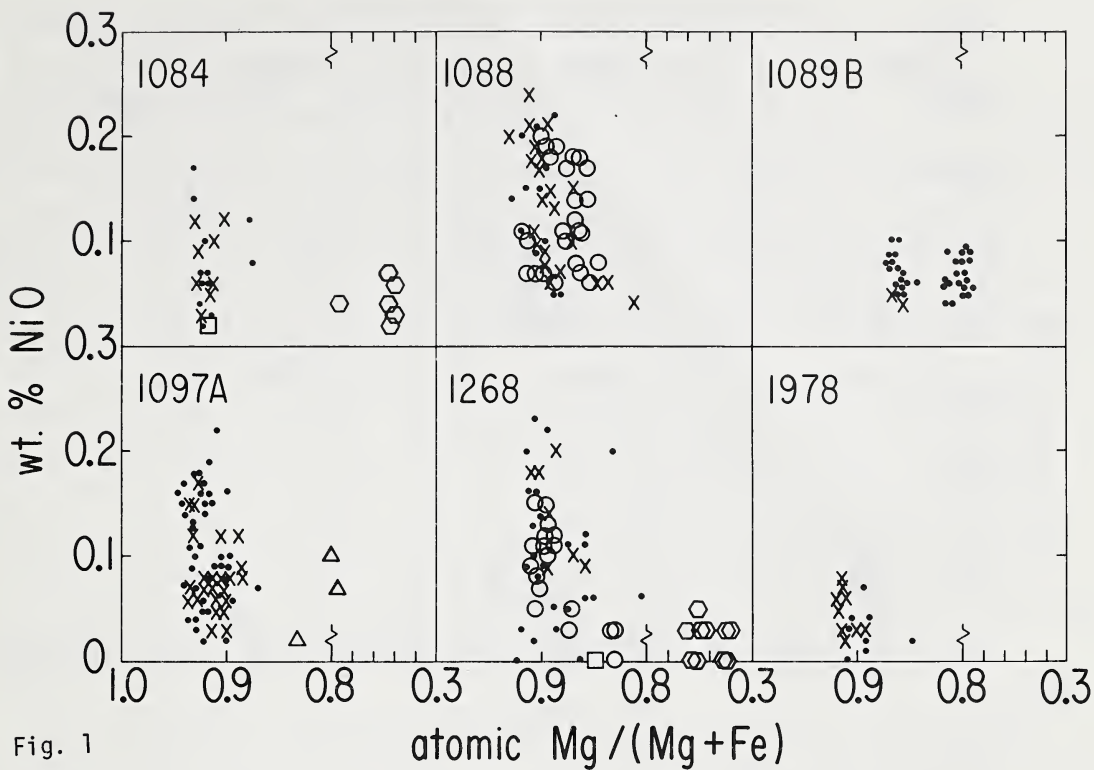


Fig. 1

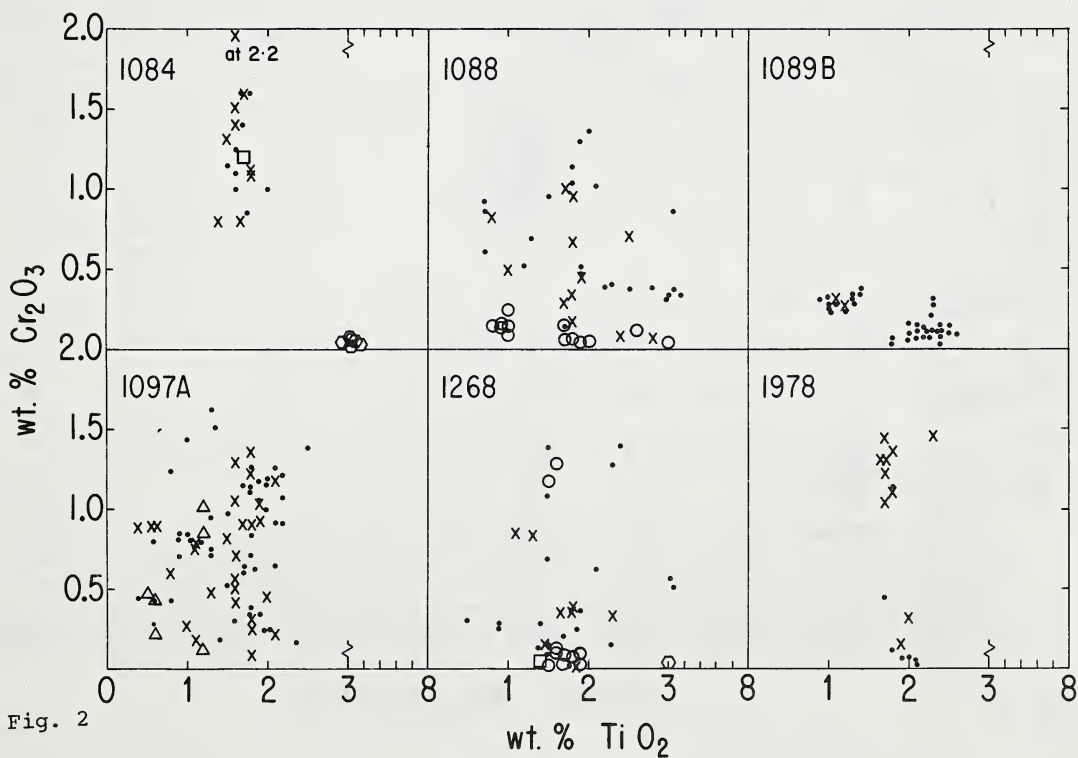


Fig. 2

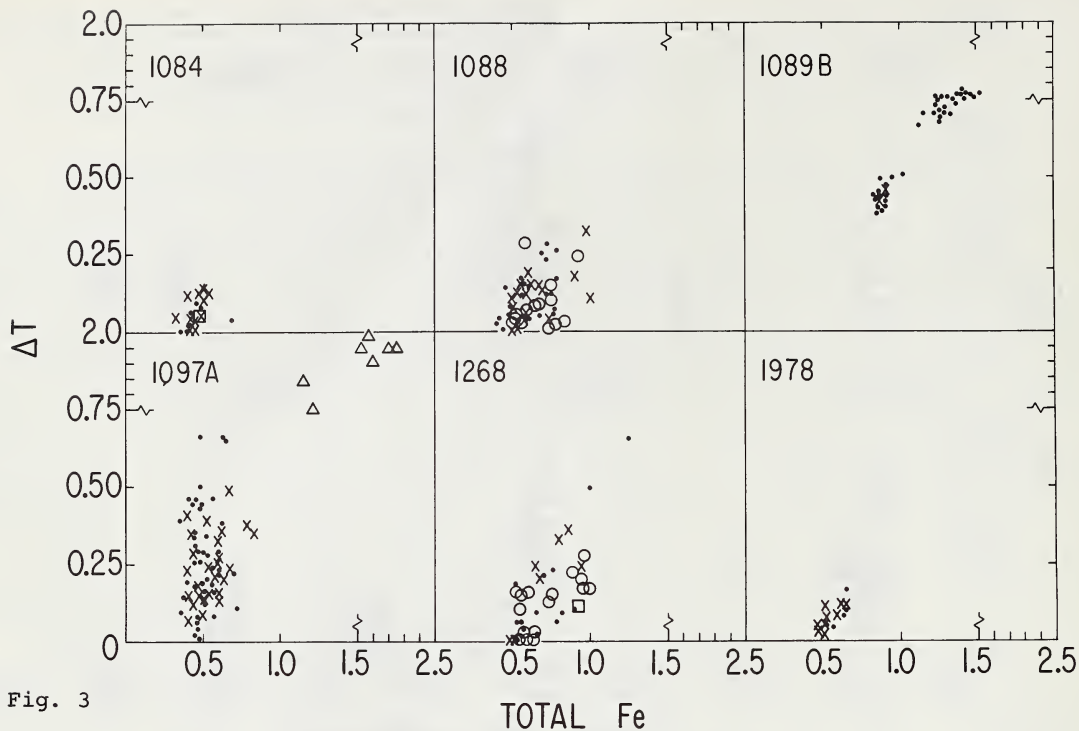


Fig. 3

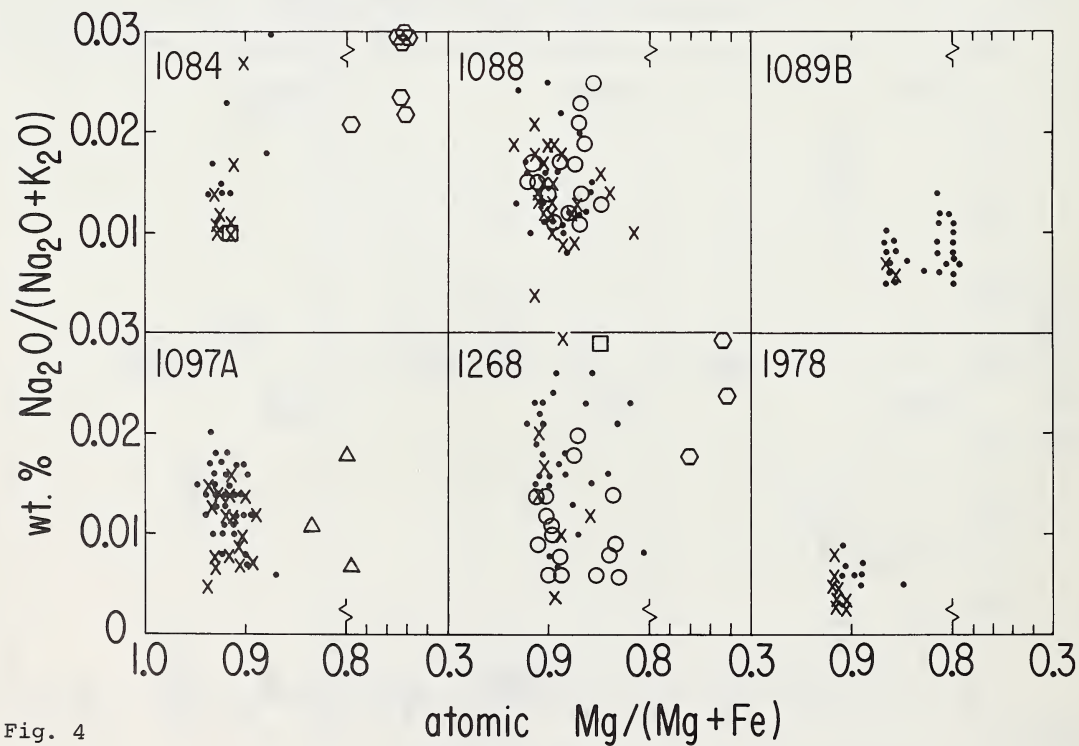


Fig. 4

K, RB AND BA IN MICAS FROM KIMBERLITE AND PERIDOTITIC XENOLITHS.

J. V. Smith and R. L. Hervig, Department of the Geophysical Sciences, The University of Chicago, Chicago, Illinois 60637 U.S.A.

D. Ackermann, Mineralogisch-Petrographisches Institut der Universität Kiel, W. Germany

J. B. Dawson, Department of Geology, University of St. Andrews, Scotland

Highly-sensitive electron microprobe analyses were made for Rb and Ba in micas from peridotitic xenoliths in kimberlites, in MARID-suite nodules, in phlogopite megacrysts, and in kimberlite groundmass minerals (Table 1). Special attention was paid to background for Rb L_{α} (Fig. 1); the standard was Corning X-glass (0.49 wt.% Rb₂O, atomic absorption analysis, J. Ito). Fig. 2 summarizes the ranges and mean for K/Rb and K/Ba.

Primary micas from peridotite xenoliths were split into two groups. High-K ones have lower Na, lower BaO (340-880) and higher Rb₂O (320-440) than low-K ones (BaO 1720-4000, Rb₂O 160-260). Phlogopites from the MARID-suite (interpreted as cumulates from kimberlite liquid crystallizing at considerable depth; Dawson and Smith, 1977) have higher Rb₂O than both types of peridotite micas, and the same range of BaO as high-K peridotite micas. Aoki (1974) recorded Rb₂O analyses for MARID micas twice greater than ours, whereas Allsopp and Barrett (1975) recorded ~400-530 for Wesselton "nodule" micas which fall in our range of 340-800 for MARID micas. The very wide ranges for megacryst micas (interpreted as phenocrysts; Smith and Dawson, 1975) overlap those for MARID micas, and our range of Rb₂O encompasses that for Monastery megacrysts (Rb₂O 683-963; Allsopp and Barrett, 1975).

The groundmass of micaceous kimberlites contains very rare, Fe-rich micas (Type I) interpreted as xenocrysts from an intrusive precursor (carbonatitic?), and abundant Type II micas interpreted as late-stage primary crystals (Smith, Brennescholtz and Dawson, see another Ext. Abstr.). Both have very wide, overlapping ranges of Rb₂O and BaO. BaO concentrations tend to be considerably greater than those for the high-K peridotite, MARID and megacryst groups, but similar to those for the low-K peridotite group. Bulk analyses of kimberlite groundmass micas should be determined essentially by Type II micas, and the K/Rb range for Wesselton groundmass mica (Barrett, 1975) is at the low end (110-160) of the range (112-1040) found by us for micaceous kimberlites from several localities. Perhaps some of these micas are partly serpentinized.

Serpentine carries substantial Rb₂O (Table 1) and somewhat less K₂O. A kimberlite with equal amounts of serpentine (K₂O 400, Rb₂O 580) and Type II mica (K₂O 10 wt.% Rb₂O 400) would have K/Rb 93. No other minerals carry substantial K and Rb. Some measured K/Rb values for bulk kimberlite are: Fesq et al. (1975a), 88-217; Barrett and Berg (1975), 93-207; Harris and Middlemost (1969), mean kimberlite 196. Until detailed mineralogical modes are obtained for samples used for bulk analysis, a definitive test cannot be made, but serpentine is apparently an important sink for Rb in kimberlite.

Unfortunately the presence of barite in many micaceous kimberlites rules out simple interpretation of K/Ba ratios of bulk kimberlite in terms of constituent minerals.

Mica and clinopyroxene (see refs. in Ext. Abstr. by Bishop et al.) are probably the significant hosts for K and Rb at depths below ~100km, and it is interesting to check whether total extraction of these minerals into magmas would yield K/Rb ratios which match those for mantle-derived volcanic rocks. Unfortunately the lack of understanding of the different origins of high-K and

low K peridotite micas provides a complication, as does possible mica-liquid fractionation (Beswick, 1976).

Values of K/Rb for bulk kimberlites (~90-220) are lower than our values for high-K peridotitic mica (210-300) and low-K peridotitic mica (330-550), but greater than the values for inclusion-bearing diamonds (20-130, mean ~70; Fesq et al., 1975b). Similarly, the values of K/Ba for kimberlites (8-39; Fesq et al., 1975) lie between those for high- and low-K peridotitic micas (112-292 and 22-51) and for diamonds (1.5-2.5; Fesq et al., 1975b). Clinopyroxenes tend to have high values of K/Rb (often over 1,000; Shimizu, 1975). We have not yet evaluated the ranges for secondary micas in peridotites, but aim to obtain data in time for the conference. Rhodes and Dawson (1975) reported K/Rb 83-234 for peridotites from Lashaine, and these relatively low values may result mainly from secondary mica.

The K/Rb ratio of Cl meteorites, probably the best representative of the primordial solar nebula, is $(544+75)/1.88+0.36 = 289 \approx 100$ (Nichiporuk and Moore, 1974; Krahenbühl et al., 1973) which lies inside our range for peridotitic micas.

K/Ba values for Basutoland flood basalts (12-46, mean 25) and dolerites (mean 36) (Cox and Hornung, 1966) overlap with the range for low-K peridotite micas but not with high-K peridotite micas, while the K/Rb values (basalts, 110-680, mean 213; dolerites, mean 435) overlap the entire range for both low- and high-K peridotite micas, but are far outside the ranges for diamond inclusions. Lloyd and Bailey (1975) reported the following average values for 17 Eifel (Germany) lavas (K/Rb 289; K/Ba 22.5) and 23 Uganda lavas (323; 22.9).

Oceanic basalts have higher K/Rb (e.g. 330-1780; O'Nions et al., 1976) and a wide range of K/Ba (e.g. 31-412; Kay et al., 1970). These values overlap considerably with those for peridotitic micas, but tend to be higher. Clinopyroxenes (Shimizu, 1975) from inclusions in kimberlite have higher variable K/Rb (160-22,300) and K/Ba (4-1140), perhaps because of contamination. Further work is needed to test whether clinopyroxene-mica-peridotite could yield oceanic basalts by partial melting, and whether other minerals must be considered to explain K, Rb and Ba.

NSF EAR 76-03604 and Materials Research Laboratory.

References, Allsopp H. L. Barrett D. R. 1975 PCE 9 605; Aoki K. 1974 CMP 48 1; Barrett D. R. Berg G. W. 1975 PCE 9 619; Beswick A. E. 1976 GCA 40 1167; Cox K. G. Hornung G. 1966 AM 51 1414; Dawson J. B. Smith J. V. 1977 GCA 41 309; Fesq H. W. Kable E. J. D. Gurney J. J. 1975a PCE 9 687; Fesq H. W. et al. 1975b PCE 9 817; Harris P. G. Middlemost E. A. 1969 L 3 77; Kay R. Hubbard N. J. Gast P. W. 1970 JGR 75 1585; Krahenbühl U. et al. 1973 GCA 37 1353; Lloyd F. E. Bailey D. K. 1966 PCE 9 389; Nichiporuk W. Moore C. B. 1974 GCA 38 1691; O'Nions, R. K. Pankhurst R. J. Grönvold, K. 1976 JP 17 315; Rhodes J. M. Dawson J. B. 1975 PCE 9 545; Shimizu N. 1975 PCE 9 655; Smith J. V. Dawson J. B. 1975 GSA Abstr. Progr. 7 1275.

Table 1. Electron microprobe analyses

Type	N	BaO ppm	Rb ₂ O ppm	K/Rb	K/Ba
Peridotite, high K	4	340-880 (635)	320-440 (380)	212-301 (254)	112-292 (173)
Peridotite, low K	3	1720-4000 (3080)	160-260 (220)	332-550 (420)	22-51 (33)
MARID	7	340-800 (390) ^a	470-700 (580)	145-203 (167)	124-286 ^a (260)
Megacryst	19	130-2070 (380) ^b	290-1060 (750)	91-319 (138)	102-726 (398)
Type I groundmass	5	1030-4320 (2670)	240-600 (470)	137-348 (209)	20-88 (42)
Type II groundmass	9	470-5780 (2450)	90-820 (400)	112-1040 (351)	16-199 (80)
serpentine ^c	-	<50ppm	530-620 (580)	0.25-1.00 (0.63)	-
amphibole ^d	-	<50ppm	780	60	-

N number of samples. ^aAll but one sample have BaO 340-380; K/Ba 248-288. ^b18 samples have BaO 130-970 (380) but one megacryst from Peiser mine is very variable (190-2070) and was omitted from the arithmetic mean. ^colivine pseudomorph, serpentinized mica, accordion types, respectively in 1097A have Rb₂O, K₂O: 620,170; 530,360; 600,660. ^d1160 (MARID).

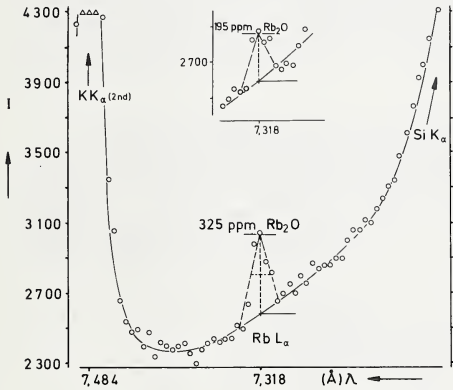


Fig. 1 X-ray counts in 120 seconds vs. λ around RbL_{α} peak for micas with 325 and 195ppm Rb_2O .

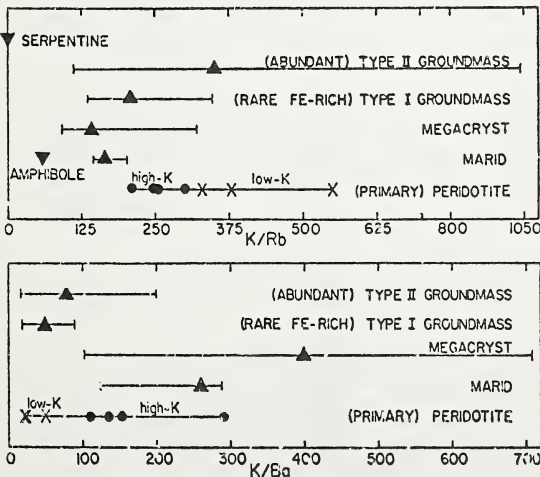


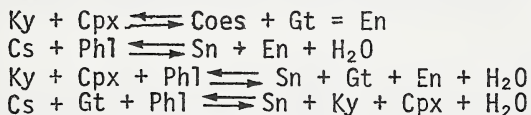
Fig. 2. Ranges and mean of K/Rb and K/Ba for mica (upright triangle) and other minerals (inverted triangle).

SILICA-BEARING ECLOGITES FROM THE ROBERTS-VICTOR KIMBERLITE

J. R. Smyth (Geological Research Group, Los Alamos Scientific Laboratory, Los Alamos, New Mexico 87545)

Recently, Smyth and Hatton (1977) described a coesite-bearing kyanite eclogite from the Roberts-Victor Kimberlite, South Africa. Since that description, two additional silica-bearing kyanite eclogites from the same locality have been found to contain quartz, apparently pseudomorphic after coesite (Smyth, 1977a). Based on several independent lines of evidence, the mineral assemblages of these specimens appear to have equilibrated near 900°C and 3.0 GPa (30 Kb). Based on bulk major element chemistry obtained from microprobe and modal analyses, these specimens appear to form a chemically distinct group of mantle-derived rocks. They are rich in both SiO₂ (52-54 wt %) and Al₂O₃ (18-23 wt %), and CIPW norm calculations yield gabbroic anorthosites with 65 to 80 percent feldspar. This set of unique mineral assemblages has provided constraint on the depth of origin and magma migration velocities of the kimberlite (Smyth and Hatton, 1977), additional insight into high pressure pyroxene crystal chemistry, and may possibly be subducted samples of a plagioclase-rich primordial crust of the earth.

The mineralogy of the specimens can be used to infer temperatures and pressures of equilibration. The disordered state of the sanidine sets a minimum temperature of 900°C, and the presence of coesite a minimum pressure of 3.0 GPa. Based on thermodynamic equilibrium of the four simplified reactions:



Wohletz (personal communication) has obtained an invariant point at 1186°K (913°C) and 3.2 GPa. Further, based on the experimental study of Råheim and Green (1974), the Fe-Mg distribution between coexisting garnet and clinopyroxene indicates a temperature of approximately 850°C, assuming the 3.0 GPa pressure minimum of the quartz-coesite transition.

The pyroxenes in these eclogites may be described as peraluminous omphacites, that is, the Al^{VI} exceeds the Al^{IV} + Na + K. In hand specimen, the clinopyroxene appears characteristically milky-white due to the exsolution of Ca-Tschermaks pyroxene and quartz according to the reaction:



(Smyth, 1977b).

The bulk chemistry may provide some insight into the ultimate origin of these rocks. The major element chemistry and CIPW norms based on microprobe and modal analyses are given in Table I. Lappin and Dawson (1975), Harte and Gurney (1975), and Gurney (1975 personal communication) have proposed a high pressure igneous cumulate origin for

many of the eclogites from Roberts-Victor. It is difficult to imagine how the silica-bearing eclogite rocks could be related to the more normal biminerally eclogites by a simple fractionation process at depth, because it is difficult to enrich a liquid in Si, Al, and Ca by the subtraction of either a clinopyroxene or garnet phase. The low-pressure equivalent of these rocks is a gabbroic anorthosite (Table 1), and samples SRV-1 and SRV-6 contain 78 wt % feldspar in the norm. Rocks of this composition are common in low pressure basic cumulate igneous complexes but are exceedingly rare as primary liquids. It therefore seems likely that these silica-bearing eclogites represent subducted bits of low-pressure cumulate rocks. The whole-rock $^{16}\text{O}/^{18}\text{O}$ of sample SRV-1 was determined by K. Muehlenbachs (University of Alberta) as +8.0‰ relative to SMOW. This value is somewhat higher than typical of mantle-derived eclogites, and would be more consistent with an origin in the lower crust. The whole-rock $^{86}\text{Sr}/^{87}\text{Sr}$ determined by J. Wooden (NASA/JSC) is 0.7074 which is also consistent with a low pressure origin of these rocks. If these silica eclogites do indeed represent subducted bits of crustal material, in order for them to have been erupted from under the stable craton of Africa, it is possible that they originated very early in the history of the earth.

REFERENCES

- Harte, D. , and J. J. Gurney, (1975), "Evolution of Clinopyroxene and Garnet in an Eclogite Nodule from the Roberts-Victor Kimberlite Pipe, South Africa," Phys. Chem. Earth 9, p. 367-387.
- Lappin, M. A., and J. B. Dawson, (1975), "Two Roberts-Victor Cumulate Eclogites and Their Re-equilibration," Phys. Chem. Earth 9, p. 351-365.
- Råheim, A., and D. H. Green, (1974), "Experimental Determination of the Temperature and Pressure Dependence of the Fe-Mg Partition Coefficient for Coexisting Garnet and Clinopyroxene," Contrib. Mineral. Petrol. 48, p. 179-203.
- Smyth, J. R., (1977a), "Quartz Pseudomorphs After Coesite," Amer. Mineral. 62, (July-August issue).
- Smyth, J. R., (1977b), "Peraluminous Omphacite: Cation Vacancies in Upper Mantle Pyroxenes," (abstract), Trans. Amer. Geophys. Union 58, p. 523.
- Smyth, J. R., and C. J. Hatton, (1977), "A Coesite-Sanidine Grosspyrite from the Roberts-Victor Kimberlite," Earth Plant. Sci. Lett. 34, p. 284-290.

TABLE I. ESTIMATED BULK COMPOSITIONS AND COMPUTED NORMS OF THREE SILICA-BEARING ECLOGITES

	SRV-1	SRV-6	SRV-7
SiO ₂	52.4	52.5	53.5
TiO ₂	.1	.3	.2
Al ₂ O ₃	22.8	22.7	18.3
Cr ₂ O ₃	.1	.0	.1
FeO	3.8	4.2	4.6
MgO	5.5	4.8	8.6
CaO	11.1	11.2	11.2
MnO	.1	.0	.1
Na ₂ O	3.7	4.3	3.2
K ₂ O	.2	.1	.1
P ₂ O ₅	.01	-	-
Total	99.8	100.1	99.9
CIPW Norm (wt %)			
OR	1.4	.7	.5
PL	76.2	76.6	62.5
(AB)	(31.1)	(34.4)	(27.0)
(AN)	(45.0)	(42.2)	(35.5)
NE		1.2	
DI	8.1	11.0	16.2
(WO)	(4.2)	(5.7)	(8.4)
(EN)	(2.6)	(3.4)	(5.6)
(FS)	(1.3)	(2.0)	(2.2)
HY	6.5		16.2
(EN)	(4.3)		(11.7)
(FS)	(2.2)		(4.5)
OL	7.3	10.2	4.1
(FO)	(4.7)	(6.1)	(2.9)
(FA)	(2.6)	(4.1)	(1.2)
CM	.1	.1	.1
IL	.2	.6	.4
AP	.02	.6	.4

MINERAL PARAGENESES OF NATURAL DIAMONDS

N.V. Sobolev (Institute of Geology and Geophysics, Siberian Branch of the Academy of Sciences of the USSR, Novosibirsk, U.S.S.R.)

Minerals coexisting with natural diamonds are specified by different relations with the latter. They are represented by isolated syngenetic crystalline inclusions, mainly as single grains, sometimes by two-, three- or even four-phase inclusions.

Intergrowths with polycrystalline diamond aggregates and monocrystals are also typical of diamond-mineral relations. Moreover, the diamonds sometimes containing inclusions are part of xenoliths of diamondiferous peridotites and eclogites. The octahedral faces established in inclusions of a majority of Yakutian samples may serve as one of the most sound indications in favour of the syngenetic nature of crystalline inclusions and diamonds.

Generalization of the results of examination of the composition of over 600 samples of olivines, pyroxenes, garnets, chromspinelides and some other minerals coexisting with diamonds as inclusions, intergrowths and contained in xenoliths, most of which are from Yakutian occurrence reveals two main types of diamond parageneses (Sobolev et al., 1969; Sobolev, 1971, 1974): ultramafic (1) and eclogitic (2).

The characteristic features relevant to Type-1 paragenesis are: presence of olivine, Mg-composition of garnets and pyroxenes, variable Cr-content in garnets, pyroxenes and spinel.

Some distinct criterions established for the mineral composition and their associations have been established permitting one to reveal a series of parageneses within Type-1 including various ultramafic rock compositions. A typomorphic nature of Mg-garnets has been recognized as one of the main criterions. The Ca-contents of these garnets are essentially a function of the nature of their parageneses. A positive correlation established for Ca- and Cr-contents in garnets typical of two-pyroxene para-

geneses (Sobolev et al., 1969) in addition to unambiguous position of the compositional field of these garnets permits one to separate the compositional field of garnets coexisting with enstatite without clinopyroxene (Ca-Cr diagram) belonging to harzburgite (dunite) paragenesis (Sobolev et al., 1969, 1973). Extremely low Na_2O contents in Ca-poor chrome pyropes (usually below 0.03 wt %) may serve as additional indication that clinopyroxene is absent in this type of paragenesis.

The finds of trimineral inclusions represented by intergrowths of Ca-poor chrome pyrope, enstatite and chromite (Sobolev et al., 1976) and even tetramineral intergrowths, such as pyrope + enstatite + chromite + olivine show an independent nature of parageneses of these garnets.

The identification of inclusions of Mg-garnets coexisting with two pyroxenes in one diamond, among them several tetramineral associations: garnet + enstatite + diopside + olivine (Sobolev et al., 1976) and five-mineral associations (+ilmenite) typical of diamondiferous lherzolite (Pokhilenko et al., 1976) permitted one to reveal websterite-lherzolite paragenesis. The garnet of this paragenesis contains moderate CaO (up to 4-6 wt%) and some Na_2O (about 0.1%).

The paragenesis of Ca-rich pyrope, olivine and clinopyroxene (wehrlite) is based on identification of trimineral association in a single diamond (Sobolev et al., 1970).

The eclogite-type paragenesis (2) is specified by a wide series of compositions from common two-mineral eclogites with rutile, coesite eclogites (Sobolev et al., 1976) to kyanite, corundum eclogites and groszpydites (Ponomarenko et al., 1976).

Type 1 generally predominates over the Type 2 in most of the diamond occurrences. Harzburgite-dunite paragenesis is most typical of Type 1, while wehrlite paragenesis is most uncommon. Coesite eclogites have been recently identified to belong to Type 2, though their distribution is still unknown. Common eclogites greatly predominate in this type.

The obtained thermobarometric data for numerous equilibrated mineral associations, such as inclusions, intergrowths and

xenoliths permit one to suggest a wide T-range for the crystallization of natural diamonds (1100-1500°C) and 50-60 kbar pressure, sometimes attaining 80 kbar.

REFERENCES

- Pokhilenko N.P., Sobolev N.V., Sobolev V.S, and Lavrent'ev Yu. G., 1976. Dokl. Akad. Nauk SSSR, 231, pp. 438-441.
- Ponomarenko A.J., Sobolev N.V., Pokhilenko N.P., Lavrent'ev Yu. G. and Sobolev V.S., 1976. Dokl. Akad. Nauk SSSR, 226, pp. 191-194.
- Sobolev N.V., 1971, J. Geophys. Res. 76, pp. 1309-1314.
- Sobolev N.V., 1974. Deep-seated inclusions in kimberlites and the problem of the composition of the Upper Mantle. Nauka Press, 264 p.
- Sobolev N.V., Botkunov A.J., Lavrent'ev Yu.G. and Usova L.V., 1976. Geologia i Geofiz., Novosibirsk, №12, pp. 3-15.
- Sobolev N.V., Lavrent'ev Yu.G., Pokhilenko N.P. and Usova L.V., 1973. Contr. Mineral. Petrol. 40, pp. 39-52.
- Sobolev N.V., Lavrent'ev Yu.G., Pospelova L.N, and Sobolev Ye. V., 1969. Dokl. Akad. Nauk SSSR, 189, pp. 162-165.
- Sobolev N.V., Yefimova E.S., Koptil V.I., Lavrent'ev Yu.G. and Sobolev V.S., 1976. Dokl. Akad. Nauk SSSR, 230, pp. 1442 - 1444.

DEEP-SEATED XENOLITHS, XENOCRYSTS IN KIMBERLITES AND CRYSTALLINE INCLUSIONS IN DIAMONDS FROM "UDACHNAYA" KIMBERLITE PIPE, YAKUTIA

N.V. Sobolev, N.P. Pokhilenko, Yu.G. Lavrent'ev and E.S. Yefimova (Institute of Geology and Geophysics, Siberian Branch of the USSR Academy of Sciences, Novosibirsk, U.S.S.R.)

A representative collection containing more than 1000 specimens of xenoliths recovered from the deep-seated rocks of "Udachnaya" kimberlite pipe in Yakutia has been examined. The following mineral associations have been identified as a result of studies: 1) olivine-garnet-enstatite-diopside, 2) olivine-garnet-enstatite-diopside-chromspinel, 3) olivine-garnet-enstatite-diopside-ilmenite, 4) olivine-enstatite-diopside-chromspinel, 5) olivine-garnet-enstatite-chromite, 6) olivine-garnet, 7) olivine-garnet-chromite, 8) olivine-garnet-diopside-chromite, 9) olivine-chromite, 10) enstatite-diopside-spinel, 11) enstatite-garnet, 12) garnet-chromspinel, 13) enstatite-diopside garnet, 14) diopside-garnet-ilmenite, 15) garnet-diopside-chromspinel, 16) garnet-omphacite-kyanite-rutile, 17) garnet-omphacite-rutile. Several diamondiferous specimens were found among the xenoliths belonging to associations 3,5,6,7,9,16,17. Most of the xenoliths from the ultramafic rocks are fragments of varying sheared pyrope peridotites belonging to associations 1,2,3 among which are the rocks containing garnets with clear zoning relevant to Cr-contents (8.2 wt % of Cr_2O_3 in the core and 1.4 at the periphery), Ti (0.3-1.4 wt% of TiO_2) as well as Ca, Fe, Mg, Al. There also occur the sheared peridotites containing garnets of tremendously varying though uniform composition within a single grain (Sp. Uv-97/76, Table 1). Table 1 lists the analyses of minerals which compose rather uncommon peculiar xenoliths of spinel (chromspinel) garnetites (Sp. Uv-958 and Uv-71/76). One of the samples contains garnet whose composition approaches to pure pyrope with extremely low iron contents (Table 1). The sheared lherzolite Uv-6 (Table 1) contains clinopyroxene with uncommonly low Na contents and rather high K admixture. The Mg-garnets from the kimberlite concentrate of "Udachnaya" Pipe have varying CaO content ranging from 0.98 to 25.4 wt %, Cr_2O_3 (0.1 to 18.7 wt %) with some variations in Ti-contents (Sobolev et al., 1973). A majority of garnets by their CaO and Cr_2O_3 contents (about 75%) belong to lherzolite paragenesis, while about 20% belong to harzburgite-dunite paragenesis and about 5% belong to wehrlite paragenesis (Fig. 1b). The variation range of CaO and Cr_2O_3 contents of the garnets from kimberlite concentrates exceeds those of garnets of xenoliths from the ultramafic rocks of "Udachnaya" Pipe (Fig. 1a).

Chromspinel (N=76) from "Udachnaya" kimberlite pipe are characterized by exceptionally varying contents of all the oxides (wt %): Cr_2O_3 (12.7-65.9), Al_2O_3 (2.1-48.9), TiO_2 (0.01-6.3), MgO (7.8-20.5), FeO (7.8-24.3), Fe_2O_3 (3.8-20.5) (Sobolev et al., 1975).

Ilmenites (N=146) have varied TiO_2 contents as well (42.3-54.3 wt %), MgO (7.0-13.2); Cr_2O_3 (0.1-4.4) with some variations in Al_2O_3 contents (0.04-0.60 wt %).

The crystalline inclusions in diamonds examined by electron probe technique (over 100 analyses) are represented by olivine, chromite, garnets (mostly Ca-poor chrome pyropes, see Fig. 1c) and pyroxenes. We have also studied along with single inclusions the compositions of coexisting minerals included in diamonds, garnets and omphacites, in particular.

Some of magnesian garnets from diamonds were found to have similar CaO and Cr_2O_3 contents with lherzolite garnets (see Fig. 1c) but proceeding from the peculiarities in the contents of some other oxides, harzburgite-dunite paragenesis predominates among the inclusions in diamonds with no indications of the presence of diamonds in the sheared lherzolites. The equilibrium conditions were established for the sheared lherzolites by geothermometry and geobarometry techniques as $T=1100-1350^\circ C$ and $P=30-45$ kbar (Sobolev, 1974).

REFERENCES

- Sobolev N.V., 1974. Deep-seated inclusions in kimberlites and the problem of the composition of Upper Mantle, Nauka, 264 p.
- Sobolev N.V., Lavrent'ev Yu.G., Pokhilenko N.P. and Usova L.V., 1973. Contr. Mineral. Petrol. 40, pp. 39-52.
- Sobolev N.V., Pokhilenko N.P., Lavrent'ev Yu.G. and Usova L.V., 1975. Geologia i Geofiz. Novosibirsk, N11.

Table 1

Selected analyses of minerals from uncommon xenoliths of the deep-seated rocks from "Udachnaya" Pipe

Sp.	Uv -958		Uv -71/76		Uv -97/76			Uv -6			
	ga	sp	ga	chr	ga1	ga2	ga3	ga	cpx		
<i>SiO₂</i>	43.9	n.d.	42.2	n.d.	42.3	41.3	41.0	41.4	55.1	59.1	
<i>TiO₂</i>	0.01	0.01	0.01	0.42	1.12	1.24	1.61	0.03	0.04	0.01	
<i>Al₂O₃</i>	24.3	66.8	21.1	7.64	20.4	17.8	14.3	16.0	0.41	0.40	
<i>Cr₂O₃</i>	0.14	1.12	3.71	58.5	1.67	5.45	8.99	9.60	0.35	0.24	
<i>FeO</i>	5.16	5.57	7.14	19.1	10.6	8.54	8.47	7.24	2.64	5.24	
<i>MnO</i>	0.28	0.01	0.36	0.25	0.27	0.27	0.28	0.27	0.14	0.11	
<i>MgO</i>	26.0	26.8	21.4	12.8	19.9	20.3	18.7	18.6	20.0	35.3	
<i>CaO</i>	0.64	-	4.19	-	4.89	5.79	7.05	7.37	20.9	0.89	
<i>NiO</i>	-	-	0.02	-	0.10	0.09	0.10	n.d.	0.16	0.03	
<i>K₂O</i>	-	-	-	-	-	-	-	-	0.13	-	
<i>Total</i>	100.4	100.3	100.1	98.7	101.2	100.8	100.5	100.5	99.9	101.3	
<i>Fe/Fe+Mn</i>	10.0	5.4	15.8	39.5	23.0	19.1	20.2	17.9	6.9	7.6	

Handwritten notes:
 P₂ - ...
 8015
 20-200

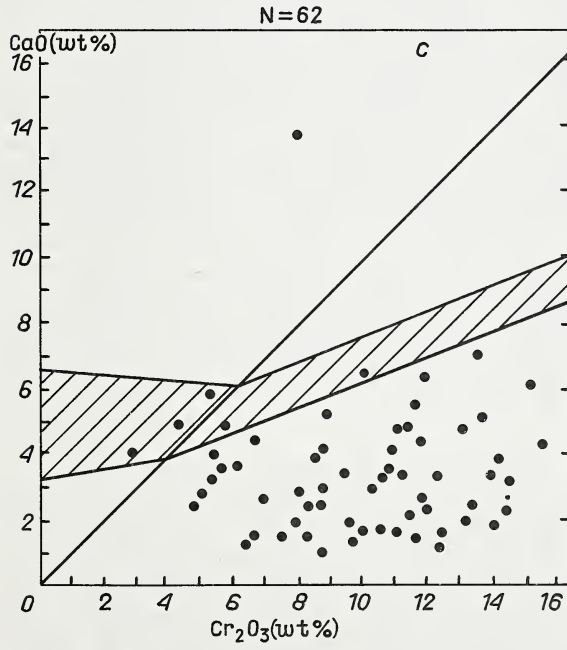
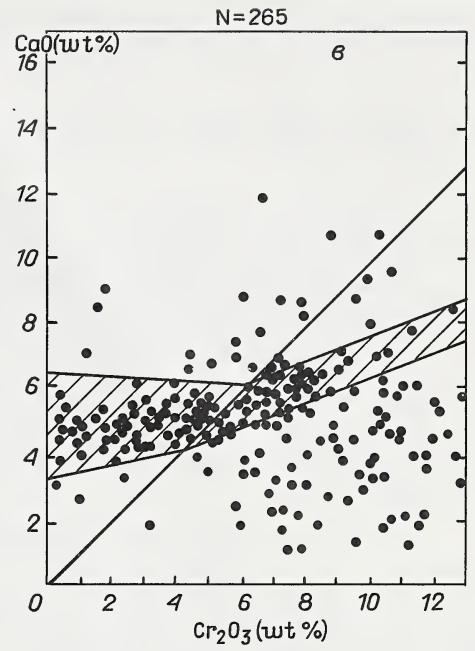
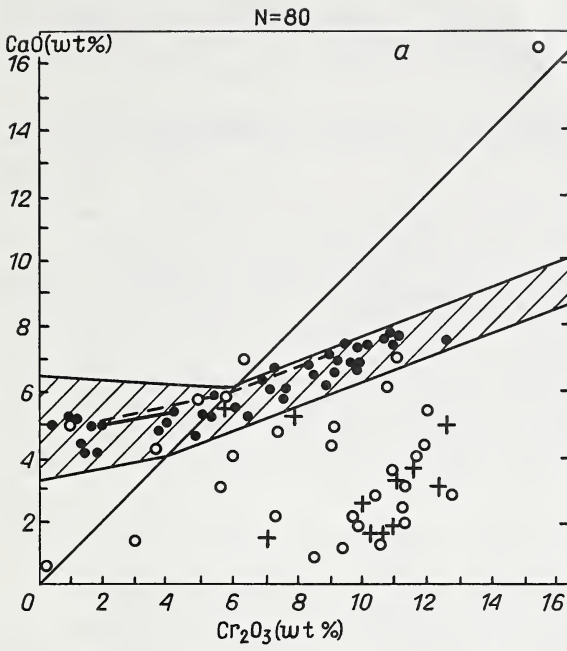


Fig.1 Features of the amounts of Cr₂O₃ and CaO in Mg-garnets from "Udachnaya" kimberlite pipe.

a. Garnets from xenoliths of ultramafic rocks: sheared lherzolites (black points), granular peridotites (open circles), granular diamondiferous peridotites (crosses).

Points of compositional variations of zoned garnet are joined by continuous line.

b. Cr-bearing garnets from kimberlite concentrate.

c. Cr-bearing garnets included in diamonds.

Shaded areas - compositions of garnets of lherzolic paragenesis.

K₂O in rpx = 0.7 wt%

≤ 0.1 wt% perov

GEOCHEMISTRY OF THE MURFREESBORO KIMBERLITE AND ITS RELATIONSHIP WITH OTHER IGNEOUS ROCKS OF ARKANSAS

K.F. Steele (Department of Geology, University of Arkansas, Fayetteville, Arkansas 72701)

G.H. Wagner (Department of Geology, University of Arkansas, Fayetteville, Arkansas 72701)

Kimberlite, lamprophyre, carbonatite and syenite are all exposed in west-central Arkansas. Samples of these rocks have been analyzed for most major and selected trace elements by atomic absorption spectrometry in order to characterize them chemically and to determine any geochemical relationships. Although these rock types are often associated, the kimberlite and some of the carbonatite exposures in Arkansas are not in close proximity to other types of igneous rocks. For example, the kimberlite at Murfreesboro in Pike County Arkansas is about 56 km southwest of tinguaitite and monchiquite dikes in Garland County, the nearest igneous outcrops. The few radiometric dates for Arkansas lamprophyre and syenite indicate that their intrusion took place during the Cretaceous.

Unlike most North American kimberlite and most of the igneous rocks of Arkansas, the Murfreesboro kimberlite does not intrude Paleozoic sediments. The Murfreesboro kimberlite is located in Pike County in the Gulf Coastal Plains at the southern edge of the Ouachita Mountain Region. The Murfreesboro kimberlite is narrowly dated geologically because it intrudes Lower Cretaceous sediments and some kimberlite is found in the lower part of an Upper Cretaceous formation (Miser and Purdue, 1929). There are four distinct occurrences of kimberlite near Murfreesboro. The Prairie Creek intrusion covering 73 acres is the major intrusion. The other three outcrops are located a few miles to the northeast and are of limited extent. The following discussion and interpretations are based on data from the Prairie Creek intrusion. Three varieties of peridotite are associated with these intrusions: 1) massive porphyritic peridotite, 2) breccia, and 3) tuff. The massive peridotite is composed primarily of olivine phenocrysts (many serpentinized) in a phlogopite groundmass. Pyroxene is also present, and perovskite and magnetite are present in minor amounts. Xenoliths of local sedimentary rocks (mostly shale) are present as well as rare fragments of igneous rocks. The mineralogy of the breccia and tuff is similar to that of the massive peridotite (Lewis et al., 1976, Miser and Ross, 1923b). Weathered breccia have produced most of the diamonds at Prairie Creek (Thoenen et al., 1949).

The three varieties of kimberlite are similar chemically; however, the tuff contains less Fe, Mg, Ni and Ba than the other two and more Na and K. The massive peridotite has the highest Cr values and the lowest Li, V, and Zn values. Differences in Ba content are difficult to ascertain because barite veins are present in the breccia. The variation of Co, Ni and V appears to be controlled by iron content. Plots of Cr, Al, K and Rb versus mafic index yield smooth trends suggestive of some differentiation. Based on chemical data (Table 1) the massive peridotite is slightly more mafic or primitive than the breccia and the tuff is least mafic. This suggests that the massive peridotite was emplaced first followed by the breccia and lastly the tuff. However, considering field, petrographic and geophysical data Bolivar et al (1976) have suggested the sequence of intrusion to be breccia, massive peridotite tuff. Meyer (1975) suggests that the scatter of points for Kimberlite from Norris Lake on an AFC diagram parallel to the CF side is a reflection of the

extensive alteration of the samples. It is of interest to note that the Murfreesboro samples exhibit a similar trend. It is also interesting that the gradual increase in Ca content corresponds with increase in felsic character.

The Murfreesboro kimberlite exhibits the general chemical characteristics of other kimberlites when compared to other peridotites, namely higher K/Na and lower Mg/Fe ratios, and relatively high Ti, Al, Fe, Cr, K, Li, Sr and Ba. However, the Murfreesboro samples contain less Ca than most other kimberlites.

A small 2 m wide peridotite sill resembling the kimberlite at Murfreesboro is exposed along Freedom Creek in Scott County. This peridotite contains phenocrysts of phlogopite and serpentinized olivine in a groundmass of phlogopite, calcite and magnetite. The Scott County peridotite differs from the Murfreesboro samples in that no diamonds have been found and there is little brecciation at this site (Miser and Ross, 1923a). The chemical composition of the Scott County peridotite reported here for the first time is similar to other kimberlite (Table 1). The greatest chemical difference between the Scott County and Murfreesboro rocks is that the Scott County peridotite contains about twice as much Ca. Slight differences in other element concentrations are also present, e.g. the Scott County peridotite also contains more Mn and V, but less Ti than the Murfreesboro samples.

A large majority of igneous rock outcrops in Arkansas are in the eastern end of the Ouachita Mountain Region or near its boundaries. Numerous tinguaitite and lamprophyre (mostly monchiquite and ouachitite) dikes and sills are located in Garland, Hot Springs and Pulaski Counties. The largest igneous intrusion in the state is located at Granite Mountain about 153 km northeast of Murfreesboro in Pulaski County. The rock is predominantly pulaskite. Twenty-four kilometers southwest of Granite Mountain in Saline County near Bauxite nepheline syenite outcrops. About 48 km west of these two large syenite intrusions are the Magnet Cove, Potash Sulfur Springs and the "V" Intrusive igneous complexes. These complexes consist chiefly of varieties of nepheline syenite and related mafic rock such as jacupiranguite.

Arkansas carbonatites can be divided into two groups, small massive bodies associated with the syenite complexes at Magnet Cove and Potash Sulfur Springs and small brecciated intrusions often occurring as dikes or sills. The later group is located in Conway and Perry Counties with no other igneous rocks exposed within 19 km. The xenoliths present are usually shale; however, igneous rock fragments are abundant at one locality.

Many of the kimberlite, lamprophyre, syenite and carbonatite samples exhibit similar chemical affinities, e.g. high K/Na ratios. All of the rocks follow the alkali-olivine basalt trend on an AFM diagram. Although, the various lamprophyre types exhibit considerable chemical overlap, the lamprophyre that has intruded the syenite complexes is characterized by both lower mafic indices and higher alkali content ($K > Na$) than the lamprophyre samples. These lamprophyre samples which intrude the syenite complexes are most similar to the kimberlite. Although the kimberlite and other igneous rocks of Arkansas are not closely related in space, they do appear to be related chemically and in time which indicates a genetic relationship of these rocks.

Table 1. Composition of Arkansas kimberlite and "average" kimberlites. Oxides are in weight percent and trace elements are in ppm by weight.

	1	2	3	4	5 ⁺	6 ⁺
TiO ₂	2.26	2.24	2.22	1.20	2.32	2.03
Al ₂ O ₃	2.94	3.92	4.60	2.46	4.4	4.9
Cr ₂ O ₃	0.37	0.16	0.04	0.11	0.26 ⁺	0.22 ⁺
Fe ₂ O ₃ [*]	9.16	9.52	6.11	10.02	10.89	11.67
MnO	0.15	0.15	0.16	0.24	0.11	0.10
MgO	20.89	19.49	10.38	18.61	27.9	23.9
CaO	5.84	5.32	5.49	11.60	7.6	10.6
NiO	0.14	0.17	0.04	0.10	0.17 ⁺	0.14 ⁺
Na ₂ O	0.48	0.35	1.72	0.19	0.32	0.31
K ₂ O	2.72	3.40	5.04	3.93	0.98	2.1
BaO	0.34	0.37	0.16	0.30	0.13 ⁺	0.23 ⁺
Sr	1272	1295	653	950	675	1100
Rb	-	-	-	-	35	80
Li	11	52	51	46	4	24
V	38	115	83	205	120	120
Co	58	92	39	70	65	70
Zn	38	66	61	62	-	-

1. Massive peridotite, Murfreesboro

2. Breccia, Murfreesboro

3. Tuff, Murfreesboro

4. Peridotite, Scott County

5. Basaltic kimberlite (Dawson, 1967)

6. Micaceous kimberlite (Dawson, 1967)

* Total iron as ferric iron

+ Trace elements and oxides indicated from Dawson (1962)

STRUCTURAL SETTING OF KIMBERLITES IN SOUTH-EASTERN AUSTRALIA

K.J. Stracke (Stockdale Prospecting Limited, 500 Collins Street, Melbourne, Victoria, 3000, Australia).

John Ferguson (Bureau of Mineral Resources, Post Office Box 378,

L.P. Black Canberra City, A.C.T., 2601, Australia).

Fourteen areas of kimberlite and kimberlitic rocks have recently been discovered in south-eastern Australia in the States of New South Wales, Victoria, Tasmania and South Australia (Fig. 1). One or more intrusives are found in each area with a maximum of twenty seven (see also Ferguson and Sheraton, this volume). Rb-Sr dating on whole-rock samples and on phlogopite separates have established Permian, Jurassic and Cainozoic ages for kimberlitic occurrences in north-western New South Wales, South Australia and south-eastern New South Wales, respectively. Field relations indicate that most of the occurrences post-date the Precambrian and that some are as young as Quaternary.

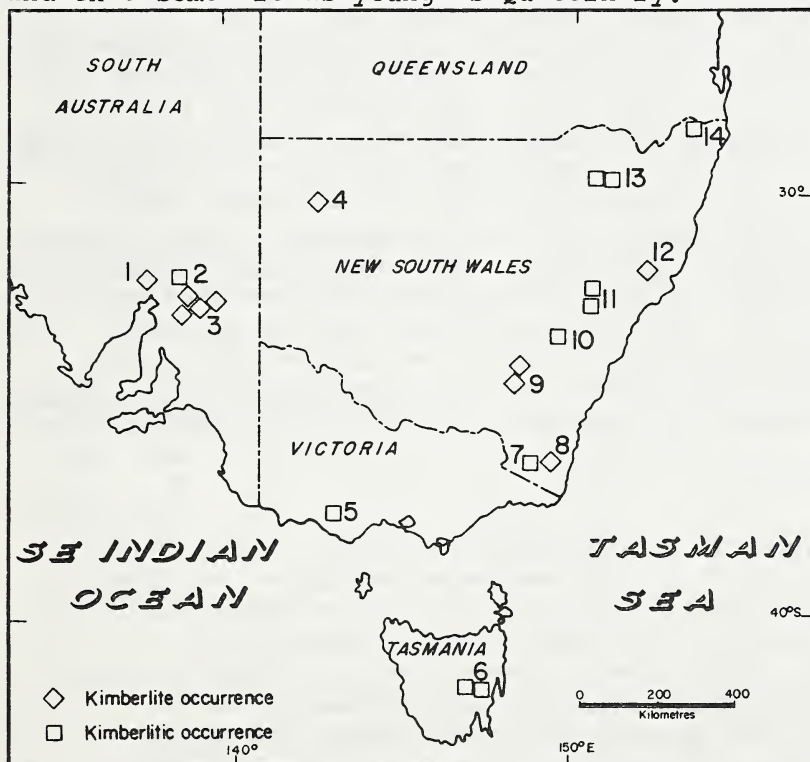


Fig. 1

- 1 Port Augusta
- 2 Walloway
- 3 Terowie
- 4 White Cliffs
- 5 Bullenmerri
- 6 Oatlands
- 7 Delegate
- 8 Bombala
- 9 Jugiong
- 10 Abercrombie
- 11 Nullo Mtn.
- 12 Gloucester
- 13 Bingara
- 14 Mt. Brown

In an attempt to relate the kimberlites and their associated rock types to a structural framework the following features were investigated: on- and off-shore structures, igneous activity, earthquake activity, general tectonics, gravity and magnetics.

Two prominent belts of earthquake activity are found in south-eastern Australia, one striking north to north-west through the Flinders Range of South Australia and extending to the north-west margin of the continent; the second belt trends north through Tasmania, across Bass Strait into Victoria, and then north-eastwards into New South Wales, and proceeds offshore in south-eastern Queensland. Cleary and Simpson (1971) have postulated that these two zones of earthquake activity correspond to projected continental extensions of oceanic transform faults originating from the Antarctic Ridge. The separation of Australia from Antarctica commenced 55 m.y. ago and is continuing to the present day (Weissel and Hayes, 1972). Nine of the areas lie on or adjacent to the projected continental extension of these oceanic transform faults.

As indicated by Cleary and Simpson (1971), the edge of epeirogenic uplift on the south-eastern seaboard of Australia, is roughly coincidental with recent earthquake activity, and in consequence, with the projected oceanic fracture zone stemming from the Antarctic Ridge. All of the kimberlite and kimberlitic areas on the south-eastern seaboard of Australia straddle the edge of this epeirogenic uplift which commenced in the Mesozoic and continued intermittently through the Cainozoic (Wellman and McDougall, 1974). Cainozoic basaltic activity is associated with this epeirogenic uplift, occurring in an approximately 300 km-wide zone which incorporates all of the kimberlite and kimberlitic areas on the south-eastern seaboard of Australia. This basaltic activity is dominantly alkaline but in two of the areas the immediate rock types are sub-alkaline. The Cainozoic mean line of hot spot migration (Wellman and McDougall, 1974), as defined by central volcano provinces and the present day hot spot sites (Sass, 1964), also passes through the zone of basaltic activity in south-eastern Australia. Areas 9, 10, 11 and 14 lie on or near this mean line of hot spot migration.

Following on the hypothesis, developed by Wilson (1965), that lines of old continental crustal weakness determine the sites of transform fault development, Ringis (1975) established that this concept has application to the south-eastern Australian continental margin. Here igneous events can be related to zones of pre-existing continental weakness that became sites of reactivation during the opening up of the Tasman Sea which commenced 80 m.y. ago and aborted 60 m.y. ago. Kimberlitic development also appears to have been governed by zones of weakness, developed during pre-breakup times, which later became the sites of continental extensions of transform faulting during Tasman Sea opening.

There is no clear-cut relationship between kimberlite and kimberlitic rocks and the distribution of granitic rocks or general tectonic units; magnetic coverage is too sketchy to draw conclusions. Thirteen of the areas occur in gravity lows and there is a broad parallelism between the trends displayed by gravity, tectonic units and granitic belts.

It is concluded that postulated continental extensions of transform faults, stemming from both the Antarctic and Tasman Sea Ridges, appear to have played the major role in the location of kimberlite and kimberlitic intrusives in south-eastern Australia.

REFERENCES

Cleary, J.R. and Simpson, D.W., 1971. Seismotectonics of the Australian Continent. *Nature, Lond.*, 230(5291), 239-241.

Ringis, J., 1975. The relationship between structures on the south-east Australian margin and in the Tasman Sea. *Bull. Aust. Soc. Explor. Geophys.*, 6(2-3), 39-41.

Sass, J.H., 1964. Heat flow values from Eastern Australia. *J. Geophys. Res.*, 69(18), 3889-3893.

Weissel, J.K. and Hayes, D.E., 1972. Magnetic anomalies of the south-east Indian Ocean. In: Hayes, D.E. (ed.), *Antarctic Oceanology II: the Australian-New Zealand Sector*, Antarctic Res. Ser., 19, 165-196.

Wellman P. and McDougall, I., 1974. Cainozoic igneous activity in eastern Australia. *Tectonophysics*, 23, 49-65.

Wilson, J.T., 1965. A new class of faults and their bearing on continental drift. *Nature, Lond.*, 207, 343-347.

KIMBERLITES IN BRAZIL: AN INITIAL REPORT.

Darcy P. Svisero: Instituto de Geociencias, Universidade de Sao Paulo, Sao Paulo, Brazil

Henry O.A. Meyer: Dept. of Geosciences, Purdue University,

Hsiao-ming Tsai: West Lafayette, Indiana 47907, U.S.A.

Diamonds were first discovered in Brazil in the early 1700's near Diamantina, central Minas Gerais State. Subsequently, other placer deposits were discovered elsewhere and as a consequence Brazil replaced the declining fields of India as the major source of diamonds. This state of affairs continued until the late 1800's and early 1900's when first South Africa and then Zaire (at that time Belgian Congo) became the foremost producers of diamond.

Unfortunately, because of several reasons the search for kimberlite as a primary source of diamonds in Brazil was never given serious consideration. The pioneering studies of Derby (1898), Porcheron (1903) and Hussak (1906) who suggested the existence of kimberlites in western Minas Gerais were largely ignored. Resurgence of this idea occurred in the late 1920's and early 1930's (Maack, 1926; Freyberg, 1932; Oppenheim, 1934) but was not readily received.

The first authenticated kimberlite to be recognized as such was discovered during a general reconnaissance geological survey in south west Piaui State - the Redondao diatreme. (Melo and Porto, 1965) Subsequently, as a result of systematic prospection in Minas Gerais a number of other kimberlitic diatremes were discovered (Barbosa et al., 1976). More recently, an examination of potential kimberlite and diamond prospects in western Minas Gerais has been extended into Mato Grosso, Goias and Rondonia Territory. At present a considerable number of kimberlite occurrences are known in Brazil of which several are diamondiferous.

The kimberlite diatremes of west Minas Gerais range in size from 50 - 500 m in diameter, although a number of narrow dikes also exist. Invariably, the rock is extensively and deeply weathered; a feature that probably contributed to the earlier lack of discovery of these bodies. At this time published geological and mineralogical data are restricted to two kimberlites in Brazil - the Vargem and Redondao diatremes (Melo and Porto, 1965; Svisero et al., 1977).

The major Vargem diatreme is approximately 22 km south-east of Coromandel, Minas Gerais. The diatreme intrudes Bambui metasediments (Upper pre-cambrian), and is capped by lateritic red soils that change with depth to a yellow-

colored material. This yellow ground is brecciated and contains serpentized olivine, red-purple garnets, green diopside and ilmenite. All these minerals display the chemical characteristics of typical kimberlitic minerals (Table 1).

The Redondao diatreme in Piauí State was first identified by Melo and Parto (1965) and is located about 15 km south-east of Santa Filomena. The diatreme is about 1 km in diameter and has intruded Palaeozoic sediments of the Parnaíba basin.

The kimberlite in the diatreme is completely serpentized at the surface but typical kimberlitic garnets can be found (Table 1). Of interest are the xenoliths of crustal and mantle origin that occur within this kimberlite. One such xenolith is a granular garnet-lherzolite whose granular fabric can be recognized in spite of serpentization of the olivine and pyroxene. Garnet, however, remains unaltered and is chemically similar to garnets in xenoliths from South Africa and elsewhere.

At the present time a study of the mineralogy and geochemistry of several other kimberlites is underway and includes the Capao da Erva, Forca, Poco Verde, Santa Clara, Brecha do Santo Antonio, Limeira and several other diatremes.

References

1. Barbosa, O., Svisero, D.P. and Hasuy, Y. (1976). Brazil. Geol. Cong., Belo Horizonte. (Abstr.).
2. Derby, O.A. (1898). Jour. Geol., 6, 121-146.
3. Freyberg, B. von (1932). Neues Jahrb. Min. Geol. Paleont., S. II.
4. Hussack, E. (1906). Zeit. Prakt. Geol., 318-333.
5. Maack, R. (1926). Zeit. Gesellsch. Erdk., 310-323.
6. Melo, U. and Porto, R. (1965). Petrobras Int. Rept. 244, Belem.
7. Oppenheim, V. (1934). Div. Fom. Prod. Min. Bol., 3, 65-74, Rio de Janeiro.
8. Porcheron, H. (1903). Rapp. Imp. Lecoq et Mathoril, Paris.
9. Svisero, D.P., Meyer, H.O.A., and Tsai, H.H. (1977). Revis. Bras. Geocien., 7, (in press).

Acknowledgement

Svisero acknowledges support from Fundacao de Amparo a Pesquisa do Estado de Sao Paulo.

TABLE 1. Representative analyses of minerals from Vargem and Redondao kimberlites, Brazil

	Vargem			Redondao	
	CPX.	ILM.	GAR.	GAR.*	GAR.
SiO ₂	54.4	0.07	42.8	42.0	41.8
TiO ₂	0.12	54.1	0.30	0.34	0.19
Al ₂ O ₃	0.21	0.46	21.2	21.1	21.3
Cr ₂ O ₃	0.71	0.59	1.35	3.39	2.68
FeO	4.39	32.6	8.42	5.99	8.13
MgO	16.7	11.4	21.1	21.4	20.7
CaO	22.0	0.02	4.66	4.91	4.89
MnO	0.11	0.27	-	-	0.36
K ₂ O	<0.01	<0.01	<0.01	<0.01	<0.01
Na ₂ O	1.11	0.03	0.05	0.09	<0.01
NiO	<0.01	<0.01	<0.01	<0.01	<0.01
	99.7	99.5	99.9	99.2	100.1

* Garnet in garnet-lherzolite xenolith. All other minerals are from mineral concentrates.

MINERAL REACTIONS IN A MODEL MANTLE: PREDICTION OF MINERAL COMPOSITIONS AND ASSEMBLAGES.

Alan Bruce Thompson (Inst.Krist.Petro., E.T.H. Zürich, CH-8092, Switzerland).

General Problem:

Despite positive attempts to calibrate mineral thermometers and barometers to evaluate physical and chemical conditions in the Upper Mantle, the possible uncertainties in data and fitting procedures can result in errors as large as 100 percent. Such uncertainties are rarely quoted if even evaluated. The difficulties arise from the existence of only a few high-variance assemblages stable over a wide range of Upper Mantle conditions, problems of defining chemical components and the minimal amount of consistent experimental, thermodynamic and chemical data. Only broad constraints upon the possible mineral associations can be supplied from observed seismic structure and viscosity limits and from inferred thermal and electrical conductivities. These bounds can be satisfied by a large range of actual and unknown rock types. Unfortunately many geochemical constraints are circularly dependent on the above properties and assumed P and T used to model the Upper Mantle. A consideration of continuous and discontinuous reactions in the CaO-Al₂O₃-MgO-SiO₂ (CAMS) system and its compositional extensions permit the available data to be more rigorously constrained and viewed in a coherent framework.

Reactions in the CAMS compositional space:

Discontinuous and continuous reactions in CAMS are most usefully discussed with reference to the CaSiO₃(Wo)-MgSiO₃(En)-Al₂O₃(Cor) plane. The four principal compositional reactions types are

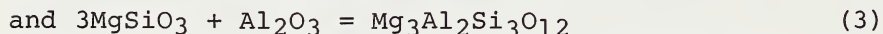
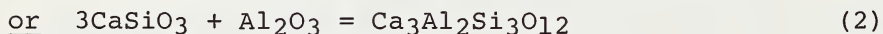
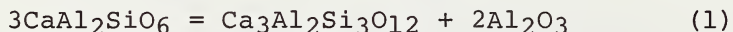
- I. in the Wo-En-Cor plane.
- II. on the SiO₂-rich side (Wo-En-Cor-Qtz).
- III. on the SiO₂-poor side (Wo-En-Cor-(CaO+MgO)).
- IV. crossing the Wo-En-Cor plane.

Of these types, those in the Wo-En-Cor plane control all the reactions in CAMS involving two or more of diopsidic clinopyroxene (Cpx), orthopyroxene (Opx) and garnet (Ca-rich=Gro, Mg-rich=Pyp). The compositions of the phases Cpx and Opx may be defined by the components CaMgSi₂O₆(Di)-MgSiO₃(En)-CaAl₂SiO₆(Ct) and those of the garnet phases Gro and Pyp by the components Ca₃Al₂Si₃O₁₂(Gr)-Mg₃Al₂Si₃O₁₂(Py).

Type I reactions in the Wo-En-Cor plane:

The compositional changes of Cpx, Opx, Gro and Pyp phases may be predicted as functions of P and T from end-member reactions in CAS or MAS and exchange reactions in Wo-En-Cor. The topology in Wo-En-Cor shown by Boyd (1970, Min.Soc.Am.Sp.Pap.3, Fig.11) shows four 3-phase fields. Cor-Gro-Cpx and Cor-Pyp-Cpx occur because of continuous reactions and Pyp-Cpx-Opx and Gro-Wol-Cpx exist by virtue of the miscibility gaps between Cpx-Opx and Wol-Cpx. Without the Cpx-Opx miscibility gap a complete bundle of two-phase tie-lines would exist with orientations determined by the pyroxene structure (because $X_{Mg} \text{Opx} > \text{Gar} > \text{Cpx}$). The behaviour of compositions of Cpx-Opx-Pyp with changing P and T may be predicted from the Di-En phase diagram and the effects of Cpx-Pyp and Opx-Pyp tie-line rotation. For example at constant P, increasing T causes greater mutual solubility of pyroxenes which is larger for Cpx (it is easier to put smaller Mg in larger Ca-sites) and an increase of Ca in Pyp (the net effect of the larger Cpx-Pyp tie-line rotation). Because of the inferred steep positive dP/dT for critical Cpx, these effects would be reversed though weaker for increasing P at constant T. For the most part the Ca-Mg exchange between Cpx-Opx-Pyp has a larger effect on composition than Tscherma's exchange except when Cpx is more aluminous than Ca-rich garnet (Gro).

The continuous reactions involving Cpx-Gro-Cor and Cpx-Pyp-Cor may be written as the end-member component reactions



coupled with the exchange reactions between Di(or Wo)-En-Ct for pyroxenes and Gr-Py for garnets. Reaction (1) has a positive dP/dT in CAS with Gr+Cor on the high-P side, consequently Cpx in Cpx-Gro-Cor becomes enriched in Ct with increasing T at constant P and depleted in Ct with increasing P at constant T.

These arguments can be extended to include continuous reactions on both sides of the Wo-En-Cor plane (Types II, III and IV).

Other reaction Types (II,III and IV):

The following discussion illustrates exactly how the reaction topologies for all Type II,III and IV reactions involving two or more of Cpx-Opx-Gar are controlled by the Wo-En-Cor plane.

Because phases such as forsterite(For), spinel(Spn), Opx, anorthite(Anr), wollastonite(Wol) do not have isostructural end-members in both CAS and MAS, no end-member reactions can be written for phases in both systems. Most relevant reactions for assemblages in the ultramafic family (Cpx+Opx+Pyp+For+Spn+Anr), eclogites (Cpx+Pyp+Cor/Kya), grospydites (Cpx+Gro+Cor/Kya) and assemblages such as Gro+Wol+Cpx+Anr+Spn+For in calc-silicates and possibly meta-rodingites, usually involve at least two of Cpx, Opx or Gar. Consequently the exact nature of the reaction is controlled by the exchange reactions in the Wo-En-Cor plane. For example, the reaction



has this form if the garnet composition (defined in Wo-En-Cor) lies between that defined by the plane Anr+En+Spn (1/6Gr 5/6Py) and Anr+Di+Spn (1/2Gr 1/2Py). However, if the data of Akella (1976,Amer.Min.,61,p.591) hold in the P-T range for (4), the reaction will have the form



because the garnet in Pyp-Opx-Cpx is more Mg-rich than (1/6Gr 5/6Py).

CAMS compositional extensions and Upper Mantle Assemblages:

The subtleties of reaction controls in CAMS are such that certain bulk compositions may easily by-pass many of the assumed reactions. While P and T may still be estimated from compositions of Cpx-Opx-Gar many bulk compositions may not exhibit a particular reaction, or the transition interval may vary in width in P-T space. Models have been developed using the above techniques to predict how a given bulk composition will behave over a wide range of P-T conditions. These models are being used to assess the likelihood of mineral reactions being the cause of seismic discontinuities and to constrain the heterogeneity of Upper Mantle compositions.

PETROLOGY OF ULTRAMAFIC XENOLITH SUITE FROM TAHITI AND REACTIONS WITH ENCLOSING BASALT

Robert J. Tracy (Dept. of Geological Sciences, Harvard Univ.,
Cambridge, Mass. 02138)
Peter Robinson (Dept. of Geology, University of Massachusetts,
Amherst, Mass. 01003)

Introduction:

Boulders of alkali olivine basalt in the Faataua valley, near Papeete, Tahiti, contain numerous xenoliths of ultramafic rock up to 10 cm in diameter. The basalt may be either a flow or hypabyssal dike or sill; in any case, it is not vesicular. The basalt is notable for its low silica and high magnesia contents (Table 1) and is interpreted to represent a primitive mantle-derived magma. Magnesian olivine phenocrysts (up to Fo 88) are nearly as magnesian as olivine in xenoliths. For a discussion of basalt petrology and mineral chemistry, see Tracy and Robinson (1977).

Petrology of Xenoliths:

Xenoliths include coarse and fine-grained spinel lherzolites, wehrlite, and dunite; no garnetiferous xenoliths have yet been found. Lherzolites are dominantly olivine (~60 modal percent) and orthopyroxene (~30 modal percent) with minor clinopyroxene and spinel. Olivines in all rock types have a limited compositional range (Fo 89 - Fo 91). Lherzolite opx is variable mainly in Al_2O_3 content, different xenoliths ranging from 3 to 6 wt.%, while CaO and Mg/Mg+Fe (.88 - .90) are relatively constant. Lherzolite cpx contains considerable Al_2O_3 (4 - 7 wt.%), Na_2O (up to 1.5 wt.%) and Cr_2O_3 (up to 1.6 wt.%). Spinel in lherzolite xenoliths show considerable variation in Cr/Al ratio (0.02 to 0.45), while spinels in wehrlite or dunite are richer in Cr. All minerals in xenoliths are homogeneous except at the periphery of the nodules where reaction with basalt has occurred. Opx, cpx and spinel within each xenolith appear to have equilibrated in terms of Cr/Al ratio (Fig. 1). Compositions of coexisting pyroxenes in lherzolites, as well as cpx in wehrlites, are shown in Figure 2, a portion of the pyroxene quadrilateral. Geothermometry of spinel lherzolites yields the following estimates: 1050 - 1100°C (Di-En solvus of Davis and Boyd, 1966, corrected by Boyd); 1100-1150°C (using Al(VI) and Ti(VI)-corrected compositions applied to corrected Di-limb of Mysen, 1976); 1150-1200°C (using the 20 Kbar Di-En solvus of Lindsley and Dixon, 1976); 1100-1200°C (using various calibrations of Al content of opx coexisting with olivine + spinel). Pressure estimates are quite crude, but suggest a maximum pressure of about 20 Kbar, based upon the absence of garnet even in xenoliths with low Cr/Al ratio.

Reaction between Xenoliths and Basalt:

The most spectacular effect is seen where opx comes in contact with basalt at the periphery of a nodule. The outermost 200-400 microns of opx has been converted to a symplectite of

silica-rich glass + olivine + high-Ca cpx which can be interpreted as representing incongruent melting of opx. The outer edge of this symplectite commonly grades into a coarse "cockscomb" overgrowth of titanite growing into basalt. The glass in the symplectite is typically very low in CaO, MgO, FeO and TiO₂ and rich but strongly zoned in SiO₂, Al₂O₃ and alkalis; representative analyses of inner and outer portions of this glass are given in Table 2. Composition trends in the glass suggest that its initial composition has been altered through element diffusion and exchange with a *residual basaltic liquid* (Table 1) rather than with a liquid close to the bulk composition of the basalt.

Normally homogeneous xenolithic olivine and spinel become zoned at xenolith edges. Olivine crystals have overgrowths of more iron-rich olivine while spinels are zoned toward Fe and Ti-rich compositions typical of basalt groundmass titanomagnetite. The zoning paths in xenolith spinels (Fig. 3) suggest that they first reacted toward intermediate Cr-Ti-Al spinel compositions which probably represented the compositions of spinel in equilibrium with partially crystallized basaltic magma. The composition trend of spinel crystallizing from the magma through most of its history has been determined by analyzing small euhedral spinel inclusions in olivine phenocrysts which apparently record virtually the entire range of equilibrium spinel compositions from liquidus to near-solidus conditions. The zoning trends of different xenolith spinels seem to be different (Fig. 3), possibly indicating relative times of xenolith incorporation into the magma.

The above data seem to be consistent with two explanations: 1) That the xenoliths represent upper mantle material which was captured by an already partially crystallized magma from deeper within the mantle, and immediately began to react with the residual liquid; 2) That the xenoliths resided in the magma for some time without reaction, and only reacted near the surface when the magma itself had begun to crystallize substantially. The second explanation is supported by the symplectite data, since incongruent melting of opx is restricted to pressures of less than about 5 Kbar in a dry system. On the other hand, it is hard to understand why the xenoliths of country rock should not begin to react immediately upon being engulfed by the basaltic magma. In answer to this, the primitive nature of the magma and the abundance of xenoliths may be taken as evidence that the magma ascended very rapidly toward the surface; the xenoliths may thus have been carried upward into the crust rapidly enough to have escaped reaction until very near the surface. The strongest argument in support of explanation (1), above, is the diversity of zoning trends in xenolith spinels. This diversity suggests that the time of xenolith incorporation, relative to the crystallization history of the basalt, is imprinted indelibly upon each xenolith. It is possible, however, that this zoning may record times when nodules break apart, exposing fresh surfaces to the magma. In any case, it is apparent that an understanding of these reaction features is essential for any interpretation of where the xenoliths came from and how they were carried to the earth's surface.

Figure 1

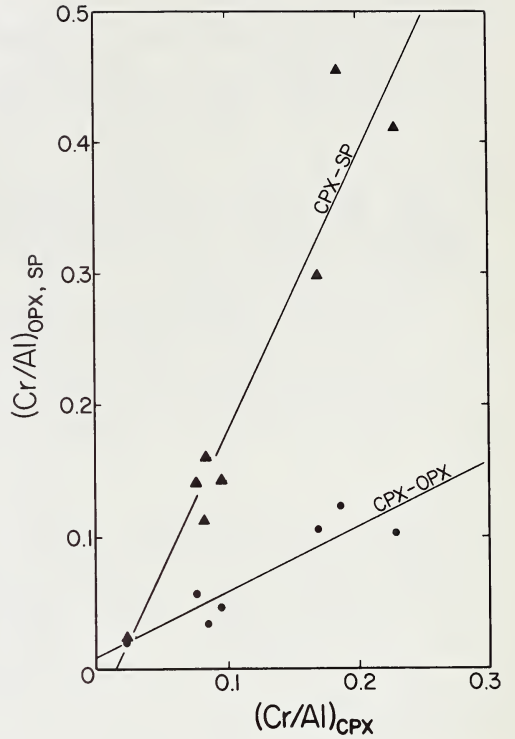


TABLE 1

Basalt*	Brown Glass**	
SiO ₂	41.8	55.5
TiO ₂	2.7	1.0
Al ₂ O ₃	9.9	21.7
Cr ₂ O ₃	0.1	0.1
FeO	12.0	5.1
MnO	0.2	0.2
MgO	18.9	0.4
CaO	10.4	1.4
Na ₂ O	2.3	6.6
K ₂ O	1.1	7.5
Total	99.4	99.5

NORMS

An	13.0	Or	43.4
Neph	12.0	Ab	19.6
Kal	3.9	An	6.8
Ol	38.1	Neph	23.0
Di	29.6	Ol	5.7
Ilm	3.6	Ilm	1.4

*Probe analysis of fused whole-rock sample.

**Patches of groundmass glass thought to represent residual liquid.

TABLE 2

Inner Glass	Outer Glass	
SiO ₂	72.2	63.5
TiO ₂	0.3	1.0
Al ₂ O ₃	17.9	20.7
Cr ₂ O ₃	0.1	0.1
FeO	0.9	0.9
MnO	0	0
MgO	0.3	0.6
CaO	0	1.3
Na ₂ O	3.4	4.5
K ₂ O	6.6	8.2
Total	101.7	101.0

NORMS

Or	38.0	46.8
Ab	30.0	39.5
An	--	6.5
Hy	1.8	1.8
Ilm	0.4	1.4
Cor	5.6	2.0
Qtz	24.0	1.7

Figure 2

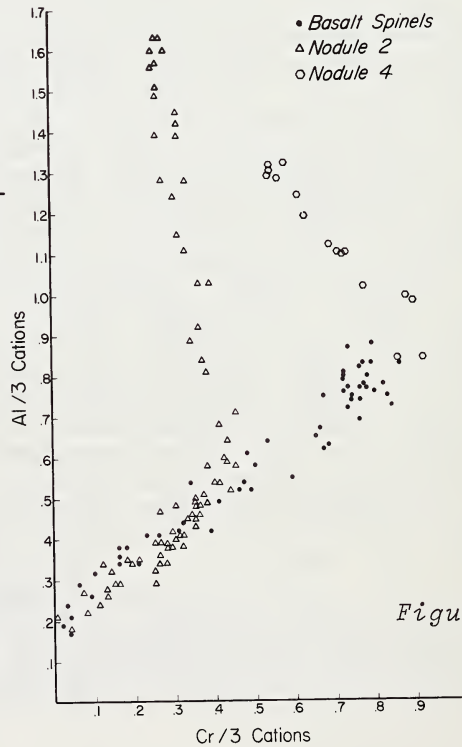
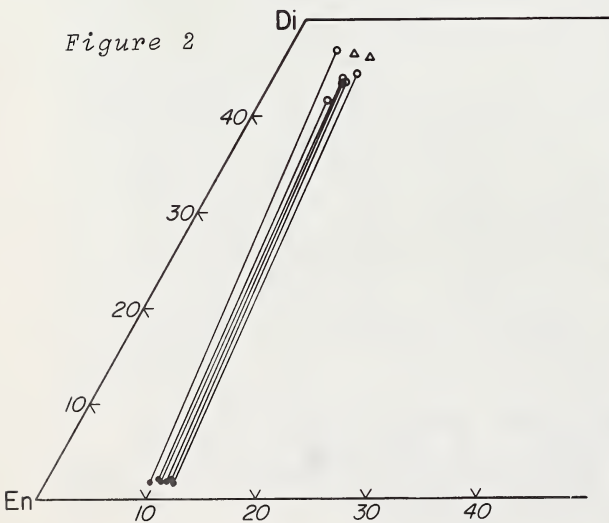


Figure 3

MINERALOGY AND S^{34}/S^{32} RATIOS OF SULFIDES ASSOCIATED WITH
KIMBERLITE, XENOLITHS AND DIAMONDS.

Hsiao-ming Tsai: Department of Geosciences
Yuch-ning Shieh: Purdue University
Henry O.A. Meyer: West Lafayette, Indiana 47907

The mineralogy of sulfides from eclogite xenoliths and inclusions in diamond, and the S^{34}/S^{32} ratios of sulfides from several eclogites and other crustal xenoliths in kimberlite have been studied:

- 1) Sulfides in thirteen eclogites (griquaites) from various localities, including Premier, Roberts Victor, Jagersfontein, Bobbejaan and Obnazhennaya (Siberia) have been examined. These sulfides are generally round in shape and often occupy interstitial positions relative to the silicate grains. The most common assemblage observed is an intergrowth of pyrrhotite-pentlandite surrounded by chalcopyrite rim. A similar assemblage has been previously described by Frick (1973), Vakhrushev and Sobolev (1973) and Meyer and Boctor (1975). However, in this study, we have also observed a small amount of chalcopyrite occurring as very fine exsolution lamellae in pyrrhotite. Nickeliferous pyrrhotite is common, and also found in association with this phase is Ni-pyrite (or Ni-marcasite). One sample from Roberts Victor appears identical to that described by Desborough and Czamanske (1973), but the new low nickel phase identified by them is probably Ni-bearing pyrrhotite. Pentlandite usually occurs as oriented exsolution lamellae in pyrrhotite and is present in various abundances. Some of the pentlandite is Co-bearing with cobalt contents of up to 3.6 wt.%. Monosulfide_{SS} is present in only one specimen. Textural relations indicate the original presence of immiscible sulfide melts having various bulk compositions. Subsequent re-equilibrium at lower temperatures accounts for the present phases and form of the intergrowths. One unique assemblage in a garnet xenocryst from Premier consists of granular aggregates of pentlandite, chalcopyrite, magnetite and silicates. Minor lamellae of pentlandite are present in some of the chalcopyrite, while pentlandite is generally free of exsolution lamellae. The silicates are interesting in that they consist of andradite, ilvaite $[CaFe_2(FeOH)(SiO_4)_2]$ and needle-shaped secondary chlorite. Pyrite observed in two samples from Bobbejaan and Roberts Victor is probably secondary, based on the presence of the well-formed crystal outlines. Analyses of major mineral phases mentioned above are presented in Tables I (sulfides) and II (silicates).
- 2) Examination of sulfide inclusions in diamonds from Premier, Finsch and Koffiefontein reveals two important features:
One is that the occurrence of sulfides as inclusions is much rarer than previously anticipated, most of the black

inclusions appear to be graphite. The second feature is the presence of a variety of sulfide assemblages, including pyrrhotite-pentlandite intergrowths with or without minor chalcopyrite; pyrrhotite-chalcopyrite intergrowths with minor pentlandite; Ni-rich pentlandite-magnetite with possible minor chalcopyrite; and pentlandite-chalcopyrite. The intimate association of these intergrowths and the small size have made it difficult to obtain satisfactory microprobe analyses. One notable difference between sulfides in diamonds and in eclogites is the much rarer occurrence of chalcopyrite in diamond than observed in eclogite. Pyrite is present in one diamond from Koffiefontein.

3) S^{34}/S^{32} ratios have been determined for sulfides in crustal and eclogitic xenoliths and discrete crystals of sulfide from Premier, Finsch, Koffiefontein, Roberts Victor and Bobbejaan. The results are shown in Fig. 1. Most pyrite-bearing crustal xenoliths as well as a secondary pyrite in a Bobbejaan eclogite give results suggestive of sedimentary origin of the sulfur (δS^{34} ranging from -37.3 to +15.1). Discrete pyrite from Premier kimberlite gives δS^{34} to be +1.3, suggesting the sulfur may be of magmatic origin. Chalcopyrite/pentlandite and pyrrhotite/pentlandite assemblages from Premier and Roberts Victor samples of supposed mantle origin give δS^{34} values of +0.2 and +2.1, respectively. These results support the inference that sulfur of mantle origin has a δ -value close to zero.

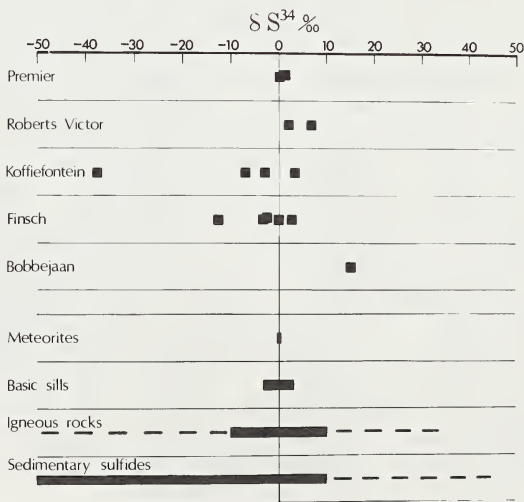


Figure 1. δS^{34} values of sulfides from kimberlites and associated xenoliths. Also included are the variations in δS^{34} for common rock types in nature (after Thode et al., 1961).

References

1. Frick (1973). Contrib. Mineral. Petrol., 39, 1-16.
2. Vakhrushev and Sobolev (1973). Int. Geol. Rev., 15, 103-110.
3. Meyer and Boctor (1975). Contrib. Mineral. Petrol., 52, 57-68.
4. Desborough and Czamanske (1973). Am. Mineral., 58, 195-202.
5. Thode, Monster and Dunford (1961). Geochim. Cosmochim. Acta, 25, 150-174.

Table I. Representative analyses of major sulfide minerals.

	Pentlandite		Pyrrhotite		Chalcopyrite		Pyrite	
Fe	27.2	33.9	56.1	61.6	30.5	30.4	46.4	44.7
Ni	38.1	28.3	2.15	0.00	0.00	0.08	0.00	1.61
Cu	0.00	0.00	0.00	0.07	33.6	33.8	0.07	0.18
Co	0.82	3.36	0.13	0.01	0.09	0.03	-	0.50
S	33.7	34.3	41.3	37.5	36.3	35.2	53.4	53.1
Total	99.8	99.9	99.7	99.2	100.5	99.5	99.9	100.1

Table II. Representative analyses of silicates.

Oxide	Andradite	Ilvaite
SiO ₂	37.2	30.1
TiO ₂	0.02	0.00
Al ₂ O ₃	5.47	0.09
Cr ₂ O ₃	0.00	0.00
FeO*	21.8	51.8
MgO	0.09	0.20
CaO	32.4	13.90
MnO	0.21	1.64
NiO	0.13	0.00
Na ₂ O	0.00	0.00
K ₂ O	0.00	0.00
Total	99.3	97.7

(+OH)

* All Fe reported as FeO

EVIDENCE FOR FRACTIONAL CRYSTALLISATION IN THE MANTLE OF LATE-STAGE KIMBERLITIC LIQUIDS

S.Y. Wass (School of Earth Sciences, Macquarie University, North Ryde, N.S.W. 2113, Australia)

Nephelinitic and basanitic dykes of Tertiary age from the Kiama area of southeastern New South Wales, Australia, contain a unique suite of amphibole-bearing xenoliths which carry apatite as an abundant and ubiquitous constituent. These xenoliths also contain biotite, clinopyroxene, olivine, magnesian ilmenite, spineliferous titanomagnetite, spinel and accessory sulphides (including chalcopyrite, pyrrhotite, pyrite and pentlandite) in varying proportions. Apatite commonly constitutes up to 20% of the mode. Carbonate is widespread as a minor constituent and may be primary. All olivine is serpentinised or altered to carbonate. Genetically distinct, but spatially associated xenoliths include Cr-spinel-bearing Cr-diopside lherzolites, Al-augite series xenoliths and granulites apparently of crustal origin. Xenoliths comprise approximately 80% of one dyke at Kiama (Wass and Irving, 1976) and it is this occurrence which has been studied in detail.

The amphibole/apatite xenoliths show a wide range of textures and modes within a restricted range of mineral assemblages, varying from monomineralic rocks to xenoliths mineralogically layered on various scales. Grainsizes vary both within individual xenoliths and from xenolith to xenolith. Extremes in grainsize are represented by large kaersutite crystals up to 10 cm in cross-sectional width to grains in layers of banded xenoliths which are less than 1 mm in diameter. Discrete mineral assemblages commonly observed include: amphibole/clinopyroxene/apatite±ilmenite, spinel, biotite, olivine, carbonate; amphibole/biotite/apatite±ilmenite, spinel, carbonate; biotite/apatite±ilmenite, spinel; amphibole/apatite±carbonate, ilmenite, spinel; Fe-rich clinopyroxene/apatite/spinel±biotite; spinel/apatite±biotite, carbonate; and monomineralic rocks consisting of amphibole, biotite, apatite and spinel. Sulphides are ubiquitous accessories.

Relict microstructures including euhedral grain shapes, mineralogical layering and adcumulus textures are consistent with a primary origin by precipitation from a melt. Excellent examples of layering are evident in some of the Fe-rich clinopyroxene/apatite/spinel xenoliths. Layers consisting only of similar modes of Fe-rich clinopyroxene and spinel, grade into a monomineralic spinel layer then into a spinel/apatite/biotite layer, culminating in a pure apatite layer. No sharp boundaries occur in this type of layered xenolith, in contrast with those consisting of sharply-delineated alternating bands of amphibole/clinopyroxene and amphibole/clinopyroxene/biotite interleaved by amphibole.

Superimposed on these primary igneous textures in some xenoliths are the effects of recrystallisation and deformation. Two distinct types are evident. The first type occurs in the spinel/apatite/biotite and in the monomineralic spinel and apatite xenoliths. A mosaic, interlocking aggregate dominated by smoothly-curved grain boundaries, triple junctions and lack of inclusions is typical. Accessory carbonate commonly forms an integral part of this microfabric. Such a microstructure suggests extensive annealing which may have occurred shortly after precipitation by grain-boundary adjustment at high but sub-solidus temperatures or significantly after precipitation by subsequent metamorphism. The other type evidences solid-state deformation by the presence of such effects as strongly kinked micas and strained clinopyroxenes showing growth of small, strain-free grains.

TABLE 1. REPRESENTATIVE MICROPROBE ANALYSES OF MAJOR MINERALS IN AMPHIBOLE/APATITE SUITE XENOLITHS, KIAMA, N.S.W.

Sample No.	K1023		K13b			K20		K1025	
	Amph.	Cpx	Biot	Amph.	Cpx	Cpx	Spinel	Apatite	Ilmenite
SiO ₂	41.8	48.3	35.1	39.2	48.4	49.5	n.d.	0.27	n.d.
TiO ₂	4.76	2.36	7.90	5.20	1.46	1.01	20.9	n.d.	51.9
Al ₂ O ₃	12.1	6.38	15.0	12.8	4.67	4.34	5.20	n.d.	0.25
Cr ₂ O ₃	0.10	0.52	n.d.	0.04	0.03	0.10	0.09	n.d.	0.08
FeO*	9.28	6.45	18.1	15.9	10.9	13.2	67.9	0.41	41.7
NiO	0.20	0.06	0.03	n.d.	n.d.	0.06	0.08	n.d.	0.00
MnO	0.08	0.12	0.12	0.20	0.29	0.33	0.80	0.06	0.53
MgO	13.7	12.8	10.5	9.20	11.3	8.90	0.52	0.23	5.20
CaO	12.0	22.3	n.d.	11.4	21.4	20.5	n.d.	54.4	n.d.
Na ₂ O	2.46	0.78	0.58	2.32	1.11	1.86	n.d.	0.18	n.d.
K ₂ O	1.75	n.d.	8.54	1.95	n.d.	n.d.	n.d.	0.02	n.d.
P ₂ O ₅	n.d.	n.d.	n.d.	n.d.	n.d.	n.d.	n.d.	38.0	n.d.
Total	98.2	100.1	95.9	98.2	99.6	99.8	95.5	93.6	99.7
100 Mg									
Mg+Fe*	72.5	78.0	50.8	50.8	64.8	54.6			

*Total Fe as Fe²⁺: n.d. = not detected

Modes of Xenoliths

K1023: Cpx 50%, amph 38%, apatite 12%, accessory spinel, ilmenite, carbonate.

K13b: Amph 35%, cpx 30%, biot 12%, apat 15%, spinel & ilmenite 8%, access. carbonate, sulphides.

K20: Fe-rich cpx 50%, spinel 30%, apatite 20%, accessory biotite, carbonate.

K1025: Amph 55%, biot 35%, apatite 5%, ilmenite 5%, accessory carbonate, sulphides.

K1023 to K13b to K20 represent xenoliths progressively enriched in Fe. Note the mutually sympathetic variation of Mg/(Mg+Fe) of coexisting amphiboles and clinopyroxenes in K1023 and K13b.

Representative microprobe analyses of the major minerals are given in Table 1. The amphiboles in this xenolith suite vary in composition from titaniferous pargasite to titaniferous kaersutite. They are relatively rich in Al₂O₃ and Mg (Mg/(Mg+Fe) where Fe is total iron as Fe²⁺) ranges from 50 to 73. NiO ranges from 0.15% to below detection limit, Cr₂O₃ up to 0.25% and MnO up to 0.30%. Biotites are low in MnO, Cr₂O₃ and NiO (maximum values 0.15, 0.08, 0.06 respectively) and Mg ranges from 58 to 66. Clinopyroxenes show the greatest compositional variation. They are generally augites, titaniferous augites and salites with moderately high Al₂O₃ (4%-8%) and TiO₂ from 1% to 3%. Cr₂O₃ varies from 0.8% for the most Mg-rich clinopyroxenes to below detection limits for the Fe-rich clinopyroxenes. Mg varies from 50 to 78, the extreme Fe-rich compositions containing up to 15% FeO. Calculation of an ideal structural formula indicates significant Fe³⁺ in these Fe-rich clinopyroxenes. Al is dominantly accommodated in the CaAl₂SiO₆ and CaTiAl₂O₆ molecules. Al^{iv}:Al^{vi} ratios are within the range for high-pressure clinopyroxenes precipitated from basic magmas (Wass, in prep.). Ilmenites are consistently low in Al₂O₃, NiO and Cr₂O₃; MnO ranges from about 0.5% to 1% and MgO from 4% to 6%. Spinel generally lacks Cr₂O₃ and contains high FeO, TiO₂, moderate Al₂O₃ and up to 5% MgO. Reverse zoning of amphiboles and clinopyroxenes in contact with the host magma is ubiquitous. The outer rims are higher in Mg and Ti than the host grain and, for the clinopyroxenes, are equivalent in composition with groundmass clinopyroxenes in the host rock. Exsolution of ilmenite is common in some amphiboles and clinopyroxenes.

A consistent pattern in the compositional differences of phases within separate xenoliths is evident. Amphiboles, clinopyroxenes and biotites show mutually sympathetic variation in Mg ratios in different xenoliths. Within some of the layered xenoliths a gradational trend towards Fe-enrichment is evident in successive layers.

Rare xenoliths containing amphibole exhibit textures and mineralogy which are distinct from those of the amphibole/apatite suite. One such xenolith is

interpreted to be an altered, partly disaggregated Cr-diopside series xenolith. Olivine is pseudomorphed by calcite and the Cr-diopside is extensively replaced by titaniferous pargasite compositionally equivalent to that in the amphibole/apatite xenoliths. Other xenoliths appear to have been originally normal, apatite-free Al-augite series xenoliths consisting of clinopyroxene, spinel and olivine. Extensive alteration of the olivine to calcite and talc(?) and of the clinopyroxene to kaersutite and to the Fe-rich clinopyroxenes typical of some of the amphibole/apatite suite xenoliths has taken place.

The range of textural and chemical features of the amphibole/apatite xenolith suite is consistent with an origin as part of a fractional crystallisation sequence. The lack of feldspar, the Mg-rich, Al-poor nature of the ilmenite and the $Al^{IV}:Al^{VI}$ ratios in the clinopyroxenes suggest high-pressure formation, probably in excess of 17 kb. The alteration of Cr-diopside series xenoliths to titaniferous pargasite indicates metasomatic penetration of mantle wall rock by a fluid phase associated with the formation of the amphibole/apatite suite xenoliths. The solid-state deformation effects observed in the amphibole/apatite suite, imply a significant time gap between their original precipitation and eventual entrainment in the host magma.

Analogous clinopyroxenes and amphiboles are recorded from ultrabasic rocks from the Fen carbonatite complex in Norway. Potassic volcanics of South West Uganda and the sodi-potassic volcanics of West Eifel, Germany contain similar Fe-rich clinopyroxene, amphibole, dark mica and apatite. Phenocryst assemblages in dykes of kimberlitic and carbonatitic affinity from Quebec closely parallel those in the amphibole/apatite suite xenoliths. Enrichment in Ti, P and Fe is characteristic also of similar mineral phases in autoliths from kimberlite pipes in Lesotho.

However, the southeastern New South Wales assemblages appear unique in their association of magnesian ilmenite and abundant apatite with the other phases. These amphibole/apatite suite xenoliths evidence the presence of mantle liquids rich in alkalis, volatiles and incompatible elements which are interpreted to have crystallised partially or fully in the upper mantle under conditions conducive to fractional crystallisation. The Fe-rich nature of the assemblages and the abundance of apatite suggests prior fractionation of the parent melt has resulted in the increased concentration of volatiles and incompatible elements and in depletion of Mg, Cr and Ni. This may have occurred at deeper levels within the mantle below the level of generation of the host basanite. The resultant high-pressure differentiation sequence was then sampled by accidental entrainment in subsequent magmas probably generated in later, unrelated, episodes of partial melting. As yet there is little evidence of low-pressure equivalents of related kimberlitic magmas in southeastern N.S.W., although stream gravels in the area contain magnesian ilmenite, pyrope-almandine garnet and rare diamonds which suggest the occurrence of kimberlitic rocks and Ferguson *et al.*, (1977) have reported rare kimberlitic diatremes further to the south-west.

References

- FERGUSON, J., ELLIS, D.J., ENGLAND, R.N. (1977) Unique spinel-garnet lherzolite inclusion in kimberlite from Australia. *Geology* 5:278-280.
- WASS, S.Y. (in prep.) Geochemistry of clinopyroxenes of diverse origins in alkali basaltic rocks from the Southern Highlands (NSW) and the Massif Central (France).
- WASS, S.Y., IRVING, A.J. (1976) XENMEG: a catalogue of occurrences of xenoliths and megacrysts in volcanic rocks of eastern Australia. Australian Museum, Sydney, 441 pp.

The chemical composition of kimberlites compared with that of three basaltic magma types

K.H. WEDEPOHL, Y. MURAMATSU (Geochemical Institute, University of Goettingen, Fed. Rep. Germany)

New data on Li, F, S, V, Cr, Mn, Co, Ni, Cu, Zn, Rb, Sr, Y, Zr, Cd, Ba, Hg, Tl, Pb, Bi and the major elements in 11 South African kimberlites (sampled during the first Kimberlite Conference) will be presented. With the exception of the alkali elements and sulfur their concentrations are rather close to their arithmetic means (\bar{x}). Most values of 26 elements range from $\bar{x}/2$ to $2\bar{x}$ only. The composition of olivine, serpentine, pyroxenes, phlogopite, perovskite, spinel, magnetite and Fe-Ni-Cu-S ores from selected kimberlites has been investigated by microprobe. In this study perovskite occurs as a major host of the REE in kimberlite. Native copper has been observed in a sample from the De Beers mine.

Additional data on 60 elements in bulk kimberlites have been compiled from the literature. The averages computed for 44 elements are based on more than 40 values each. The element averages for geographic subgroups scatter about the total average in a range which is specific for certain elements. These ranges generally increase with the rate in which a certain element is accumulated in kimberlites relative to ultramafic rocks. Good correlations between the following elements have been observed in kimberlites: Cr-Ni-Co, K-Rb. But expected correlations between Pb-Tl-K and Na-K are apparently not existent. The detailed chemical information has been published by MURAMATSU (1977).

Analytical data for the same group of elements in olivine nephelinites, alkali olivine basalts, tholeiitic basalts and ultramafic rocks have been compiled and evaluated by WEDEPOHL (1975 and unpublished; major source: Handbook of Geochemistry).

The number of values on element concentrations in basaltic rock types used for averages is comparable to that in kimberlites. Less chemical information is available on ultramafic rocks and nephelinites. It has to be kept in mind that some ultramafics, used for this compilation, are residual material from partial melting.

Magmas of kimberlites, nephelinites and basalts are thought to be melting products of mantle rocks. Therefore, they are to be compared chemically with ultramafics from the upper mantle. Ratios of element concentrations in the 4 magmatic rock types to those in ultramafic rocks, indicating accumulations or depletions from mantle materials, are plotted in Fig. 1. There exists a surprisingly similar behavior of large groups of elements in the 4 magma series shown in this diagram. The specific difference between the 4 series is the degree of element accumulations relative to ultramafics.

Elements like Cr, Ni, Mg, Co are incorporated in the residual ultramafic material, increasingly from kimberlites to tholeiites. Mn, Fe, Sc must have distribution coefficients

between the total of mantle minerals and the four melts which are close to one. Al and Ga have a tendency towards the residual minerals garnet and orthopyroxene and are low in kimberlites exclusively. The so-called incompatible elements Th, U, light REE, Nb, Ta etc. are almost consistently increasing from tholeiites to kimberlites. The heavy alkalis, alkaline earths, Pb, Tl and Li follow this tendency but in a less pronounced way. From these regularities it can be concluded that the rocks have been formed from magmas which represent increasing fractions of partially melted mantle rocks. In this case, tholeiitic basalt has been formed from the relative largest and kimberlite from the smallest fraction of partial melt; the other rock types are intermediate.

Melting experiments of olivine melilitite under high CO₂ and H₂O pressure (30 kb) have demonstrated the persistence of garnet and orthopyroxene as near-liquidus phases at increasing CO₂-H₂O proportions (BREY and GREEN, 1977). They indicate an increasing contribution of olivine and clinopyroxene from mantle rocks to partial melts under these specific vapor pressures. The specific accumulation of Ni and Co and depletion of Al, Ga and heavy REE in kimberlites relative to basalts can be explained by the increased melting of olivine and loss of garnet and orthopyroxene to the residual mantle respectively. Sodium could have been lost from kimberlitic magmas to country rocks by means of CO₂ vapor transport (finitization).

The degree of element accumulation in magmas relative to mantle rocks seems to depend on the deviations of their ionic size from that of the host ions in mantle minerals.

A constant increase of the heavy sulfur isotope and of the Fe³⁺/Fe²⁺ ratio can be observed in the 4 rock groups from tholeiitic basalts ($\delta^{34}\text{S} - 0.3\%$; Fe₂O₃/FeO = 0.32) to kimberlites ($\delta^{34}\text{S} + 4.6\%$; Fe₂O₃/FeO = 1.3). It must be due to an increase of the oxygen fugacity in this sequence. For $\delta^{34}\text{S}$ values of basalts see SCHNEIDER (1970).

References

- BREY, G., GREEN, D.H.: Systematic study of liquidus phase relations in olivine melilitite + H₂O + CO₂ at high pressures and petrogenesis of an olivine melilitite magma. *Contrib.Mineral.Petrol.* 61, 141 (1977).
- MURAMATSU, Y.: Geochemische Untersuchungen an Kimberliten, einem Granatperidotit und einem Eklogit-Einschluß aus Kimberley, Südafrika. PhD-Thesis Göttingen (1977).
- SCHNEIDER, A.: The sulfur isotope composition of basaltic rocks. *Contrib.Mineral.Petrol.* 25, 95 (1970).
- WEDEPOHL, K.H.: The contribution of chemical data to assumptions about the origin of magmas from the mantle. *Fortschr.Mineral.* 52, 141 (1975).

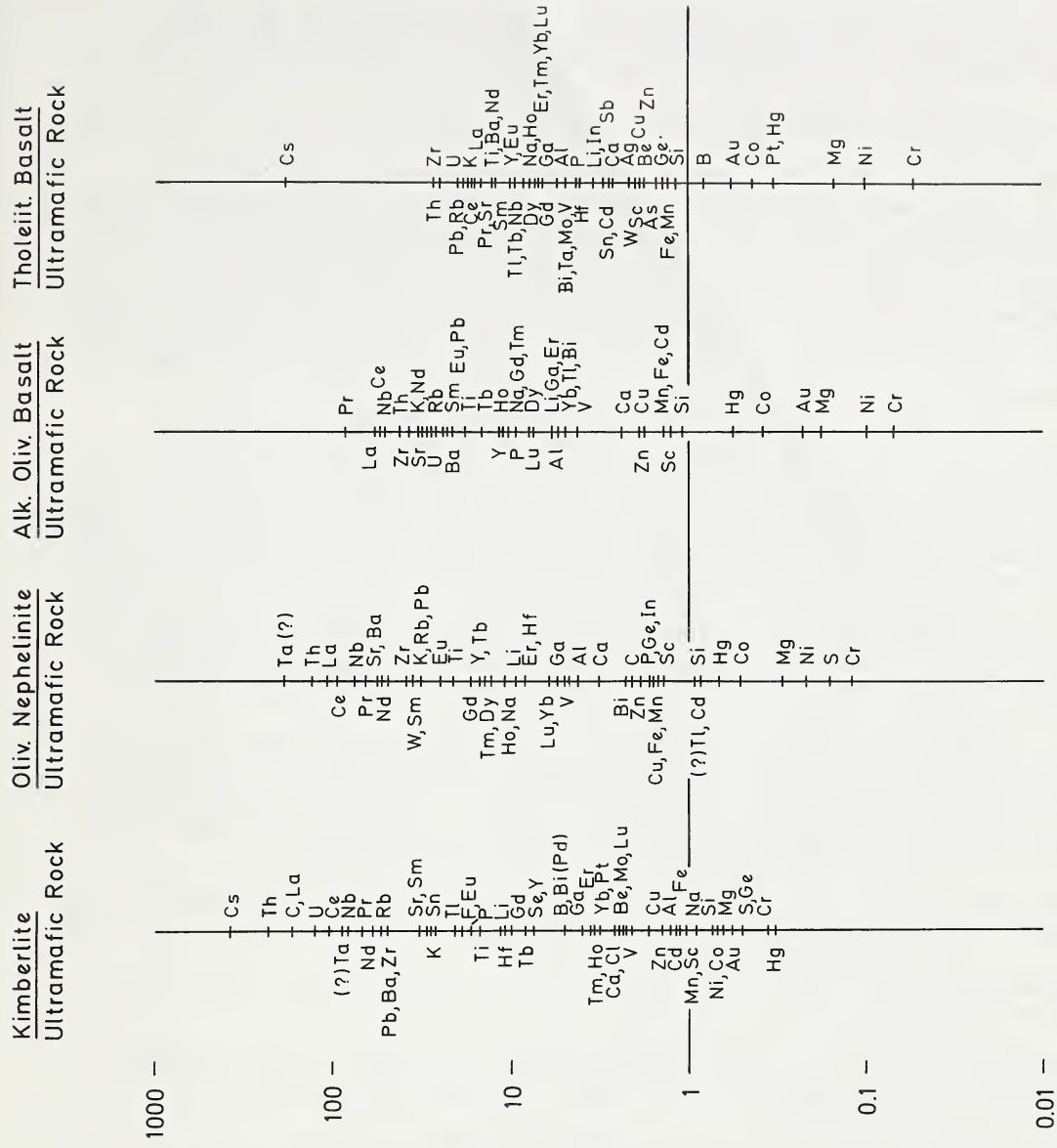


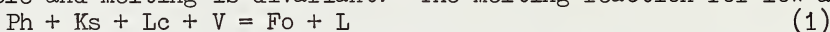
Figure 1: Ratios of concentrations in rock series

THE SYSTEM $K_2O-MgO-Al_2O_3-SiO_2-H_2O-CO_2$: PHASE RELATIONS OF THE JOINS
 $Ph-H_2O-CO_2$ AND $Ph-En-Mag$ AT HIGH TEMPERATURES AND HIGH PRESSURES AND
 APPLICATIONS TO THE GENESIS OF ALKALIC MAGMAS

R. F. Wendlandt (Geophysical Laboratory, 2801 Upton St., N. W.,
 Washington, D. C. 20008)

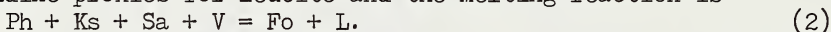
Volatile-bearing minerals in the upper mantle, such as carbonate and phlogopite, can buffer the composition of a coexisting vapor and can restrict the range of temperatures of melting and of melt compositions (Eggler and Holloway, 1977; Wyllie, 1977). While carbonates have been the subject of considerable experimental attention in the past several years, the role of phlogopite in the genesis of alkalic magmas, especially in the presence of a CO_2-H_2O vapor, and the melting behavior of coexisting phlogopite and carbonate are less well understood.

The stability of phlogopite has been investigated at 20 kbar as a function of X_{CO_2} , with emphasis on low total volatile contents (Fig. 1). Melting can occur either under conditions of high a_{H_2O} , such that all potential phlogopite in the system is saturated, or under conditions of low a_{H_2O} , in which case phlogopite coexists at subsolidus temperatures with its breakdown products. In the former case, the vapor and liquid compositions are variable and melting is divariant. The melting reaction for low a_{H_2O}

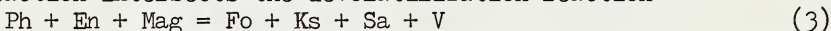


is univariant; the CO_2-H_2O vapor composition is buffered at subsolidus conditions (a "zone of invariant vapor composition"; Eggler and Holloway, 1977) and the liquid composition is independent of the volatile content of the system.

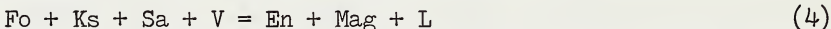
Reaction (1) is characterized by a vapor composition that becomes increasingly CO_2 -rich with increasing pressure. The reaction originates at the CO_2 -absent invariant point, I_{10} in Fig. 2, located at approximately 1.5 kbar and 1160°C (Yoder and Kushiro, 1969). At pressures between 22-30 kbar, sanidine proxies for leucite and the melting reaction is



The liquid produced is silica-undersaturated and alkalic. At 30 kbar, the melting reaction intersects the devolatilization reaction

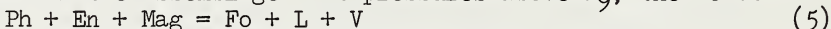


generating I_9 and introducing magnesite as a solidus phase. The phlogopite-absent reaction



emanates from the H_2O -absent invariant point, I_8 , and is characterized by decreasing X_{CO_2} as it trends toward I_9 . The vapor composition at I_9 is approximately $X_{CO_2}=0.60$.

Reactions involving the assemblage $Ph+En+Mag$ have been investigated to pressures of 50 kbar and the results are presented in P-T projection in Fig. 3. The devolatilization reaction (3) represents the low pressure stability limit of the assemblage. At pressures above I_9 , the reaction



involves two volatile-bearing minerals as solidus phases. At 32.5 kbar, phlogopite persists above the solidus for most compositions in the $Ph-En-Mag$ join and the liquid generated is haplocarbonatitic. At 40 kbar, liquids are more potassic; the supersolidus volume for magnesite is enlarged and that of phlogopite is diminished relative to the situation at 32.5 kbar. Pyrope is encountered as a product of reaction (5) at pressures of 40 kbar and higher. At 50 kbar, magnesite persists above the solidus over a wide

range of compositions in the Ph-En-Mag join. Phlogopite is believed to be a solidus phase, however, none of the compositions investigated provided direct evidence of a supersolidus volume. The vapor composition along reaction (5) is initially CO₂-rich at pressures above I₉ but becomes increasingly H₂O-rich with increasing pressure.

The system K₂O-MgO-Al₂O₃-SiO₂-H₂O-CO₂ models a Ca-deficient mantle and portions of the system have been investigated to elucidate the origins of potassic magmas, carbonatites, and kimberlites. Theory and experiment show that melting of peridotite in the presence of small amounts of volatiles is restricted by the volatile-mineral assemblage. In the present investigation, vapor compositions are buffered by phlogopite and magnesite and the compositions of liquids in equilibrium with these vapors are restricted. The fundamental peridotite melting reaction was found to be

- (1) at P less than 22 kbar,
- (2) at P = 22-30 kbar, and
- (5) at P greater than 30 kbar.

The pressure of magma generation appears to be the critical variable; pressure determines the volatile-mineral assemblage and this in turn buffers the vapor composition. Accordingly, different liquids are produced by partial melting at different pressures. The liquids produced by reactions (1) and (2) are silica-undersaturated and alkalic, whereas those produced by reaction (5) are carbonatitic at pressures slightly above I₉ but become increasingly alkalic and silicic with increasing pressure.

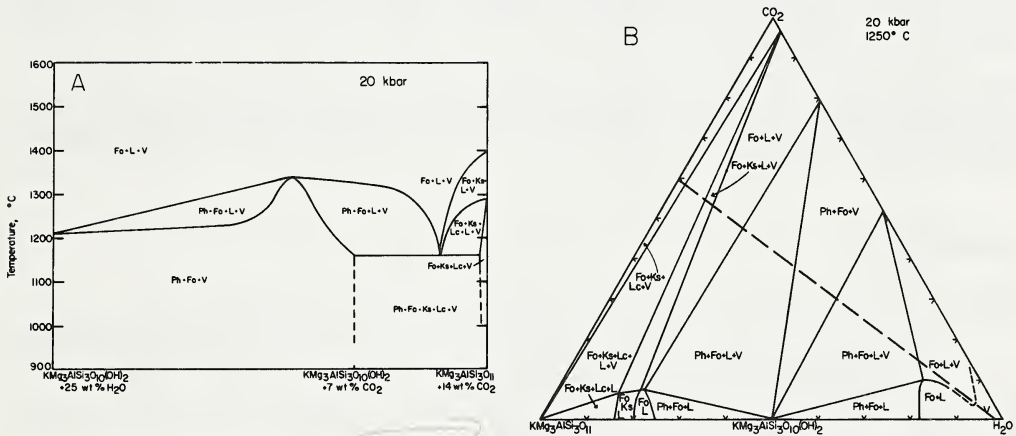


Figure 1-(A). An isobaric section through the join $\text{KMg}_3\text{AlSi}_3\text{O}_{11}\text{-H}_2\text{O-CO}_2$ illustrating the stability of phlogopite as a function of volatile composition at 20 kbar (the location of the section is shown in Fig. 1B). Compositions to the left of the azeotropic-like point are characterized by high $a_{\text{H}_2\text{O}}$ and divariant melting behavior. Compositions to the right of the point are characterized by low $a_{\text{H}_2\text{O}}$ and the liquid is generated by eutectic-like melting. (B). A schematic isobaric-isothermal section of the join $\text{KMg}_3\text{AlSi}_3\text{O}_{11}\text{-H}_2\text{O-CO}_2$. Compositions are in mole per cent and vapor compositions are schematic.

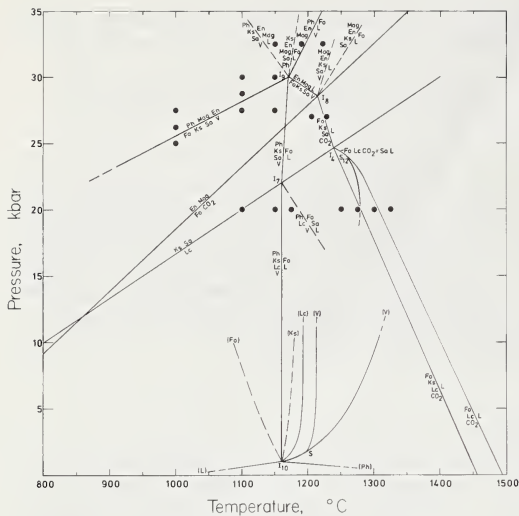


Figure 2 (left)-A P-T projection of phase relations involving Ph, En, Mag, Fo, Sa, Ks, Lc, L and V. The invariant point, I_0 , involves six components and an H_2O-CO_2 vapor; I_8 and I_7 are quinary and I_4 and I_{10} are quaternary. The data for I_{10} is from Yoder and Kushiro (1969). The reaction $Lc = Ks + Sa$ is from Lindsley (1966) and the reaction $En + Mag = Fo + CO_2$ is from Newton and Sharp (1975).

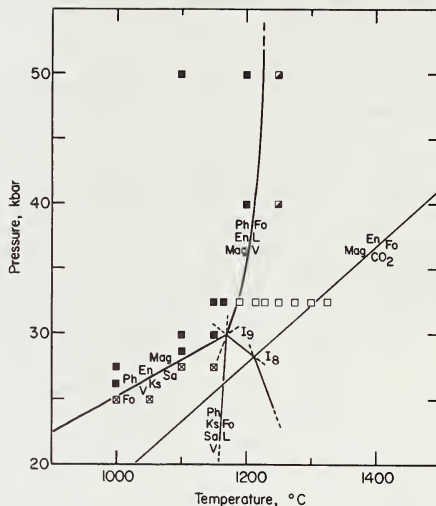


Figure 3 (right)-A preliminary P-T projection of reactions involving the assemblage Ph + En + Mag. Pyrope is observed in the products at pressures greater than 40 kbar.

REFERENCES

Eggler, D. H., and J. R. Holloway, Partial melting of peridotite in the presence of H_2O and CO_2 : principles and review, in Chapman Conference on Partial Melting in the Upper Mantle, Oreg. Dep. Geol. Miner. Ind. Bull., in press, 1977.

Lindsley, D. H., P-T projection for part of the system kalsilite-silica, Carn. Inst. Wash. Yb. 65, 244-247, 1966.

Newton, R. C., and W. E. Sharp, Stability of forsterite + CO_2 and its bearing on the role of CO_2 in the mantle, Earth Planet. Sci. Lett., 26, 239-244, 1975.

Wyllie, P. J., Mantle fluid compositions buffered by carbonates in peridotite- CO_2-H_2O , J. Geol., 85, 187-207, 1977.

Yoder, H. S., Jr., and I. Kushiro, Melting of a hydrous phase: Phlogopite, Am. J. Sci., Schairer Vol., 267A, 558-582, 1969.

328
 0-600s
 Pyrope
 more to now Si
 K_{7c}
 (poly on solidus)

THE STABILITY OF GRAPHITE IN THE SYSTEM C-O.

Woermann, E.; Knecht, B. (Aachen); Rosenhauer, M. (Frankfurt)
and Ulmer, G.C. (Philadelphia).

On the basis of the CCO-buffer equation (graphite-CO₂-CO-O₂) from French and Eugster (1965) :

$$\log f_{O_2} = - \frac{20586}{T} - 0.044 + \log P - \frac{0.028(P-1)}{T} \text{ for atm and K} \quad (1)$$

the stability of graphite can be calculated in the system C-O. The derivation of this equation was, however, based on the assumption that:

$$\log f_{CO_2} = \log P_{\text{gas}}$$

which also means that their assumptions were :

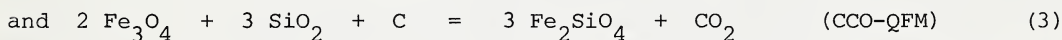
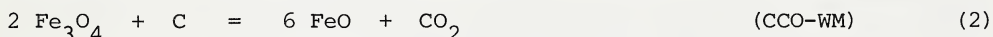
$$1) \quad P_{CO_2} = P_{\text{total}} \quad \text{and} \quad P_{CO} = 0,$$

$$\text{and } 2) \quad f_{CO_2} = P_{CO_2} \quad (\text{or that } CO_2 \text{ is an ideal gas})$$

Recent experiments on PVT relations of CO₂ (Shmulovich and Shmonov (1975) and Holloway (1976)) however indicate a significant pressure dependence of the fugacity coefficient of carbon dioxide. Therefore it seemed desirable to determine the oxygen fugacity of the CCO-buffer experimentally.

Redox equilibria of the CCO-assemblage were studied under controlled oxygen fugacities of the QFM- (quartz-fayalite-magnetite) and WM- (wüstite-magnetite) buffers respectively in the temperature range 800-1200°C and pressures up to 30 kbar.

Experiments were carried out to study the monovariant equilibria :



CO₂ was introduced in the form of FeCO₃ or Ag(COO)₂, both of which decomposed under the conditions of the experiment with liberation of CO₂.

Assuming that neither carbon is introduced into wüstite, magnetite, quartz or fayalite, nor iron into graphite or the carbon oxide species it appeared to be unnecessary to separate the buffer assemblages by membranes. The reagents were thus intimately mixed. The samples were welded in silver-palladium or platinum capsules and reacted in a piston cylinder apparatus. The run products were investigated microscopically and by X-ray diffractometry.

The results (figure 1) plot between theoretical estimates, assuming

- 1) ideal gas behavior after equation (1) (French and Eugster(1965)) (= "b")
- and 2) real gas behavior of CO₂, applying a modified equation after Redlich and Kwong (Holloway(1976)) (= "c").

By least squares fit the present data for the CCO equilibrium may be expressed by :

$$\log f_{O_2} = 2.74 - \frac{19559}{T} + \frac{0.13}{T} (P-1) \quad \text{in bar and K, for } 5 < P < 30 \text{ kbar.}$$

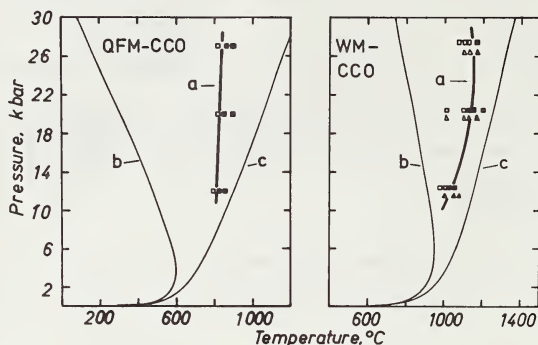


Figure 1.

Monovariant equilibria QFM-CCO and WM-CCO.

"a" = experimental results.

"b" = theoretical estimates assuming ideal gas behavior after equation (1), (French and Eugster, (1965)).

"c" = theoretical estimates assuming real gas behavior of CO_2 applying a modified equation after Redlich and Kwong "MRK". (Holloway, (1976)).

References :

French, B.M, and Eugster, H.P.: J.Geophys.Res. 70, (1965), 1529-1539.

French, B.M.: Rev. Geophys. 4, (1966), 223-253.

Holloway, J.R.: in: Thermodynamics in Geology, D.G.Fraser, ed.,

D.Reidel Publishing Co., Dordrecht, 1976, pp. 161-181.

Shmulovich, K.I., and Shmonov, V.M.: Geochem.Intern. 12, (1975), 202-206.

THE INFLUENCE OF Cr_2O_3 ON THE RELATIONSHIPS BETWEEN SPINEL- AND GARNET-PERIDOTITES

B. J. Wood (Department of Geology, University of Manchester, Manchester M13 9PL, England)

Introduction

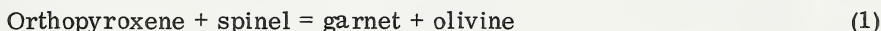
The main object of this study has been to determine the stability fields of spinel- and garnet-peridotites in the system $\text{MgO-Al}_2\text{O}_3\text{-Cr}_2\text{O}_3\text{-SiO}_2$ as a function of the $(\text{Cr}/\text{Cr}+\text{Al})$ ratio of the spinel. Extrapolation of these experimental data to natural systems is, to some extent, complicated by interactions in high-Ca, high-Cr garnets. The magnitudes of these interactions and their influence on relevant equilibria have been estimated from partitioning in natural assemblages.

Experimental

All experiments were performed in an 0.5" piston-cylinder apparatus using crystalline starting materials. Forsterite, pyrope and orthopyroxene (with 2% and 11% Al_2O_3) were separately prepared by crystallising gel starting materials under appropriate P-T conditions. MgAl_2O_4 spinel and MgCr_2O_4 spinel were synthesized from oxides at 1 atmosphere and 1400°C . Sealed Pt capsules and either an H_2O or a CO_2 vapour phase were used.

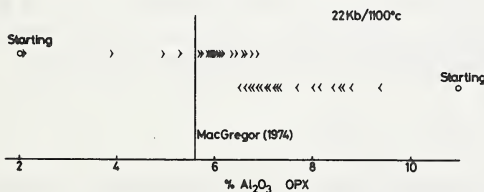
$\text{MgO-Al}_2\text{O}_3\text{-SiO}_2$ system :

The reaction :



was found to lie between 23.5 and 24 kb at 1100°C and 22 and 23.2 kb at 1000°C . These results are reversals with crystalline starting material using piston-out procedure and CO_2 vapour.

The Al_2O_3 content of orthopyroxene coexisting with garnet has been determined at 22 kb/ 1100°C using the crystallised gel starting materials. Results starting with $(\text{MgSiO}_3)_{0.98}(\text{Al}_2\text{O}_3)_{0.02}$ opx and $(\text{MgSiO}_3)_{0.89}(\text{Al}_2\text{O}_3)_{0.11}$ opx are shown in figure 1. Despite the considerable scatter, agreement with the experiments of MacGregor (1974) is reasonably good. These results do not support the contention that the "primary" starting material, gel in this case, affects the Al_2O_3 content of the product orthopyroxene.



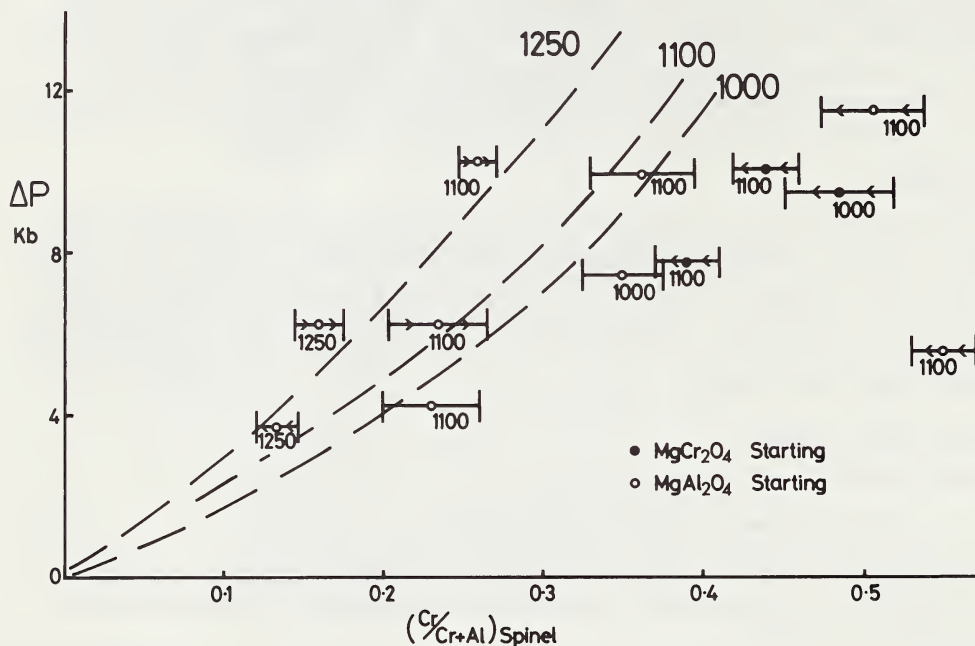
$\text{MgO-Al}_2\text{O}_3\text{-SiO}_2\text{-Cr}_2\text{O}_3$ system :

Experiments were performed with two starting materials :

- (a) Forsterite + pyrope + orthopyroxene (All Cr-free) + MgCr_2O_4 spinel

(b) Forsterite + pyrope + orthopyroxene (all Cr-free) + $MgAl_2O_4$ spinel

+ Cr_2O_3 . Results are shown in figure 2 as ΔP (run pressure minus equilibrium pressure in MAS system) versus $Cr/(Cr+Al)$ in the spinel. Arrow pointing to the left denotes olivine absent from products. Arrow pointing right denotes orthopyroxene absent. Labelled curves were calculated (at the temperature indicated) by assuming that the spinel behaves as an ideal solution.

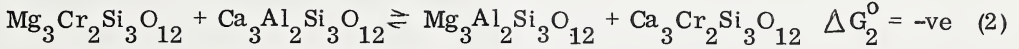


The compositions of product spinels were determined by microprobe and with EMMA-IV. They are, in general, closely grouped in any one experiment and results from starting material (b) are consistent with those from starting material (a). It may be seen from figure 2 that stabilisation of spinel + olivine due to a given $(Cr/Cr+Al)$ of the spinel is close to that which would be predicted on the basis of ideal two-site $MgAl_2O_4$ - $MgCr_2O_4$ solution.

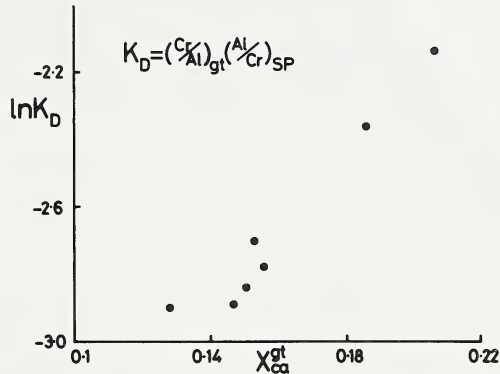
Extension to natural systems :

In order to extrapolate these results to natural systems it is necessary to take account, in particular, of the presence of Fe^{2+} in all phases and of Ca in garnet. If we make the common assumption of ideal Mg-Fe mixing, then the main non-ideal terms will involve Ca in a garnet, the composition of which may be approximated by $(Mg_x Fe_y Ca_{(1-x-y)})_3 (Al_z Cr_{(1-z)})_2 Si_3 O_{12}$. Treating double site garnet using the reciprocal salt approach the principal contribution to the activity coefficient of

$\text{Mg}_3\text{Al}_2\text{Si}_3\text{O}_{12}$ component arises from the standard state free energy change of the exchange reaction :



Note that for the garnet solid solution to be ideal, ΔG_2^0 must be zero. ΔG_2^0 may be estimated from the magnitude of the well-known coupling between Ca and Cr in the garnet. A plot of $\ln (\text{Cr}/\text{Al})_{\text{garnet}} \cdot (\text{Al}/\text{Cr})_{\text{spinel}}$ versus $X_{\text{Ca}}^{\text{gt}}$ in spinel + garnet herzolites (figure 3) yields ΔG_2^0 of about -50 kcal.



From this we have :

$$RT \ln \gamma_{\text{Mg}_3\text{Al}_2\text{Si}_3\text{O}_{12}}^{\text{gt}} \approx X_{\text{Ca}}^{\text{c}} \cdot X_{\text{Cr}} \quad (50\ 000) \quad (3)$$

$$RT \ln a_{\text{Mg}_3\text{Al}_2\text{Si}_3\text{O}_{12}}^{\text{gt}} \approx RT \ln (X_{\text{Mg}}^{\text{c}3} \cdot X_{\text{Al}}^{\text{o}2}) + X_{\text{Ca}}^{\text{c}} X_{\text{Cr}}^{\text{o}} \quad (50\ 000)$$

Where X_{Mg}^{c} , X_{Al}^{o} refer to the atomic fractions of Mg and Al in cubic and octahedral sites respectively.

The P-T curve for a natural garnet-spinel-olivine-clinopyroxene assemblage can thus be represented by (from reaction 1) :

$$RT \ln K = 1.987 \ln \left(\frac{a_{\text{Mg}_3\text{Al}_2\text{Si}_3\text{O}_{12}} \cdot X_{\text{Fo}}^{\text{ol}2}}{(X_{\text{Mg}}^{\text{t}})_{\text{sp}} (X_{\text{Al}}^{\text{o}})_{\text{sp}}^2 \cdot X_{\text{Mg}}^{\text{M1}2} \cdot X_{\text{Mg}}^{\text{M2}2}} \right) \quad (4)$$

$$= -4420 + 0.54 T + 0.1895 P$$

In equation (4) t and o refer to tetrahedral and octahedral sites in the spinel phase and the P term appropriate for low Al_2O_3 contents of the orthopyroxene (4 wt % or less).

PHASE RELATIONSHIPS IN THE SYSTEM PICOILMENTITE - CLINOPYROXENE - Cr_2O_3

B. Wyatt: Anglo American Research Laboratories,
P.O. Box 106, Crown Mines, 2025. R.S.A.

Preliminary experiments have been carried out between 15 - 35 kb and 1000-1550°C on the natural system picroilmenite - clinopyroxene - Cr_2O_3 using graphite capsules, in an attempt to determine phase relationships relevant to the petrogenesis of titanium and chromium bearing opaque oxides which occur in upper mantle xenoliths, and as megacrysts in kimberlite. A chromium-rich system, picroilmenite (21 wt%) - clinopyroxene (69.5 wt%) - Cr_2O_3 (9.6 wt%) and a relatively chromium-poor system, picroilmenite (66.5 wt%) - clinopyroxene (28.5 wt%) and Cr_2O_3 (5.0 wt%) have been examined.

In the chromium-rich system, two subsolidus runs at 15 and 35kb and 1100° and 1286°C respectively, both produced titanian chromite, chrome diopside and chromian rutile. The 15kb run also probably contained small laths of armalcolite. In the chromium-poor system, however, chromian ulvöspinel, chromian ilmenite and chrome diopside appeared in the runs at 20, 27.5 and 35kb within the temperature range studied (Figure 1). Chromian ulvöspinel is the liquidus phase, followed by chromian picroilmenite with the proportion of ilmenite relative to spinel increasing with decreasing temperature. Spinel is absent on the solidus at 35 kb but is retained as a solidus phase at 20 and 27.5 kb. Very small spinels were encountered in the subsolidus runs at 35 kb, but it is uncertain whether they are metastable phases or the products of subsolidus reaction and further experimentation is required. Clinopyroxene was encountered for the first time at 20-30°C above the solidus. In general, both the Cr_2O_3 and MgO contents of the ilmenite and the spinel decrease with decreasing temperature at each pressure studied. Some representative results are given in Table 1. Tie lines between ilmenite - spinel pairs are given in Figure 2.

The more important phase relationships which emerge from this initial experimental study are (i) the coexistence of titanian chromite and chromian rutile in the Cr_2O_3 - rich system, (ii) the coexistence of chromian ilmenite and chromian ulvöspinel in the Cr_2O_3 - poor system, and (iii) the absence of armalcolite above 20 kb. (The projected curves for the breakdown of armalcolite (Kesson and Lindsley, 1975; Friel et al, 1977) intersect the solidus between 8 and 18 kb depending on the composition of the armalcolite). In addition, it appears as if chromian ulvöspinel has a reaction relationship to ilmenite of the type,
 $\text{Fe}_2\text{TiO}_4 + \text{TiO}_2$ (from liquid) \longrightarrow 2FeTiO_3 .

A new suite of chromian ilmenite megacrysts containing lamellae of chromian spinel similar to those previously described by Danchin and d'Orey (1972) and Haggerty (1975) have also been analysed (Table 1). Some of these lamellae are also associated with chromian rutile. The high MgO content (>13 wt%) of these megacrysts when compared to the MgO content of the experimentally produced ilmenites (<10 wt%) possibly indicates that the former crystallized in equilibrium with an MgO-rich phase such as olivine or orthopyroxene, whereas the latter have crystallized from a clinopyroxene-rich system. Using these data and previously recorded associations of ilmenite, spinel and rutile from kimberlite and upper mantle xenoliths (Dawson and Smith, 1976; Smith and Dawson, 1975; Haggerty, 1975; Boyd and Nixon, 1975) as well as the present experimental data, it has been possible to compile a phase compatibility diagram for the system
 $\text{TiO}_2 - (\text{MnO} + \text{FeO} + \text{MgO}) - (\text{Fe}_2\text{O}_3 + \text{Al}_2\text{O}_3 + \text{Cr}_2\text{O}_3)$ relevant to upper mantle conditions (Figure 3). It is to be noted that the 3 phase assemblage, spinel - ilmenite - rutile replaces the low pressure assemblage, spinel - ilmenite^{ss} - ferropseudobrookite^{ss} determined at atmospheric pressure within the synthetic^{ss} system $\text{TiO}_2 - \text{MgO} - \text{FeO} - \text{Al}_2\text{O}_3 - \text{Cr}_2\text{O}_3$ (Maun et al 1971; Schreifels and Maun, 1975). The solubility of Cr_2O_3 and $\text{Al}_2\text{O}_3(?)$ in picroilmenite is temperature dependant and

probably reach maxima of approximately 13 and 1.2 (?) wt% respectively. Under subsolidus conditions the breakdown of chromian picroilmenite would be towards chromian ulvöspinel, rutile and Cr_2O_3 - depleted picroilmenite, with decreasing temperature. At low temperatures (less than approximately 1000°C) the spinel compositions may be complicated by miscibility gaps in system $\text{Mg Al}_2\text{O}_4$ - Mg_2TiO_4 and FeAl_2O_4 and Fe_2TiO_4 (Maun et al, 1972).

REFERENCES

- Boyd, F.R. and Nixon, P.H. (1975). In: Physics and chemistry of the earth, 9, L.H. Ahrens, J.B. Dawson, A.R. Duncan, A.J. Erlank, (eds.), 431-453. Oxford: Pergamon Press.
- Danchin, R.V. and D'Orey, F. (1972). Contr. Mineral. Petrol. 35, 43-49.
- Dawson, J.B. and Smith J.V. (1977). Geochim. Cosmochim. Acta 41, 309-323.
- Friel, J.J., Harker, R.I. and Ulmer, G.C. (1977). Geochim. Cosmochim. Acta 41, 403-410.
- Haggerty, S.E. (1973). In: Lesotho kimberlites (ed. P.H. Nixon), 350pp. Lesotho National Development Corporation, Maseru.
- Haggerty, S.E. (1975). In: Physics and chemistry of the earth, 9, L.H. Ahrens, J.B. Dawson, A.R. Duncan, A.J. Erlank (eds.), 295-307. Oxford: Pergamon Press.
- Kesson, S.E. and Lindsley, D.H. (1975). Proc. Lunar Sci. Conf. 6th, 911-920.
- Maun, A. Hank, J., Osborn, E.F. (1971). Proc. Lunar Sci. Conf. 2nd, 497-505.
- Maun, A. Hank, J. and Löfall, T. (1972). Proc. Lunar Sci. Conf. 3rd, 185-196.
- Schreifels, W.A. and Maun, A. (1975). Proc. Lunar Sci. Conf. 6th, 973-985.
- Smith, J.V. and Dawson, J.B. (1975). In: Physics and chemistry of the earth, 9, L.H. Ahrens, J.B. Dawson, A.R. Duncan, A.J. Erlank (eds.), 309-322. Oxford: Pergamon Press.

TABLE 1. Representative analyses of coexisting minerals from three experimental runs and a natural chromian picroilmenite containing lamellae of spinel and rutile.

P (kb) T ($^\circ\text{C}$) PHASE	EXPERIMENTAL RUNS						SPINEL AND RUTILE LAMELLAE IN ILMENITE		
	27,5 1402		27,5 1500		35 1286		I	S	R
	I	S	I	S	R	S			
SiO_2	0.02	0.63	0.00	0.13	0.10	0.49	0.0	0.16	0.05
TiO_2	50.39	24.66	51.21	24.18	89.94	6.34	48.46	8.11	87.86
Al_2O_3	0.41	1.81	0.70	2.62	0.30	3.24	1.02	11.40	0.21
Cr_2O_3	7.14	20.19	11.25	26.73	7.72	57.16	11.18	41.56	4.18
Fe_2O_3^*	2.60	1.71			0.42	1.90	7.35	4.93	1.78
FeO	29.90	40.06	26.70	34.28		17.66	18.48	19.25	
MnO	0.11	0.21	0.13	0.19		0.28	0.18	0.26	0.03
MgO	8.31	9.19	9.70	12.08	0.11	13.63	13.96	14.22	0.48
CaO	0.40	0.62	0.26	0.30	0.46	0.39	0.03		0.11
TOTAL	99.28	99.07	99.95	100.51	99.05	101.09	100.68	99.89	94.70

* Fe_2O_3 calculated from mineral formula. I=ilmenite, S=spinel, R=rutile

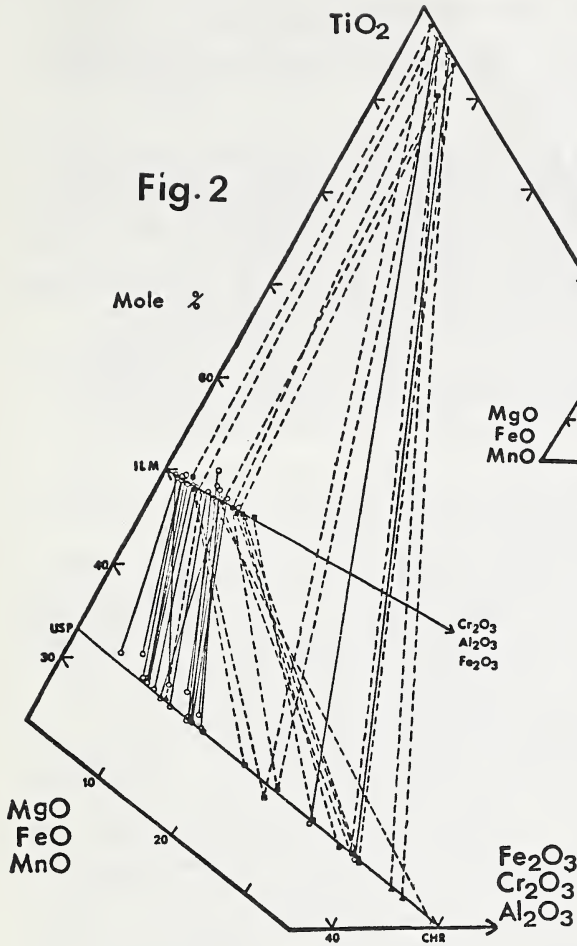


Fig. 2

Tie lines for coexisting ilmenite, spinel and rutile. Solid lines—experimental runs, dashed lines—data for natural assemblages from this study and the literature. NB. For experimental runs, Fe_2O_3 is absent or present in very low concentrations. ILM=ilmenite, CHR=chromite, USP=ulvöspinel.

Fig. 1

Isopleth for the composition, microilmenite (66.5 wt%) - clinopyroxene (28.5 wt%) - Cr_2O_3 (5.0 wt%). Solid squares indicate data points. ilm=chromian microilmenite, sp=chromian ulvöspinel, cpx=clinopyroxene, liq=liquid.

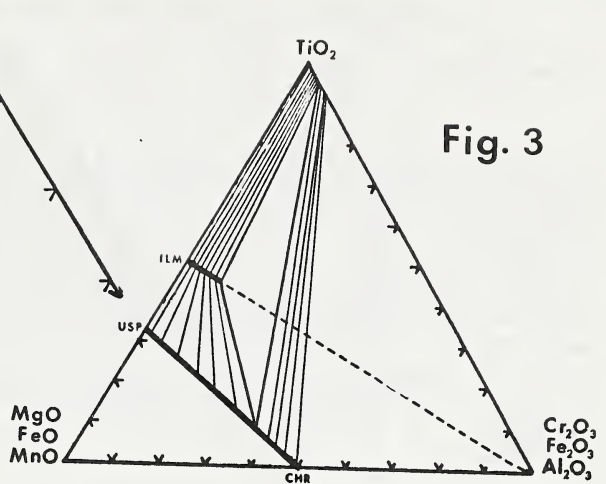
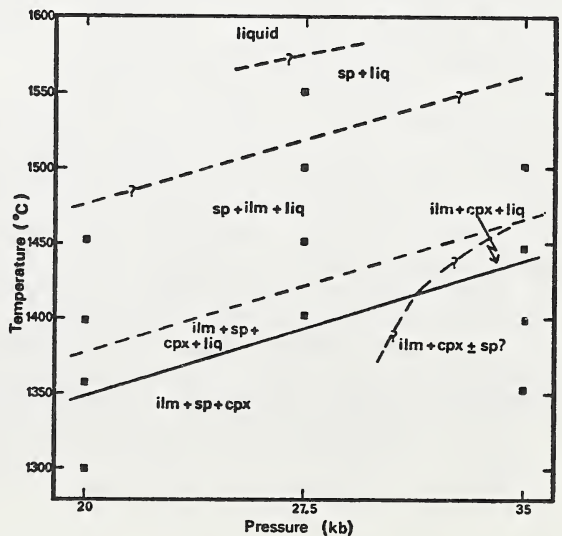


Fig. 3

Fig. 3

Phase compatibility diagram (mole %) constructed from Fig.2 and relevant to upper mantle conditions (>20 kb). Apices in the 3 phase triangle, usp_{ss} - rutile - ilm_{ss} will vary with temperature. ss Åbrev. as for Fig.2.

Fig. 1



KIMBERLITE MAGMAS FROM THE SYSTEM PERIDOTITE-H₂O-CO₂

Peter J. Wyllie (*University of Chicago, Department of Geophysical Sciences, Chicago, Illinois 60637*)

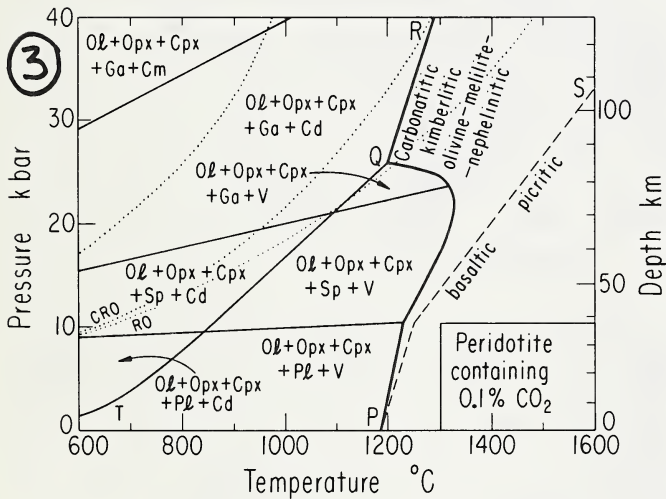
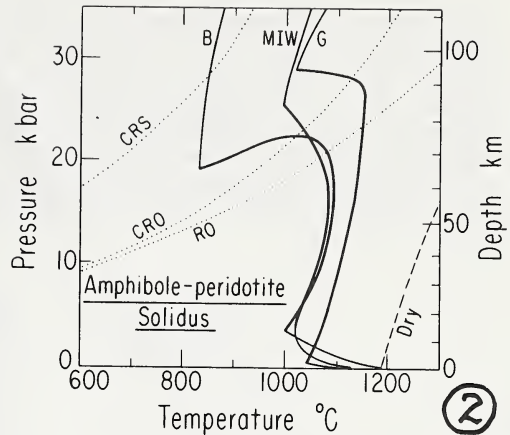
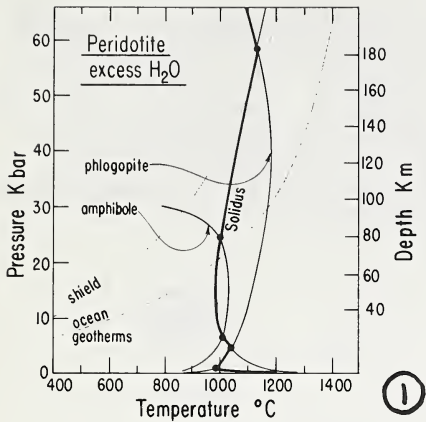
Kimberlite magmas are generated by a small degree of partial melting of mantle peridotite containing H₂O and CO₂, normally at depths greater than about 100 km. The presence of CO₂ is crucial for the development of melts sufficiently low in SiO₂. Phlogopite is an obvious candidate for the source of K₂O. Available experimental data from the systems peridotite-H₂O-CO₂, CaO-MgO-SiO₂-H₂O-CO₂, and pyrope-magnesite can be combined to construct phase diagrams for peridotite containing H₂O and CO₂. Direct experimental measurement of many parts and features of these phase diagrams would be difficult, perhaps impossible. Uncertainties in results and interpretations up to 30 or 35 kbar have been discussed extensively. Results at higher pressures, for the specific problem of kimberlite genesis, are virtually non-existent.

Wyllie (1977) extrapolated available experimental data from 30 to 60 kbar in order to outline the relationships among carbonate (calcic dolomite or magnesite), phlogopite, and amphibole on the solidus surface of peridotite-H₂O-CO₂. Ellis and Wyllie (this volume) calculated to 100 kbar the positions of specific reactions involving carbonates and hydrous minerals in the system MgO-SiO₂-H₂O-CO₂. The detailed phase relationships in this model system revealed intricacies in the peridotite-H₂O-CO₂ system that will be drafted into diagrams by the time of the Conference.

Initial melting of mantle peridotite may involve (1) vapor-absent or (2) vapor-present assemblages. If we consider H₂O and CO₂ as the only volatile components present in significant amounts, the minerals amphibole, phlogopite, and carbonate are the most likely crystalline hosts. There are three possible subsolidus vapor-absent assemblages: (a) H₂O in hydrous minerals, (b) CO₂ in carbonate, and (c) H₂O and CO₂ in hydrous minerals and carbonate. There are six possible subsolidus vapor-present assemblages: (a) all H₂O+CO₂ in vapor phase, (b) H₂O in hydrous minerals with excess in vapor phase, (c) H₂O distributed between hydrous minerals and H₂O-CO₂ vapor phase, (d) CO₂ in carbonate with excess in vapor phase, (e) CO₂ distributed between carbonate and H₂O-CO₂ vapor phase, (f) H₂O and CO₂ distributed between hydrous minerals, carbonate, and H₂O-CO₂ vapor phase. All nine examples can be examined in the system peridotite-H₂O-CO₂ for various pressures, temperatures, and H₂O/CO₂.

Fig. 1 shows the effect of excess H₂O on the peridotite solidus, the maximum stability ranges of amphibole and phlogopite with peridotite and excess H₂O, and the effect of phlogopite melting in lowering the peridotite solidus at pressures below 5 kbar and above about 60 kbar. Fig. 2 shows three experimentally-based versions of the solidus for different peridotites with a trace of H₂O. The heavy lines show the solidus where vapor-absent amphibole-peridotite begins to melt. Fig. 3 shows the effect of a trace of CO₂ on peridotite. This exists as vapor at pressures below the reaction TQ, and as carbonate above TQ. CO₂ solubility in the near-solidus liquid increases from 1-4% to almost 40% between 20-26 kbar as the solidus drops through more than 100°C. Dolomite and peridotite melt together along QR, producing low-SiO₂, high-K₂O, carbonatitic liquids.

Fig. 4 shows the effect of H₂O on the system peridotite-CO₂. With



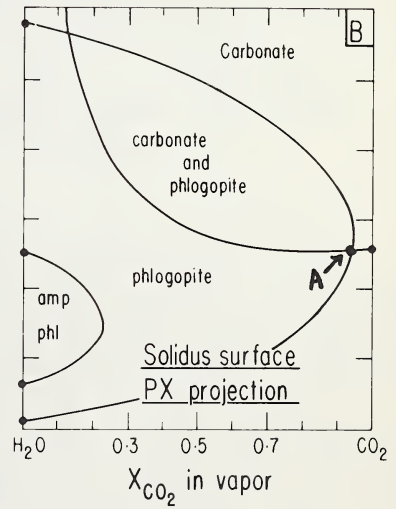
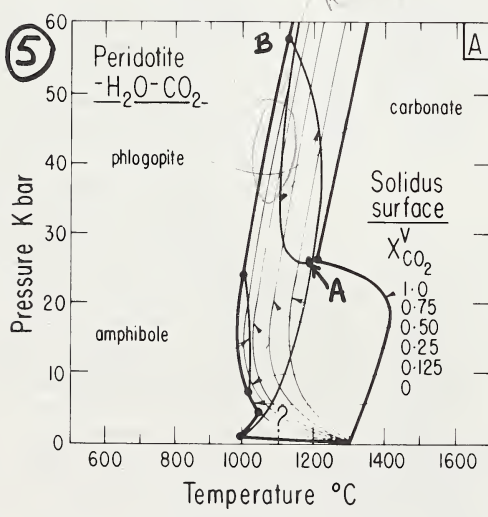
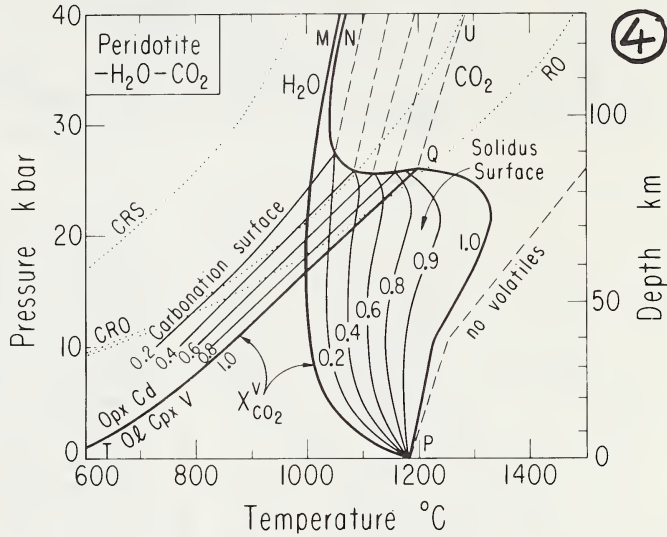
excess volatiles, the solidus of Fig. 3 becomes a divariant surface, PQUM. This surface is intersected by the divariant surface for the carbonation reaction QT, along the univariant line QN. Unless there is enough CO₂ present to carbonate all of the clinopyroxene (unlikely in the mantle), conditions in the area QNU for melting of carbonated peridotite are not reached. Partially carbonated peridotite begins to melt along the line QN, with the vapor phase compositions buffered as shown by the contours.

Fig. 5A shows an early version of Fig. 4, with buffer lines added for the estimated maximum ranges of existence of carbonate, amphibole and phlogopite on the solidus surface. Using curve G from Fig. 2, amphibole and carbonate may just overlap on the solidus surface. Using the solidus B from Fig. 2, the solidus surface expands and the intersections change again.

Additional analysis of Fig. 5 shows that there is a univariant curve for the coexistence of carbonate and phlogopite, extending from A on the solidus surface, just below the carbonate buffer line in both temperature (Fig. 5A) and pressure (Fig. 5B). This passes below the peridotite-H₂O solidus near point B (Fig. 5A, compare Fig. 1). Phlogopite and carbonate can jointly dominate near-solidus melts from depths of 80 km to about 230 km, with vapor phase buffered to very high H₂O/CO₂. High H₂O/CO₂ in vapor lowers the solidus compared to that for vapor-absent carbonate-phlogopite-

peridotite, but coexistence of the first liquid with carbonate ensures generation of CO_2 -rich, SiO_2 -poor melt, and phlogopite ensures high K_2O in the very small amount of liquid first produced. The temperature maxima on the solidus contours (absent on Fig. 5A, see Fig. 4), now known to be much more accentuated than illustrated, show that magma rising through about 85-70 km from greater depths must evolve CO_2 and H_2O .

Research supported by the National Science Foundation through Grant EAR 76-20410 and the Materials Research Laboratory.



LATE ABSTRACTS

EMPLACEMENT AND CRYSTALLISATION OF A KIMBERLITE DYKE FROM THE DE BEERS MINE,
KIMBERLEY, SOUTH AFRICA.

Colin H. Donaldson (Department of Geology, University of Manchester,
Manchester, M13 9PL, U.K.)

Arch M. Reid (Department of Geology, University of Cape Town, Rondebosch,
7700 South Africa).

Introduction: A narrow (24 cm) vertical kimberlite dyke was sampled at the 585 m level in the De Beers Mine, Kimberley, where it intrudes the country rock adjacent to the main pipe. Prominent features of the dyke are the well-developed banding parallel to the dyke walls and the presence in some bands of abundant horizontally elongate light-coloured 'amygdales' set in a dark kimberlitic matrix.

Petrography: Petrographic study of a series of thin sections across the dyke allows the recognition of discrete bands which are described below in sequence from the margin to the centre of the dyke (bands I to VI). Band I (0.5 cm thick) is a narrow fine-grained band immediately adjacent to the dyke wall. Microphenocrysts of phlogopite, ilmenite and serpentine occur in a matrix of sub-parallel calcite laths, granular opaques and interstitial serpophite. There are no amygdales and the calcite and phlogopite grains show a preferred orientation parallel to the dyke wall. Band II (1 cm thick) contains elongate irregular white amygdales up to 6 mm long oriented normal to the dyke wall. They are filled by calcite and serpophite and make up about one third of the area of band II. We interpret some of the complex amygdales as having formed by coalescence of two or more individuals moving toward the interior of the dyke. The remainder of the band resembles band I but lacks the well-developed preferred orientation. Band III (2 cm thick) is uniformly fine-grained without amygdales. Like band I the microphenocrysts are oriented parallel to the dyke wall but band III differs from band I in having a much higher abundance of opaque oxides. The amygdales in band II do not transgress the boundary with band III. Band IV (1.5 cm thick) is characterised by the presence of elongate amygdales, 3 to 15 mm long, oriented normal to the dyke wall. These amygdales commonly have a broad rounded end facing the centre of the dyke with a narrower tail or tails pointing toward the dyke margin. Megacrysts of phlogopite, serpentine, calcite pseudomorphs after olivine, and rarer rutile are set in a matrix of serpophite, calcite and opaque oxides. Phlogopite is less abundant than in band III. Between the amygdales and oriented normal to the banding are narrow elongate branching calcite crystals up to 10 mm long. Band V (3 cm thick) lacks calcite laths and the amygdales present are fewer in number but are larger with more complex shapes. Carbonate-bearing amygdales contain either coarse plates of calcite and dolomite or elongate parallel-growth skeletons of calcite. Some of the large complex amygdales have a 'root zone' in band IV and become wider and more complex in band V. Towards the interior of the dyke the serpophite and carbonate of the amygdales either terminate abruptly or, in some cases, merge into the kimberlite matrix. Band V contains more abundant megacrysts (phlogopite, ilmenite and calcite and serpentine pseudomorphs after olivine) than band IV. The matrix consists of serpophite, carbonate and opaque minerals. Band VI (13 cm thick), occupying the middle of the dyke, does not carry amygdales but is otherwise similar to and grades into band V. Band VI has a still higher content of megacrysts which are mostly olivine or serpentine. Sharp boundaries divide zones with no fresh olivine from zones of partly serpentinised olivine. Megacrysts of pyrope and amphibole are rare and one inclusion of a serpentinised phlogopite-rutile-ilmenite peridotite was noted. The remainder of the dyke consists of a repetition of

band V plus a thin marginal band that has not yet been properly sampled. The two sides of the dyke are asymmetric and the sequence of bands on one side is not wholly represented on the other. Amygdales in bands II, IV and V are filled with carbonate, serpophite, or a mixture of both phases. All have at least a thin lining of carbonate. Some amygdales are zoned with calcite cores and dolomite rims or with serpophite cores and calcite rims. Euhedral serpentine grains in some amygdales may be pseudomorphs after phlogopite.

Modal Variations: The modal variation across the dyke is complex, involving both abrupt and gradational changes across conformable contacts. Phlogopite, serpentine and ilmenite are present throughout the dyke as megacrysts or microphenocrysts. Fresh olivine is prominent only in the innermost band (band VI). The matrix comprises calcite, serpophite, ilmenite, perovskite, apatite, magnetite and chromite. Phlogopite is most abundant at the dyke margins and opaque oxides are most abundant in band III. Amygdales occupy about one third of some bands but the total carbonate and serpophite content of these bands is similar to that in adjacent amygdale-free bands. Total carbonate content is greatest in band V, where calcite pseudomorphs after olivine are most common, and decreases toward the centre of the dyke. Olivine is most abundant in band VI where the highest concentration of megacrysts occurs.

Mineral Chemistry: Olivine compositions range from $Fe_{91.6}$ to $Fe_{88.4}$ and normally zoned olivines are commonly mantled by a narrow reverse zoned rim. Phlogopite is magnesian ($Mg/Mg+Fe=0.9$), low in Ti and commonly shows evidence of reaction with the matrix. Serpentine is also highly magnesian but with a range of Ti, Al, Na and K contents. Calcite grains show a range of Fe and Mg contents with the higher values occurring in the carbonates in the amygdales. Dolomite was found only in the amygdales. Ilmenite is also Mg-rich but a range of Cr contents is present. Rutile occurs as rare-earth rich and rare-earth poor varieties. The complex oxide phases indicate a paragenetic sequence with the early crystallisation of Mg-Al-rich chromite and rutile followed by microilmenite and Mg-Al-poor chromite, followed by titanomagnetite. Perovskite granules with up to 3 wt percent Nb_2O_5 occur throughout the matrix. Chalcopyrite, millerite and an Fe-Ni sulphide were also noted.

Emplacement and crystallisation of the dyke: The multiple shapes of calcite grains in the matrix and particularly the presence of elongate branching calcite crystals indicate crystallisation from a melt at different degrees of undercooling. The presence of amygdales also testifies to the presence of a melt whether they are filled gas cavities or immiscible liquid segregations. The contrasting textural and mineralogical character of the various bands within the dyke indicate that the dyke was emplaced as a sequence of discrete pulses of magma of similar composition. At least three pulses of magma would be required, corresponding to a) bands I and II, b) band III and c) bands IV to VI. Compositions of the first and second magma pulses (calculated from mineral compositions and abundances) are richer in CO_2 and K than the aphyric Benfontein kimberlite (Dawson and Hawthorne, 1973) and poorer in Mg and Fe. The second pulse (band III) is enriched in Cr, Ti and Fe over the first, and depleted in calcite components. It is difficult to calculate an average composition for the third pulse of magma. All three pulses carry similar megacryst phases. We conclude that the intrusions were nearly contemporaneous and derive from a common parent magma. The first magma pulse contained 20-30 percent microphenocrysts (serpentine and phlogopite) in a melt of 40-50 percent calcium carbonate, with the remainder equivalent to hydrous Mg-Fe silicate and Fe-Ti-Al-Cr oxides. Rapid cooling produced the chilled margin represented by band I. Slower cooling allowed the formation of amygdales in band II which has a similar total calcite content. The second magma pulse contained approx-

imately the same proportion of megacrysts but in a melt that was considerably richer in Fe and Ti. Rapid cooling and continuous flow produced the oriented fine-grained texture of band III. The formation of band III was abruptly terminated by the third magma pulse consisting of 40 percent olivine, serpentine, phlogopite and opaque megacrysts in a carbonate-rich melt. The oriented branching calcites in band IV are evidence of stagnant conditions along the margins of the third intrusion and of supercooling prior to calcite crystallisation. Super-saturation was relieved by rapid dendritic crystallisation of calcite, by the formation of carbonate-rich amygdales, and by extensive metasomatic alteration of olivine to calcite. The concentration of megacrysts towards the centre of the dyke is ascribed to a combination of flow differentiation and increase in megacryst abundance with time. We assume that the three magma pulses are derived from a homogeneous mantle-derived kimberlite magma. Fractionation of crystals and melt in a shallow magma chamber and consequent tapping of the chamber provided the sequence of broadly similar magmas represented in this multiple intrusion. The sequence may represent sampling of successively deeper portions of a magma chamber or conduit that had differentiated by preferential settling of megacryst phases.

Formation of the amygdales: The amygdales may have formed as segregations of melt, as globules of an immiscible liquid, or as infilled gas cavities. The similarity in total carbonate content between amygdaloidal zones and adjacent zones free from amygdales (e.g. bands I and II) suggests that the material filling the amygdales crystallised contemporaneously with and probably derived from the kimberlite matrix. This indication is further reinforced by the similarity in phase compositions between the amygdales and the matrix. Carbonate and serpophite phases were crystallising contemporaneously in both amygdales and matrix and in some cases merge into one another (band V). These relationships are not consistent with formation as immiscible liquid droplets. We suggest the following model for the formation of the amygdales (cf. Smith, 1967; Mackenzie and White, 1970). Zones in the dyke that are characterised by amygdales have crystallised under stagnant conditions as evidenced by the development of delicate elongate carbonate laths at right angles to the direction of flow in the dyke. The presence of a vapour phase in association with a carbonate-rich melt allowed the nucleation of vesicles at relatively few equally spaced centres along the dyke margins. The vesicles then grew and expanded inward to the hotter more plastic interior. Cooling of the melt continued to a stage where carbonate and serpophite were crystallising directly from a residual fluid. This fluid in part migrated into the vesicles forming the carbonate-serpophite amygdales. Where the cavity walls effectively separated the fluid from the remainder of the dyke it could internally differentiate to produce the zoned amygdales. This physical separation was not always maintained towards the interior of the dyke and the carbonate and serpophite of the amygdales in some cases grade indistinguishably into the matrix of the kimberlite. The amygdales are thus interpreted as gas cavities infilled by the residual fluid resulting from crystallisation of the kimberlite.

References:

- Dawson, J.B. and Hawthorne J.B. (1973) *J. Geol. Soc.* 129, 61-85.
Mackenzie D.E. and White A.J.R. (1970) *Lithos* 3, 309-317.
Smith R.E. (1967) *Amer. J. Sci.* 265, 696-713.

STRONTIUM AND STRONTIUM ISOTOPE DISTRIBUTIONS IN SOME KIMBERLITE NODULES AND MINERALS.

A.J. Erlank, Dept. of Geochemistry, University of Cape Town, Rondebosch, S.A.
N. Shimizu, Laboratoire de Géochimie et Cosmochimie, Institut de Physique du
Globe, Université de Paris 6, Paris, France.

Introduction: An accompanying paper in this volume (Erlank and Rickard) concludes that a suite of potassic richterite bearing peridotites, mostly from the Bultfontein pipe, are the products of upper mantle metasomatism. It is suggested that the formation of K-richterite by metasomatic replacement marks the final stage of this process, with phlogopite + diopside forming in these nodules at an earlier stage. Many phlogopite bearing nodules which lack K-richterite are also interpreted as members of the same metasomatic suite, and since they are much more abundant than the K-richterite bearing varieties, a widespread upper mantle metasomatic event, specifically as indicated by nodules from the major pipes in the Kimberley area, is implied. The conclusions reached above are based on bulk rock, mineralogical and textural evidence and the purpose of this communication is to provide further evidence for the proposed mantle metasomatic process.

Sr-isotope relationships: Many of the peridotite nodules in kimberlite have such low concentrations of Rb and Sr (e.g. Barrett, 1975) that we would not advocate bulk rock isotopic analysis, in view of the potentially large contribution of Rb and Sr contamination from the enclosing kimberlite (e.g. Erlank, 1970). However, the metasomatic rocks chosen for study (freshest varieties from the Bultfontein pipe only have been used) contain much higher concentrations of Rb and Sr, with the bulk of these elements being contained in diopside, phlogopite and K-richterite. Thus we consider that the nett effect of potential kimberlite contamination is minimized in these nodules. Rb and Sr concentrations (in ppm), as measured by XRF (28 \sim 0.5 ppm for both elements) are: K-richterite bearing nodules, Rb = 34-75, Sr = 55-237; others, Rb = 17-31, Sr = 37-165. Mass spectrometric measurements were made on two Micromass 30 instruments (28 averaged 0.00007). The results are shown in the form of an isochron diagram in Fig. 1. Our interpretation is directed towards the questions of whether the isotopic data can provide evidence for the nature and timing of the metasomatic process, and to what extent the isotopic data are influenced by kimberlite emplacement. In passing, it is pertinent to note that most kimberlite nodules (i.e. the common peridotites lacking K-richterite and with minor phlogopite) have Rb/Sr ratios that are lower than the sample with the lowest Rb/Sr ratio in Fig. 1.

Reference to Fig. 1 shows that (a) all K-richterite bearing nodules but one define an apparent "age" of 148 ± 7 m.y. (1 δ) by York Model 1 regression, (b) the other K-richterite bearing nodule, together with two phlogopite-rich nodules have isotopic relationships which are roughly consistent with the age of pipe emplacement, i.e. 90 m.y., (c) the data for the garnet bearing sample plot near the intersection of the two age lines shown in Fig. 1 and (d) all nodules have Sr^{87}/Sr^{86} ratios markedly higher than that for fresh Bultfontein kimberlite (data from Barrett and Berg, 1975). Since the initial Sr^{87}/Sr^{86} ratios for all nodules at 90 m.y. are much higher than for the kimberlite it is clear that the metasomatic process is not related to kimberlite formation and intrusion. Thus we infer that the isotopic relationships observed in the nodules are of mantle origin.

The 148 m.y. event implied in Fig. 1 is considered to represent the last time the six K-richterite bearing nodules involved comprised a single closed isotopic system, and we suggest that it indicates the Rb-Sr closure age for the postulated metasomatic process. We consider that the agreement of this age with the apparent cessation of Karroo intrusive activity at about 155 m.y. (Fitch and Miller, 1971) is highly significant. Furthermore, unpublished

$\text{Sr}^{87}/\text{Sr}^{86}$ measurements of Karroo basalts and dolerites from the central Karroo basin by one of us (AJE) are generally in the range 0.705 - 0.707. The initial $\text{Sr}^{87}/\text{Sr}^{86}$ ratio of 0.7054 at 148 m.y. for the K-richterite bearing nodules is within this range. Thus there may be a genetic connection between the postulated mantle metasomatic and Karroo events, with representatives of both indicating derivation from an isotopically modified mantle region.

Mass spectrometric analysis (by J.F. Minster) of co-existing phlogopite and K-richterite (supplied by K. Aoki) for one of the K-richterite bearing nodules plotting on the 148 m.y. line in Fig. 1 yields a two point age of 85 m.y. with initial $\text{Sr}^{87}/\text{Sr}^{86} = 0.7078$. This indicates approximate mineral isotopic equilibration on the scale of a hand specimen, from 148 m.y. until pipe emplacement, and is in agreement with the work of Barrett (1975), who noted that co-existing phlogopite and diopside from kimberlite nodules (K-richterite free) were in approximate isotopic equilibrium at pipe emplacement.

Two interpretations may be offered for the nodules which are aligned along the 90 m.y. reference line in Fig. 1. Either these are representative of a system (presumably smaller than that pertaining to the other nodules discussed above) which continued to equilibrate (approximately) until pipe emplacement or they are products of a younger mantle metasomatism just prior to, and unrelated to, the Bultfontein kimberlite emplacement. If the latter is true, then the two metasomatic events are of the same nature, with K-richterite being the last forming mineral in both sequences. The prima facie evidence is for the second interpretation given above.

Sr content of diopsides: Combination of the data given by Barrett (1975) and Shimizu (1975) for diopsides shows that those from discrete and sheared (Lesotho) nodules have lower Sr contents than those from granular nodules. There is also a tendency for the former to have lower $\text{Sr}^{87}/\text{Sr}^{86}$ ratios when compared to the latter. As noted by Shimizu (1975), the high Sr contents of the diopsides from the granular nodules are difficult to explain because experimentally determined solid/liquid partition coefficients ($D=0.05-0.08$, Shimizu, 1974) indicate a very high Sr content for any magma or fluid that may have equilibrated with these diopsides. The concentrations implied (which could be at the percentage level) rule out any known type of basaltic magma, and only carbonatites are known to possess the necessary high Sr concentrations. The suggestion arises that the high Sr diopsides could have equilibrated with CO_2 (and Sr) - rich fluids within the upper mantle during the previously postulated metasomatic process.

A secondary ion mass spectrometric (SIMS) technique (Shimizu and Allègre, this volume) has been used for measuring the Sr content of diopsides, in order to monitor possible variations in concentration due to alteration and inhomogeneity between and within grains. Replicate analysis of different spots ($\sim 30-50\mu\text{m}$) on the same grain, and of different grains from the same nodule, showed Sr to be homogeneously distributed within counting statistics ($2\sigma=5-10\%$) for diopsides from all but two nodules. The SIMS data and published isotope-dilution data for Sr in diopsides are shown in Fig. 2. Nodules which are considered to be representative of the metasomatised suite (phlogopite \pm richterite \pm garnet bearing) have much higher Sr contents in their diopsides than the least metasomatised peridotite nodule, which contains no primary phlogopite. Thus we consider that the SIMS data provide supporting evidence that the diopsides from the metasomatised suite acquired their high Sr contents by equilibration with Sr-rich fluids during the postulated metasomatic process.

References: Barrett, D.R. (1975) *Phy. Chem. Earth* 9, 637; Barrett, D.R. and Berg, G.W. (1975) *Phy. Chem. Earth* 9, 619; Erlank, A.J. (1970) *Carnegie Instit. Wash. Year Book* 68, 433; Fitch, F.J. and Miller, J.A. (1971) *Bull. Volcanologique* 35, 64; Kramers, J.D. (1977) *Earth Planet. Sci. Lett.* 34, 419; Shimizu, N. (1974) *Geochim. Cosmochim. Acta* 38, 1789; Shimizu, N. (1975) *Phy. Chem. Earth* 9.

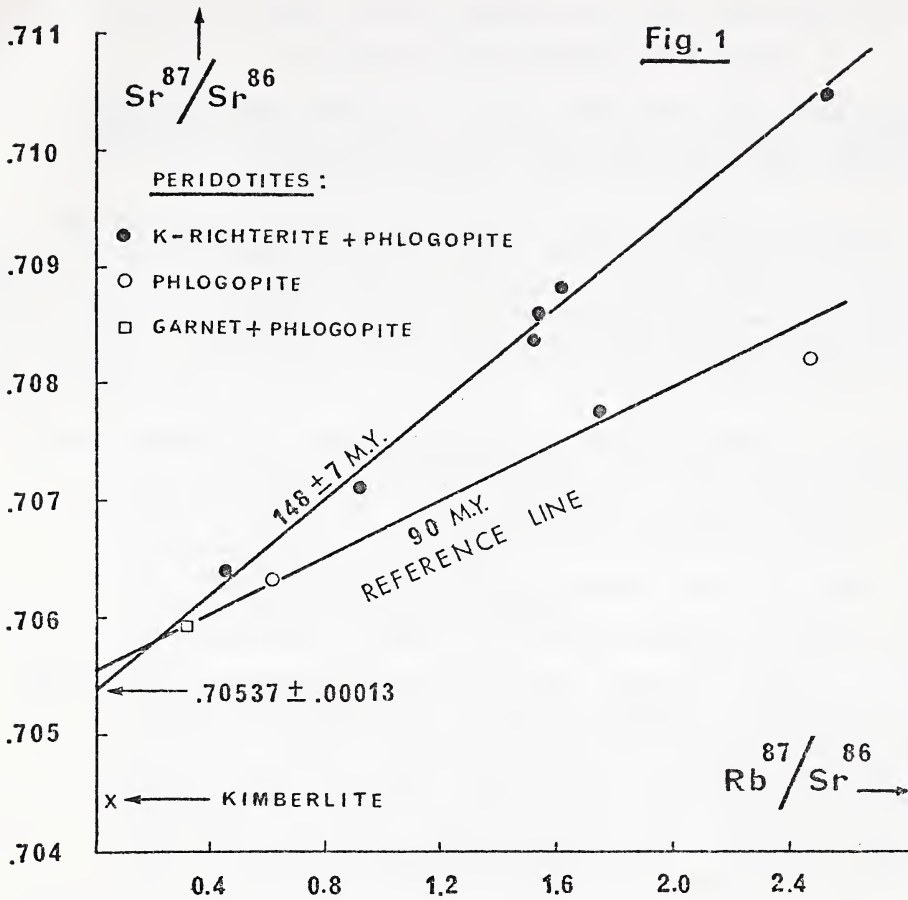
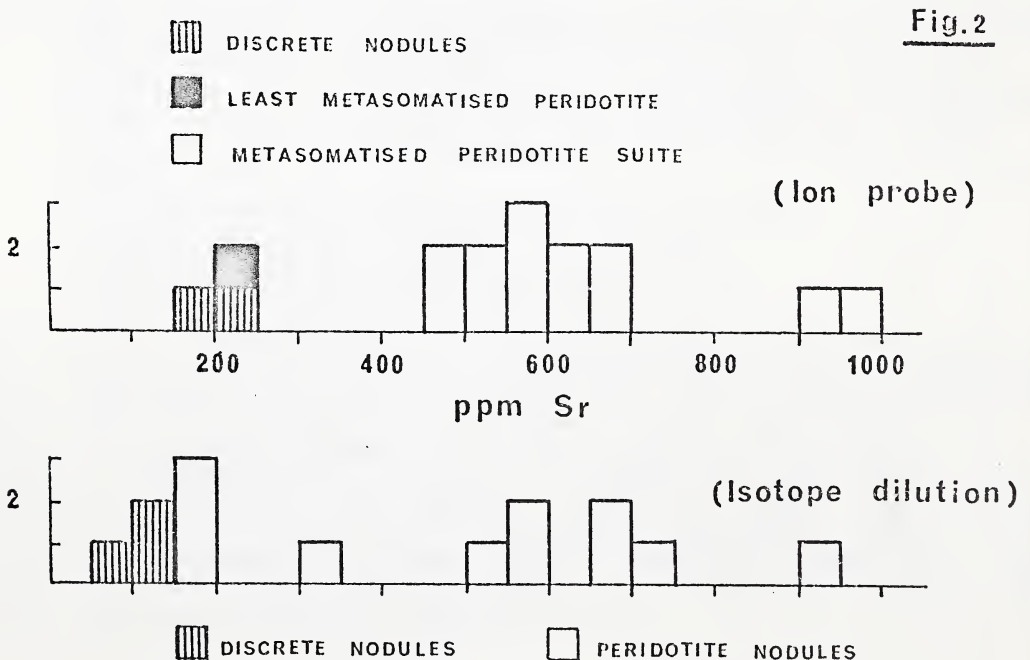


Fig. 1. Isotopic relationships in nodules and kimberlite from the Bultfontein pipe.

Fig. 2. Sr contents of diopsides from nodules from the five major Kimberley pipes. Isotope dilution data from Barrett (1975), Shimizu (1975) and Kramers (1977).



Variations in Stable Isotope Compositions for Carbon and Oxygen in some
South African and Lesothan Kimberlites

B.J. Kobelski, Exxon Co., U.S.A. Box 496, Harvey, Louisiana 70058.
D.P. Gold, and P. Deines, Department of Geosciences, The Pennsylvania
State University, University Park, Pa. 16802.

The 142 samples studied are of kimberlite matrix from some diamond-bearing pipes and other kimberlite bodies visited on the field trips associated with the First International Kimberlite Conference in 1973. These rocks were grouped into three types in a compound classification scheme based on, (a) descriptions in the literature, (b) textural, mineralogical and petrographic descriptions on the hand specimens and thin sections, and (c) field relationships within each kimberlite body. They are:

Type 1 kimberlite or massive kimberlite lacks fragments and has a dense, dark matrix composed of olivine, serpentine, ilmenite, small fibrous aggregates of phlogopite, and carbonates. The carbonates in the 42 samples analysed occur in one or more of the following habits:

- (a) segregations or ocelli,
- (b) irregular bladed carbonate crystals that look like a quench product,
- (c) disseminated anhedral grains,
- (d) replacement products in sub- and anhedral olivine grains.

Type 2 group, represented by 23 samples, occurs generally in tabular bodies composed predominantly (>60%) of anhedral carbonate, with minor magnetite or ilmenite and serpentine, and accessory phlogopite in a medium to fine-grained hypautomorphic granular textured rock. These "dikes" differ in color (grey) and texture (granular and locally poikilitic) from the adjacent kimberlite, and they are considered to be "late stage" carbonatite-kimberlites. Carbonate metasomatism of the host rock has produced the "piebald kimberlite" at Premier Mine.

Type 3 group (77 samples) is termed fragmental kimberlite due to their brecciated appearance. Phenocrysts of "rounded" olivine, serpentinized olivine, pyroxene, pyrope garnet, and angular fragments of country rocks occur in a dense matrix of serpentine, phlogopite, and carbonates. Lapilli of earlier generated kimberlite are an important but rare autolithic component. The carbonate minerals occur in the following habits:

- (a) large "rounded" nodules of crystalline limestone,
- (b) angular limestone fragments (sedimentary),
- (c) small aggregates of carbonates in the matrix,
- (d) finely dispersed grains in the matrix.

The only carbonate minerals detected by XRD analysis were calcite and dolomite. Figure 1 is $\delta^{13}\text{C}$ versus $\delta^{18}\text{O}$ plot of the isotopic data obtained with geographic locality. The carbon values are more variable than has been determined previously by other workers. The average carbon and oxygen isotopic compositions of the kimberlites by location are summarized in Table 1, under title of matrix, inclusions or segregations, and the total. In Figure 2 the mean $\delta^{13}\text{C}$ and $\delta^{18}\text{O}$ values have been plotted for each locality, together with "error" bars to represent standard deviations from the mean. Each location is numbered except for the solid square, which represents the mean isotopic composition of the Premier Mine carbonatite-kimberlite dikes (type 2), and the solid circle which indicates the fragmental kimberlite (type 3) at this same location.

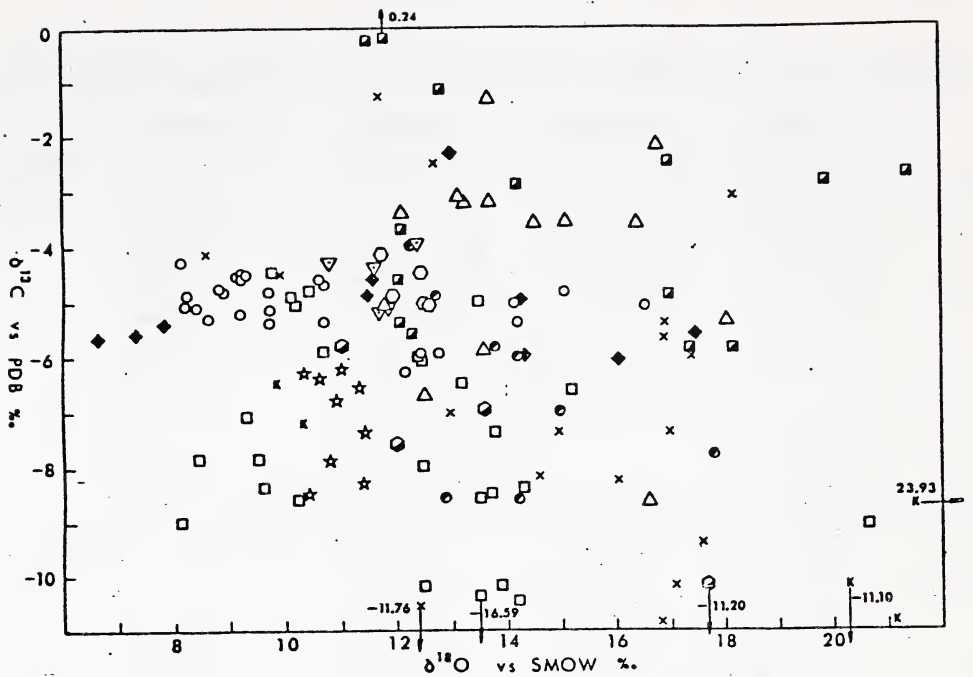


Figure 1 The isotopic composition of South African and Lesothan kimberlite carbonates of this investigation. Symbols are for localities and represent: ○ = Benfontein Sill, × = DeBeers Mine, ◆ = Wesselton, △ = Monastery Mine, ■ = National, □ = Premier, ▽ = Ngopetsau, ☆ = Star Mine, ● = Pipe 200, K = Kao, ● = Marakabei, ⊙ = Roberts Victor.

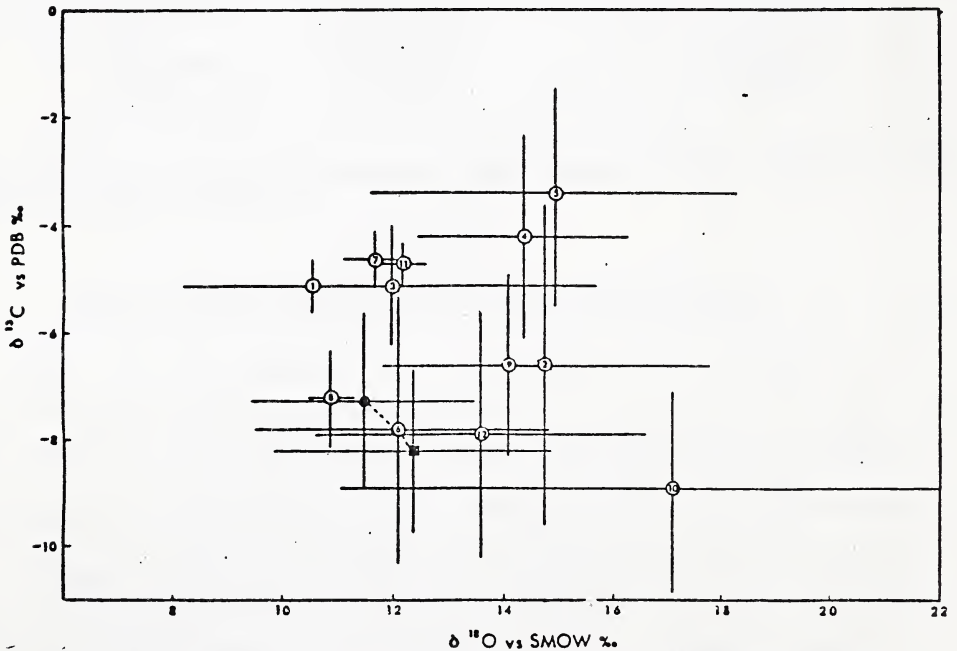


Figure 2 The mean isotopic composition for kimberlite carbonates this investigation by location. Numbers within circles represent: 1 = Benfontein Sill, 2 = DeBeers Mine, 3 = Wesselton, 4 = Monastery Mine, 5 = National, 6 = Premier Mine, 7 = Ngopetsau, 8 = Star Mine, 9 = Pipe 200, 10 = Kao, 11 = Marakabei, 12 = Roberts Victor.

TABLE 1

The Mean Carbon and Oxygen Isotopic Composition of Kimberlites of this Study

	<u>Location</u>	<u>Matrix</u>	<u>Inclusion</u>	<u>Total</u>
$\delta^{13}\text{C}$ vs PDB ($^{\circ}/\text{oo}$)	Benfontein Sill	-5.21 \pm 0.54 (13)	-4.91 \pm 0.38 (12)	-5.07 \pm 0.48 (25)
	DeBeers	-5.99 \pm 2.29 (7)	-7.11 \pm 3.45 (10)	-6.65 \pm 3.00 (17)
	Wesselton	-4.88 \pm 1.32 (6)	-5.44 \pm 0.65 (4)	-5.12 \pm 1.10 (10)
	Monastery	-4.50 \pm 2.30 (6)	-4.03 \pm 1.73 (8)	-4.23 \pm 1.92 (14)
	National	-4.41 \pm 1.17 (5)	-2.90 \pm 2.29 (9)	-3.44 \pm 2.05 (14)
	Premier	-7.18 \pm 1.86 (18)	-9.10 \pm 3.37 (8)	-7.77 \pm 2.52 (26)
	Ngopetsou	-4.60 \pm 0.41 (3)	-4.59 \pm 0.86 (2)	-4.59 \pm 0.52 (5)
	Star	-7.61 \pm 0.80 (6)	-6.33 \pm 0.04 (3)	-7.18 \pm 0.90 (9)
	Pipe 200	-6.84 \pm 1.51 (5)	-6.22 \pm 2.29 (3)	-6.61 \pm 1.71 (8)
	Kao	-8.89 \pm 2.09 (5)		-8.89 \pm 2.09 (5)
	Marakabei	-4.74 \pm 0.41 (5)		-4.74 \pm 0.41 (5)
	Roberts Victor	-6.81 \pm 0.89 (3)	-11.20 (1)	-7.91 \pm 2.31 (4)

$\delta^{18}\text{O}$ vs SNOW ($^{\circ}/\text{oo}$)	Benfontein Sill	11.62 \pm 2.86	9.42 \pm 0.92	10.56 \pm 2.39
	DeBeers	12.82 \pm 2.72	16.22 \pm 2.23	14.82 \pm 2.93
	Wesselton	10.62 \pm 4.21	13.98 \pm 1.85	11.97 \pm 3.74
	Monastery	16.26 \pm 1.29	12.96 \pm 0.72	14.37 \pm 1.94
	National	13.70 \pm 3.47	15.70 \pm 3.31	14.98 \pm 3.38
	Premier	11.38 \pm 2.11	13.87 \pm 3.14	12.14 \pm 2.68
	Ngopetsou	11.40 \pm 0.51	12.09 \pm 0.46	11.68 \pm 0.57
	Star	11.04 \pm 0.38	10.66 \pm 0.32	10.91 \pm 0.39
	Pipe 200	14.71 \pm 1.95	13.14 \pm 1.02	14.12 \pm 1.77
	Kao	17.10 \pm 6.56		17.10 \pm 6.56
	Marakabei	12.23 \pm 0.39		12.23 \pm 0.39
Roberts Victor	12.23 \pm 1.31	17.74	13.61 \pm 2.95	

The mean carbon and oxygen isotopic compositions for the different kimberlite types are given in Table 2.

TABLE 2

Mean Isotopic Composition of Kimberlites by Type

	Item	Matrix	Inclusion	Total
$\delta^{13}\text{C}$ ($^{\circ}/\text{oo}$)	Type 1	-5.67 \pm 1.46(29)	-4.84 \pm 0.44(13)	-5.41 \pm 1.29(42)
	Type 2	-7.09 \pm 2.19(15)	-7.58 \pm 1.17(7)	-7.24 \pm 3.64(22)
	Type 3	-6.01 \pm 2.08(38)	-5.38 \pm 3.00(39)	-5.67 \pm 2.59(77)
$\delta^{18}\text{O}$ ($^{\circ}/\text{oo}$)	Type 1	11.98 \pm 2.11	9.64 \pm 1.18	11.26 \pm 2.16
	Type 2	11.73 \pm 2.30	14.33 \pm 3.59	12.56 \pm 2.96
	Type 3	13.40 \pm 4.04	14.39 \pm 2.68	13.90 \pm 3.43

Angular carbonate xenoliths have similar $\delta^{13}\text{C}$ values as the matrix carbonate. Xenocrystic carbonates tend to be enriched in $\delta^{13}\text{C}$ (heavier) with respect to the matrix. Unzoned and "rounded" carbonate nodules yield similar isotopic values to the matrix carbonates, and are interpreted as cognate xenoliths. Ocelli in the Benfontein sill have a similar $\delta^{13}\text{C}$ value to the matrix carbonates, but are heavier by about 1‰ than early "quench" carbonate needles. Pisolitic kimberlite lapilli and the carbonate matrix, that occur in pipe-like habit in the Star Mine, have similar $\delta^{13}\text{C}$ values, suggesting they originated from the same source. Both the $\delta^{13}\text{C}$ and $\delta^{18}\text{O}$ values of "replacement" carbonates are highly variable and distinctive from those of the matrix carbonates.

Statistical treatments of the data were utilized to construct frequency distributions and to test the various categories for normality. Each of the several groups of kimberlites were analysed with regard to their mean carbon isotopic composition by an Analysis of Variance procedure (ANOVES/ANOVUM). The mean $\delta^{13}\text{C}$ of type 2 (carbonatite-kimberlite) was found to test significantly different from either type 1 (massive) or type 3 (fragmental) kimberlites, and the type 1 and type 3 kimberlites were found to be isotopically similar. The mean $\delta^{13}\text{C}$ of the three general groups of kimberlites are:

Type 1 = -5.41 ‰, \pm 1.29;

Type 2 = -7.24 ‰, \pm 3.64;

Type 3 = -5.67 ‰, \pm 2.59.

Another test (ANOVUM) showed that the mean $\delta^{13}\text{C}$ of isotopically similar kimberlite types (e.g., 1 and 3) may be significantly different with locality. A similar analysis of the $\delta^{18}\text{O}$ data yielded inconclusive results. However, a comparison of the mean $\delta^{18}\text{O}$ values of kimberlites by their geographic location reveals a possible significant difference.

Dolomite samples from the Benfontein kimberlite sills were found to be significantly heavier in $\delta^{13}\text{C}$ (+0.65 ‰) than coexisting calcites. It was noted that the enrichment in $\delta^{13}\text{C}$ in dolomites is characteristic of primary carbonatites.

A comparison between subsamples with different habits of carbonate indicates there is a high "in-sample" variability, and that steep isotopic gradients can occur between different phases. This comparison, the statistical tests of the $\delta^{13}\text{C}$ and the $\delta^{18}\text{O}$ data, and a search of the recent literature suggests that the observed isotopic variation may be a number of factors, the most likely being:

- (1) Carbon isotopic fractionation process between an initial "heavy" silicate + CO_2 kimberlite phase, and a later "light" carbonatite phase;
- (2) meteoric-hydrothermal fluid interaction with the kimberlite after emplacement, evidenced by isotopically distinctive replacement carbonates within the kimberlite;
- (3) a degassing process of the isotopically heavy CO_2 - H_2O phase during emplacement;
- (4) isotopic inhomogeneities due to geography and elevation, which may be a function of, (a) a "combined isotopic effect" of all the above factors, (b) isotopic inhomogeneity of the kimberlite magmas, and (c) isotopic inhomogeneity of carbon in the mantle.

Summary and Conclusions

1. The mean isotopic composition of carbonates in 142 kimberlite samples from 12 kimberlite localities in Southern Africa were determined as $\delta^{13}\text{C} = -5.92\text{‰}$ vs PDB ($\sigma_{\pm} 2.42$), and $\delta^{18}\text{O} = 12.91\text{‰}$ vs SMOW ($\sigma_{\pm} 3.23$).
2. Although the mean isotopic (carbon) composition is comparable to the values established for diamonds and carbonatites (see Figure 3), the mean oxygen isotopic composition of these kimberlites is enriched in $\delta^{18}\text{O}$ by several permil with respect to carbonatites.
3. The $\delta^{13}\text{C}$ and $\delta^{18}\text{O}$ values range from 0.24 ‰ to -11.76 ‰, and 6 ‰ to 24 ‰, respectively.
4. Three main types of kimberlite (massive, fragmental, and carbonatite-kimberlite) were distinguished on textural, petrographic and isotopic criteria.
5. There is a significant difference in the mean $\delta^{13}\text{C}$ of some kimberlites from different localities. For those kimberlite locations where the differences between their mean $\delta^{13}\text{C}$ and $\delta^{18}\text{O}$ values are too great to be explained by a "combined isotopic effect process", then an inhomogeneous source reservoir of carbon isotopes is inferred.
6. Many samples and analyses are needed for a meaningful isotopic characterization of a kimberlite body.

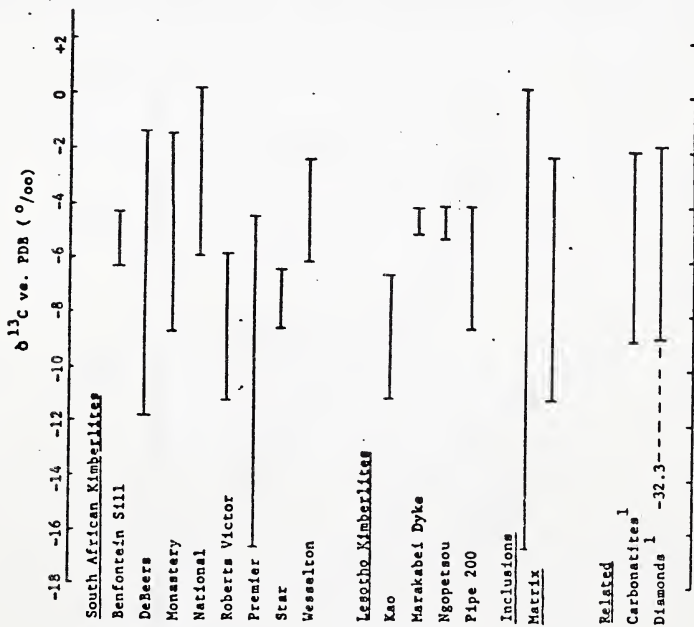
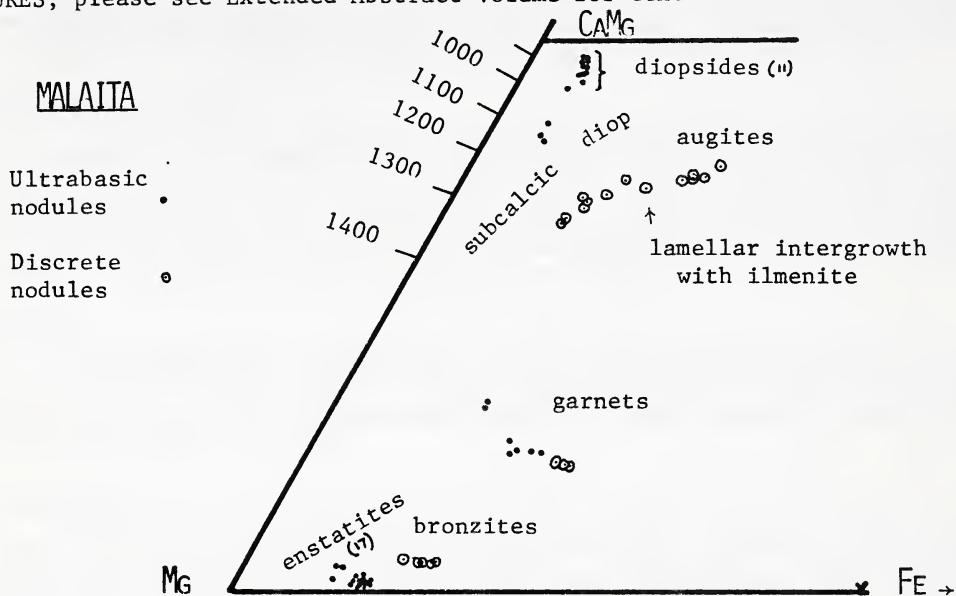


Figure 3 The overlap of the carbon isotopic composition for kimberlite carbonates from the kimberlite localities of this study. Data for carbonatites and diamonds are from : 1. compiled by Deines and Gold (1973) from various works.

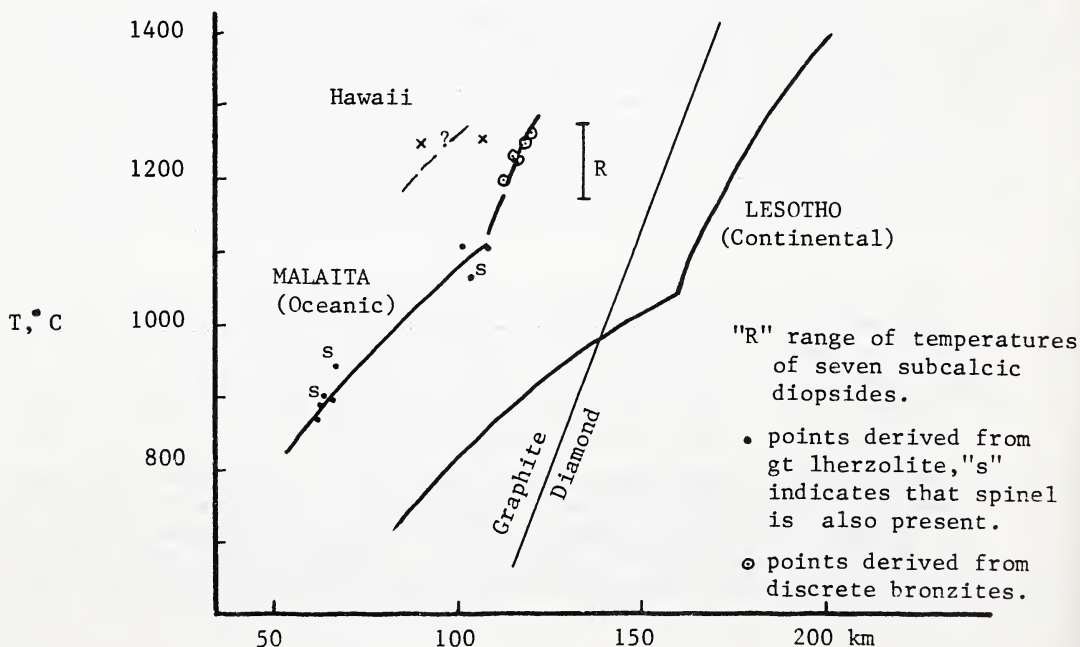
GARNET BEARING ULTRABASIC AND DISCRETE NODULE SUITES FROM MALAITA, SOLOMON ISLANDS, S.W. PACIFIC, AND THEIR BEARING ON AN OCEANIC GEOTHERM

P.H. Nixon (Dept. Geology, The University, Port Moresby, Papua/New Guinea)
 F.R. Boyd (Geophysical Laboratory, Washington, D.C., U.S.A.)

FIGURES; please see Extended Abstract Volume for text



Compositions of minerals from the ultrabasic and discrete nodule suites from the alnoitic pipe, Babaru'u, Malaita, Solomon Islands, S.W. Pacific.



Comparison of Oceanic (Malaita) geotherm with that of Continental (Lesotho) geotherm. Two points calculated from reconstituted unexsolved pyroxene data of Beeson and Jackson (1970) for Hawaiian garnet pyroxenite nodules are also shown. The graphite/diamond equilibrium boundary is from Kennedy and Kennedy (1976).

D.K. Paul (Geological Survey of India, Calcutta 16, India)

Samples analysed:

Concentrations of rubidium, strontium and isotopic compositions of strontium are reported for twenty three kimberlites from India. The samples are from six diatremes occurring in two petrographic provinces and have been collected from surface, underground mine and bore hole core.

Analytical method:

Concentrations of Rb and Sr have been determined by isotope dilution. The procedure for separation and purification of Rb and Sr and mass spectrometry is similar to that described by Burwell (1975). Blank levels varied from 12 to 25 ng for Sr. Measured $^{87}\text{Sr}/^{86}\text{Sr}$ ratios have been normalized to a $^{86}\text{Sr}/^{88}\text{Sr}$ ratio of 0.1194. The mean value for Eimer and Amend standard Sr obtained during the course of the work is 0.7081.

Results:

Abundances of Rb, Sr and the $^{87}\text{Sr}/^{86}\text{Sr}$ ratios are presented in Table 1. The initial $^{87}\text{Sr}/^{86}\text{Sr}$ ratios from the Majhgawan pipe (Central India) range from 0.7030 to 0.7064 corresponding values in three pipes from south India vary from 0.7027 to 0.7102.

Discussion:

The kimberlites of the present study exhibit large variations in Sr isotope ratios, but the spread is within the range established earlier for kimberlites (Mitchell and Crocket, 1971; Berg and Allsopp, 1972; Barrett and Berg, 1975). General geological and petrographical description of the Indian kimberlites have been given by Paul et al., (1975 a). Based on the criteria of Berg and Allsopp (1972), the south Indian occurrences would be classified as 'fresh' and those from central India as 'altered'. From Table 1, it is observed that the $^{87}\text{Sr}/^{86}\text{Sr}$ ratios are not related to the degree of alteration. Leaching experiments on three whole rock kimberlites with dil. H_3PO_4 showed no significant difference in the Sr isotopic composition of the leached solution and residue. The Indian kimberlites have been emplaced through Precambrian granites and gneisses, estimated to be 40 - 45 km thick. One sample of basement granite from Wajrakarur (south India) gave a $^{87}\text{Sr}/^{86}\text{Sr}$ ratio of 0.7101 and a strontium content of 668 ppm. A significant amount of contamination of crustal rocks of this composition would be required to obtain the Sr isotope ratios of kimberlites (Table 1). There is no evidence for such assimilation.

The mineralogy of kimberlites and associated nodules indicate their deep-seated nature. Some of the Indian kimberlites are, however, enriched in ^{87}Sr compared to the normal mantle region. Two explanations can be offered to explain this : (a) disequilibrium partial melting in the source region where no isotopic equilibration was attained between the melt and the residue, and (b) equilibrium melting of a heterogeneous source. In the first hypothesis, the isotopic composition of Sr in the initial melt would be mainly controlled by phlogopite on account of its high Rb/Sr and $^{87}\text{Sr}/^{86}\text{Sr}$ ratios (Sun and Hanson, 1975), leading to higher $^{87}\text{Sr}/^{86}\text{Sr}$ ratios in the melt compared with the parent. When other minerals e.g. olivine, orthopyroxene contribute to the melt, the $^{87}\text{Sr}/^{86}\text{Sr}$ ratios will tend to decrease. This agrees with the REE

distribution patterns (Paul et al. 1975 b) in that kimberlites are derived by small amounts of partial melting in a peridotitic mantle. Accordingly, isotopic composition of Sr would depend on the extent of melting. Alternatively, the isotopic characters of kimberlites may be inherited from the source region which had undergone enrichment of LIL elements in small sub-systems with variable Rb/Sr ratios. Indeed, Brooks et al., (1976) showed that subcontinental mantle has Sr isotope ratios from 0.703 to 0.710, a range encompassed by the kimberlites. In this case, variable isotopic composition of kimberlites would be a necessary consequence of melting in the heterogeneous source region.

References:

Barrett D.R. and Berg G.W. (1975). *Physics and Chemistry of the Earth*, 9, 619 - 636.

Berg G.W. and Allsopp, H.L. (1972). *Earth Planet. Sci. Lett.*, 6, 27 - 30.

Brooks C., James D.E. and Hart S.R. (1976). *Science*, 193, 1086 - 1094.

Burwell A.D.M. (1975). *Earth Planet. Sci. Lett.*, 29, 69 - 78.

Mitchell R.H. and Crocket J.H. (1971). *Contrib. Mineral. Petrol.*, 30, 277 - 290.

Paul, D.K. Rex D.C. and Harris P.G. (1975 a). *Bull. Geol. Amer.*, 86, 364 - 366.

Paul D.K., Potts P.J., Gibson I.L. and Harris P.G. (1975 b). *Earth Planet. Sci. Lett.*, 25, 151 - 158.

Sun S.S. and Hanson G.N. (1975). *Geology*, 3, 296 - 302.

TABLE 1: Rb, Sr and $^{87}\text{Sr}/^{86}\text{Sr}$ ratios of Indian Kimberlites.

Sample No.	Rb ppm	Sr ppm	$^{87}\text{Rb}/^{86}\text{Sr}$	$^{87}\text{Sr}/^{86}\text{Sr}$ measured	$^{87}\text{Sr}/^{86}\text{Sr}$ @ initial
------------	-----------	-----------	---------------------------------	---	--

Central India

MG 21	20.3	1206.6	0.049	0.7036	0.7030
MG 50	43.1	1513.4	0.083	0.7044	0.7033
MG 11	15.8	87.8	0.052	0.7045	0.7038
MG 40	37.3	1343.2	0.080	0.7048	0.7038
MG 6	36.3	1207.7	0.087	0.7050	0.7038
MG 25	39.3	1343.9	0.085	0.7051	0.7040
UG 11A	81.1	1558.1	0.151	0.7066	0.7045
UG 136	97.6	1577.8	0.179	0.7069	0.7043
UG 84	60.0	1316.0	0.132	0.7073	0.7064
HV 4/4	99.1	1824.6	0.157	0.7063	0.7041
HV 4/7	63.6	1047.6	0.176	0.7074	0.7050
HV 4/1	29.8	605.6	0.143	0.7086	0.7067
HV 4/6	37.0	628.0	0.171	0.7093	0.7068

South India

WK 1/1	6.3	760.5	0.024	0.7044	0.7044
--------	-----	-------	-------	--------	--------

Table 1 contd.

Sample No.	Rb ppm	Sr ppm	$^{87}\text{Rb}/^{86}\text{Sr}$	$^{87}\text{Sr}/^{86}\text{Sr}$ measured	$^{87}\text{Sr}/^{86}\text{Sr}$ initial @
WK 2/7	146.1	858.6	0.493	0.7102	0.7060
WK 2/6	174.5	936.3	0.540	0.7106	0.7043
WK 2/9	206.6	1089.3	0.550	0.7121	0.7057
WK 2/5	185.0	774.7	0.692	0.7142	0.7061
LM 3/5	4.5	560.4	0.024	0.7094	0.7091
LM 3/4	125.9	863.7	0.422	0.7160	0.7102
LM 4/6	120.8	666.3	0.525	0.7102	0.7027
LM 4/7	108.9	508.7	0.620	0.7132	0.7046
LM 4/9	153.6	642.4	0.699	0.7141	0.7043
WK granite	38.1	667.9	0.165	0.7101	

@ assumed age for samples with prefix WK is 840 Ma; for others assumed age is 1000 Ma (Paul et al., 1975 a)



